Composition and microstructure of concrete mixtures subjected to biogenic acid corrosion and their role in corrosion prediction of concrete outfall sewers

Moses Wopicho Kiliswa

Thesis submitted in fulfillment of the requirements for the degree of **Doctor of Philosophy** in the University of Cape Town

March 2016

Declaration

I declare that this thesis is essentially my own work and is being submitted for the degree of Doctor of Philosophy in the University of Cape Town. It has not been submitted before for any degree or examination at any other university. In addition, I know the meaning of plagiarism and declare that all the work in this document, save for that which is properly acknowledged, is my own.

Signed: Signed by candidate Date: 19 March 2016

Moses Wopicho Kiliswa

Abstract

Wastewater conveyance and treatment facilities, which include outfall sewers, manholes, and treatment works, are among the key constituents of a country's infrastructure. Most of these facilities are made of concrete due to its low production costs, versatility, inherent strength and durability under most conditions. However, under certain conditions, sewage that is conveyed through outfall sewers becomes septic and hydrogen sulphide (H_2S) gas is generated. When this gas is released from the sewage and absorbed onto the moist concrete sewer pipe walls, it is microbially converted by sulphide-oxidising bacteria to sulphuric acid (biogenic H_2SO_4) which reacts with the acid-soluble components of concrete causing it to corrode. In principle, the biogenic H_2SO_4 concrete corrosion mechanism entails simultaneous destruction of the calcium hydroxide (CH) in the hydrated cement paste (HCP) and substituting a larger molecule of calcium sulphate into the concrete matrix thus causing pressure and spalling of the adjacent concrete and aggregate particles. In addition, the calcium sulphate precipitates as gypsum which reacts with various aluminates to form secondary ettringite. These mechanisms lead to the loss of stiffness and strength, accompanied by expansion and cracking, and eventually transformation of the affected concrete matrix into a soft and pulpy non-cohesive layer.

The biogenic concrete corrosion rate depends, inter alia, on the chemical composition of binders (cement and supplementary cementitious materials (SCMs)) and microstructural characteristics of concrete mixtures used in the manufacture of sewer pipes. The needed properties of concrete mixtures for sewer pipe applications can be determined by biogenic corrosion prediction models, such as the widely used deterministic (mechanistic) Life Factor Method (LFM). The service life of wastewater treatment facilities made of concrete depends on the input parameters in corrosion prediction models. The motivation behind the current study was based on the need to improve the ability to predict the design life of concrete sewers by improving the input parameters in the LFM, which is used in South Africa. The design life of concrete sewers in South Africa has traditionally been 40 years.

The main objective of the current study was to characterise the microstructure of both Portland cement (PC) and calcium aluminate cement (CAC) based concrete mixtures that had been subjected to biogenic corrosion mechanisms in an operational sewer environment for approximately 127 months (10½ years); further, based on the understanding of the underlying mechanisms of attack, proposals were made to improve the LFM, for which the corrosion rate-controlling input parameter, referred to as *alkalinity* (or equivalent $CaCO_3$, as a summation for both binder and aggregate) is based on the characteristics of plain PC-based binder systems. In addition to the main objective above, a parallel study was undertaken to characterise parameters that influence biogenic concrete corrosion rates based on measurements taken in two sewer environments/sites in different geographical locations in South Africa. One of the study sites was the Virginia Experimental Sewer (VES) in Virginia, Free State Province, while the other site was a manhole within the Langa Pump Station in Cape Town, Western Cape Province. The VES consists of 900 mm diameter by 300 mm long concrete pipe samples made from both PC- and CAC-based (plain and blended) binder systems, the top 120° being cut to form 'lids', so that they are removable. The removable 'lids' enable scheduled observations and sample recovery to be undertaken. Moreover, the 'lids' also act as windows through which core samples can be placed in plastic baskets that are hung at certain sections in the sewer headspace, so that they can be accessed for monitoring.

To address the objectives of the current study, experimental programs were run concurrently on two sites. One of the experimental programs entailed monitoring certain sewer parameters in-situ, in both the VES and in the manhole at Langa. These parameters included sewage pH and temperature, sewer headspace temperature, relative humidity (RH), and gas (hydrogen sulphide

(H_2S)) concentration. Moreover, in order to understand the mechanisms of attack in different sewer exposure conditions, newly cast concrete cores with similar properties (density, compressive strength, oxygen permeability and water sorptivity) as concrete sewer pipes were installed in the VES and manhole at Langa after 28 d of curing at a temperature of 22 ± 2 °C and RH of 50% for surface pH vs. time profiling. The surface pH vs. time profiling was undertaken for a period of approximately 6 months (185 d) after installation of the cores in the sewer environments. Surface pH can be used to characterise activities of acid-generating microbes. The other experimental program entailed (i) determination of biogenic corrosion rates, (ii) microstructural characterisation of concrete mixtures subjected to biogenic acid attack, and (iii) characterising the microbial diversity on the surfaces of concrete sewer pipes under biogenic acid attack. Biogenic corrosion rates were based on the measurement of mass and changes in dimensions of the 'lid' and core samples installed in the VES, while microstructural studies were based on scanning electron microscopy (SEM) and energy-dispersive spectroscopy (EDS), quantitative X-ray diffraction (XRD), and thermogravimetric analysis (TGA) techniques. SEM/EDS analysis was undertaken both on products of corrosion and on polished concrete sections. Microbial speciation was based on the bacteria community fingerprinting technique by assaying genomic deoxyribonucleic acid (gDNA).

Samples used in the SEM/EDS, XRD and TGA analysis consisted of products of corrosion that were carefully scraped from the surfaces of the 'lids'. Immediately after scraping, they were placed in clean 50 ml air-tight plastic bottles, leaving a space of about 10 mm from the bottle top. These bottles were then stored in an insulated 'Cooler Box' and transported from the field to the laboratory within 36 hours after sampling. In the laboratory, the samples were dried using the solvent-exchange method in isopropanol before being gently 'ground' using a pestle and mortar to obtain a powder. This powder was then sieved through a 63 µm sieve to obtain the respective final test specimens. The products of corrosion used for microbial speciation were not subjected to the solvent-exchange drying process, but were air-dried for 24 h prior to undertaking the test regime. The polished concrete sections used for SEM/EDS analysis consisted of approximately 20 mm^3 resin-embedded blocks sawn from larger sections taken from the lower portion, not the 'lid' of the 300 mm long pipes in the VES, which had also been subjected to biogenic acid attack.

Results from the comparison of mechanisms of attack in different sewer environments showed that despite the different environmental characteristics (both geographical and operational) of the VES and manhole at Langa, the surface pH vs. time profiles were similar during the 6-month monitoring period, although generally, the surface pH on samples installed in the manhole at Langa decreased at a slightly higher rate (factor of approximately 1.04) than those in the VES. After exposing the core samples in the two sewer environments for approximately 6 months, the surface pH range on PC-based mixtures was between 2.42 and 5.68, whereas that on CAC-based mixture was between 3.73 and 4.40. Moreover, from the results on microbial speciation, the phylogenetic relatives of microbes found in the products of corrosion taken from both PC- and CAC-based concrete mixtures consisted of those that (i) can grow at low levels of nutrients (alphaproteobacteria), (ii) those that use nutrient substances that emanate from areas of anaerobic decomposition such as H_2S (betaproteobacteria), and (iii) those that oxidise H_2S instead of water to produce sulphur as a waste product (gammaproteobacteria), all growing optimally between pH 2 and 7.

The backscattered electron (BSE) micrographs from SEM analysis of the polished concrete sections showed three distinct layers within the depth of the concrete matrices; (i) the sound matrix that had not been subjected to biogenic acid attack, (ii) the deteriorated matrix that had been completely transformed into a non-cohesive layer through biogenic acid attack mechanisms, and (iii) the semi-deteriorated matrix that had been partially subjected to biogenic acid attack, and which formed an interface between the sound and deteriorated matrices. Results from microstructural characterisation of concrete mixtures subjected to biogenic acid attack showed that the deteriorated matrices on both PC- and CAC-based mixtures consist predominantly of gypsum. Within the semi-deteriorated matrices of both PC- and CAC-based concrete mixtures, the

concentration of calcium species was lower than that in both the deteriorated and sound matrices of the respective mixtures. Within the semi-deteriorated matrices of CAC-based concrete mixtures, the concentration of the alumina species was higher than that of the sound matrix. From the EDS point analyses, the alumina-rich layer within the semi-deteriorated matrices of CAC-based mixtures was identified as AH_3 (or AH_x gel). On the other hand, a comparative EDS point analysis of the ratios Fe/Ca and Al/Ca in the sound matrices of PC- and CAC-based concrete mixtures showed a higher concentration of Fe (FeO(OH) and Al (AH_x) in the sound matrices of CAC-based concrete mixtures than in PC-based concrete mixtures. The characteristics of these three distinct layers influence the deterioration rate of the respective binder systems, when they are subjected to biogenic acid attack.

A comparison of the biogenic concrete corrosion rates between various binder systems showed that CAC-based mixtures have a lower corrosion rate than PC-based mixtures. This improved performance was attributed to the neutralisation capacity of the CAC hydrates, and to the bacteriostatic effect caused by higher concentrations of Al^{3+} and Fe^{3+} in CAC.

Based on the experimental results, a framework was proposed to increase the range of input parameters in the LFM with the view of improving the prediction of biogenic concrete corrosion rates, considering binder systems other than plain PC. In this regard, (i) the influence of equivalent CH, AH_3 and FeO(OH) were incorporated within the *alkalinity* (equivalent $CaCO_3$, which was distinguished between binder and aggregate) component of the LFM, resulting in a part of the equation that addresses the neutralisation capacity (*NC*) of binders, and (ii) additional input parameters relating to the nature of the hydrates ((Al + Fe)/Ca) were incorporated within the *NC* component to further address the influence of the respective HCP phases in suppressing the activities of acid-generating sulphide-oxidising bacteria. These additional parameters resulted in what is termed the *effective resistance capacity* ($RC_{eff.}$) of concrete mixtures. This proposed improved LFM equation contributes to achieving a wider scope of design parameters, and thus more accurate prediction of design lives of concrete sewers through application of an understanding of the microstructure of various concrete mixtures used in the manufacture of concrete sewer pipes, although further work is required.

Dedication

To my dear wife Gathoni, and our dear daughters Nekoye and Wangũi

Acknowledgements

Much appreciation is extended to my supervisor, Professor Mark Alexander, and advisors, Associate Professor Hans Beushausen and Professor Pilate Moyo for their guidance and support.

I would like to thank the following organisations for their valuable support in one way or another: Rocla (Pty) Ltd; Kerneos SA (Pty) Ltd; Haw & Inglis Group; Aveng Grinaker-LTA; The Concrete Institute; The National Research Foundation; Sika South Africa (Pty) Ltd; Pretoria Portland Cement (PPC) Ltd; AfriSam South Africa (Pty) Ltd; The Water Research Commission; Dedan Kimathi University of Technology (Kenya).

I would also like to express my appreciation to Alaster Goyns, PrEng, for his invaluable guidance; Professor Karen Scrivener of EPFL, Switzerland; Dr Hervé Fryda of Kerneos, France; Prof Manu Santhanam of IIT Madras, India; Anic Smit, Nigel Ireland and Freddie Williams of the City of Cape Town; Dr Robin Beddoe of the Technical University of Munich, Germany; Dr Rob van Hille and Dr Rob Huddy of the Centre for Bioprocess Engineering Research, Department of Chemical Engineering, UCT; Dr Bjorn Hohlig of Leipzig University of Applied Sciences, Germany; Tanya Dreyer and Nicholas Laidler of the X-Ray Diffraction Unit, Department of Geological Sciences, UCT; Miranda Waldron of the Electron Microscope Unit, Centre for Imaging and Analysis, UCT; Nooredien Hassen, Charles May and all Civil Engineering laboratory staff, UCT; all administrative staff, Department of Civil Engineering, UCT; Kassie Botha of Virginia, Free State Province.

Special thanks to the Kamau-Kiliswa family.

Finally, I wish to give thanks to all CoMSIRU members for upholding an extremely conducive environment for research.

Each age produces its own architecture out of its own materials and technology
- Eero Saarinen (1910 – 1961)

Ours is the age of concrete.

Table of Contents

List of Figures

List of Tables

Glossary

The following definitions clarify terms used in this thesis that are either not commonly used in concrete technology or their use here does not necessarily apply to normal use.

Abiotic	Not derived from living organisms (involves physical rather than biological mechanisms)
Acidophilic	Microorganisms that survive in environments with pH below 4
Adenosine triphosphate	A molecule that is used in cells as a coenzyme for intracellular energy transfer. It transports chemical energy within cells for metabolism
Aerobic	Condition of cellular respiration in the presence of oxygen
Alkalinity	A conventional quantitative capacity of an aqueous solution to neutralise an acid to the equivalence point of carbonate or bicarbonate. In concrete technology, it is taken as equivalent total $CaCO_3$ content in a concrete mixture (or g $CaCO_3$ per g concrete material), not basicity as measured by pH
Anaerobic	Condition of cellular respiration in the absence of oxygen
Anoxic	An environment without oxygen (microorganisms utilise nitrate instead of oxygen as an electron acceptor)
Bacteriostatic	Limits the growth bacteria by interfering with bacterial protein production, DNA replication, or other aspects of bacterial cellular metabolism
Biodegradable	Decomposes by action of living organisms, usually bacteria
Biofilm	A densely packed community of microbial cells that grow on living or inert surfaces and surround themselves with secreted polymers (long chains)
Biogenic	Generated by living organisms or biological processes
Biogeochemical cycle	A pathway by which a chemical substance moves through both abiotic and biotic environments
Biotic	Derived from or related to living organisms (involves biological mechanisms)
Brownian motion	The random motion of particles suspended in a fluid resulting from their collision with the fluid's atoms or molecules
Catabolism	A set of metabolic pathways that breaks down molecules into smaller units that are primarily oxidised to release energy for maintenance and growth of cells in (micro) organisms
Chemotrophs	Organisms that derive their energy from oxidation of electron donors (reduced inorganic compounds such as hydrogen sulphide, ammonia or hydrogen)
Composite cement	A hydraulic cement composed of Portland cement (PC) and one or more inorganic materials added (blended or interground) during the manufacturing process. The inorganic materials take part in the hydration reactions and thereby make a contribution to the properties of the hydrated cement paste (HCP)
Diprotic	Contains within its molecular structure two hydrogen atoms per molecule capable of dissociating in water
Electrostatic forces	Forces between particles that are caused by their electric charges
Fingerprinting	To profile the diversity of a (microbial) community
Heterotrophic	Utilises only organic substances (carbon) as source of food
Hydraulicity	Ability to set or harden while in contact with water
Hydrodynamic	Forces that are produced by flowing liquids
Hydrogen bonding	Electrostatic attraction between polar molecules that occurs when a hydrogen atom bound to a highly electronegative atom such as nitrogen or

	oxygen experiences attraction to some other nearby highly electronegative atom
Hydrolysis	A reaction involving the breaking of a bond in a molecule using water
Hydrophobic	Tendency of nonpolar substances to aggregate in aqueous solution and exclude water molecules
Isotherm	A line or curve on a diagram connecting points having the same temperature at a given time
Microbially	Formed by the interaction of single-cell organisms
Neutrophilic	Microorganisms that survive in environments with a pH range of approximately 6 to 9
Oxidation-reduction potential	A measure of an aqueous system's capacity to either release or accept electrons from chemical reactions
Polymerase	An enzyme that synthesises long chains (polymers) of nucleic acids
Polythionic acid	An oxoacid (contains oxygen) which has a straight chain of sulphur atoms
Prokaryote	Single-celled microorganism that lacks a membrane-bound nucleus
Proteobacteria	A group of bacteria that are important contributors to the biogeochemical cycles, such as the sulphur, carbon, oxygen and nitrogen cycles
Protoplasm	Living content of a cell that is surrounded by a plasma membrane. It is composed of a mixture of small micro-molecules (such as ions and amino acids) and macro-molecules (such as nucleic acids and proteins)
Septic	Characterised by foul decay or decomposition
Sound matrix	Not subjected to biogenic H_2SO_4 attack
Spectrophotometric	Measures the concentration of solutes in a solution based on the amount of light that is absorbed by the solution in a cuvette.
Stale sewage	Domestic sewage which has remained in the sewer long enough to become anaerobic
Stoichiometry	Calculation of the relative quantities of reactants and products in chemical reactions
Topochemical reaction	A chemical reaction that occurs at the boundary of solid phases
Van der Waals forces	Attraction of intermolecular forces between molecules (excludes covalent bonds or electrostatic interaction)

Abbreviations

AC	Asbestos Cement
ACPA	American Concrete Pipe Association
AE	Auger Electrons
ARISA	Automated Ribosomal Intergenic Spacer Analysis
BOD	Biochemical Oxygen Demand
BSE	Backscattered Electrons
CAC	Calcium Aluminate Cement
COD	Chemical Oxygen Demand
CSIR	Council for Scientific and Industrial Research
DNA	Deoxyribonucleic Acid
DO	Dissolved Oxygen
DOL	Dolomite
DS	Dissolved Sulphide
EDS	Energy Dispersive Spectroscopy
EPS	Extracellular Polymeric Substances
FA	Fly Ash
GGBS	Ground Granulated Blast-furnace Slag
HCP	Hydrated (or Hardened) Cement Paste
HDPE	High Density Polyethylene
HRT	Hydraulic Retention Time
IHCP	Incompletely Hydrated Cement Particles
IM	Inlet Manhole
ITZ	Interfacial Transition Zone
LFM	Life Factor Method
NCBI	National Centre for Biotechnology Information
OD	Outside Diameter
ORP	Oxidation-reduction Potential
PC	Portland Cement
PCR	Polymerase Chain Reaction
PE	Primary Electrons
RH	Relative Humidity
rRNA	Ribosomal Ribonucleic Acid
SATIR	Säure (acid), Angriff (attack), Transport, Instationär (non-stationary), Reaktion (reaction)
SE	Secondary Electrons
SF	Silica Fume
SIL	Siliceous
SOB	Sulphide-oxidising Bacteria
SRB	Sulphate-reducing Bacteria
SRT	Solids Retention Time
T-RFLP	Terminal Restriction Fragment Length Polymorphism
VES	Virginia Experimental Sewer
WATS	Wastewater Aerobic-anaerobic Transformations in Sewers
WD	Wavelength Dispersive
WWTF	Wastewater Treatment Facilities

Cement chemistry abbreviations used are as follows.

A = Al_2O_3 *(alumina)*
C = CaO *(lime)*

$\bar{C}$ = CO_2 *(carbon dioxide)*
F = Fe_2O_3 *(ferric oxide)*
f = FeO *(ferrous oxide)*
H = H_2O *(water)*
S = SiO_2 *(silica)*
$\bar{S}$ = SiO_3 *(silicate)*
C_3S = $3CaO.SiO_2$ *(Alite)*
C_2S = $2CaO.SiO_2$ *(Belite)*
C_3A = $3CaO.Al_2O_3$ *(Aluminate)*
C_4AF = $4CaO.Al_2O_3.Fe_2O_3$ *(Ferrite)*

Notations

Å	Angstrom (= 10^{-10} m or 1 nm)
AFm	Calcium aluminate monosulphate hydrate (monosulphate)
AFt	Calcium aluminate trisulphate hydrate (ettringite)
Al	Aluminium
atm	Atmosphere (= 101.325 pascal)
Ca	Calcium
H_2S	Hydrogen sulphide molecules
H_2SO_4	Sulphuric acid
HCl	Hydrochloric acid
HS^-	Hydrogen sulphide ions
kV	kilovolts
mA	milliampere
mol	Molarity
O_2	Oxygen gas
ppm	Parts per million (mg/l)
S	Sulphur
S^{2-}	Sulphide/sulphide ions
Si	Silica
SO_4^{2-}	Sulphate
w/b	Water/binder ratio
w/c	Water/cement ratio

Chapter One: Introduction

1.1 Background

Concrete is the most commonly used material for large diameter outfall sewers due to its inherent strength, durability under most conditions, and low cost of production. Furthermore, the fact that concrete pipes can generally be rehabilitated by application of cementitious or non-cementitious linings even when the cover to their reinforcing steel is corroded justifies why they are preferred to other sewer pipe materials for use in wastewater disposal pipelines, bearing in mind the high cost that is associated with premature replacement of such deteriorated facilities (Hewayde et al., 2006). Notably, approximately 40% of the total damage of concrete sewer pipes in a given sewer section can be attributed to corrosion by biogenic (microbially-induced) sulphuric acid (H_2SO_4) attack as a result of long flow periods and insufficient ventilation of the wastewater conduits (Kaempfer and Berndt, 1999). The remaining 60% can be attributed to improper foundation design and pipe installation, inadequate specifications, and lack of proper pre- and post-installation inspections (ACPA, 2008).

Fresh sewage entering a wastewater collection system contains compounds such as sulphur (S) and nitrogen (N), which are the main energy sources needed for microbial growth-related processes in sewers and for maintaining the life of already existing biomass (Hvitved-Jacobsen et al., 2013). Both S- and N-compounds are capable of being oxidised to sulphate (SO_4^{2-}) and nitrate (NO_3^-) respectively. Initially, aerobic microorganisms flourish in the sewage but as oxygen used for catabolising organic compounds becomes depleted, anaerobic-anoxic microorganisms occur. It is these anaerobic-anoxic microorganisms such as heterotrophic anaerobic bacteria (these are Proteobacteria that include sulphate-reducing bacteria (SRB) and nitrate-reducing bacteria (NRB)) that are involved in the initial processes of biogenic corrosion mechanisms in sewers. The final processes of biogenic corrosion involve other aerobic microorganisms, namely, sulphide-oxidising bacteria (SOB) that flourish on the non-submerged walls of concrete sewers.

Therefore in the first instance, there is SRB and NRB in the sewer's biofilm, and in the absence or depletion of dissolved oxygen (DO) in the sewage, SRB reduces SO_4^{2-} to sulphide (S^{2-}) while NRB reduces NO_3^- to nitrite (NO_2^-) (and eventually to ammonia (NH_3)) as alternative sources of oxygen (Hvitved-Jacobsen et al., 2013; Kohsaka et al., 2008). The rate at which sulphide and nitrite (ammonia) are produced from the activity of SRB and NRB respectively depends on a variety of environmental conditions including DO concentration, the concentration of organic food source represented by biochemical oxygen demand (BOD), temperature, pH, wastewater velocity, and the area of the normally wetted surface of the sewer pipe (Pisano et al., 1998).

Ammonia (from the nitrogen cycle) exists in the stale sewage as a gas, and it is not corrosive. However, its reaction with other acids such as H_2SO_4 (from the sulphur cycle) to form ammonia salts such as ammonium sulphate and ammonium bisulphate promotes the attack of concrete sewer pipes (Baek and Aneja, 2004). Therefore the influence of the sulphur cycle in biogenic corrosion processes in sewers extends to other (non-sulphur) biogeochemical cycles such as the nitrogen, oxygen and carbon cycles as highlighted further in Chapter Two, Part One. On the other hand, sulphide exists in the stale sewage as sulphide ions (S^{2-}), hydrogen sulphide ions (HS^-), and hydrogen sulphide molecules (H_2S) both in aqueous and gaseous states, depending primarily on pH. At pH less than 7, H_2S predominates in aqueous solutions (Figure 1-1) and is readily released into the sewer headspace especially under turbulent flow conditions in sewers flowing partly full. Some of the factors that contribute to this release of H_2S from the sewage include H_2S concentration in the sewage, and high sewage velocities and turbulence (Goyns et al., 2008; Kiliswa et al., 2015).

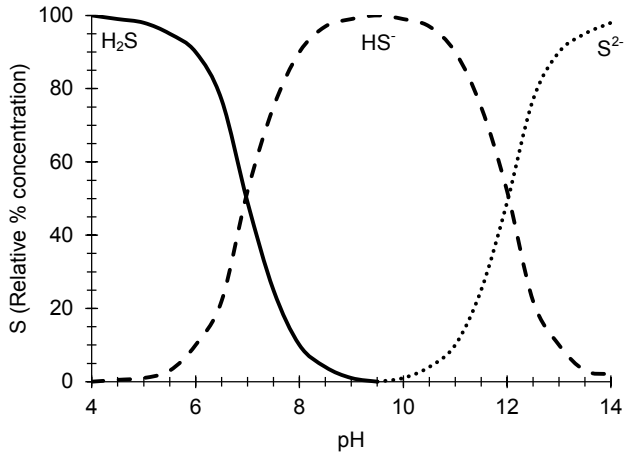

Figure 1-1: Sulphide species concentration as a function of pH (Morel, 1983).

In the second instance, there is SOB typically on the moist walls of the sewer pipe above the flowing sewage, which oxidises the available H_2S in the sewer headspace to generate energy for assimilation of carbon for synthesis of cell materials, and in the process forms H_2SO_4 on the sewer pipe walls. This process is generally referred to as biogenic H_2SO_4 formation. It therefore follows that oxidation of H_2S to H_2SO_4 occurs in two ways; microbially and through auto-oxidation by a spontaneous reaction of H_2S with O_2 in an aqueous solution (O'Connell et al., 2010).

A schematic of this process of H_2S generation in the stale sewage, release from the sewage into the sewer headspace, and formation of H_2SO_4 on the sewer pipe walls is shown in Figure 1-2.

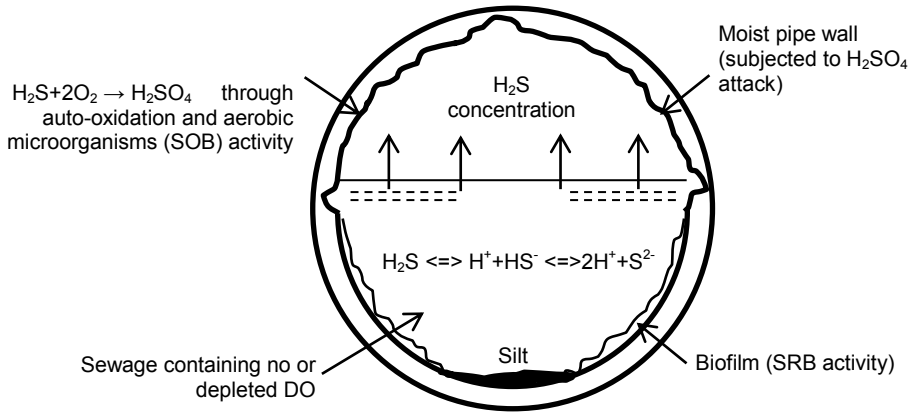

Figure 1-2: Generation, emission and absorption of sulphide from stale sewage in a pipe (Alexander et al., 2008).

Most researchers agree that attack in sewers is mainly caused by biogenic H_2SO_4 produced by S-oxidising bacteria. Others like Tazawa et al. (1994) have also reported that biogenic corrosion in sewers can be caused by aerobic bacteria alone, where they metabolise organic and carbonic acids leading to the flux of the calcium salts and decomposition of the cement hydrates respectively. However, as will be discussed in subsequent sections of the current study, the latter mechanism is not a viable representation of the scale of biogenic corrosion experienced in outfall sewers. Therefore the current study is based on the former hypothesis based on biogenic corrosion mechanisms. These are discussed further in Chapter Two, Part One.

In Portland cement (PC)-based systems, the H_2SO_4 that is formed on the concrete sewer pipe walls attacks the acid-soluble portions of the concrete matrix in two principle processes. The first process entails simultaneous destruction of the polymeric nature of calcium hydroxide (CH) and

substituting a larger molecule (calcium sulphate ($C\bar{S}$)) into the concrete matrix thus causing pressure and spalling of the adjacent concrete and aggregate particles. In the second process, $C\bar{S}$ precipitates as gypsum ($C\bar{S}H_2$) and reacts with various aluminates to form secondary ettringite ($C_6A\bar{S}_3H_{32}$ - AFt). These mechanisms lead to the loss of stiffness and strength, followed by expansion and cracking, and eventually transformation of the affected concrete matrix into a soft and pulpy non-cohesive layer (Sahmaran, 2010). More discussion on these mechanisms is given in Chapter Two, Part Two.

Depending on the severity of the sewer environment that is responsible for the generation of biogenic H_2SO_4, concrete sewer pipes can be made of two components that are defined by their functions; (i) the outer, often steel-reinforced host pipe for structural strength, and (ii) the inner pipe lining or sacrificial layer for corrosion resistance due to exposure to biogenic H_2SO_4 (Goyns, 2013). In most applications, both the host pipe and the sacrificial layer are PC-based. However, in severe sewer environment conditions as discussed later in Chapters Two and Three, these components can be manufactured from different binder systems such as PC-based (for host pipe) and calcium aluminate cement (CAC)-based (for lining). This is because the characteristics of PC-based concrete differ from those of CAC-based concrete when subjected to H_2SO_4 attack, particularly the nature of their hydrates.

When CAC (or monocalcium aluminate (CA)) comes into contact with water, calcium ions (Ca^{2+}) and aluminate ions ($Al(OH)_4^-$) dissolve to give a solution. This solution can combine as several different types of hydrate phases that include AFm (Al_2O_3–Fe_2O–mono), hydrogarnet (CAH_{10}, C_2AH_8, and C_3AH_6) and gibbsite (alumina gel) (AH_3) plus poorly crystallized gel-like phases (Gosselin, 2009; Scrivener et al., 1999). The structure of these phases is discussed in Chapter two, Part Two.

From notions of thermodynamics, when different phases are mixed together, they tend to react and recombine to give a new mixture of phases that have the lowest energy. These are the stable phase assemblages. However, sometimes it is difficult for the stable phases to form immediately due to the rearrangement of ions that needs to occur, a process called nucleation. In this case, it often happens that different phases form temporarily, which are metastable. At all temperatures the stable hydrates of CA are C_3AH_6 and AH_3. CAH_{10} and C_2AH_8 are metastable at temperatures below 50 °C, but convert to stable hydrates at higher temperatures, and also with time at normal temperatures (Gosselin, 2009; Scrivener, 2003; Taylor, 1997).

Both the stable and metastable hydrates of CAC play a significant role when CAC-based binder systems are subjected to biogenic H_2SO_4. For instance, the formation of the amorphous alumina gel (AH_3) and the dissolution of the calcium component of the other hydrates lead to the creation of additional quantities of the alumina gel, which is a stable compound at pH of approximately 4. It therefore presents greater neutralisation of the attacking acid (Equation 1.1). This is not the case with PC-based binder systems where CH, which is the major acid-neutralising phase, completely dissociates in biogenic H_2SO_4 (Equation 1.2). Equation 1.1 shows that six moles of acid are needed to neutralise one mole of alumina in CAC-based binder systems. This implies that CAC-based binder systems have an increased capacity to neutralise the attacking acid; this capacity, referred to as the *neutralisation capacity* (or g ($CaCO_3$ + AH_3) per g concrete material) of a concrete mixture will be discussed further in Chapter Two, Part Two.

$$C_3AH_6 + 6H^+ \rightarrow 3Ca^{2+} + 2AH_3 + 6H \quad (1.1)$$

$$CH + 2H^+ \rightarrow Ca^{2+} + 2H \quad (1.2)$$

According to Herisson et al. (2014), the alumina gel (AH_3) supresses or stifles the succession activities of SOB (from neutrophilic to acidophilic) due to its stability at pH of approximately 4, thus

preventing the most aggressive low-pH environments (< 2) that are responsible for greater rates of biogenic corrosion in outfall sewers. Therefore, the characteristics of CAC-based binder systems differ from those of PC-based binder systems when they are subjected to biogenic H_2SO_4 attack in that they have an increased neutralisation capacity and the ability to stifle succession of SOB. More discussion on these characteristics is given in Chapter Two, Part Two.

In addressing biogenic H_2SO_4 attack of concrete sewer pipes, earlier research in South Africa culminated in the publication of a book on the subject in which several recommendations were made (CSIR, 1959). The most significant of these recommendations was to pay attention to sewer hydraulics in order to avoid high velocities and turbulence so as to minimise the release of H_2S, and to use an acid-soluble aggregate. Acid-soluble aggregates generally increase the amount of bases in the concrete matrix's pore solution, which can be converted to uncharged species by an attacking acid. Therefore it is hypothesised that acid-soluble aggregates provide more alkalinity to a concrete matrix thereby contributing to the overall neutralisation of the attacking acid. Similar studies in the US led to the formulation of equations (EPA, 1974), which later became known as the Life Factor Method (LFM) that are used to predict the rate of sulphide (S) generation in the sewage, H_2S flux from the sewage surface, and the annual corrosion rate (influenced by the concrete's alkalinity) due to biogenic H_2SO_4 attack in PC-based concrete sewer pipes (EPA, 1985). Recent studies in South Africa (Motsieloa, 2013) and elsewhere such as in France (Herisson, 2012), Denmark (Hvitved-Jacobsen et al., 2013), Germany (Beddoe and Schmidt, 2009), the UK (Romanova et al., 2014), Australia (Wells and Melchers, 2014), Lebanon (Ayoub et al., 2004), Belgium (De Belie et al., 2003), China (Zhaohui et al., 2003) and the US (Kienow and Kienow, 2004) tend to confirm the earlier research findings that H_2S (gas) concentration in the sewer headspace and the concrete sewer pipe material properties (alkalinity) are the most significant factors that influence the rate of biogenic H_2SO_4 attack of the acid-soluble portions in a PC-based concrete matrix.

Notwithstanding the considerable research on the factors that influence biogenic H_2SO_4 attack in concrete sewer pipes reported in literature, its application by design engineers remains a challenge due to limited transfer of knowledge to the existing design methods, some of which were developed more than 30 years ago. A variety of concrete sewer (biogenic) corrosion prediction methods have been proposed in literature as discussed in detail in Chapter 2. These methods are based on relationships between the observed sewer conditions and factors deemed to influence the rates of corrosion. However, the methods differ in (i) the mathematical description of the corrosion process, (ii) the input data requirements, and (iii) the mode of calibration (Kley and Caradot, 2013; Scheidegger et al., 2011). Therefore, some of the reasons as to why the process of knowledge transfer from research findings to design applications has lagged include the following:

(i) The concrete sewer pipe corrosion rate is a function of many variables dependent on different sewer environment characteristics such as the composition and temperature of the sewage, gas (H_2S) concentrations, temperature of the sewer headspace, and sewer pipe material properties, some of which are still not well understood. These variables are interrelated in such a complex manner that their influence may be synergistic, similar, or opposing (WERF, 2007).
(ii) Lack of sufficient database.
(iii) There are no standardised corrosion assessment techniques in concrete sewer environments. Different corrosion assessment techniques have been reported to give varied corrosion rate results for the same parameters under the same measurement conditions (Islander et al., 1991).

As mentioned earlier, past studies have mainly focused on biogenic corrosion prediction based on the generation and concentration of the sulphide species in outfall sewers. However, bearing in mind that the final steps in biogenic corrosion prediction revolve around the characteristics of sewer pipe materials, it is prudent that in-depth (microstructural) understanding of these materials

be pursued with the view of improving on the composition or design of cementitious materials that are used in the manufacture of concrete sewer pipes and linings (Herisson et al., 2014; Goyns et al., 2008; Kienow and Kienow, 2004). This approach of studying the concrete sewer pipe material characteristics is critical, since it could allow for additional material modification factors to be incorporated in the final steps of design of the existing biogenic corrosion prediction methods (Motsieloa, 2013; Alexander et al., 2008, Goyns et al., 2008).

1.2 Definition of outfall sewer environment phases in terms of the current study

The concrete sewer environment can broadly be described in four phases with regard to biogenic corrosion (refer to Figure 1-2): (i) the water or aqueous (sewage) phase, (ii) the gaseous phase, (iii) the biological (specific to the sulphur cycle) phase, and (iv) the mineralogical (concrete material) phase.

The aqueous phase as considered in the current study refers to the sewage containing S compounds, and its immediate surrounding (sewage-pipe interface (biofilm) and sewage-headspace interface). Due to certain sewer parameters such as the composition of sewage, sewage velocity and temperature, the sewage becomes septic under certain operational conditions and sulphide species begin to occur (S^{2-}, HS^- and H_2S). Therefore the factors (characteristics) that result in the generation and release of H_2S in the sewage will be discussed in light of the aqueous phase. The chemistry of the sulphide system (both mass balance and mass transfer) will also be considered in this phase.

Due to certain characteristics that exist in the aqueous phase such as the pH of the sewage, total dissolved sulphide species concentration and turbulence, H_2S is released to the gaseous phase of the sewer. Therefore the factors that govern gas concentrations and temperature gradients will be considered in this phase. The difference in temperature results in water vapour escaping from the sewage stream and condensing on the non-submerged walls of sewers. This condensate, however, will be considered under the biological phase.

The amount of moisture on the non-submerged walls of sewers governs the rate of oxidation of H_2S that is absorbed on these walls, and also leads to the establishment of habitats for SOB. Therefore the factors that result in the formation of both auto-oxidised and biogenic H_2SO_4 on the non-submerged walls of sewers will be considered under the biological phase of the sewer environment.

The formation of H_2SO_4 (particularly, biogenic) on the non-submerged walls of sewers leads to the attack of the acid-soluble components on the concrete sewer pipe surfaces. The characteristics of the different binder systems (both PC- and CAC-based) used in concrete sewer pipes will be considered under the mineralogical phase of the sewer environment.

These outfall sewer environment phases are discussed in Chapter Two, Part One.

1.3 Research motivation and knowledge contribution

According to Sullivan and Sheffrin (2003), industrialisation can be defined as the period of social and economic change that involves extensive re-organisation of an economy for the purpose of manufacturing. This period commenced during the mid-18th century. One of the social consequences of industrialisation is urbanisation, which is the increase in the proportion of people living in urban areas. Therefore urbanisation is relevant to a range of disciplines such as urban planning and public health, which involves development of sewer networks (Watson, 1993).

Most sewer networks in many countries around the world, including South Africa, were built during the late 19th and 20th centuries (1850 to 1950) (Metcalf and Eddy, 1922). The design life of sewers in South African cities has traditionally been 40 years (Da Silva and Goyns, 2009). However, many of the sewers in the older cities have been in operation for far longer than 40 years and have

deteriorated due to biogenic corrosion, yet they have not been replaced or rehabilitated due to the high costs associated with replacement or rehabilitation of such systems (DWA, 1986; Hewayde et al., 2006).

The widely used concrete sewer rehabilitation technique in South Africa is the application of thermoplastic-based liners, which are deemed to withstand biogenic corrosion (Goyns, 2001). However, these liners have two significant limitations when used in deteriorated concrete sewers: (i) they are not designed to perfectly fit the rugged surface profiles of concrete sewers that have been subjected to acid attack, and are susceptible to piercing by acid-insoluble aggregates that may stand proud (after acid attack of the acid-soluble components), (ii) they experience structural failures due to the groundwater pressure that accumulates between them and the rough surface of concrete host pipes. Similarly, such structural failures are also experienced in sewer pipes that are manufactured *ab initio* with a concrete host pipe and a thermoplastic-based liner (Goyns et al., 2008).

The limitations associated with thermoplastic-based liner application in new and deteriorated concrete sewers can be overcome by developing or improving the existing cement-based (concrete) liners or sacrificial layers, since they consist of similar materials as the host pipes. The successful development of such concrete liners requires an in-depth understanding of the performance of various concrete mixtures that are used in the manufacture of sewer pipes, particularly through studies of samples installed in active sewer environments. Therefore, it is imperative that certain concrete mixtures (and sewer environments) be characterised in order to improve on the understanding of the biogenic corrosion mechanisms. The current study is aimed at (i) characterising and studying the biogenic corrosion mechanisms of certain concrete mixtures that have been subjected to biogenic corrosion for more than 10 years in a 'live' sewer, and (ii) reviewing the sewer environment under which these concrete mixtures have been exposed. Thus the outcome of the current study will contribute towards the development of a database that is relevant to the advancement of cement-based (concrete) liners for both sewer rehabilitation and for new applications.

Moreover, advances in cement chemistry coupled with the utilisation of supplementary cementitious materials (SCMs) in various concrete binder systems that are used in the manufacture of concrete sewer pipes have, over time, led to changes in the properties of these binder systems, which influence biogenic corrosion (and prediction) (Alexander and Fourie, 2011). Therefore for practical applications by design engineers responsible for service life prediction of concrete sewer pipes, various tools such as biogenic corrosion prediction models which were developed based on earlier cement chemistry and binder systems also need to be improved. This is the main contribution of the current study.

1.4 Aims and objectives of study

The main aims of the current study are:

(1) To critically review the widely used deterministic (mechanistic) biogenic corrosion prediction model – the LFM, with the view of improving it based on the microstructural studies of certain concrete mixtures used in the manufacture of concrete sewer pipes. These concrete mixtures have been exposed in a 'live' experimental sewer section, the so-called Virginia Experimental Sewer (VES) in Free State Province, South Africa for more than 10 years.
(2) To demonstrate that the improved LFM is a practical tool for design engineers with regard to adaptation to the cement and SCM industries.

In order to achieve the aims given above, the current study will focus on the following objectives:

(i) To review other biogenic corrosion prediction models (both deterministic and statistical) that incorporate properties of concrete mixtures as rate-controlling parameters, with the view of highlighting respective shortcomings based on the characteristics of different binder systems.

(ii) To review the general sewer hydraulics and sewer environment considerations based on three sets of factors; (a) those that lead to the generation and release of H_2S from the sewage, (b) those that govern the concentration of H_2S in the sewer's headspace and formation of moisture on the non-submerged walls of concrete sewer pipes, and (c) those that lead to the formation of biogenic H_2SO_4 on the non-submerged walls of concrete sewer pipes, with the view of highlighting their interdependence and influence on the performance of different binder systems used in the manufacture of concrete sewer pipes.
(iii) To study certain sewer environment phases in two localities in South Africa; (a) the VES, and (b) the Northern Area Sewer section at Langa pump station in the City of Cape Town.
(iv) To better characterise parameters that influence rates of biogenic corrosion of concrete sewer pipe materials and relate these to an understanding of the sewer environment and material properties.
(v) To evaluate the distinction between the neutralisation capacity of a concrete mixture and its ability to stifle succession of SOB.
(vi) To study and draw conclusions on the potential impact of varying exposure conditions on the performance of different concrete sewer pipe materials.

1.5 Scope and limitations of study

Biogenic corrosion in outfall sewers is a complex phenomenon that involves multi-phase factors that exist in the sewer environment such as the chemical equilibrium characteristics of the aqueous, gaseous and mineralogical phases, and the transport mechanisms within these phases. Nonetheless, all these complex inter-relationships in biogenic corrosion prediction models of outfall sewers address only one aspect, the corrosion rate. It would be ideal to simultaneously consider all the multi-phase factors in the sewer environment in order to precisely quantify the biogenic corrosion rate, particularly with a sufficient database for reference. The current study aims at relating certain parameters of two sewer environments in South Africa and the material properties (characteristics) of concrete mixtures used in the manufacture of sewer pipes (as influenced by the sewer environment conditions (or phases)), and will thus contribute towards a better understanding of the multi-phase factors involved in biogenic corrosion.

However, due to experimental set-up limitations, only a certain combination of parameters can be investigated in depth in order to quantify related corrosion rates. Therefore the scope of the current study was limited to the following:

1. Mechanisms of attack on the non-submerged walls of concrete sewer pipes due to the activities of SOB only. The role of other *acidophilic bacteria* such as iron-oxidising bacteria (IOB) that are also present at different stages of corrosion of the concrete sewer pipes, and which possibly contribute to the overall biogenic corrosion mechanisms, was not considered.
2. Two geographical locations within South Africa; Virginia, Free State Province and Cape Town, Western Cape Province. These locations have distinct differences in (i) their topography (Virginia is characterised by an expansive flat terrain while Cape Town is characterised by steep mountainous ranges and the sea level), thus different sewer hydraulic considerations (ii) their economic activities (Virginia is characterised by agricultural and mining activities while Cape Town is characterised by tourism (human population)), thus different sewage composition, and (iii) their climatic conditions (Virginia is characterised by an annual mean precipitation of 600 mm, temperatures of up to 38 °C in summer and 18 °C in winter, and an annual mean relative humidity (RH) of 56%; Cape Town is characterised by an annual mean precipitation of 580 mm, temperatures of up to 36 °C in summer and 16 °C in winter, and an annual mean RH of 74%), thus potential different sewer environment cycles. However, they are not representative of other locations in South Africa such as those in Gauteng Province which are characterised by a higher annual mean precipitation (720 mm), lower temperatures (up to 33 °C in summer and 15 °C in winter), and an intermediate annual mean RH of 61%.

3. Focus on the microstructural characteristics of the mineralogical phase (concrete materials) of concrete sewer pipes, which has not been widely studied in depth in comparison to the other sewer environment phases such as the aqueous and biological phases. The latter phases have been widely studied in other fields such as wastewater engineering and environmental microbiology.
4. The quality of concrete samples was checked based on the South African Durability Indices (Oxygen Permeability Index and Water Sorptivity). However, some of the samples that were used in the current study were made 10 years ago, and due to revisions in Cement Standards, which resulted in some cements being phased out, these samples could not be reproduced with a similar type of cement for such quality checks. Therefore certain indicative checks were based on the most recent cement types. This is discussed in Chapter Four.

1.6 Outline of the thesis document

This thesis consists of seven chapters.

Chapter One presents a background, research motivation and knowledge contribution, aims and objectives, and scope and limitations of the current study.

Chapter Two presents a review of literature, and it is divided into three parts. *Part One* reviews the sewer hydraulics and environment considerations. It focusses on certain basic principles of sewer design (hydraulics) that are deemed generally to govern rates of biogenic corrosion, and also reviews the characteristics of the aqueous, gaseous, biological and mineralogical phases in outfall sewers. The chemistry of the sulphide system is also covered in detail in this part. *Part Two* reviews the characteristics of the concrete sewer pipe materials. It focusses on the properties of PC, CAC and SCMs, and on the microstructure of both plain and blended PC- and CAC-based binder systems. Certain properties of the acid-soluble and acid-insoluble aggregates used in the manufacture of concrete sewer pipes are also reviewed in this part. *Part Three* reviews three concrete sewer pipe biogenic corrosion prediction models. It focusses on deterministic (mechanistic) and statistical models with the view of justifying the applicability of certain results from the current study in one of the widely used deterministic (mechanistic) model, the LFM.

*Chapter Three p*resents a review of previous and current work undertaken in relation to, and in the Virginia Experimental Sewer (VES) in Free State Province, South Africa. It outlines the reasons that led to the establishment of three documented (two of them, Boksburg and Klerksdorp have only been partially documented) experimental sewers in South Africa, and reviews the different phases of study that have been undertaken in the VES since its commissioning during 1989. The performance of a range of cement-based mixtures for both concrete host pipe and lining applications subjected to both biogenic and mineral (laboratory) H_2SO_4 is also reviewed in the chapter.

Chapter Four presents a description of the materials and experimental work undertaken in the current study. The experimental methods include in-situ and laboratory-based testing. Other laboratory analytical techniques including scanning electron microscopy (SEM), energy dispersive spectroscopy (EDS), X-ray diffraction (XRD), thermogravimetric analysis (TGA), and microbial speciation are also presented.

Chapter Five presents a general overview of the time development trends of biogenic concrete corrosion rates, and experimental results, related analyses and discussion of the significance of the evaluated results.

Chapter Six presents the practical applications of the characteristics of concrete mixtures subjected to biogenic corrosion in deterministic (mechanistic) corrosion prediction models. It focusses on the inter-relationships between (i) the actual (measured) biogenic corrosion rates, (ii) the predicted biogenic corrosion rates based on the widely used LFM, which considers the

conventional alkalinity of concrete mixtures as the rate-controlling parameter in biogenic corrosion, (iii) the alkalinity and neutralisation capacity of both PC- and CAC-based concrete mixtures, (iv) Al/Ca and Fe/Ca ratios of the sound matrices of different concrete mixtures investigated in the current study, and (v) other parameters within the VES, such as H_2S concentration in the sewer headspace, sewer temperature and relative humidity. These inter-relationships show that the use of conventional alkalinity as a biogenic corrosion rate-controlling parameter is limited, and a new proposal is presented to incorporate the *effective resistance capacity* ($RC_{eff.}$) instead of *alkalinity* (A) in the denominator of LFM equation, resulting in the so-called *Improved LFM*.

Chapter Seven presents the conclusions and recommendations for further work, based on the current study.

Appendix A presents temperature and RH profiles at Boksburg, Klerksdorp, and Virginia where experimental sewer sections were constructed during the 1980s.

Appendix B presents the H_2S profiles in the VES and Langa.

Appendix C presents a layout of the nine different types of sewer pipes and the mixture composition of the unprotected cementitious category of samples installed in the VES during 1988.

Appendix D presents details of concrete mixtures used in Phase II studies in the VES (1995 to 2001).

Appendix E presents the layout and mixture details of the seventeen different types of concrete sewer pipe samples installed in the VES during 2004.

Appendix F presents the composition of concrete mixtures used for laboratory-based studies of physicochemical properties, and also installed in the VES during 2011.

Appendix G presents details of concrete mixtures installed in the VES and Langa during 2015 for a comparative study on surface pH vs. time profiles

Appendix H presents particle size distribution of aggregates used in the current study

Appendix I presents a summary of test procedures and results for density, compressive strength, and durability indices of concrete core samples used for surface pH vs. time profiling

Appendix J presents test procedures for the laboratory analytical techniques used in the current study

Appendix K presents temperature and relative humidity profiles in the manhole at Langa

Appendix L presents detailed results from the current study

Appendix M presents the EBE Faculty's Assessment of Ethics in Research Projects form.

Appendix N presents a list of papers that were published in the course of the current study.

The structure of this thesis is such that references are provided at the end of each chapter.

1.7 References

Alexander, M. G., & Fourie, C. W. 2011. Performance of sewer pipe concrete mixtures with portland and calcium aluminate cements subject to mineral and biogenic acid attack. *Materials and Structures*. 44 (1): 313 – 330.

Alexander, M. G., Goyns, A. M., & Fourie, C. W. 2008. Experiences with a full-scale experimental sewer made with CAC and other cementitious binders in Virginia, South Africa. *Proceedings of*

the Centenary Conference on Calcium Aluminate Cements. June 30 – July 2, Avignon. 279 – 292.

American Concrete Pipe Association. 2008. *The infrastructure is collapsing*. Irving: ACPA.

Ayoub, G. M., Azar, N., El Fadel M., & Hamad, B. 2004. Assessment of hydrogen sulphide corrosion of cementitious sewer pipes: A case study. *Urban Water*. 1(1): 39 – 53.

Baek, B. H., & Aneja, V. P. 2004. Measurement and analysis of the relationship between ammonia, acid gases, and fine particles in eastern North Carolina. *Journal of the Air and Waste Management association.* 54(5): 623 – 633.

Beddoe, R. E., & Schmidt, K. 2009. Effect of concrete composition on resistance of concrete to acid attack. *International conference on Concrete in Aggressive Aqueous Environments, Performance, Testing and Modeling*. June 3 – 5. Toulouse. 187 – 195.

Council for Scientific and Industrial Research. 1959. *Corrosion of concrete sewers*. Pretoria: CSIR. Series DR12.

Da Silva, V. A., & Goyns, A. 2009. The aging of concrete sewers: Replace or rehabilitate. *Concrete Repair, Rehabilitation and Retrofitting II*. London: Taylor & Francis.

De Belie, N., Monteny, J., Vincke, E., & Beeldens, A. 2003. Testing and modelling biogenic sulphuric acid corrosion of concrete sewer pipes in function of aggregate type, cement type and production method. In: Naus, D. J. Eds. *Life prediction and aging management of concrete structures, Proceedings of the 2nd International RILEM Workshop.* May 5 – 6. Paris.

Department of Water Affairs. 1986. *Management of the water resources of the Republic of South Africa - Report*. Pretoria: DWA.

Environmental Protection Agency, Centre for Environmental Research Information. 1985. *Design Manual: Odor and Corrosion Control in Sanitary Sewerage Systems and Treatment Plants*. Cincinnati: EPA.

Environmental Protection Agency. 1974. *Process design manual for sulphide control in sanitary sewerage systems*. Washington: EPA.

Gosselin, C. 2009. Microstructural development of calcium aluminate cement based systems with and without supplementary cementitious materials. PhD dissertation. École Polytechnique Fédérale de Lausanne, Lausanne.

Goyns, A. M. 2001. Calcium aluminate cement linings for cost-effective sewers. *International Conference on Calcium Aluminate Cements*. July 16 – 19, Edinburgh. 617 – 631.

Goyns, A. M. 2003. Virginia sewer rehabilitation: Progress Report 1. Pretoria: Concrete Manufacturers Association.

Goyns, A. M. 2004. Virginia sewer rehabilitation: Progress Report 2. Pretoria: Concrete Manufacturers Association.

Goyns, A. M. 2013. *Design manual for concrete pipe outfall sewers.* Midrand: Concrete Manufacturers Association.

Goyns, A. M., Alexander, M. G., & Fourie, C. W. 2008. Applying experimental data to concrete sewer design and rehabilitation. *Proceedings of the Centenary Conference on Calcium Aluminate Cements.* June 30 – July 2. Avignon. 293 – 308.

Herisson, J. 2012. Biodeterioration of cementitious materials in the wastewater – Comparative study of calcium aluminate cement and Portland cement. PhD dissertation. Université Paris-Est, Paris.

Herisson, J., Guéguen-Minerbe, M., van Hullebusch, E. D., & Chaussadent, T. 2014. Behaviour of different cementitious material formulations in sewer networks. *Water Science and Technology*. 69(7): 1502 – 1508.

Hewayde, E., Nehdi, M., Allouche, E., & Nakhla, G. 2006. Effect of geopolymer cement on microstructure, compressive strength and sulphuric acid resistance of concrete. *Magazine of Concrete Research*. 58(5): 321 – 331.

Hvitved-Jacobsen, T., Vollertsen, J. & Nielsen, A.H. 2013. *Sewer processes: Microbial and chemical process engineering of sewer networks*. 2nd ed. Boca Raton: CRC Press.

Islander, R. L., Devinny, J. S., Mansfeld, F., Postyn, A., & Hong, S. 1991. Microbial ecology of crown corrosion in sewers. *Journal of Environmental Engineering*. 117(6): 751 – 770.

Kaempfer, W., & Berndt, M. 1999. Estimation of service life of concrete pipes in sewer networks. *Proceedings of the 8th Conference on Durability of Building Materials and Components*. May 30 – June 3. Vancouver. 36 – 45.

Kelly, M. J., & Krüger, J. E. 1996. *Consolidated Report on Phase 1 of Sewer Corrosion Research: The Virginia Sewer experiment and related research.* Pretoria: CSIR.

Kienow, K. K., & Kienow, K. E. 2004. Evaluation of sanitary sewer sulphide, odor and corrosion potential. *Proceedings of the Pipelines 2004 International Conference*. August 1 – 4. San Diego.

Kiliswa, M. W., Alexander, M. G., & Beushausen, H. 2015. Durability design of concrete mixtures for sewer pipe applications: A review of the Life Factor Method. *Proceedings of the 4th International Conference on Concrete Repair, Rehabilitation and Retrofitting*. October 5 – 7. Leipzig. 163 – 167.

Kley, G. & Caradot, N. 2013. *Review of sewer deterioration models*. Berlin: KWB.

Kohsaka, K., Abdul-Talib, S., & Yin, C-Y. 2008. Effect of anoxic transformation processes in municipal wastewater on pH and oxidation reduction potential. *International Symposium on Sanitary and Environmental Engineering.* June 24 – 27. Florence.

Mehta, P. K., & Monteiro, P. J. M. 2013. *Concrete: Microstructure, properties, and materials*. 3rd ed. New Delhi: McGraw Hill.

Metcalf, L., & Eddy, H. P. 1922. *Sewerage and sewage disposal: A textbook*. New York: McGraw Hill.

Morel, F. M. M. 1983. *Principles of aquatic chemistry.* New York: John Wiley and Sons.

Motsieloa, N. 2013. Acid resistance of sewer pipe concrete. MSc (Eng) dissertation. University of Cape Town, Cape Town.

O'Connell, M., McNally, C., & Richardson, M. G. 2010. Biochemical attack on concrete in wastewater applications: *A state-of-the-art review*. University College Dublin, Dublin.

Pisano, W. C., Barsanti, J., Sorensen, H., & Joyce, J. 1998. Sewer and tank sediment flushing: Case studies. Washington: EPA.

Romanova, A., Mahmoodian, M., & Alani, M. A. 2014. Influence and interaction of temperature, H_2S and pH on concrete sewer pipe corrosion. *International Scholarly and Scientific Research & Innovation*. 8(6): 607 – 610.

Sahmaran, M. 2010. Deterioration mechanisms – chemical. In: Soutsos, M. Eds. *Concrete durability: A practical guide to the design of durable concrete structures*. London: Thomas Telford.

Scheidegger, A., Hug, T., Rieckermann, J., & Maurer, M. 2011. Network condition simulator for benchmarking sewer deterioration models. *Water Research*. 45: 4983 – 4994.

Scrivener, K. L. 2003. Calcium aluminate cements. In: Newmann, J., & Choo, B. S. Eds. *Advanced Concrete Technology – Constituent Materials*. Oxford: Elsiever.

Scrivener, K. L., Cabiron, J., & Letourneux, R. 1999. High-performance concretes from calcium aluminate cements. *Cement and Concrete Research*. 29: 1215 – 1223.

Sullivan, A., & Sheffrin, S. M. 2003. *Economics: Principles in action.* New Jersey: Pearson Prentice Hall.

Taylor, H. F. W. 1997. *Cement chemistry*. 2nd ed. London: Thomas Telford Publishing.

Tazawa, E. I., Morinaga, T., & Kawai, K. 1994. Deterioration of concrete derived from metabolites of microorganisms. *Proceedings of the 3rd CANMET/ACI International Conference on Durability of Concrete*. May 21 – 26. Nice. 1087 – 1097.

Vollertsen, J., Nielsen, A. H., Jensen, H. S., Rudelle, E. A., & Hvitved-Jacobsen, T. 2011. Modeling the corrosion of concrete sewers. *12th International Conference on Urban Drainage*. September 11 – 16. Porto Alegre.

Water Environment Research Foundation. 2007. Minimisation of odors and corrosion in collection systems (Phase 1). *Final Report: Project Number 04-CTS-1*. Alexandria: WERF.

Watson, C. 1993. Trends in world urbanisation. *Proceedings of the 1st International Conference on Urban Pests*. June 30 – July 3. Cambridge.

Wells, T., & Melchers, R. E. 2014. An observation-based model for corrosion of concrete sewers ubder aggressive conditions. *Concrete and Cement Research*. 61: 1 – 10.

Zhaohui, C., Qiang, H., & Wentao, Y. 2003. Research on the corrosion of sewer system pipelines from domestic wastewater. *Proceedings of the International Conference on Pipeline Engineering and Construction*. July 13 – 16. Baltimore.

Chapter Two: Literature review

2.0 Outline

The main objectives of this chapter are to (i) review the governing principles of general sewer hydraulics and sewer environment phases with the view of highlighting the significance of these principles and phases on the performance cementitious mixtures used in the manufacture of concrete sewer pipes, (ii) review the characteristics of certain binders, binder systems and aggregates that are used in the manufacture of concrete sewer pipes with the view of highlighting the significance of various properties when these materials are subjected to biogenic H_2SO_4 attack, (iii) review different biogenic corrosion prediction models with the view of highlighting the rate-controlling parameters based on the characteristics of concrete mixtures (materials); improvements on the rate-controlling parameters in deterministic (mechanistic) models are proposed. These discussions are presented in Part One, Part Two and Part Three respectively.

Before proceeding, it is important to note that most of the data presented in the current study (as discussed later in Chapter Five), which include the performance of certain concrete sewer pipe materials (both PC- and CAC-based) has been recorded for more than 10 years following research in a 'live' experimental sewer in Free State Province, South Africa. Moreover, the analytical techniques used in the current study for characterising the concrete mixtures subjected to biogenic H_2SO_4 for more than 10 years provide comparative quantifiable parameters that fit the description of deterministic (mechanistic) models. It is for these reasons that the current study focusses on deterministic models.

Even though the main focus of the current study is to propose improvements to the Life Factor Method (LFM), which is largely mechanistic (deterministic), a review of other models, both deterministic and statistical is presented to highlight the significance of material properties (concrete) in their execution. The reasons for proposing improvements on the LFM are threefold; (i) its parameters have direct, quantifiable interpretation of the biogenic corrosion processes of PC-based concrete mixtures, (ii) it has been used and tested in various geographical locations with reasonable concurrence on the performance of PC-based concrete mixtures, (iii) its fundamental characteristics are well understood and can be extended to a wider range of service environments and material properties such as different binder systems.

Literature review: Part One

Sewer hydraulics and environment considerations

2.1 General sewer hydraulics and sewer environment considerations

The problem of biogenic corrosion affects parts that are above the average sewage flow level (non-submerged walls) in sewers that flow partly full. Therefore other forms of corrosion such as those resulting due to the presence of aggressive chemicals in the sewage itself are not part of the current study. There are three sets of factors within the sewer environment that contribute to biogenic corrosion; those resulting in the generation of H_2S in the sewage, those resulting in the release of H_2S from the sewage, and those resulting in the formation of biogenic H_2SO_4 on the non-submerged walls of sewers (Goyns et al., 2008). However, before these factors are discussed, certain principles of sewer design (hydraulics) that are deemed to generally govern the three sets of factors mentioned above will be highlighted in the following section.

2.2 Basic principles of sewer hydraulics

The design of outfall sewers involves, among other considerations such as the population density, estimation of sewage flow rates and evaluation of any local conditions that may affect the hydraulic operation of the sewer system. These local conditions include: the applicability of certain hydraulic design equations; availability of alternative sewer pipe materials and sewer pipe sizes; minimum and maximum flow velocities; evaluation of alternative alignments. Therefore there are two important considerations in the design of outfall sewers; (i) alignment (both vertical and horizontal), and (ii) sewer pipe materials. This Part One will focus mainly on alignment and related significances. Materials (in this case, concrete) will be reviewed in detail in Part Two of this literature review.

2.2.1 Flow velocity

Outfall sewers are generally gravity pipelines that flow partly full and follow natural watercourses. These watercourses often have alignments that are not ideal for sewers such as relatively flat grades interspersed with short steep sections, and bends. Therefore outfall sewers are designed to cope with both vertical and horizontal changes in alignment (and the energy losses that occur due to these changes) to ensure effective performance, for example, by maintaining recommended flow velocities.

As will be discussed later, silt deposition in outfall sewers due to inadequate flow (self-cleansing) velocities is one of the contributors towards the inception of biogenic corrosion. The maintenance of minimum flow velocities (generally between 0.6 and 0.8 m/s) so that silt does not accumulate at invert levels in sewers is an accepted principle in sewer design (Goyns, 2013; Bizier, 2007; EPA, 1985). One of the widely used equations for determining flow velocity in sewers, the Manning's equation, is given below (Equation 2.1):

$$v = \frac{1}{n} R^{2/3} S^{1/2} \tag{2.1}$$

where v = velocity (m/s)
n = Manning's roughness coefficient (0.013, for centrifugally spun concrete)
R = hydraulic radius (m)
S = gradient of conduit (m/m)

Equation 2.1 shows that the flow velocity is proportional to both the diameter and gradient, so smaller diameter sewers are often at gradients that are insufficient to ensure self-cleansing velocities while larger diameter sewers often experience flow disruptions in the form of, for example, super-critical flows. These different types of flows (subcritical, critical, and super-critical)

are defined in the following section, together with certain significant numbers (ratios) that are used to describe such flow velocities and other related characteristics that are incorporated in biogenic corrosion prediction models as discussed in Part Three of this literature review.

2.2.1.1 Specific energy and critical flow

The flow in outfall sewers is similar to that in open channels. Therefore for a uniform flow section between any two points (such as point 1 and 2, see Figure 2-1), the specific energy, *E* is defined as the sum of the depth of flow and the velocity head (Equation 2.2).

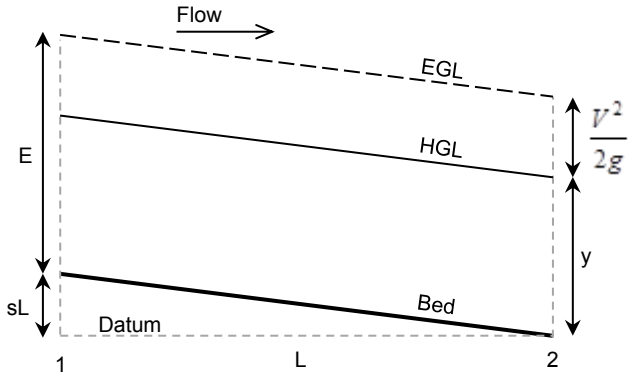

E – Specific energy (m)
EGL – Energy grade line (= total head available to the fluid)
HGL – Hydraulic grade line (or fluid surface) (= EL minus the velocity head)
$V^2/2g$ – Velocity head (m)
y – Depth of flow (m)
s – Slope of EL and HGL
L – Distance between points 1 and 2 under consideration (m)

Figure 2-1: Specific energy diagram for uniform flow (Daugherty and Franzini, 1965).

$$E = y + \frac{V^2}{2g} \tag{2.2}$$

where y = depth of flow (m)
V = mean velocity (m/s)
g = gravitational acceleration (m/s^2)

Assuming an infinitely short section (essentially no friction losses and no change in elevation) of an open channel, the general energy equation (Equation 2.2) can be re-written as an equality of specific energies (Equation 2.3).

$$E_1 = y_1 + \frac{V_1^2}{2g} = y_2 + \frac{V_2^2}{2g} = E_2 \tag{2.3}$$

According to Equation 2.1, flow velocity is directly related to the area of flow (by the hydraulic radius), and the area of flow is a function of channel depth. Therefore the flow velocity can be related to a discharge rate per unit width, q (Equation 2.4), and Equation 2.3 can be re-written as Equation 2.5.

$$q = \frac{Q}{b}; v = \frac{q}{y} \tag{2.4}$$

$$E = y + \frac{q^2}{2gy^2} \tag{2.5}$$

For a given flow (discharge), the specific energy at each point is solely a function of channel depth, so we may have the same specific energy for various depths. This can be illustrated by the specific energy diagram (Figure 2-2).

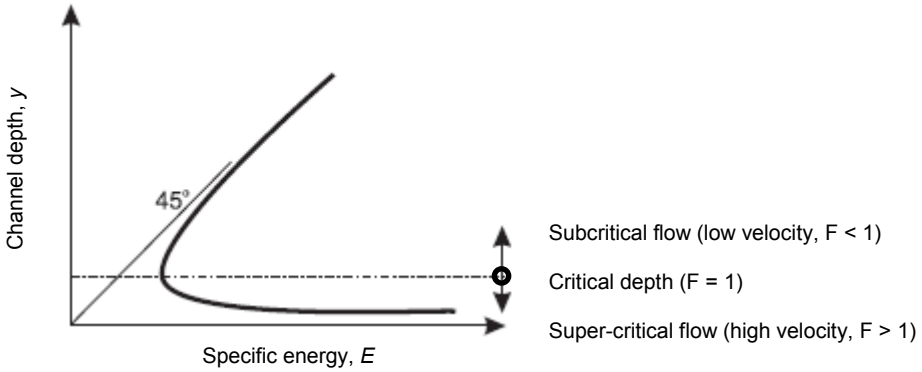

Figure 2-2: Relationship between specific energy and depth of flow (after Haestad Methods, 2002).

The relationship given in Figure 2-2 is described by a dimensionless number known as the Froude number, *F* (Equation 2.6).

$$F = \frac{V}{\sqrt{gD}} \tag{2.6}$$

where D = hydraulic mean depth (= flow area/top width of flow) (m)
V = mean velocity (m/s)
g = gravitational acceleration (m/s^2)

A depth (depth of flow or channel depth) at which the specific energy is at a minimum is known as the critical depth (F = 1). Sections where the depth of flow is less than the critical depth (or velocity is higher than the critical velocity) experience super-critical flows (F > 1). Sections where the depth of flow is more than the critical depth (or velocity is less than the critical velocity) experience subcritical flows (F < 1).

The Froude number is one of the significant parameters (others are sediment volumetric concentration and relative size of particles) that influence the design criteria for self-cleansing velocities in sewers (Ebtehaj et al., 2014; Vongvisessomjai et al., 2010).

2.2.1.2 Laminar flow and turbulent flow

Laminar flow occurs with low velocities and/or high viscosity. It is characterised by smooth, predictable streamlines. Turbulent flow, on the other hand, occurs with high velocities and/or low viscosity. It is characterised by the formation of eddies within a certain flow, resulting in erratic and unpredictable streamlines (Bengtson, 2011). In sewers, the flow of sewage is characterised by low-velocity flow near the sewer walls (due to effects of friction and drag) and higher-velocity flow towards the centre, and so they experience a continuous mixing of flow resulting in turbulence. Therefore flows in sewers are, in principal, turbulent, and the velocity at any given point within a turbulent section will be closer to the mean velocity of the entire section than with laminar flow conditions. It is also important to mention that (i) turbulent flows are typical in sewer sections located downstream of pump stations due to the pumping cycles of the sewage, and (ii) turbulent flows occur where there is an abrupt change in the direction of flow in a sewer section (Goyns, 2013).

In order to classify flow as either laminar or turbulent, a dimensionless number, known as the Reynolds number, *Re* is used (Equation 2.7).

$$\mathrm{Re} = \frac{4VR}{v} \tag{2.7}$$

where V = mean velocity (m/s)
R = hydraulic radius (m)
v = kinematic viscosity (m^2/s)

In sewers, laminar flow occurs when *Re* < 500, and turbulent flow occurs when *Re* > 2000. For 500 > *Re* < 2000, the flow is known as transitional.

The hydraulic principles reviewed above have a significant impact on biogenic corrosion since the flow velocity and turbulence will determine whether air is entrained or released from the sewage, and whether there is solid deposition on the sewer invert. At high flow velocities, air is entrained in the sewage and most solids are carried in suspension throughout the sewer, while at low velocities, there is less air entrainment in the sewage and solids are deposited on the sewer's invert. Air entrainment will in turn determine whether the effluent will be aerobic or anaerobic. Under anaerobic conditions, there is insufficient oxygen in the sewage to support microbial activities within the biofilm. Therefore, SRB and NRB will obtain oxygen by reducing SO_4^{2-} to S^{2-} and NO_3^- to NO_2^- respectively. Under aerobic conditions, there is sufficient oxygen in the sewage to support microbial activities so reduction of the SO_4^{2-} and NO_3^- will not be of the same magnitude as in the case of anaerobic conditions (EPA, 1985). At low flow velocities, solids are deposited on the sewer's invert in form of sludge and silt to form additional habitat for the Proteobacteria (both SRB and NRB).

Therefore due to sewer hydraulics, the minimum and maximum flow velocities and energy losses could vary along a particular sewer section due to changes in both vertical and horizontal alignments. This means that S^{2-} (H_2S) (and also other gases such as NH_3) could be generated in one section of the sewer and due to factors such as turbulence, be released at another section. It therefore follows that, fundamentally, sewer hydraulics is one of the significant parameters that influence the characteristics of different phases of the sewer environment as discussed in the following sections.

Before proceeding, it is important to note that even though biogenic corrosion mechanisms in concrete sewers involve more than one biogeochemical cycle (includes among others the sulphur, carbon, oxygen and nitrogen), the sulphur cycle is the most significant because, under certain conditions, it is directly responsible for the generation of biogenic H_2SO_4 that attacks concrete sewer pipes. Therefore the sewer environment phases that are reviewed in the current study mostly make specific references to mechanisms that are involved in the sulphur cycle alone, although this does not negate the influence of the other cycles.

2.3 Characteristics of the aqueous phase

The aqueous phase as considered in the current study refers to the sewage containing sulphur compounds, and its immediate surrounding (sewage-conduit interface (biofilm) and sewage-headspace interface). The characteristics of the sewage that influence biogenic corrosion are simplistically defined by low flow velocities, and the retention time in sewerage facilities.

Retention time refers to a period in which sewage is stored within facilities such as rising mains, pumping stations, sumps, tanks and sewers. Retention time may be desirable to allow for settling of solids for biological and chemical processes to take place in wastewater treatment facilities (WWTF), or for operational considerations. Retention time can therefore be categorised into (i) solid retention time (SRT), and (ii) hydraulic retention time (HRT) (Malik, 1996). Microbial activities (establishment of bacteria populations) responsible for generation of S^{2-} in sewers are attributed to HRT, and these occur in the sewer's biofilm under the influence of the sewage temperature, biochemical oxygen demand (BOD), dissolved oxygen (DO), dissolved sulphide (DS), and pH (Barjenbruch, 2003).

2.3.1 Aerobic and anoxic microbial processes

Microbial activities under aerobic and anoxic conditions in sewer environments are an essential part for the establishment of anaerobic environments due to the consumption of oxygen. Microorganisms in aerobic and anoxic environments use DO and nitrate (bonded O_2) respectively

as terminal electron acceptors; the aerobic and anoxic pathways of organic compound degradation are identical (Hvitved-Jacobsen et al., 2013).

Under aerobic conditions, organic compounds such as carbon (a major constituent of domestic sewage), which are electron donors are oxidised through a respiration process by passing electrons to molecular oxygen that is thereby reduced (Tchobanoglous et al., 2003). Therefore aerobic respiration with DO as the terminal electron acceptor is an efficient process for energy metabolism. Anoxic conditions require the absence of DO and presence of nitrates (bonded O_2), although the similarity in the microbial reactions under aerobic (O_2 - based) and anoxic (NO_3^- - based) processes is, for example, given in Equations 2.8 and 2.9 respectively.

$$6C_6H_{12}O_6 + O_2 \rightarrow CO_2 + H_2O \tag{2.8}$$

$$5C_6H_{12}O_6 + 24NO_3^- + 24H^+ \rightarrow 12N_2 + 30CO_2 + 42H_2O \tag{2.9}$$

The depletion of total oxygen due to both aerobic and anoxic processes leads to the establishment of anaerobic conditions, discussed in the following section.

2.3.2 Anaerobic microbial processes

Under anaerobic conditions with available SO_4^{2-}, there are two basic processes that support energy requirements of present microorganisms. These processes are (i) respiration, and (ii) fermentation (Sharma, 2007). Generally, respiration processes require participation of external electron acceptors such as prokaryotes, but fermentation processes do not. During fermentation, the organic compounds undergo a series of alternative oxidative and reductive reactions such that the organic compounds are reduced in one step of the process and are oxidised in another step. As a result, the partial breakdown of organic compounds through fermentation processes yields organic products with a low molecular weight such as volatile fatty acids (carboxylic acids) and CO_2. The low molecular weight products can be used by SRB that make use of SO_4^{2-} as the terminal electron acceptor (Nielsen and Hvitved-Jacobsen, 1988). Fermentation processes are involved in certain microbial systems such as the sewage, and the biofilm.

2.3.3 Establishment of biofilm on the submerged walls of sewers

A biofilm is a densely packed community of microbial cells that grow on living or inert surfaces and surround themselves with secreted polymers (long chains). Due to HRT conditions and low flow velocities in sewer systems, biofilms grow. Biofilm formation involves a series of distinct stages consisting of reversible attachment, irreversible attachment, maturation and detachment. On the onset of the reversible attachment stage, biofilm formation begins at the solid-liquid (sewer pipe wall-sewage) interface by bacteria weakly associating with surfaces through non-specific interactive forces such as Van der Waals forces, electrostatic forces, hydrogen bonding, and Brownian motion forces. In order to make this attachment, bacteria overcome various repulsive forces such as hydrophobic interactions at the solid-liquid interface (Kjelleberg and Givskov, 2007; Gottenbos et al., 1999). Therefore the nature of the substrate surface and other characteristics of the aqueous medium such as hydrodynamic strength (including low flow velocities or shear stress) enable bacteria to overcome prevailing repulsive forces and thus establish the initial reversible attachment through production of extracellular polymeric substances (EPS) which bind the bacteria cells to surfaces (Cohn et al., 2010; Andersson, 2009).

Bacteria that thrive in the biofilm that forms on the submerged sewer pipe walls include SRB and NRB. Oxygen cannot normally penetrate this biofilm and this leads to the formation of two inert zones next to the pipe wall where sulphide and nitrate are reduced as alternative sources of oxygen, although the respective thicknesses of these zones have not been characterised. In the inert anaerobic zone SO_4^{2-} is reduced to S^{2-} (S^{2-}, HS^- and H_2S) while in the inert anoxic zone NO_3^- is reduced to NO_2^- (Hvitved-Jacobsen et al., 2013; Alexander et al., 2008; Kaempfer and Berndt,

1999). However, studies have shown that under anaerobic-anoxic conditions, the reduction of nitrate suppresses the generation of sulphide (Hvitved-Jacobsen et al., 2013; Heukelekian, 1943). This will be discussed later in Part Three of this literature review. A schematic of typical characteristics of such a biofilm are shown in Figure 2-3.

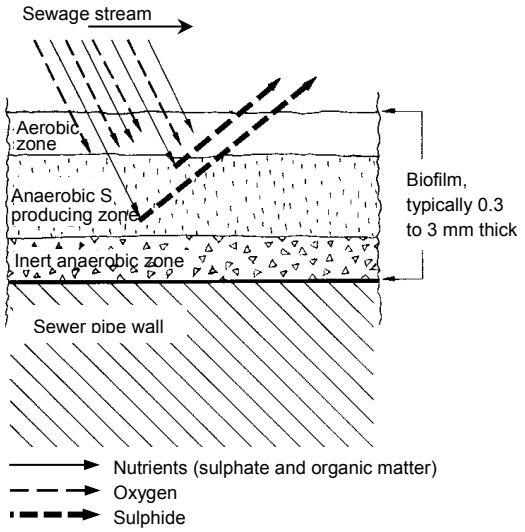

Figure 2-3: A schematic of typical characteristics of a biofilm in sewers (Boon and Pomeroy, 1990).

The thickness of the biofilm, typically 0.3 mm to 3 mm, depends partly on the flow velocity of the sewage and its abrasive content. Increased flow velocity tends to reduce the generation of S^{2-} because of the reduced thickness of the biofilm due to increased shear. It therefore follows that apart from the low sewage flow (below the self-cleansing velocities) being responsible for deposition of solids on the invert of sewer pipes (additional habitat for SRB), it also positively influences microbial activities within the biofilm (Pickell, 1993).

2.3.4 Temperature of the sewage

Biological based processes and reactions are generally influenced by temperature. Not only does an increase in temperature lead to an increase in the rate of biochemical reactions, it also impacts the growth rate of microorganisms, and therefore has a pronounced influence on microbial population density in the sewer's biofilm (Neethling et al., 1989). Viehl (1950) reported that an increase in the temperature of sewage tends to 'destroy' the still layer between the flowing sewage and the biofilm due to the sewage becoming less viscous. The less viscous sewage creates a rather turbulent flow near the surface of the biofilm, and this leads to more nutrient supply into the biofilm resulting in the generation of more S^{2-}. Baumgartner (1934) reported that the production rate of S^{2-} is greatly retarded at temperatures below 7 °C whereas the highest production rate occurs at about 30 °C. According to Pomeroy and Bowlus (1946), the generation rate of S^{2-} increases by approximately 7% per °C increment between a temperature range of 15 °C to 38 °C. Mara and Horan (2003) also reported that temperature impacts on the rate of biological based processes in sewage by influencing the solubility of gases such as oxygen. Warmer sewage leads to less solubility of oxygen and this increases the activity of SRB due to limited DO in the sewage.

2.3.5 Dissolved oxygen (DO) in the sewage

Sulphur species in sewage occur mainly in two forms, as organic sulphur compounds and as inorganic salts. According to Eliassen et al. (1949), the initial production of sulphides in sewage occurs through biochemical reactions in which the organic sulphur compounds are broken down. Under anaerobic conditions, SRB attack complex organic sulphur compounds, particularly sulphur-containing proteins which are first hydrolysed to sulphur-containing amino acids, then to S^{2-} (H_2S). Waksman (1932) stated that SRB can grow at a fairly high oxidation-reduction potential (ORP) (> -50 mV), but owing to among other factors, the competition with other microorganisms for any

available DO in the sewage, the ORP of sewage falls steadily to values less than -50 mV leading to further generation of S^{2-} by SRB (Michael, 2007). The formation of S^{2-} in sewers is non-existent when DO levels are greater than 1 mg/l, but this is seldom the case (Boon and Lister, 1975; Hollerbach, 1985).

2.3.6 Biochemical (and chemical) oxygen demand (BOD (and COD)) of the sewage

BOD is a measure of the amount of oxygen absorbed by microorganisms in the sewage (organic strength), and it is usually expressed as a measure of how much DO is consumed by aerobic bacteria in 5 days at a sewage temperature of 20 °C (BOD_5) (Abdalla and Hammam, 2014). SRB derive food for growth from many types of organic sulphur compounds such as dimethyl sulphide ($(CH_3)_2S$), which can also be oxidised to SO_4^{2-}. In the absence or depletion of DO, SRB further reduce SO_4^{2-} to S^{2-}. It is hypothesised that in typical municipal sewage, the organic nutrients available for the generation of S^{2-} (thus H_2S) are proportional to the BOD of the sewage (Davy, 1950). High BOD leads to an increase in the growth of bacteria and consumption of DO (House and Weiss, 2014).

Similar in function to BOD (BOD_5) is COD since they are both measures of the amount of organic compounds in sewage that can be oxidised. However, COD is less specific because it is a measure of all organic compounds that can be chemically oxidised, rather than the levels of biologically active organic compounds only. Nonetheless, a quantifiable correlation exists between BOD_5 and COD, known as the *biodegradability index* (BI). The use of the BI overcomes certain disadvantages that are related to the use of BOD_5 as a means of characterising sewage. Such disadvantages include (i) a test duration of 5 d (whereas for COD, it takes approximately 2 to 4 h) during which the in-situ characteristics of the sewage are likely to change, (ii) the possibility of inaccurate measurements where the bacteria encountered take longer than 5 days to break down (Hammam, 2013). Still, the use of COD has its limitations, which includes the inability to measure the oxygen consuming potential of certain compounds such as acetate that can be metabolised by microorganisms. Therefore, although COD is a reliable measure for sewage characterisation, it is not a direct substitute for BOD_5.

2.3.7 pH of the sewage

Typical pH values of municipal sewage range from 6.0 to 8.0, and it influences several factors that contribute to biogenic corrosion (EPA, 1985; Herisson, 2012; Hvitved-Jacobsen et al., 2013; House and Weiss, 2014). Studies have shown that (i) optimal conditions for the generation of S^{2-} in sewage exist when the pH is between 6.5 and 8 (Mara and Horan, 2003), (ii) the tolerance of SRB is between a pH of 5.5 and 9 (Barjenbruch et al., 2008), (iii) a decrease in the pH of the sewage from 7.9 to 7.2 corresponds to an increase in H_2S gas concentration in the sewer's headspace from 3 to 11 ppm (Figure 2-4) (Nielsen et al., 2006).

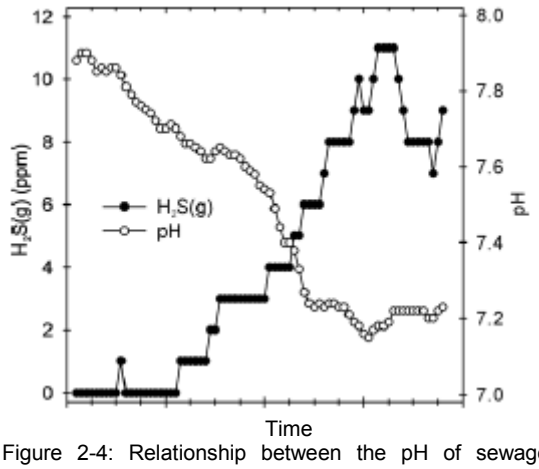

Figure 2-4: Relationship between the pH of sewage and the concentration of H_2S in the sewer's headspace (Nielsen, 2006).

2.3.8 Dissolved sulphides (DS) in the sewage

If the concentration of DO is 'low', S^{2-} (H_2S) diffuses through the biofilm and enters the sewage (Dux, 1999). H_2S is fairly soluble in water (sewage). When it dissolves in sewage, it is partially ionised so that it exists as a mixture of H_2S and HS^- (the proportions depend principally upon the pH of the sewage) (Herisson, 2012). However, when the sewage becomes completely anaerobic, the generation of S^{2-} occurs not only in the biofilm but also in the flowing sewage. The amount of sulphide produced in the sewage, however, is small in comparison with the output by the biofilm except where the flow depth is more than 600 mm (Pomeroy and Bowlus, 1946).

2.3.9 Chemistry of the sulphide system in the aqueous phase of sewers

The mere production of $H_2S_{(aq)}$ in the sewage itself does not mean that H_2S will exist in the gaseous phase. In the aqueous phase, the sulphide species occur as $H_2S_{(aq)}$, HS^-, S^{2-} together with other complexes. The concentration of these species in solutions is governed by both equilibrium equations and mass balance considerations, and varies with pH and total dissolved sulphide concentration (Lu, 2001).

H_2S is a diprotic weak acid which exist in equilibrium with its conjugate bases according to the following equilibria (Equations 2.10 and 2.11):

$$H_2S \leftrightarrow HS^- + H^+ \qquad \rho K_{a1} = 7.04 \tag{2.10}$$

$$HS^- \leftrightarrow S^{2-} + H^+ \qquad \rho K_{a2} = 11.96 \tag{2.11}$$

where K_{a1} and K_{a2} are thermodynamic equilibrium constants as expressed in Equation 2.12.

$$K_{a1} = \frac{(H^+)[HS^-]}{[H_2S]} \tag{2.12(a))}$$

$$K_{a2} = \frac{(H^+)[S^{2-}]}{[HS^-]} \tag{2.12(b))}$$

At a temperature of 25 °C, the values of K_{a1} and K_{a2} ,as functions of pH are given approximately as (Equations 2.13) (Lu, 2001):

$$-\log K_{a1} = \rho K_{a1} = 7.04 \tag{2.13(a))}$$

$$-\log K_{a2} = \rho K_{a2} = 11.96 \tag{2.13(b))}$$

According to Neethling et al. (1989), acid-base reactions proceed rapidly to reach equilibrium. Consequently, as sulphide is produced by bacteria, it rapidly gains and loses protons to establish a new equilibrium with other sulphide species. It is therefore convenient to consider the total sulphide species i.e. the total dissolved sulphide species concentration, $C_{d,s}$ in the liquid rather than specific, individual sulphide species when initially looking at these resultant equilibriums.

2.3.9.1 Mass balance equation in the aqueous phase of sewers

For a fixed $C_{d,s}$, the relevant mass balance equation is given by Equation 2.14.

$$C_{d,s} = [H_2S_{(aq)}] + [HS^-] + [S^{2-}] \tag{2.14(a))}$$

or

$$C_{d,s} = C_{H_2S_{aq}} + C_{HS^-} + C_{S^{2-}} \quad (2.14(b))$$

where [*X*] = molarity of species X

In order to assess the impact of sulphide reactions with other compounds in the sewage, the specific sulphide species concentration in the sewage must be known. The various species can be expressed as a fraction of $C_{d,s}$ as given in Equations 2.15, 2.16, and 2.17 (Jenkins et al., 1980).

$$C_{H_2S_{aq}} = \alpha_0 C_{d,s} \quad (2.15)$$

$$C_{HS^-} = \alpha_1 C_{d,s} \quad (2.16)$$

$$C_{S^{2-}} = \alpha_2 C_{d,s} \quad (2.17)$$

where α_i = the fraction of the sulphide species that lost *i* number of protons and can be calculated as shown in Equations 2.18, 2.19, and 2.20.

$$\alpha_0 = \frac{[H^+]^2}{[H^+]^2 + K_{a1}[H^+] + K_{a1}K_{a2}} \quad (2.18)$$

$$\alpha_1 = \frac{K_{a1}[H^+]^2}{[H^+]^2 + K_{a1}[H^+] + K_{a1}K_{a2}} \quad (2.19)$$

$$\alpha_2 = \frac{K_{a1}K_{a2}}{[H^+]^2 + K_{a1}[H^+] + K_{a1}K_{a2}} \quad (2.20)$$

α_i depends, to a larger extent, on the pH of the effluent, and on the equilibrium constants which have some dependence on the temperature of the effluent. For known $C_{d,s}$, a relationship of log [sulphide species concentration] or relative percentage sulphide species concentration vs. pH can be plotted (Figure 2-5). This reveals that at normal sewer environments with pH values in the order of 7, the H_2S and HS^- species concentrations occur in almost equal levels. At pH less than 7, H_2S predominates in aqueous solutions.

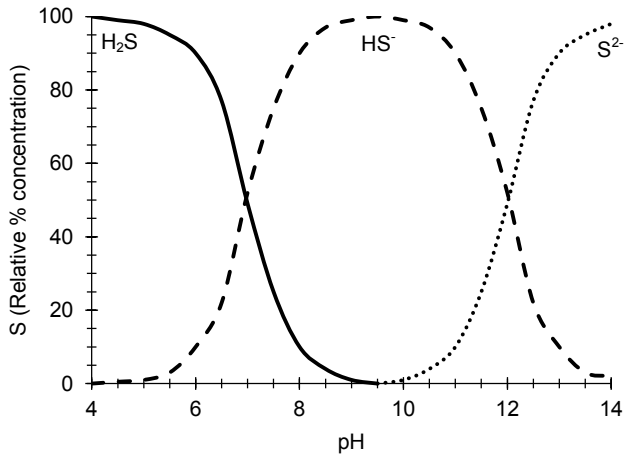

Figure 2-5: Sulphide species concentration as a function of pH (Morel, 1983).

2.3.10 Discussion – characteristics of the aqueous phase in sewers

The presence of both organic substances and SO_4^{2-} is necessary for the biological production of H_2S in the sewage (Equation 2.21), and the majority reduction of SO_4^{2-} takes place in anaerobic zones of biofilms (below the daily sewage flow levels) due to depreciation of DO.

$$SO_{4(aq)}^{2-} + 2C + H_2O \rightarrow 2HCO_{(aq)}^{3-} + H_2S_{(aq)} \quad (2.21)$$

where C = organic matter

Factors that significantly influence the concentration of DO in the sewage include temperature, BOD and turbulence (and flow velocity), while those that influence the concentration of S^{2-} in the sewage include pH and also temperature. The characteristics of the aqueous phase that influence the generation and build-up of S^{2-} in the sewage are summarised in Table 2-1.

The factors summarised in Table 2-1 are commonly used in biogenic corrosion prediction models (EPA, 1985; Vollersten and König, 2005; Tran et al., 2007; Kley and Caradot, 2013; Hvitved-Jacobsen et al., 2013). However, there is difficulty in securing input data from these factors for accurate prediction and various assumptions are made in order to generate prediction equations. Such assumptions include; that sufficient sulphate is present so that it is not limiting, that oxygen concentration is low, that no nitrate is present in the sewage, and that there is no toxic condition or factor that would inhibit the activities within the biofilm (Boon and Pomeroy, 1990). These assumptions are too simplistic for accurate biogenic corrosion prediction in concrete sewers as discussed in Part Three of this literature review.

Table 2-1: Factors affecting sulphide concentration in sewage (House and Weiss, 2014).

Factor	Effect
DO	Low DO encourages activity of SRB and the reduction of sulphate to sulphide
SO_4^{2-}	Source of sulphide
Temperature	Increased temperatures encourages microbial activity and lower oxygen solubility
BOD/COD	Represents nutrients available for bacteria that deplete DO
Turbulence	Encourages re-aeration of sewage resulting in lowered potential for sulphide build-up

2.4 Characteristics of the gaseous phase

The gaseous phase in outfall sewers consists of a mixture of both toxic and non-toxic gases that may be present in varying concentrations. The composition of these gases include those that are normally found in air as well as those that are formed due to (i) microbial respiration, and (ii) decomposition of organic matter in the sewage. Thus the sewer gases that are involved in biogenic corrosion typically consist of oxygen (O_2), carbon dioxide (CO_2), hydrogen sulphide (H_2S), sulphur dioxide (SO_2), ammonia (NH_3), and nitrogen (N_2) (Hvitved-Jacobsen et al., 2013). The formation of gases due to the decomposition of organic matter takes place in the biofilm that is established on the submerged walls of sewers, and under certain conditions, they are released to the sewer's headspace. Therefore most of these gas species occur in the sewer's headspace through certain mass transfer conditions between the aqueous and gaseous phases.

The mass transfer for an arbitrary gas species x can be expressed as (Equation 2.22) (Neethling et al., 1989):

$$N_x = (K_L a)_x \left(C_x^* - C_x\right) \quad (2.22)$$

where x = species under consideration (such as H_2S)
N_x = flux of species x from the biofilm into the aqueous phase (g/m^2-h)
$(K_L a)_x$ = mass transfer coefficient for species x into the aqueous phase (m/h)
C_x = concentration of species x in the aqueous phase (g/m^3)
C_x^* = saturation coefficient of species x in the aqueous phase, in equilibrium with the concentration in the gaseous phase (g/m^3).

C^* is calculated using Henry's law (Equation 2.23)

$$C_x^* = H_x P_x \quad (2.23)$$

where P_x = partial pressure of species x in the gaseous phase (atm)

H_x = Henry's law coefficient for species *x* (mg/L-atm)

Henry's constant is temperature-dependent (Smith and Harvey, 2007). This implies that gas concentrations in the sewer's headspace are dependent on the prevailing sewer temperature.

The roles of typical sewer gases in biogenic corrosion processes can be distinguished into two; abiotic-based and biotic-based. Nonetheless, most of these gases are involved in both roles. This section of literature review (Section 2.4) will focus on abiotic-based mechanisms. Biotic-based mechanisms will be discussed under the characteristics of the biological phase in Section 2.5.

2.4.1 Oxygen (O_2)

O_2 normally found in air is also available in the sewer's headspace where it is used, in combination with other gases, in abiotic-based mechanisms. Also, depending on the concentration of DO in the sewage, O_2 can flux into the sewer's aqueous phase where it is involved in biotic-based mechanisms on the submerged walls of sewers (Nielsen et al. 2008b). At the onset of H_2S generation in the sewage, the concentration of DO in the aqueous phase may be considered negligible ($C_{O_2}^* = 0$) and, applying Equation 2.22, the rate of transfer of O_2 can be expressed as (Equation 2.24):

$$N_{O_2} = +(K_L a)_{O_2}\left(C_{O_2}\right) \quad (2.24)$$

The positive sign in Equation 2.24 indicates that the transfer of O_2 is from the gaseous to the aqueous phase. Assuming that the oxygen concentration in the gaseous phase remains essentially constant, then the re-aeration rate of the sewage becomes solely dependent on the mass transfer coefficient, $(K_L a)_{O2}$, which is controlled by the flow velocity, depth of flow and temperature (Smith et al., 1981). Therefore, apart from the rate of consumption of O_2 in the sewage, these three factors (flow velocity, depth of flow and temperature) also influence the concentration of O_2 in the sewer's headspace.

The influence of O_2 (in moisture) in the gaseous phase of the sewer on the biogenic corrosion processes will be discussed in relation to reactions with other respective sewer gases such as CO_2 and H_2S.

2.4.2 Carbon dioxide (CO_2)

Apart from the CO_2 normally found in air, it is also generated by microbial activities in the sewer (Joseph et al., 2012). In the presence of moisture (H_2O), CO_2 dissolves to form a weak carbonic acid (H_2CO_3) solution, which reacts with the calcium in both PC-based and CAC-based hydrates (CH, C-S-H (in PC), and C-A-H (in CAC)) to form calcium carbonate ($CaCO_3$) (a process known as carbonation) at a RH of approximately 50% to 80% (Wierig, 1984).

According to Juvekar and Sharma (1973), the physicochemical processes involved in CH carbonation are (i) the diffusion of CO_2 in the gaseous phase of the concrete pores (ii) the dissolution of CO_2 in the pore water as H_2CO_3 (iii) the dissociation of H_2CO_3 as HCO_3^- and CO_3^{2-} ions (iv) the dissolution of solid CH releasing Ca^{2+} and OH^- ions, and (v) the precipitation of Ca^{2+} with CO_3^{2-} to form $CaCO_3$ when the pH of the concrete pore > 8.2 (Equation 2.25).

$$CH + CO_2 \rightarrow CaCO_3 + H \quad (2.25)$$

The solubility of CH (K_{sp} = 5.5 x 10^{-6}) is higher than that of $CaCO_3$ (K_{sp} = 0.99 x 10^{-8}); $CaCO_3$ also has lower permeability than CH. Therefore, although on one hand it is hypothesised that the low

permeability and low solubility of $CaCO_3$ offers some protection against external aggressive medium such as acid attack, the effect of carbonation which on the other hand includes reduction of concrete surface pH, need to be considered in context of the effect of other corrodents such as H_2SO_4, H_2SO_3 and HNO_3 (Islander et al., 1991; Rahman and Bassuoni, 2014). Therefore the concentration of CO_2 in the sewer's headspace is dependent on (i) the rate of generation and release of CO_2 from the aqueous phase, and (ii) the rate of dissolution of CO_2 on the non-submerged moist (depending on the RH in the sewer) walls.

2.4.3 Hydrogen sulphide (H_2S)

At the onset of H_2S generation, its concentration in the gaseous phase may be considered negligible ($C^*_{H2S} = 0$) and, applying Equation 2.22, the rate of transfer of H_2S can be expressed as (Equation 2.26):

$$N_{H_2S} = -(K_L a)_{H_2S}\left(C_{H_2S}\right) \tag{2.26}$$

The negative sign in Equation 2.26 indicates that the transfer of H_2S is from the aqueous to the gaseous phase.

As discussed in Section 2.3.9, the various sulphide species are expressed as a fraction of the total dissolved sulphide concentration the sewage. Therefore by substituting Equation 2.15 into Equation 2.26, it can be shown that the rate of transfer of H_2S from the aqueous to gaseous phase is also dependent on the pH of the sewage (Equation 2.27) (Nielsen, 2006).

$$N_{H_2S} = -\alpha_0 (K_L a)_{H_2S}\left(C_{d,S}\right) \tag{2.27}$$

H_2S is alkaline and when available in the sewer's headspace, it is readily adsorbed on the moist concrete surfaces where it is chemically (abiotic) oxidised to form elemental sulphur (S), and a weak H_2SO_4 in the absence of SOB (a process known as auto-oxidation (Equation 2.28)) (Jolley and Forster, 1985). Greater H_2S oxidation occurs on concrete surfaces with higher carbonation potential (Ismail et al., 1993).

$$H_2S + 2O_2 \rightarrow H_2SO_4 \tag{2.28}$$

This H_2SO_4 formed through auto-oxidation contributes to the lowering of concrete surface pH (Islander et al., 1991). Also, in PC-based binder systems, it simultaneously destroys the polymeric nature of CH and substitutes a larger molecule of $C\bar{S}$ which precipitates as $C\bar{S}H_2$ (Equation 2.29). $C\bar{S}H_2$ reacts with the aluminates to form secondary ettringite (Equation 2.30).

$$CH + H_2SO_4 \rightarrow C\bar{S}H_2 \tag{2.29}$$

$$C_3\overline{S_3}H_6 + C_3AH_{12} + H_{14} \rightarrow C_6A\overline{S_3}H_{32} \tag{2.30}$$

2.4.4 Sulphur dioxide (SO_2)

SO_2 is one of the gases generated during biodeterioration of sulphur-based organic matter in the sewage (in the aqueous phase), and is released into the gaseous phase depending on the mass transfer conditions discussed earlier. In the presence of moisture, SO_2 will form weak sulphurous acid (H_2SO_3) that can dissociate to form HSO_3^- in solution. H_2SO_3 can react with H_2S to form weak polythionic acids which can be oxidised to H_2SO_4 and SO_2 (Equations 2.31 and 2.32). Most of these polythionic acids contribute to the reduction of the surface pH of concrete, and also react with CH to form $C\bar{S}$ (Islander et al., 1991; Parande et al., 2006; Gutiérrez-Padilla et al., 2010).

$$H_2SO_3 + H_2S \rightarrow H_2S_2O_2 + H_2O \tag{2.31}$$

$$H_2S_2O_2 + 2O_2 \rightarrow H_2SO_4 + SO_2 \quad (2.32)$$

2.4.5 Ammonia (NH_3)

NH_3 is generated in the sewer's biofilm during anaerobic processes, and it is the only base in the mixture of sewer gases (Weissenberger et al., 2004; Bi et al., 2015). Therefore NH_3 itself is not corrosive but its reaction with other acids such as H_2SO_4 to form ammonia salts (ammonium sulphate (Equation 2.33) and ammonium bisulphate (Equation 2.34)) promotes the attack of concrete sewer pipes (Huntzicker et al., 1980; McMurry et al., 1983; Baek and Aneja, 2004).

$$NH_3 + H_2SO_4 \rightarrow NH_4HSO_4 \quad (2.33)$$

$$2NH_3 + H_2SO_4 \rightarrow (NH_4)_2SO_4 \quad (2.34)$$

In sewers where the RH is generally > 65%, ammonia salts will decompose to dissolved salts. Solutions of NH_4HSO_4 are known to have corrosive effects, and their mechanisms of attack follow the two-step H_2SO_4 attack given by Equations 2.29 and 2.30 (Equations 2.35 and 2.36) (Lea, 1965; Werner et al., 2000).

$$CH + NH_4HSO_4 \rightarrow C\bar{S}H_2 + NH_3 \quad (2.35)$$

$$C_3\overline{S_3}H_6 + C_3AH_{12} + H_{14} \rightarrow C_6A\overline{S_3}H_{32} \quad (2.36)$$

The role of NH_3 in abiotic-based concrete sewer corrosion is considered aggressive with rapid progression internally since (i) $C\bar{S}H_2$ has a higher solubility in NH_4HSO_4 (Lea, 1970), (ii) the regeneration of NH_3 as shown in Equation 2.35 indicates that there is more of the corroding reagents re-occurring (see Equation 2.33) (Lea, 1965).

2.4.6 Discussion – characteristics of the gaseous phase in sewers

The sources and concentrations of gases in the sewer's headspace are varied, and even though most researchers have reported that the concentration of H_2S has the most significant impact during biogenic corrosion processes, the role of other gases as discussed above cannot be generally deemed to be of less significance (Pomeroy and Bowlus, 1946; Pomeroy and Parkhurst, 1977; Boon and Pomeroy, 1990; Hvitved-Jacobsen et al., 2013). The composition and concentration of the gaseous phase in sewers is primarily dependent on the characteristics of the aqueous phase and sewer hydraulics. These characteristics that include (i) species concentration in the sewage, (ii) the flow velocity, depth of flow, temperature, and pH of the sewage, and (iii) the relative humidity and temperature of the sewer's headspace are reflected in commonly used biogenic corrosion prediction models with bias towards the sulphur species (EPA, 1985; Vollersten and König, 2005). However, it is not always necessary for the concentrations of H_2S to be 'very high' for biogenic corrosion to occur. A 'low' H_2S concentration of between 2 ppm and 6 ppm can result in the generation of biogenic H_2SO_4 (on sewer walls) of concentrations in the order of 6% v/v (approximate pH 1.2) when the temperature in the sewer headspace is approximately 18 °C (Thistlethwayte, 1972). It is therefore hypothesised that mechanisms involving gases other than H_2S play a significant role in biogenic corrosion of concrete in sewers.

Therefore, better characterisation of the sewer corrosion mechanisms can be obtained by, among others, inclusion of the influence of other sewer gases in biogenic corrosion prediction models. However, the combination of these gases kinetics remains complex because not all interactions are synergistic (Nixon, 1997).

2.5 Characteristics of the biological phase

At most sewer depths, the temperature of the sewage is generally higher than the temperature of the surrounding earth (and sewer pipe material) (Boon and Pomeroy, 1990). Due to this

temperature difference, water vapour escapes from the sewage stream and condenses on the non-submerged walls of sewers depending on the sewer's RH (typically > 65%). As discussed in Section 2.4, certain gases and salts dissolve in this condensate to form (weak) acids that are mostly responsible for lowering the pH of the concrete sewer pipe surfaces (typically between 12 and 13 for newly cast pipes), and also become habitats for various types of microorganisms that includes SOB once the pH of the concrete surfaces drops to about 9 (Rigdon and Berdsley, 1956).

Several researchers have described the growth of microorganisms, regulated by the pH of the concrete surface as successive, and dependent on (i) the oxidation of the various gases found in the sewer's headspace, and (ii) the microbial activities of the respective bacteria and fungi species (Islander et al., 1991; Mori et al., 1992; Okabe et at., 2007; Valix et al., 2012). The succession of microorganisms occurs because different species thrive in a specific range of pH. At pH of about 9, the neutrophilic SOB (NSOB) and fungi start to grow. NSOB such as *Acidithiobacillus thioparus* (*A. thioparus*), *Starkeya novella, Halothiobacillus neapolitanus,* and *Thiomonas intermedia*, which influence the conversion of thiosulphate ($S_2O_3^{2-}$) to S are predominant at pH 8 to 6 (Islander et al., 1991; Kelly et al., 2000; Kelly and Wood, 2000). Acidophilic SOB (ASOB) and fungi grow at pH < 6. ASOB which includes heterotrophic bacteria, and fungi such as *Aspergillus niger* grow at pH 6.5 to 4 and excrete organic acids (Cho and Mori, 1995; Gu et al., 1998; Valix et al., 2012). Other ASOB such as *Acidithiobacillus thiooxidans* (*A. thiooxidans*) and *Acidithiobacillus ferrooxidans* (*A. ferrooxidans*), which oxidise H_2S and other sulphur compounds ($S_2O_3^{2-}$ and S) to H_2SO_4 thrive at pH 5.5 to 1 (Hernandez et al., 2002; Okabe et al., 2007).

Microbial sulphur oxidation is a biological energy conservation process that is key for the biogeochemical sulphur cycle, which is responsible for biogenic corrosion in sewer environments (Wachtershauser, 1990). Many microorganisms can carry out dissimilatory sulphur oxidation of reduced inorganic sulphur compounds such as $S_2O_3^{2-}$ and S (Brüser et al., 2000). The microbial ecosystem is discussed in the following section.

2.5.1 Microbial ecosystem

The microbial ecosystem on concrete sewer pipe surfaces that are not submerged is dominated by a single source of energy – sulphide, and chemotrophs (Islander et al., 1991; Lenk, 2006). The sulphur chemolithotrophs grow primarily aerobic, using molecular O_2 as terminal electron acceptor and CO_2 as a source of carbon (Brüser et al., 2000).

According to Islander et al. (1991), biogenic acid production is dominated by species of the genus *Acidithiobacillus*. The *Acidithiobacillus thiooxidans* excretes as much as 20% of the CO_2 it fixes as organic substances, as well as pyruvic acid and oxalacetic acid which are self-inhibitory (Karavaiko and Pivovarova, 1973; Borichewski, 1967). Therefore the growth of the acid-producing bacteria (*A*-species) requires a mutualistic relationship with certain heterotrophs that can degrade the organics excreted by these *A*-species. Sand and Bock (1984) reported abundance of heterotrophs on deteriorated concrete surfaces with pH 6.2 to 1.5.

At the inception of biogenic corrosion processes, a biofilm forms on the non-submerged walls of concrete sewer pipes. This biofilm is created by the *A. thioparus* which are among the first NSOB to colonise new concrete pipe surfaces (at pH of about 9), although the biofilm disappears as biogenic corrosion progresses (Rigdon and Beardsley, 1956). Therefore the microbial structure system can be visualised as individual organisms in a volume of porous material (concrete), at abundances varying with depth. The microorganisms interact with chemical gradients between the highly alkaline environment nearest to the un-attacked concrete surface and the acidic environments within the deteriorated concrete matrix (Islander et al., 1991).

Islander et al. (1991) reported that microbial activities on concrete sewer pipes are influenced by pH, and that the microorganisms may produce acid until it becomes self-inhibitory. This means that

microbial activities are limited by 'very low' pH. Concrete sewer pipe surfaces with pH < 1.0 experiences a lower growth rate of *A. thiooxidans* (Kempner, 1966).

However, according to Gu et al. (1998), *Acidithiobacillus* are not solely responsible for corrosion of concrete in sewers. Their study showed that fungi, particularly *Fusarium sp.*, appear to act synergistically with the *Acidithiobacillus* to release Ca^{2+} and degrade the concrete matrix. Organic acids such as acetic, oxalic and glucuronic produced by the *Fusarium sp.,* may form soluble calcium complexes with concrete matrix, resulting in dissolution.

2.5.2 Discussion – characteristics of the biological phase in sewers

The microbial communities on both un-attacked and attacked (deteriorated) concrete sewer pipe surfaces vary in composition and with depth. Generally, fungi and bacteria other than SOB coexisted with SOB during the microbial succession in the corroding concrete. Certain species of fungi that thrive in neutrophilic environments front the biogenic corrosion processes. On the other hand, even at a concrete surface pH of about 2, bacteria other than SOB still accounted for approximately 50% of the total microbial community, and they are most likely responsible for removal of toxic substances such as pyruvate and oxalate (that are excreted by SOB (particularly *A. thiooxidans*)) thereby funnelling the activities of SOB (Okabe et al., 2007).

Nonetheless, in concrete sewer pipes that utilise binder systems that are rich in Al_2O_3 and Fe_2O_3 such as CAC, this ecosystem is often disrupted in the presence of Al^{3+} and Fe^{3+} at approximately pH 3. Al^{3+} has a bacteriostatic effect on sulphide-oxidising bacteria since it can (i) penetrate the bacteria's cell envelope, and (ii) associate with (bind to) the nucleic acid (DNA) of the bacteria. Once inside the cell, the Al^{3+} forms predominantly positively-charged polymeric complexes that cross-link with other DNA strands that have near-neutral pH (O'Hara et al., 1989). It is therefore hypothesised that the binding of the Al^{3+} to the DNA halts the replication of acidophilic bacteria cells (Johnson and Wood, 1990). On the other hand, Fe^{3+} results in oxidative stress, inflammation and consequent damage to proteins and DNA through the production of reactive oxygen species (ROS) in bacteria (Soenen et al., 2012; Chatterjee et al., 2011; Trun and Gottesman, 1990).

2.6 Characteristics of the mineralogical phase

Concrete is a moderately porous mixture of inorganic precipitates and mineral aggregate. It is highly alkaline and dissolves on contact with aggressive media such as acids. Generally, acids will react first with the calcium hydroxide (CH), and then with the calcium oxides (C) thereby destroying the structural integrity of a concrete matrix.

The characteristics of the concrete sewer pipe surface (mineralogical phase) are mostly influenced by the characteristics of the gaseous and biological phases in the sewer environment. Due to the porous nature of the concrete, certain compounds and microorganisms are distributed both on the concrete sewer surfaces and beneath (in the pores of the concrete matrix). These pores act as sinks for both abiotic and biotic sulphur-based processes that result in the formation of biogenic H_2SO_4. This H_2SO_4 diffuses inward as it gets neutralised by the alkalinity of the concrete matrix. Eventually, the dissolution of the calcium hydroxide by the attacking acid leads to an increase in the porosity of the concrete matrix, particularly in PC-based binder systems which are widely used in the manufacture of concrete sewer pipes.

However, other binder systems apart from PC-based are also used in the manufacture of concrete sewer pipes, albeit mainly for lining applications. These include CAC-based binder systems whose characteristics differ from those of PC-based binder systems, particularly the nature of their hydrates. The characteristics of these two binder systems (with and without SCMs) in a sound state and when subjected to biogenic H_2SO_4 are discussed in detail in Part Two of this literature review.

2.7 Summary – general sewer hydraulics and sewer environment considerations

This part presented a review of various aspects of the sewer environment, where it was noted that:

(1) Sewer hydraulics, which includes flow velocity, depth of flow, and system turbulence, is one of the significant parameters that define the different phases of the sewer environment that are responsible for biogenic corrosion processes.
(2) The presence of both organic substances and SO_4^{2-} is necessary for the biological production of H_2S in the sewage, and the majority of SO_4^{2-} reduction takes place in anaerobic zones of the biofilms (below the daily sewage flow levels) due to depreciation of DO. Factors that significantly influence the concentration of DO in the sewage include temperature, BOD and turbulence (and flow velocity), while those that influence the concentration of S^{2-} in the sewage include pH and also temperature.
(3) Most researchers have reported that the presence of H_2S in the sewer's headspace has the most significant impact during biogenic corrosion processes. However, the role of other gases such as CO_2 and O_2 cannot be generally deemed to be of less significance.
(4) The microbial communities on both un-attacked and attacked (deteriorated) concrete sewer pipe surfaces vary in composition and with depth. Generally, fungi and bacteria other than SOB coexisted with SOB during the biogenic H_2SO_4 attack mechanisms of concrete sewer pipes.
(5) The corrosion mechanism of concrete sewer pipes entails reduction of the surface pH, abiotic and biotic formation of H_2SO_4, dissolution of CH, and increase in the porosity of (attacked) concrete surfaces which accelerates the rate of attack. This cycle is repetitive.
(6) The characteristics of the different binder systems viz. PC-based and CAC-based used in the manufacture of concrete sewer pipes vary when subjected to biogenic H_2SO_4, and are dependent on the nature of their hydrates.
(7) The Al^{3+} resulting from the dissolution of certain alumina hydrates in CAC-based binder systems has a bacteriostatic effect to acidophilic SOB through DNA-binding processes that halt replication of the bacteria cells.
(8) It is probable that the Fe^{3+} from the dissolution of iron hydroxides in binders results in oxidative stress, inflammation and consequent damage to proteins and DNA through the production of reactive oxygen species (ROS) in bacteria, thereby suppressing the acid-generating activities of the microbes.

The outfall sewer environment phases discussed in this section (Part One of literature review) are interdependent and in most cases give rise to aggressive situations that are responsible for the corrosion of materials used in the manufacture of sewer conduits (pipes). Even though the governing principles of general sewer hydraulics and sewer environment phases are relatively well understood, their direct application in biogenic corrosion prediction of cement-based materials has not been widely researched and documented. The current study focusses on cement based materials – particularly, concrete, whose performance in sewers depends on the characteristics of the binder systems that are used in the manufacture of concrete pipes. The characteristics of concrete mixtures for sewer pipe application are discussed in Part Two of this literature review.

2.8 Characteristics of the concrete sewer pipe materials

The service life of concrete sewers depends on various design and operational considerations. Such considerations include parameters such as system hydraulics, headspace gas (particularly CO_2, O_2 and H_2S) concentrations and properties of sewer pipe materials. Most of these parameters are related in the form of service life or corrosion prediction models (these are reviewed in Part Three of this Chapter Two), which are readily available for use by design engineers (EPA, 1985; Goyns, 2013; Hvitved-Jacobsen et al., 2013). The ultimate objective of such prediction models is to enable engineers to choose the most durable and economical concrete mixtures for the intended service life of sewers. As briefly mentioned in Section 2.6, the two binder types that are mainly used in the manufacture of different components in concrete sewer pipes are Portland cement (PC) and calcium aluminate cement (CAC). The characteristics of these binder systems (with and without SCMs), and the nature of their products of corrosion when they are subjected to biogenic H_2SO_4 are discussed in detail in the following sections.

2.8.1 Background and composition of Portland cement (PC)

PC is made by heating a mixture of limestone ($CaCO_3$) and clay (or other materials of similar bulk composition (aluminosilicate) and sufficient reactivity) in a kiln, ultimately to a temperature of about 1450 °C, where partial fusion occurs, and nodules of clinker are produced. The clinker is mixed with a certain percentage of $C\bar{S}$ and the mixture is finely ground to make cement. The $C\bar{S}$ controls the rate of set and influences the rate of strength development. The typical chemical composition (main oxides) and major phases of PC clinker are given in Table 2-2.

Table 2-2: Typical chemical composition (main oxides) and major phases of PC clinker (Taylor, 1997; Neville, 2011).

PC (clinker)	Chemical composition (%)				Major phases (%)			
	S	A	F	C	C_3S	β-C_2S	C_3A	C_4AF
	17 – 25	3 – 8	0.5 – 6	60 – 67	45 - 65	10 - 30	5 - 12	6 - 12

The two calcium silicate phases, C_3S and C_2S are largely responsible for the development of strength and other properties such as permeability that are associated with durability performance of PC (Graeme, 2003). C_2S is known to have three forms, α-C_2S, which exists at high temperatures (> 1500 °C), inverts to the form β-C_2S at about 1450 °C. β-C_2S undergoes further inversion to γ-C_2S at about 670 °C but, at the rates of cooling of commercial cements (approximately 1450 °C), β-C_2S is preserved in the clinker (Neville, 2011).

During the manufacturing process of clinker, the reaction between C (lime from limestone) and S (silica from sand) is difficult to achieve even at higher firing temperatures (> 1500°C), and their chemical combination is facilitated by addition of small quantities of A (typically 5%) and F (typically 3%). The A and F help to form a molten flux or liquid phase (at temperatures in the order of 1500°C) through which C and S partially dissolve prior to crystallisation to form C_3S and β-C_2S.

Therefore, although the process of formation of PC clinker occurs at temperatures of approximately 1450°C, higher temperatures are generally involved during this process, which can be distinguished into two basic temperature-dependent stages; (i) Temperature range greater than 1500°C that constitutes the liquid phase from which C_3S and β-C_2S are formed by crystallisation, and (ii) Temperature range of about 1450°C where clinkering reactions proceed in the solid state, in the presence of very low quantities of the liquid phase.

A basis for the preliminary understanding of the chemistry underlying the formation of PC can be provided by the major oxide components through a pure $CaO–SiO_2–Al_2O_3$ system (Figure 2-6),

that can be used to predict the solid phases that will be present for various bulk chemical compositions (Taylor, 1997).

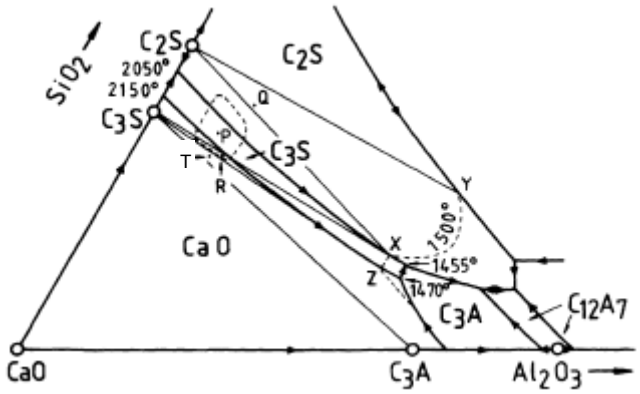

Figure 2-6: Part of the pure CaO-SiO_2-Al_2O_3 system used to illustrate the formation of PC clinker (Taylor, 1997).

According to Figure 2-6, the compositions in a pure CaO–SiO_2–Al_2O_3 system that correspond closely to those of typical PC lie within the ringed area surrounding point P. This point lies within a triangle whose apices are the compositions of C_3S, C_2S and the point X, which lies at the intersection of the boundary of the C_3S and C_2S primary phase fields with the 1500°C isotherm. To explain the major phase compositions of PC further, for example, if a liquid composition of P that is at a temperature higher than 1500 °C is cooled, C_3S crystallises first and the remaining liquid composition will move away from C_3S until the boundary between the primary phase fields C_3S and C_2S is reached. At this boundary, both C_3S and C_2S then crystallise and the remaining liquid composition will continue to move along this boundary until the 1500 °C isotherm is reached.

Similarly, for any bulk composition of Q in triangle C_2S–X–Y, the equilibrium phases at 1500°C will be C_2S, and a liquid having a composition XY. Any bulk composition of R in triangle C_3S–X–Z (1455 °C isotherm), the equilibrium phases at 1455°C will be C_3S, and a liquid having a composition XZ. Any bulk composition lying below the C_3S–Z line (1470 °C isotherm), such as that of point T will give an assemblage that includes C as the solid phase. Therefore, this line C_3S–Z (or clinker cooling temperatures of approximately 1470 °C) sets a practical limit of the C content in clinker.

During the manufacture of PC clinker, it is essential to maximise the amounts of C_3S, and to avoid the presence of more than minimal amounts of free lime or calcium oxide (C) in the final product. The free C is one of the key parameters that is used in the regulation of the composition of clinker, and is often expressed in terms of a quantity known as the Lime Saturation Factor (LSF) (Equation 2.37) (Lawrence, 1998). The LSF expresses the maximum amount of lime that can be combined with the various major oxides present in PC clinker, based on the chemical formulae for the major PC clinker phases being formed (C_3S, β-C_2S, C_3A, and C_4AF), and on the CaO–SiO_2–Al_2O_3 system.

$$LSF = \frac{C}{2.8S + 1.1A + 0.7F} \tag{2.37}$$

The significance of the LSFs in the manufacture of PC has been reported in literature (Lawrence, 1998). Stark et al. (1981) reported that a reduction in the LSF leads to an increase in the content of β-C_2S and reduction in C_3S. Ludwig and Pöhlmann (1986) also reported that the strength development for cements with LSFs above 0.84 was adequate with regard to various design guidelines, whereas a marked decrease in strength development was reported for cements with LSFs less than 0.8. According to Locher (1986), a certain minimum content of C_3S is therefore required in clinker for general satisfactory performance of PC in most environments. However, in aggressive acid environments such as those subjected to biogenic H_2SO_4, higher contents of C_3S

are disadvantageous because they provide higher amounts of CH, which is the main acid-soluble component in a concrete matrix. The hydration and significance of these silicate phases in PC is discussed in Section 2.8.2.

The other key parameters that regulate the composition and properties of clinker are the proportion of the silicate phases and the quantity of flux formed at relatively low temperatures (< 1338°C). The former is often described by a quantity known as the Silica Ratio (SR) (Equation 2.38) and the latter by a quantity known as the Alumina Ratio (AR) (Equation 2.39) (Taylor, 1997).

$$SR = \frac{S}{A + F} \tag{2.38}$$

$$AR = \frac{A}{F} \tag{2.39}$$

The SR governs the proportion of silicate phases in the clinker. Increase in SR lowers the proportion of the liquid phase at any given temperature in the kiln, and thus makes the clinker more difficult to burn and fuse. For a given LSF, the higher the SR, the more C_3S and the less C_3A and C_4AF will be produced. On the other hand, the AR is used to optimise the temperatures at which partial fusion of the clinker first occurs. For a given LSF, a higher AR results in a higher C_3A content in clinker. This implies that the composition and properties of clinker (thus the PC), are mostly dependent on the three ratios – LSF, SR, and AR, as defined by Equations 2.37, 2.38 and 2.39 respectively.

When used in the manufacture of concrete, PC can attain adequate respective mechanical properties (such as strength, shrinkage, and permeability) that generally ensure good durability under a variety of conditions. However, it has not been possible to find in the composition of cement a complete solution to the problem of the durability of concrete; hence several Standards have specific limits for the contents of constituents of PC for various applications (Neville, 2011). Nonetheless, the durability of PC-based concrete mixtures when subjected to biogenic H_2SO_4 in sewer environments has broadly been unsatisfactory (Goyns, 2003; Fourie, 2007; Alexander et al., 2008; Goyns et al., 2008; Herisson, 2012, Scrivener and De Belie, 2013; Herisson, 2014). This is principally related to the nature of their hydrates, which are discussed in the following section.

2.8.2 Mechanism of hydration of PC

There are two mechanisms of hydration of PC proposed in literature (Mehta and Monteiro, 2013). The first of these is the *through-solution hydration* where hydration occurs by a process of dissolution and precipitation. This means that the anhydrous phases in the grains of cement dissolve in water to give ions in solution. These ions can recombine in different proportions with water, and the new combinations precipitate, due to their lower solubility, as the hydrate phases. The second mechanism is the *solid-state hydration* where reactions take place directly at the surface of the anhydrous cement compounds without the compounds going into solution. The through-solution mechanism is dominant in the early stages of PC hydration, while at later stages when the ionic mobility of the solution becomes restricted, the hydration of the residual cement particles may occur in solid-state reactions.

Since PC is composed of a heterogeneous mixture of several compounds or phases, the hydration process consists of simultaneously occurring reactions of the anhydrous phases with water, albeit at different rates to form a hydrated cement paste (HCP), which constitutes of solids and various types of voids as discussed later. The two major anhydrous phases in PC are the silicates and the aluminates, and their mechanisms of hydration are discussed below.

2.8.2.1 Hydration of the silicates

The hydration of C_3S and β-C_2S in PC produces a family of calcium silicate hydrates (C-S-H) (which are structurally similar but vary in their Ca/Si ratios and the content of chemically combined water) and calcium hydroxide (CH) (Equations 2.40 and 2.41).

$$2C_3S + 6H \rightarrow C_3S_2H_3 + 3CH \tag{2.40}$$

$$2C_2S + 4H \rightarrow C_3S_2H_3 + CH \tag{2.41}$$

The fact that the term C-S-H is hyphenated signifies that it is not a well-understood phase yet, even though it makes up to 60% (making it an important phase in determining the strength properties) of the volume of solids in HCP (Neville, 2011). Also, the chemical composition of C-S-H in HCP varies with the w/c ratio, temperature and age of hydration. On complete hydration of PC, the approximate composition of this phase corresponds to $C_3S_2H_3$, and it is this composition that is used in stoichiometric calculations involving C-S-H (Equations 2.40 and 2.41). Therefore C-S-H does not have definite stoichiometry, and its morphology varies from poorly crystalline fibers to reticular network.

Even though similar reaction products are formed on hydration of both C_3S and *β*-C_2S in PC, it is important to note that stoichiometric calculations show that the hydration of C_3S would produce 61% C-S-H and 39% CH, while the hydration of *β*-C_2S would produce 82% C-S-H_3 and 18% CH. CH constitutes 20 to 25% of the volume of solids in HCP, and unlike the C-S-H, CH has definite stoichiometry. The strength-contributing potential of CH in HCP is limited due to its considerably lower surface area in comparison to C-S-H. The morphology of CH varies from nondescript to stacks of large plates of distinctive hexagonal prisms (Mehta and Monteiro, 2013).

2.8.2.2 Hydration of the aluminates

The major aluminate phases in PC are C_3A and C_4AF. C_3A reacts rapidly with water to form the phases C_2AH_8 and C_4AH_{19}, which subsequently convert to C_3AH_6. This is a rapid and highly exothermic reaction. This rapid reaction is controlled by blending the C_3A with $C\bar{S}$. Therefore the initial reactions of PC with water are controlled by the formation of a protective layer of ettringite ($C_6A\bar{S}_3H_{32}$) on the surface of the C_3A crystals. This is a topochemical reaction. The mechanism of retardation of the reactions involving C_3A and $C\bar{S}$ in water can be explained as follows (Mehta and Monteiro, 2013):

Since $C\bar{S}$ and alkalis go into solution quickly, the solubility of C_3A is depressed in the presence of hydroxyl, alkali, and sulphate ions. Depending on the concentration of aluminate and sulphate ions in the solution, the precipitating crystalline product is either calcium aluminate trisulphate hydrate (AFt) or the calcium aluminate monosulphate hydrate (AFm). In solutions saturated with calcium and hydroxyl ions, the former crystallises as short prismatic needles (ettringite) (Equation 2.42). The monosulphate (Equation 2.43) crystallises as thin hexagonal plates.

$$[AlO_4]^- + 3[SO_4]^{2-} + 6[Ca]^{2+} + aq \rightarrow C_6A\overline{S_3}H_{32} \tag{2.42}$$

$$[AlO_4]^- + [SO_4]^{2-} + 4[Ca]^{2+} + aq \rightarrow C_4A\bar{S}H_{18} \tag{2.43}$$

Even though the rate of hydration of C_4AF is slower than that of C_3A, the crystal structure of its resultant phases, $C_6A(F)\bar{S}_3H_{32}$ and $C_4A(F)\bar{S}H_{18}$ is similar to that of ettringite (Equation 2.42) and monosulphate (Equation 2.43) respectively. These calcium sulphoaluminates ($C_6A\bar{S}_3H_{32}$ and $C_4A\bar{S}H_{18}$) occupy 15 to 20% of the volume of solids in the HCP.

Therefore ettringite is usually the first hydrate to crystallise because of the high sulphate/aluminate ratio in the solution phase during early hydration. However, after the depletion of sulphate when

the concentration of aluminate ions in the solution increases due to renewed hydration of C_3A and C_4AF, ettringite becomes unstable and is gradually also converted into the monosulphate phase (Equation 2.44), which is the final product of hydration of aluminates in PC.

$$C_6A\overline{S_3}H_{32} + 2C_3A + H_{22} \rightarrow 3C_4A\overline{S}H_{18} \quad (2.44)$$

The monosulphate phase is susceptible to various forms of attack mechanisms including that of biogenic H_2SO_4 attack as discussed later in Section 2.10.

2.8.2.3 Other phases in the hydrated cement paste

Hydration occurs by a process of dissolution and precipitation. Depending on the particle size distribution of the anhydrous PC and the degree of hydration, some unhydrated cement grains may be found in the microstructure of HCP. The reason for this is that with the progress of the hydration process, the smaller grains dissolve first as the larger grains reduce in size. But because of the limited available space between the grains in the system undergoing hydration, the products of hydration tend to crystallise in close proximity to the hydrating grains and 'coats' the unhydrated grains. This 'coated' system of unhydrated grains may eventually form a 'dense product' whose morphology resembles that of the original cement grains (Mehta and Monteiro, 2013).

Apart from the hydration resulting in solids constituting the HCP as discussed in sections above, several types of voids also occur. Such voids include the inherent interlayer space in C-S-H, capillary voids, and air voids. Several researchers have reported that the interlayer spaces in C-S-H may be 'too small' (0.5 to 2.5 nm) to have an adverse effect on the strength and other durability-related properties such as permeability of HCP (Powers, 1958; Feldman and Sereda, 1968; Mehta and Manmohan, 1980).

The capillary voids represent the irregularly-shaped spaces not filled by the solid phases of the HCP (Basheer and Barbhuiya, 2010). In well-hydrated low w/c ratio pastes, the capillary voids may range from 10 to 50 nm in size, whereas in high w/c ratio pastes, at early stages of hydration, they may be as large as 3 to 5 μm (Mehta and Manmohan, 1980). Capillary voids can broadly be described by their sizes; *macropores* are larger than 50 nm in size whereas the *micropores* are smaller than 50 nm in size. The macropores are more influential in characterising the strength and transport processes in HCP while the micropores play a significant role in drying shrinkage and creep (Basheer and Barbhuiya, 2010; Mehta and Monteiro, 2013).

Air usually gets trapped in the cement paste during mixing, and results in spherical voids upon hardening of the HCP. This entrapped air voids may be as large as 3 mm. Under certain circumstances where chemical admixtures are used in cement-based mixes to purposely entrain air, entrained air voids ranging from 50 to 200 μm in size form upon hardening of the HCP. Therefore both entrapped and entrained air voids in the HCP are generally larger than the capillary voids, and are capable of adversely affecting the strength and other transport-related processes such as permeability.

Therefore the characteristics of the PC's HCP are influenced by certain ratios such as the LSF, SR and AR as applied during the manufacturing stages of PC clinker, coupled with the w/c used during the mixing of the cement paste. From the literature reviewed so far on PC, it has been highlighted that the preferred phases for strength development are C_3S and β-C_2S, but these also result in the formation of a high quantity of CH during hydration, which is disadvantageous during chemical or acid attack.

Before proceeding, it is important to note that from the discussions on the hydration processes of the major PC phases, it has been highlighted that the hydration and strength development of PC involves, among other reactions, the formation of C-S-H and CH, where the C-S-H is assumed to be the main strength-giving phase. Nonetheless, the processes leading to the formation of both C-

S-H and CH are complementary to each other since for a given degree of cement hydration, an increase in the Ca/Si molar ratio of C-S-H lowers the proportion of CH. Several researchers have reported Ca/Si molar ratios of C-S-H in PC-based mixtures of between approximately 1 and 2 (Pelisser et al., 2012; Hughes and Trtik, 2004; Ulm et al., 2001; Famy et al., 2000). However, Chatterji (1995) correlated certain durability characteristics of PC-based concrete mixtures and their Ca/Si molar ratios and reported that a fully leached PC-based paste has a molar ratio of about 1.5. Higher molar ratios (of up to 1.8) were related to excess loosely-bound C (CaO). The excess C does not contribute to strength characteristics, and under certain prevailing conditions is liable to cause deterioration of the concrete matrix through various chemical reactions such as those involving biogenic H_2SO_4.

Two other points are worth noting in PC-based mixtures. First, under certain conditions, the Ca^{2+} are bound by the carbonate ions (CO_3^{2-}) in the pore solution thereby forming $CaCO_3$, which in effect, defines the alkalinity of such mixtures. Secondly, somewhat opposing mechanisms are involved in PC-based mixtures in aggressive (acid) environments; (i) there is the provision of sites for acid reaction through the available CH, which is readily acid-soluble and (ii) the same available CH provides a basis for neutralising the attacking acid. Therefore, a distinction between these two mechanisms and their relationship with the respective Ca/Si (or Si/Ca) and Ca/Al (or Al/Ca) molar ratios is necessary in order to better understand the mineralogical transformations during biogenic corrosion processes. This is one of the focus areas of the current study.

2.8.3 Blended PC-based binder systems

In order to improve certain durability requirements of the HCP of PC (and PC-based concrete mixtures in general) without additional clinkering processes involved in the manufacture of PC, various supplementary cementitious materials (SCMs) are used to partially replace PC in concrete mixtures (Lothenbach et al., 2011). SCMs consist of (i) naturally occurring materials such as pozzolana and fine limestone, and (ii) by-products of certain manufacturing processes such as ground granulated blast-furnace slag (GGBS), fly ash (FA), and condensed silica fume (SF). The current study focusses on the latter, and in particular GGBS, FA, and SF (as SCMs, not as part of composite cements).

In general, the chemistry of GGBS, FA and SF is characterised by lower calcium content than that of plain PC, and also the characteristics of the respective hydrates (predominantly C-S-H) formed during hydration differ. These hydrates influence both strength and durability characteristics (Lothenbach et al., 2011). Figure 2-7 shows the CaO-SiO_2-Al_2O_3 ternary diagram of PC and certain SCMs together with the respective (approximate) hydrate phases.

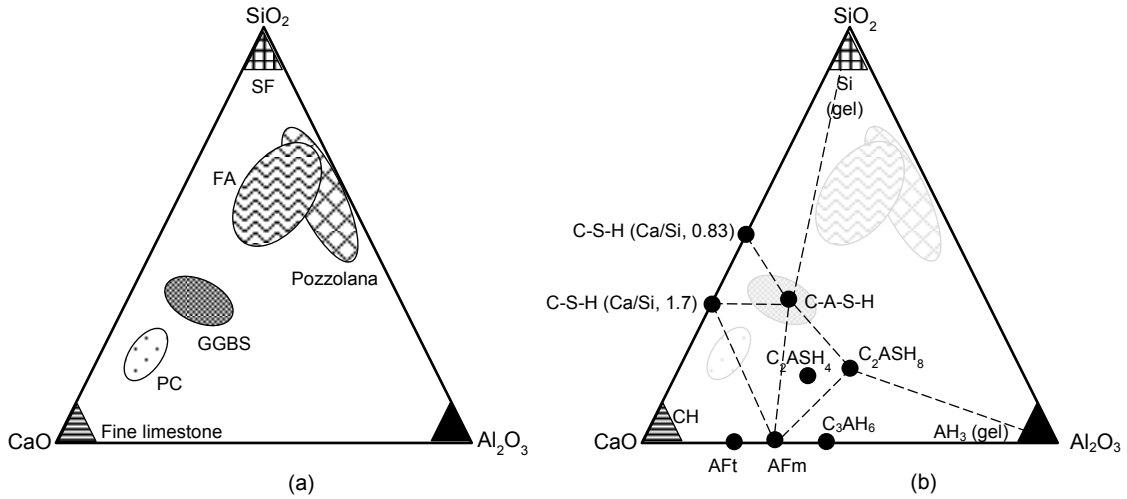

Figure 2-7: (a) CaO-SiO_2-Al_2O_3 diagram of cementitious materials; (b) Approximate hydrate phases in the CaO-SiO_2-Al_2O_3 system (Lothenbach, 2011).

2.8.3.1 PC – GGBS binder system

GGBS is a non-metallic by-product (produced using the granulation technique) from a blast-furnace during the manufacture of iron. It results from the fusion of a limestone flux ($CaCO_3$) with ash from coke (carbon (C)) and the siliceous (S) and aluminous (Al_2O_3) residue after the reduction and separation of the iron from the ore (Lewis et al., 2003). The typical (mean) chemical composition (main oxides) of GGBS is given in Table 2-3.

Table 2-3: Typical (mean) chemical composition (main oxides) of GGBS (Taylor, 1997).

GGBS	Chemical composition (%)							
	C	S	A	F	M	$\bar{S}$	K	N
	42.2	33.5	13.3	1.2	6.0	0.04	0.7	0.4

GGBS possesses latent hydraulicity, and therefore in the presence of water, its chemical reaction rate is slow in comparison to other cementitious materials such as PC. However, in the presence of sulphates and/or alkalis, the reactivity of GGBS is activated, and it begins to react with water thus forming its own hydrates (cementitious gels) (Lewis et al., 2003). PC contains both alkalis ($Ca(OH)_2$, NaOH and KOH) and sulphates. Therefore by blending GGBS with PC, and in the presence of water, their reaction mechanisms involve; (i) the activation of the GGBS by alkalis and sulphates to form its own hydration products (C-S-H and S) (Equation 2.45), and (ii) some of the hydration products from GGBS combine with those of PC (CH) to form further hydrates (Equation 2.46). These parallel yet synergistic reaction mechanisms are complex, but can be expressed simplistically as:

$$3CS + 3H \rightarrow C_3S_2H_3 + S \tag{2.45}$$

$$2S + 3CH \rightarrow C_3S_2H_3 \tag{2.46}$$

Generally, PC – GGBS binder systems (i) contain less free lime (CH), most of which is consumed by the products of hydration of GGBS, and (ii) are less reactive to S-based attack since GGBS does not contain C_3A. The influence of both free lime and C_3A in PC-based binder systems was discussed in Section 2.8.2. Furthermore, the PC – GGBS HCP has (more) smaller gel pores and fewer large capillary pores in comparison to PC's HCP. This finer pore structure gives PC – GGBS binder systems lower permeability than plain PC-binder systems (Siddique and Khan, 2011).

2.8.3.2 PC – FA binder system

FA is a by-product separated (by electrostatic precipitation) from flue gas produced in power stations during the burning of pulverised coal. As the coal burns, the incombustible materials coalesce to form spherical glassy droplets (ash) of silica (S), alumina (A), iron oxide (F), and other minor elements. This ash consists of coarser fractions that collect at the bottom of the furnace, and finer fractions that 'fly out' of the furnace with the flue gas. These finer fractions are known as FA (Taylor, 1997; Mehta and Monteiro, 2013). Generally, FA has significant differences in its mineralogical composition mainly due to the varying calcium content. Therefore FA is divided into two main categories; the first category contains <10% C, whereas the second category contains between 15 and 35% C. The FA used in the current study falls within the first category, and its typical (mean) chemical composition (main oxides) is given in Table 2-4.

Table 2-4: Typical (mean) chemical composition (main oxides) of FA (Taylor, 1997).

FA	Chemical composition (%)							
	C	S	A	F	M	$\bar{S}$	K	N
	2.4	48.7	27.9	9.5	1.6	1.2	4.2	1.5

In the presence of water, the reaction mechanism of the PC – FA binder system differs from that of the PC – GGBS binder system since FA does not undergo a separate reaction process as in the

case of GGBS. In PC – FA systems, a pozzolanic reaction occurs between the silica and the CH from hydration of PC (Equation 2.47).

$$2S + 3CH \rightarrow C_3S_2H_3 \tag{2.47}$$

Generally, the PC – FA binder systems have improved reactivity in comparison to plain PC-systems since the finer FA improves the dispersion of PC particles in the pore solution, making them more available for reactions. This results in better long-term strength and durability (low permeability) characteristics (Keck and Riggs, 1997). However, it is also important to note that the depletion of CH at early-age reactions (Equation 2.47) only affects strength development during this period, but not at a later age since, with time, there is provision of nucleation sites on the surface of the FA particles (Taylor, 1997). Figure 2-8 shows a comparison of available CH vs. time and strength development in plain PC- and in PC – FA binder systems (Lewis et al., 2003).

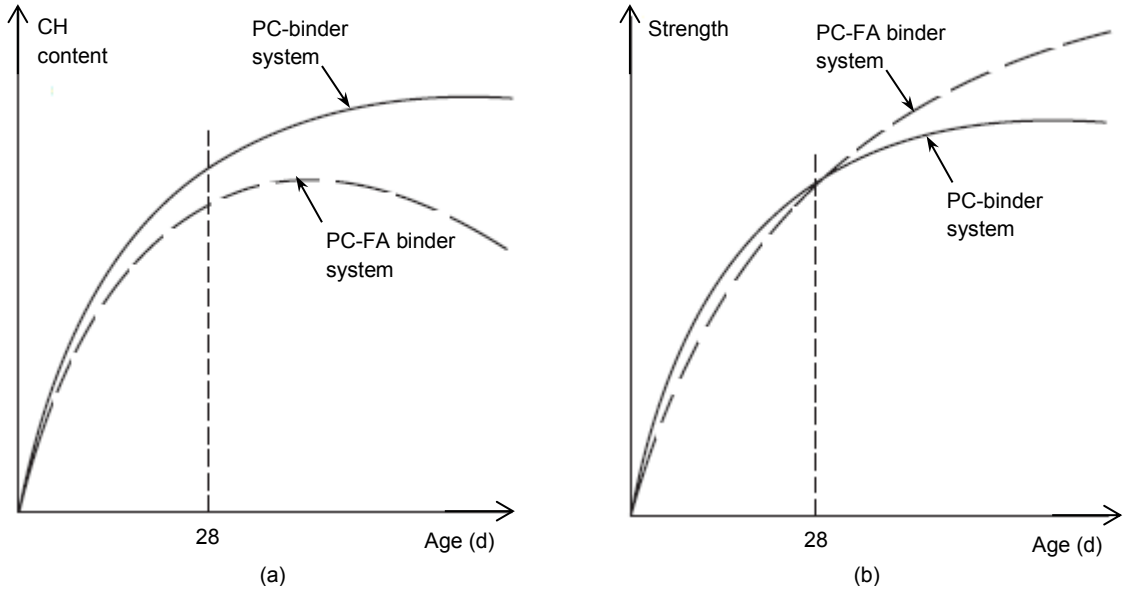

Figure 2-8: (a) Available CH; (b) Strength development in plain PC- and in PC – FA binders systems (Lewis et al., 2003).

The microstructure of PC – FA binder systems is characterised by a finer pore structure (lower permeability) and less CH content than plain PC-binder systems. This characteristic microstructure of PC – FA binder systems gives them better durability performance characteristics (than plain PC-binder systems) in most exposure environments.

2.8.3.3 PC – SF binder system

SF is a by-product of the production of silicon or silicon alloys by reducing quartz in an electric (induction arc) furnace. The reduction of quartz to silicon (at temperatures of up to 2000 °C) produces SiO vapour, which oxidise and condense in a lower temperature zone to fine spherical particles consisting of non-crystalline silica (silica fume) (which may require some beneficiation). The typical (mean) chemical composition (main oxides) of SF is given in Table 2-5.

Table 2-5: Typical (mean) chemical composition (main oxides) of SF (Taylor, 1997).

	Chemical composition (%)							
SF	C	S	A	F	M	$\bar{S}$	K	N
	0.2	96.0	0.3	0.1	0.6	0.2	0.5	0.3

In the presence of water, the reaction mechanism of the PC – SF binder system is similar to that of the PC – FA binder system (Equation 2.47). Moreover, due to its higher specific surface area (more than that of GGBS and FA), SF has been found to be more reactive (Altcin and Regourd,

1985). It is hypothesised that this increased reactivity increases the rate of hydration of the C_3S fraction in PC thereby liberating more CH, but also results in consumption of more CH during the hydration process (Lewis et al., 2003).

According to Taylor (1997), the microstructure of PC – SF binder systems is characterised by (i) a dense paste due to the fine SF particles occupying the spaces between the clinker grains, and (ii) a denser interfacial transition zone (ITZ) at the paste-aggregate interface. Thus PC – SF binder systems have increased strength and lower permeability than plain PC-systems.

From the review presented above, it is shown that generally, the use of SCMs in PC-based binder systems has long-term positive effects as characterised by binder matrices with (i) densified and finer pore structures within the HCP and the ITZ resulting in lower permeability, and (ii) increased strength development. However, it has also been highlighted that during the hydration process of blended PC-based binder systems, the SCMs lead to an increased consumption of CH, which provides the alkalinity of concrete mixtures. This means that, consequently, the use of SCMs reduces the neutralising effect of an attacking acid by a PC-based binder system.

2.8.4 Phenomenon of the neutralisation capacity (or alkalinity) of PC

When a PC-based binder system is exposed to an acid such as biogenic H_2SO_4, two phenomena occur; (i) the materials in the binder system are altered by the attacking acid, and (ii) the attacking acid is also consumed by the materials under attack (Equation 2.48). In such an aggressive environment, the consumption of acid is the primary indicator of corrosion and this allows for quantification of the phenomena independent of other secondary processes that may be involved in such mechanisms.

$$nH^{+} + material \rightarrow Ca^{++} + altered\ material \tag{2.48}$$

Therefore the consumption of a certain quantity of available acid corresponds to the 'destruction' of a certain amount of material. Depending on the material, the greater the quantity of acid necessary to destroy a given quantity of material, the longer the material is capable of tolerating an aggressive (acid) environment (Espinosa et al., 1996). Hence, neutralisation capacity (NC) can be defined as the quantity of acid H atoms (in milliMoles (mM)) necessary to neutralise a given quantity of material (in grams (g)), as expressed in Equation 2.49.

$$\text{NC (mM/g)} = \text{No of acid H atoms (mM)} / \Delta \text{ mass of material (g)} \tag{2.49}$$

The potential neutralisation capacity of PC can be calculated if its chemical composition is known, and bearing in mind that S is acid-insoluble. For example – with reference to Table 2-2, consider 1 g of unhydrated PC with 67% (or 0.67 g) C (molar mass of C is 56 g) and 3% (or 0.03 g) A (molar mass of A is 102 g). The elementary equations giving the number of H^+ ions per mole of oxide show that 2H are required to neutralise C (Equation 2.50), and 6H are required for A (Equation 2.51).

$$C + 2H^{+} \rightarrow Ca^{2+} \tag{2.50}$$

$$A + 6H^{+} \rightarrow 2Al^{3+} \tag{2.51}$$

Using the stoichiometric (equivalence) point, the neutralisation capacity of C is calculated as 24 mMol and that of A as 1.7 mMol, giving the total neutralisation capacity of the PC considered in this example as approximately 26 mM/g. This example illustrates that if the chemical compositions of the various acid-soluble components of a concrete mixture are known, then the neutralisation capacity of the mixture can be calculated using stoichiometric points.

However, the conventional neutralisation capacity of PC-based binder systems is related to their alkalinity or the equivalent total $CaCO_3$ in a mixture (g $CaCO_3$/g concrete) (EPA, 1985). Therefore, the alkalinity can be calculated from experimentally determined CaO contents of the concrete mixture or from the CaO contents of individual constituents of concrete such as cement and aggregates as shown in Equation 2.52.

$$Alkalinity = \frac{\left((c \times CaO_{cement}) + (a \times CaO_{aggr})\right)}{d} \times \frac{100}{56} \quad (2.52)$$

where c = cement content (kg cement/m^3 concrete)
CaO_{cement} = CaO content of the cement (kg CaO/kg cement)
a = aggregate content (kg/m^3 concrete)
CaO_{aggr} = CaO content of the aggregates (kg CaO/kg aggregates)
d = density of concrete (kg/m^3)
The factor 100/56 is the ratio between the molar masses of $CaCO_3$ and CaO

A critique of this approach will follow after similar discussions based on another binder type – CAC, in the following section.

2.8.5 Background and composition of calcium aluminate cement (CAC)

CAC is made by heating limestone ($CaCO_3$) and bauxite (or other aluminous materials low in SiO_2) at between 1450 °C and 1600 °C in a reverberatory open hearth furnace to form molten clinker. Bauxite is an aluminium ore that consists mainly of aluminium hydroxide ($Al(OH)_3$), aluminium oxide hydroxide (γ- and α-AlO(OH)), iron oxide hydroxide (FeO(OH)), and iron (III) oxide (Fe_2O_3). The molten clinker is tapped off continuously from the furnace, solidifies and then crushed and ground to make cement. Generally, CAC has significant differences in its mineralogical composition mainly due to the varying iron content. Therefore CAC is divided into two main categories; the dark iron-rich (up to 20% Fe_2O_3), and the white low-iron (< 2% Fe_2O_3) CAC (Taylor, 1997). The widely used CAC in concrete mixtures is the dark iron-rich type, commonly known as *Ciment Fondu (CF)*, and it is the one utilised in the current study; herein simply referred to as CAC.

Unlike in PC where $C\bar{S}$ is added to regulate the setting time, no additional mineral is added to the raw materials during the manufacture (at grinding stage) of CAC. The typical chemical composition (main oxides) of CAC is given in Table 2-6.

Table 2-6: Typical chemical composition (main oxides) of CAC (Taylor, 1997).

CAC (CF)	Chemical composition (%)								
	C	S	A	F	f	T	$\bar{S}$	M	K + N
	37 – 39	3 – 5	38 – 40	15 – 18	3 – 6	2 – 4	< 0.2	< 1.5	< 0.4

According to Pöllmann (2001), the chemistry of CAC is complicated. It can be considered in the system $CaO–Al_2O_3–Fe_2O_3–SiO_2$, although MgO and TiO_2 may be present in various percentages. The possible equilibrium assemblages of four solid phases are $CA–C_2S–C_2AS$–ferrite and $CA–C_2S–C_{12}A_7$–ferrite, where CA, C_2AS and ferrite represent solid solutions (Taylor, 1997). The main reactive phases in CAC at an early age are CA and $C_{12}A_7$, and they are greatly influence by temperature (Gosselin, 2009).

2.8.6 Mechanism of hydration of CAC

According to Scrivener (2003), when CA comes into contact with water, calcium ions (Ca^{2+}) and aluminate ions ($Al(OH)_4^-$) dissolve in the water to give a solution. These ions can combine as several different types of calcium aluminate hydrates generally known by their chemical formulas as CAH_{10} (monocalcium aluminate hydrate), C_2AH_8 (dicalcium aluminate hydrate), and C_3AH_6 (tricalcium aluminate hexahydrate) (and AH_3 (aluminium hydroxide)) (Equations 2.53, 2.54, 2.55 respectively).

$$CA + 10H \rightarrow CAH_{10} \quad (2.53)$$

$$2CA + 16H \rightarrow C_2AH_8 + AH_3 \quad (2.54)$$

$$3CA + 12H \rightarrow C_3AH_6 + 2AH_3 \quad (2.55)$$

From notions of thermodynamics, when different phases are mixed together, they tend to react and recombine to give a new mixture of phases that has the lowest energy. “This is the stable phase assemblage. However, sometimes it is difficult for the stable phases to form immediately due to the rearrangement of ions that needs to occur, a process called nucleation. In this case, it often happens that different phases form temporarily, which are metastable. They have a lower energy than the starting phase assemblage, which provides a driving force for their formation, but they have a higher energy than the stable phase assemblage. Thus a driving force remains for the metastable phases to in turn react to give the stable phase assemblage” (Figure 2-9) (Scrivener, 2003).

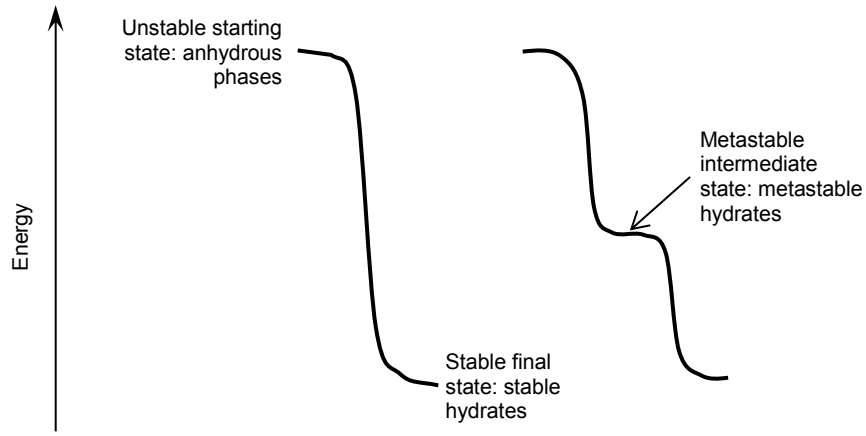

Figure 2-9: A schematic definition of metastable and stable hydrates (Scrivener, 2003).

The formation of these hydrates is dependent on temperature (Figure 2-10) and time (Taylor, 1997).

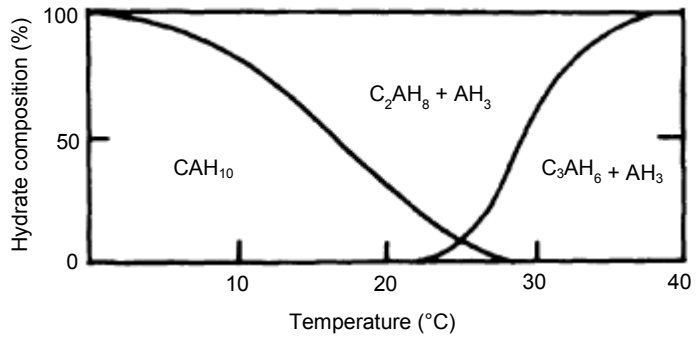

Figure 2-10: Major hydration products of CAC at various temperatures (Taylor, 1997).

At temperatures of up to about 65 °C, the nucleation of C_3AH_6 is very slow. The first hydrate to form at temperatures of up to about 27 °C is usually CAH_{10}, and predominates at temperatures of about 15 °C. C_2AH_8 and AH_3 start to form at temperatures of about 5 °C to 38 °C, and predominate at temperatures of about 25 °C. C_3AH_6 (and AH_3) start to form at temperatures of about 23 °C, and predominates at temperatures > 40 °C. This progressive replacement of the metastable hydrates (CAH_{10} and C_2AH_8) by the stable hydrates (C_3AH_6 and AH_3) due to increase in temperature (and/or

with time) is known as *conversion*. These subsequent conversion reactions are given in Equations 2.56 and 2.57.

$$2CAH_{10} \rightarrow C_2AH_8 + AH_3 + 9H \quad (2.56)$$

$$3C_2AH_8 \rightarrow 2C_3AH_6 + AH_3 + 9H \quad (2.57)$$

All these reactions take place mostly through solution, that is, the reacting phases dissolve and the resultant phases are precipitated from solution. Once the stable phases are present, they will continue to form even if there is a fall in temperature (Scrivener, 2003).

2.8.6.1 Impact of conversion

According to Scrivener (2003) and Gosselin (2009), the impact of conversion is greatest at w/b ratios greater than 0.7. In this case, if the temperature is kept below 20 °C, there is sufficient water and space available for nearly all the reactive anhydrous phases to react to give the metastable hydrates (CAH_{10} and C_2AH_8), and since they have a low solid density, they fill most of the space originally occupied by water resulting in a HCP with low porosity. When conversion occurs and dense stable hydrates (C_3AH_6 and AH_3) form, there is a considerable decrease in the solid volume resulting in a HCP with higher porosity and lower strength.

On the other hand, when the w/b ratio is kept below 0.4, there is insufficient water and space available for all the cement to react to form the metastable hydrates. In this case, the water released during conversion process is available to react with more of the unreacted cement to form more metastable hydrates. Therefore the net reduction in solid volume and subsequent increase in porosity is lessened. Therefore, a denser, lower-porosity microstructure is obtained (after conversion) at low w/b ratios.

2.8.6.2 Basic structure of the CAC hydrates

Most of the known CAC hydrates are also found in other binder systems, except for the CAH_{10} which is unique to the hydration of CAC. The structure of CAH_{10} consists of hexagonal prismatic crystals, whose stability is very sensitive to RH since much of the water in these crystals is loosely bound (Taylor, 1997). The loss of this loosely-bound water may begin at a RH of about 80% and also upon heating (increased temperature), and it results in the deterioration of crystallinity, subsequently converting to lower hydrates (with lower water content) such as C_2AH_8. CAH_{10} is thermodynamically unstable with respect to C_3AH_6 (Odler, 2005).

The structure of C_2AH_8 is of two forms; α-C_2AH_8 and β-C_2AH_8 depending on the water content. The structure is hexagonal and belongs to the AFm phases. Similar to CAH_{10}, C_2AH_8 is highly sensitive to RH and it easily converts into a lower hydrate $C_2AH_{7.5}$ at a RH of about 46% and a temperature of about 26 °C (Scheller et al., 1976). C_2AH_8 is also thermodynamically unstable with respect to C_3AH_6.

C_3AH_6 is the only phase in the C–A–H system that is thermodynamically stable at ordinary temperature (about 25 °C). All the other CAC hydrates eventually convert to C_3AH_6. C_3AH_6 belongs to a group of hydrogarnet phases and it is characterised by a cubic structure in which A and C are octahedrally and distorted-cubic coordinated, respectively (Odler, 2005; Gosselin, 2009).

In addition to the hydrates described above, AH_3, which is an amorphous aluminate hydrate (also known as alumina gel), also forms during hydration. According to Gosselin (2009), the study of this hydrate remains difficult due to its instability under drying conditions. Renaudin (1998) reported that AH_3 has three crystalline polymorphs – nordstrandite, bayerite and gibbsite. Gibbsite, which is widely reported in literature about the hydration processes of CAC has a monoclinic structure.

2.8.7 Blended CAC-based binder systems

The characteristics and influence of certain SCMs when used in PC-based binder systems were discussed in Section 2.8.3. Broadly, similar principles relating to (i) the reduction in permeability of the HCP, and (ii) improved strength characteristics in comparison to plain CAC-based binder systems apply, although the nature of the resultant hydrates differ from those of blended PC-based binder systems as discussed in the following sections.

2.8.7.1 CAC – GGBS binder system

Several researchers have studied various properties of CAC – GGBS binder systems and reported that (i) during the hydration process at temperatures of up to 40 °C, the predominant hydrate is C_2ASH_8 (stratlingite), (ii) C_3SH_6 also started forming at temperatures above 40 °C, and was predominant at temperatures greater than 45 °C (Edmonds and Majumdar, 1989; Fentiman et al., 1990; Singh and Majumdar, 1992; Osborne, 1994; Quillin et al., 2001; Dunster et al., 2008). The formation of C_2ASH_8 is due to reactions with the soluble silica in GGBS, as simplistically expressed in Equation 2.58.

$$C_2AH_8 + S \rightarrow C_2ASH_8 \tag{2.58}$$

It is hypothesised that the formation of C_2ASH_8 reduces the extent of conversion and formation of C_3AH_6 since it is stable relative to C_3AH_6 at ambient temperatures (Gosselin, 2009). However, it does not eliminate the formation of C_3AH_6 at temperatures > 40 °C or with time (Majumdar and Singh, 1992). According to Midgley and Rao (1978), the effect of the formation of C_2ASH_8 is particularly significant during the conversion process. For instance, during the conversion of C_2AH_8 to C_3AH_6 (Equation 2.57), there is a decrease in the solid volume of up to 34%. On the other hand, the reaction between soluble silica and C_2AH_8 to form C_2ASH_8 (Equation 2.58) leads to an increase in the solid volume up to 1.4%. Subsequently, the net reduction in the solid volume is decreased (therefore reduced porosity and loss of strength) in instances where C_2AH_8 is still available for conversion in CAC – GGBS binder systems. It has also been reported that C_2ASH_8 has relatively high strength in comparison to C_3AH_6 (Ding et al., 1995).

C_2ASH_8 is an AFm phase whose structure is closely related to that of C_2AH_8, although it is characteristically defined by double tetrahedral sheets of aluminosilicate (Rinaldi et al., 1990).

2.8.7.2 CAC – FA binder system

The influence of FA in CAC – FA binder systems is similar to that of GGBS, which results in the formation of C_2ASH_8 due to the reactive silica (Equation 2.58). Although studies have shown that in order for FA to have an impact in reduction of the transformation mechanisms of the metastable hydrates into the stable hydrates at temperatures of between 20 °C and 60 °C, a minimum quantity of 40% by weight (of total binder) is required (in the CAC – FA binder system) (Collepardi, 1995; Fernández-Carrasco and Vázquez, 2009). This implies that at lower replacement levels of CAC by FA in blended binder systems, there is less C_2ASH_8 in comparison to that formed in CAC – GGBS binder systems.

2.8.7.3 CAC – SF binder system

Even though SF contains higher amounts of silica than that found in both GGBS and FA, studies by Rivas-Mercury et al. (2006; 2007; 2008) revealed a different reaction mechanism in CAC – SF binder systems. Binder systems with a composition of 60% CAC and 40% SF showed that up to 87% of the SF was still unreacted and available in the matrix after 1 year hydration at 50 °C. It was also observed that the silica particles were surrounded by AH_3 which reduced their dissolution. Moreover, C_2ASH_8 was only observed in this AH_3 phase that was surrounding clusters of SF, but with siliceous C_3AH_6 being predominant elsewhere in the binder matrix.

2.8.8 Phenomenon of the neutralisation capacity of CAC

A background to the phenomenon of the neutralisation capacity of unhydrated cement and that of a PC-based concrete mixture were presented in Section 2.8.4. In this section, the same concept will be applied to calculate the neutralisation capacity of 1 g of unhydrated CAC with 38% (or 0.38 g) C (molar mass of C is 56 g) and 40% (or 0.4 g) A (molar mass of A is 102 g) – with reference to Table 2-6, and Equations 2.50 and 2.51.

Using the stoichiometric (equivalence) point, the neutralisation capacity of C is calculated as14 mMol and that of A as 24 mMol, giving the total neutralisation capacity of the CAC considered in this example as approximately 38 mM/g.

These stoichiometric (equivalence) point computations show that CAC has a higher neutralisation capacity of an attacking acid than PC. However, unlike in the case of PC where the major contributor towards the neutralisation capacity is C, for CAC the major contributor is A. Therefore, the expression for conventional *alkalinity* as given in Equation 2.52 does not apply in CAC-based binder systems. More discussions on these phenomena are presented in Sections 2.9 and 2.10.

2.8.9 Fe_2O_3 in the hydrated cement paste of both PC- and CAC-based systems

Several researchers have reported that during the hydration process of both PC and CAC, iron (III) oxide-hydroxide (FeO(OH)) is also formed due to a higher ratio of Al/Fe in the hydrated phases than in the unhydrated material. These ratios were studied using various techniques such as XRD, TGA, and SEM (Chatterji and Jeffery, 1962; Ball et al., 1987; Taylor, 1997). However, there is limited experimental evidence to show that an iron hydroxide gel is formed in cement pastes, and Harchand et al (1980) concluded that the 'absence' of this gel was due to Fe^{3+} entering an AFm phase that was so poorly crystalline that it cannot be detected. Scrivener (1989), using backscattered electron imaging, also reported that Fe^{3+} does not migrate through the pore solution on hydration, but remains in the products formed in-situ. Therefore the potential significance of FeO(OH) during biogenic acid attack mechanisms is presented in Chapter Six.

2.8.10 Discussion – binder types used in concrete sewer pipes

All the binders discussed in this Section 2.8 (PC, CAC, GGBS, FA, and SF) have a similar chemical description of oxides, although these oxides vary quantitatively. It is this chemical composition that gives each binder their characteristic properties, both in an unhydrated and in a hydrated state. The hydration mechanism of a PC-based binder system involves both the silicate and aluminate phases, which play a synergistic role in ensuring durability under most exposure conditions. However, in aggressive environments such as those involving acid attack, the plain PC hydrates require refinement of their microstructure by inclusion of certain SCMs which help in (i) improving (lowering) the permeability characteristics of the resultant binder matrices, and (ii) lowering the quantity of the highly acid-soluble sites such as CH. The same applies to CAC-based binder systems, although an additional significant contribution of the SCMs in CAC binder systems is the suppression of the conversion process.

When used in the manufacture of sewer pipes, these binder systems are subjected to biogenic corrosion. Therefore they are required to have sufficient neutralisation capacities in order to last their design or service life. It has been demonstrated in this section that PC- and CAC-based binder systems have different mechanisms of providing the neutralisation capacity against acid attack; PC significantly utilises the C (or CH) component while CAC mostly utilises the A component. Therefore, describing the neutralisation capacity of both PC- and CAC-based binder systems using a quantitative expression relating to *equivalent* $CaCO_3$ is not a reliable hypothesis. The current study addresses this phenomenon in Chapters Five and Six.

2.9 Challenges associated with measuring the neutralisation capacity of PC- and CAC-based binder systems

Apart from the stoichiometric (equivalence) point computational approach of determining the neutralisation capacity of concrete mixtures presented in Section 2.8, various design manuals and standards outline procedures using chemical analysis (ACPA, 1988; CSIR, 1996). This analysis will be simplistically highlighted in this section. A concrete sample to be analysed is first ground to a fine powder. HCl (molarity = 12.1 moles/l) is then added to this powder (to complete submersion) resulting in some effervescence. Once the effervescence subsides, the mixture is heated to boiling point and allowed to boil for 30 seconds and thereafter allowed to cool. The excess HCl is then titrated with a normal sodium hydroxide (NaOH) solution – a neutralisation reaction, and the result is presented in the form of the quantity of NaOH required to neutralise the excess HCl. Moreover, in order to express the results of the neutralisation capacity of different cement-based materials in a comparative (more practical) form, the neutralisation capacities of various materials are compared to that of pure limestone ($CaCO_3$) (which contains 90% – 95% C), and presented as a ratio. This ratio is known as the *alkalinity* of a given material.

Nonetheless, this method is useful for materials with a high C content and relatively low A content such as PC-based binder systems (Espinosa et al., 1996). In the case of CAC, whose A content is in the order of 40% or more, the results are biased since the titration of the excess acid with NaOH turns the Al^{3+} (which are dissolved from the $AlCl_{3\,(aq)}$ by the excess HCl – see Equation 2.59(b)) to $Al(OH)_3$ (AH_3), and the Cl^- to NaCl (Equation 2.59(c)).

$$Al_2O_{3(s)} + 6HCl_{(aq)} \rightarrow 2AlCl_{3(aq)} + 3H_2O \qquad (2.59(a))$$

$$2AlCl_{3(aq)} + HCl_{(aq)} \rightarrow 2Al^{3+} + 3Cl^- \qquad (2.59(b))$$

$$Al + 3Cl + 3NaOH \rightarrow Al(OH)_3 + 3NaCl \qquad (2.59(c))$$

The acid that is consumed during the dissolution of $AlCl_{3\,(s)}$ does not reflect in the final result (Equations 2.59(b) and (c)). This renders the use of *alkalinity* as a measure of the neutralisation capacity of other cement-based materials other than PC unreliable, and its application in certain biogenic corrosion models needs to be reviewed. More highlights are presented in Part Three of this literature review (Section 2.14), and in Chapter Three. Work on other proposed biogenic corrosion rate-controlling parameters is presented in Chapter Six.

2.10 Characteristics of PC-based and CAC-based binder systems subjected to biogenic H_2SO_4 attack

Concrete is a multiphase, porous, and strongly basic material whose pore solution has a pH of around 12 to 13. Because of its mineralogical and chemical nature, concrete is naturally in dis-equilibrium with its environment. The characteristics of the pore network, size and connectivity of the capillary porosity in particular, determine the transfer of aggressive species inside a matrix. The chemical nature of the matrix is also a key parameter of the resistance of concrete to aggressive aqueous environments (Alexander et al., 2013).

As discussed in Section 2.8, the major hydrates in PC-based binder systems are CH and C-S-H. When these hydrates are subjected to biogenic H_2SO_4, they are transformed in two principle phases:

(i) Simultaneous destruction of the polymeric nature of calcium hydroxide (CH) and the amorphous C-S-H, and substituting a larger molecule (calcium sulphate ($C\bar{S}$)) (Equation 2.60) into the matrix thus causing pressure and spalling of the adjacent concrete and aggregate particles.

$$CH + H_2SO_4 \rightarrow C\bar{S} + 2H \quad (2.60(a))$$

$$C - S - H + H_2SO_4 \rightarrow C\bar{S} + S + 2H \quad (2.60(b))$$

(ii) $C\bar{S}$ precipitates as gypsum ($C\bar{S}H_2$) and reacts with the hydrated calcium aluminates (CAH), hydrated calcium sulfoaluminates ($C_4A\bar{S}H_{12}$) or unhydrated tricalcium aluminates (C_3A) to form secondary ettringite ($C_6A\bar{S}_3H_{32}$ - AFt) according to the following equations (Equation 2.61).

$$C_3\overline{S_3}H_6 + C_3AH_{12} + H_{14} \rightarrow C_6A\overline{S_3}H_{32} \quad (2.61(a))$$

$$C_2\overline{S_2}H_4 + C_4A\bar{S}H_{12} + H_{16} \rightarrow C_6A\overline{S_3}H_{32} \quad (2.61(b))$$

$$C_3\overline{S_3}H_6 + C_3A + H_{26} \rightarrow C_6A\overline{S_3}H_{32} \quad (2.61(c))$$

Therefore, on one hand, gypsum leads to the deterioration of the hardened PC paste through a process that first leads to the loss of stiffness and strength, followed by expansion and cracking, and eventually transformation of the affected concrete matrix into a soft and pulpy non-cohesive layer (Sahmaran, 2010). On the other hand, deterioration of concrete by formation of secondary ettringite is supported by several hypotheses; exertion of pressure within the concrete matrix by growing ettringite crystals, and swelling due to absorption of water in alkaline environment by poorly crystalline ettringite are two major schools of thought supported in literature (Mehta and Monteiro, 2013). Ettringite-based form of deterioration also leads to the formation of a non-cohesive layer. Nonetheless, both processes leading to the deterioration of concrete are complimentary, and are seldom discussed in isolation.

The soft and pulpy non-cohesive layer formed on PC-based concrete sewer pipes due to biogenic H_2SO_4 attack is acidic (pH < 2), and it influences (lowers) the pH of the adjacent concrete surface that has not been subjected to this acid (Alexander and Fourie, 2011). This layer also creates excellent conditions (high humidity and low pH) for the growth of SOB. Due to the increased porosity of this non-cohesive layer, the SOB can penetrate deeper towards the low-pH concrete surface where they continue to generate H_2SO_4 that attacks the acid-soluble portions of the concrete matrix.

On the other hand, the major hydrates in CAC-based binder systems are the hydrogarnet (CAH_{10}, C_2AH_8, and C_3AH_6) and gibbsite (alumina gel) (AH_3). When these hydrates are subjected to biogenic H_2SO_4, they are transformed in three principle phases:

(i) The dissolution of the calcium component of the hydrogarnet leads to the creation of additional quantities of AH_3 (Equations 2.62 – 2.64).

$$CAH_{10} + H_2SO_4 \rightarrow C\bar{S} + AH_3 + 9H \quad (2.62)$$

$$C_2AH_8 + 2H_2SO_4 \rightarrow 2C\bar{S} + AH_3 + 9H \quad (2.63)$$

$$C_3AH_6 + 3H_2SO_4 \rightarrow 3C\bar{S} + AH_3 + 9H \quad (2.64)$$

(ii) The initially formed AH_3 together with the additional quantities released from the dissolution of the hydrogarnet reacts with H_2SO_4 to form aluminium sulphate ($Al_2(SO_4)_3$) (Equation 2.65).

$$2AH_3 + 3H_2SO_4 \rightarrow Al_2(SO_4)_3 + 12H \quad (2.65)$$

(iii) $C\bar{S}$ precipitates as gypsum ($C\bar{S}H_2$) and reacts (through-solution) with the stable aluminates to form secondary ettringite ($C_6A\bar{S}_3H_{32}$ - AFt) according to the following equations (Equation 2.66).

$$C_3\overline{S_3}H_6 + C_3AH_6 + H_{20} \rightarrow C_6A\overline{S_3}H_{32} \quad (2.66)$$

Unlike in PC-based binder systems where the hydrates (CH and C-S-H) that provide the neutralisation of the attacking acid are completely broken down during initial reactions, CAC hydrates provide a longer chain of dissolution and neutralisation by various hydrates (Equations 2.62 – 2.65). Moreover, AH_3 is a stable compound at pH of between 3 and 4, and it presents greater neutralisation of the attacking acid at such pH levels.

In aqueous solution $Al_2(SO_4)_3$ (Equation 2.65) forms a number of hydrolysis species such as $Al(OH)^{2+}$, $Al(OH)_2^+$, $Al(OH)_3$, and $Al(OH)_4^-$, depending on pH. Therefore during the generation of biogenic H_2SO_4 and attack mechanisms of CAC-based binder systems presented above, the free Al^{3+} (mostly formed through hydrolysis) bind to the DNA of acidophilic bacteria and halts the replication of cells, thus providing a bacteriostatic effect in the microbial ecosystem on corroding CAC-based sewer pipes (Johnson and Wood, 1990).

It is hypothesised that the secondary ettringite that forms by the reaction of C_3AH_6 with gypsum does not portray highly detrimental characteristics found in PC-based binder systems because it forms through-solution reactions, and not through topochemical reactions like in the case of PC (Odler, 2005).

The current study aims at revealing and quantifying the attack mechanisms discussed above through microstructural characterisation of certain PC- and CAC-based binder systems that have been subjected to biogenic H_2SO_4 in a 'live' sewer for more than 10 years. These are presented in Chapter Four.

2.11 Certain characteristics of aggregates used in concrete mixtures for sewer pipes

Generally, fine and coarse aggregates occupy between 60% and 75% of the volume of concrete and therefore, they significantly influence the properties of both freshly mixed and hardened concrete (Kosmatka et al., 2003; Alexander and Mindess, 2005; Neville, 2011). According to Mehta and Monteiro (2013), the characteristics of aggregates used in concrete are derived from three main conditions; (i) the mineralogical composition of the parent rock, (ii) the exposure conditions of the parent rock (prior to processing for aggregates), and (iii) the production processes of the aggregates. The significance of these conditions on the characteristics of aggregates is briefly highlighted in the following sections.

2.11.1 Mineralogical composition of the parent rock

Rocks are geologically categorised into three groups according to their origin; (i) igneous rocks, which are formed on cooling of magma above, below or near the earth's surface, (ii) sedimentary rocks, which are stratified rocks mostly formed under water bodies, but can also accumulate through wind and glacial action, and (iii) metamorphic rocks, which are either igneous or sedimentary rocks that have changed their original crystal structure or mineralogical composition in response to physical and chemical conditions below the earth's surface (Carlson and Plummer, 2010).

Moreover, each of the three geological groups of rocks can further be chemically classified into three types; (i) siliceous rocks, whose principal constituent is silica, (ii) calcareous rocks, whose principal constituent is calcium and magnesium carbonate, and (iii) argillaceous rocks, whose principal constituent is argil (clay). Both siliceous and calcareous rocks are sources of aggregates used in the manufacture of concrete sewer pipes based on certain properties such as crushing

strength, water absorption, specific gravity, resistance to weathering and acid attack (Punmia et al., 2004).

2.11.2 Exposure conditions of the parent rock

Due to the rock fracture mechanics associated with weathering, the characteristics of aggregates that are dependent on the exposure conditions of the parent rock include particle size (grading), shape and texture. These characteristics affect the aggregate proportions in a concrete mixture as well as the binder and water requirements; these in turn affect the workability of fresh mixtures and strength of hardened concrete. Therefore, various Standards and design processes specify certain limits such as maximum aggregate size (MAS) and flakiness indices for various applications. Apart from workability and strength issues, the cross-sectional dimensions of respective concrete elements can dictate, for example, the MAS used. For concrete sewer pipes, which have typical wall thicknesses in the order of 75 mm, the MAS mostly used is approximately 13 mm (Goyns, 2003).

2.11.3 Production processes of aggregates

The processes through which both fine and coarse aggregates are produced can be broadly categorised into two; natural and manufactured (through crushing). Generally, deposits of coarse-grained soil are a good source of natural sand and gravel, which are characterised by rounded shapes and smooth surfaces due to transformations (attrition) that occur during transportation. The advantages associated with naturally occurring aggregates include improved workability of fresh concrete. However, aggregates sourced from natural sources often contain deleterious substances and further processing that may include washing or screening is often required in certain instances.

On the other hand, manufactured aggregates are produced under 'controlled' environments and are seldom contaminated. Moreover, due to the crushing technique used during production, manufactured aggregates are characterised by angular shapes and rough surfaces, which increase the water (and binder) demand for workability requirements of fresh concrete. However, it is hypothesised that the shape and texture characteristics of manufactured aggregates can result in improved early strength through the formation of a stronger physical bond between the aggregate and binder paste (Mehta and Monteiro, 2013).

The use of aggregates of certain mineralogical composition, exposure conditions of the parent rock, or production processes is not undertaken in isolation since respective aggregates are characterised by properties that are synergistic when used in combination. Generally, the manufacturing processes of concrete sewer pipes take advantage of this synergy, particularly in South Africa.

2.12 Summary – characteristics of the concrete sewer pipe materials

This part presented a review of various characteristics of concrete sewer pipe materials, where it was demonstrated that:

(1) Even though various binders (PC, CAC, GGBS, FA, and SF) have a similar chemical description of oxides, these oxides vary quantitatively and consequently influence differently the characteristics of their respective hydrates.
(2) Under biogenic H_2SO_4 attack, PC- and CAC-based binder systems rely on different hydrate phases for neutralisation of the attacking acid. PC-based binder systems (with or without SCMs) rely on CH and C-S-H, or the equivalent $CaCO_3$ content (conventional alkalinity) in a concrete mixture, while CAC-based binder systems (with or without SCMs) rely on the content of the stable hydrates, C_3AH_6 and C_2ASH_8, and the amorphous AH_3 in a concrete mixture.
(3) Under biogenic H_2SO_4 attack, both PC- and CAC-based binder systems are transformed into calcium sulphate ($C\bar{S}$), which precipitates as gypsum ($C\bar{S}H_2$) and reacts with the aluminates to form secondary ettringite ($C_6A\bar{S}_3H_{32}$ - AFt). However, it is hypothesised that the formation of the AFt in these binder systems follow different reaction mechanisms; for PC-based systems, it

mostly occurs topochemically, while for CAC-based systems, it mostly occurs through solution. According to Paulini (1994), topochemical reactions are influenced by factors such as the fineness of the binder, while through solution reactions are controlled by the pore structure of the C-S-H or C-A-H gel. Moreover, it is hypothesised that the pressure of expansive AFt formed in topochemical reactions may cause nucleation and propagation of micro-cracks in the HCP, while that generated in through-solution reactions is insufficient to cause micro-cracks via nucleation and growth (Basista and Weglewski, 2008; Kurdowski, 2014).

(4) The standard chemical analysis method (HCl test) of determining the neutralisation capacity (alkalinity) of PC-based binder systems does not apply to CAC-based binder systems due to its inability to account for the total acid consumed in the final result.

(5) The characterisation of aggregates based on mineralogical (chemical) properties, particularly with regard to their performance in aggressive aqueous (acidic) environments may play a significant role during durability design of concrete mixtures for sewer pipe applications.

The (durability) design of concrete mixtures for applications in outfall sewer networks is a function of the interaction of multi-phase factors that exist in these networks. These interactions are expressed as mathematical equations in the form of biogenic corrosion prediction models. Nonetheless, the choice of which corrosion prediction model to use should clearly define the pros and cons with regard to the prevailing design considerations. The following section, Part Three, critically reviews the widely used deterministic (mechanistic) biogenic corrosion prediction model – the LFM, and also critiques certain components in other biogenic corrosion models that incorporate properties of concrete mixtures as rate-controlling parameters.

2.13 Concrete sewer biogenic corrosion prediction models

2.13.1 Introduction

Biogenic concrete corrosion prediction in sewers is not only controlled by chemical equilibrium characteristics pegged on the features of the different phases (aqueous, gaseous, biological, and mineralogical) in the sewer system but also by the transport mechanisms within these phases (as previously discussed in Section 2.1). Therefore the basic concept of biogenic corrosion prediction models is to relate the different multi-phase factors in the sewer systems, but this relationship is always complex. Hence, biogenic corrosion prediction models can be developed based on one or a combination of the following approaches; (i) description of the microbial and chemical transformation processes of organic matter, oxygen, and oxidised nitrogen and sulphur-based compounds (EPA, 1985; Vollersten and König, 2005; Hvitved-Jacobsen et al., 2013), (ii) description of the mineralogical (chemical) characteristics of concrete materials (EPA, 1985; Hvitved-Jacobsen et al., 2013), (iii) and statistical analysis of experimental data (Beddoe and Dorner, 2005). An outline of biogenic corrosion prediction models, with examples of the most commonly used tools, is given in Figure 2-11 (Kley and Caradot, 2013).

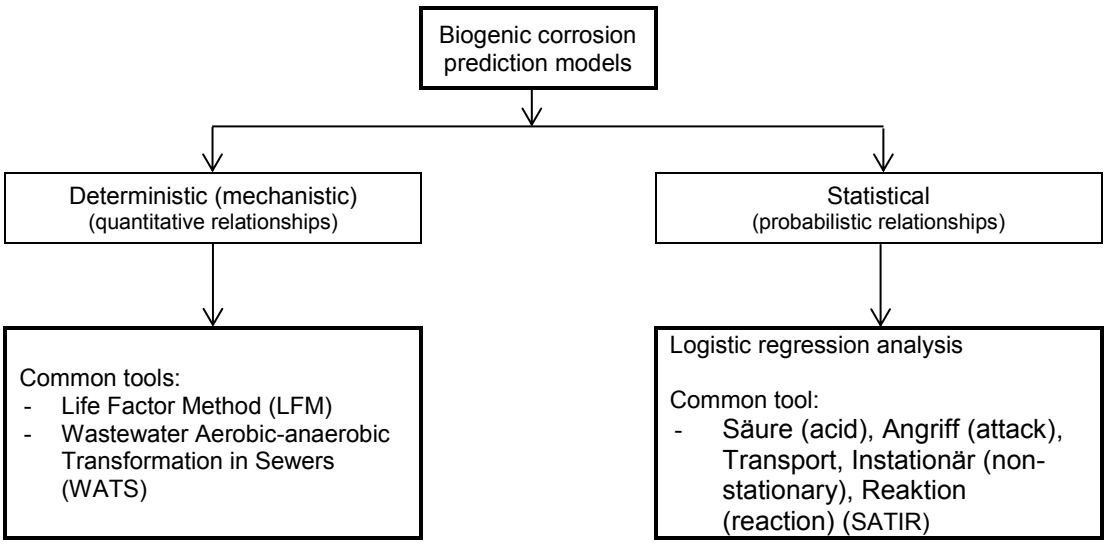

Figure 2-11: Most commonly used models for biogenic corrosion prediction (Kley and Caradot, 2013).

One of the main focuses of the current study is to characterise material (mineralogical) properties of various PC-based and CAC-based binder systems that have been exposed in a 'live' sewer environment. This characterisation includes quantifying certain parameters such as rates of deterioration vis-à-vis binder system transformations. Therefore the practical application of findings such as those from the current study closely relate to theories behind deterministic (mechanistic) models and these will be presented in Chapter Five – particularly using the LFM. Nonetheless, a review of another mechanistic and statistical model will also be undertaken in order to highlight the significance of material properties in biogenic corrosion prediction models.

2.13.2 Deterministic concrete sewer biogenic corrosion prediction models

Deterministic models use mathematical equations to evaluate the quantitative relationship between deterioration (corrosion) factors and sewer conditions. They can be empirical, mechanistic or a combination of both, based on the physical, chemical or engineering science knowledge of the phenomenon of interest (understanding the physical mechanisms of sewer corrosion processes).

Whereas empirical models are based solely on direct observations, measurements and extensive data records, mechanistic models have a similar basis but with an added component of an understanding of the behaviour of various system parameters (Wolfram, 2002). Therefore both the LFM and WATS are mechanistic models as discussed in the following sections.

2.13.2.1 The LFM model (EPA, 1985)

The LFM is one of the most widely used deterministic (mechanistic) model to describe the biogenic corrosion process in sewers (EPA, 1985, 1991, 1992; Vollertsen et al., 2011). This model is based on a series of relationships that considers sulphide generation within the sewage and hydrogen sulphide (H_2S) release from the sewage, and relates these to the concrete corrosion rate via two functions; (i) the rate of H_2S consumption (through auto-oxidation and by SOB) on the moist concrete surface, and (ii) the alkalinity of the concrete materials, expressed as $CaCO_3$ equivalent. Various relationships that define the LFM are discussed in the following sections.

2.13.2.1.1 Sulphide generation within the sewage

The occurrence of sulphide in sewage results principally from biochemical reduction of inorganic sulphur compounds (sulphate to sulphide) in the absence of oxygen and in the presence of organic matter. This reduction involves various bacteria, (i) assimilatory microbes, which assimilate inorganic sulphur and reduce it to sulphide within their protoplasm, (ii) proteolytic bacteria, which hydrolyse proteins and amino acids under anaerobic conditions resulting in the release of sulphides, and (iii) sulphate-reducing bacteria (SRB), which use inorganic sulphate as the hydrogen acceptor in their energy cycle. SRB are the principal mechanism of sulphate reduction in sewage (EPA, 1985).

The presence of both organic substances and sulphate (SO_4^{2-}) is necessary for the biochemical production of sulphide (S^{2-}, H_2S) in the sewage (Equation 2.67), and the majority reduction of SO_4^{2-} takes place in anaerobic zones of biofilms (below the daily sewage flow levels) due to depreciation of DO.

$$SO_{4(aq)}^{2-} + 2C + H_2O \xrightarrow{\text{bacteria}} 2HCO_{(aq)}^{3-} + H_2S_{(aq)} \qquad (2.67)$$

where C = organic matter

The rate at which sulphide is generated within the slime layer depends on the concentration of organic material and nutrients, sulphate concentration, DO in the sewage, pH and temperature of the sewage, flow velocity and surface area of the sewage. Sulphide generation generally occurs at sewage temperatures above 15 °C (EPA 1974). Pomeroy and Parkhurst (1977) assumed that the concentration of nutrients supporting SRB that thrive in the biofilm of the sewage is proportional to the biological oxygen demand (BOD) of most municipal wastewater. BOD is dependent on sewage temperature as discussed earlier in Section 2.3. The quantity of available nutrients that provide energy to the SRB is measured by the 5-day BOD (BOD_5) (McLaren 1984). However, since for design purposes a seasonal effect is required, sulphide generation is determined from the effective BOD (EBOD) as shown in Equation 2.68 (EPA 1985).

$$[EBOD] = [BOD_5] \times 1.07^{(T-20)} \qquad (2.68)$$

where $[EBOD]$ = effective $[BOD_5]$ (mg/l)
$[BOD_5]$ = composite average BOD_5 (mg/l)
T = wastewater (sewage) temperature (°C)

However, for sewers flowing partly full, there is an air-water interface, and the sewage entrains air resulting in stifling some sulphide generation. Also, some of the generated H_2S (in aqueous form) escapes via this interface. This means that sulphide accumulation in the sewage is slower than it would be in an equivalent system with the pipe flowing full. Assuming there is little or no dissolved

oxygen [DO] in the sewage, SRB would reduce the sulphate in the sewage to sulphide, and the total sulphide generation in the sewage can be determined from Equation 2.69.

$$\frac{d[S]}{dt} = M'\left(\frac{EBOD}{R}\right) - \frac{m[S](sV)^{0.375}}{d_m} \tag{2.69}$$

where $d[S]/dt$ = rate of change of total sulphide (mg/l.hr)
[S] = total sulphide concentration (mg/l)
M' = effective sulphide flux coefficient for H_2S generated in the biofilm for a sewer flowing partly full under gravity (m/hr)
$EBOD$ = effective BOD_5 (mg/l)
R = hydraulic radius of flow area (m)
m = sulphide loss coefficient due to oxidation and escape into headspace
s = slope of energy grade line (m/m)
V = mean sewage velocity (m/s)
d_m = mean hydraulic depth (m)

There will be a theoretical upper limit to the sulphide concentration in the sewage when the losses equal the total sulphide concentration, i.e. when $d[S]/dt$ = 0. This will occur as shown in Equation 2.70.

$$[S]_{\text{lim}} = \frac{M'}{m} EBOD(sV)^{-0.375}\left(\frac{P}{W}\right) \tag{2.70}$$

where $[S]_{\text{lim}}$ = upper limit for H_2S generation in an open channel gravity system (mg/l)
P = wetted perimeter (m)
W = flow width (m)

The limiting value of [S], $[S]_{\text{lim}}$, is approached asymptotically in a sewer flowing partly full under gravity and will not be reached under these conditions. However, when a sewer flowing partly full under gravity receives discharge from a closed system, the [S] concentration may exceed the limiting value and H_2S will be stripped rapidly from the sewage to re-establish equilibrium between gas concentrations in the sewer headspace and sewage. The downstream sulphide concentration is calculated from Equation 2.71 (EPA 1985).

$$S_2 = S_{\text{lim}} - \frac{(S_{\text{lim}} - S_1)}{\log_{10}^{-1}\left[\frac{m(sV)^{0.375}\Delta t}{2.31 d_m}\right]} \tag{2.71}$$

where S_2 = predicted downstream sulphide concentration (mg/l)
S_1 = upstream sulphide concentration (mg/l)
Δt = flow time in a given reach of sewer (hr)

Due to biological activities in the sewage, several sulphur compounds are formed but it is the gaseous H_2S that can escape causing odour and corrosion problems. Therefore, for corrosion-related analysis, it is necessary to determine the proportion of [S] formed that is dissolved, and the proportion of this dissolved sulphide [DS] that is H_2S. The proportion of [S] that is [DS] is variable and dependent upon the pH and metal content of the sewage. The proportion of [DS] that is H_2S is directly related to the pH of the sewage (see Figure 2-5) (Bealey et al., 1982; Herisson, 2012).

The rate of sulphide production in the sewage is influenced by several factors such as temperature (it increases with increase in temperature), and the concentrations of both organic nutrients and sulphate. It is worthwhile to note that the rate of sulphide production can be limited by a scarcity of

either sulphate or organic nutrients, and since both are consumed in the biological reactions that produce H_2S (Equation 2.67), they are required in a certain ratio (Boon and Pomeroy, 1990). If there is an excess of organic nutrients, then the rate of sulphide production is limited by the amount of sulphate and if there is an excess of sulphate, it is limited by the amount of organic nutrients.

Equations 2.68 to 2.71 express the rate of sulphide build-up as a function of the various factors that influence generation by the biofilm and the losses by oxidation and escape to the air. As they stand, these equations are limited due to the difficulty in securing relatively accurate input information (Hvitved-Jacobsen et al. 2013). For example, absorption of oxygen at the surface of the sewage stream can be predicted if the relative concentrations of O_2 in the sewer headspace, slope, pipe size and sewage flow quantity are known, but extra oxygen will be added at junctions, drops, and other points of turbulence. It is also difficult to predict the rate at which oxygen will be consumed.

Boon and Pomeroy (1990) stated that the practical approach to the difficulty in H_2S prediction is to consider 'worst-case' scenarios in which unpredictable factors are considered favourable for sulphide build-up. That is, it will be assumed that sufficient sulphate is present so that it is not limiting, that oxygen concentration is low, that no nitrate is present, and that there is no toxic condition or other factor that inhibits the action of the biofilm. These assumptions vary in-situ even within a section of the same sewer, and their applications to different sewer environments could result in unreliable outcomes. However, under typical sewer conditions, indicative dissolved sulphide concentrations can be determined from these equations for use in estimating H_2S flux from the sewage surface.

2.13.2.1.2 Hydrogen sulphide release from the sewage

When there is no equilibrium between the concentrations of gaseous H_2S in the sewage and the sewer headspace, interface movement of this gas occurs. Since H_2S concentration is invariably lower in the sewer headspace than in the sewage, its release is usually from the sewage to the sewer headspace.

Under typical sewer conditions, once [DS] in the sewage has been determined using Equations 2.68 to 2.71, the rate of H_2S release can be calculated from Equation 2.72.

$$\varphi_{sf} = 0.69(sV)^{0.375} J[DS] \tag{2.72}$$

where φ_{sf} = H_2S flux from the sewage surface (g/m^2/h)
s = hydraulic gradient (m/m)
V = mean flow velocity (m/s)
J = proportion of dissolved sulphides in sewage present as H_2S (%)
[DS] = dissolved sulphide concentration in the sewage (mg/l)

Assuming that all H_2S escaping to the sewer headspace is oxidised on the pipe wall, the average H_2S flux to the pipe wall can be obtained by multiplying φ_{sf} by the ratio of sewage surface width, W, to exposed perimeter of the pipe wall above the sewage surface, P', to give Equation 2.73.

$$\varphi_{sw} = 0.69(sV)^{0.375} J[DS]\left(\frac{W}{P'}\right) \tag{2.73}$$

where $\varphi_{sw} = \varphi_{sf}\,(W/P')$ = average H_2S flux to the pipe wall (g/m^2/h)

However, apart from the flow velocity, the rate at which H_2S is released from the sewage is also influenced by local turbulence and whether the flow is sub- or super-critical (Goyns 2013). This

particular equation, therefore, is also limited due to the absence of additional parameters that contribute to H_2S release from the sewage.

2.13.2.1.3 Corrosion rate

H_2SO_4 that is generated on the moist sewer surfaces may react with the alkaline (or acid-soluble) constituents, specifically the calcareous fractions, in the concrete as shown in Equation 2.74.

$$H_2SO_4 + CaCO_3 \rightarrow H_2O + CO_2 + CaSO_4 \quad (2.74)$$

If the formation rate of the H_2SO_4 is 'low', a major part of it will react with the acid-soluble components such as any PC-based binder matrix. On the other hand, if the formation rate of the H_2SO_4 is relatively 'high', part of it will trickle down the sewer walls before reaction. This 'excess' acid will reach the sewage and may react with the alkaline components therein to form sulphate ions. The liquid film on the sewer walls around the sewage daily flow level may contain these ions that could, through association, cause chemical sulphate attack on the concrete (Hvitved-Jacobsen et al. 2013).

Equation 2.74 shows that 1 mol of H_2S (32 g) resulting in the formation of H_2SO_4 has a potential for reaction with 1 mol (100 g) of cement and/or calcareous aggregate in the concrete (as equivalent $CaCO_3$). Based on this mass balance, a quantitative method was developed for predicting the corrosion rate of concrete in relation to the alkalinity of the concrete (as discussed in Section 2.8) material and the rate of H_2S absorption in the moisture on the concrete surface. This is expressed in Equation 2.75 (EPA 1974).

$$r_{corr} = \frac{100}{32} \cdot \frac{\phi_{sw}}{A} \quad (2.75)$$

where r_{corr} = corrosion rate per unit area of the concrete surface (g/m^2/h)
ϕ_{sw} = average H_2S flux to the moist pipe wall (g/m^2/h)
A = alkalinity of the concrete material (g $CaCO_3$ per g concrete material)

If the right-hand side of Equation 2.75 is divided by the density of concrete, estimated to be 2.4 x 10^6 g/m^3, the area-based corrosion rate, r_{corr} can be expressed as an average corrosion rate, c_{avg} in units of depth per time as shown in Equation 2.76.

$$c_{avg} = 11.4 \frac{\phi_{sw}}{A} \quad (2.76)$$

where c_{avg} = average (annual) corrosion rate (mm/year)

In Equation 2.76, it is assumed that all H_2SO_4 formed on the concrete wall will react with the acid-soluble portion of the concrete matrix. However, this is not usually the case and an efficiency coefficient is necessary for acid reaction based on an estimated fraction of acid remaining on the sewer wall. This can be expressed as shown in Equation 2.77.

$$c_{avg} = 11.4k \frac{\phi_{sw}}{A} \quad (2.77)$$

where k = efficiency factor < 1 (rate constant for H_2S adsorption and oxidation kinetics as a function of temperature and air-flow (Reynolds number)). For systems where ϕ_{sw} is 'low' (such as in large diameter (> 1 m) pipes with less condensate forming on their walls), the value of k approaches 1; for systems where ϕ_{sw} is 'high' (such as in smaller diameter (< 1 m) pipes with more condensate forming on their walls), k may decrease to about 0.3.

To ensure that a sewer remains serviceable after a certain period, Equation 2.77 can be used together with the design life in order to determine the required additional concrete cover to reinforcing steel as shown in Equation 2.78.

$$Az = 11.4k\,\phi_{sw}L \tag{2.78}$$

where $z = cL$ = additional concrete cover required over reinforcing steel (mm)
L = required design life of a sewer (years)

The term 'Az' on the left-hand side of Equation 2.78, called the Life Factor, is used for comparing different concrete mixtures by their alkalinity. The term on the right-hand side describes the conditions within the sewer in terms of certain characteristics of the sewage and sewer headspace, and the required service life.

Up to this point, the review of the LFM has revealed the following hypotheses (Table 2-7), in addition to those given in Table 2-1, Section 2.3.10:

Table 2-7: Factors influencing biogenic concrete corrosion in sewers (EPA, 1991)

Factor	Effect
Slope and velocity	Affects degree of reaeration, H_2S release from the sewage
Sub- and super-critical flow	Affects O_2 transfer at the aqueous-gaseous phase, H_2S release from the sewage
Concrete alkalinity	Higher alkalinity reduces the corrosion rate

However, the factors given in Table 2-7 will be critiqued further in light of certain case studies and subsequent calibrations to the LFM (based on these case studies) as discussed in the following sections.

2.13.2.2 Case studies – performance of the LFM (EPA, 1985, 1991, 1992; McWilliams and Parmer, 2010)

The first documented extensive biogenic corrosion investigation was undertaken by the county of Sacramento in the State of California U.S. during 1976 on a 21 km outfall sewer having sections of varying diameters (between 700 mm and 1500 mm) (Figure 2-12), the so-called Central Trunk Sewer, which was designed using the LFM. The sewer was commissioned during 1963. After two years in operation, the total and dissolved sulphide concentration was monitored (since 1965), whereas visual inspections were conducted during 1964, 1968, 1969, 1974, and 1976. Severe corrosion was not apparent during the first three visual inspection regimes. However in 1974, severe corrosion was apparent and this spurred a more extensive sampling program to establish the cause and extent of biogenic corrosion, based on the total sulphide concentration in the sewage and the depth of corrosion in different sections of the sewer.

Table 2-8 gives a comparison between predicted and measured total sulphide concentrations in the sewage flowing through the Central Trunk Sewer. The predicted values were calculated to account for gains and losses of sulphide from tributary streams based on Equation 2.71.

Table 2-8: Comparison of predicted and measured total sulphides in the Sacramento Central Trunk (EPA, 1985)

Distance upstream from CWTP* (m)	Total sulphides (mg/l)	
	Predicted[#]	Measured[+]
2 438 (1.5 m dia.)	1.5	1.4
6 705 (1.4 m dia.)	1.8	1.5
10 668 (1.2 m dia.)	1.9	1.8
16 764 (1.0 m dia.)	1.4	0.9

*Central Wastewater Treatment Plant
[#]Value of m (in Equation 2.71) = 0.96
[+]Average of 48 samples

Figure 2-12: Layout of the Central Trunk Concrete Sewer (McWilliams and Parmer, 2010).

A comparison was also made between the measured corrosion depth due to biogenic H_2SO_4 attack and that predicted based on Equation 2.77 with the following parameters; measured alkalinity, A of 0.16 (indicating use of acid-insoluble aggregates); efficiency factor, k was assumed to be 1; ϕ_{sw} was calculated based on 15-years data, which included dissolved sulphide concentrations, sewage velocities, pH values, and slopes at manhole locations. The measured and predicted depths due to biogenic corrosion are presented in Figure 2-13.

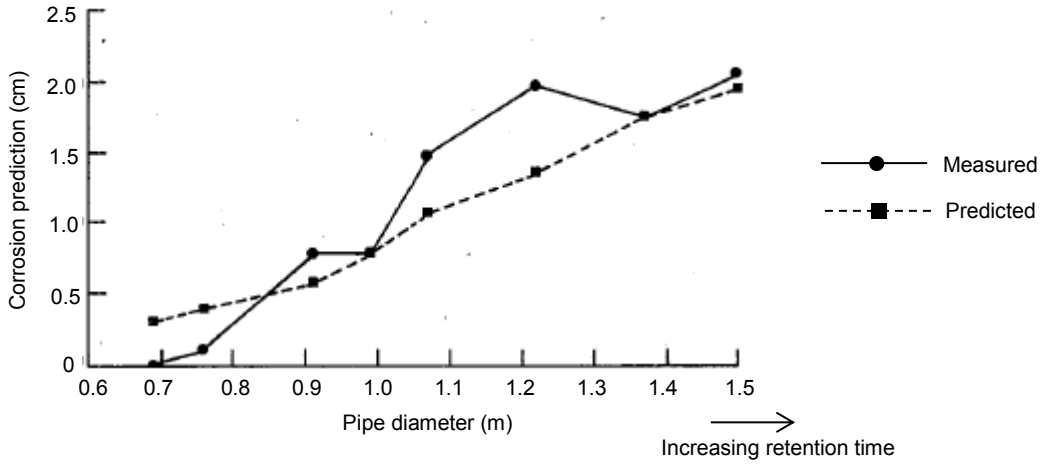

Figure 2-13: Measured and predicted biogenic corrosion rates for the Sacramento Central Trunk (EPA, 1985).

The comparisons presented from the Sacramento Central Trunk Sewer seem to give mixed but relatively comparable results for a PC-based mixture with acid-insoluble aggregates. Generally, the predicted total sulphide compared well with the measured values except for the section that is approximately 16.8 km upstream from CWTP (with 1 m diameter pipes) whose predicted concentration was approximately 1.5 times the measured concentration. Similarly, the predicted corrosion depth compared well with the measured values except for the approximately 1100 mm and 1200 mm diameter pipe sections, whose measured corrosion depths were up to 1.4 times the predicted values. Notably, the sewer section where the measured and the predicted total sulphide

concentration in the sewage varied most had precise predicted corrosion depth. These contradictory results can be attributed to various factors that may include (i) certain assumptions made while developing the LFM (such as the accuracy of the efficiency factor '*k*' in Equation 2.77 or H_2S flux in Equation 2.72), (ii) certain parameters that were not included in the LFM but are known to influence rates of biogenic corrosion in sewer (such as the effect of local turbulence within the sewage flow), or (iii) both factors (i) and (ii) above. Also, it is possible that the neutralisation capacity mechanisms of concrete mixtures, based on conventional alkalinity in this case, were not well understood since other acid-soluble components (other than $CaCO_3$) could be involved in neutralising the attacking acid. From this point of view, opportunities exist to calibrate the LFM based on these aspects as will be discussed in later sections.

From the revelations on the performance of the Central Trunk Sewer, various inspections were further undertaken during early 1980's, and these were expanded to the entire State of California. Results showed that the rates of corrosion had increased markedly in comparison to the predicted rates using the LFM as given by Equation 2.77, and so a nationwide study was commissioned in the U.S. to explain the observed corrosion mechanisms. Around this time, similar studies were being undertaken in other countries that used the LFM concept in the design of concrete sewer pipes. These countries included South Africa, France, Germany, Italy, United Kingdom, Netherlands, Denmark, Japan, Singapore, Kuwait, Venezuela, Brazil and Australia. The major common conclusions from most of these studies relating to the LFM included; (i) that the actual corroded depths in most sections of the sewers were greater than the predicted values, (ii) that the most corroded areas on the concrete pipes were around the daily sewage flow level and at the crown, (iii) that the most corroded sections in the sewers coincided with sites which had turbulent sewage flows.

Based on conclusions from these studies, EPA (1992) proposed that the LFM given by Equation 2.77 could be modified for use in areas that were deemed to have severe conditions for the generation of biogenic H_2SO_4, resulting in greater concrete corrosion. In this regard, a 'crown corrosion factor' and a 'turbulence corrosion factor' were introduced to predict peak (maximum) corrosion rates, c_{max} (Equation 2.79).

$$c_{\max} = c_{avg} \times CCF \times TCF \tag{2.79}$$

where c_{max} = maximum corrosion rate (mm/year)
c_{avg} = average corrosion rate (mm/year) (Equation 2.77)
CCF = crown corrosion factor, ranging from 1.5 to 2.0
TCF = turbulence corrosion factor, ranging from (i) 1.0 to 2.5 for areas with typical turbulent flow conditions, and (ii) 5.0 to 10.0 for turbulent junctions

Therefore, following can be noted from this review of the LFM:

(i) The LFM can be used to predict total sulphide build-up in the sewage relatively accurately.
(ii) The LFM can be used to predict biogenic corrosion rates relatively accurately for plain PC-based concrete mixtures with 16% PC.
(iii) Even though the LFM can be calibrated using either the CCF, TCF or both factors, the material properties of the concrete mixtures, which are responsible for neutralising the attacking acid have not been investigated.
(iv) It may be more appropriate to first investigate and consider improvement on aspects of the neutralisation capacity of concrete mixtures before incorporating, for example, the CCF or TCF, which may result in unnecessarily thick concrete sewer pipe walls.
(v) The influence of other binder systems (apart from PC-based) has not been considered in the LFM, due to the assumption that conventional alkalinity (equivalent g $CaCO_3$ per g concrete material) is the rate-controlling parameter in biogenic H_2SO_4 attack of concrete sewer pipes. This hypothesis needs further examination.

A critique of the widely used LFM summarised above merit the methodology of the current study.

As mentioned earlier, a review of another deterministic (mechanistic) and one statistical model will also be undertaken in order to highlight the significance of material properties in biogenic corrosion prediction models. Even though results from the current study can be incorporated in these models, focus will be on the LFM since (i) it is the most widely used model in the design of concrete sewer pipes (EPA, 1992; McWilliams and Parmer, 2010; Kley and Caradot, 2013), and (ii) data presented in the current study is based on the principles of the LFM for designing concrete mixtures for sewer pipe applications.

2.13.2.3 The WATS model (Hvitved-Jacobsen et al., 2013)

A more recently developed deterministic (mechanistic) model for the prediction of biogenic corrosion of concrete sewers is the so-called WATS (Wastewater Aerobic-anaerobic Transformations in Sewers) (Hvitved-Jacobsen et al., 2013). This model, expressed in terms of various mass balances, is based on the resolution of non-linear differential equations describing microbial and chemical transformation processes of organic matter, oxygen, oxidised nitrogen and sulphur-based compounds (Vollersten and König, 2005).

The process elements of the WATS model are based on the following descriptions:

(i) The sulphur cycle
(ii) Aerobic, heterotrophic transformations of organic matter
(iii) Aerobic transformations of organic carbon and sulphur
(iv) Anoxic, heterotrophic transformations of organic matter
(v) Aerobic and anaerobic transformations or organic carbon and sulphur

Therefore the backbone of the WATS process concept is the sulphur and carbon cycles including related aerobic, anoxic, or anaerobic transformations. This concept, expressed in process matrix formulations is considered as the WATS model approach. Certain matrix formulations for the WATS process descriptions are given in Table 2-9 (Hvitved-Jacobsen et al., 2013).

Table 2-9: WATS sewer process model for aerobic, heterotrophic transformations of organic matter in wastewater expressed as a process matrix (Hvitved-Jacobsen et al., 2013).

Process	X_{Hw}	S_s[##]	X_{s1}	X_{s2}	S_o
Growth of biomass in bulk water phase	1	$-1/Y_{Hw}$			$(1 - Y_{Hw})/Y_{Hw}$
Growth of biomass in biofilm	1	$-1/Y_{Hf}$			$(1 - Y_{Hf})/Y_{Hf}$
Maintenance energy requirement	(-1)	-1			1
Hydrolysis, fast		1	-1		
Hydrolysis, slow		1		-1	
Reaeration					-1

X_{Hw} = Heterotrophic active biomass in the water phase (g COD m^{-3})
X_{s1} = Hydrolysable substrate, fast biodegradable (g COD m^{-3})
X_{s2} = Hydrolysable substrate, slowly biodegradable (g COD m^{-3})
Y_{Hw} = Yield constant for aerobic growth of heterotrophic biomass in the water phase (g COD (g COD)$^{-1}$)
Y_{Hf} = Yield constant for aerobic growth of heterotrophic biomass in the biofilm (g COD (g COD)$^{-1}$)
S_O = Dissolved oxygen (g O_2 m^{-3})
S_S = Readily biodegradable substrate (S_F + S_A) (g COD m^{-3})

[##] $S_S = S_F + S_A$
S_F = Fermentable substrate (g COD m^{-3})
S_A = Fermentation products (g COD m^{-3})

As an example to illustrate the use of the process matrix in Table 2-9, the mass balance of S_S as a differential equation can be expressed as (Equation 2.80):

$$\frac{\partial S_S}{\partial t} = -\frac{1}{Y_{Hw}} r_{grw} - \frac{1}{Y_{Hf}} r_{grf} - r_{maint} + r_{hydr.1} + r_{hydr.2} \quad (2.80)$$

where r_{grw}, r_{grf}, r_{maint}, $r_{hydr.1}$, and $r_{hydr.2}$ = formation rates (day^{-1})

The aerobic, heterotrophic transformations of organic matter in wastewater presented in Table 2-9 are essential when simulating sewer processes since, for example, the mass balance of S_O determines when anaerobic conditions occur (thus growth of SRB).

As discussed in Section 2.4, the end products of biological sulphide oxidation are primarily elemental sulphur (S^0) and sulphate (SO_4^{-2}). The WATS sewer process model for formulation of the sulphur cycle in both the sewage phase and on the concrete pipe surface is presented in Table 2-10.

Table 2-10: WATS sewer process model for formulation of sulphur cycle (Hvitved-Jacobsen et al., 2013).

Process	S(-II)	S_{SO4}	MeS	P_{H2S}	S_{H2SO4}	S_O	d_{corr}
H_2S formation	1	-1					
Chemical oxidation of sulphide	-1	1				$-(1/R_{Cwc})$	
Biological oxidation of sulphide	-1	1				$-(1/R_{Cwb})$	
Oxidation of sulphide in biofilm	-1	1				$-(1/R_{Cfb})$	
Precipitation of sulphide by metals	-1		1				
H_2S emission	-1			$(RT/32)(V_w/V_g)$			
H_2S oxidation at concrete surfaces		$(32(1-\partial_{corr}))/RT$		-1	$32/RT$		$(100\partial_{corr}V_g)/(\sigma_{conc}ARTA_c)$

$S(-II)$ = Dissolved sulphide (g S m^{-3})
S_{SO4} = Concentration of sulphate in the water phase (g S m^{-3})
MeS = Precipitated metal sulphide phase (g S m^{-3})
P_{H2S} = Partial pressure of H_2S in the sewer atmosphere (ppm)
S_{H2SO4} = Sulphuric acid concentration in the water film of moist sewer surfaces (g S m^{-3})
S_O = Dissolved oxygen (g O_2 m^{-3})
d_{corr} = Rate of concrete corrosion (surface corrosion depth) (m day^{-1})
R = Hydraulic radius of flow area (m)
T = Temperature (°C)
R_C = Reaction coefficients (S g O_2^{-1})
A_c = Concrete surface area
V_g = Gas volume in sewer
V_w = Water volume in sewer
A = Alkalinity of concrete, expressed in g $CaCO_3$ per g concrete material
σ_{conc} = Specific mass of the concrete material (g m^{-3})
∂_{corr} = Fraction of sulphuric acid resulting in corrosion
S_S = Readily biodegradable substrate (S_F + S_A) (g COD m^{-3})

From the sewer process models described in Table 2-9 and Table 2-10, it is shown that the WATS model is developed to include both water phase and gas phase processes. The model is therefore suited to simulate, for example, corrosion where the process relationships between the water phase and the gas phase are significant (Hvitved-Jacobsen et al., 2013).

From Table 2-10, the rate of concrete corrosion due to biogenic H_2SO_4 attack is given as (Equation 2.81):

$$d_{corr} = \frac{100\partial_{corr}}{\sigma_{conc}ART} \frac{V_g}{A_c} \quad (2.81)$$

The following can be noted from this review of the WATS model:

(i) It incorporates more variables than the LFM during prediction of the formation of biogenic H_2SO_4.

(ii) Other material properties, apart from the conventional alkalinity of PC-based concrete mixtures, which are responsible for neutralising the attacking acid have not been investigated.

(iii) Since WATS also considers conventional alkalinity (equivalent g $CaCO_3$ per g concrete material) as the rate-controlling parameter in biogenic H_2SO_4 attack of concrete sewer pipes, it faces similar critique as the LFM in this regard.

The main advantage of deterministic (mechanistic) models is that the developed relationships are based on an understanding of actual mechanisms (physical, chemical) of the sewer deterioration process. The main disadvantage of these models is that even though some single aspects, such as corrosion, can be modelled mechanistically, involvement of other degradation mechanisms of sewer conditions remains a complex process that is not completely understood and it depends on a large amount of factors (Ana, 2009; Marlow et al. 2009; Schmidt, 2009; Kley and Caradot, 2013).

2.13.3 Statistical concrete sewer biogenic corrosion prediction models

These models comprise a set (or sets) of mathematical equations which when solved, describe the sewer condition as a random variable. They take into account the probabilistic nature of the corrosion process and use historical data to provide correlations between factors that are deemed to control the rate of corrosion (such as concrete pipe material) and condition data (such as temperature and characteristics of the attacking acid) (Kley and Caradot, 2013). One important aspect of these models is that they need to be calibrated against experimental test results, either from laboratory or field data, before they can be applied. The widely used statistical model for biogenic corrosion prediction, the so-called SATIR (Säure (acid), Angriff (attack), Transport, Instationär (non-stationary), Reaktion (reaction)) (Beddoe and Dorner, 2005) is reviewed in the following section.

2.13.3.1 The SATIR model (Beddoe and Dorner, 2005)

This model, for simulation of acid attack on concrete sewer pipes and other concrete surfaces, is based on the characteristics of several media. The corrosion process can be simulated for concrete of known composition, which is exposed to acids that are either in a static or flowing condition (Beddoe and Schmidt, 2009). The concrete may contain acid-soluble or acid-insoluble aggregate. Also, the conditions of attack are defined by parameters which may be determined based on the material characteristics at the point of attack and properties (chemical analysis) of the attacking acid. The result from the simulation of this model is in the form of the time needed to reach a given depth of corrosion based on four mechanisms; (i) the dissolution of aggregates, (ii) the dissolution of the binder matrix, (iii) the flux density of the diffusion (charged chemical) species, and (iv) the characteristics of the pore solution. A schematic of these mechanisms is presented in Figure 2-14 (Beddoe and Dorner, 2005).

SATIR is based on the modified Nernst-Planck equation (Equation 2.82(a)) for one dimensional diffusion to calculate the diffusion of species in the pore solution of concrete, based on their concentration distribution in the pore solution, $c_i(x)$.

$$J_i = -D_i^{eff} P_c \left(\frac{\partial c_i}{\partial x} + \frac{F z_i}{RT} c_i \frac{\partial \psi}{\partial x} + c_i \frac{\partial \ln \gamma_i}{\partial x} \right) \qquad (2.82(a))$$

where J_i = flux density for a series of diffusing species in the bulk material (C/m^2)
D_i^{eff} = effective diffusion coefficients for individual species
P_c = volume fraction of the pore space in which diffusion takes place
F = Faraday constant (C/mol)
z_i = valence of ionic species
R = gas constant (J/mol.K)
T = temperature (°C)

Ψ = local potential
γ_i = activity coefficients (from Wateq Debye-Hückel Equation 2.82(b))

$$\log\gamma_i = -Az_i^2 \frac{\sqrt{I}}{I + B\dot{a}\sqrt{I}} \qquad (2.82(b))$$

where I = ionic strength; z = charge number of the ion; $å$ = ion size parameter; A and B = temperature-dependent constants

As corrosion proceeds, the pore space increases due to dissolution of the binder matrix (and acid-soluble aggregate). J_i is primarily determined by the porosity of the corroded materials (it is assumed that the effect of diffusion in the un-corroded materials is less than that of the corroded materials) (Beddoe and Hilbig, 2007; Beddoe and Schmidt, 2009).

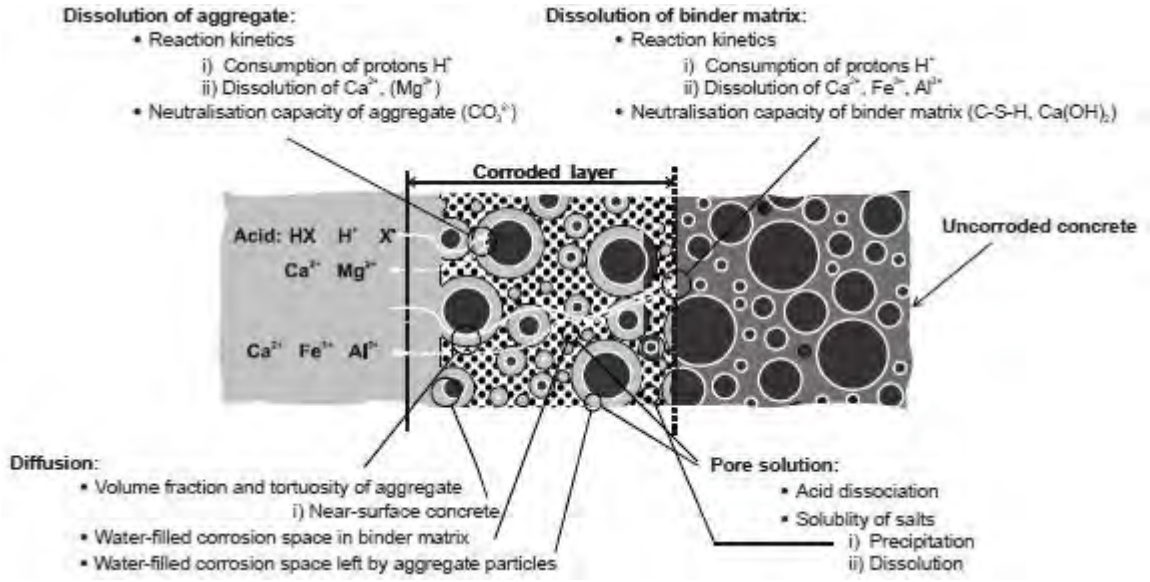

Figure 2-14: Mechanisms involved in the corrosion process (acid attack) of concrete (Beddoe and Dorner, 2005).

The dissolution of the binder matrix results in the transfer of Ca^{2+} ions from the binder matrix into the pore solution as described by the reaction kinetics in Equation 2.83.

$$\frac{\partial c_{Ca}}{\partial t} = k_{Ca} S_{Ca} c_H \qquad (2.83)$$

where C_{Ca} = concentration of Ca^{2+} ions in solution
S_{Ca} = amount of potentially soluble calcium in concrete with respect to pore solution volume
C_H = proton concentration of the pore solution
k_{Ca} = rate constant

At the beginning of corrosion, S_{Ca} is basically the neutralisation capacity of the concrete given by the total quantity of calcium calculated from the CaO content of the cement and the cement content of the concrete. The increase in the porosity of concrete due to the removal of calcium from the binder matrix is calculated from the increase in calcium concentration of the pore solution. It is important to note here that since the dissolution of Fe^{3+} and Al^{3+} in aluminate and ferrite hydrates occurs along with Ca^{2+}, their effect on porosity is considered together.

In order to calibrate SATIR, Beddoe and Schmidt (2007) simulated corrosion of PC-based concrete (with siliceous aggregate) in mineral H_2SO_4 at pH 2 and pH 4 to mimic exposure classes XA1 and

XA3 (according to EN 206-1) respectively. These exposure classes fulfil the requirements for concrete exposed to chemical attack. The concrete mixtures had Portland cement contents of between 280 kg/m^3 and 320 kg/m^3, and w/c ratios between 0.45 and 0.6.

Results indicated that the corrosion resistance of concrete can be improved by use of low cement contents and low w/c ratios. Also, the time, t needed for the corrosion depth to reach the target 10 mm was dependent on the proton concentration, C_H of acid molecules in the attacking medium. Therefore, in this simulation, it was reported that the corrosion depth increased with the square root of time and proton concentration (Equation 2.84). The constant 'a' depends on the composition of the concrete (alkalinity).

$$d = a\sqrt{tC_H} \tag{2.84}$$

Gypsum precipitation and measurements of loss of surface material were not considered during this test regime.

The following can be noted from this review of the SATIR model:

(i) The model considers the flux density for a series of diffusing species in the bulk material, J_i while computing the diffusion of species in the pore solution. However, this flux density should be calibrated since the properties of the attacking acid are changed during this reaction.

(ii) Similarly, the reaction kinetics for the dissolution of the binder matrix considers the amount of potentially soluble calcium in the concrete with respect to the pore solution volume. However, it should be noted that the potentially soluble calcium in this case is virtually infinite.

(iii) The computation of the increase in porosity of the concrete due to the removal of calcium from the binder matrix is based on the increase in Ca^{2+} ion concentration in the pore solution. However, it is not clear whether there is a counter diffusion of these ions out of the pore space since the removal of calcium from the binder matrix can rapidly result in Ca^{2+} saturation of the pore solution.

(iv) The neutralisation capacity of the attacking acid is defined by conventional alkalinity (equivalent $CaCO_3$), similar to the deterministic (mechanistic) models reviewed above – the LFM and WATS. Therefore the characteristics of other binder systems apart from PC-based have not been investigated.

2.14 Summary – concrete sewer biogenic corrosion prediction models

This part presented a review of certain concrete sewer biogenic corrosion prediction models, where it was demonstrated that there are still significant challenges that need to be addressed with regard to biogenic corrosion prediction in concrete sewers. This review established that:

(1) Prediction of biogenic corrosion of concrete sewers is principally a two-step process. The first step entails the generation of H_2S in the sewer, and the second step entails the prediction of the corrosion rate of the concrete pipe materials based on the concentration of H_2S in the sewer's headspace. Whereas the former has been widely researched and documented in other fields such as wastewater engineering and environmental microbiology, the latter has lagged particularly in view of advancement in the cement and SCM industries.

(2) Recent models, both deterministic and statistical, still adopt equivalent $CaCO_3$ only as the rate-controlling parameter of the corrosion rate of concrete mixtures. This therefore excludes other binder systems such as blended PC- and CAC-based.

(3) The biogenic corrosion prediction models reviewed present contradictory hypotheses with regard to the characteristics of the most effective concrete mixture composition in sewer pipe applications. According to the deterministic (mechanistic) models (LFM and WATS), the corrosion rate of concrete sewer pipes is reduced with increased alkalinity of the concrete mixtures, whereas according to the statistical model (SATIR), the corrosion resistance of

concrete can be improved by use of low cement (PC) contents. This indicates a knowledge gap that needs further investigation – this has been undertaken in the current study.

In summary, it is evident that (i) the prediction of H_2S concentration in the sewer's headspace for application in corrosion prediction is difficult due to turbulence mechanisms, (ii) a reliable correlation between H_2S concentration in the sewer's headspace and prediction of the concrete corrosion rate based on conventional alkalinity as a rate-controlling parameter remains a challenge. Even so, there are limited studies that have focussed on characterising various binder systems with the view of understanding the overall neutralisation capacity (apart from equivalent $CaCO_3$) mechanisms of concrete mixtures when subjected to biogenic H_2SO_4 attack, and applying these to corrosion prediction models. This is the main objective of the current study, which particularly focuses on the widely used LFM.

2.15 General conclusions – Literature review

From the literature reviewed in Part One, Part Two and Part Three of this Chapter Two, it has been highlighted that the governing principles of general sewer hydraulics and sewer environment phases are relatively well understood, although their direct application in biogenic corrosion prediction of cement-based materials has not been widely researched and documented. Moreover, the currently available binders that can be used in the manufacture of concrete sewer pipes have varying properties, particularly the nature of their hydrates, and this limits their application in the existing corrosion prediction methods. Therefore, further work is required to address these gaps by (i) characterising the microstructure of various binder systems subjected to biogenic acid attack, (ii) applying an understanding of the microstructural characteristics in biogenic corrosion prediction, and (iii) providing a framework for knowledge transfer to existing design methods commonly used by design engineers in predicting biogenic corrosion rates of concrete sewers. These gaps have been addressed in the current study.

2.16 References

Abdalla, K. Z., & Hammam, G. 2014. Correlation between biochemical oxygen demand and chemical oxygen demand for various wastewater treatment plants in Egypt to obtain the biodegradability indices. *International Journal of Sciences: Basic and Applied Research.* 13(1): 42 – 48.

Alani, A., Faramarzi, A., Mahmoodian, M., & Tee, K. F. 2014. Prediction of sulphide build-up in filled sewer pipes. *Environmental Technology.* 35: 1721 – 1728.

Alexander, M. G., & Fourie, C. W. 2011. Performance of sewer pipe concrete mixtures with portland and calcium aluminate cements subject to mineral and biogenic acid attack. *Materials and Structures*. 44 (1): 313 – 330.

Alexander, M. G., & Mindess, S. 2005. *Aggregates in concrete*. Oxford: Taylor & Francis.

Alexander, M. G., Goyns, A. M., & Fourie, C. W. 2008. Experiences with a full-scale experimental sewer made with CAC and other cementitious binders in Virginia, South Africa. *Proceedings of the Centenary Conference on Calcium Aluminate Cements.* June 30 – July 2, Avignon. 279 – 292.

Alexander, M., Bertron, A., & De Belie, N. Eds. 2013. Performance of cement-based materials in aggressive aqueous environments. *State-of-the-Art Report, RILEM TC 211-PAE*. Netherlands: Springer.

Altcin, P., & Regourd, M. 1985. The use of condensed silica fume to control alkali-silica reaction – a field case study. *Cement and Concrete Research.* 15(4): 711 – 719.

American Concrete Pipe Association. 1988. *Concrete pipe handbook*. Vienna: ACPA.

Ana, E. V. 2009. Sewer asset management – sewer structural deterioration modeling and multicriteria decision making in sewer rehabilitation projects prioritisation. PhD dissertation. Vrije Universiteit Brussel, Brussel.

Andersson, S. 2009. Characterisation of bacterial biofilms for wastewater treatment. PhD dissertation. Royal Institute of Technology, Stockholm.

Baek, B. H., & Aneja, V. P. 2004. Measurement and analysis of the relationship between ammonia, acid gases, and fine particles in eastern North Carolina. *Journal of the Air and Waste Management association.* 54(5): 623 – 633.

Ball, M. C., Simmons, R. E., & Sutherland, I. 1987. Surface composition of anhydrous tricalcium aluminate and calcium aluminoferrite. *Journal of Materials Science.* 22: 1975 – 1979.

Barjenbruch, M. 2003. Prevention of odour emergence in sewage network. *Water Science and Technology*. 47(7): 357 – 363.

Barjenbruch, M., Hinkelmann, R., Hüttl, R., Huhnt, W., Nehrig, M., & Röben, R. 2008. An online-monitoring and operating system to prevent odour and corrosion in sewer networks. Feasibility study. Berlin: KompetenzZentrum Wasser.

Basheer, P. A. M., & Barbhuiya, S. 2010. Pore structure and transport process. In: Soutsos, M. Eds. *Concrete durability: A practical guide to the design of durable concrete structures*. London: Thomas Telford.

Basista, M., & Weglewski, W. 2008. Micromechanical modelling of sulphate corrosion in concrete: Infuence of ettringite forming reaction. *Theoretial and Applied Mechanics.* 35(1 – 3): 29 – 52.

Baumgartner, W. H. 1934. Effect of temperature and seeding on hydrogen sulphide formation in sewage. *Sewage Works Journal*. 6(3): 399 – 412.

Beddoe, R. E., & Dorner, H.W. 2005. Modelling acid attack on concrete, Part I: The essential mechanisms. *Cement and Concrete Research.* 35 (1). 2333 – 2339.

Beddoe, R. E., & Hilbig, H. 2007. Acid attack on concrete – A new computer model. In: Setzer, M. J. Eds. *Proceedings of the 5th International Essen Workshop.* Essen: Aedification. 387 – 398.

Beddoe, R. E., & Schmidt, K. 2009. Effect of concrete composition on resistance of concrete to acid attack. *Proceedings of the RILEM Conference on Concrete in Aggressive Aqueous Environments: Performance, Testing and Modelling.* June 3 – 5. Toulouse. 187 – 195.

Bengtson, H. H. 2011. Uniform open channel flow and the manning equation. Morrisville: PDH.

Bi, E. G., Monette, F., Gasperi, J., & Perrodin, Y. 2015. Assessment of the ecotoxicological risk of combined sewer overflows for an aquatic system using a coupled "substance and bioassay" approach. *Environmental Science and Pollution Research.* 22(6): 4460 – 4474.

Bizier, P. 2007. *Outfall sanitary sewer design and construction*. 2nd ed. Virginia: American Society of Civil Engineers.

Boon, A. G., & Lister, A. R. 1975. Formation of sulphide in rising main sewers and its prevention by injection of oxygen. *Progress in Water Technology*. 7(2): 289 – 300.

Boon, A. G., & Pomeroy, R. D. 1990. *The problem of hydrogen sulphide in sewers*. 2nd ed. Westminster: Acer John Taylor.

Borichewski, R. M. 1967. Keto acids as growth-limiting factors in autotrophic growth of *Thiobacillus thiooxidans*. *Journal of Bacteriology.* 93(2): 597- 599.

Brüser, T., Lens, P. N. L., & Trüper, H. G. 2000. The biological sulphur cycle. In: Lens, P. N. L. Eds. *Environmental technologies to treat sulphur pollution.* London: IWA Publishing. 47 – 76.

Carlson, D., & Plummer, C. 2010. *Physical geology: Earth revealed.* 9th ed. New York: McGraw-Hill.

Chatterjee, S., Bandyopadhyay, A., & Sarkar, K. 2011. Effect of iron oxide and gold nanoparticles on bacterial growth leading towards biological application. *Journal of Nanobiotechnology.* 9: 34.

Chatterji, S. 1995. Concrete durability and CaO/SiO_2 mole ratio of C-S-H. *Cement and Concrete Research.* 25(5): 929 – 932.

Chatterji, S., & Jeffery, J. W. 1962. Studies of early stages of paste hydration of cement compounds. *Journal of the American Ceramic Society.* 45(11): 536 – 543.

Cho, K. S., & Mori, T. 1995. A newly isolated fungus participates in the corrosion of concrete sewer pipes. *Water Science and Technology*. 31(7): 263 – 271.

Cohn, S., Hayes, A., & Renault, K. 2010. The effect of substrate variation on biofilm growth for use in wastewater treatment. Project report number TAC-MQP-FR20. Worcester Polytechnic Institute, Worcester, MA.

Collepardi, M., Monosi, S., & Piccioli, P. 1995. The influence of pozzolanic materials on the mechanical stability of aluminous cement. *Cement and Concrete Research.* 25(5): 961 – 968.

Council for Scientific and Industrial Research. 1996. *Consolidated report on phase 1 of sewer corrosion research: The Virginia sewer experiment and related research*. Pretoria: CSIR. Report No BOU/C128.

Daugherty, R. L., & Franzini, J. B. 1965. *Fluid mechanics with engineering applications.* 6th ed. New York: McGraw-Hill.

Davy, W. J. 1950. The influence of velocity on sulphide generation in sewers. *Sewage and Industrial Wastes*. 22: 1132 – 1139.

Ding, J., Fu, Y., & Beaudoin, J. J. 1995. Stratlingite formation in high alumina cement – silica fume systems: Significance of sodium ions. *Cement and Concrete Research.* 25(6): 1311 – 1319.

Dunster, A. M., Moulinier, F., Quillin, K. C., & Osborne, G. J. 2008. Durability of concrete made with calcium aluminate cement and ground granulated blast-furnace slag in sulphate and marine envrinments. *Proceedings of the Centenary Conference on Calcium Aluminate Cements.* June 30 – July 2, Avignon. 443 – 454.

Dux, P. 1999. Asbestos cement pipes in aggressive ground water: A case study. In: Dhir, R. K., & McCarthy, M. J. Eds. Concrete durability and repair technology. *Proceedings of the International Conference on Creating with Concrete*. September 8 – 10. Dundee. 373 – 379.

Ebtehaj, I., Bonakdari, H., & Sharifi, A. 2014. Design criteria for sediment transport in sewers based on self-cleansing concept. *Journal of Zhejiang University (Applied Physics & Engineering).* 15(11): 914 – 924.

Edmonds, R. N., & Majumdar, A. J. 1989. The hydration of mixtures of monocalcium aluminate and blastfurnace slag. *Cement and Concrete Research.* 19(5): 779 – 782.

Eliassen, R., Heller, A. N., & Kirch, G. 1949. The effect of chlorinated hydrocarbons on hydrogen sulphide production. *Sewage Works*. 21: 457.

Environmental Protection Agency. 1974. Process design manual for sulphide control in sanitary sewerage systems. Washington: EPA.

Environmental Protection Agency. 1985. Design manual: Odor and corrosion control in sanitary sewerage systems and treatment plants. Cincinnati: EPA.

Environmental Protection Agency. 1991. Hydrogen sulphide corrosion in wastewater collection and treatment systems, Technical Report to Congress, 430/09-91-010. Cincinnati: EPA.

Environmental Protection Agency. 1992. Detection, control, and correction of hydrogen sulphide corrosion in existing wastewater systems. Cincinnati: EPA.

Espinosa, B., Letourneux, R., & Marcdargent, S. 1996. Acid attack of hydraulic cement-bound materials: Corrosion kinetics and neutralisation capacity. *Proceedings of the 13th International Corrosion Congress.* November 25 – 29. Melbourne. 494 – 503.

Famy, C., Scrivener, K. L., Atkinson, A., & Brough, A. R. 2000. Effects of an early or late heat treatment on the microstructure and composition of inner C-S-H products of Portland cement mortars. *Cement and Concrete Research.* 32(2): 269 – 278.

Feldman, R. F., & Sereda, P. J. 1968. A model for hydrated Portland cement paste as deduced from sorption-length change and mechanical properties. *RILEM Bulletin.* 1(6): 509 – 520.

Fentiman, C. H., & Rashid, S. 1990. The effect of curing conditions on the hydration and strength development in Fondu: Slag. *Calcium aluminate cements, International Symposium.* July 9 – 11. London.

Fernández-Carrasco, L., & Vásquez, E. 2009. Reactions of fly ash with calcium aluminate cements and calcium sulphate. *Fuel.* 88(9): 1533 – 1538.

Fourie, C. W. 2007. Acid resistance of sewer pipe concrete. MSc (Eng) dissertation. University of Cape Town, Cape Town.

Gosselin, C. 2009. Microstructural development of calcium aluminate cement based systems with and without supplementary cementitious materials. PhD dissertation. École Polytechnique Fédérale de Lausanne, Lausanne.

Gottenbos, B., Van der Mei, H. C., & Busscher, H. J. 1999. Models for studying initial adhesion and surface growth in biofilm formation on surfaces. *Methods in Enzymology*. 310: 523 – 534.

Goyns, A. M. 2003. Virginia sewer rehabilitation: Progress Report 1. Pretoria: Concrete Manufacturers Association.

Goyns, A. M. 2013. *Design manual for concrete pipe outfall sewers.* Midrand: Concrete Manufacturers Association.

Goyns, A. M. 2014. Virginia sewer rehabilitation: Progress Report 6. Pretoria: Concrete Manufacturers Association.

Goyns, A. M., Alexander, M. G., & Fourie, C. W. 2008. Applying experimental data to concrete sewer design and rehabilitation. *Proceedings of the Centenary Conference on Calcium Aluminate Cements.* June 30 – July 2, Avignon. 293 – 308.

Graeme, M. 2003. Cements. In: Newmann, J., & Choo, B. S. Eds. *Advanced Concrete Technology – Constituent Materials*. Oxford: Elsiever.

Gu, J. D., Mitton, D. B., Ford, T. E., & Mitchell, R. 1998. Microbial degradation of polymeric coatings measured by electrochemical impedance spectroscopy. *International Biodeterioration & Biodegradation*. 9: 39 – 45.

Gutiérrez-Padilla, M. G. D., Bielefeldt, A., Ovtchinnikov, S., Hernandez, M., & Silverstein, J. 2010. Biogenic sulphuric acid attack on different types of commercially produced concrete sewer pipes. *Cement and Concrete Research.* 40: 293 – 301.

Haestad Methods. 2002. *Computer applications in hydraulic engineering*. Michigan: Haestad Press.

Hammam, G. 2013. Influence of raw wastewater biodegradability on optimal selection and performance of treatment processes. MSc dissertation. Cairo University, Cairo.

Harchand, K. S., Vishwamittar, K., & Chandra, K. 1980. Infrared and Mössbauer study of two Indian cements. *Cement and Concrete Research.* 10(2): 243 – 252.

Herisson, J. 2012. Biodeterioration of cementitious materials in the wastewater – Comparative study of calcium aluminate cement and Portland cement. PhD dissertation. Université Paris-Est, Paris.

Herisson, J., Guéguen-Minerbe, M., van Hullebusch, E. D., & Chaussadent, T. 2014. Behaviour of different cementitious material formulations in sewer networks. *Water Science and Technology*. 69(7): 1502 – 1508.

Hernandez, M., Marchand, E. A., Roberts, D., & Peccia, J. 2002. In-situ assessment of active Thiobacillus species in corroding concrete sewers using fluorescent RNA probes. *International Biodeterioration & Biodegradation.* 49(4): 271 – 276.

Heukelekian, H. 1943. Effect of addition of sodium nitrate to sewage on hydrogen sulphide production and BOD reduction. *Sewage Works.* 15(2): 255 – 261.

Hollerbach, G. H. Jr. 1985. Controlling sulphides in sewage by direct injection of oxygen. *Public Works*. 116(3): 82 – 83.

House, M. W., & Weiss, W. J. 2014. Review of microbially induced corrosion and comments on needs related to testing procedures. *4th International Conference on the Durability of Concrete Structures.* July 24 – 26. West Lafayette.

Hughes, J. J., & Trtik, P. 2004. Micro-mechanical properties of cement paste measured by depth-sensing nanoindentation: A preliminary correlation of physical properties with phase type. *Materials Characterisation.* 53(2 – 4): 223 – 231.

Huntzicker, J. J., Cary, R. A., & Ling, C. S. 1980. Neutralisation of sulphuric acid aerosol by ammonia. *Environmental Science and Technology.* 14(7): 819 – 824.

Hvitved-Jacobsen, T., Vollertsen, J., & Nielsen, A. H. 2013. *Sewer processes: Microbial and chemical process engineering of sewer networks*. 2nd ed. Boca Raton: CRC Press.

Islander, R. L., Devinny, J. S., Mansfeld, F., Postyn, A., & Hong, S. 1991. Microbial ecology of crown corrosion in sewers. *Journal of Environmental Engineering*. 117(6): 751 – 770.

Ismail, N., Nonaka, T., Noda, S., & Mori, T. 1993. Effect of carbonation on microbial corrosion of concretes. *Journal of Construction Management and Engineering.* 20(474): 133 – 138.

Jenkins, R. L., Gute, J. P., Krasner, S. W., & Baird, R. B. 1980. The analysis and fate of odorous sulphur compounds in wastewater. *Water Research*. 14: 441 – 448.

Jensen, H. S., Nielsen, A. H., Hvitved-Jacobsen, T., & Vollertsen, J. 2008. Hydrogen sulphide initiated corrosion in concrete sewers – a conceptual approach for prediction. *11th International Conference on Urban Drainage.* August 31 – September 5. Edinburgh.

Johnson, A. C., & Wood, M. 1990. DNA, a possible site aluminium toxicity in *Rhizobium*. *Applied and Environmental Microbiology*. 56: 3629 – 3633.

Jolley, R. A., & Forster, C. F. 1985. The kinetics of sulphide oxidation. *Environmental Technology.* 6: 1 – 10.

Joseph, A. P., Keller, J., Bustamante, H., & Bond, P. L. 2012. Surface neutralization and H_2S oxidation at eraly stages of sewer corrosion: Influence ot temperature, relative humidity and H_2S concentration. *Water Research.* 46(13): 4235 – 4245.

Juvekar, V. A., & Sharma, M. M. 1973. Absorption of CO_2 in a suspension of lime. *Chemical Engineering Science.* 28: 825 – 837.

Kaempfer, W., & Berndt, M. 1999. Estimation of service life of concrete pipes in sewer networks. *Proceedings of the 8th Conference on Durability of Building Materials and Components*. May 30 – June 3. Vancouver. 36 – 45.

Karavaiko, G. I., & Pivovarova, T. A. 1973. Oxidation of elementary sulphur by *Thiobacillus thiooxidans. Microbiology.* 42(3): 389 – 395.

Keck, R. H., & Riggs, E. H. 1997. Specifying fly ash for durable concrete. *Concrete International.* 19(4): 35 – 38.

Kelly, D. P., & Wood, A. P. 2000. Reclassification of some species of Thiobacillus to the newly designated genera Acidithiobacillus gen. nov., Halothiobacillus gen. nov., and Thermithiobacillus gen. nov. *International Journal of Systematic and Evolutionary Microbiology.* 50: 511 – 516.

Kelly, D. P., McDonald, I. R., & Wood, A. P. 2000. Proposal for the reclassification of Thiobacillus novellus as Starkeya novella gen. nov., in the alpha-subclass of the Proteobacteria. *International Journal of Systematic and Evolutionary Microbiology.* 50: 1797 – 1802.

Kempner, E. S. 1966. Acid production by *Thiobacillus thiooxidans*. *Journal of Bacteriology.* 92(6): 1842 – 1843.

Kjelleberg, S., & Givskov, M. Eds. 2007. *The biofilm mode of life: Mechanisms and adaptations*. Norfolk: Horizon Bioscience.

Kley, G. & Caradot, N. 2013. *Review of sewer deterioration models*. Berlin: KWB.

Kosmatka, S. H., Kerkhoff, B., & Panarese, W. C. 2003. *Design and control of concrete mixtures.* 14th ed. Skokie: Portland Cement Association.

Kurdowski, W. 2014. *Cement and concrete chemistry*. Dordrecht: Springer.

Lawrence, D. C. 1998. The production of low-energy cements. In: Hewlett, P. C. Eds. *Lea's chemistry of cement and concrete*. 4th ed. Oxford: Elsiever.

Lea, F. M. 1965. The action of ammonia salts on concrete. *Magazine of Concrete Research.* 17(52): 115 – 116.

Lea, F. M. 1970. *The Chemistry of Cement and Concrete.* 3rd ed. London: Edward Arnold.

Lenk, S. 2006. Diversity and abundance of sulphur-oxidising bacteria in Wadden Sea sediments revealed by DsrAB phylogeny and *dsrAB*-targeted real-time PCR. MSc dissertation. University of Bremen, Bremen.

Lewis, R., Sear, L., Wainwright, P., & Ryle, R. 2003. Cementitious additions. In: Newmann, J., & Choo, B. S. Eds. *Advanced Concrete Technology – Constituent Materials*. Oxford: Elsiever.

Locher, F. W. 1986. Low energy clinker. *Proceedings of the 8th International Congress on the Chemistry of Cement.* September 22 – 27. Rio de Janeiro. 57 – 67.

Lothenbach, B., Scrivener, K., & Hooton, R. D. 2011. Supplementary cementitious materials. *Cement and Concrete Research.* 41(12): 1244 – 1256.

Lu, Y. 2001. Modelling of sulphide emission from the Virginia sewer system. MSc (Eng) dissertation. University of Cape Town, Cape Town.

Ludwig, U., & Pöhlmann, R. 1986. Investigation on the production of low lime Portland cements. *Proceedings of the 8th International Congress on the Chemistry of Cement.* September 22 – 27. Rio de Janeiro. 363 – 371.

Majumdar, A. J., & Singh, B. 1992. Properties of some blended high-alumina cements. *Cement and Concrete Research*. 22(6): 1101 – 1104.

Malik, M. 1996. In-sewer treatment of domestic wastewater. PhD dissertation. University of Newcastle upon Tyne, Newcastle.

Mara, D., & Horan, N. Eds. 2003. *The Handbook of Water and Wastewater Microbiology*. London: Elsevier.

Marlow, D., Davis, P., Trans, D., Beale, D., & Burn, S. 2009. Remaining asset life: A State-of-the-Art Review – Final Report. Alexandria: WERF.

McLaren, F.R. 1984. *Design manual: Sulphide and corrosion prediction control*. Virginia: American Concrete Pipe Association.

McMurry, P. H., Takano, H., & Anderson, G. R. 1983. Study of the ammonia (gas) sulphuric acid (aerosol) reaction rate. *Environmental Science and Technology.* 17(6): 347 – 352.

McWilliams, N., & Parmer, A. 2010. The largest cured-in-place-pipe rehabilitation project in the country. *The 18th Annual Sharing Technologies Seminar.* February 18. Berkeley.

Mehta, P. K., & Manmohan, D. 1980. Pore size distribution and permeability of hardened cement pastes. *Proceedings of the 7th International Symposium of the Chemistry of Cement.* June 30 – July 4. Paris. 181 – 185.

Mehta, P. K., & Monteiro, P. J. M. 2013. *Concrete: Microstructure, properties, and materials*. 3rd ed. New Delhi: McGraw-Hill.

Michael, H. G. 2007. Oxidation reduction potential and wastewater treatment. Interstate Water Report. New England Interstate Water Pollution Control Commission, NE.

Midgley, H. G., & Rao, P. B. 1978. Formation of stratlingite, $2CaO.SiO_2.Al_2O_3.8H_2O$), in relation to the hydration of high alumina cement. *Cement and Concrete Research.* 8(2): 169 – 172.

Morel, F. M. M. 1983. *Principles of aquatic chemistry.* New York: John Wiley and Sons.

Mori, T., Nonaka, T., Tazaki, K., Koga, M., Hikosaka, Y., & Noda, S. 1992. Interactions of nutrients, moisture and pH on microbial corrosion of concrete sewer pipes. *Water Research*. 26(1): 29 – 37.

Neethling, J. B., Mah, R. A., & Stenstrom, M. K. 1989. Causes and control of concrete pipe corrosion. Annual report to County Sanitation Districts of Los Angeles. University of California, Los Angeles, CA.

Neville, A. M. 2011. *Properties of concrete*. 5th ed. Harlow: Pearson.

Nielsen, A. H., & Hvitved-Jacobsen, T. 2008. Effect of sulphate and organic matter on the hydrogen sulphide formation in biofilms of filled sanitary sewers. *Water Pollution Control Federation.* 60: 627 – 634.

Nielsen, A. H., Hvitved-Jacobsen, T., & Vollertsen, J. 2006. Recent findings on sinks for sulphide in gravity sewer. *Water Science Technology*. 54(6): 127 – 134.

Nielsen, A. H., Hvitved-Jacobsen, T., Vollertsen, J. 2008a. Effect of pH and iron concentrations on sulphide concentrations in wastewater collection systems. *Water Environment Research*. 80(4): 380 – 384.

Nielsen, A. H., Vollertsen, J., Jensen, H. S., Wium-Andersen, T., & Hvitved-Jacobsen, T. 2008b. Influence of pipe material and surfaces on sulphide related odor and corrosion in sewers. *Water Research*. 42(15): 4206 – 4214.

Nixon, R. 1997. Future material selection guidelines for coatings on concrete for changing exposure conditions in large municipal wastewater collection and treatment systems. *National Association of Corrosion Engineers Annual Conference.* March 9 – 14. New Orleans.

Odler, I. 2005. *Special inorganic cements.* London: Taylor & Francis.

O'Hara, G. W., Goss, T. J., Dilworth, M. J., & Glenn, A. J. 1989. Maintenance of intracellular pH and acid tolerance in *Rhizobium meliloti*. *Applied and Environmental Microbiology.* 155: 1870 – 1876.

Okabe, S., Odagiri, M., Itoh, T., & Satoh, H. 2007. Succession of sulphur-oxidizing bacteria in the microbial community on corroding concrete in sewer systems. *Applied and Environmental Microbiology*. 73(3): 971 – 980.

Osborne, G. 1994. BRECEM: A rapid hardening cement based on high alumina cement. *Structures and Buildings.* 104(1): 93 – 100.

Parande, A. K., Ramsamy, P. L., Ethirajan, S., Rao, C. R. K., & Palanisamy, N. 2006. Deterioration of reinforced concrete in sewer environments. *Municipal Engineer.* 159: 11 – 20.

Parker, C. D., & Prisk, J. 1953. The oxidation of inorganic compounds of sulphur byvarious sulphur bacteria. *Journal of General and Applied Microbiology.* 8(3): 344 – 364.

Paulini, P. 1994. A Through Solution Model for volume changes of cement hydration. *Cement and Concrere Research.* 24(3): 488 – 496.

Pelisser, F., Gleize, P. J. P., & Mikowski, A. 2012. Effect of the Ca/Si molar ratio on the micro/nanomechanical properties of synthetic C-S-H measured by nanoindentation. *Physical Chemistry.* 116: 17219 – 17227.

Pickell, M. B. Eds. 1993. Pipeline infrastructure II. *Proceedings of the American Society of Civil Engineers Conference*. August 16 – 17. San Antonio. 647 – 670.

Pomeroy, R. D., & Parkhurst, J. D. 1977. *Progress in water technology.* London: Pergammon.

Pomeroy, R., & Bowlus, F. D. 1946. Progress report on sulphide control research. *Sewage Works Journal*. 18(4): 597 – 640.

Powers, T. C. 1958. Structure and physical properties of hydrated Portland cement paste. *Journal of the American Ceramic Society.* 41(1): 1 – 6.

Punmia, B. C., Jain, A. K., & Jain, A. K. 2004. *Basic civil engineering.* New Delhi: Laxmi Publications

Quillin, K., Osborne, G., Majumdar, A., & Singh, B. 2001. Effects of w/c ratio and curing conditions on strength development in BRECEM concretes. *Cement and Concrete Research.* 31(4): 627 – 632.

Rahman, M. M., & Bassuoni, M. T. 2014. Thaumasite sulphate attack on concrete: Mechanisms, influential factors and mitigation. *Construction and Building Materials.* 73: 652 – 662.

Renaudin, G. 1998. Study of a single aluminium hydroxide: The bayerite, II. Study of a family of layered double hydroxides of aluminium and calcium: AFm phases. PhD dissertation. University Henri Poincaré, Nancy.

Rigdon, J. H., & Berdsley, C. W. 1956. Corrosion of concrete by autotrophs. *Corrosion*. 5: 60 – 62.

Rinaldi, R., Sacerdoti, M., & Passaglia, E. 1990. Stratlingite: Crystal structure, chemistry and a re-examination of its polytype vertumnite. *European Journal of Mineralogy.* 2(6): 841 – 849.

Sahmaran, M. 2010. Deterioration mechanisms – chemical. In: Soutsos, M. Eds. *Concrete durability: A practical guide to the design of durable concrete structures*. London: Thomas Telford.

Sand, W., & Bock, E. 1984. Concrete corrosion in the Hamburg sewer system. *Environmental Technology Letters.* 5(12): 517 – 528.

Scheller, T., & Kuzel, H. 1976. Studies on calcium aluminate hydrates. *6th International Congress on the Chemistry of Cement.* 2(1): 217.

Schmidt, T. 2009. Modelling sewer deterioration processes with condition data. PhD dissertation. Technical University Dresden, Dresden.

Scrivener, K. L. 1989. The microstructure of concrete. In: Skalny, J. P. Eds. *Materials Science of Concrete.* Westerville: The American Ceramic Society. 127.

Scrivener, K. L., & De Belie, N. 2013. Biogenic sulphuric acid attack of cementitious materials in sewage systems. In: Alexander, M., Bertron, A., & De Belie, N. Eds. *Performance of cement-based materials in aggressive aqueous environments: State-of-the-Art Report, RILEM TC 211-PAE*. Netherlands: Springer. 305 – 318.

Sharma, P. D. 2007. *Microbiology.* 2nd ed. New Delhi: Rakesh Kumar Rastogi.

Siddique, R., & Khan, M. I. 2011. *Supplementary cementing materials.* Berlin: Springer.

Singh, B., & Majumdar, A. J. 1992. The hydration of calcium dialuminate and its mixtures containing slag. *Cement and Concrete Research.* 22(6): 1019 – 1026.

Smith, F. L., & Harvey, A. H. 2007. Avoid common pitfalls when using Henry's law. *Chemical Engineering Progress.* September. 33 – 39.

Smith, J. H., Bomberger, D. C., & Haynes, D. L. 1981. Volatilization rates of intermediate and low volatility chemicals from water. *Chemosphere*. 10: 281.

Soenen, S. J., Cuyper, M., Smedt, S. C., & Braeckmans, K. 2012. Investigating the toxic effects of iron oxide nanoparticles. *Methods in Enzymology.* 509: 195 – 224.

Stark, J., Müller, A., Schrader, R., & Rümpler, K. 1981. Existence conditions of hydraulically active belite cement. *ZKG International.* 34: 476 – 481.

Taylor, H. F. W. 1997. *Cement chemistry*. 2nd ed. London: Thomas Telford Publishing.

Tchobanoglous, G., Burton, F. L., & Stensel, H. D. Eds. 2003. *Wastewater engineering: Treatment and reuse.* 4th ed. New York: McGraw-Hill.

Thistlethwayte, D. K. 1972. *Control of sulphide in sewage systems*. Michigan: Ann Arbor.

Tran, D. H., Perera, B. J. C., & Ng, A. W. M. 2007. Neural network based prediction models for structural deterioration of urban drainage pipes. In: Oxley, L. & Kulasiri, D. Eds. *MODSIM 2007 International Congress on Modelling and Simulation*. December 10 – 13. Christchurch.

Trun, N. J., & Gottesman, S. 1990. On the bacterial cell cycle: Escherichia coli mutants with altered ploidy. *Genes and Development.* 4: 2036 – 2047.

Ulm, F. J., Bazant, Z. P., Wittmann, F. H. Eds. 2001. *Creep, shrinkage and durability mechanics of concrete and other quasi-brittle materials.* Cambridge: Oxford, Elsevier.

Valix, M., Zamri, D., Mineyama, H., Cheung, W. H., Shi, J., & Bustamante, H. 2012. Microbiologically induced corrosion of concrete and protective coatings in gravity sewers. *Chinese Journal of Chemical Engineering.* 20(3): 433 – 438.

Viehl, K. 1950. The influence of temperature on biological changes in water and sludge with special consideration of the effect of warm water discharges on the receiving stream. *Sewage and Industrial Waste*s. 23: 943.

Vollersten, J., & König, A. 2005. WP2 Report D6: Model testing and evaluation. *Computer Aided Rehabilitation of Sewer Networks (Care-S)*. SINTEF Technology and Society, Trondheim.

Vollertsen, J., Nielsen, A. H., Jensen, H. S., Rudelle, E. A., & Hvitved-Jacobsen, T. 2011. Modelling the corrosion of concrete sewers. *12th International Conference on Urban Drainage*. September 11 – 16. Porto Alegre.

Vongvisessomjai, N., Tingsanchali, T., & Babel, M. S. 2010. Non-deposition design criteria for sewers with part-full flow. *Urban Water.* 7(1): 61 – 77.

Wachtershauser, G. 1990. The case for the chemoautotrophic origin of life in an iron-sulphur world. *Origins of Life and Evolution of the Biosphere.* 20: 173 – 176.

Waksman, S. 1932. *Principles of soil microbiology*. Baltimore: Williams and Wilkins.

Weissenberger, J., Duffourg, J. M., & Vdi/Vde, V. 2004. Avoidance of odour emission from biosolids with the help of the Nutriox® concept - results from a trial at La Crau treatment plant (France). *International Conference on Environmental Odour Management*. November 17 – 19. Cologne.

Werner, K. C., Chen, Y. X., & Odler, I. 2000. Invetsigations on stress corrosion of hardened cement pastes. *Cement and Concrete Research.* 30(9): 1443 – 1451.

Wierig, H. 1984. Long time studies on the carbonation of concrete under normal outdoor conditions. *Proceedings of the RILEM Seminar on the Durability of Concrete Structures under Normal Outdoor Exposure.* March 26 – 29. Hannover. 239 – 249.

Wolfram, S. 2002. *A new kind of science.* Chapaign: Wolfram Media.

Chapter Three: A review of work undertaken in relation to the Virginia Experimental Sewer, South Africa

3.1 Background

The problem of concrete sewer pipe corrosion due to biogenic H_2SO_4 attack is prevalent in South Africa, as in many countries, particularly sub-tropical and tropical countries mainly due to the climatic characteristics. In 1949, the Town Engineer of Springs in Gauteng, South Africa produced a report on severe corrosion of the outfall sewer serving the town. Based on this report, the Transvaal Association of City and Town Engineers recommended further research to determine the fundamental reasons for the failure of cement-based sewers in South Africa, and to endeavour to find a solution to this problem. In this regard, a team consisting of consultants, pipe manufacturers, municipalities, and the South African Council for Scientific and Industrial Research (CSIR) proposed that the problem be considered in three aspects (CSIR, 1959):

(1) The microbiological aspects to elucidate or confirm the mechanisms by which H_2SO_4 was produced in a sewer environment, and a study of means by which this process could be interrupted or inhibited.
(2) Field aspects involving study of factors related to design, construction and operation of sewers having a bearing on location and severity of corrosion.
(3) A study of the possibilities of using construction materials which were more resistant to biogenic H_2SO_4 attack.

These three extensive studies took place simultaneously and culminated in the publication of a book on the subject in which several recommendations were made (CSIR, 1959). These recommendations included (i) minimising the retention time in the rising mains, the sumps or in both facilities (ii) using pneumatic ejectors or air pumps in pumping stations (iii) having the rising main discharge into some form of stilling chamber which is ventilated and separated from the sewer by a water seal (iv) installing sewers at 'optimal' depths to minimise the effect of (high) temperature on sulphide generation (v) occasional dosing of suitable alkalis to alter the pH of the sewage in order to suppress the generation of hydrogen sulphide (vi) flooding sewers to disrupt the activities of SOB, and to dilute and wash away H_2SO_4 formed on the non-submerged walls. However, the most significant of these recommendations was to pay attention to sewer hydraulics in order to avoid high velocities and turbulence so as to minimise H_2S (gas) release from the sewage, and to use calcareous aggregate, usually dolomite (DOL) ($CaMg(CO_3)_2$) which provides more alkalinity to a concrete matrix thereby contributing to the neutralisation of the biogenic H_2SO_4 attack.

Based on these recommendations, it was decided by a study group, established under the auspices of CSIR in 1986, to set up facilities that would allow for monitoring the actual performance of various cement-based mixtures that are used in the manufacture of sewer pipes (CSIR, 1996). These facilities were to be designed and incorporated in new outfall sewers in order to act as 'live' laboratories. Three outfall sewer sections were designed for this experimental work in South Africa, based on the potential H_2S concentration in the sewer headspace, since their climatic characteristics were similar. Two of these experimental outfall sewer sections, Boksburg and Klerksdorp are briefly discussed in Sections 3.2 and 3.3 respectively, whereas the Virginia experimental sewer, the main subject of this Chapter, is discussed in Section 3.4.

3.2 Boksburg experimental sewer

This outfall sewer, located in Boksburg Gauteng Province, was completed in November 1989. The location of the Boksburg sewer experiences a wide range of temperature and RH gradients. The monthly average-high ambient temperature is 27 °C in summer (occasionally 18 °C in winter) while the monthly average-low ambient temperature is 2 °C in winter (occasionally 15 °C in summer). From time to time, the monthly ambient temperatures reach 35 °C in summer (occasionally 25 °C in winter) and -8 °C in winter (occasionally 7 °C in summer. The monthly average ambient RH varies between

46% and 68%. These profiles are given in Appendix A. Boksburg's experimental sewer section consisted of 1300 mm OD pipes that were categorised in three groups; unprotected asbestos-cement (AC), protected AC, and unprotected Portland cement with dolomite aggregate (PC/DOL). The protected samples consisted of AC coated with epoxy tar, epoxy, polyurethane and bitumen.

The first inspection was done after the sewer had been in operation for 15 months, in February 1991. At the time of inspection, the average sewage flow was about 8 Ml/day (the dry weather and wet weather peak flows were 12 Ml/day and 16 Ml/day respectively). No H_2S was detected in the sewer headspace at the time of inspection even though this was during the summer period. Generally, all the pipes appeared to be in a 'very good' condition, although a 'thin and soft' layer had formed on the unprotected AC and PC/DOL (CSIR, 1996). Data on temperature in the sewer headspace was not recorded during this inspection. No documented information on the performance of the pipe samples that were installed in this experimental sewer section has been found beyond the first inspection.

3.3 Klerksdorp experimental sewer

This outfall sewer, located in Klerksdorp North West Province, was completed around July 1987. The location of the Klerksdorp sewer also experiences a wide range of temperature and RH gradients. The monthly average-high ambient temperature is 29 °C in summer (occasionally 20 °C in winter) while the monthly average-low ambient temperature is 1 °C in winter (occasionally 15 °C in summer). From time to time, the monthly ambient temperatures reach 44 °C in summer (occasionally 26 °C in winter) and -9 °C in winter (occasionally 6 °C in summer. The monthly average ambient RH varies between 45% and 64%. These profiles are given in Appendix A. Klerksdorp's experimental section consisted of 1300 mm OD pipes that were categorised in two groups; unprotected AC and protected AC. The protected samples consisted of AC coated with epoxy tar, epoxy and polyurethane.

The first inspection was done after the sewer had been in operation for about 42 months, in February 1991. At the time of inspection, the average sewage flow was about 12 Ml/day (the dry weather and wet weather peak flows were 19 Ml/day and 35 Ml/day respectively). The H_2S concentration in the headspace of the entrance manhole to this experimental section was 5 ppm. Generally, all the pipe samples appeared to be in a 'good' condition (CSIR, 1996). Data on temperature in the entrance manhole (and sewer) headspace was not recorded during this inspection. Similarly, no documented information on the performance of the pipe samples that were installed in this experimental sewer section has been found beyond the first inspection.

3.4 Virginia experimental sewer (VES)

3.4.1 Introduction

This 63 m experimental line of 900 mm diameter (by 2.44 m length) sewer pipes installed alongside a bypass line (at a depth of approximately 3 m), both being part of the Virginia sewer located in Free State Province (Figure 3-1), was completed in 1988 and commissioned in March 1989 (CSIR, 1996). The Virginia sewer consists of the Virginia town reticulation system (Town pump station, Oryx Avenue and Prisons ground networks) whose sewers and interceptors all empty into a main pump station. The rising main from this main pump station discharges into a manhole that is located approximately 600 m upstream of an inlet manhole (IM) to both the bypass line and experimental line (Figure 3-2). This experimental line is the so-called Virginia Experimental Sewer (VES). Photographs of typical samples installed in the VES are shown in Figure 3-3.

The IM to the VES and the bypass line has two gate valves that are used to control sewage flow from the upstream section. These gate valves are used to ensure that the sewage flows either through the VES or the bypass line at any particular time, depending on the inspection schedules for data collection from the VES.

Figure 3-1: Geographical location of the Virginia Experimental Sewer (VES), Free State Province.

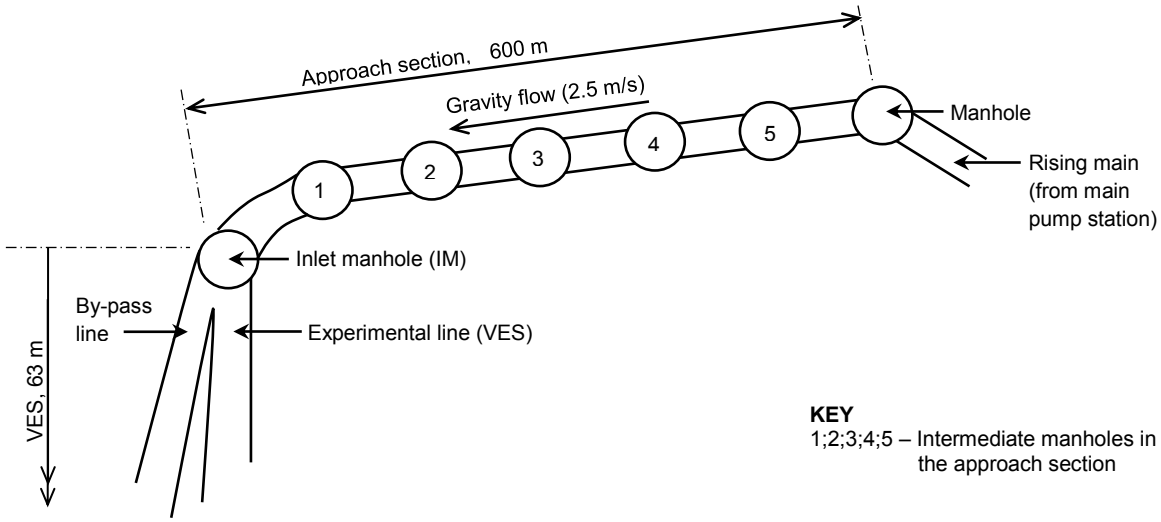

Figure 3-2: Schematic of a section of the Virginia sewer showing gravity sewer feeding into the VES, 600 m downstream of the rising main (Alexander et al., 2008).

(a) Pipe sections (samples) of different concrete mixtures

(b) Typical 'lid' samples removed for inspection and core samples suspended in the sewer

Figure 3-3 (a) and (b): Photos showing typical samples at the VES.

Similar to the locations of both Boksburg and Klerksdorp experimental sewers, the location of the Virginia sewer also experiences a wide range of temperature and RH gradients. The monthly average-high ambient temperatures are 30 °C in summer (occasionally 18 °C in winter) while the monthly average-low ambient temperatures are -1 °C in winter (occasionally 15 °C in summer). From time to time, the monthly ambient temperatures reach 38 °C in summer (occasionally 25 °C in winter) and -9 °C in winter (occasionally 5 °C in summer. The monthly average ambient RH varies between 45% and 66%. Within the sewer's headspace of the VES, daily temperatures reach 27 °C in summer (occasionally 22 °C in winter), and the daily RH is above 70%. These profiles are given in Appendix A.

Certain conditions (such as flat terrain that necessitates pumping, and turbulence where there is change in direction of sewage flow) upstream of the VES tend to lead to higher concentrations of H_2S in the VES' headspace, when compared to both Boksburg and Klerksdorp. It is important to note that the VES was designed with a sewage flow velocity of 2.5 m/s, which does not allow for sulphide build-up within this section (CSIR, 1996). The average daytime H_2S concentration in the IM is up to 86 ppm in summer and 20 ppm in winter. Most of this H_2S 'escapes' downstream to VES (when the gate valve to the bypass line is closed) where concentrations reach up to 50 ppm in summer and 10 ppm in winter. Typical H_2S profiles in the IM and the VES during summer and winter months recorded during the current study are given in Figure 3-4, whereas the typical H_2S profiles in the IM and the VES for all climatic seasons (summer, autumn, winter and spring) recorded during the current study are given in Appendix B.

The characteristic sewer parameters that include temperature and H_2S concentration prevailing in the VES headspace are ideal for the generation of biogenic H_2SO_4 that attacks the acid-soluble portions in concrete (and cement-based) matrices (Krüger, 1990). A sewer containing an H_2S concentration of between 2 ppm to 6 ppm results in the formation of biogenic H_2SO_4 of 6% v/v (pH <1) on the sewer's non-submerged moist walls when the headspace temperature is in the order of 18 °C (Schremmer, 1972). This acid concentration is typical of that found on the corroded non-submerged surfaces of cement-based pipes in sewers (CSIR, 1996). Therefore the conditions in the VES can be said to be aggressive with regard to biogenic acid (H_2SO_4) attack of cement-based sewer pipes. It is for this reason that the VES has been used continually for over 25 years to monitor the actual performance of various cement-based mixtures that are used in the manufacture of concrete sewer pipes.

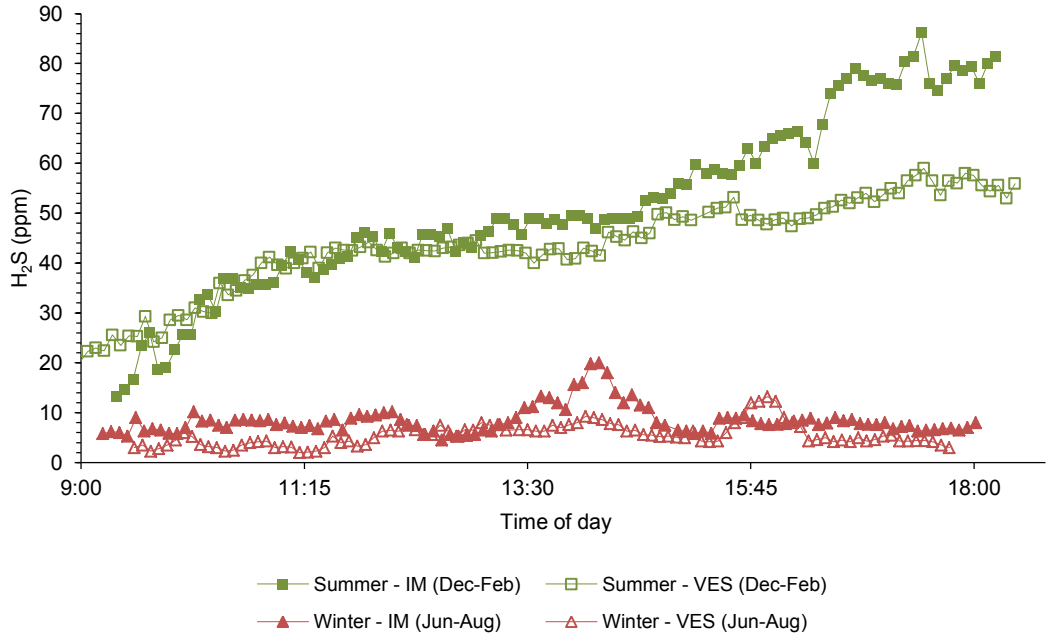

Figure 3-4: Typical H_2S profiles in the IM and VES during summer and winter months (data from current study (2013-2015)).

Since inception, studies in the VES have been undertaken by different researchers in phases.

3.4.2 Phase I work by CSIR

CSIR was responsible for the design and installation of various cement-based sewer pipe samples in VES prior to the actual monitoring of their performance in this 'live' environment. Therefore, this first phase commenced in 1986 (planning, design and implementation) and ended in 1995. The main objectives of this phase of study included the following (CSIR, 1996):

(1) Monitoring the temperature, pH, COD and sulphide content of the sewage flowing through the VES, and the H_2S concentration in the VES headspace.
(2) Monitoring and recording the condition of the various pipe samples installed in the VES on a regular basis.

In order to meet these objectives, nine different types of sewer pipe materials (samples), in three categories, were installed in the VES. Eight of these sewer pipes were cement-based samples while one was a high-density polyethylene (HDPE) pipe. The three categories of samples were (i) unprotected cementitious, (ii) protected cementitious, and (iii) HDPE. The unprotected cementitious category consisted of Portland cement (PC)-based with siliceous aggregate (PC/SIL) concrete, PC-based with dolomite aggregate (PC/DOL) concrete, calcium aluminate cement (CAC)-based with siliceous aggregate (CAC/SIL) concrete, and asbestos-cement (AC)-based samples. The protected samples consisted of PC/SIL with a post-installed HDPE lining, and AC coated with epoxy tar, polyurethane and epoxy (Goyns et al., 2003). The layout of these nine different types of sewer pipes and the mix composition (also given in Table 3-1) of the unprotected cementitious category of samples are given in Appendix C (Goyns, 2003; CSIR, 1996).

Table 3-1: Mixture composition of the unprotected cementitious category of samples installed in the VES during 1988 (Goyns, 2003; CSIR, 1996).

Sewer pipe materials/description	Binder		Aggregate					
			Stone		Sand		Other	
	Type	%	Type	%	Type	%	Type	%
Unprotected PC/SIL	PC*	15	SIL	50	SIL	35	-	-
Unprotected PC/DOL	PC*	15	DOL	50	SIL	35	-	-
Unprotected CAC/SIL	CAC[#]	20	SIL	42	SIL	38	-	-
Unprotected AC	PC**	85	-	-	-	-	Asbestos fibre	15

*Rapid-hardening Portland cement
**Portland blastfurnace cement
[#]Calcium (high) aluminate cement

The findings from this phase of study, which was undertaken between 1988 and 1995, are highlighted below.

3.4.2.1 Findings on measured sewer environment parameters (from 1989 to 1995)

(i) The temperature of the sewage varied from 16 °C in winter to 28 °C in summer, whereas the mean temperature in the sewer headspace throughout all the climatic seasons was 22 ± 2 °C. These relatively warm temperatures are considered favourable for microbial (SOB) activity. The temperature of the sewage was reported to have a low diurnal variation in any particular climatic season since the ground provides effective insulation against heat transfer.
(ii) The pH of the sewage measured from 1989 to 1995 ranged between 6.0 and 7.7, with a mean of 7.0. This pH range indicates that the sewage is virtually neutral, and any dissolved sulphides in the sewage would predominantly be present as H_2S.
(iii) The COD measured from 1988 to 1993 ranged between 112 ppm and 912 ppm, with a mean of about 400 ppm. These values of COD, which are typical in outfall sewers, had no clear relationship with specific seasons of the year.
(iv) The total dissolved sulphide content of the sewage varied from zero to 1.4 ppm. Such contents could be a significant source for the generation of H_2S under septic sewage conditions.
(v) The H_2S concentration in the sewer headspace was, on average, 49 ppm, occasionally up to 60 ppm whereas that in the IM reached 85 ppm at certain periods of the day. Under certain

conditions, these levels of H_2S concentration result in aggressive environments for the generation of biogenic H_2SO_4.

3.4.2.2 Findings on the performance of the various cement-based pipe samples installed in VES

Generally, the unprotected samples showed greater depths of attack than coated and lined samples during this period of study. Of the three binder systems used in these unprotected samples, CAC-based mixtures offered the best resistance against biogenic H_2SO_4 attack, followed by AC-based mixtures, whereas PC-based mixtures had the worst performance. Coated samples showed minimal attack whereas HDPE-lined samples did not experience biogenic H_2SO_4 attack. The respective performances of these samples are further highlighted below.

(i) The PC/SIL pipe samples with 70 mm thick walls had depths of attack of about 30 mm in some sections. This depth of attack, representing about 43% loss of wall thickness was greater than the cover to reinforcing steel. Reinforcing steel was visible in most sections of the samples and particularly around the daily sewage flow level where the products of corrosion were consistently being washed away and 'fresh' surfaces exposed to biogenic H_2SO_4 attack.
(ii) The PC/DOL pipe samples with 70 mm thick walls had depths of attack of between 10 mm and 15 mm, representing a loss of wall thickness of between 14% and 21%, approximately.
(iii) The AC-based pipe samples with 47 mm thick walls had depths of attack of about 10 mm to 12 mm, representing a loss of the wall thickness of between 21% and 25%.
(iv) The CAC/SIL pipe samples with 70 mm thick walls had depths of attack of about 5 mm to 10 mm, representing a loss of the wall thickness of between 7% and 14%.
(v) The epoxy tar, polyurethane and epoxy coatings appeared to offer resistance to biogenic H_2SO_4. The only areas that experienced severe attack in these pipes were around the pipe joints, and this relates more to improper laying techniques of the pipes which exposes unprotected surfaces rather than to the performance of the material (coatings).
(vi) The HDPE-lined pipe samples did not experience any biogenic H_2SO_4 attack.

3.4.2.3 Conclusions from Phase I work by CSIR

Phase I work by CSIR was undertaken between 1988 and 1995. During this period, the main objectives of the study were satisfactorily addressed. The following significant conclusions were drawn from this phase of study:

(i) Even though the flow velocity of 2.5 m/s within VES is too high for sulphide build-up to occur, aggressive conditions exist for generation of biogenic H_2SO_4. This is due to relatively high average concentrations of H_2S gas (> 49 ppm) in VES headspace. The sulphide build-up leading to the release of these levels of H_2S occurs in the upstream section of the pump station (located more than 1300 m from the VES).
(ii) Certain unprotected cement-based materials can be used successfully in sewers where less aggressive conditions exist.
(iii) CAC-based concrete mixtures exhibited superior performance in comparison to other cementitious mixtures (PC- and AC-based).
(iv) If correctly installed, coated and HDPE-lined concrete pipes afford protection against biogenic H_2SO_4 attack.

From the conclusions presented above, particularly with regard to the superior performance of CAC-based concrete mixtures in comparison to PC-based concrete mixtures, opportunities exist for further research focussing on the characteristics of these concrete mixtures. Results from such research will provide a better understanding of the respective mechanisms of attack when these mixtures are subjected to biogenic H_2SO_4 attack, and subsequently be incorporated in certain principles of concrete mix design. This is one of the objectives of the current study.

3.4.3 Phase II work by CMA, assisted by UCT

This phase of study was undertaken by the Concrete Manufacturers Association (CMA) of South Africa, assisted by the Department of Civil Engineering at UCT from 1995 to 2003. The main objectives of this phase, undertaken by different researchers at different periods, were:

(1) To develop a laboratory test to measure acid resistance of concrete used in the manufacture of sewer pipes (Fourie, 2007).
(2) To evaluate the impact of the composition of concrete mixtures on the resistance (mass loss) and attack mechanisms (hydrogen ion consumption) when these mixtures are subjected to both mineral and biogenic H_2SO_4 (Fourie, 2007).
(3) To model (develop a kinetic equation) for H_2S emission in the Virginia sewer in terms of flow characteristics using a computer program that is used for the identification and simulation of aquatic systems (AQUASIM) as the mathematical integrator (Lu, 2001).
(4) To establish the actual corrosion rates of certain cement-based sewer pipe materials by undertaking actual measurements of wall thicknesses of pipes samples that were to be removed from VES based on their state of deterioration (Goyns, 2003).

The set up for these studies was twofold; at UCT's Department of Civil Engineering (concrete materials laboratory) and in VES. In order to undertake studies within the laboratory to address objectives (1) and (2) above, a rig was designed to test core concrete specimens (80 mm in diameter x 150 mm) in strong acid solutions. The rig had rollers that allowed the concrete core specimens to be continuously rotated and brushed so as to mimic the situation in the zone between daily sewage flow levels, where corroded concrete is continuously removed by action of flowing sewage thereby exposing 'fresh' (un-attacked) concrete matrices. The rig consisted of a 72-litre (length 800 mm, width 300 mm, depth 300 mm) compartment made of 10 mm thick polyvinyl chloride (PVC) sheeting. Two rubberised steel rollers approximately 50 mm apart at the bottom-centre, and a soft PVC-bristle brush supported at the top-centre, span the compartment length. A motor driving a rubber belt over pulleys attached to the axle on the outside of the compartment rotates the rubberised steel rollers at approximately 16 revolutions per minute. A schematic of the rig's cross-section is given in Figure 3-5.

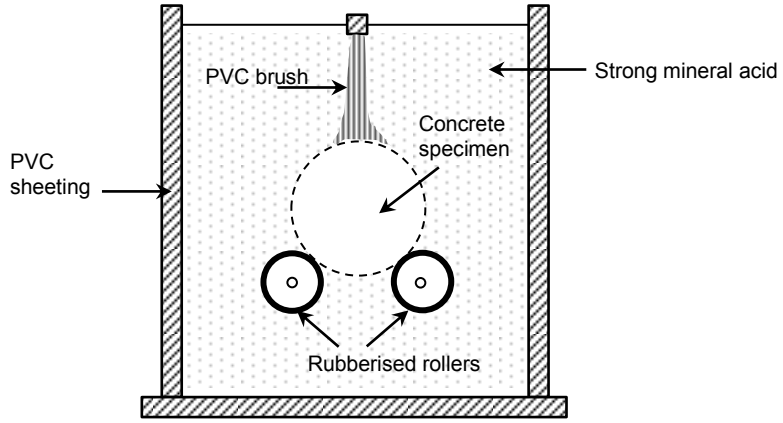

Figure 3-5: Schematic of the cross-section of rig used to rotate and brush concrete specimens in a strong mineral acid solution (Alexander and Fourie, 2011).

As discussed in Part Two of Chapter Two, when concrete sewer pipes are subjected to biogenic H_2SO_4 attack, there is a build-up of a gypsum layer on the surface of these pipes, which is continuously dissolved and removed by the action of flowing sewage at the daily flow level. In order to simulate acid attack of concrete in a sewer environment, preliminary tests were undertaken on PC/DOL concrete cylinders (made from similar concrete mixtures as those used in the industry for the manufacture of sewer pipes) immersed in a mineral H_2SO_4 solution (at pH = 1.00) to assess the rate of build-up of this gypsum layer (as well as the rate of saturation of the acid solution with Ca^{2+} and other ions). Generally, two types of dolomite aggregates were used in this phase of study; high quality (DOL 3) and low quality (DOL 2) (see details in Table 3-2 and Table 3-3, and also in Appendix D).

The mineral acid studies incorporated DOL 3 aggregate only (in-situ studies discussed in later sections incorporated both DOL 2 and DOL 3 aggregates). The concrete cylinders were cast using a specially developed heavy mechanical compaction technique (see details in Chapter Four) that gave similar properties of concrete (density, acid insolubility, oxygen permeability, water sorptivity, porosity, splitting tensile and compressive strength) as the roller suspension manufacturing process used in South Africa in which compaction is achieved by the kneading action and centrifugal force during casting (Fourie, 2007).

Table 3-2: Concrete mixture proportions (ratio by mass to total binder content) of core samples used in the laboratory for mineral acid tests (Alexander and Fourie, 2011).

Mixture[#]	% binder	w/b	Binder		DOL aggregate	
			SCM	Cement	Stone**	Crusher sand
Sewer pipe mixtures:						
PC/DOL 3	18	0.30	-	1.00	2.28	2.28
PC/GGBS/DOL 3	18	0.30	0.50	0.50	2.28	2.28
PC/FA/DOL 3	18	0.30	0.30	0.70	2.28	2.28
PC/SF/DOL 3*	18	0.28	0.10	0.90	2.28	2.28
PC/MK/DOL 3*	18	0.30	0.10	0.90	2.28	2.28
CAC/DOL 3	18	0.30	-	1.00	2.28	2.28
Lining mixtures:						
PC/DOL 3	23	0.28	-	1.00	1.67	1.67
CAC/DOL 3	23	0.28	-	1.00	1.67	1.67
CAC/ Alag^{TM}	18	0.33	-	1.00	2.28	2.28
CAC/Alag^{TM}	23	0.28	-	1.00	1.67	1.67
CAC/SF/Alag^{TM}	23	0.24	0.1	0.90	1.67	1.67

[#]All aggregates crushed; DOL 3 = high quality dolomite (acid insolub. < 6%, 10% FACT = 354); Alag^{TM} = aluminate aggregate
*SF = silica fume; MK = metakaolin; superplasticiser (1%) used for workability and dispersion
**Nominal 13 mm maximum size used for sewer pipe mixtures and nominal 6 mm maximum size for lining mixtures

Results from these preliminary tests showed that the rate of attack was high directly after immersion of the specimens in mineral H_2SO_4 but decreased rapidly thereafter. Analysis and stoichiometric saturation calculations showed that the solution became saturated with $C\bar{S}$ within 2 h of immersion, thereby slowing attack. After saturation, $C\bar{S}$ precipitated onto the specimens and further slowed the attack resulting in a continuous decrease in both hydrogen ion consumption rate and corresponding (specimen) mass loss rate. After 30 h, this attack was virtually stifled. This was clearly not representative of the corrosion mechanisms at the daily sewage flow level in concrete sewers.

Therefore, in order to simulate the corrosion mechanism at the daily sewage flow level in the laboratory, an alternative acid solution, hydrochloric acid (HCl) which possesses similar attack properties but forms soluble reaction products was used. Both H_2SO_4 and HCl completely dissociate in solution, and consequently solutions that contain equal amounts of hydrogen ions possess the same ability to attack concrete. However, unlike in the case of H_2SO_4 attack, calcium that dissolves in HCl to form calcium chloride ($CaCl_2$) does not precipitate due to its much greater solubility (> 0.1 mol/l) compared with the solubility of $C\bar{S}$ (0.01 – 0.1 mol/l) (Ebbing, 1984).

A total of twenty different concrete mixtures (PC and CAC-based), whose details are given in Appendix D, were used in this study. They consisted of eleven mixtures used in the manufacture of sewer pipes, and nine mixtures used in the manufacture of sewer pipe linings. Both PC and CAC-based mixtures, some with SCMs were used to cast core specimens (80 mm in diameter x 150 mm) by means of the heavy compaction technique. One set of these specimens, consisting of six sewer pipe mixtures and five lining mixtures was studied in the laboratory under mineral HCl attack (see details in Table 3-2), while another set of specimens consisting of five sewer pipe mixtures and four

lining mixtures was installed in the inlet manhole to VES for studies on biogenic H_2SO_4 attack (see details in Table 3-3).

Table 3-3: Concrete mixture proportions (ratio by mass to total binder content) of core samples installed in the inlet manhole to VES (Alexander and Fourie, 2011).

Mixture[#]	% binder	w/b	Binder		Aggregate		
			SCM	Cement	Stone**	Crusher sand	Filler sand
Sewer pipe mixtures:							
PC/SIL	14	0.30	-	1.00	3.25	2.89	-
PC/DOL 2	16	0.36	-	1.00	3.45	1.32	0.53
PC/DOL 3	18	0.30	-	1.00	2.28	2.28	-
PC/SF/DOL 2	16	0.32	0.10	0.90	3.45	1.32	0.53
PC/Ag-Zn-Cu/DOL 3[+]	18	0.30	0.01	0.99	2.28	2.28	-
Lining mixtures:							
PC/SIL	23	0.32	-	1.00	1.64	0.82	0.82
PC/DOL 3	23	0.26	-	1.00	1.67	1.67	-
CAC/DOL 3	23	0.26	-	1.00	1.67	1.67	-
CAC/Alag^{TM}	23	0.26	-	1.00	1.67	1.67	-

[#]All aggregates crushed; DOL 3 = high quality dolomite (acid insolub. < 6%, 10% FACT = 354); DOL 2 = low quality dolomite (acid insolub. > 9%, 10% FACT = 130)

[+]Silver-zinc-copper based biocide was used as a corrosion inhibiting additive

**Nominal 13 mm maximum size used for sewer pipe mixtures and nominal 6 mm maximum size for lining mixtures

3.4.3.1 Findings on the performance of concrete sewer pipe samples in mineral HCl

After a 96 h test cycle of the sewer pipe specimens in mineral HCl at pH of 1.00, mass loss of the CAC-based specimens (51.3%) and PC/Metakaolin-based specimens (46.7%) was higher than that of the unblended PC-based specimens (39.3%). PC/FA and PC/SL-based specimens performed identically in respect of mass loss, while the PC/SF-based specimens showed greater resistance to mineral HCl attack, probably due to the combined effects of slower dissolution of the silica fume, generally denser microstructure, and improved interfacial transition zone (ITZ) that prevents acid penetrating readily into the concrete matrix (Alexander and Fourie, 2011).

Results for hydrogen ion consumption from the same test regime showed that the CAC-based specimens (47.5 mg/cm^2) and PC/Metakaolin-based specimens (48.0 mg/cm^2) had higher values than for the unblended PC-based and PC/FA-based specimens (37.5 mg/cm^2). Likewise, the PC/SF-based specimens showed greater resistance to mineral HCl attack.

3.4.3.2 Findings on the performance of concrete sewer pipe lining samples in mineral HCl

After a 96 h test cycle of the sewer pipe lining specimens in mineral HCl at pH of 1.00, mass loss rates were similar. Specimens made with an aluminate aggregate (Alag^{TM}) showed lower mass loss rates than those made with dolomite aggregate. In summary, the mass loss for (a 23% binder content) calcium aluminate cement (CAC-based) and dolomite aggregate (CAC/DOL) (50.9%) specimens was higher than that for (a 23% binder content) PC/DOL (43.2%) specimens. The mass losses for 23% CAC/Alag^{TM} (15.2%), 18% CAC/ Alag^{TM} (11.8%), and 23% CAC/SF/Alag^{TM} (10.9%) specimens were lower than that for 23% PC/DOL (43.2%) specimens. The mass loss for 23% PC/DOL (43.2%) specimens was higher than that for 18% PC/DOL (39.3%) specimens. The mass loss for 23% CAC/DOL (50.9%) specimens was similar to that of 18% CAC/DOL (51.3%) specimens. These results are given in Figure 3-6 together with those for 18% PC/DOL and 18% CAC/DOL sewer pipe concrete mixtures for comparison.

Figure 3-7 shows that the hydrogen ion consumption rates of the Alag^{TM} aggregate specimens were constant with time and also lower than the hydrogen ion consumption rates for specimens containing dolomite aggregates, which increased with time. The constant consumption rate of the CAC/Alag^{TM}

specimens was due to the similar acid insolubility of the CAC binder and Alag™ aggregate (Alexander and Fourie, 2011).

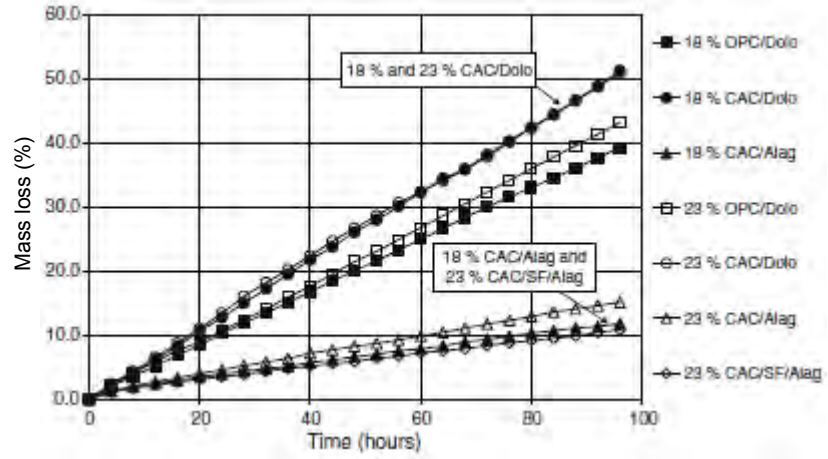

Figure 3-6: Mass loss with time of sewer pipe lining concrete specimens in HCl at pH of 1.00 (Alexander and Fourie, 2011)

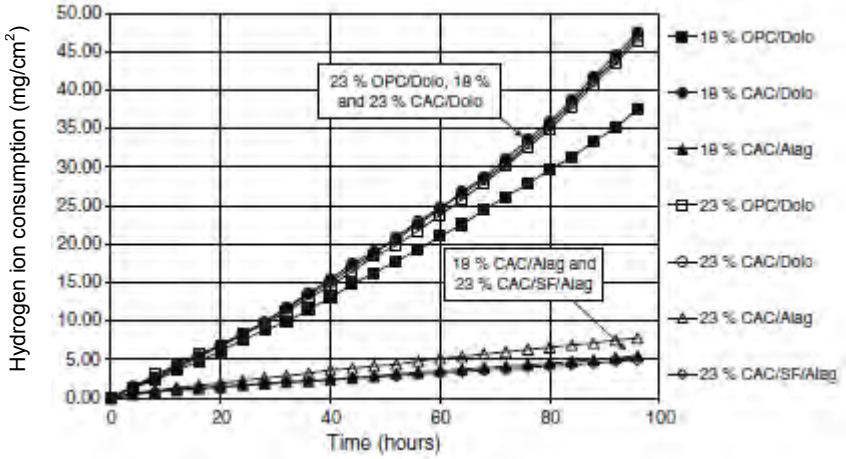

Figure 3-7: Hydrogen ion consumption with time of sewer pipe lining concrete specimens in HCl at pH of 1.00 (Alexander and Fourie, 2011).

Even though the use of mineral HCl instead of mineral H_2SO_4 under laboratory conditions provides opportunities to simulate the corrosion mechanism at the daily sewage flow level in sewers, the findings presented above do not confirm those presented in Phase I work by CSIR with regard to the performance of various cement-based samples subjected to biogenic acid attack. For example, whereas CAC-based concrete mixtures showed superior performance to PC-based concrete mixtures under biogenic acid (H_2SO_4) attack with regard to loss of wall thickness, results under mineral acid (HCl) attack showed that PC-based concrete mixtures had superior performance to CAC-based concrete mixtures (which can be related to changes in dimensions such as wall thickness) and hydrogen ion consumption (which can be related to the neutralisation capacity of concrete mixtures). These results clearly demonstrate that the biogenic acid attack mechanisms in sewers cannot be reliably simulated using mineral acid attack mechanisms.

3.4.3.3 Findings on the performance of concrete sewer pipe and sewer pipe lining samples installed in the inlet manhole to VES

This investigation entailed measuring the effects of deterioration mechanisms (mass loss and drop in surface pH) of 80 mm diameter x 150 mm core specimens that were installed in plastic holders (placed directly above the maximum sewage flow level) on the walls of the IM to the VES (Figure 3-8), commencing December 2000 (during summer).

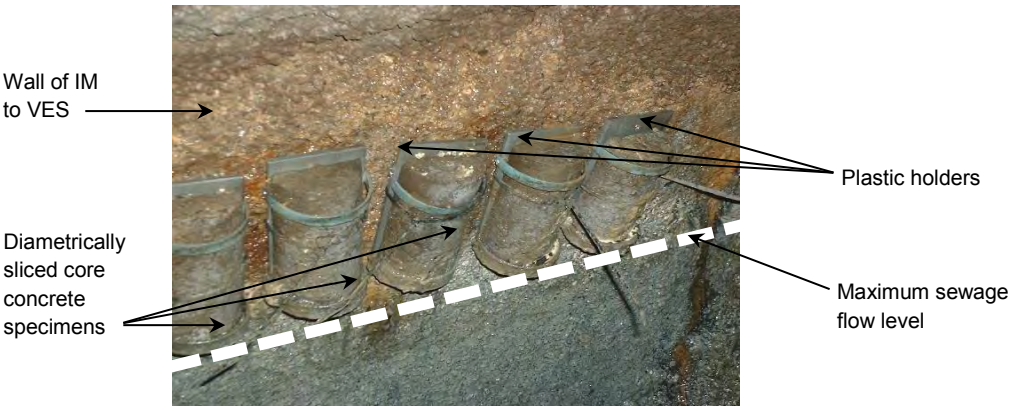

Figure 3-8: Concrete specimens installed in the IM to VES (Alexander et al., 2008).

The mix composition of these specimens represented five concrete mixtures that are used in the manufacture of sewer pipes and four concrete mixtures that are used in the manufacture of sewer pipe linings. The materials used included the following:

(i) PC-based specimens to compare attack on concretes containing siliceous aggregates and dolomite aggregates of varying quality (high quality (DOL 3), and low quality (DOL 2)).
(ii) Blended PC (with silica fume) specimens to assess the influence of silica fume on biogenic corrosion rate.
(iii) CAC/DOL and CAC/Alag^{TM} specimens to assess the influence of calcium aluminate materials on biogenic corrosion rate.
(iv) PC/DOL specimens containing an antibacterial biocide to assess the influence of materials (silver, copper and/or zinc) toxic to bacteria.

These specimens were visually inspected 5 months (May 2001) and 17 months (May 2002) after installation, and the surface pH was also measured during these inspections. After 17 months, the specimens were removed from their plastic holders and cleaned under running tap water using a stiff nylon brush to remove corrosion debris. The mass loss of each specimen was then determined. These results (together with certain mixture details also given in Appendix D) are presented in Table 3-4.

5 months after installation, all PC-based specimens were evidently attacked as characterised by moist slimy layers of corrosion debris covering their surfaces (see Figure 3-8), and their surface pH was less than 2.00. After 17 months exposure to biogenic H_2SO_4, all PC-based specimens experienced mass losses greater than 2.4%. Comparing the performance of PC-based specimens, it was shown that sewer pipe mixtures with lower PC contents experienced less mass losses regardless of aggregate type (SIL vs. DOL) and quality (DOL 2 vs. DOL 3) (14% PC/SIL = 4.14%; 16% PC/DOL 2 = 4.71%; 18% PC/DOL 3 = 6.30). However, at equal PC contents in lining mixtures, DOL-based specimens experienced less mass loss than SIL-based specimens (23% PC/DOL 3 = 2.46; 23% PC/SIL = 6.09). The silica fume and biocide had no beneficial effect in PC-based mixtures with regard to the reported mass losses.

Generally, the PC-based specimens were attacked more severely than the CAC-based specimens. Also, even though the biogenic H_2SO_4 attack was negligible on CAC-based specimens, the CAC/Alag^{TM} specimens seemed to have experienced less (or no) mass loss in comparison to the CAC/DOL 3 specimens (0.35%).

Table 3-4: Mixture proportions (ratio by mass to total binder content), and attack on specimens in the inlet manhole to VES 5 and 17 months after installation (Alexander and Fourie, 2011).

Mixture[#]	% binder	Binder		5 months		17 months		
		SCM	Cement	Attack[##]	pH	Attack[##]	pH	Mass loss (%)
Sewer pipe mixtures:								
PC/SIL	14	-	1.00	S	-	S	-	4.14
PC/DOL 2	16	-	1.00	S	1.20	S	2.40	4.71
PC/DOL 3	18	-	1.00	S	0.50	S	1.44	6.30
PC/SF/DOL 2	16	0.10	0.90	S	1.20	S	2.40	4.72
PC/Ag-Zn-Cu/DOL 3[+]	18	0.01	0.99	S	0.40	S	1.45	5.92
Lining mixtures:								
PC/SIL	23	-	1.00	S	-	S	6.70	6.09
PC/DOL 3	23	-	1.00	N	6.00	M	6.70	2.46
CAC/DOL 3	23	-	1.00	N	6.00	N	6.70	0.35
CAC/Alag[TM]	23	-	1.00	N	6.50	N	7.14	0.00

[#]All aggregates crushed; DOL 3 = high quality dolomite (acid insolub. < 6%, 10% FACT = 354); DOL 2 = low quality dolomite (acid insolub. > 9%, 10% FACT = 130)

[+]Silver-zinc-copper based biocide was used as a corrosion inhibiting additive

**Nominal 13 mm maximum size used for sewer pipe mixtures and nominal 6 mm maximum size for lining mixtures

[##] 'S' = severe; 'M' = moderate; 'N' = negligible

The findings presented above confirm those reported during Phase I work, which showed superior performance of CAC-based mixtures under biogenic acid attack, and are contradictory to those presented from the mineral (laboratory) based test regime, which was intended to mimic biogenic acid attack mechanisms. Also, a significant hypothesis from the findings on the performance of PC-based mixtures tested in-situ is that as the PC content is increased, there is greater provision of sites for acid reaction through the increasing CH content, which is readily acid-soluble as discussed in Chapter Two, Section 2.8.

3.4.3.4 The development of a kinetic equation for H_2S emission in the Virginia sewer in terms of flow characteristics

The main objective of this study (see objective (3) of this Phase II work) was to predict H_2S (gas) emission from sewage, along a line of flow of the Virginia sewer section upstream of the VES. Most of the H_2S released from the turbulent sewage in this section feeds into the VES, when the gate valve in the IM is opened for sewage to flow through the VES and not through the bypass line. In order to address this objective, an understanding of both the flow hydraulics in the Virginia sewer and a model (kinetic equation) for H_2S emission in terms of flow characteristics were required. Therefore this study presented a theory for predicting hydraulic characteristics (including the velocity gradient, *G*) in outfall sewers. This theory was then used to establish a dynamic model for the Virginia sewer line using AQUASIM as a mathematical integrator. The kinetics of H_2S emission was measured in the laboratory.

The laboratory set-up consisted of a standard flocculation batch reactor (115 mm, length, 115 mm, width, and 230 mm, height) (Figure 3-9) that was capable of imparting desired values of *G* into a water sample containing dissolved sulphide species, and maintained at pH of 7. Depending on *G*, the rate of H_2S emission was measured with time. Such emission from this batch reactor simulates H_2S release from a plug flow reactor, which simulates H_2S release in an outfall sewer. A series of these laboratory tests were undertaken at a room temperature of 20 °C where H_2S emission rates with time, at various values of *G* were measured. The specific experimental conditions included the following:

(i) 0.72 mg of sodium sulphide dihydrate ($Na_2S.2H_2O$) flakes were added to 2 litres of distilled water to give an initial dissolved sulphide concentration of 10 ppm in the solution that was used in the batch reactor.

(ii) The pH of the solution of $Na_2S.2H_2O$ in water was maintained at 7 by adding equal molar concentrations of potassium dihydrogen phosphate (KH_2PO_4) (3.2 mg) and dipotassium phosphate (K_2HPO_4) (2.7 mg) to the 2-litre solution.

(iii) The solution's temperature was maintained between 18 °C and 20 °C.

(iv) The batch reactor's motor was rotated at a frequency of between 25 Hz (120 rpm) (G = 115/s) and 60 Hz (275 rpm) (G = 350/s) in order to create turbulence to release the H_2S from the test solution.

(v) Dissolved sulphide concentrations for each value of G (115/s, 150/s, 178/s, 212/s, 241/s, 278/s, 313/s, and 350/s) were measured every 5 minutes, up to a maximum of 300 minutes.

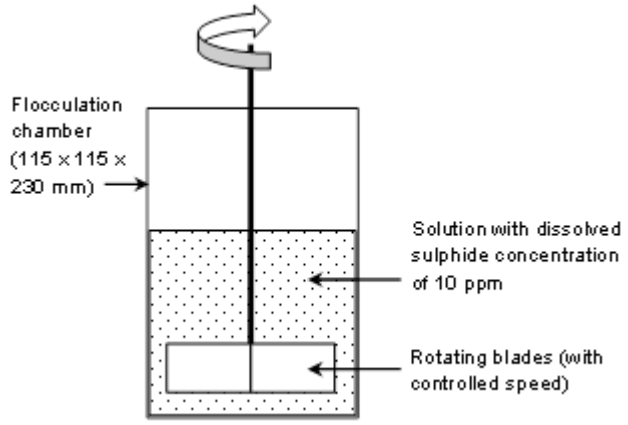

Figure 3-9: Schematic of the cross-section of a batch reactor used to impart desired velocities and turbulence in a solution with dissolved sulphide species (Lu, 2001).

The batch reactor's rotating blades generated turbulence within the test solution and the velocity of rotation of these blades was linked to G. In modelling the data measured in the laboratory, it was assumed that the rate of change of total sulphide concentration was dependent on the mixing conditions G (in this experiment G^2 was found to be more appropriate) (/m), the solution's free surface area A_s (m^2), the batch reactor's volume V (m^3), the hydraulic depth of batch reactor d_{mean} (m), and the concentration of dissolved sulphide (H_2S) and H_2S gas (ppm). This relationship is given in Equation 3.1.

$$-\frac{d[S_T]}{dt} \propto G^2 \times \frac{A_s}{V} \times d_{mean} \times \left([H_2S] - H_K \times P_{H_2S}\right) \quad (3.1)$$

where $d[S_T]/dt$ = rate of change of total sulphide concentration (ppm/s)
S_T = total sulphide concentration (ppm)
H_K = Henry's law coefficient for H_2S (mg/L-atm)
P_{H2S} = partial pressure of H_2S in the gaseous phase (atm)

However, during the test exercise, P_{H2S} was zero, resulting in Equation 3.2.

$$-\frac{d[S_T]}{dt} = K_1 \times G^2 \times \frac{A_s}{V} \times d_{mean} \times [H_2S] \quad (3.2)$$

where K_1 = constant

AQUASIM was used to fit Equation 3.2 to the experimental data. Selected curves fitted on the experimental data are given in Figure 3-10.

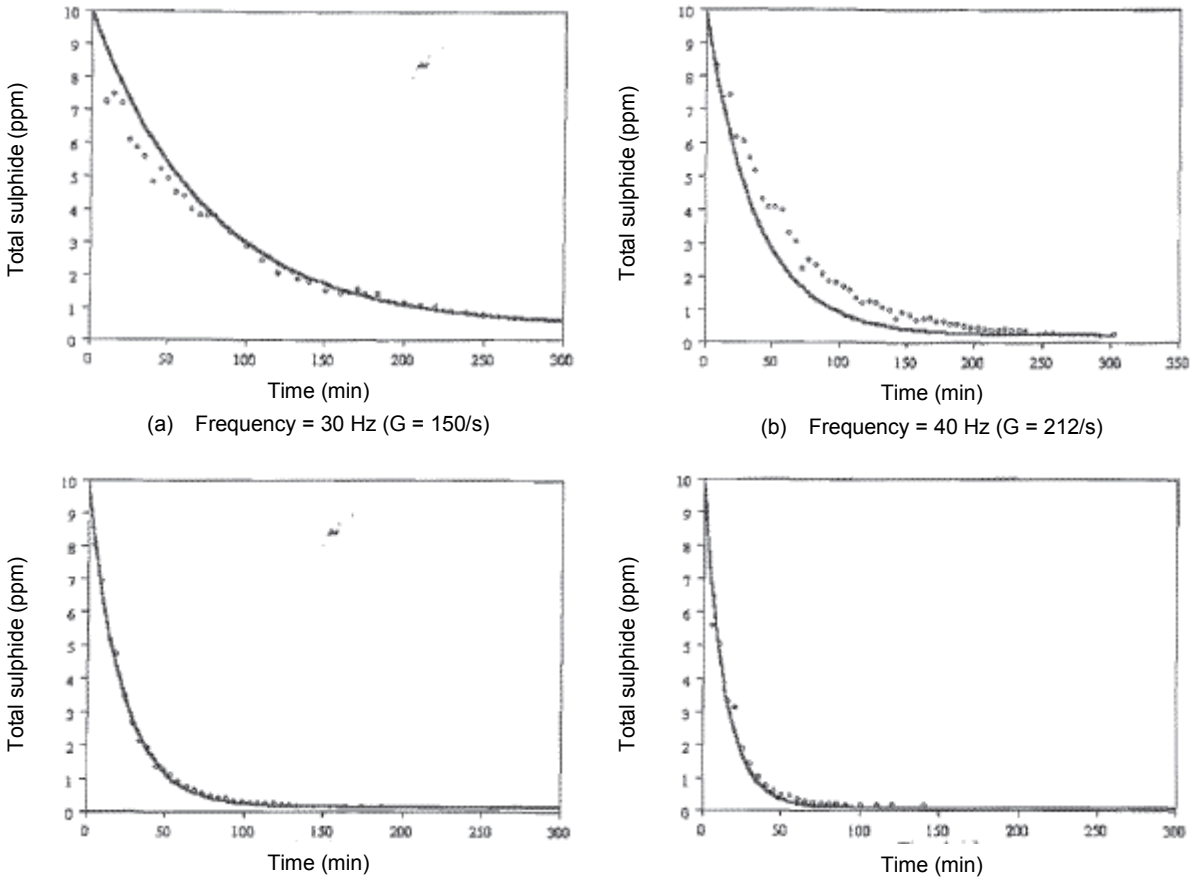

Figure 3-10 (a) – (d): Experimental data at different frequencies (varying values of *G*) fitted with modelled curves from AQUASIM (Lu, 2001).

Also, in order to improve the curve fitting in low H_2S concentration regions such as those beyond a test period of 150 minutes in Figures 3.10 (c) and (d), Equation 3.2 was modified to Equation 3.3.

$$-\frac{d[S_T]}{dt} = K_1 \times G^2 \times \frac{A_s}{V} \times d_{mean} \times [H_2S] - K_2 \tag{3.3}$$

where K_2 = constant

From this experiment, the values of K_1 = *9.33 x* 10^{-8} and K_2 = *8.3 x* 10^{-5} were determined by regression from the fitted curves given in Figure 3-10. Therefore the general equation for the rate of change in total sulphide concentration from this test regime is given by Equation 3.4.

$$-\frac{d[S_T]}{dt} = 9.33 \times 10^{-8} \times G^2 \times \frac{A_s}{V} \times d_{mean} \times [H_2S] - 8.3 \times 10^{-5} \tag{3.4}$$

In order for the general Equation 3.3 to be applied to sewer hydraulics and related H_2S emission rates, the parameters therein were related to a typical circular sewer's (flowing partly full) geometrical characteristics shown in Figure 3-11, where α is linked to the sewer radius and depth of flow (under any flow conditions) as given in Equation 3.5.

$$\alpha = a\cos\left(\frac{r-d}{r}\right) \tag{3.5}$$

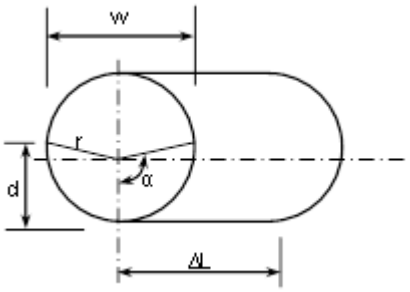

Figure 3-11: Typical circular sewer's geometrical characteristics (Lu, 2001).

Also, the following parameters (Equations 3.6 and 3.7) apply in defining certain characteristics of the circular sewer's geometry, for any flow condition:

$$w = 2 \times r \times sin(\alpha) \tag{3.6}$$

where w = sewage surface width (m)

$$A = r \times r \times (\alpha - sin(\alpha) \times cos(\alpha) \tag{3.7}$$

where A = cross sectional area (m^2)

For a sewer length ΔL, the surface area exposed to sewer atmosphere, the mixed sewage volume, surface width and cross-sectional area can be related (Equation 3.8).

$$\frac{A_s}{V} = \frac{w \times \Delta L}{A \times \Delta L} = \frac{w}{A} \tag{3.8}$$

Therefore Equation 3.3 can be written as:

$$-\frac{d[S_T]}{dt} = K_1 \times G^2 \times \frac{w}{A} \times d_{mean} \times [H_2S] - K_2 \tag{3.9}$$

With regard to the velocity gradient G, this parameter reflects the mixing conditions in hydraulic systems such as batch reactors and sewers, and it depends on the system's dissipation function and the absolute viscosity of the liquid being mixed (Equation 3.10) (Bratby, 1980).

$$G = \sqrt{\frac{W}{\mu}} \tag{3.10}$$

where W = dissipation function ($N/s/m^2$)
μ = absolute viscosity of liquid (for water = 10^{-3} $N/s/m^2$ at 20 °C)

In a batch reactor set-up, G can be calculated from the torque generated by rotating blades whereas in a sewer, G is a function of system hydraulic parameters (Lu, 2001). According to Bratby (1980), for a straight line flow (straight length of pipe) in sewers, W is given by Equation 3.11.

$$W = \frac{r \times H_L}{T} \tag{3.11}$$

where r = unit weight of liquid
T = retention period (s)
H_L = head loss in a straight length of pipe (m)

and

$$H_L = f \times \frac{\Delta L}{D_H} \times \frac{v^2}{2g} \tag{3.12}$$

where f = Darcy friction factor
D_H = hydraulic diameter (m)

v = average flow velocity along distance ΔL (m/s)

Substituting Equations 3.11 and 3.12 into Equation 3.10 and further manipulation, the velocity gradient G can be expressed as given in Equation 3.13.

$$G = \sqrt{\frac{r \times f \times v^3}{\mu \times D_H \times 2g}} \tag{3.13}$$

Substituting Equation 3.13 into Equation 3.9 gives the general expression for the rate of change of total sulphide concentration ($d[S_T]/dt$) in a sewer system, assuming that sulphide generation occurs in the pumping section of the system and not along the line of flow (Equation 3.14) (Lu, 2001).

$$-\frac{d[S_T]}{dt} = K_1 \times \frac{r \times f \times v^3}{\mu \times D_H \times 2g} \times \frac{w}{A} \times d_{mean} \times [H_2S] - K_2 \tag{3.14}$$

Using AQUASIM, Equation 3.14 was integrated and theoretical predictions of sulphide concentrations along a line of flow were generated. These were then compared with the actual residual sulphide in the 600 m sewer section, upstream of the VES. These comparisons showed reasonable agreement, and that sulphide (H_2S) emitted between any two points along a line of flow relates to a decrease in total sulphide concentration between these points.

3.4.3.5 Corrosion rates of certain cement-based sewer pipe materials determined from actual measurements of pipe wall thicknesses at the end of their 'service life'

Towards the end of this Phase II work (see objective (4)), after 12 years since commissioning of the VES, i.e. in 2001, a physical inspection of the VES was undertaken. This inspection showed that (i) the unprotected PC/SIL pipe sections had virtually corroded away (Figure 3-12(a)), (ii) the reinforcing steel particularly at the daily sewage flow level in unprotected PC/DOL pipe sections was corroded, and (iii) at certain places on the unprotected CAC/SIL pipe sections, the reinforcing steel was exposed and had started corroding (Figure 3-12(b)). In general, deterioration in the VES was so severe that the sewage flow was diverted to the bypass line with the view of minimising H_2S concentrations in the VES' headspace. This practically marked the end of the service life of some unprotected concrete sewer pipe samples that were originally installed in the VES during 1988. Therefore, rehabilitation was required in order to continue monitoring the pipe sections that were serviceable (Goyns, 2003).

(a) Remaining (socket) section of a PC/SIL pipe (originally 2.44 m)

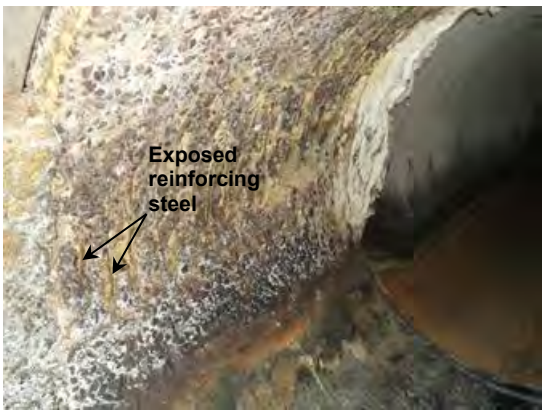

(b) Reinforcing steel in a CAC/SIL pipe exposed at the daily sewage flow level

Figure 3-12(a) and (b): Condition of certain concrete pipes after 12 years of exposure to biogenic H_2SO_4 in the VES.

Therefore, the unprotected PC/SIL pipe samples (together with a half of each adjacent pipe sample – see comments on the samples layout in Appendix C) were removed from the VES 14 years after installation, i.e. in 2002, and the residual wall thicknesses were measured in order to establish the corrosion rates of these mixtures when subjected to biogenic H_2SO_4 attack. These corrosion rates,

together with the predicted corrosion rates deduced from the LFM, the 5-year estimates undertaken during Phase I of this study (by CSIR), and the 12-year estimates undertaken independently by Goyns (2001) are given in Table 3-5.

Table 3-5: Estimated and measured corrosion rates of concrete mixtures at VES (Goyns, 2003).

Material	Measured alkalinity*	Predicted corrosion rate (mm/yr.)#	5-year estimate (mm)		12-year estimate (mm)		14-year measured (mm)	
			Total	Ave./yr.	Total	Ave./yr.	Total	Ave./yr.
PC/SIL	0.20	6.3	> 30.0	> 6.0	> 64.0	> 5.0	> 105.0	> 7.5
PC/DOL	0.70	1.8	10 – 15	2 – 3	20 – 30	1.7 – 2.5	43	3.1
CAC/SIL	0.45	NA	5 – 10	1 – 2	10 – 15	0.8 – 1.2	26	1.9
AC	0.65	1.9	10 – 12	2+	20 – 25	1.7 – 2.1	**	**

*Values based on insolubility tests ($CaCO_3$ equivalent) by CSIR

**Measurements were not taken on AC-based pipes as walls were swollen and soft due to products of corrosion

#Predicted corrosion rate based on the Life Factor Method (LFM)

The average concrete corrosion rates estimated at 5 years after commissioning of the VES varied slightly from the average corrosion rates estimated at 12 years, and the actual average measurements undertaken after 14 years of service. The most significant findings with regard to these rates of corrosion were that (i) CAC-based mixtures performed better than both PC-based and AC-based mixtures, and (ii) the LFM could be used to predict the performance of PC-based mixtures with siliceous aggregates, but when a calcareous aggregate or different binder system such as CAC-based or AC-based is used, the LFM does not apply. The findings from this phase of study, which was completed in 2003 after about 8 years of study, are outlined below.

3.4.3.6 Findings and recommendations from Phase II work by CMA, assisted by UCT

Pursuant to objectives (1) to (4) outlined in this Phase II work, primarily undertaken between 1995 and 2003, the following significant conclusions were drawn:

(i) A laboratory mineral acid test, using HCl at a pH of 1.00, was developed for assessing the performance of concrete mixtures that are used in the manufacture of sewer pipes. This test was able to distinguish between the influence of different binders and different aggregates when subjected to aggressive acid conditions.

(ii) Binder-aggregate systems in concrete mixtures that are characterised by dense microstructures and the inferred absence of an ITZ perform better under aggressive acid conditions.

(iii) The relative rates of dissolution of binder and aggregate are important in the overall performance of concrete mixtures. Uniform rates of dissolution are preferable since these eliminate aggregate fallout which exposes 'fresh' surfaces to aggressive acid conditions.

(iv) CAC-based concrete mixtures did not outperform PC-based concrete mixtures in the mineral acid test, but exhibited substantially superior performance under biogenic acid attack.

(v) Mineral acid testing cannot model conditions in a real sewer where acids are microbially generated due to the influence of other mechanisms involved.

(vi) The total sulphide emission rate along a line of flow in a sewer can be predicted under laboratory conditions in terms of the velocity gradient.

(vii) The most commonly used and referenced concrete sewer corrosion prediction model, the Life Factor Method cannot be reliably used for other concrete mixtures apart from those with certain plain PC-based binders.

Based on the conclusions above, recommendations for further investigation were proposed with the view of generating quantifiable parameters that could be incorporated in sewer design processes such as design of corrosion control linings on concrete host pipes. This was to be done by considering (i) two binder systems (PC-based and CAC-based), (ii) three binder contents (16%, 18%, and 23%), (iii) two aggregate types (siliceous and calcareous), (iv) inclusion of SCMs (to investigate the effect of blended binders), and (v) mortar versus concrete mixtures (Alexander et al., 2008; Goyns et al., 2008; Goyns, 2010). The execution of these recommendations formed Phase III of study.

3.4.4 Phase III work by UCT (CMA was involved up to 2010)

Broadly, this phase of study is on-going. It is currently being undertaken by UCT. Different researchers have been involved in this phase of study at different stages since inception in 2004 (Goyns, 2003; Alexander et al., 2008; Goyns et al., 2008; Goyns, 2010; Alexander and Fourie, 2011; Motsieloa, 2013). The main objectives of this study include:

(1) Rehabilitation of certain sections of VES in order to allow for further in-situ studies of concrete materials used in the manufacture of sewer pipes.
(2) Monitoring mass changes (loss) of new concrete sewer pipe materials with greater accuracy in order to develop a reliable comparison of corrosion rates.
(3) Investigating the physicochemical properties of certain concrete sewer pipe materials consisting of blended binder systems.
(4) Drawing conclusions on (i) the benefits of various binder systems and (ii) concrete pipe production technologies for application in aggressive sewer environments.

As mentioned earlier in Section 3.4.1, the VES originally consisted of a 900 mm diameter and 63 m long (individual pipes of 2.44 m length) section of sewer in which nine different types of pipes were installed during 1988. After 12 years of service, three unprotected PC/SIL pipes had corroded away in places, and these together with a half-length of each adjacent pipe at either end (see comments on the layout of samples in Appendix C) were removed from the VES after 14 years since installation. In the spaces left, three manholes – the so-called Manhole I, Manhole II and Manhole III were built in 2004. A new set of seventeen pipe samples (each 300 mm long – see manufacturing technique in Chapter Four) of different binder systems (both PC-based and CAC-based) and aggregates (siliceous and calcareous) were installed in each manhole after taking their masses. The layout and mix composition of these seventeen different types of concrete sewer pipe samples (in triplicate) is given in Appendix E (Goyns, 2010). The top 120° of some of these pipe samples was cut to form 'lid' samples that can be removed so that observations and measurements can be made. In Manhole II, these 'lids' also act as windows through which additional core samples (these formed part of later studies by Motsieloa (2013) as discussed in Section 3.4.4.2) that are suspended in the sewer headspace can be accessed for observations and measurements (Figure 3-13).

(a) Typical 'lid' sample removed for inspection

(b) 'Window' for accessing core samples, and core samples suspended in Manhole II at VES

Figure 3-13 (a) – (b): Typical 'lid' and core samples installed in VES.

During 2006, various cement manufacturers from Europe requested to have their concrete mixtures (in the form of both 'lid' and core samples) installed in the VES for monitoring under biogenic H_2SO_4 attack. This led to the removal of some of the AC-based samples coated with epoxy and epoxy tar (Figure 3-14, also see comments on the layout of samples in Appendix C) and a fourth manhole, the so-called Manhole IV was constructed in 2007. New 'lid' and core samples supplied by these cement manufacturers were installed in this manhole in January 2010.

(a) Condition of typical AC-based sample coated with epoxy tar removed from VES during 2007

(b) New 'lid' and core samples installed in Manhole IV; some lid samples have been removed for inspection

Figure 3-14 (a) – (b): Condition of typical AC-based sample coated with epoxy tar removed from VES during 2007 and new samples installed in Manhole IV in January 2010.

In order to address the aims and certain objectives of the current study as outlined in Chapter One, (triplicate) 'lid' samples installed in Manholes I, II, and III (see details in Table 3-6) were used for characterisation of various concrete mixtures subjected to biogenic H_2SO_4, and results are presented in Chapter Five. Lid samples installed in Manhole IV do not form part of the current study due to (i) reproducibility limitations since each concrete mix is represented by one sample, and (ii) certain ownership rights held by the various cement manufacturers who supplied these samples.

Table 3-6: Mixture composition (percentage of total mass) of certain samples installed in Manholes I, II and III in the VES during 2004 (Goyns, 2010).

Mixture[†]	% total binder	Binder type				% Aggregate		
		% SCM			% Cement	Stone*	Crusher sand**	Filler sand[##]
		GGBS	FA	SF				
Concrete pipe mixtures:								
PC/DOL 16	16	-	-	-	16	48	18	18
PC/DOL 18	18	-	-	-	18	47	18	17
PC/DOL 23	23	-	-	-	23	44	17	16
PC/GGBS/DOL	18	6	-	-	12	47	18	17
PC/FA/DOL	18	-	4.5	-	13.5	47	18	17
PC/SF/DOL	18	-	-	1.5	16.5	47	18	17
Concrete lining mixtures:								
CAC/SIL 23	23	-	-	-	23	44	17	16
CAC/DOL 16	16	-	-	-	16	48	18	18
CAC/DOL 18	18	-	-	-	18	47	18	17
CAC/DOL 23	23	-	-	-	23	44	17	16
CAC/FA/SF/DOL	17	-	4.5	1.5	11	47	18	18
CAC/Alag™	20	-	-	-	20	40	-	40

[†]PC = CEM I (42.5R); CAC = Ciment Fondu. See chemical composition (also of SCMs) in Appendix E.3

*Nominal 13 mm maximum size used for sewer pipe mixtures and nominal 6 mm maximum size for lining mixtures

**Crusher sand used = dolomite

[##]Filler sand used = siliceous, except for the aluminate-based

All the manholes (Manhole I – IV) were fitted with overhead steel I-beams (spanning from respective upstream and downstream sections) at the roof slab soffit level, on which equipment used to measure masses of the 'lid' samples, were attached during the exercise.

3.4.4.1 Findings on changes in mass of concrete sewer pipe samples prior to the current study (2004 to 2013)

During the first four years (2005 to 2008) after installation of the triplicate 'lid' samples in Manholes I, II and III, inspections were undertaken every six months, but no significant material loss could be

observed. Therefore, it was decided to undertake mass measurements in order to capture possible trends that could not be confirmed visually since inception. The first mass measurements were undertaken during 2008. Subsequent mass measurements taken in 2009 and 2010 were compared to the initial masses and a trend was observed. Results showed that for about six years after the installation of the samples in the VES, they generally gained mass. However, during 2011, 2012 and 2013, a mixed pattern of mass loss and gain was observed (Figure 3-15) (Goyns, 2014).

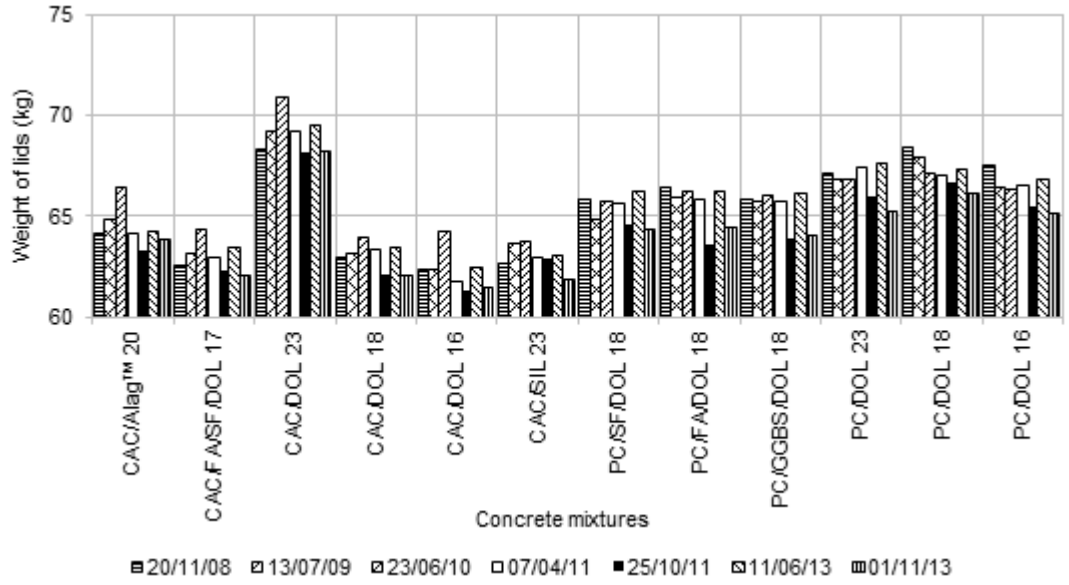

Figure 3-15: Average of mass changes (taken between 2008 and 2013) of 'lid' samples installed in Manholes I, II and III in the VES in 2004 (Goyns, 2014).

Goyns (2014) stated that the reasons for the observed pattern of mass gain and loss over the duration of study are:

(i) Due to the RH characteristics in the sewer headspace, the samples initially absorb moisture and become saturated leading to mass gain.
(ii) At inception of biogenic H_2SO_4 attack, the products of concrete corrosion that are formed stay intact on the pipe surface. These products of corrosion also absorb moisture leading to mass gain.
(iii) The products of biogenic concrete corrosion have little or no (bond) strength, and as they absorb moisture over time, they become heavy and eventually fall off the pipe surface leading to mass loss.
(iv) The products of concrete corrosion that form on the 'freshly' exposed pipe surface absorb moisture leading to mass gain.

It is hypothesised that cycle (iii) and (iv) above continues over the 'service-life' of these samples.

Drawing conclusions about the relative performance of the different samples from Figure 3-15 is difficult, as they were not initially of the same mass. However, by expressing the mass changes of the samples at the end of the five-year (2008 to 2013) period as percentages of the initial masses taken, the performance of these concrete mixtures could be compared. Results show that (Goyns, 2014):

(i) The CAC-based mixtures, irrespective of binder content and aggregate type, outperformed the PC-based mixtures.
(ii) Considering the CAC-based mixtures, the binder content appears to have a significant influence on the rate of material loss. The higher the CAC content, the lower is the material loss.
(iii) The CAC-based ternary mixtures (CAC+FA+SF) with 17% binder content appear to have similar mass losses as some of the plain CAC-based mixtures with higher binder content (18% and 23%).

(iv) Certain PC-based binary mixtures (PC+SF and PC+GGBS) with 18% binder content appear to outperform some of the plain PC-based mixtures with higher binder content (23%) and PC-based binary mixtures with FA at a binder content of 18%.

3.4.4.2 Findings on physicochemical properties of certain concrete sewer pipe materials consisting of blended binder systems

This study was intended to primarily characterise certain blended binder systems used in the manufacture of concrete sewer pipes based on laboratory tests. The main aim of this study was to determine the mass loss and hydrogen ion consumption of certain concrete mixtures as a measure of the rate of acid attack and corrosion resistance (neutralisation capacity) respectively. The concrete mixtures under investigation included CAC-based binary mixtures (CAC + FA, and CAC + GGBS at various percentages), PC-based binary mixtures (70% PC + 30% FA, and 90% PC + 10% SF), PC-based ternary mixtures (72% PC + 20% FA + 8% SF), plain (100%) CAC mixtures and plain (100%) PC mixtures. The mixture details of these binder systems are given in Table 3-7, and also in Appendix F (Motsieloa, 2013). A similar set of concrete mixtures was installed in the VES during 2011 for in-situ observations and measurements, and forms part of the current study; results from these measurements are given in Chapter Five.

Table 3-7: Concrete mixture proportions (ratio by mass to total binder content) of core samples used in Phase III work by Motsieloa (2013).

Mixture[†]	% total binder	Binder type			Cement	Aggregate		
		SCM				Stone*	Crusher sand**	Filler sand[##]
		GGBS	FA	SF				
Concrete lining mixtures:								
PC 100	16	-	-	-	1.00	2.89	1.10	1.10
PC 70/FA 30	16	-	0.30	-	0.70	3.04	0.98	0.98
PC 90/FA 10	16	-	0.10	-	0.90	2.89	1.08	1.08
PC 72/FA 20/SF 8	16	-	0.20	0.08	0.72	3.02	0.99	0.99
CAC 100	16	-	-	-	1.00	2.89	1.11	1.11
CAC 85/FA 15	16	-	0.15	-	0.85	2.93	1.04	1.04
CAC 75/FA 25	16	-	0.25	-	0.75	3.01	1.02	1.02
CAC 60/FA 40	16	-	0.40	-	0.60	3.07	0.94	0.94
CAC 75/GGBS 25	16	0.25	-	-	0.75	2.89	1.10	1.10
CAC 60/GGBS 40	16	0.40	-	-	0.60	2.89	1.09	1.09
CAC 40/GGBS 60	16	0.60	-	-	0.40	2.89	1.08	1.08
CAC 50/GGBS 50	16	0.50	-	-	0.50	2.89	1.08	1.08

[†]PC = CEM I (42.5R); CAC = Ciment Fondu. See chemical composition (also of SCMs) in Appendix F.2
*Nominal 13 mm maximum size
**Crusher sand used = dolomite
[##]Filler sand used = siliceous

The physicochemical properties of the concrete mixtures investigated in the laboratory included 28 d compressive strength, 14 h tensile strength, density, permeability (using the Oxygen Permeability Index (OPI)), water sorptivity and porosity, acid insolubility, and hydrogen ion consumption in hydrochloric acid solution at pH = 1 (Motsieloa, 2013; Fourie, 2007). Results from this study are summarised below.

3.4.4.2.1 Compressive strength

(i) The 28 d compressive strength of the plain (100%) PC concrete mixture (57.1 MPa) was higher than that of the 70% PC + 30% FA blend (44.4 MPa) and 72% PC + 20% FA + 8% SF blend (47.0 MPa). However, the 90% PC + 10% SF blend had higher compressive strength (62.5 MPa).

The higher compressive strength development in mixtures containing SF was attributed to the high pozzolanic reactivity of SF. FA has a tendency for slow strength development depending on the curing regime.

(ii) The 28 d compressive strength of the plain (100%) CAC concrete mixture (54.0 MPa) was lower than that of the 85% CAC + 15% FA blend (56.4 MPa) and 75% CAC + 25% GGBS blend (56.7 MPa), but higher than that of the 75% CAC + 25 % FA blend (47.8 MPa), 60% CAC + 40% FA blend (33.8 MPa), 60% CAC + 40% GGBS blend (40.1 MPa), 50% CAC + 50% GGBS blend (31.5 MPa) and 40% CAC + 60% GGBS blend (26.1 MPa).

These results show that increasing the CAC replacement levels by more than 25% FA or more than 40% GGBS leads to lower compressive strength development at 28 d than plain CAC mixtures. It is hypothesised that an increase in the FA or GGBS content in CAC-based mixtures increases the dicalcium aluminate silicate (C_2AS) phase which has very low hydraulicity thus reduced hardening properties (Majumdar and Singh, 1992; Robson, 1962).

3.4.4.2.2 Tensile strength

(i) The 14 h tensile strength of the plain (100%) PC concrete mixture (3.17 MPa) was higher than that of the 70% PC + 30% FA blend (1.70 MPa), 90% PC + 10% SF blend (2.90 MPa), and 72% PC + 20% FA + 8% SF blend (2.25 MPa).

(ii) The 14 h tensile strength of the plain (100%) CAC concrete mixture (4.01 MPa) was higher than all the other CAC-based blends; 85% CAC + 15% FA (2.74 MPa), 75% CAC + 25% FA (2.21 MPa), 60% CAC + 40% FA (1.93 MPa), 75% CAC + 25% GGBS (2.85 MPa), 60% CAC + 40% GGBS (1.64 MPa), and 40% CAC + 60% GGBS (1.64 MPa).

The 14 h results presented in (i) and (ii) above for PC-based and CAC-based binder systems show that the inclusion of SCMs has no beneficial effect on early tensile strength development.

3.4.4.2.3 Density (oven-dry)

(i) The 28 d oven-dried density of the plain (100%) PC concrete mixture (2575 kg/m^3) was higher than all the other PC-based concrete mixtures; 70% PC + 30% FA (2390 kg/m^3), 90% PC + 10% SF (2464 kg/m^3), and 72% PC + 20% FA + 8% SF (2510 kg/m^3).

(ii) The 28 d oven-dried density of the plain (100%) CAC concrete mixture (2604 kg/m^3) was lower than that of the 75% CAC + 25% GGBS blend ((2657 kg/m^3), but higher than all the other CAC-based blends; 85% CAC + 15% FA (2533 kg/m^3), 75% CAC + 25% FA (2559 kg/m^3), 60% CAC + 40% FA (2555 kg/m^3), 60% CAC + 40% GGBS (2551 kg/m^3), 50% CAC + 50% GGBS (2504 kg/m^3), and 40% CAC + 60% GGBS (2416 kg/m^3).

3.4.4.2.4 Oxygen permeability index (OPI)

(i) The 28 d OPI of the plain (100%) PC concrete mixture (10.55 – log scale) was similar to that of the 70% PC + 30% FA blend, but lower than that of the 90% PC + 10% SF blend (10.93 – log scale) and 72% PC + 20% FA + 8% SF blend (10.95 – log scale).

These results show that inclusion of SF in PC-based mixtures leads to the densification of the concrete matrix thus lower permeability (higher OPI value).

(ii) The 28 d OPI of the plain (100%) CAC concrete mixture (9.89 – log scale) was similar to that of all CAC + FA blends; 85% CAC + 15% FA (9.90 – log scale), 75% CAC + 25% FA (9.89 – log scale), 60% CAC + 40% FA (9.90 – log scale), but higher than that of all the other CAC + GGBS blends; 75% CAC + 25% GGBS (9.54 – log scale), 60% CAC + 40% GGBS (9.58 – log scale), 50% CAC + 50% GGBS (9.83 – log scale), and 40% CAC + 60% GGBS (9.84 – log scale).

These results show that inclusion of FA and GGBS in CAC-based mixtures does not improve the permeability characteristics at 28 d. This could be attributed to compensation mechanisms where the potential influence of SCMs in densifying the HCP was affected by conversion processes during hydration (which leads to formation of more voids).

3.4.4.2.5 Sorptivity

(i) The 28 d sorptivity of the plain (100%) PC concrete mixture (6.1 mm/√hr) was lower than that of the 70% PC + 30% FA blend (6.4 mm/√hr), but higher than that of the 90% PC + 10% SF blend (3.2 mm/√hr) and 72% PC + 20% FA + 8% SF blend (3.7 mm/√hr).

These results show that inclusion of SF in PC-based mixtures leads to low water sorptivity characteristics because of the inferred property of refined pore structure due to its fine filler effect that densify the ITZ. Moreover, more calcium silicate that is formed from the pozzolanic reactions provides more binding characteristics (Chandra, 2002; Alexander and Fourie, 2011).

(ii) The 28 d sorptivity of the plain (100%) CAC concrete mixture (13.2 mm/√hr) was lower than that of the 85% CAC + 15% FA blend (14.4 mm/√hr), but higher than that of all the other CAC-based blends; 75% CAC + 25% FA (11.7 mm/√hr), 60% CAC + 40% FA (13.0 mm/√hr), 75% CAC + 25% GGBS (9.5 mm/√hr), 60% CAC + 40% GGBS (10.5 mm/√hr), 50% CAC + 50% GGBS (9.5 mm/√hr), and 40% CAC + 60% GGBS (11.7 mm/√hr).

These results show that inclusion of less than 15% FA in CAC-based mixtures has no beneficial effects on the water sorptivity characteristics of such concrete matrices.

3.4.4.2.6 Porosity

(i) The 28 d porosity of the plain (100%) PC concrete mixture (7.4%) was higher than that of the 90% PC + 10% SF blend (7.0%), but lower than that of the 70% PC + 30% FA blend (8.8%) and 72% PC + 20% FA + 8% SF blend (8.3%).

These results show that inclusion of SF as the only SCM in the PC-based mixture refines the concrete matrices' microstructure thus low porosity (Chandra, 2002; Fourie, 2007; Goyal et al., 2009)

(ii) The 28 d porosity of the plain (100%) CAC concrete mixture (7.6%) was higher than that of the 85% CAC + 15% FA blend (7.3%) and 50% CAC + 50% GGBS (6.9%), but lower than all the other CAC-based blends; 75% CAC + 25% FA (7.7%), 60% CAC + 40% FA (8.0%), 75% CAC + 25% GGBS (8.2%), 60% CAC + 40% GGBS (8.3%), and 40% CAC + 60% GGBS (8.6%).

These results do not show a clear relationship between the binder replacement levels and porosity in these CAC-based mixtures.

3.4.4.2.7 Acid insolubility

(i) The acid insolubility of the plain (100%) PC concrete mixture (19.9%) was lower than that of the PC-based blends; 70% PC + 30% FA (23.5%), 90% PC + 10% SF (27.1%), and 72% PC + 20% FA + 8% SF (30.8%).

It is hypothesised that the mineral additives consumed the free lime in a pozzolanic reaction to give more calcium silicate that provides higher acid insolubility than the calcium hydroxide (Goyal et al., 2009).

(ii) The acid insolubility of the plain (100%) CAC concrete mixture (15.3%) was lower than that of all the CAC-based blends; 85% CAC + 15% FA (19.0%), 75% CAC + 25% FA (20.4%), 60% CAC + 40% FA (22.8%), 75% CAC + 25% GGBS (17.2%), 60% CAC + 40% GGBS (18.2%), 50% CAC + 50% GGBS (22.0%), and 40% CAC + 60% GGBS (20.5%).

The high acid insolubility of the blended binders was attributed to the formation of the silica-bearing compound stratlingite (C_2ASH_8) which provides significant acid insolubility (Hildalgo et al., 2009).

3.4.4.2.8 Hydrogen ion consumption

(i) The acid resistance, evaluated using hydrogen ion consumption (in hydrochloric acid solution maintained at pH = 1), of the plain (100%) PC concrete mixture (17.79 mg/cm^2) was lower than that of the PC-based blends (8.79 mg/cm^2 to 17.72 mg/cm^2). Generally the PC-based blends ((PC + SF), (PC + FA +SF), and (PC + FA)) had better acid resistance (lower hydrogen ion consumption) than the CAC + FA blends, but both had better acid resistance than plain unconverted CAC mixtures. The acid resistance of the plain converted CAC mixtures was similar to that of 70% PC + 30% FA blended mixtures (17.72 mg/cm^2).

(ii) The acid resistance of the CAC + GGBS blends was higher than that of the plain unconverted CAC (20.98 mg/cm^2) and plain PC mixtures (17.79 mg/cm^2). The plain converted CAC had similar acid resistance to 60% CAC + 40% GGBS blends (approximately 15 mg/cm^2).

3.4.4.2.9 Mass loss

(i) Considering PC-based mixtures, the mass loss of the PC + SF blends had the lowest mass loss (13.43%) while the PC + FA blends had the highest mass loss (17.72%), which was even higher than that of the plain PC-based mixtures (16%) probably due to the fallout of the acid-insoluble particles.

(ii) Considering CAC-based mixtures, the mass loss of the plain converted CAC mixtures (25%) was less than that of all the other CAC-based (plain unconverted and blended) mixtures (29% to 40%).

(iii) Generally, the mass loss for all the PC-based concrete mixtures was less than that of all the CAC-based concrete mixtures investigated.

From the findings on the physicochemical properties of various concrete mixtures presented above, they further confirm that (i) mineral acid tests cannot mimic biogenic acid attack mechanisms in sewers, and (ii) the corrosion mechanisms in sewers are significantly influenced by microbial activities.

3.5 Summary – significance of findings from the VES

This chapter presented a review of certain aspects that led to the establishment of the VES, and its significance, with regard to studies on biogenic corrosion mechanisms, since inception. The understanding of the sewer environment phases (aqueous, gaseous, biological and mineralogical) in the VES will help in (i) revealing the significance of certain intensities of sewer headspace characteristics such as temperature, RH, CO_2 and H_2S concentration on the generation of biogenic H_2SO_4 on the moist, non-submerged walls of concrete sewer pipes (ii) highlighting the influence of certain parameters of concrete materials such as alkalinity and certain products of hydration on the neutralisation capacity of concrete mixtures used in the manufacture of sewer pipes (iii) highlighting the influence in (ii) above on the activity of SOB on the moist non-submerged walls of concrete sewers, and (iv) the interpretation of experimental data presented in Chapter 5.

In summary, the review presented in this chapter demonstrated that:

(1) Biogenic H_2SO_4 attack of cement-based sewer pipes occurs along sewer sections in which sewer hydraulics allow for generation and release of H_2S (gas) within the same regions under attack or in other sections that are not within the vicinity of the H_2S-generating regions. This means that under certain sewer environment conditions, aggressive conditions still exist even if the generation and release of H_2S (gas) occurs elsewhere (such as upstream) in the system.

(2) The physical and chemical interactions of concrete sewer pipe mixture components (with and without SCMs) are important as reflected in acid resistance tests undertaken in the laboratory. However, the performance of PC-based and CAC-based concrete mixtures under laboratory conditions does not mimic in-situ conditions (Alexander and Fourie, 2011; Motsieloa, 2013).

(3) The interaction between mechanisms leading to aggressive conditions on the non-submerged walls of sewers and the features of the mineralogical phases (both sound and deteriorated) of concrete mixtures used in the manufacture of sewer pipes should be characterised. This

characterisation can be used to explain and quantify the underlying mechanisms of biogenic acid attack.

(4) In contradiction to the hypothesis of the LFM that the higher the equivalent $CaCO_3$ in a mixture the lower the corrosion rate, PC-based mixtures with less cement content (for example, 16%) performed better than PC-based mixtures with higher cement contents (for example, 18%) when subjected to biogenic H_2SO_4 attack.

(5) A comparison of most of the physicochemical characteristics of PC- and CAC-based concrete mixtures do not give a consistent relationship with observed corrosion rates when these mixtures are subjected to biogenic H_2SO_4. For example;

   a. The 28 d compressive strength of plain PC mixtures (57.1 MPa) is higher than that of plain CAC mixtures (54.0 MPa)
   b. PC mixtures have lower permeability (OPI, > 10.55 – log scale) than CAC mixtures (OPI, < 9.90 – log scale)
   c. PC mixtures have lower sorptivity (< 6.1 mm/√hr) than CAC mixtures (> 9.5 mm/√hr)

   Despite PC mixtures showing superior physicochemical characteristics, findings on the performance of concrete mixtures subjected to biogenic H_2SO_4 attack show that CAC mixtures perform better than PC mixtures. Therefore characterising concrete mixtures based on physicochemical properties does not merit applications in biogenic corrosion prediction.

(6) There is need to develop effective resistance capacity or materials factors that incorporate relationships between various biogenic corrosion rates and substrate types, for incorporation in certain deterministic (mechanistic) biogenic corrosion prediction models such as the LFM, which is widely used by design engineers.

3.6 Scope for further work

The literature review presented in Chapter Two together with the review of work undertaken in the VES (Chapter Three) have shown that characterising certain aspects of the sewer environment, particularly factors that individually contribute to the generation and release of sulphides, and their interrelationships that lead to the formation of biogenic H_2SO_4 and subsequently, attack of concrete sewer pipes is needed. Certain significant factors which have not been dealt with sufficiently in past studies are (i) characterisation of the mineralogical phases in the corroded layers of concrete sewers, and (ii) means of improving biogenic corrosion prediction models that are used in practice based on long-term studies in 'live' environments. The current study will focus on these factors.

3.7 References

Alexander, M. G., & Fourie, C. W. 2011. Performance of sewer pipe concrete mixtures with portland and calcium aluminate cements subject to mineral and biogenic acid attack. *Materials and Structures*. 44 (1): 313 – 330.

Alexander, M. G., Goyns, A. M., & Fourie, C. W. 2008. Experiences with a full-scale experimental sewer made with CAC and other cementitious binders in Virginia, South Africa. *Proceedings of the Centenary Conference on Calcium Aluminate Cements.* June 30 – July 2, Avignon. 279 – 292.

Bratby, J. 1980. *Coagulation and flocculation*. Croydon: Uplands Press.

Chandra, S. 2002. Properties of concrete with mineral and chemical admixtures. In: Barnes, P., & Bensted, J. Eds. *Structure and performance of cements*. London: Spon Press. 141 – 185.

Council for Scientific and Industrial Research. 1959. *Corrosion of concrete sewers*. Pretoria: CSIR. Series DR12.

Council for Scientific and Industrial Research. 1996. *Consolidated report on phase 1 of sewer corrosion research: The Virginia sewer experiment and related research*. Pretoria: CSIR. Report No BOU/C128.

Ebbing, D. D. 1984. *General Chemistry*. Boston: Houghton Mifflin.

Fourie, C. W. 2007. Acid resistance of sewer pipe concrete. MSc (Eng) dissertation. University of Cape Town, Cape Town.

Goyal, S, Kumar, M., Sidhu, S. D., & Bhattacharjee, B. 2009. Resistance of mineral admixture concrete to acid attack. *Journal of Advanced Concrete Technology*. 7: 273 – 283.

Goyns, A. M. 2003. Virginia sewer rehabilitation: Progress Report 1. Pretoria: Concrete Manufacturers Association.

Goyns, A. M. 2010. Virginia sewer rehabilitation: Progress Report 4. Pretoria: Concrete Manufacturers Association.

Goyns, A. M. 2014. Virginia sewer rehabilitation: Progress Report 6. Pretoria: Concrete Manufacturers Association.

Goyns, A. M., Alexander, M. G., & Fourie, C. W. 2008. Applying experimental data to concrete sewer design and rehabilitation. *Proceedings of the Centenary Conference on Calcium Aluminate Cements.* June 30 – July 2, Avignon. 293 – 308.

Goyns, A. M., Alexander, M. G., & Fourie, C. W. 2008. Applying experimental data to concrete sewer design and rehabilitation. *Proceedings of the Centenary Conference on Calcium Aluminate Cements.* June 30 – July 2, Avignon. 293 – 308.

Krüger, J. E. 1990. *First Interim Report on Sewer Corrosion Research – Virginia Sewer.* Pretoria: CSIR.

Lu, Y. 2001. Modelling of sulphide emission from the Virginia sewer system. MSc (Eng) dissertation. University of Cape Town, Cape Town.

Majumdar, A. J., & Singh, B. 1992. Properties of some blended high-alumina cements. *Cement and Concrete Research*. 22(6): 1101 – 1104.

Motsieloa, N. 2013. Acid resistance of sewer pipe concrete. MSc (Eng) dissertation. University of Cape Town, Cape Town.

Robson, T. D. 1962. *High Alumina Cements and Concretes*. New York: John Willey & Sons.

Schremmer, H. 1972. Report of the ATV working party concerning parameters of the ATV Code of Practice A115. *Wastewater Correspondence*. 33(8): 729.

South African National Standard. SANS 6242: 2008. *Acid insolubility of aggregates*. Pretoria: SABS.

South African National Standard. SANS 676: 2010. *Reinforced concrete pressure pipes*. Pretoria: SABS.

Chapter Four: Materials and experimental methods

4.1 Introduction

This chapter presents details of concrete materials, experimental arrangements and related tests that were carried out in the current study. The main focus is to characterise three sets of samples that have been exposed to biogenic H_2SO_4 with the view of understanding the underlying mechanisms of attack, and incorporating these in a biogenic corrosion prediction model, the Life Factor Method (LFM). One set, consisting of 'lid' samples, has been exposed to biogenic H_2SO_4 in a 'live' environment (the VES) for approximately 127 months. The second set, consisting of discs, has also been exposed in the VES for approximately 48 months, while the third set, consisting of discs for comparative studies in different sewer environments, has been exposed in the VES and a manhole at Langa for approximately 6 months.

Before proceeding, it is important to note that since the 1960s most concrete sewers installed in South Africa were made using calcareous aggregates, usually dolomite (DOL), and the sacrificial layer principle (CSIR, 1959). In practice, a distinction has been made between the conventional sacrificial layer system where the whole pipe is made using the same material (PC-based), and the corrosion control layer system where two different materials are used, one for the host pipe and another for the lining (Goyns, 2001). The use of CAC/DOL concrete as a corrosion resisting layer for concrete sewers has been based on information obtained from the testing of various cementitious materials in an aggressive 'live' sewer (VES). This technique has been in use in South Africa since 1997, and has proved to be both technically sound and cost-effective for sewers where conditions are deemed to be highly aggressive (Goyns, 2003), although there is no documented biogenic prediction model or method that provides a basis for the design of these sacrificial or corrosion resisting layers.

From the literature review presented in Chapter Two, and further review of work undertaken in the VES presented in Chapter Three, it was shown that biogenic H_2SO_4 attack or corrosion in sewers is affected by several parameters in the aqueous, gaseous, biological, and mineralogical phases that are interrelated. However, even though there is vast research on characteristics of the aqueous, gaseous, and biological phases particularly in other fields such as wastewater engineering and environmental microbiology, the same is not true for the mineralogical phase (concrete materials), yet the rate-controlling parameter in biogenic corrosion mechanisms is the neutralisation capacity of materials (concrete mixtures). Researchers focussing on biogenic corrosion prediction define this neutralisation capacity of concrete mixtures as conventional alkalinity (g $CaCO_3$ per g concrete material) (EPA, 1992; Beddoe and Dorner, 2005; Hvitved-Jacobsen et al., 2013). However, based on the reviewed literature, this hypothesis is not reliable, and the current study will focus on improving this aspect through microstructural characterisation of various concrete mixtures used in the manufacture of concrete sewer pipes.

The following sections present details of concrete materials, experimental arrangements and related tests that were carried out in the current study with the view of addressing knowledge gaps relating to characterisation of the mineralogical phase (including the microbial ecosystem on concrete sewer pipe surfaces), and also the gaseous phase. Although the current study focussed on the VES, certain studies were also being undertaken simultaneously at the Langa pump station in Cape Town. Therefore details of materials presented herein include those that were used by other researchers during 2004 (for 'lid' samples in the VES for corrosion rate measurements) and 2010 (for core samples in the VES for corrosion rate measurements), and those used to cast 'new' samples during the current study in 2015. The latter involved surface pH vs. time profiling investigations only on core samples in the VES and Langa since this aspect, which is significant during the biogenic corrosion processes in sewers, has not been investigated before in South African sewer environments.

4.2 Materials

As highlighted in Chapters Two and Three, certain characteristics of concrete materials (binder types (cements and SCMs) and aggregates) play a significant role in neutralising biogenic acid attack in sewers, and thus provide biogenic corrosion rate control mechanisms. Therefore a study of the materials presented in this section is intended to reveal an in-depth understanding of the ability of certain concrete mixtures to improve performance with regard to reducing the biogenic corrosion rate in concrete sewer environments.

4.2.1 Cement types and SCMs (binders)

Portland cement (PC) used in the current study was supplied by PPC Ltd. Two types of PC were used; (i) CEM I 42.5R was used in all samples cast during 2004 and 2010, and (ii) CEM II/A-L 52.5N was used in samples cast during 2015 due to unavailability of the CEM I. The other cement used was CAC (*Ciment Fondu* (CF)), supplied by Kerneos SA (Pty) Ltd. The SCMs used included GGBS supplied by Afrisam SA (Pty) Ltd, FA supplied by Ash Resources (Pty) Ltd, and SF supplied by Silicon Smelters (Pty) Ltd. In principal, there are two binder systems under study; (i) PC-based, with and without SCMs, and (ii) CAC-based, with and without SCMs. In practice, PC-based concrete mixtures are mainly used for host pipe applications, but can also be used for lining applications (as sacrificial layers) while CAC-based mixtures are solely used for lining applications because of cost limitations. The cost of CAC is approximately fourfold that of PC (Scrivener et al., 1999). The typical chemical composition of these binders is given in Table 4-1, and also in Appendices D, E and F (Goyns, 2010; Alexander and Fourie, 2011; Motsieloa, 2013).

Table 4-1: Typical chemical composition of different binders used in the current study (Goyns, 2010; Alexander and Fourie, 2011; Motsieloa, 2013).

Binder type	Chemical composition (%)											
	CaO	MgO	SiO_2	Al_2O_3	Fe_2O_3	Mn_2O_3	TiO_2	SO_3	Na_2O	P_2O_5	K_2O	LOI
CEM I (42. R)	64.5	0.8	21.2	4.0	3.0	0.1	0.3	2.9	0.1	0.2	0.7	2.87
CEM II/A-L (52.5N)*	63.2	0.91	20.2	4.03	3.19	0.1	0.24	2.64	0.18	0.15	0.67	4.08
CAC (CF)	37.6	0.7	4.4	39.5	15.1	0.2	1.8	0.2	0.1	0.1	0.2	0.2
FA	4.1	1.0	54.9	31.3	3.7	0.06	1.67	0.19	0.36	0.49	0.71	0.78
SF	0.68	0.2	96.0	< 0.1	< 0.1	-	-	0.25	0.18	-	0.45	1.8
GGBS	36.4	8.1	37.1	12.8	0.72	0.98	0.59	2.24	0.5	-	1.07	-

*Data from current study, supplied by PPC

4.2.2 Aggregates

As discussed in Chapter Two, the choice of aggregates influences the neutralisation capacity of concrete mixtures subjected to biogenic H_2SO_4 attack in sewers. The current study mainly focussed on concrete mixtures with calcareous coarse aggregates and a blend of calcareous and siliceous fine aggregates. However, certain concrete mixtures with siliceous coarse aggregates were also studied with the view of distinguishing the deterioration mechanisms between calcareous and siliceous aggregates under biogenic H_2SO_4 attack.

The calcareous aggregates used in all the samples included 13 mm maximum aggregate size (MAS) dolomite and dolomite crusher sand supplied from Rocla Roodepoort (sourced from Olifantsfontein) in Gauteng Province (this is a source of 'high quality' dolomite (DOL 3 as described in section 3.4.3)), while the siliceous coarse aggregate used in certain CAC-based samples cast during 2004 is a 13 mm MAS quartzite (SIL) supplied from Rocla Roodepoort. The siliceous pit (filler) sand used in all the samples was also supplied from Rocla Roodepoort. The typical chemical composition of the calcareous (dolomite) aggregate is given in Table 4-2, while certain mechanical and acid solubility properties of both calcareous and siliceous aggregates are given in Table 4-3. The particle size distribution of these aggregates is given in Figure 4-1 and also in Appendix H.

Table 4-2: Typical chemical composition of Olifantsfontein dolomite (Motsieloa , 2013).

Aggregate/ type	Chemical composition (%)				
	CaO	MgO	Mn_2O_3	Fe_2O_3	LOI
Olifantsfontein dolomite	30.8	21.2	< 1.0	< 1.0	46.0

Table 4-3: Certain mechanical and acid solubility properties of aggregates.

Aggregate/type	Properties of aggregates			
	Specific gravity*	10% FACT** (kN)	Fineness Modulus#	Acid insolubility ## (%)
Olifantsfontein dolomite stone, 13 mm	2.87	354	-	4.18
Roodepoort quartzite stone, 13 mm	2.65	360	-	90.00
Olifantsfontein dolomite crusher sand	-	-	3.76	6.28
Roodepoort siliceous pit (filler) sand	-	-	1.74	93.90

*SANS 5844: 2014
**SANS 5842: 2006
#SANS 201: 2008
##SANS 6242: 2008

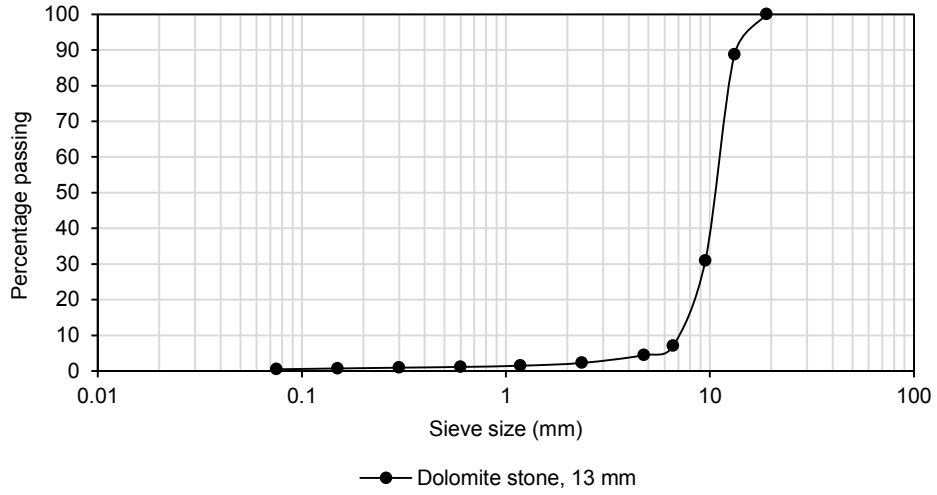

(a) Particle size distribution of Olifantsfontein dolomite stone, 13 mm

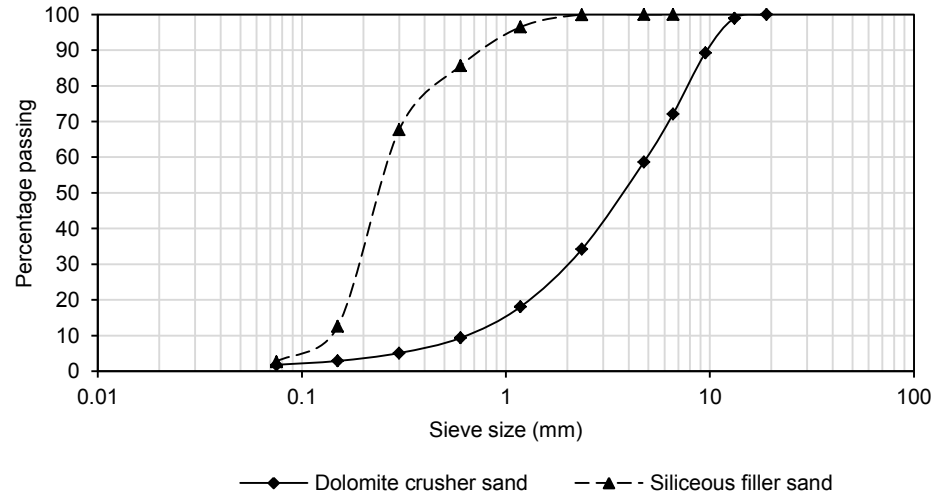

(b) Particle size distribution of fine aggregates
Figure 4-1(a) and (b): Particle size distribution of coarse and fine aggregates.

4.2.3 Concrete mix proportions

All the PC-based concrete mix proportions were based on three principal guidelines used in South Africa's concrete sewer pipes industry; (i) the target alkalinity as defined by the LFM, (ii) the consistency (or measure of workability) suitable for precast manufacturing process using the horizontal roller suspension technique as described in Section 4.3, and (iii) high early strength to allow for stripping and steam curing. The proportions for CAC-based mixtures were simplistically matched to those of PC-based mixtures (with regard to the cement or total binder content) for comparative studies. Since PC and CAC have different chemical compositions and products of hydration, optimising the CAC-based mixtures based on, for example, the LFM or early strength would be misleading. Therefore certain binder contents in both PC- and CAC-based mixtures were used in similar quantities, which included 16%, 18%, and 23% by mass in the total concrete mixture.

These binder contents in PC-based mixtures resulted in concrete that met the three principal guidelines mentioned above (Goyns, 2003), namely; (i) design life of 50 years or a sacrificial layer approximately 40 mm in thickness, which based on the LFM, requires alkalinity values in the order of 0.9 (for PC/DOL mixtures), (ii) 'zero-slump' mixes, due to the manufacturing technique of these pipes, thus w/b ratios of between 0.3 and 0.36 and appropriate water content, and (iii) early strength considerations with target 14 h compressive strengths of 30 MPa (Fourie, 2007; Motsieloa, 2013).

The concrete mix proportions used for the manufacture of the 'lid' samples installed in the VES during 2004, and which formed the main focus of the current study, are given in Table 4-4 (also in Appendix E). These 'lid' samples were manufactured at Rocla's Roodepoort precast plant. The mix proportions for core samples installed in the VES during 2010, and for those installed in the VES and Langa during 2015, are given in Table 4-5 (also Appendix F) and Table 4-6 (also Appendix G) respectively. The core samples were cast in the laboratory, targeting similar characteristics (compressive strength, density, OPI) as those of the 'lid' samples. The respective manufacturing techniques are discussed in Section 4.3.

Table 4-4: Mixture composition (percentage of total mix mass) of certain 'lid' samples installed in Manholes I, II and III in the VES during 2004 (Goyns, 2010).

Mixture†	% total binder	Binder type				% Aggregate		
		% SCM			% Cement	Stone*	Crusher sand**	Filler sand##
		GGBS	FA	SF				
Concrete pipe mixtures:								
PC/DOL 16	16	-	-	-	16	48	18	18
PC/DOL 18	18	-	-	-	18	47	18	17
PC/DOL 23	23	-	-	-	23	44	17	16
PC/GGBS/DOL	18	6	-	-	12	47	18	17
PC/FA/DOL	18	-	4.5	-	13.5	47	18	17
PC/SF/DOL	18	-	-	1.5	16.5	47	18	17
Concrete lining mixtures:								
CAC/SIL 23	23	-	-	-	23	44	17	16
CAC/DOL 16	16	-	-	-	16	48	18	18
CAC/DOL 18	18	-	-	-	18	47	18	17
CAC/DOL 23	23	-	-	-	23	44	17	16
CAC/FA/SF/DOL	17	-	4.5	1.5	11	47	18	18
CAC/Alag™	20	-	-	-	20	40	-	40

†PC = CEM I (42.5R); CAC = Ciment Fondu. See chemical composition (also of SCMs) in Appendix E.3; Alag™ = aluminate aggregate

*Nominal 13 mm maximum size used for sewer pipe mixtures and nominal 6 mm maximum size for lining mixtures

**Crusher sand used = dolomite

##Filler sand used = siliceous, except for the aluminate-based

Table 4-5: Concrete mixture proportions (ratio by mass to total binder content) of core samples installed in the VES during 2010 (Motsieloa, 2013).

Mixture†	% total binder	Binder type				% Aggregate		
		SCM			Cement	Stone*	Crusher sand**	Filler sand##
		GGBS	FA	SF				
Concrete lining mixtures:								
PC 100	16	-	-	-	1.00	2.89	1.10	1.10
PC 70/FA 30	16	-	0.30	-	0.70	3.04	0.98	0.98
PC 90/FA 10	16	-	0.10	-	0.90	2.89	1.08	1.08
PC 72/FA 20/SF 8	16	-	0.20	0.08	0.72	3.02	0.99	0.99
CAC 100	16	-	-	-	1.00	2.89	1.11	1.11
CAC 85/FA 15	16	-	0.15	-	0.85	2.93	1.04	1.04
CAC 75/FA 25	16	-	0.25	-	0.75	3.01	1.02	1.02
CAC 60/FA 40	16	-	0.40	-	0.60	3.07	0.94	0.94
CAC 75/GGBS 25	16	0.25	-	-	0.75	2.89	1.10	1.10
CAC 60/GGBS 40	16	0.40	-	-	0.60	2.89	1.09	1.09
CAC 40/GGBS 60	16	0.60	-	-	0.40	2.89	1.08	1.08
CAC 50/GGBS 50	16	0.50	-	-	0.50	2.89	1.08	1.08

†PC = CEM I (42.5R); CAC = Ciment Fondu. See chemical composition (also of SCMs) in Appendix F.2
*Nominal 13 mm maximum size
**Crusher sand used = dolomite
##Filler sand used = siliceous

Table 4-6: Concrete mixture proportions (ratio by mass to total binder content) of core samples installed in the VES and Langa during 2015.

Mixture†	% total binder	Binder type				% Aggregate		
		SCM			Cement	Stone*	Crusher sand**	Filler sand##
		GGBS	FA	SF				
Concrete lining mixtures:								
PC 100	16	-	-	-	1.00	2.89	1.09	1.09
PC 67/GGBS 33	16	0.33	-	-	0.67	2.89	1.09	1.09
PC 75/FA 25	16	-	0.25	-	0.75	2.89	1.09	1.09
PC 92/SF 8	16	-	-	0.08	0.92	2.89	1.09	1.09
CAC 100	16	-	-	-	1.00	2.89	1.09	1.09
CAC 65/GGBS 10/FA 25	16	0.10	0.25	-	0.65	2.89	1.09	1.09

†PC = CEM II/A-L (52.5N); CAC = Ciment Fondu. See chemical composition (also of SCMs) in Appendix G.1; w/b = 0.36
*Nominal 13 mm maximum size
**Crusher sand used = dolomite
##Filler sand used = siliceous

4.3 Experimental methods

4.3.1 Casting and curing of samples

As mentioned in earlier sections, the samples used in the current study included ‘lids’ and cores. The ‘lid’ samples were cast as part of a complete sewer pipe, in a precast factory (Rocla Roodepoort) using the horizontal roller suspension technique. This technique incorporates an outer steel form that rotates on a horizontal mandrel during the pipe manufacturing process (Figure 4-2). A zero-slump concrete mixture was fed into the steel mould using a conveyor system that is capable of distributing the concrete throughout the entire length of the mould. During this process of filling the steel mould, the horizontal mandrel rotates in a certain direction while the mould together with the fresh concrete rotates in the opposite direction. Therefore compaction of the concrete is achieved in two ways; (i) initially, by centrifugal force, and (ii) as the mould fills up, by compaction via the rotating mandrel.

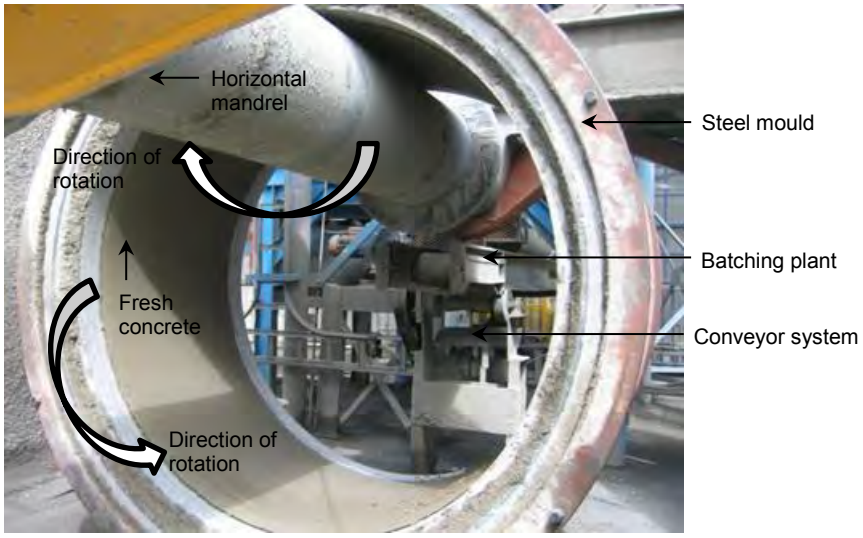

Figure 4-2: Horizontal roller suspension sewer pipe manufacturing technique.

On completion of the casting exercise, the freshly made pipe, while still in the mould, was immediately moved to the curing area where it was left to set for 4 h, then steam-cured at 50 °C for a further 4 h prior to demoulding. Thereafter, the concrete pipe was air-cured for at least 7 d before respective sections were cut (Figure 4-3) and installed in the VES. It is important to note that for samples incorporating two binder systems (such as PC-based for the host pipe and CAC-based for lining), the host pipe was cast first then allowed to achieve its initial set (after approximately 45 min) before proceeding to cast the lining layer.

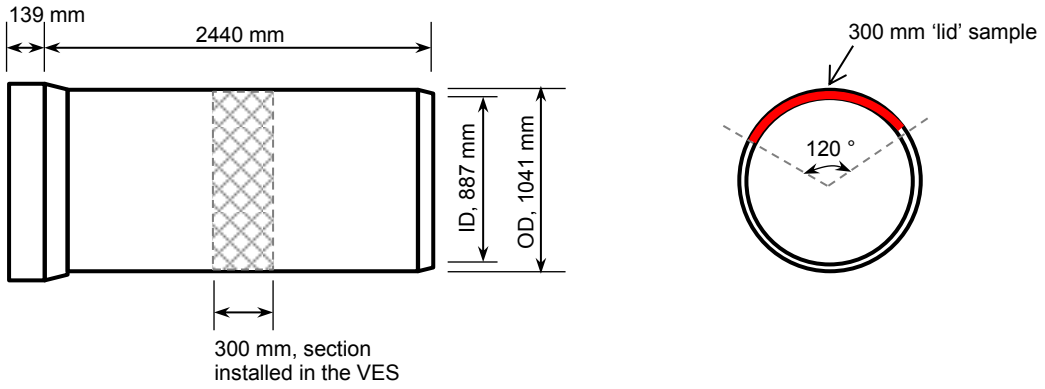

(a) Whole concrete sewer pipe (b) 'lid' sample(s) installed in the VES

Figure 4-3: Schematic of how concrete sewer pipe samples were cut from whole pipe sections.

These 'lids' also act as windows through which additional core samples can be suspended in the sewer headspace, and accessed for observations and measurements as discussed in Chapter Three.

Motsieloa (2013) cast core samples using a dynamic heavy compaction technique developed by Fourie (2007), while the core samples cast during 2015 for surface pH vs. time profiling were cast using a static (heavy) compaction technique; however, both techniques resulted in cores with similar characteristics as the 'lid' samples manufactured using the horizontal roller suspension technique described above. Concrete mixtures for the core samples were batched by mass and mixed using a 5-litre bench-mounted mixer (Hobart®) (Figure 4-4(a)) and cast in a 75 mm diameter by 300 mm steel mould (see mould and accessories in Figure 4-4(b)).

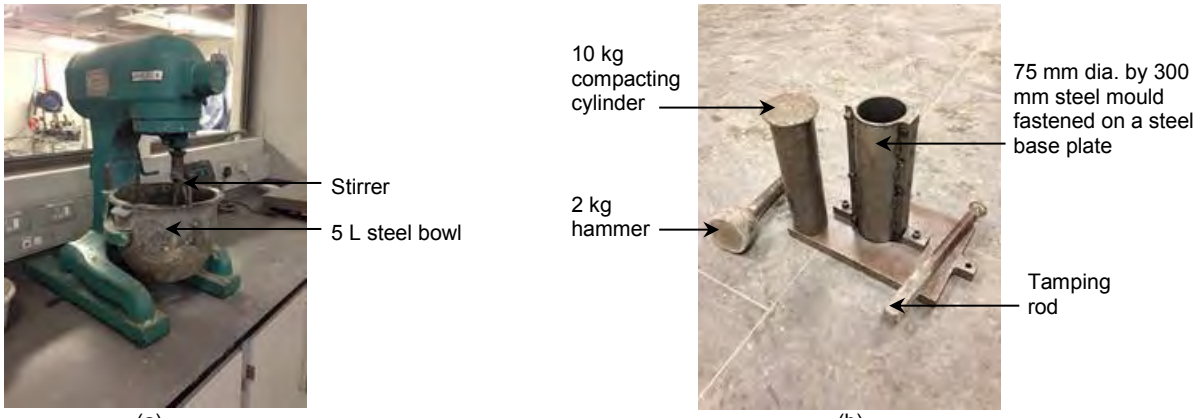

Figure 4-4: (a) 5 L bench-mounted mixer (Hobart®) ; (b) Steel mould and accessories used for casting core samples using heavy compaction techniques.

The freshly-mixed concrete was placed and compacted in the steel mould using different techniques by different researchers; (i) the dynamic heavy compaction technique was used for core samples installed in the VES during 2011, (ii) the static compaction technique was used for core samples installed in the VES and Langa during 2015. For the dynamic heavy compaction technique, the freshly-mixed concrete was placed in the mould in four layers. Each layer was first lightly compacted 20 times using a tamping rod; thereafter, the 10 kg compacting cylinder was placed on the top surface of the lightly compacted layer and struck 5 times using the 2 kg hammer. The freshly-compacted sample was then left to set in the mould for 4 h. Thereafter, the sample was stripped and immediately cured in water at 38 ± 2 °C (Figure 4-5(a)) for 10 h, based on the concept of Saul's Law of Maturity as described by Motsieloa (2013) and Fourie (2007). After the 10 h of curing in water, the core sample was air dried for 28 d in a room maintained at a temperature of 22 ± 2 °C and RH of 50% in order to achieve similar maturity characteristics as concrete manufactured in the industry (Fourie, 2007). However, for samples meant for early strength testing, they were tested after the 10 h period of curing in water (total, 14 h after casting).

For the static compaction technique, a greater part of the procedure in the dynamic technique was followed except that instead of striking each of the four layers via the 10 kg compacting cylinder using the 2 kg hammer, a static load was applied using a compression machine (Figure 4-5(b)), targeting a load of 160 kN per layer in order to achieve similar characteristics (density, strength, OPI) as for core and 'lid' samples cast using the dynamic and roller compaction techniques respectively. The total height of the samples was 220 ± 10 mm. The curing regime was similar to that described above (after dynamic compaction).

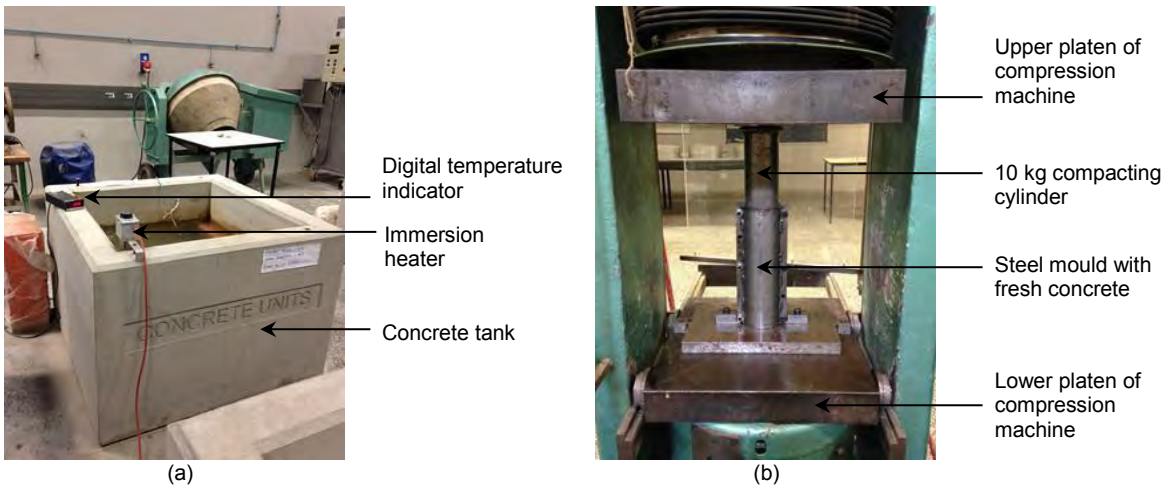

Figure 4-5: (a) Water curing bath maintained at 38 ± 2 °C; (b) Static compaction technique of core samples.

4.3.2 Tests for quality checks of hardened concrete

As described in previous sections, most of the samples used in the current study were prepared during earlier studies by other researchers. Therefore the required tests, which included compressive and tensile strength, density, oxygen permeability, water sorptivity and porosity, acid insolubility, and hydrogen ion were undertaken at respective ages of testing (Fourie, 2007; Goyns, 2008; Motsieloa, 2013). The 'new' samples cast during the current study were used for surface pH vs. time profiling only since this aspect, which is significant during the biogenic corrosion processes in sewers, has not been investigated before in South African sewer environments. In this regard, the 'new' samples, which utilised concrete mixtures similar to those of the 'lid' samples installed in the VES during 2004 were not subjected to all the previous tests, but to (i) density (saturated) (SANS 6251, 2006) and compressive strength (SANS 5863, 2006) using 75 mm diameter by 80 mm cores, (ii) oxygen permeability, water sorptivity and porosity (SA DI Manual, 2009) using 70 ± 2 mm diameter by 30 ± 2 mm discs, and (iii) surface pH, using powder in suspension (Kakade, 2014). A description of these standard test procedures and respective outcomes are given in Appendix I.

4.3.3 Exposure conditions for 'lid' and core samples

The experimental work is based on samples exposed in-situ. The reasons for utilising in-situ exposure conditions as opposed to laboratory-based exposure conditions are (i) laboratory-based mineral acid testing cannot model conditions in a real sewer where acids are microbially generated due to the influence of other mechanisms involved, (ii) availability of long-term data (more than 127 months) from the VES, which could be used to reliably characterise concrete mixtures used in the manufacture of concrete sewer pipes, (iii) access to sewer environments (the VES and Langa) that are deemed to possess ideal conditions (such as average sewer temperature > 18 °C, average H_2S gas concentration > 50 ppm, and average RH > 70% in the sewer's headspace) for generation of aggressive biogenic H_2SO_4. The conditions in the VES were described in Section 3.4. The other site used in the current study is a manhole located within the Langa Pump Station in Cape Town.

The Langa (minor and main) Pump Station is one of the catchment areas for Athlone Wastewater Treatment Works. The Minor Pump Station receives domestic sewage only while the Main Pump Station receives mostly domestic and some industrial sewage. The manhole, where samples used for a comparative study (with those in the VES) on surface pH vs. time profiling were suspended, is located between the Minor and Main (Langa) Pump Stations (see Figure 4-6).

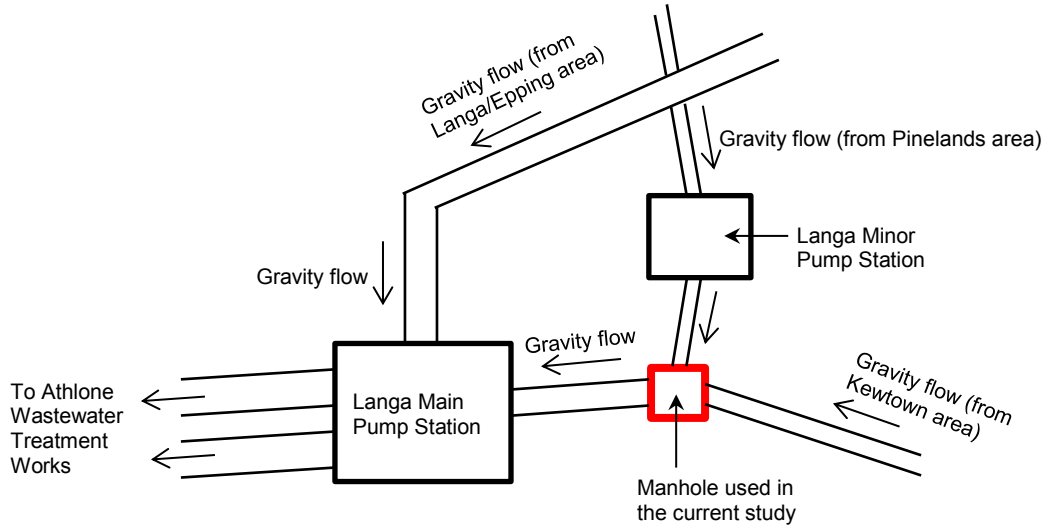

Figure 4-6: Schematic of the sewer network at Langa Pump Station showing two feeders into the manhole used in the current study (20 m downstream of the Minor Pump Station).

Figure 4-7 shows an aerial view of the 3 m deep manhole at Langa (with the steel cover removed) and core samples suspended therein.

Figure 4-7: (a) Aerial view of the 3 m deep manhole at Langa with the steel cover removed; (b) Some core samples for surface pH vs. time profiling, suspended in the manhole at Langa.

Similar to studies in the VES, the sewer environment characteristics (that influence biogenic corrosion mechanisms in concrete sewers) that were measured at Langa included H_2S gas concentration, temperature and RH in the manhole's headspace. Figure 4-8 shows the H_2S gas profiles in the manhole at different climatic seasons. The cyclic peaks are mainly due to turbulent flows generated when sewage is released from the Minor Pump Station.

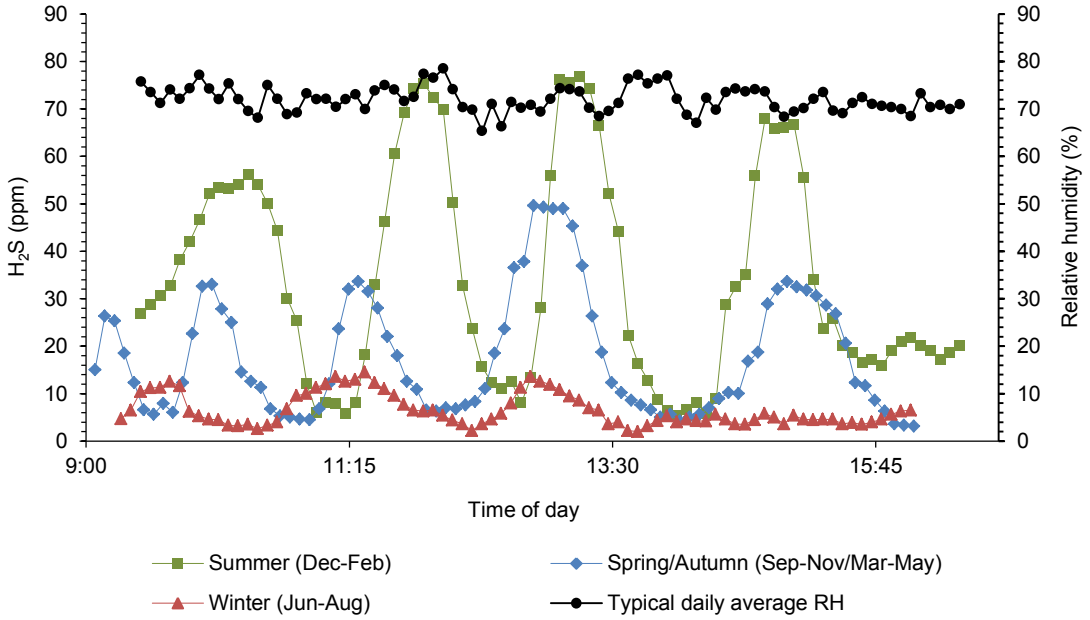

Figure 4-8: Typical daily H_2S and RH profiles in the manhole at Langa during summer, spring/autumn and winter months (data from current study (2013-2015)).

The (3 point moving) average headspace temperatures in winter (June – August), spring ((September – November) (and autumn (March – May)), and summer (December – February) in the manhole at the time of profiling the H_2S gas concentrations (given in Figure 4-8) were 18 °C, 22 °C and 26 °C

respectively. The typical daily RH in the manhole is above 72%. The temperature and RH profiles in the manhole at Langa are also given in Appendix K.

4.3.4 Measurement of in-situ sewer environment parameters that influence biogenic corrosion processes

The main focus of the current study is to characterise concrete mixtures subjected to biogenic acid attack mechanisms in a sewer environment, and to apply the findings in biogenic concrete corrosion prediction, specifically the LFM. It is therefore important that, together with the corrosion rates established based on the performance of the various concrete mixtures, relationships with parameters that are deemed to influence the biogenic concrete corrosion mechanisms (such as pH and temperature of the sewage, temperature and RH of the sewer's headspace, gas (H_2S, CO_2, O_2) concentrations in the sewer's headspace, and surface pH of concrete) be defined. In this regard, these parameters were measured during the current study as discussed in the following sections.

4.3.4.1 pH and temperature of the sewage

The pH and temperature of the sewage were measured using a portable digital spear-tip (pH and temperature) meter (Oakton®). Prior to undertaking these measurements in the VES, the flow of sewage was diverted from the experimental to the by-pass section (see Section 3.4.1), and the 'lid' samples in the respective locations in the experimental section removed in order to provide a window to access the residual sewage (Figure 4-9). The test locations were accessed via Manholes I, II, III and IV. After switching on the digital meter, 20 readings were taken randomly within each access location (manhole) by dipping the spear-tip approximately 20 mm into the sewage. Measurements were taken during (i) different climatic seasons, and (ii) different time of day (morning and afternoon sessions). These measurements were taken every 3 to 4 months over a period of 24 months.

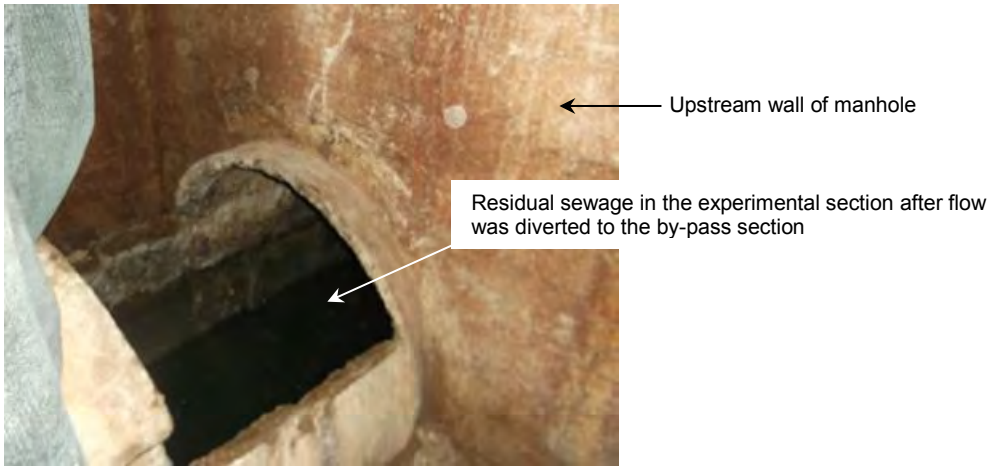

Figure 4-9: 'lid' samples removed in the experimental section of the VES to enable sewage pH and temperature measurements.

Due to access restrictions into the manhole at Langa, the pH and temperature of the sewage in this location were not measured, but data was available for use from the City of Cape Town.

4.3.4.2 Temperature and RH in the headspace of the VES and manhole at Langa

The temperature and RH in the headspace were measured (logged) using a portable dual data logger (Huato S100-TH series). In order to take measurements in the experimental section at the VES, the flow of sewage was first diverted to the by-pass section. One 'lid' sample at each respective test location was then removed to create an access window. The data logger was then switched on, fastened to a 'lid' that was adjacent to the access window using a 2 mm diameter plastic-coated wire rope, and allowed to suspend in the headspace (approximately 300 mm above the sewage flow level). The removed 'lid' was then gently put back in place (any gaps between adjacent 'lids' were sealed using porcelain clay), and the diverted flow of sewage was redirected through the experimental section, marking the beginning of the logging session.

In order to take measurements in the manhole at Langa, the manhole's steel cover was lifted approximately 150 mm off its resting position, and the portable data logger that was attached to a 2 mm diameter plastic-coated wire rope was switched on, lowered into the manhole and allowed to suspend approximately 300 mm above the inlet pipes from the Langa Minor Pump Station (see Figure 4-7 (a)) (which are approximately 1 m from the base of the manhole). The manhole's steel cover was then gently returned to its resting position thus holding the wire rope in place. Any gaps between the steel cover and the manhole's top surface were sealed using porcelain clay. This marked the beginning of the logging session.

Each data logging session lasted for 4 h during (i) different time of day (morning and afternoon sessions), and (ii) different climatic seasons. These measurements were taken every 3 to 4 months over a period of 24 months in the VES and manhole at Langa.

4.3.4.3 Gas (H_2S, CO_2 and O_2) concentration in the headspace of the VES and manhole at Langa

H_2S, CO_2 and O_2 gas concentrations (in ppm) in the headspace were measured using a portable multi-gas meter (MX6 iBrid®) fitted with a 2 mm diameter silicone tube (Figure 4-10(a)). Prior to undertaking the gas readings, an inspection was undertaken to ensure that all joints between the 'lid' samples were sealed using porcelain clay to minimise gas leakages. In order to take measurements in the experimental section at the VES, the gas meter was switched on and allowed to 'warm-up' for approximately 2 minutes. Thereafter, the silicone tubing attached to the gas meter was inserted through a pre-drilled 3 mm diameter hole on the crown of the lid samples in respective test locations (the test locations were accessed via Manholes I, II, III and IV), and allowed to suspend approximately 300 mm above the sewage flow level. The gap between the silicone tube and the pre-drilled hole was sealed using porcelain clay. This marked the beginning of the gas logging session.

In order to take measurements in the manhole at Langa, the manhole's steel cover was lifted approximately 50 mm off its resting position, and the gas meter's silicone tube inserted through this opening (after the 2-minute warm-up), and allowed to suspend approximately 300 mm above the inlet pipes from Langa Minor Pump Station. The manhole's steel cover was then gently returned to its resting position thus holding the silicone tube in place. Any gaps between the steel cover and the manhole's top surface were sealed using porcelain clay. This marked the beginning of the gas logging session.

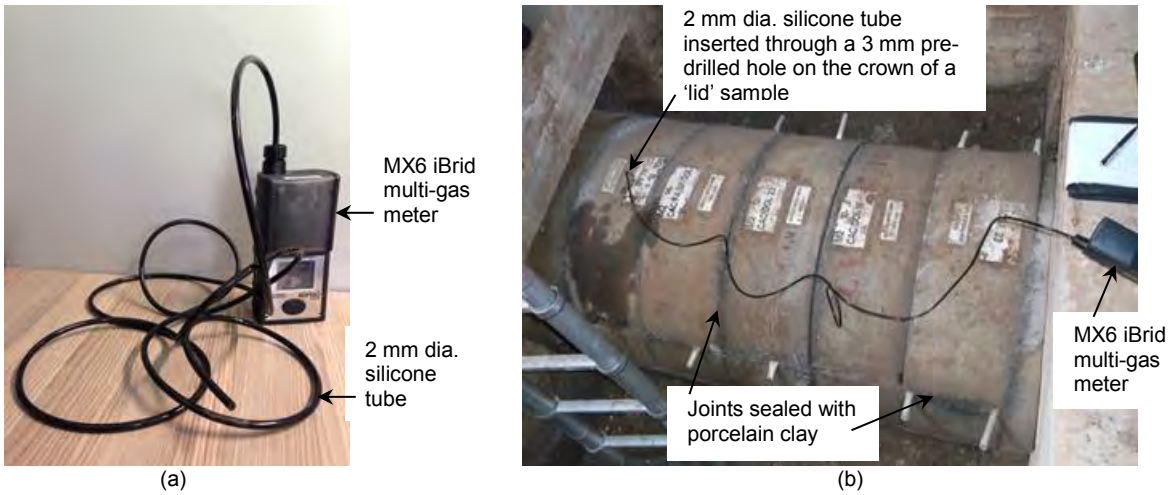

Figure 4-10: (a) MX6 iBrid multi-gas meter; (b) Set-up of gas measurement in the VES.

Each gas logging session lasted for 8 h on any particular day of different climatic seasons. These measurements were taken every 3 to 4 months over a period of 24 months in the VES and manhole at Langa.

4.3.4.4 Mass changes of samples exposed to biogenic H_2SO_4 in the VES

The mass changes of the 'lid' and core samples were measured using different equipment. For the 'lid' samples, a 100 ± 0.01 kg S-type load cell (TDC®) with a rechargeable digital display (for measured mass) attachment were used. Prior to undertaking mass measurements of the 'lid' samples in the VES, the flow of sewage was diverted from the experimental to the by-pass section. The load cell, while connected to the digital display was then attached to an overhead I-beam via steel rollers, which enabled movement of the load cell across the entire length of the manhole for ease of loading samples during measurements. Once the load cell was secured on the I-beam, steel forks, which acted as sample holders were attached to the load cell via a stainless steel chain. The digital display was then switched on before loading 'lid' samples (one at a time) for mass measurements (Figure 4-11(a)).

For the core samples, a 2 ± 0.001 kg portable bench-top scale with a digital display was used. Measurement of masses of the core samples was taken at the same period as that of the 'lid' samples. As the 'lid' samples (in sections where cores were suspended in the sewer's headspace) were removed from their positions during mass measurement, windows were created through which core samples were accessed and weighed (see Section 3.4.4 and Figure 4-11(b)). These measurements were taken every 3 to 4 months over a period of 24 months.

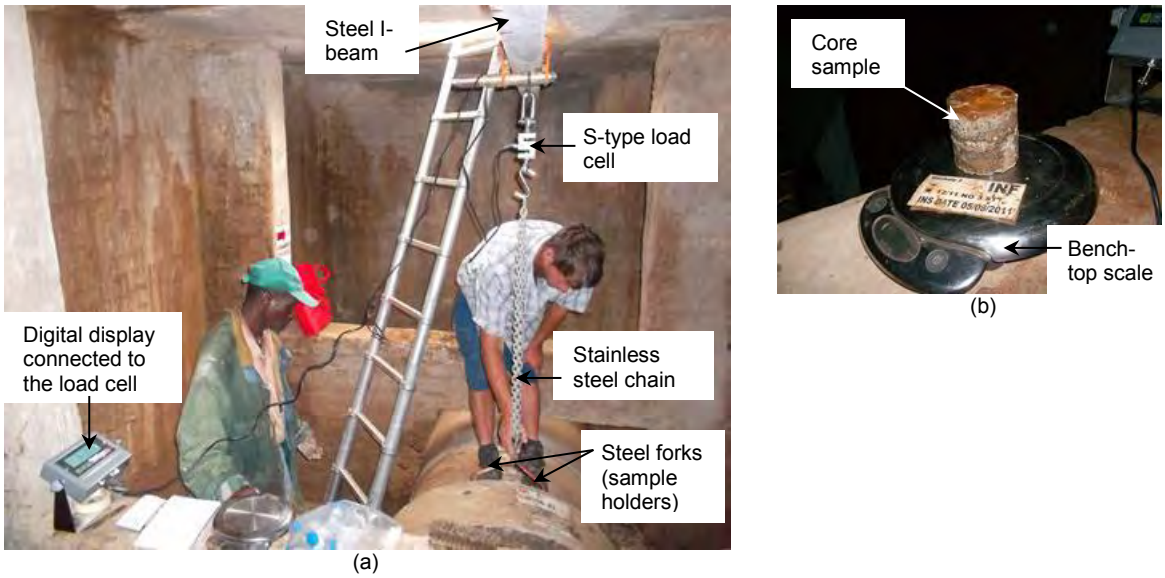

Figure 4-11: (a) Load cell assembly attached on an overhead I-section, and mass measurement of 'lid' samples; (b) Mass measurement of a core sample (the mass of the label was subtracted from the reading).

It is important to note that mass measurements taken by other researchers since the inception of this phase of study (Phase III) in 2004 were used in computing the corrosion rates of various concrete mixtures in the VES (Goyns et al., 2008; Goyns, 2010; Alexander and Fourie, 2011; Motsieloa, 2013).

4.3.4.5 Dimensional changes of samples exposed to biogenic H_2SO_4 in the VES

Dimensional changes of the 'lid' and core samples were measured using a digital outside caliper with pin tips (INSIZE®). These measurements were undertaken at the same period as mass measurements. After recording mass readings of the respective samples, the samples were removed from the weighing equipment (load cell or scale) and placed on a stable surface ('lid' samples were placed on adjacent 'lid' samples that were still in place, and the core samples were placed on a cross beam in the manhole(s)) before taking measurements. However, prior to undertaking these measurements on 'lid' samples, certain positions were marked on these samples in order to ensure that same locations were measured during subsequent exercises. A specially-made steel template with slots (Figure 4-12(a)) was used for these markings. Therefore, the dimensions (thickness) of each 'lid' sample were measured in a total of 18 locations, 50 mm from the edge (Figure 4-12(b).

Figure 4-12(c) shows measurement of the dimensions of a core sample in the VES. These measurements were taken every 3 to 4 months over a period of 18 months.

(a) Steel template used for marking dimension-measurement positions on 'lid' samples; picture shows a 'lid' sample in position

(b) Measurement of the thickness of a 'lid' sample (50 mm from the edge) in progress

(c) Measurement of the dimensions of a core sample in progress

Figure 4-12: Processes of undertaking dimensional measurements of samples installed in the VES.

4.3.4.6 pH on surfaces of samples exposed to biogenic H_2SO_4 in the VES and manhole at Langa

The pH on the surfaces of the 'lid' and core samples installed in the VES and core samples installed in the manhole at Langa was measured using a portable digital spear-tip meter (Oakton®) (Figure 4-13). Measurements at the VES were undertaken at the same period as the mass and dimension measurements. However, pH measurements were undertaken (every 3 to 4 months over a period of 18 months) before either mass or dimensions measurements were taken, since this provided the shortest time of exposure to 'outside environment' after the removal of samples from their in-situ positions.

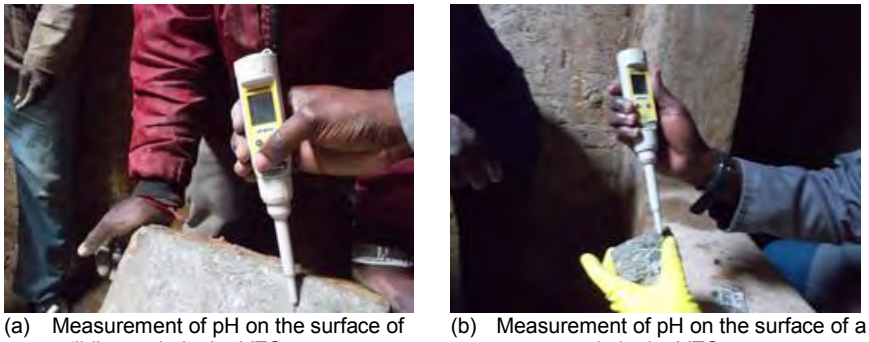

(a) Measurement of pH on the surface of a 'lid' sample in the VES

(b) Measurement of pH on the surface of a core sample in the VES

Figure 4-13: Measurement of pH on surfaces of 'lid' and core samples in the VES.

After taking in-situ measurements of the parameters discussed above, samples in the form of 'products of biogenic concrete corrosion' and concrete blocks whose surfaces had been exposed to biogenic H_2SO_4 were sampled from the VES (as described in the following section) and transported to the laboratory at UCT for further testing.

4.3.5 Sampling of specimens from the VES for laboratory tests

Sampling of the products of biogenic concrete corrosion from the 'lid' samples for laboratory testing was undertaken twice during the current study. The first set of samples was removed during November 2013 and the second set during November 2014, 109 months and 121 months respectively after installation of the 'lid' samples in the VES. These samples were removed immediately after undertaking surface pH, mass and dimensional measurements as described in Section 4.3.4. The sampling procedure entailed gently scraping and brushing off from the internal faces of the concrete sewer pipes (Figure 4-14(a)). Each scraping was first weighed using a bench-top scale before being placed in a clean 50 ml air-tight plastic bottle (Figure 4-14(b)), leaving a space of about 10 mm from

the bottle top. These bottles were then stored in an insulated 'Cooler Box' and transported from the field to the laboratory within 36 hours after sampling.

(a) Brushing the products of biogenic concrete corrosion from an internal surface of a 'lid' sample

(b) Products of corrosion being placed in a 50 ml plastic bottle after weighing using a bench-top scale

Figure 4-14: Sampling the products of biogenic corrosion from a 'lid' sample in the VES.

The concrete blocks exposed to biogenic H_2SO_4 were sampled once during the current study in March 2015, 127 months after installation in the VES. Prior to removing these samples, the flow of sewage was diverted from the experimental to the by-pass section. All the 'lid' samples in the respective sample locations (accessed via Manhole I, II or III) were then removed from their in-situ positions, enabling the blocks to be cut from the lower section (adjacent to the 'lid') (see Figure 4-15(a)) of the concrete pipe using a grinding disc.

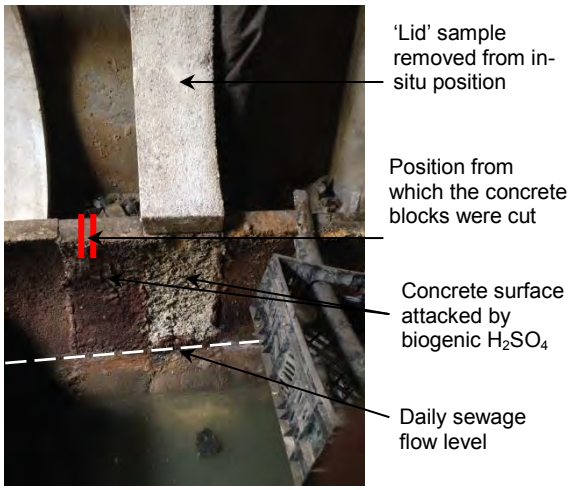

(a) Position at which concrete blocks were sampled from. 'Lid' samples have been removed from the positions to enable the sampling exercise

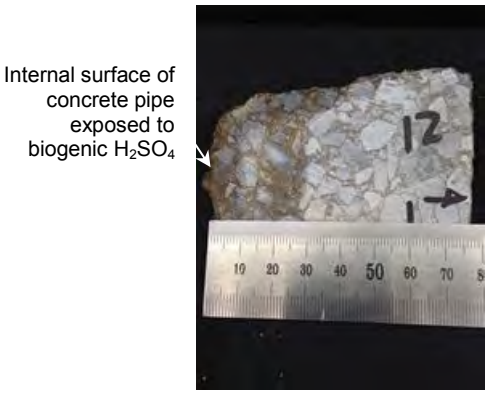

(b) Concrete block cut from a 77 mm thick pipe; block size approx. 77 mm x 50 mm x 15 mm thick

Figure 4-15: Sampling position of the concrete blocks from the VES.

The concrete blocks were placed in plastic bags, sealed and stored in an insulated 'Cooler Box' prior to transportation to the laboratory for further testing. Both the products of biogenic concrete corrosion and the concrete blocks were subjected to microstructural characterisation using various techniques as discussed in Section 4.3.6. Moreover, the products of corrosion were also used for microbial speciation in order to characterise the microbial ecosystem within such corroded layers.

4.3.6 Laboratory analytical techniques

Cements are made using many of the same rocks, ores, or minerals that are used as aggregates in concrete. Thus, elemental differentiation between the cement and the aggregates is often difficult. Fortunately, modern analytical instruments such as the scanning electron microscope, X-ray diffractometer and thermogravimetric analyser allow reliable analyses for various components of concrete. These instruments were used in the current study for microstructural characterisation of

concrete mixtures subjected to biogenic H_2SO_4 in the VES. For microbial speciation, the genomic DNA and PCR template purification kits were used. The analytical techniques that make use of these equipment are discussed in the following sections.

4.3.6.1 Scanning electron microscopy (SEM) and energy-dispersive spectroscopy (EDS)

SEM can be a powerful technique used for the identification and quantification of cementitious materials (Scrivener, 2004). In this technique, a beam of primary electrons (PE) strikes a bulk of solid (sample) where the electrons are either reflected (scattered) or absorbed, producing various signals (Figure 4-16). The incident electrons disperse into a 'pear shaped' volume in the solid. The reflected electrons (responses) include secondary electrons (SE), backscattered electrons (BSE), X-rays and Auger electrons (AE). Different modes of observation and/or microanalysis can thus be employed on a solid (sample) under examination. The most frequently used modes in SEM involve the capture of secondary and backscattered electrons, while the most commonly used micro-analytical techniques, based on detection of X-rays are the energy dispersive spectroscopy (EDS) and the wavelength dispersive (WD) analysis (Sarkar et al., 2001). BSE and EDS techniques were used in the current study.

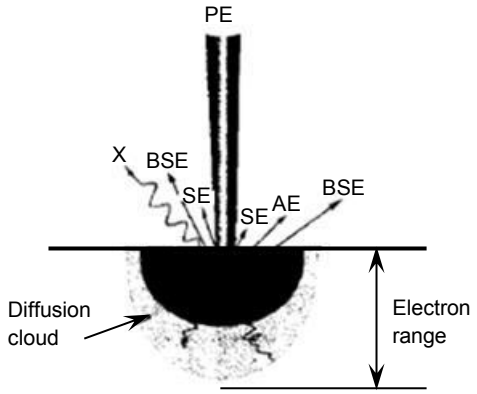

Figure 4-16: Different interactions of an electron beam (Sarkar et al., 2001).

The intensity of the reflected electrons is proportional to the atomic number of the substances in the solid (sample) and the density of the respective material. In BSE mode, the reflection of PE by a specimen is higher when the atomic density of the specimen is higher, meaning that a material having a high atomic number results in more efficient reflection. A cement paste provides some good examples in this respect. For example, an unreacted cement particle appear brighter than C-S-H due to the presence of iron whose atomic number (= 26) is higher than that of silica (= 14) (Figure 4-17).

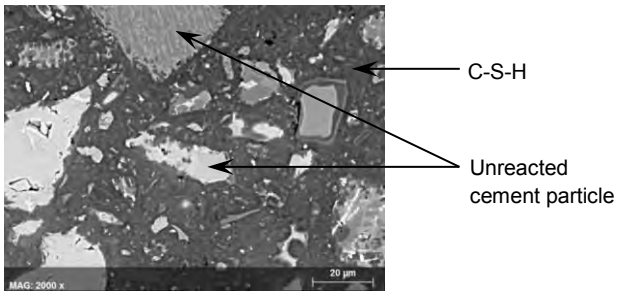

Figure 4-17: Monograph of cement paste (Nuytten, 2014).

This technique was used on both powder samples (products of biogenic concrete corrosion) and polished sections prepared following standard procedures as outlined in Appendix J. BSE imaging and EDS analysis were undertaken twice using different equipment. Initially, a Nova NanoSEM 230 scanning electron microscope was used, and later a Philips Quanta 200 with PGT EDS was used. A summary of this test regime is given in Appendix J.

4.3.6.2 Quantitative X-ray diffraction (QXRD)

XRD is a powerful technique for the study of crystalline materials (Scrivener et al., 2004). It is the elastic scattering of X-ray photons by atoms in a periodic lattice. The scattered monochromatic X-rays that are in phase give constructive interference (Chatterjee, 2001). Figure 4-18 shows a beam of parallel X-rays penetrating a stack of planes of spacing '*d*', at an angle of incidence, *θ*. Each plane is pictured as reflecting a portion of the incident beam. The 'reflected' rays combine to form a diffracted beam if they differ in phase by a whole number of wavelength, that is, if the path difference AB – AD = nλ, where 'n' is an integer (Connolly, 2012). It can be seen that:

$$AB = \frac{d}{\sin\theta}; AD = AB\cos 2\theta = \frac{d}{\sin\theta}(\cos 2\theta) \tag{4.1}$$

and

$$n\lambda = \frac{d}{\sin\theta} - \frac{d}{\sin\theta}(\cos 2\theta) = \frac{d}{\sin\theta}(1 - \cos 2\theta) = \frac{d}{\sin\theta}(2\sin^2\theta) \tag{4.2}$$

therefore

$$n\lambda = 2d\sin\theta \tag{4.3}$$

In this regard, Figure 4-18 illustrates how diffraction of X-rays by crystal planes allows derivation of lattice spacing using the so-called Bragg's law (Bragg's law calculates the angle where constructive interference from X-rays scattered by parallel planes of atoms will produce a diffraction peak), which is an equation that allows diffraction to be treated mathematically as reflection from the diffracting planes (Equation 4.3).

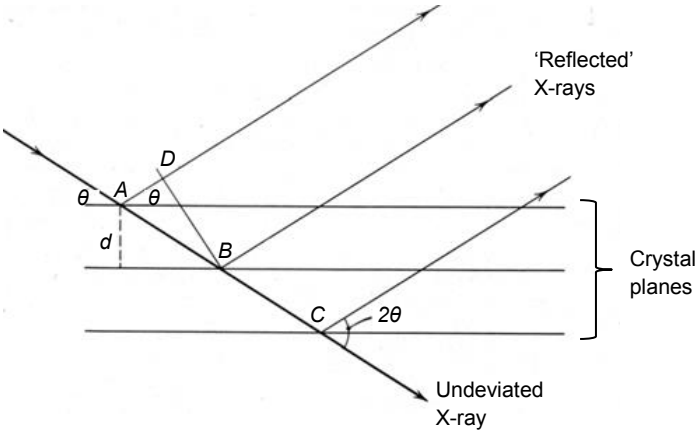

Figure 4-18: The condition for reflection – Bragg's law (Connolly, 2012).

By measuring the angles, *θ*, under which the constructively interfering X-rays leave the crystal, the inter-planar spacing, *d*, of every single crystallographic phase can be determined (Chatterjee, 2001). Therefore XRD was used for qualitative mineralogical identification of crystalline phases in the products of concrete corrosion prepared following standard procedures as outlined in Appendix J. An example of an XRD pattern (at different ages) of CAC hydrated at 20 °C is given in Figure 4-19.

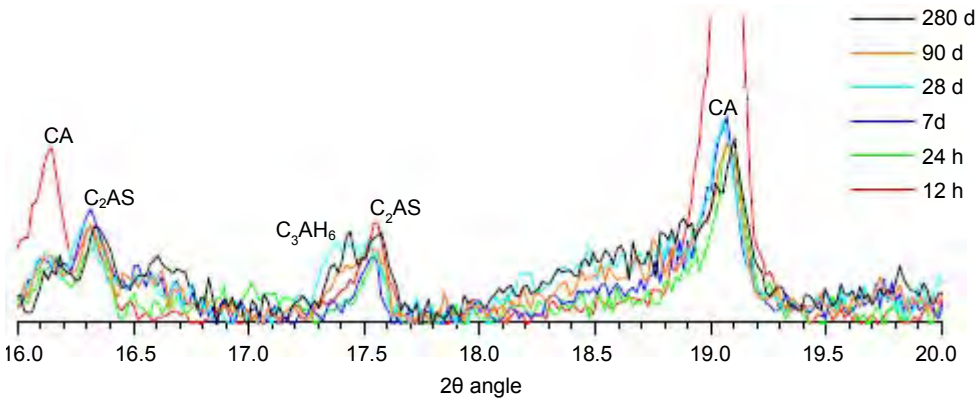

Figure 4-19: XRD pattern (at different ages) of CAC hydrated at 20 °C (Gosselin, 2009).

Quantitative analysis (QXRD) was based on Rietveld analysis (Rietveld, 1969; Scrivener et al., 2004). This method compares the measured and calculated powder diffraction patterns, based on known crystalline phases (lattice parameters and atomic positions).

XRD was carried out using a Philips PW 1390 X-ray diffractometer with copper radiation, Cu Kα (wavelength, K = 1.5418 Å), operated at 40 kV and 20 mA over an angular rotation (2θ) from 0° to 70° with a step size of 0.02° and total scan of 20 minutes. Rietveld analysis was undertaken using HighScore® Software. A summary of this test regime is given in Appendix J.

4.3.6.3 Thermogravimetric analysis (TGA)

A thermogravimetric analyser is equipped with a thermobalance which continuously measures the mass loss of materials during progressive heating (Gosselin, 2009). The output is normally in the form of a TGA curve. Differentiation of the TGA curve results in a derivative thermogravimetry (DTG) curve, in which specific peaks of mass loss are related to the different products of hydration (Figure 4-20). Interpretation of TGA/DTG results is aided by another curve based on the simultaneous differential thermal analysis (SDTA), which monitors the difference in temperature between the sample under test and an inert reference material.

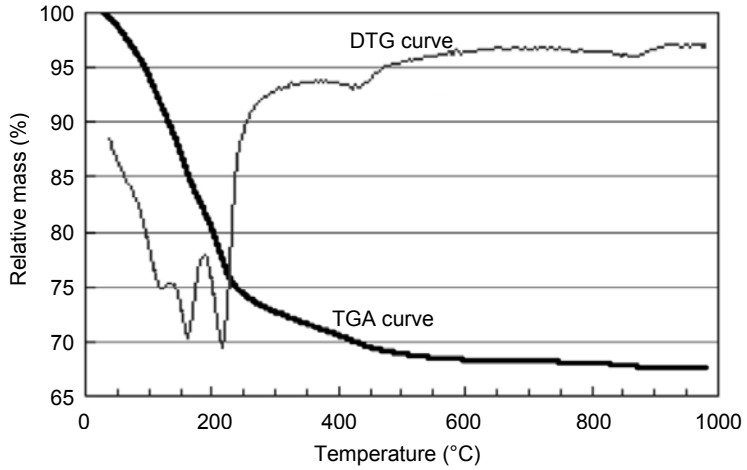

Figure 4-20: TG and DTG curves of stratlingite (tested at 10 °C/min) (Matshei et al., 2007).

TGA was undertaken on the products of concrete corrosion prepared following standard procedures as outlined in Appendix J, using a Mettler Toledo TGA/SDTA 851e microbalance. Samples were tested over a temperature range of 25 °C to 1000 °C, with a heating rate of 10 °C/min, under nitrogen atmosphere.

4.3.6.4 Microbial speciation

The (bacteria) community fingerprinting technique was used to profile the diversity of the microbial community. This method analyses samples by assaying genomic DNA (gDNA). Specifically, the automated ribosomal intergenic spacer analysis (ARISA) technique was used since it has a higher resolution in detecting microbial diversity as compared to other techniques such as the terminal restriction fragment length polymorphism (T-RFLP) (Danovaro et al., 2006). Amplification (making multiple identical copies (replicates)) of the gDNA was done by the polymerase chain reaction (PCR) method followed by sequencing (determining the precise order of nucleotides within a DNA molecule) of the resulting fragment. Identification to the species level was performed by comparison to the Basic Local Alignment Search Tool (BLAST) database. BLAST is an algorithm for comparing primary biological sequence information, such as the amino-acid sequences of different proteins or the nucleotides of DNA sequences (Altschul et al., 1990).

gDNA was extracted from the respective samples using a Macherey-Nagel Genomic DNA kit, while amplification was done using a Roche PCR Template Purification kit, after neutralisation with sequential phosphate buffered saline washes. A total of three separate gDNA extractions were conducted on the various samples. The quantity and quality of the extracted nucleic acid material was assessed spectrophotometrically using a Nanodrop, ND-1000.

4.4 Summary of experimental arrangements

The experimental arrangement presented in this chapter encompasses both site and laboratory based test regimes. A summary of the respective tests is given in Table 4-7.

Table 4-7: Summary of experimental work

Test location/facilities	Test regime	Sample type/location	Description of age during test
VES	pH	Sewage; surface of concrete 'lids'/cores	Every 3 to 4 months between Month 104 and Month 127**
	Temperature	Sewage; sewer headspace	
	Relative humidity	Sewer headspace	
	Gas (H_2S, CO_2, O_2) concentration	Sewer headspace	
	Mass changes	Concrete 'lids'/cores	
	Dimensional changes	Concrete 'lids'/cores	Month 120**
Manhole at Langa	Temperature	Manhole headspace	Every 3 to 4 months between Jan 2014 and Dec 2015
	Relative humidity		
	Gas (H_2S, CO_2, O_2) concentration		
UCT (Geol.), EPFL*	X-ray diffraction (XRD)	Products of biogenic corrosion (powder)	Month 120 and Month 131**
UCT (Chem. Eng.), EPFL*	Thermogravimetric analysis (TGA)		
UCT (Surface Sci.), EPFL*	Scanning electron microscopy (SEM)	Polished concrete blocks; products of biogenic corrosion	Month 127; Month 120 and Month 131**
	Energy dispersive spectroscopy (EDS)		
UCT (Chem. Eng.)	Microbial speciation	Products of biogenic corrosion	Month 120 and Month 131**
UCT (Civil Eng.)	Density of concrete	Concrete cores	28 d##
	Compressive strength of concrete		
	Oxygen permeability index (OPI)	Concrete discs	
	Water sorptivity index (WSI)		

*EPFL = Laboratory of Construction Materials, École Polytechnique Fédérale de Lausanne

**Since the start of Phase III work in the VES (see Chapter Three)

##Tests used only for characterisation of concrete prior to exposure in sewer environments

4.5 References

Alexander, M. G., & Fourie, C. W. 2011. Performance of sewer pipe concrete mixtures with portland and calcium aluminate cements subject to mineral and biogenic acid attack. *Materials and Structures*. 44 (1): 313 – 330.

Altschul, S., Gish, W., Miller, W., Myers, E., & Lipman, D. 1990. Basic local alignment search tool. *Journal of Molecular Biology*. 215(3): 403 – 410.

Beddoe, R. E., & Dorner, H.W. 2005. Modelling acid attack on concrete, Part I: The essential mechanisms. *Cement and Concrete Research.* 35 (1). 2333 – 2339.

Chatterjee, A. K. 2001. X-ray diffraction. In: Ramachandran, V. S., & Beaudoin, J. J. Eds. *Handbook of analytical techniques in concrete science and technology*. New York: Noyes/William Andrew. 275 – 332.

Connolly, J. R. 2012. Introduction to X-ray powder diffraction for EPS400-001. Trinity College, Hartford.

Council for Scientific and Industrial Research. 1959. *Corrosion of concrete sewers*. Pretoria: CSIR. Series DR12.

Danovaro, R., Luna, G. M., Dell'Anno, A., & Pietrangeli, B. 2006. Comparison of two fingerprinting techniques, terminal restriction fragment length polymorphism and automated ribosomal intergenic spacer analysis, for determination of bacterial diversity in aquatic environments. *Applied and Environmental Microbiology.* 72: 5982 – 5989.

Environmental Protection Agency. 1992. Detection, control, and correction of hydrogen sulphide corrosion in existing wastewater systems. Cincinnati: EPA.

Fourie, C. W. 2007. Acid resistance of sewer pipe concrete. MSc (Eng) dissertation. University of Cape Town, Cape Town.

Gosselin, C. 2009. Microstructural development of calcium aluminate cement based systems with and without supplementary cementitious materials. PhD dissertation. École Polytechnique Fédérale de Lausanne, Lausanne.

Goyns, A. M. 2001. Calcium aluminate cement linings for cost-effective sewers. *International Conference on Calcium Aluminate Cements*. July 16 – 19, Edinburgh. 617 – 631.

Goyns, A. M. 2003. Virginia sewer rehabilitation: Progress Report 1. Pretoria: Concrete Manufacturers Association.

Goyns, A. M. 2010. Virginia sewer rehabilitation: Progress Report 4. Pretoria: Concrete Manufacturers Association.

Goyns, A. M., Alexander, M. G., & Fourie, C. W. 2008. Applying experimental data to concrete sewer design and rehabilitation. *Proceedings of the Centenary Conference on Calcium Aluminate Cements.* June 30 – July 2, Avignon. 293 – 308.

Hvitved-Jacobsen, T., Vollertsen, J., & Nielsen, A. H. 2013. *Sewer processes: Microbial and chemical process engineering of sewer networks*. 2nd ed. Boca Raton: CRC Press.

Kakade, A. M. 2014. Measuring concrete surface pH – A proposed test method. *Concrete Repair Bulletin.* 16 – 20.

Matshei, T., Lothenbach, B., Glasser, F. P. 2007. Thermodynamic properties of Portland cement hydrates in the system CaO-Al_2O_3-SiO_2-$CaSO_4$-$CaCO_3$-H_2O. *Cement and Concrete Research.* 37(10): 1379 – 1410.

Motsieloa, N. 2013. Acid resistance of sewer pipe concrete. MSc (Eng) dissertation. University of Cape Town, Cape Town.

Nuytten, S. 2014. Microstructure and durability against sulphate attacks of ettringite-based rapid repair binders. MSc (Eng) dissertation. École Polytechnique Fédérale de Lausanne, Lausanne.

Rietveld, H. M. 1969. A profile refinement method for nuclear and magnetic structures. *Journal of Applied Crystallography.* 2: 65 – 71.

Sarkar, S. L., Aimin, X., & Jana, D. 2001. Scanning electron microscopy, X-ray microanalysis of concrete. In: Ramachandran, V. S., & Beaudoin, J. J. Eds. *Handbook of analytical techniques in concrete science and technology.* New York: Noyes/William Andrew. 231 – 274.

Scrivener, K. L. 2004. Backscattered electron imaging of cementitious microstructures: understanding and quantification. *Cement and Concrete Composites*. 26(8): 935 – 945.

Scrivener, K. L., Cabiron, J., & Letourneux, R. 1999. High-performance concretes from calcium aluminate cements. *Cement and Concrete Research*. 29: 1215 – 1223.

Scrivener, K. L., Füllmann, T., Gallucci, E., Walenta, G., & Bermejo, E. 2004. Quantitative study of Portland cement hydration by X-ray diffraction/Rietveld analysis and independent methods. *Cement and Concrete Research*. 34(9): 1541 – 1547.

South African Durability Index Testing Procedure Manual. 2009. Department of Civil Engineering, University of Cape Town, Cape Town.

South African National Standard. SANS 201: 2008. *Sieve analysis, fines content and dust content of aggregates*. Pretoria: SABS.
South African National Standard. SANS 5842: 2006. *FACT value (10% fines aggregate crushing value) of coarse aggregates*. Pretoria: SABS.
South African National Standard. SANS 5844: 2014. *Particle and relative densities of aggregates*. Pretoria: SABS.
South African National Standard. SANS 5863: 2006. *Concrete tests – compressive strength of hardened concrete*. Pretoria: SABS.
South African National Standard. SANS 6242: 2008. *Acid insolubility of aggregates*. Pretoria: SABS.
South African National Standard. SANS 6251: 2006. *Concrete tests – density of hardened concrete*. Pretoria: SABS.

Chapter Five: Results, analyses and discussions

5.1 Introduction

This chapter presents results, analyses and discussion of concrete mixtures subjected to biogenic corrosion mechanisms for durations ranging from approximately 6 months to 127 months in two different sewer environments – Langa and the VES. The main focus lies in microstructural characterisation of concrete mixtures exposed to biogenic H_2SO_4 attack for approximately 127 months in the VES in relation to respective measured corrosion rates, based on changes in both mass and dimensions of samples. Other aspects discussed in this chapter include, (i) characteristics of the microbial ecosystem on different concrete substrates exposed to biogenic corrosion for approximately 120 months in the VES, and (ii) concrete surface pH vs. time profiling of concrete mixtures exposed in the VES and Langa for approximately 6 months. However, before proceeding, it is important to note the following:

(i) Even though, while determining the corrosion rates of different concrete mixtures, focus was on measurement of changes in mass of samples at a later-age, it is also important to characterise the inception period of this mass loss due biogenic corrosion. However, mass measurements of the 'lid' samples commenced during 2008, 38 months after installation of the samples in the VES, and the initial mass was not recorded. Therefore, in effect, 'month 38' was taken as 'month zero' while calculating the corrosion rates of the 'lid' samples. Nevertheless, at the age of 38 months, most concrete mixtures, particularly PC-based would have undergone deterioration (see Section 3.4), therefore characterisation of the inception period of biogenic corrosion was based on mass measurements of core samples (made from similar mixtures as the 'lid' samples) which commenced during 2011, 3 months after installation in the VES (Motsieloa, 2013).

(ii) Direct measurement of lost concrete pipe wall thickness due to biogenic acid attack was undertaken during 2014, approximately 120 months (10 years) after installation of the samples in the VES. Direct measurement of the lost pipe wall thickness was used to validate the calculated average corrosion rates based on changes in mass of the respective samples.

(iii) The products of biogenic concrete corrosion that were used for XRD and TGA analysis were first sampled (carefully scraped) from the 'lid' samples during 2014, approximately 120 months (10 years) after installation in the VES. Subsequent sampling was done approximately 12 months after the first exercise (approximately 131 months after installation in the VES).

(iv) Although the results for changes in mass of the 'lid' samples presented in this chapter cover durations of up to 127 months, mass measurements in the current study were taken over a period of 24 months (2 years). Earlier measurements were taken by other researchers (Alexander et al., 2008; Goyns et al., 2008; Goyns, 2010; Motsieloa, 2013).

5.2 Objective of the chapter

The main objective of this chapter is to analyse changes in mass loss of different concrete mixtures subjected to biogenic acid attack in order to understand the relationship between biogenic corrosion rates and certain characteristics of the binders (binder type and binder content). The characteristics of the binders are based on the microstructure of the respective concrete mixtures, studied using the SEM/EDS technique. These characteristics form a basis for the development of mechanistic correlations between certain elemental ratios (from the SEM/EDS technique) of the sound (un-attacked) concrete matrices and the respective corrosion rates, which will be used in Chapter Six to develop effective resistance capacity factors that can be incorporated within the alkalinity (A) component (see Chapter Two, Equation 2.77) in the widely used LFM for biogenic corrosion prediction of concrete sewer pipes.

5.3 Biogenic corrosion rates – a general overview of time-development trends

The corrosion rate time-development trends of various concrete mixtures subjected to biogenic H_2SO_4 attack were calculated based on changes in mass. For the core samples, the time-development

trends were calculated using data collected over a period of 48 months (2011 to 2015), while for the 'lid' samples, these trends were calculated using data collected over a period of 89 months (between 'month 38' and 'month 127') – see details in Appendix L (L.1). The corrosion rates were calculated using Equation 5.1.

$$c = \frac{m_1 - m_2}{d \times A \times \Delta t} \tag{5.1}$$

where c = corrosion rate (mm/year)
m_1 = initial mass (g)
m_2 = final mass after time t (g)
d = density of concrete (taken as 2500 kg/m^3)
A = surface area exposed to biogenic acid (mm^2)
Δt = time lapse between measurement of mass m_1 and m_2 (years)

The typical average corrosion rate time-development trends for biogenic corrosion rates based on changes in mass of the core samples are given in Figure 5-1, while those based on changes in mass of the 'lid' samples are given in Figure 5-2 and Figure 5-3 for PC- and CAC-based mixtures respectively. Before proceeding, it is important to note that the subsequent mass measurements of the 'lid' samples after those taken at 'month 38' were undertaken at 'month 57'. This explains the start period of the time-development trends in Figure 5-2 and Figure 5-3.

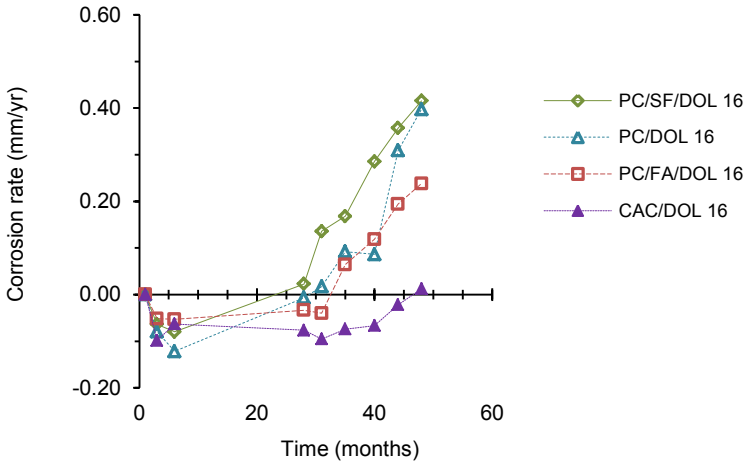

Figure 5-1: Typical average corrosion rate time-development trends based on core samples

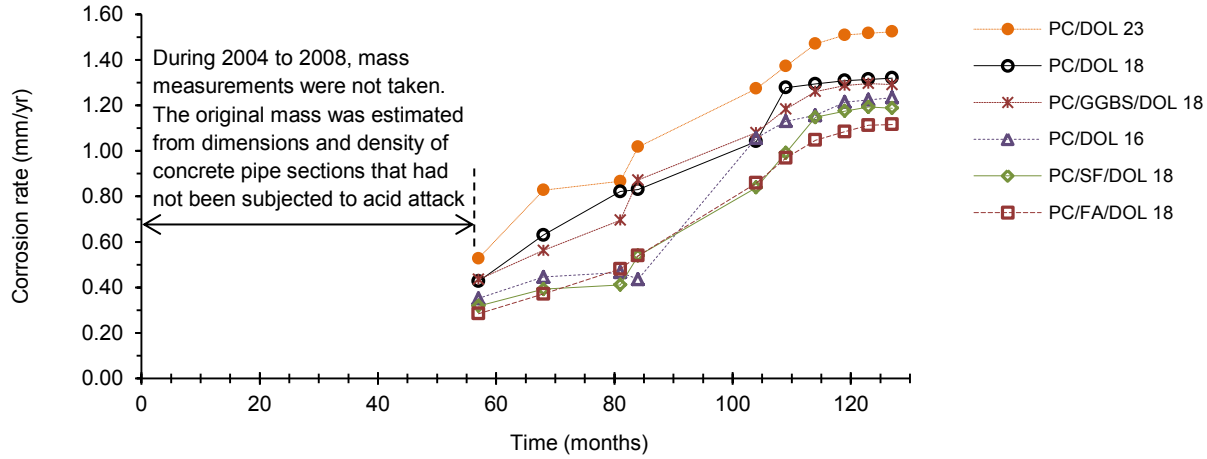

Figure 5-2: Typical average corrosion rate time-development trends based on PC-based 'lid' samples

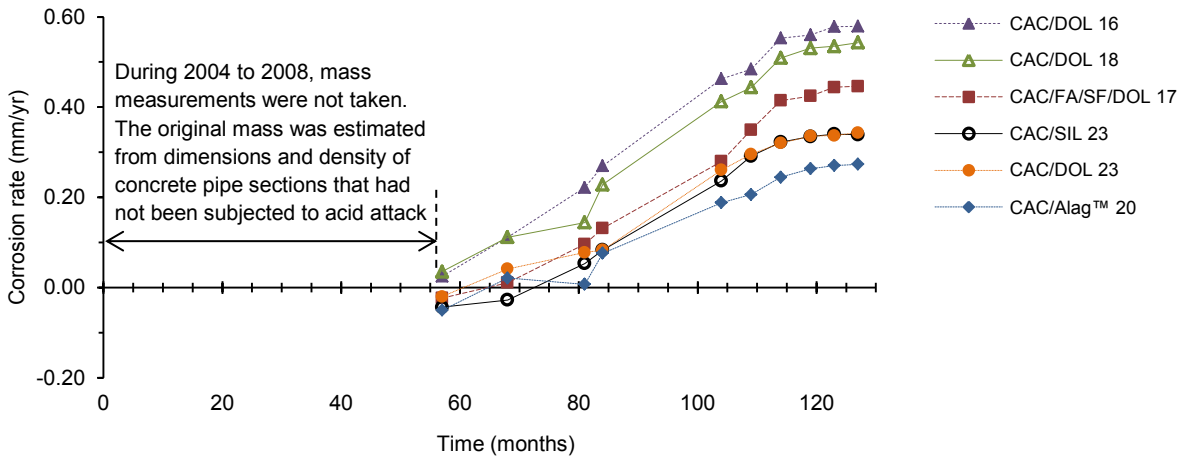

Figure 5-3: Typical average corrosion rate time-development trends based on CAC-based 'lid' samples

The average corrosion rate time-development trends presented in Figure 5-1 to Figure 5-3 are arithmetic mean values obtained from three sets of samples. Individual results for these samples are given in Appendix L.

The following general and phenomenological trends were noted in the biogenic corrosion rate results presented in Figure 5-1 to Figure 5-3:

(i) During early ages when outfall concrete sewers commence operations, both PC- and CAC-based mixtures gained mass (depicted by negative corrosion rates) due to absorption of moisture that is available in the sewer's headspace. However, concrete mixtures incorporating supplementary cementitious materials (SCMs) (FA and SF) experienced less mass gain (water absorption) than plain mixtures. According to Siddique and Khan (2011), concrete mixtures with SCMs have a finer pore structure resulting in systems with lower permeability than plain binder systems.

(ii) At similar binder contents, PC-based concrete mixtures started losing mass approximately 24 months earlier than CAC-based mixtures.

(iii) At similar binder contents, PC-based concrete mixtures incorporating FA and SF experienced less mass loss than those incorporating GGBS and plain systems.

(iv) PC-based concrete mixtures with a lower amount of PC (16%) experienced less mass loss than those with higher amounts of PC (18% and 23%).

(v) CAC-based concrete mixtures with a lower amount of CAC (16%) experienced more mass loss than those with higher amounts of CAC (18% and 23%).

(vi) Certain CAC-based mixtures incorporating SCMs but with a lower total binder content (such as CAC + FA + SF ternary mixtures with a total binder content of 17% (content of CAC only at 11%)) experienced less mass loss than those with a slightly higher amount of CAC (18%). However, CAC-based concrete mixtures with a higher amount of CAC (23%) experienced less mass loss than the ternary mixtures.

(vii) Regardless of the aggregate type (acid-soluble or acid-insoluble), CAC-based concrete mixtures with approximately 23% cement content had similar biogenic corrosion rates.

(viii) The use of artificial aluminate aggregate (such as alag^{TM}) in CAC-based concrete mixtures resulted in a lower biogenic corrosion rate, even at a lower cement content. CAC/alag^{TM} mixtures with 20% CAC experienced less mass loss than both CAC/DOL and CAC/SIL mixtures with 23% cement content.

Based on the general trends summarised above, a further comparative analysis of biogenic corrosion rate time-development trends between different binder systems with similar cement contents was undertaken, and results presented in the following Section 5.3.1.

5.3.1 Comparative biogenic corrosion rate time-development trends and average corrosion rates of PC- and CAC-based binder systems with similar cement contents

From the literature review presented in Part Two of Chapter Two, it was highlighted that CAC-based concrete mixtures deteriorated at a slower rate than PC-based concrete mixtures when subjected to biogenic H_2SO_4 attack. Similar results were found in the current study as given by comparative trends in Figure 5-4.

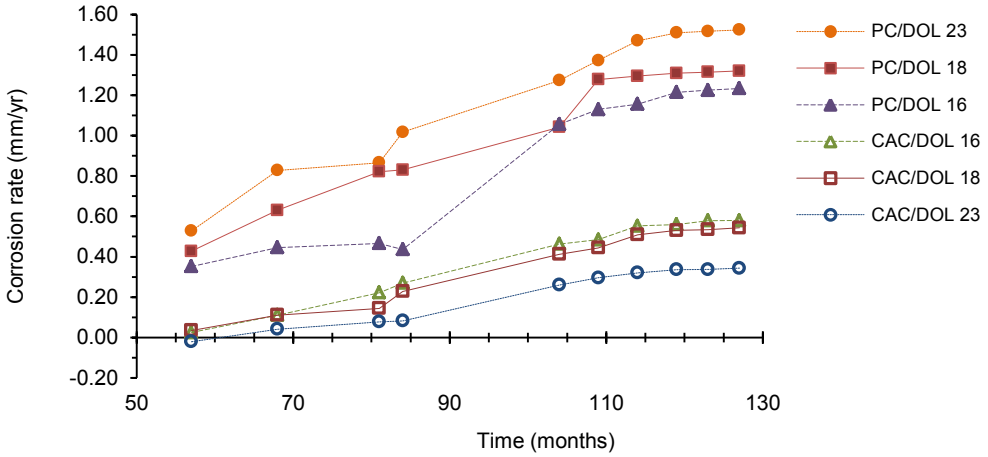

Figure 5-4: Comparative average corrosion rate time-development trends based on PC- and CAC-based 'lid' samples

From the trends presented in Figure 5-4, it is shown that the biogenic corrosion rate of PC-based concrete mixtures is proportional to the PC content in the mixture, whereas that of CAC-based concrete mixtures is inversely proportional to the CAC content in the mixture. These results are similar to findings reported in the literature reviewed, where it was highlighted that (i) available CH and C-S-H (in PC) provide preferred sites for increased biogenic H_2SO_4 reactions, and (ii) available C_3AH_6 and AH_3 (in CAC) provide a higher neutralisation capacity and bacteriostatic effect to acid-generating SOB (Johnson and Wood, 1990; Scrivener, 2003; Goyns, 2003; Alexander et al., 2008; Goyns et al., 2008; Gosselin, 2009; Sahmaran, 2010; Alexander and Fourie, 2011; Herisson, 2012).

It is important to note that the biogenic corrosion rates presented herein will be compared to predicted values calculated from one of the biogenic corrosion prediction models, the LFM with the view of improving it. In order to achieve this, a comparison of the average biogenic corrosion rates of both PC- and CAC-based concrete mixtures were deduced from the corrosion rate time-development trends presented in Figure 5-2 and Figure 5-3, from month 109 to month 127. This duration was chosen since it represents a stage in which the corrosion rates tend to start levelling off or attaining peak corrosion rates. The range of confidence (error bars) was calculated from statistical analysis of the average biogenic corrosion rates based on a standard *t*-distribution at a 95% confidence level using Equation 5.2.

$$c_{max} = c_{average} + \sigma t \;; \qquad c_{min} = c_{average} - \sigma t \tag{5.2}$$

where c_{max} = maximum corrosion rate (mm/year)
c_{min} = minimum corrosion rate (mm/year)
$c_{average}$ = mean corrosion rate (mm/year)
t = value obtained from the critical value chart at a 95% confidence level
σ = standard deviation (see Appendix L for computation)

A comparison of these average biogenic corrosion rates is given in Figure 5-5.

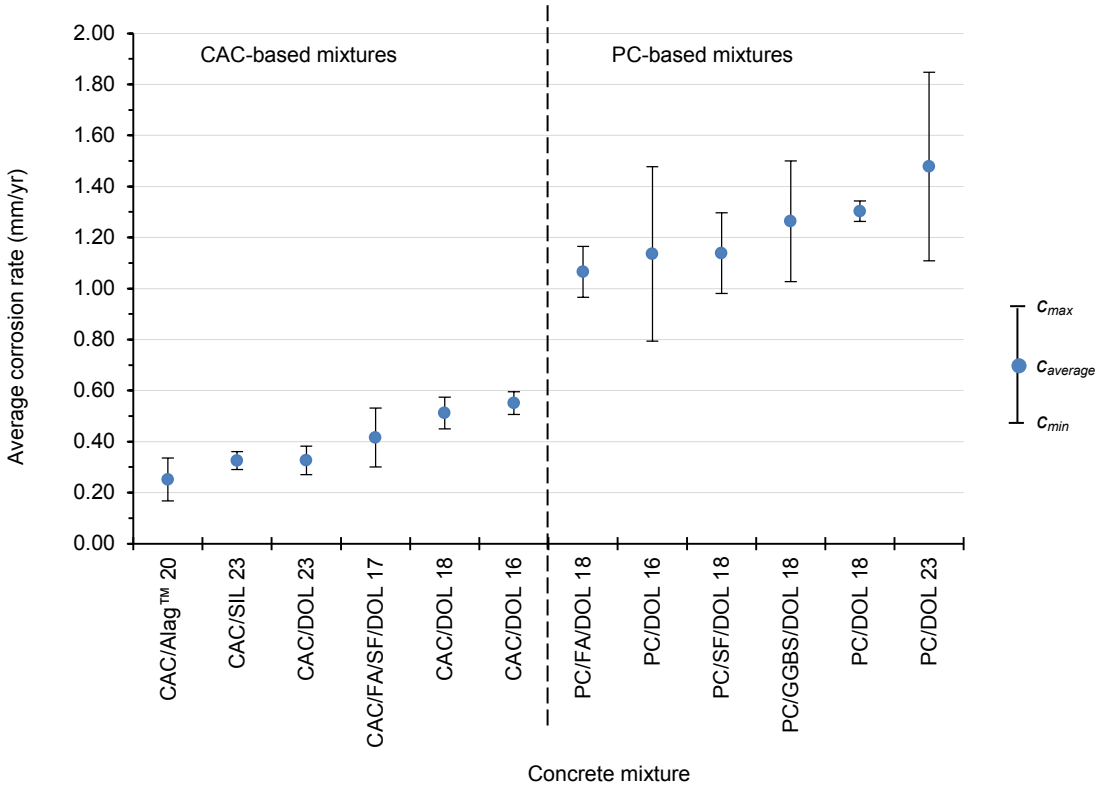

Figure 5-5: Average corrosion rates of PC- and CAC-based concrete mixtures subjected to biogenic H_2SO_4 for 127months in a 'live' sewer

The results presented in Figure 5-5 generally show that binder systems with a high alumina content (such as mixtures with aluminate aggregate and 23% CAC in the case of CAC-based concrete, and mixtures with PC/FA blends in the case of PC-based concrete) experience lower corrosion rates. The average biogenic corrosion rates presented in Figure 5-5 were compared with direct measurements of the lost wall thicknesses of the respective 'lid' samples, and the results are summarised in Table 5-1.

Table 5-1: Summary of biogenic corrosion rates – A comparison of corrosion rates calculated from changes in mass of samples vs. direct measurements of lost wall thickness of the same samples.

	Biogenic corrosion rates based on:						Standard deviation of averages (mm/yr.)
	(i) Changes in mass (mm/yr)			(ii) Lost wall thickness (mm/yr)			
Concrete mixture	Average*	Range#		Range**		Average##	
		Minimum	Maximum	Minimum	Maximum		
CAC/Alag™	0.25	0.17	0.34	0.17	0.30	0.23	0.01
CAC/SIL 23	0.33	0.29	0.36	0.23	0.47	0.35	0.01
CAC/DOL 23	0.33	0.27	0.38	0.27	0.43	0.35	0.02
CAC/FA/SF/DOL 17	0.42	0.30	0.53	0.27	0.63	0.45	0.02
CAC/DOL 18	0.51	0.45	0.57	0.33	0.77	0.55	0.03
CAC/DOL 16	0.55	0.51	0.60	0.40	0.80	0.60	0.03
PC/FA/DOL 18	1.07	0.97	1.17	0.80	1.30	1.05	0.01
PC/DOL 16	1.14	0.79	1.48	0.87	1.37	1.12	0.01
PC/SF/DOL 18	1.14	0.98	1.30	0.87	1.50	1.18	0.03
PC/GGBS/DOL 18	1.26	1.03	1.50	0.97	1.60	1.28	0.01
PC/DOL 18	1.30	1.26	1.34	0.90	1.53	1.22	0.06
PC/DOL 23	1.48	1.11	1.85	1.13	2.00	1.57	0.06

*Changes in mass recorded for approximately 127 months. Refer to Figure 5.5 and Appendices L.1 and L.2

**Direct measurements taken approximately 120 months after installation in the sewer. See Appendix L.3 for details

#Calculated using Equation 5.2

##Arithmetic mean

In order to understand the underlying mechanisms of acid attack resulting in the presented biogenic corrosion rates, when concrete mixtures are subjected to biogenic H_2SO_4, it is paramount that the microstructure of both attacked and sound matrices be characterised and certain rate-controlling parameters be quantified. In order to achieve this, the microstructure of the respective concrete mixtures was studied using the SEM/EDS, XRD and TGA techniques. Results for PC- and CAC-based mixtures are presented in Section 5.4 and 5.5 respectively.

5.4 PC-based binder systems

The PC-based samples (with dolomite coarse aggregates) that were characterised included three plain mixtures with a PC content of 16%, 18% and 23%, and three blended mixtures, each with a total binder content of 18%, consisting of (i) 12% PC + 6% GGBS, (ii) 13.5% PC + 4.5% FA, and (iii) 16.5% PC + 1.5% SF. See mixture composition in Appendix E.

5.4.1 SEM/EDS

The BSE micrographs for the six PC-based concrete mixtures are given in Figure 5-6.

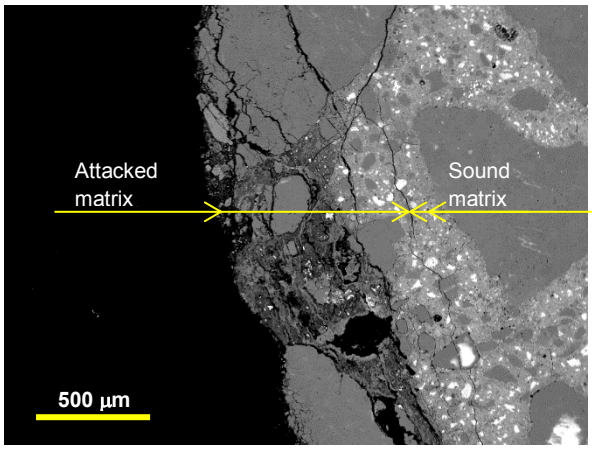

(a) 16% PC total binder*

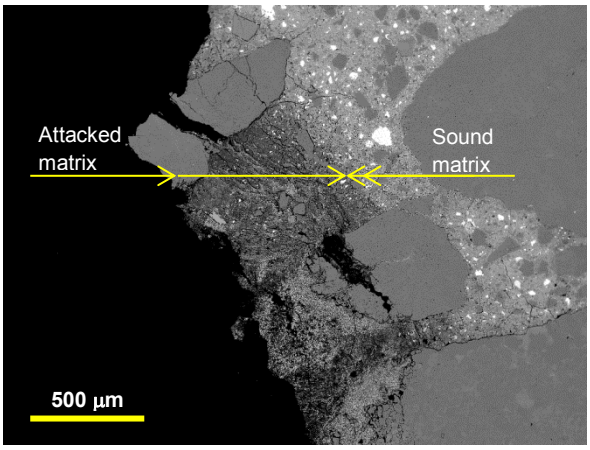

(b) 18% PC total binder*

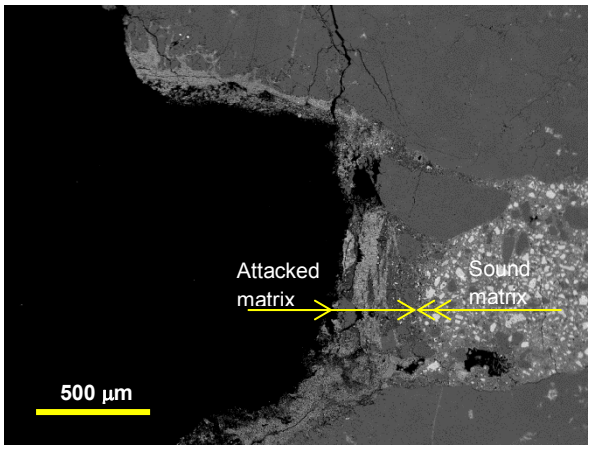

(c) 23% PC total binder*

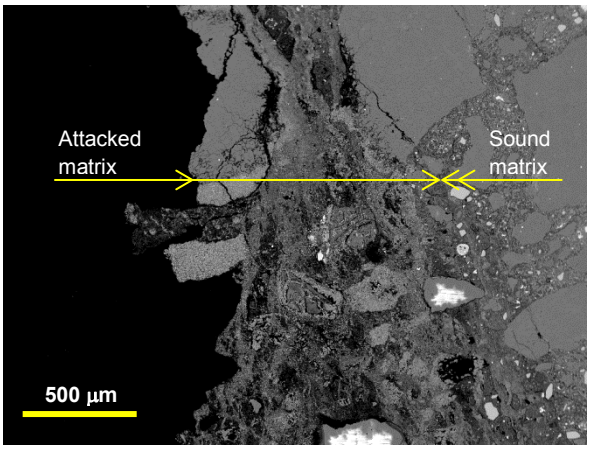

(d) 12% PC + 6% GGBS total binder*

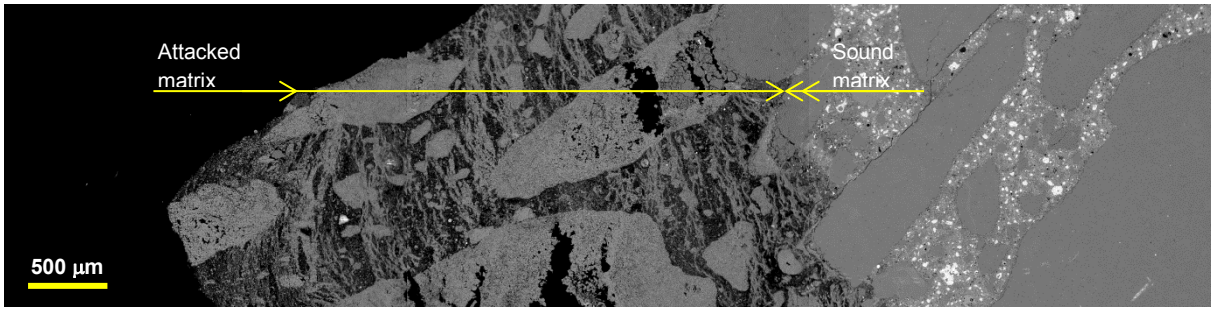

(e) 13.5% PC + 4.5% FA total binder*

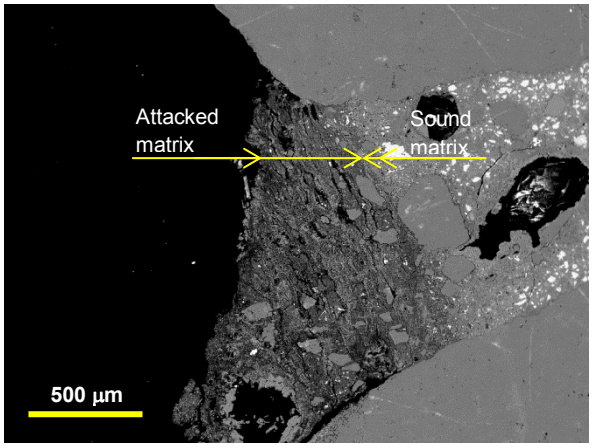

(f) 16.5% PC + 1.5% SF*

*Concrete mixtures with DOL coarse aggregate and 50/50 blend of DOL and SIL fine aggregates.

*See the BSE micrographs of the attacked matrix (products of corrosion) in Appendix L.

NB: The backscattered electrons (BSE) micrographs from SEM analysis of the polished concrete sections showed three distinct layers within the depth of the concrete matrices; (i) the sound matrix that had not been subjected to biogenic acid attack, (ii) the deteriorated matrix that had been completely transformed into a non-cohesive layer through biogenic acid attack mechanisms, and (iii) the semi-deteriorated matrix that had been partially subjected to biogenic acid attack, and which formed an interface between the sound and deteriorated matrices.

Figure 5-6 (a) to (f) : BSE micrographs of PC-based concrete mixtures exposed to biogenic H_2SO_4 for 127 months in the VES.

As discussed in Chapter Two and Chapter Three, corrosion mechanisms in concrete sewers are mostly influenced by the sulphur cycle, through microbial generation of sulphuric acid, which attack the acid-soluble components in concrete. Therefore, discussions in the current chapter will focus on sulphur-based attack mechanisms.

The depth of attacked matrices, measured from the current exposed surface, and not the original pipe surface (see approximate lost thicknesses of the respective 'lid' wall material in Table 5-2) in the PC-based concrete mixtures given in Figure 5-6 varies. The depth of attack in mixtures with 16%, 18%, and 23% PC is approximately 500 µm, while in 12% PC + 6% GGBS, 13.5% PC + 4.5% FA, and 16.5% PC + 1.5% SF, the depth of attack is approximately 1 mm, 3 mm, and 1 mm respectively. Generally, it can also be noted that the microstructure of PC-based concrete (with and without SCMs) exposed to biogenic H_2SO_4 attack is characterised by micro-cracks within both the HCP and aggregates. The varying depths of attack and development of micro-cracks within various matrices can be explained by certain properties of the products of corrosion, certain chemical reactions such as topochemical reactions, and the theory of crystallisation pressure (Taber, 1916; Paulini, 1994; Bizzozero et al., 2014).

However, before these mechanisms are discussed, it is important to understand the distribution, concentration and composition of various species involved in biogenic corrosion mechanisms within the concrete matrices. Therefore, elemental mapping with respective concentration profiles plotted from area segments using ImageJ Software (EMPA, 2015), and EDS point analysis for each of the concrete mixtures given in Figure 5-6 are presented in sub-sections 5.4.1.1 to 5.4.1.6 (Figure 5-7 to Figure 5-18). These elemental mapping include species responsible for generation of the attacking acid – sulphur, and species within the HCP that are responsible for neutralising the attacking acid – calcium and aluminium. Moreover, in order to understand the behaviour and potential role of aggregates in concrete mixtures exposed to biogenic H_2SO_4, mapping for magnesium and silica, which are major constituents of acid-soluble and acid-insoluble aggregates respectively, is also presented.

Table 5-2: Summary of approximate thicknesses of lost PC-based 'lid' wall material due to biogenic H_2SO_4 attack for 127 months

Mixture	Total binder content (%)	Lost wall thickness (mm)*
PC/DOL 16	16	11.2 ± 2.5
PC/DOL 18	18	12.2 ± 3.1
PC/DOL 23	23	15.7 ± 4.3
PC/GGBS/DOL 18	18	12.8 ± 3.2
PC/FA/DOL 18	18	10.5 ± 2.5
PC/SF/DOL 18	18	11.8 ± 3.2

*Based on direct measurements - See Table 5.1 for details

5.4.1.1 Elemental mapping of concrete mixture with 16% PC and dolomite coarse aggregate

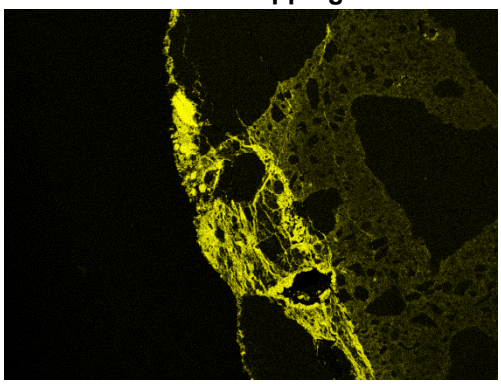

(a) Sulphur mapping (16% PC)

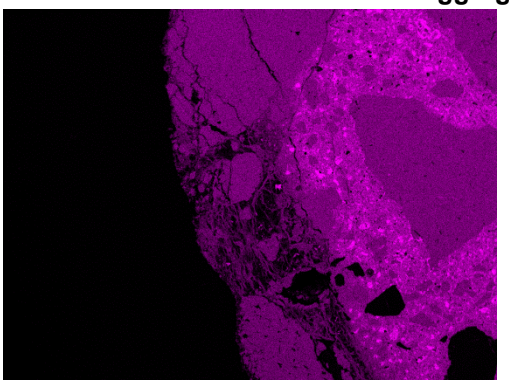

(b) Calcium mapping (16% PC)

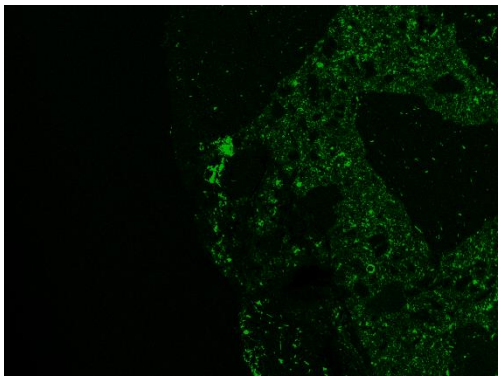

(c) Aluminium mapping (16% PC)

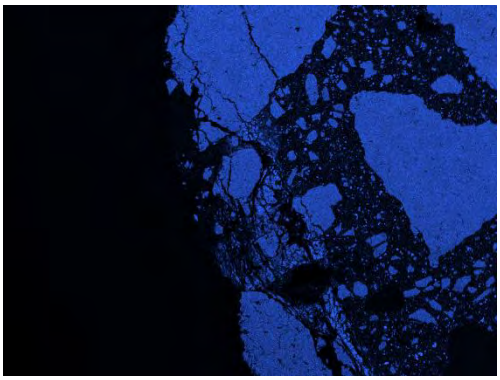

(d) Magnesium mapping (16% PC)

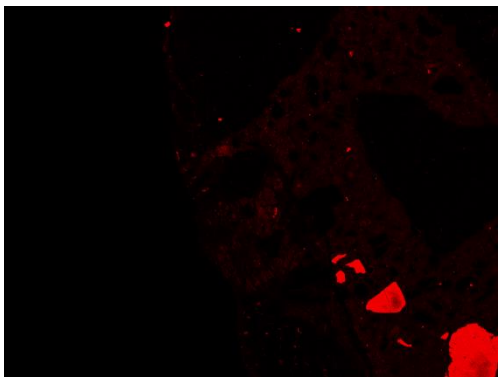

(e) Silica mapping (16% PC)

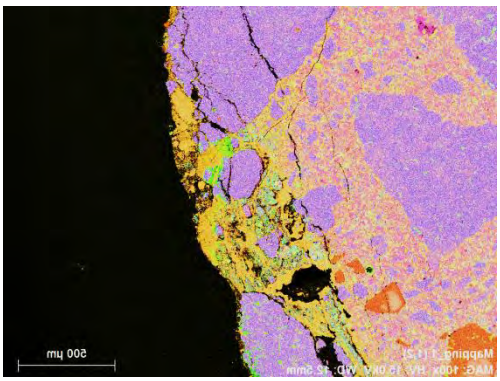

(f) Combined-element (S-Ca-Al-Mg-Si) mapping (16% PC)

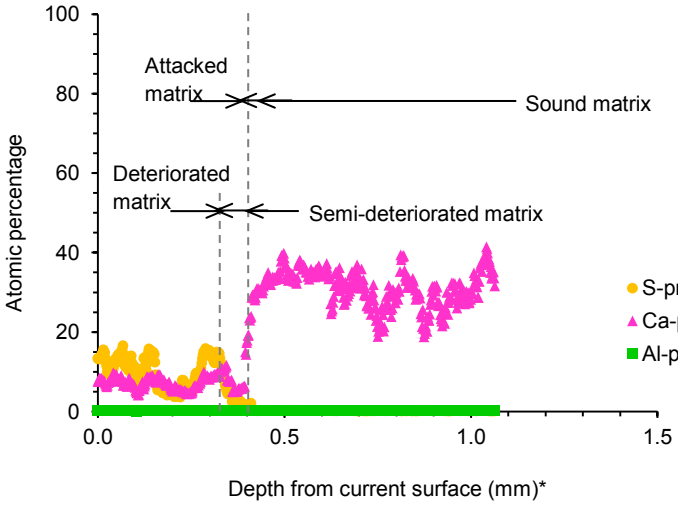

*Lost pipe wall thickness is approximately 11.2 mm; therefore depth 0.0 mm = 11.2 mm. See Table 5.2.

(g) S-Ca-Al concentration vs. depth profiles, up to approximately 0.65 mm into the sound matrix (16% PC)

Figure 5-7 (a) to (g): Elemental mapping/concentration profiles for concrete mixture with 16% PC.

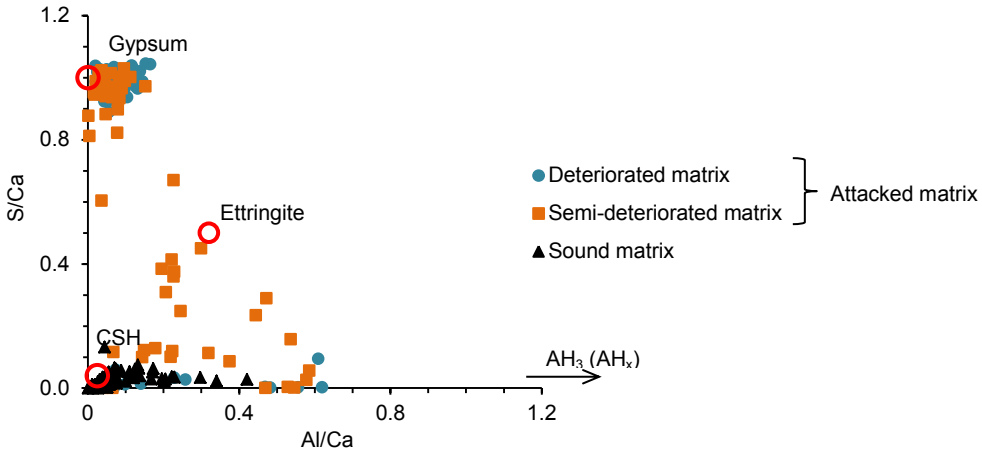

Figure 5-8: EDS point analysis for concrete mixture with 16% PC, exposed to biogenic H_2SO_4 for 127 months.

5.4.1.2 Elemental mapping of concrete mixture with 18% PC and dolomite coarse aggregate

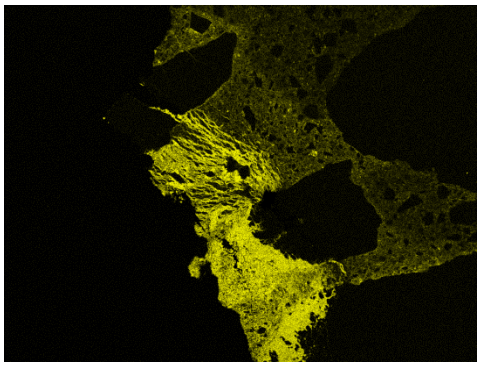

(a) Sulphur mapping (18% PC)

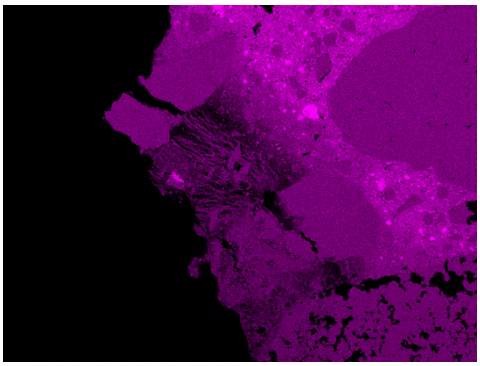

(b) Calcium mapping (18% PC)

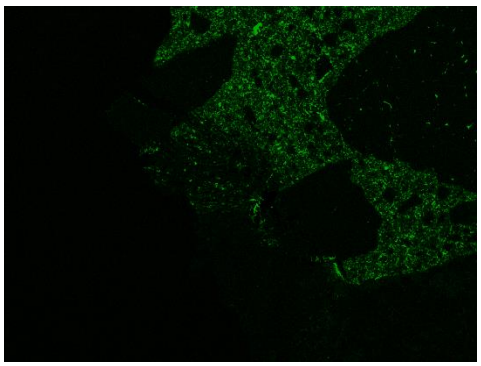

(c) Aluminium mapping (18% PC)

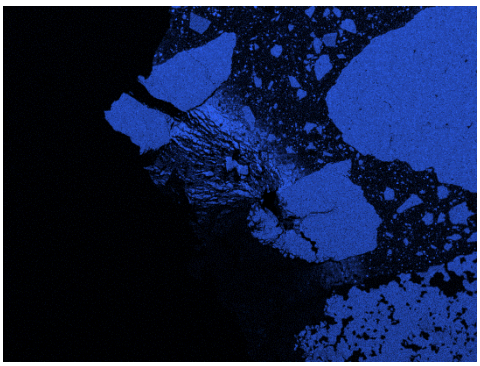

(d) Magnesium mapping (18% PC)

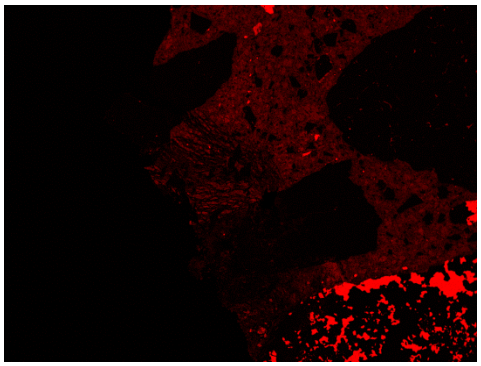

(e) Silica mapping (18% PC)

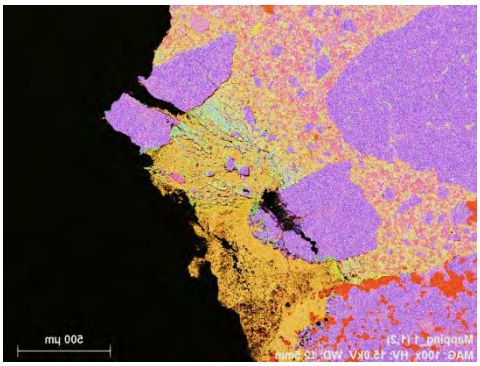

(f) Combined-element (S-Ca-Al-Mg-Si) mapping (18% PC)

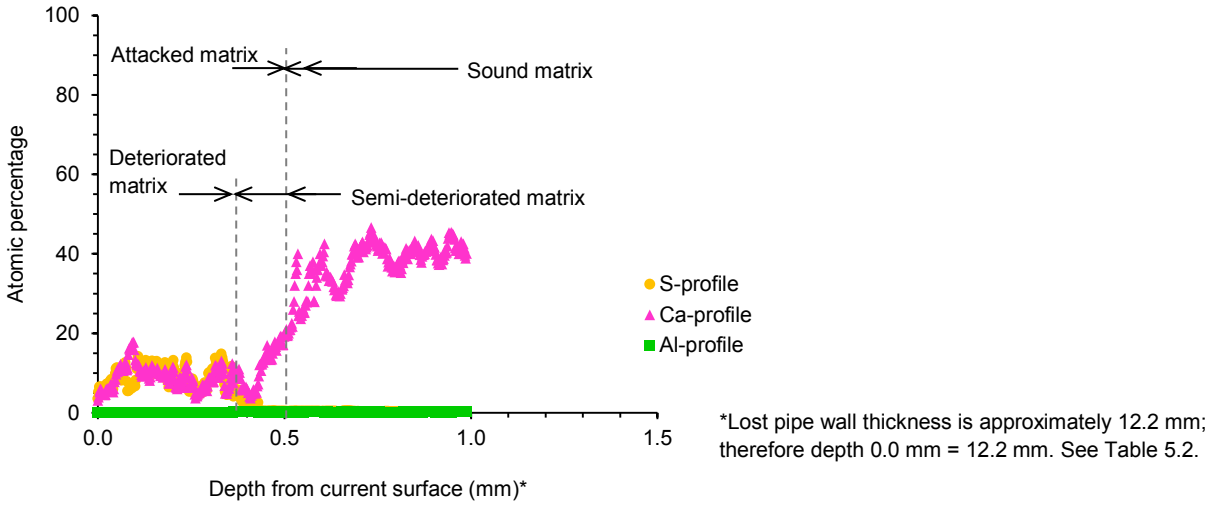

(g) S-Ca-Al concentration vs. depth profiles, up to approximately 0.5 mm into the sound matrix (18% PC)
Figure 5-9 (a) to (g): Elemental mapping/concentration profiles for concrete mixture with 18% PC.

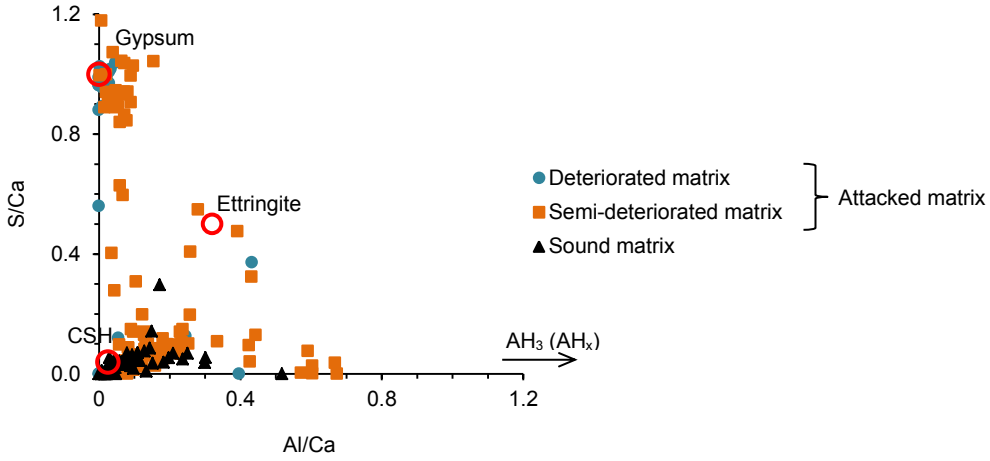

Figure 5-10: EDS point analysis for concrete mixture with 18% PC, exposed to biogenic H_2SO_4 for 127 months.

5.4.1.3 Elemental mapping of concrete mixture with 23% PC and dolomite coarse aggregate

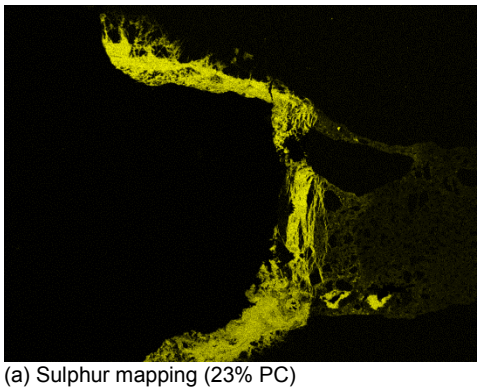

(a) Sulphur mapping (23% PC)

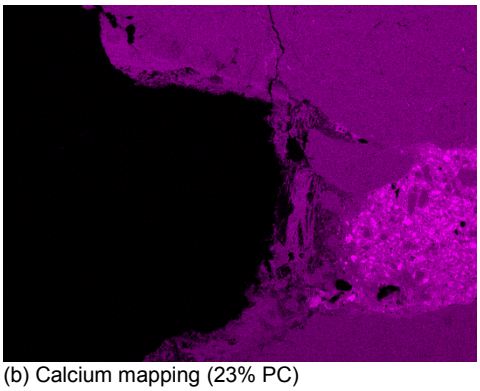

(b) Calcium mapping (23% PC)

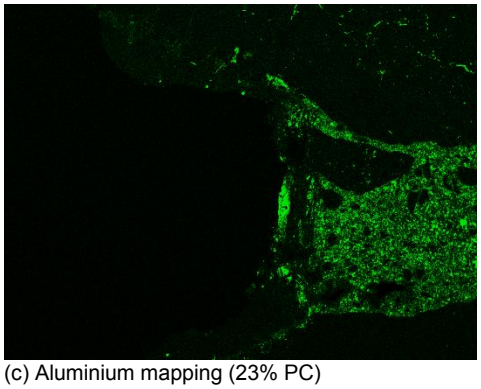

(c) Aluminium mapping (23% PC)

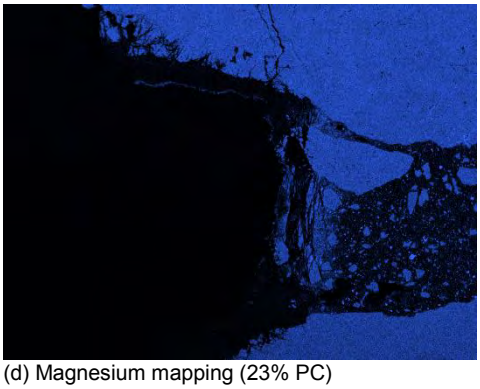

(d) Magnesium mapping (23% PC)

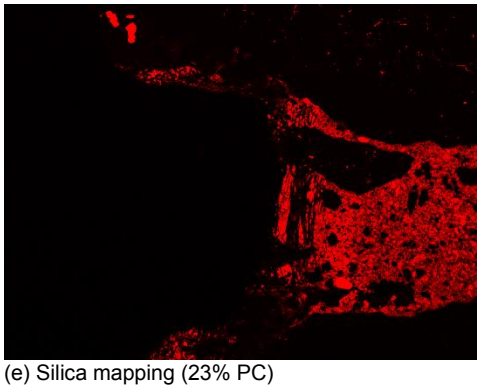

(e) Silica mapping (23% PC)

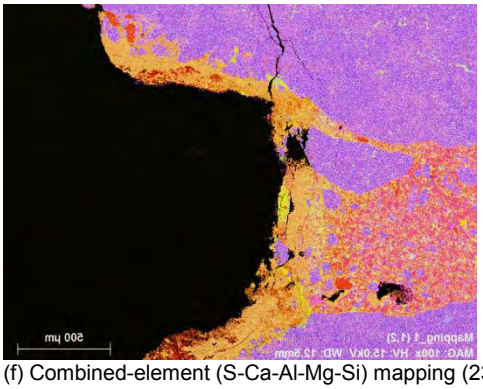

(f) Combined-element (S-Ca-Al-Mg-Si) mapping (23% PC)

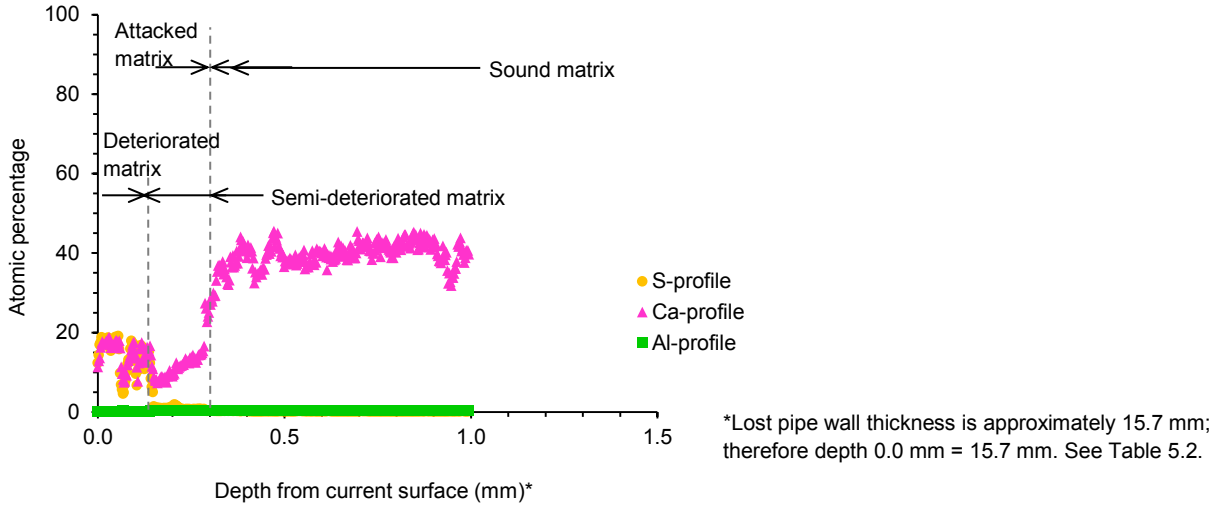

*Lost pipe wall thickness is approximately 15.7 mm; therefore depth 0.0 mm = 15.7 mm. See Table 5.2.

(g) S-Ca-Al concentration vs. depth profiles, up to approximately 0.7 mm into the sound matrix (23% PC)

Figure 5-11 (a) to (g): Elemental mapping/concentration profiles for concrete mixture with 23% PC.

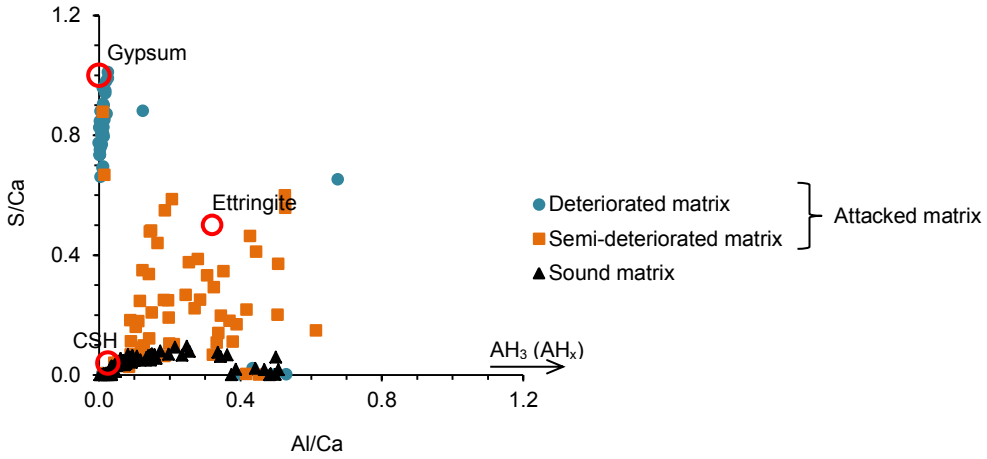

Figure 5-12: EDS point analysis for concrete mixture with 23% PC, exposed to biogenic H_2SO_4 for 127 months.

5.4.1.4 Elemental mapping of concrete mixture with 12% PC + 6% GGBS and dolomite coarse aggregate

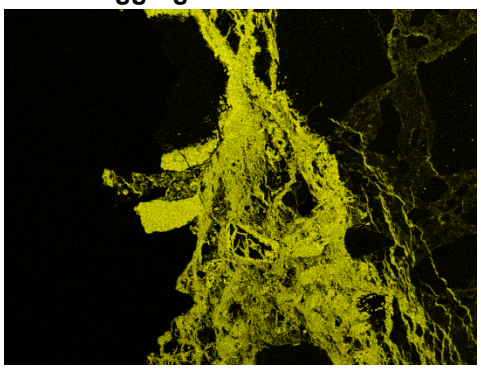

(a) Sulphur mapping (12% PC + 6% GGBS)

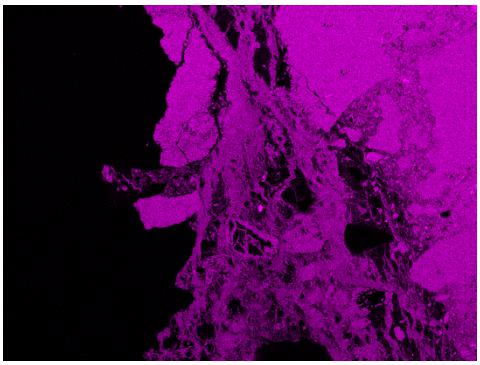

(b) Calcium mapping (12% PC + 6% GGBS)

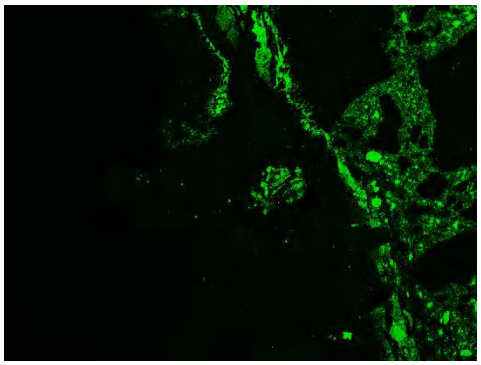

(c) Aluminium mapping (12% PC + 6% GGBS)

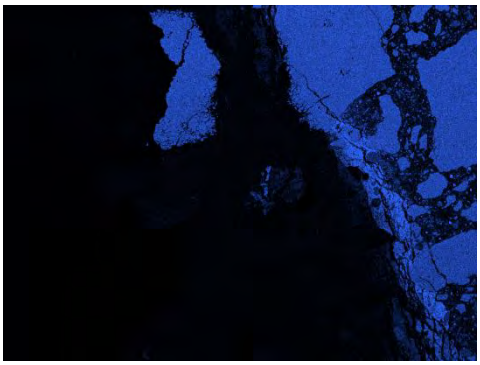

(d) Magnesium mapping (12% PC + 6% GGBS)

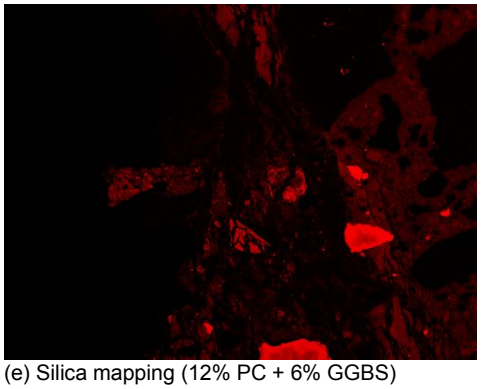

(e) Silica mapping (12% PC + 6% GGBS)

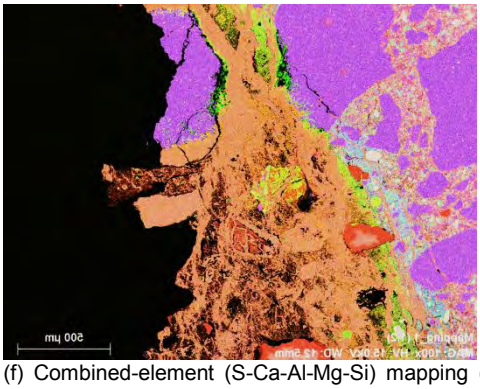

(f) Combined-element (S-Ca-Al-Mg-Si) mapping (12% PC + 6% GGBS)

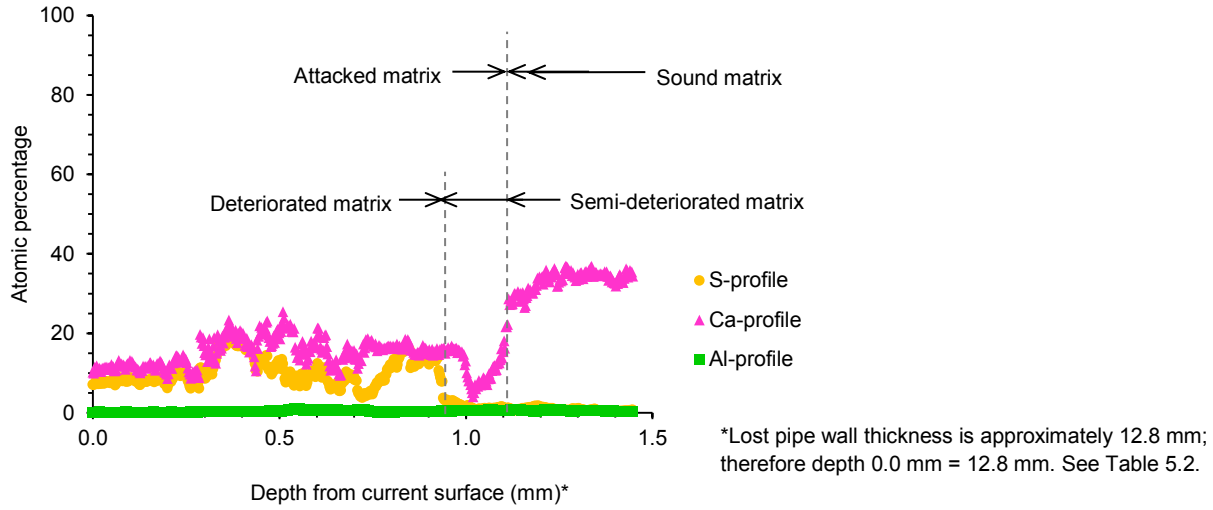

(g) S-Ca-Al concentration vs. depth profiles, up to approximately 0.4 mm into the sound matrix (12% PC + 6% GGBS)
Figure 5-13 (a) to (g): Elemental mapping/concentration profiles for concrete mixture with 12% PC + 6% GGBS.

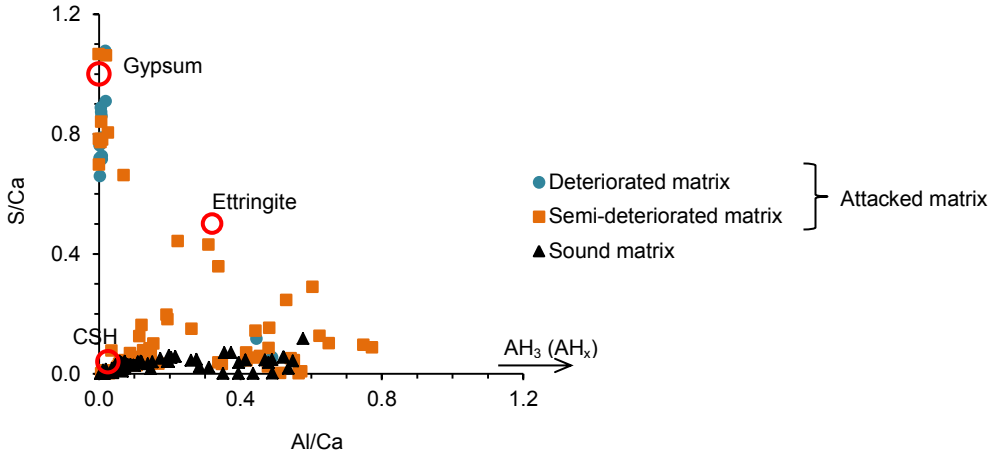

Figure 5-14: EDS point analysis for concrete mixture with 12% PC + 6% GGBS, exposed to biogenic H_2SO_4 for 127 months.

5.4.1.5 Elemental mapping of concrete mixture with 13.5% PC + 4.5% FA and dolomite coarse aggregate

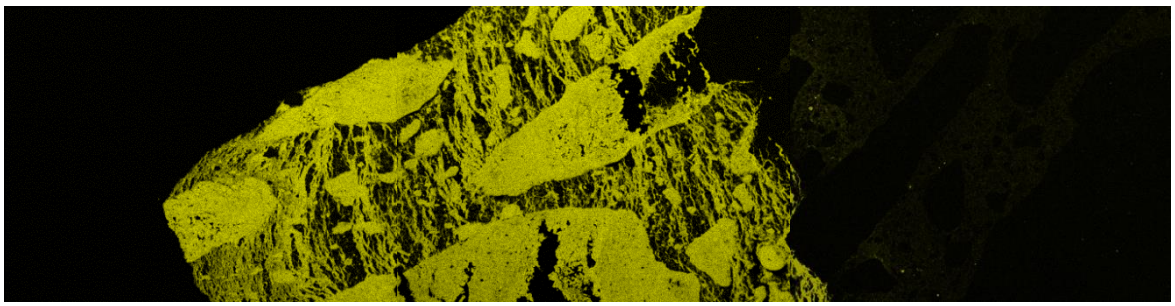

(a) Sulphur mapping (13.5% PC + 4.5% FA)

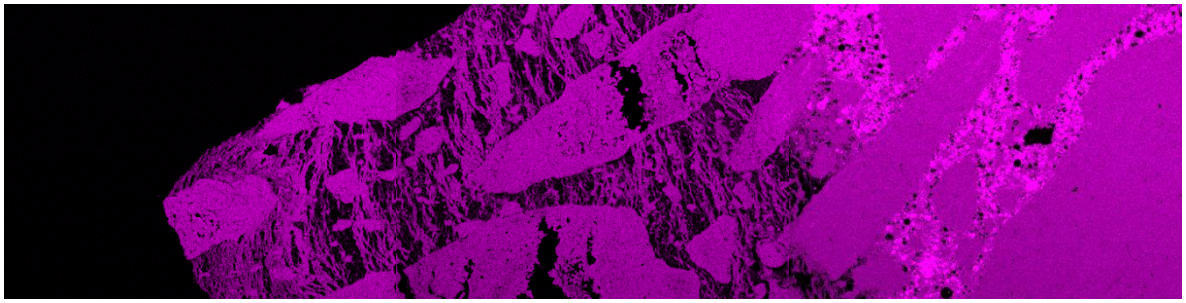

(b) Calcium mapping (13.5% PC + 4.5% FA)

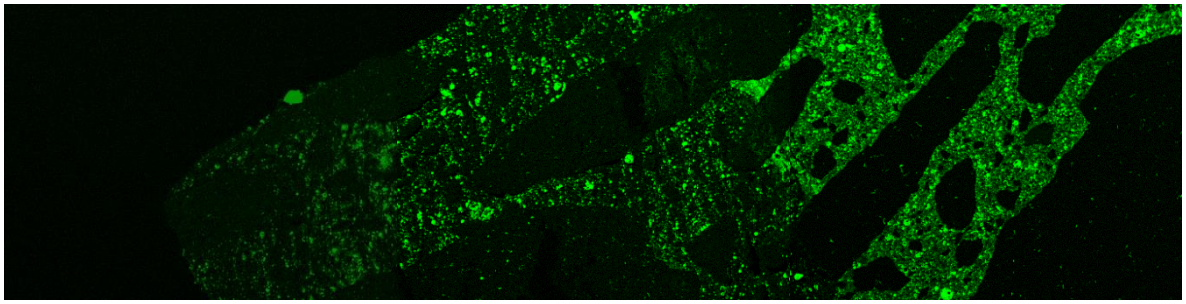

(c) Aluminium mapping (13.5% PC + 4.5% FA)

(d) Magnesium mapping (13.5% PC + 4.5% FA)

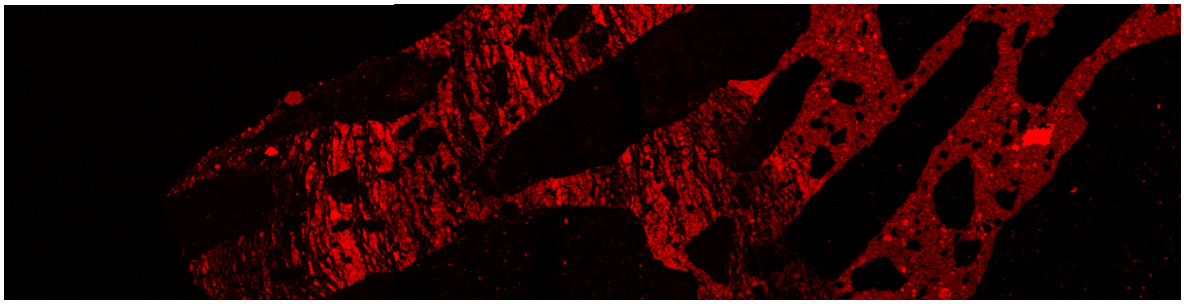

(e) Silica mapping (13.5% PC + 4.5% FA)

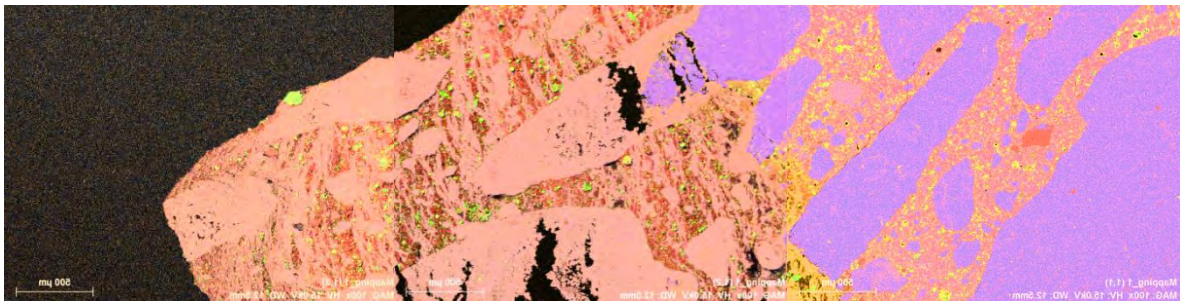

(f) Combined-element (S-Ca-Al-Mg-Si) mapping (13.5% PC + 4.5% FA)

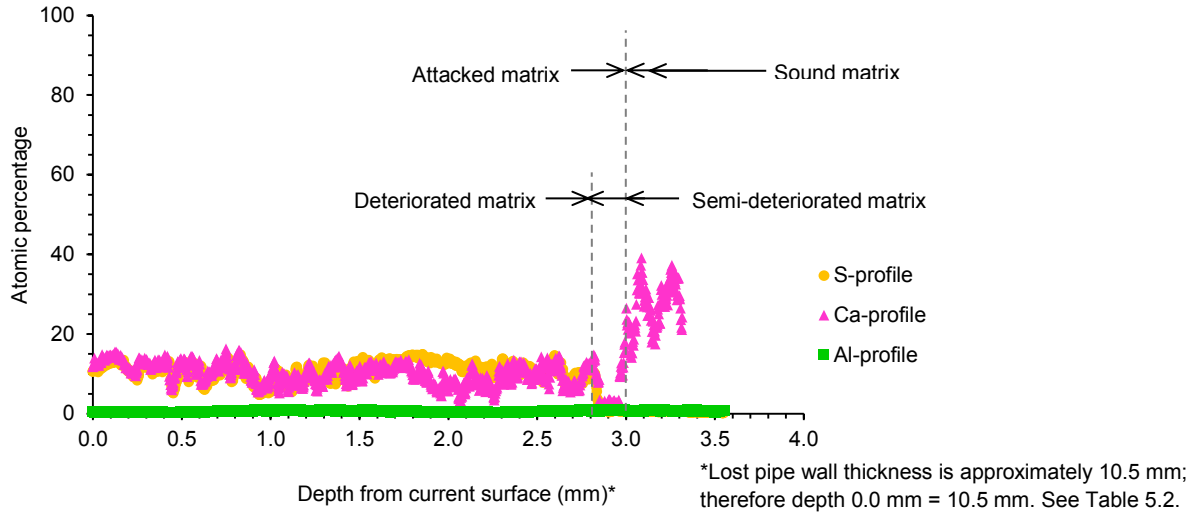

(g) S-Ca-Al concentration vs. depth profiles, up to approximately 0.5 mm into the sound matrix (13.5% PC + 4.5% FA)
Figure 5-15 (a) to (g): Elemental mapping/concentration profiles for concrete mixture with 13.5% PC + 4.5% FA.

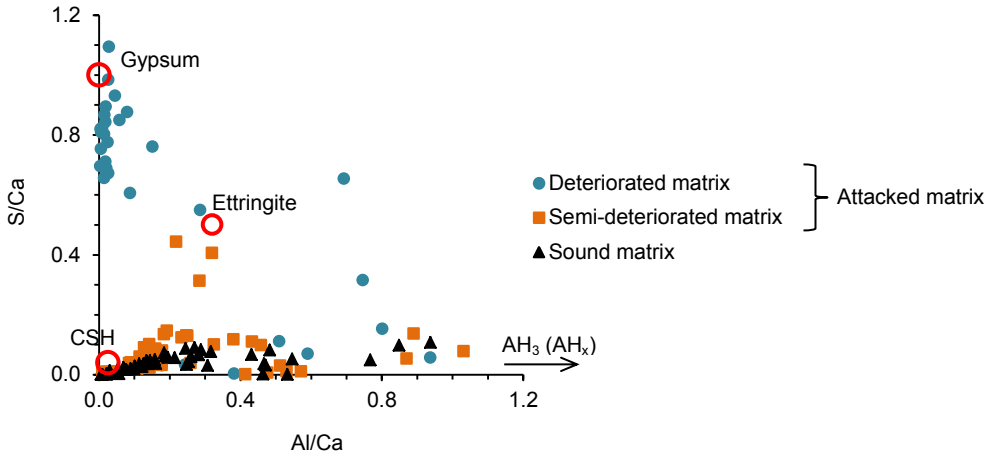

Figure 5-16: EDS point analysis for concrete mixture with 13.5% PC + 4.5% FA, exposed to biogenic H_2SO_4 for 127 months.

5.4.1.6 Elemental mapping of concrete mixture with 16.5% PC + 1.5% SF and dolomite coarse aggregate

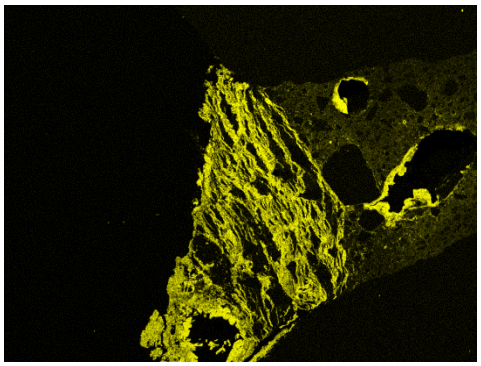

(a) Sulphur mapping (16.5% PC + 1.5% SF)

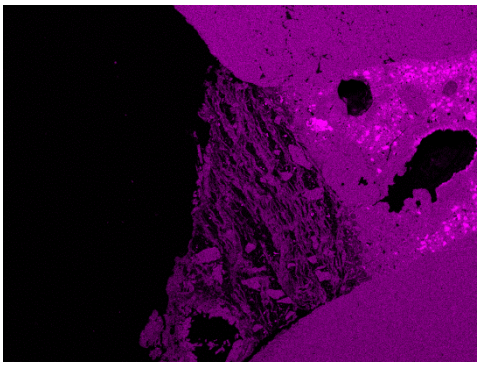

(b) Calcium mapping (16.5% PC + 1.5% SF)

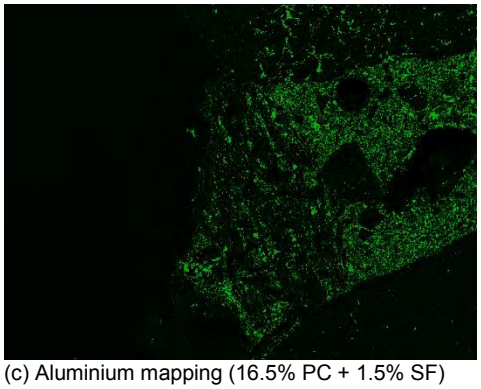

(c) Aluminium mapping (16.5% PC + 1.5% SF)

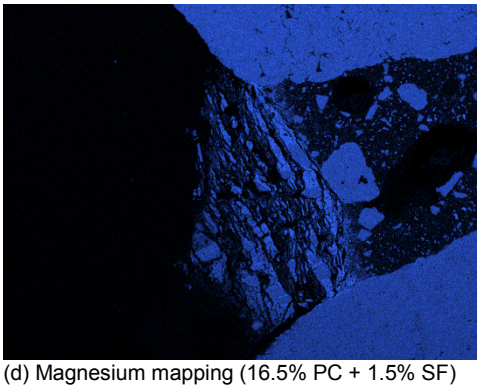

(d) Magnesium mapping (16.5% PC + 1.5% SF)

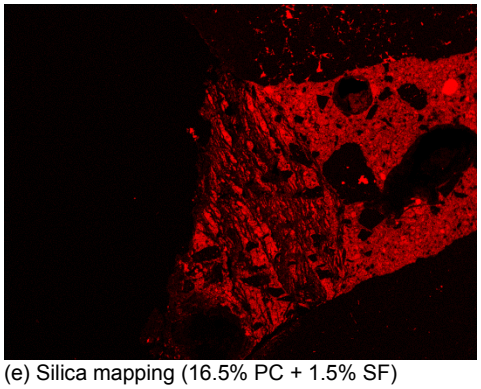

(e) Silica mapping (16.5% PC + 1.5% SF)

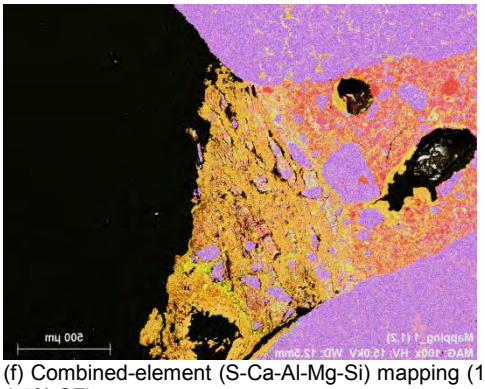

(f) Combined-element (S-Ca-Al-Mg-Si) mapping (16.5% PC + 1.5% SF)

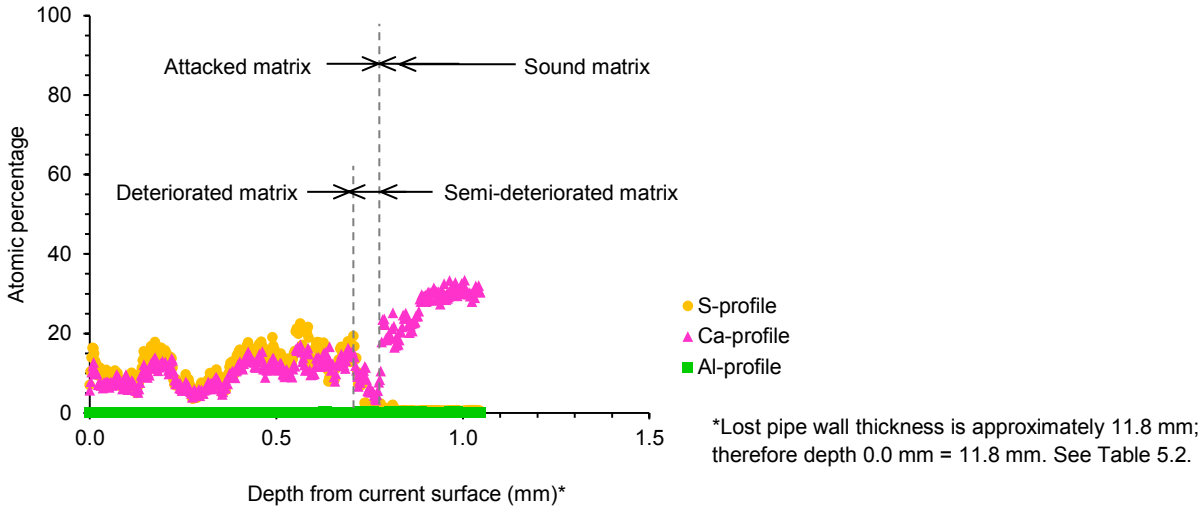

(g) S-Ca-Al concentration vs. depth profiles, up to approximately 0.3 mm into the sound matrix (16.5% PC + 1.5% SF)

Figure 5-17 (a) to (g): Elemental mapping/concentration profiles for concrete mixture with 16.5% PC + 1.5% SF.

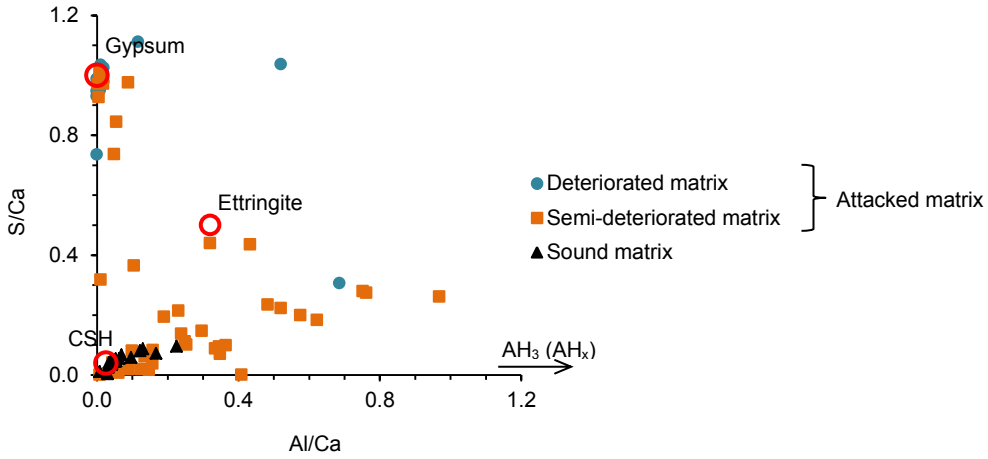

Figure 5-18: EDS point analysis for concrete mixture with 16.5% PC + 1.5% SF, exposed to biogenic H_2SO_4 for 127 months.

The following can be noted from the results presented in Figure 5-7 to Figure 5-18:

(i) The concentration (atomic percentage) of the sulphur (S) species within the attacked (deteriorated and semi-deteriorated) matrices of PC-based concrete mixtures is in the order of 13%, and this concentration is attributed to the deposition of elemental sulphur through abiotic transformations (Wilmot et al., 1988; EPA, 1991; Kotronarou and Hoffmann, 1991; Herisson et al., 2014). However, the progression of the micro-cracks in the concrete matrices is due to biogenic sulphuric acid attack mechanisms which will be discussed in detail in Section 5.7. The concentration of sulphur species in the sound matrices of PC-based concrete mixtures is less than 0.3%.

(ii) The concentration (atomic percentage) of the calcium species varies across the attacked (deteriorated and semi-deteriorated) and sound matrices of PC-based concrete mixtures. Within the sound and semi-deteriorated matrices, the concentrations are in the order of 40% and 5% respectively in all the mixtures. Within the deteriorated matrices, the concentrations are in the order of 9%, 14%, 18%, 20%, 13%, and 8% for PC 16, PC 18, PC 23, PC/GGBS 18, PC/FA 18, and PC/SF 18 respectively.

(iii) The concentration (atomic percentage) of the aluminium species across the attacked (deteriorated and semi-deteriorated) and sound matrices of all the PC-based concrete mixtures is less than 1%.

(iv) The Al/Ca ratios of the sound matrices in all the PC-based concrete mixtures are less than 0.1.

(v) The acid-soluble (dolomite) aggregate that has been subjected to biogenic sulphuric acid attack is characterised by micro-cracks, indicating typical acid-aggregate dissolution characteristics.

(vi) From the EDS point analyses, the deteriorated matrix is characterised as predominantly gypsum, the semi-deteriorated matrix is characterised as predominantly ettringite (AFt), while the sound matrix is principally C-S-H (and CH).

Since the sound concrete matrices subjected to biogenic corrosion process undergo external-based attack, both the deteriorated and semi-deteriorated matrices (products of corrosion) play a significant role in the attack mechanisms, for example, by providing a protective barrier to the attacking acid. In this regard, in order to further understand the underlying mechanisms of attack, the products of corrosion were characterised in detail using quantitative XRD (QXRD) and TGA techniques. Results from these techniques are presented in sub-sections 5.4.2 (QXRD) and 5.4.3 (TGA).

5.4.2 Quantitative XRD

The mineralogical characterisation by XRD shows that the deteriorated and semi-deteriorated matrices (products of corrosion) consist predominantly of gypsum, and also silica, dolomite, and calcite. Results for quantitative XRD, determined by Rietveld analysis are presented in Figure 5-19.

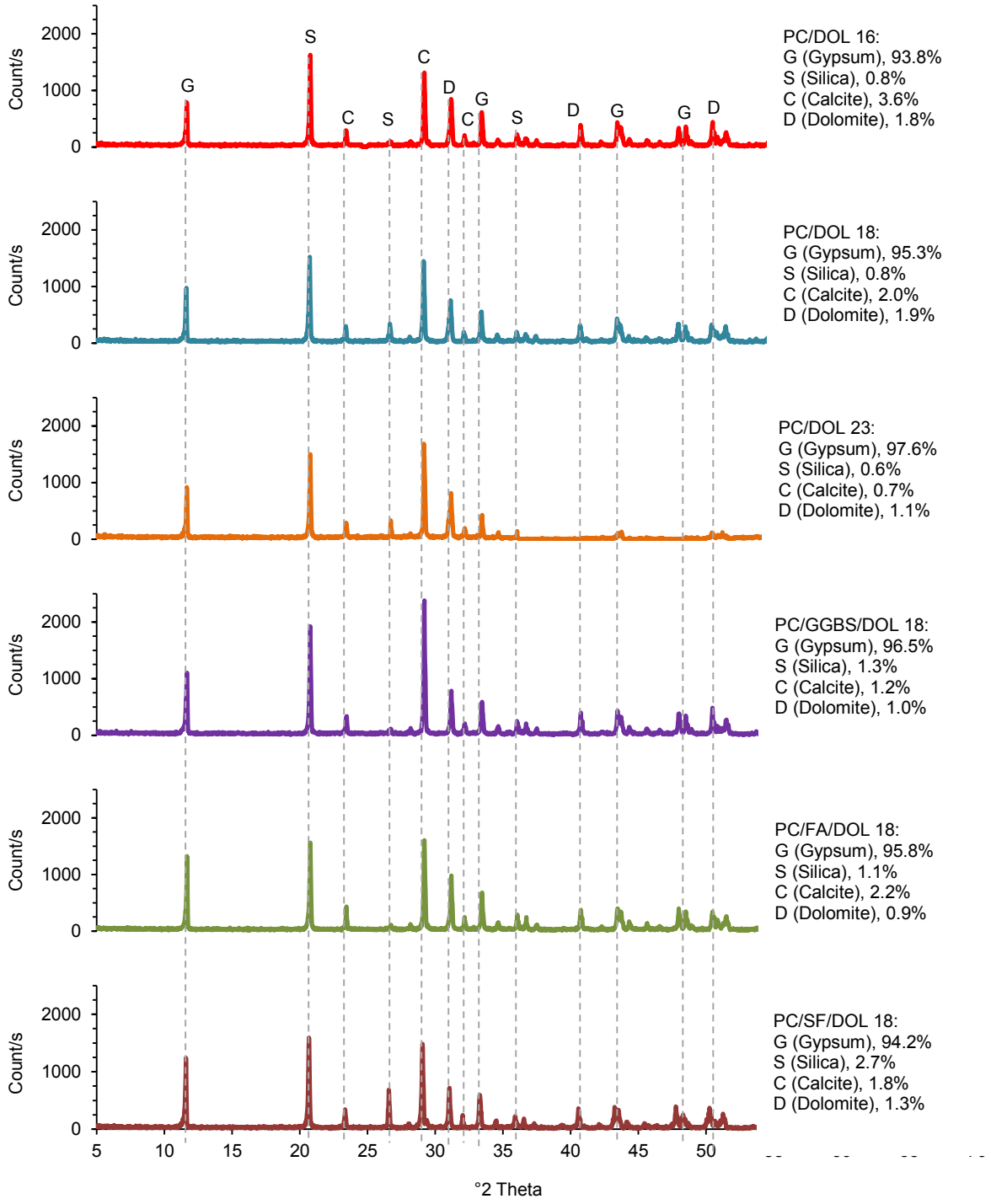

Figure 5-19: QXRD for 'products of corrosion' sampled from PC-based concrete subjected to biogenic H_2SO_4 for 127 months.

QXRD results presented above show a slight increase in the amount of gypsum in the products of corrosion as the cement content in plain PC mixtures increased from 16% (gypsum content approximately 93.8%) to 23% (gypsum content approximately 97.6%). For blended PC mixtures with 6% GGBS (and 12% PC), 4.5% FA (and 13.5% PC) and 1.5% SF (and 16.5% PC), the amount of gypsum in their products of corrosion was approximately 96.5%, 95.8% and 94.2% respectively. Results for mixtures with SCMs show an inverse correlation (in comparison to plain PC mixtures) between cement content and the amount of gypsum in the products of corrosion. For example, mixtures with 12% PC (and 6% GGBS) have a higher amount of gypsum in their products of corrosion

than those with 16.5% PC (and 1.5% SF). Apart from the gypsum, the other phases (silica, calcite, and dolomite) within the products of corrosion do not show a clear correlation with binder content in the respective concrete mixtures. More discussion will be given in Section 5.7.

5.4.3 TGA

TGA results on the products of corrosion taken from PC-based concrete mixtures are presented in Figure 5-20 to Figure 5-25.

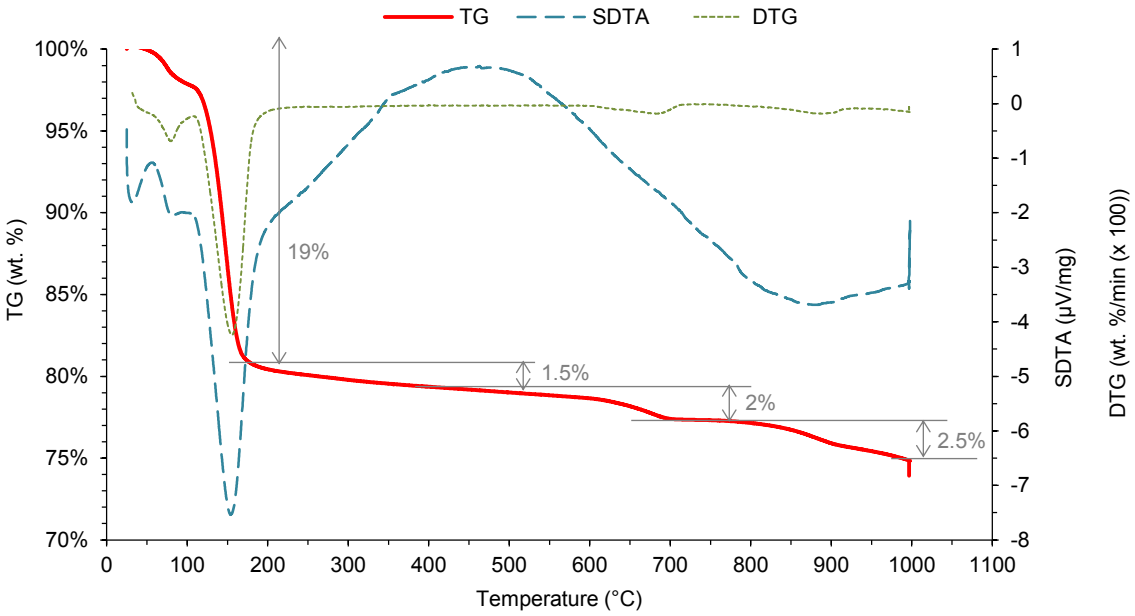

Figure 5-20: TG/SDTA/DTG curves for 'products of corrosion' taken from a concrete sample with 16% PC.

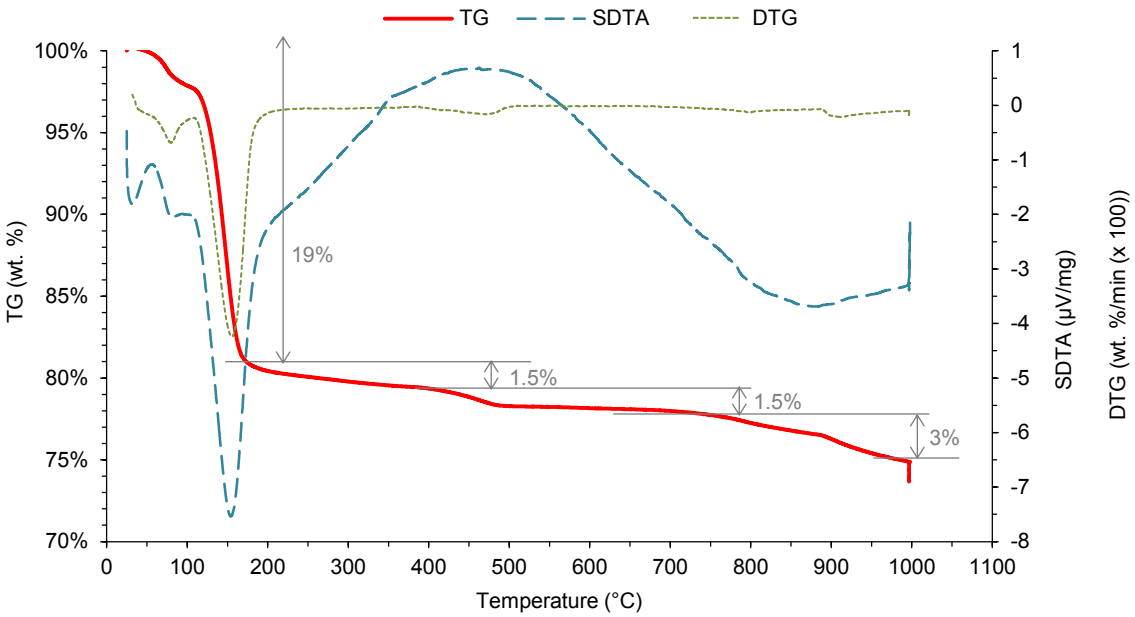

Figure 5-21: TG/SDTA/DTG curves for 'products of corrosion' taken from a concrete sample with 18% PC.

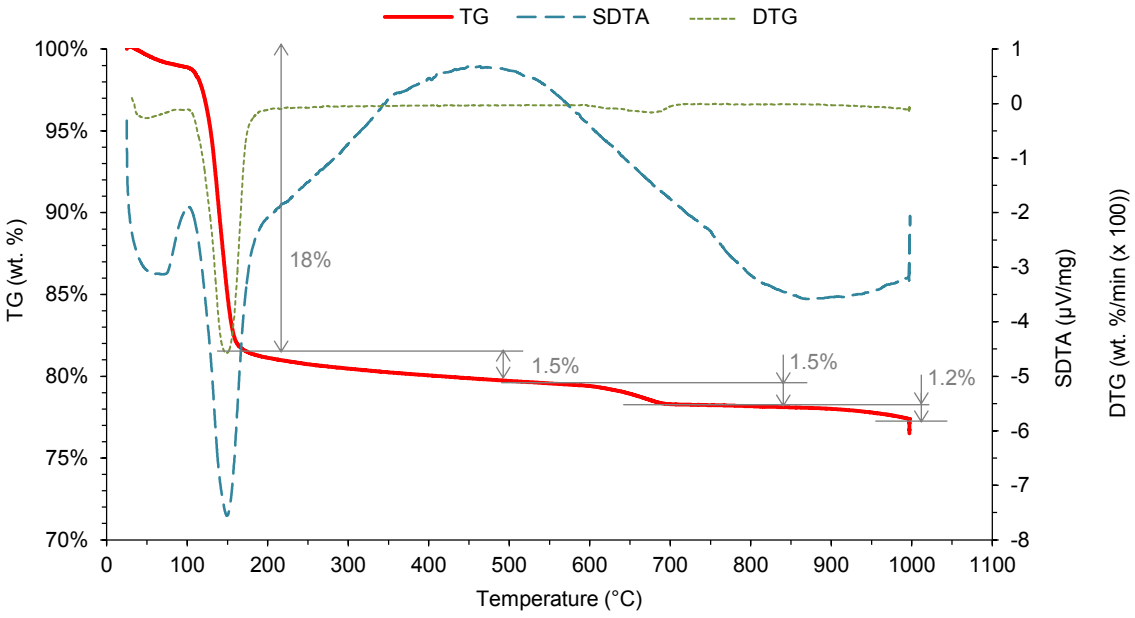

Figure 5-22: TG/SDTA/DTG curves for 'products of corrosion' taken from a concrete sample with 23% PC.

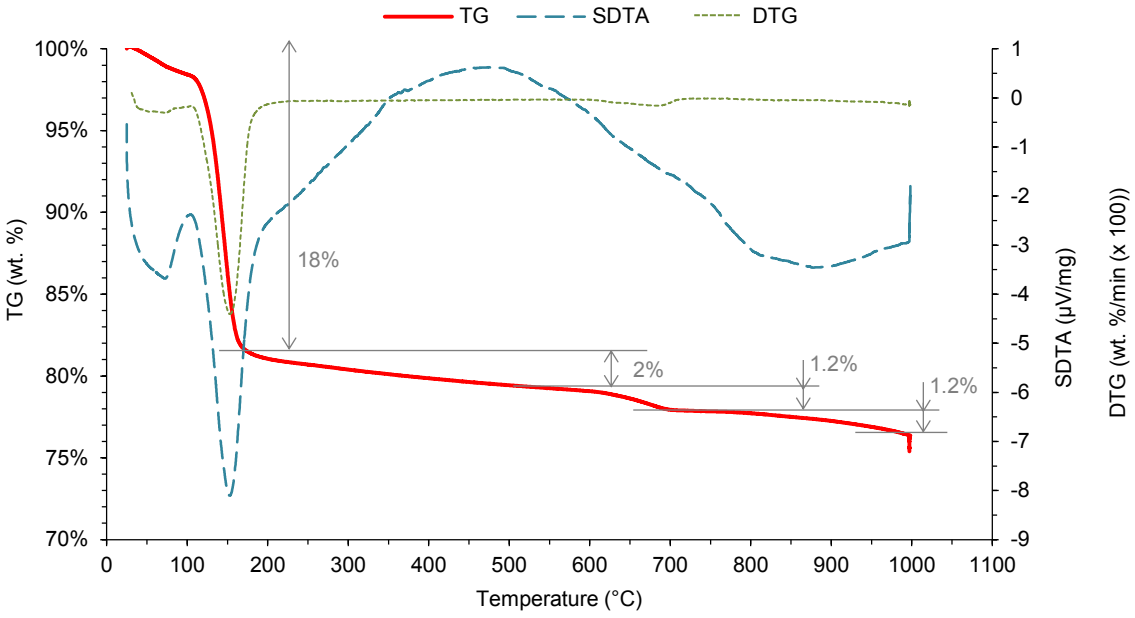

Figure 5-23: TG/SDTA/DTG curves for 'products of corrosion' taken from a concrete sample with 12% PC + 6% GGBS.

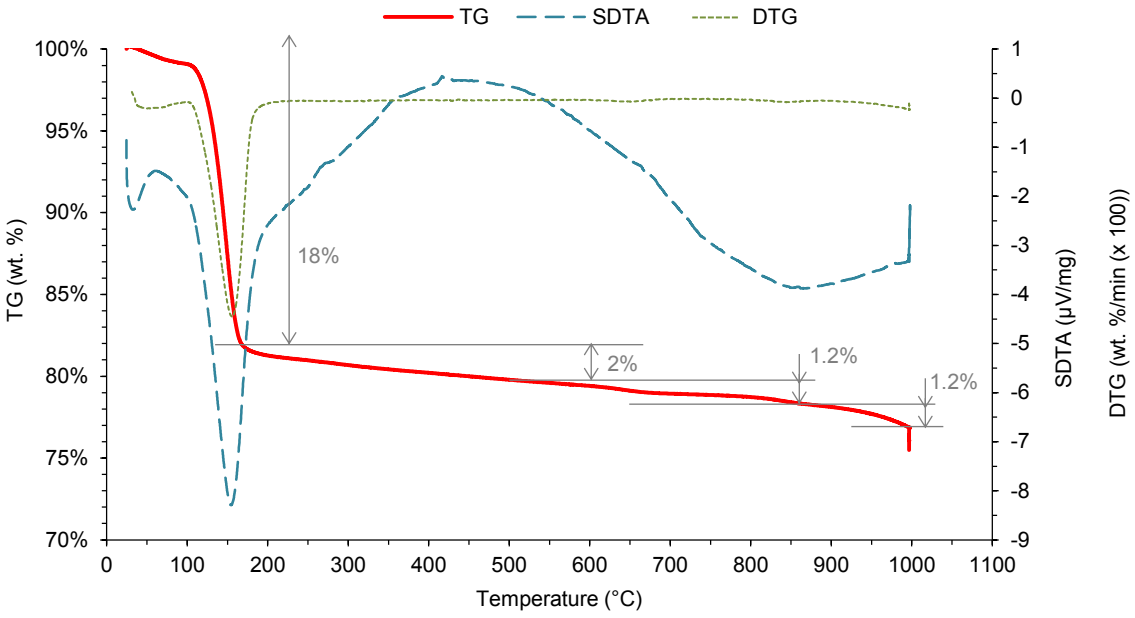

Figure 5-24: TG/SDTA/DTG curves for 'products of corrosion' taken from a concrete sample with 13.5% PC + 4.5% FA.

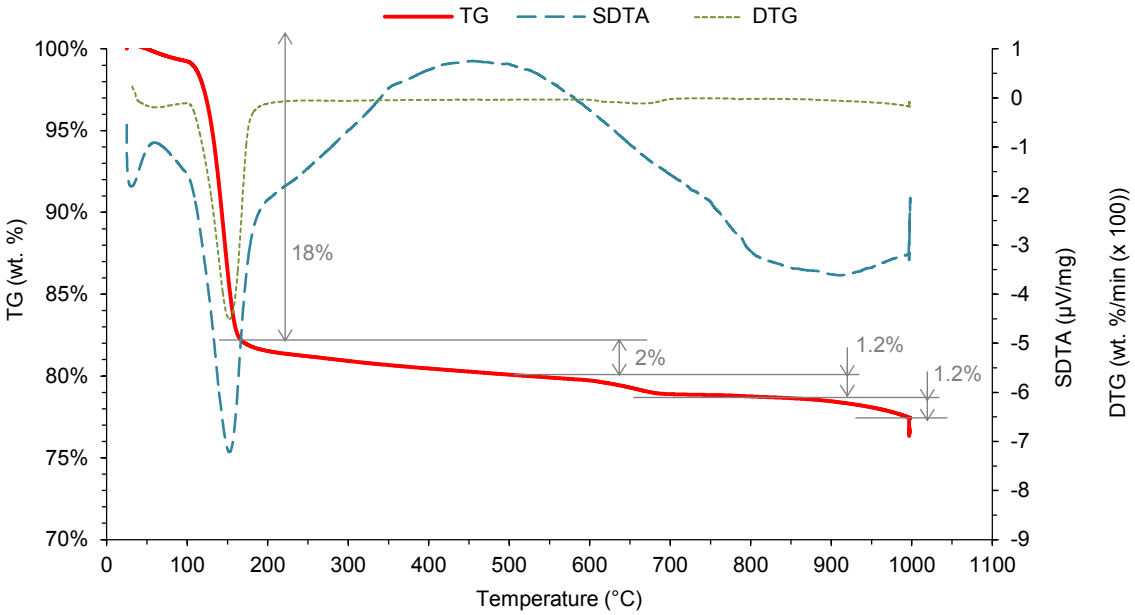

Figure 5-25: TG/SDTA/DTG curves for 'products of corrosion' taken from a concrete sample with 16.5% PC + 1.5% SF.

All the TGA graphs presented above are typical for the dehydration of gypsum, indicating a total weight loss of approximately 22% to 25%. The graphs show multiple weight losses (2-stage weight decrease) of approximately 18% to 19% due to evaporation of water at a temperature peak of approximately 50 °C and 154 °C. The thermal ratio of the two peaks is approximately 3 to 1, which corresponds well with the ratio of evaporated water molecules as given in Equation 5.3.

$$CaSO_4.2H_2O \xrightarrow{-3/2\,H_2O} CaSO_4.\tfrac{1}{2}H_2O \xrightarrow{-1/2\,H_2O} CaSO_4 \qquad (5.3)$$

A third broad peak, at approximately 450 °C represents further decomposition of dehydrated gypsum (weight loss of approximately 1.5% to 2%). At a temperature of approximately 675 °C, there is a weight loss of approximately 1.2% to 2% corresponding to the decomposition of silica. Beyond a temperature of approximately 675 °C, there is a weight loss of approximately 1.2% to 3% corresponding to the decomposition of carbonates (in calcite and dolomite).

Discussion of the SEM/EDS, XRD, and TGA results presented above from the analysis of PC-based concrete mixtures subjected to biogenic H_2SO_4 will be done (in Section 5.7) together with those from CAC-based concrete mixtures presented in Section 5.5.

5.5 CAC-based binder systems

The CAC-based samples that were characterised included four mixtures with dolomite (DOL) coarse aggregates, one mixture with quartzite (SIL) coarse aggregate, and one mixture with an artificial aluminate (Alag^{TM}) aggregate. Mixtures with DOL included three plain mixtures with a total binder content of 16%, 18% and 23% CAC, and one blended mixture incorporating 11% CAC + 4.5% FA + 1.5% SF. Mixtures incorporating SIL and Alag^{TM} had binder contents of 23% CAC and 20% CAC respectively. See mixture composition in Appendix E.

5.5.1 SEM/EDS

The BSE micrographs for the six CAC-based concrete mixtures are given in Figure 5-26.

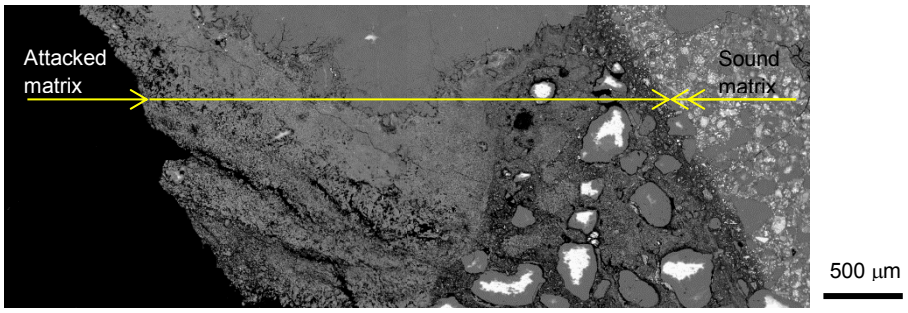

(a) 16% CAC total binder*

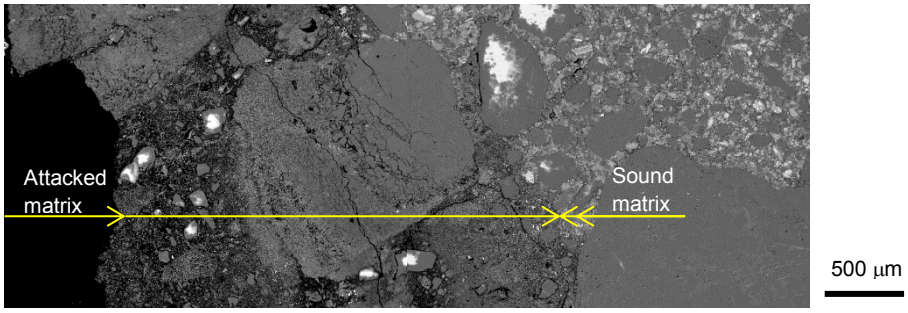

(b) 18% CAC total binder*

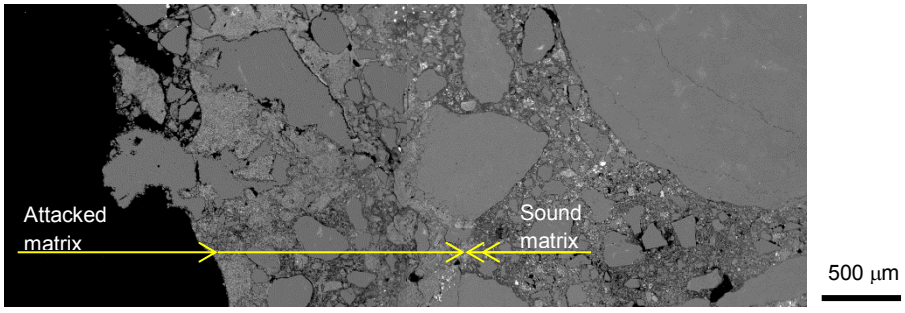

(c) 23% CAC total binder*

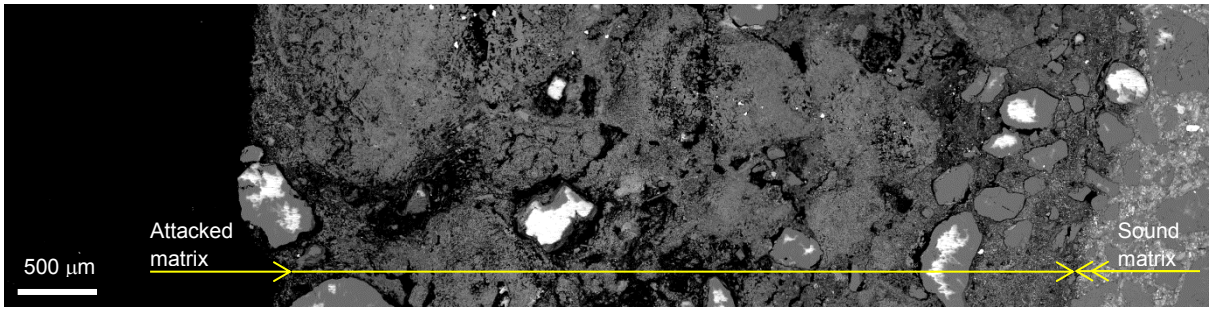

(d) 23% CAC total binder**

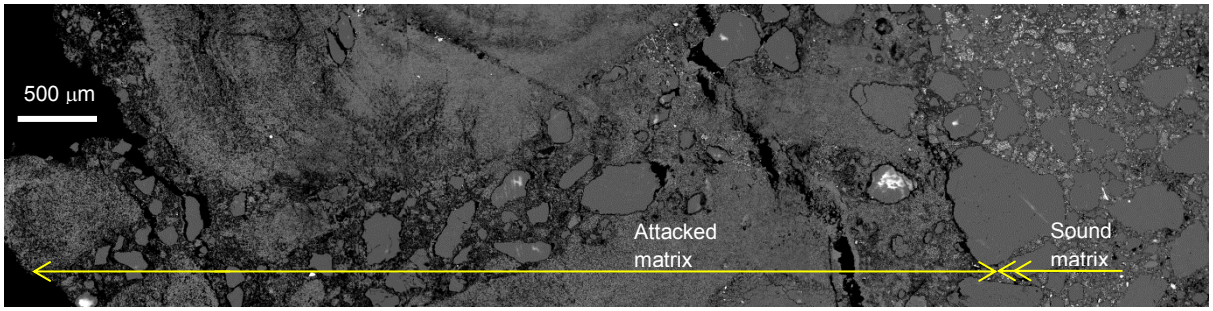

(e) 11% CAC + 4.5% FA + 1.5% SF total binder*

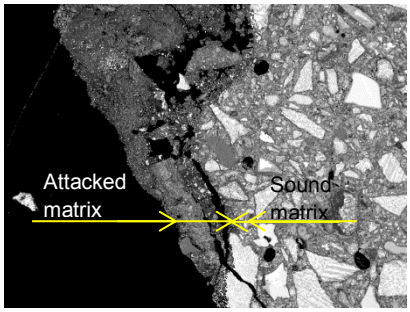

(f) 20% CAC total binder#

*Concrete mixtures with DOL coarse aggregate and 50/50 blend of DOL and SIL fine aggregates

**Concrete mixture with SIL coarse aggregate and 50/50 blend of DOL and SIL fine aggregates

#Concrete mixture with aluminate coarse aggregate and SIL filler sand

*See the BSE micrographs of the attacked matrix (products of corrosion) in Appendix L.

Figure 5-26 (a) to (f) : BSE micrographs of CAC-based concrete mixtures exposed to biogenic H_2SO_4 for 127 months in the VES.

The depth of attacked matrices, measured from the current exposed surface, and not the original pipe surface (see approximate lost thicknesses of the respective 'lid' wall material in Table 5-3) in the CAC-based concrete mixtures given in Figure 5-26 varies. The depth of attack in mixtures with 16%, 18%, and 23% CAC/DOL is approximately 3 mm, 2.5 mm, and 1.5 mm respectively, while in 23% CAC/SIL, 11% CAC/DOL + 4.5% FA + 1.5% SF, and 20% CAC/Alag^{TM}, the depth of attack is approximately 3.5 mm, 4 mm, and 400 μm respectively. Generally, it can also be noted that the microstructure of CAC-based concrete (with and without SCMs) exposed to biogenic H_2SO_4 attack is characterised by less micro-cracks within both the HCP and aggregates, in comparison to PC-based concrete. The varying depths of attack and development of micro-cracks within various CAC-based matrices can also be explained by certain properties of the products of corrosion, certain chemical reactions such as topochemical reactions, and the theory of crystallisation pressure (Taber, 1916; Paulini, 1994; Bizzozero et al., 2014).

However, before these mechanisms are discussed, it is important to understand the distribution, concentration and composition of various species involved in biogenic corrosion mechanisms within the concrete matrices. Therefore, elemental mapping with respective concentration profiles plotted from area segments using ImageJ Software (EMPA, 2015), and EDS point analysis for each of the concrete mixtures given in Figure 5-26 are presented in sub-sections 5.5.1.1 to 5.5.1.6 (Figure 5-27 to Figure 5-38). These elemental mapping include species responsible for generation of the attacking

acid – sulphur, and species within the HCP that are responsible for neutralising the attacking acid – calcium and aluminium. Moreover, in order to understand the behaviour and potential role of aggregates in concrete mixtures exposed to biogenic H_2SO_4, mapping for magnesium and silica, which are major constituents of acid-soluble and acid-insoluble aggregates respectively is also presented.

Table 5-3: Summary of approximate thicknesses of lost CAC-based 'lid' wall material due to biogenic H_2SO_4 attack for 127 months

Mixture	Total binder content (%)	Lost wall thickness (mm)*
CAC/DOL 16	16	6.0 ± 2.0
CAC/DOL 18	18	5.5 ± 2.2
CAC/DOL 23	23	3.5 ± 0.8
CAC/SIL 23	23	3.5 ± 1.2
CAC/FA/SF/DOL 17	17	4.5 ± 1.8
CAC/Alag^{TM} 20	20	2.3 ± 0.7

*Based on direct measurements - See Table 5.1 for details

5.5.1.1 Elemental mapping of concrete mixture with 16% CAC and dolomite coarse aggregate

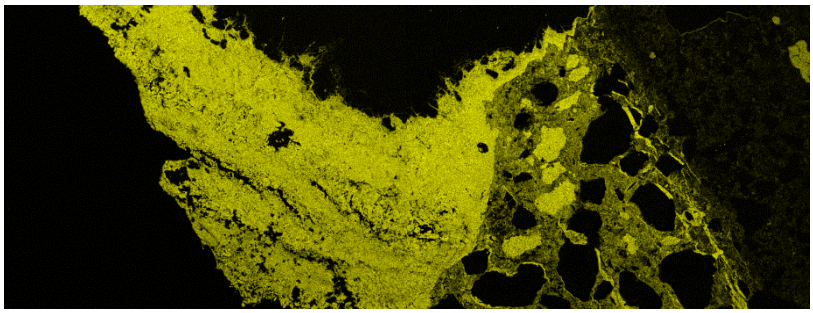

(a) Sulphur mapping (16% CAC)

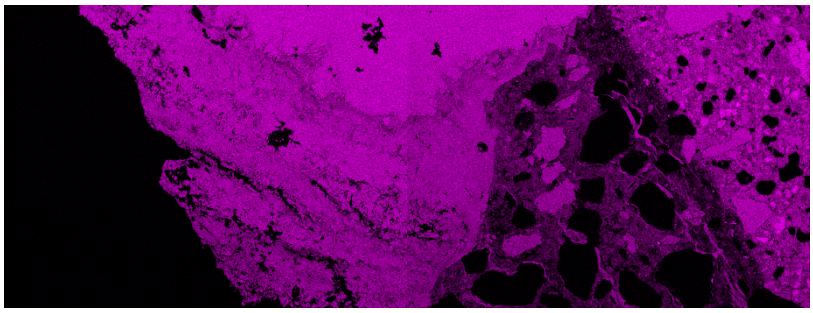

(b) Calcium mapping (16% CAC)

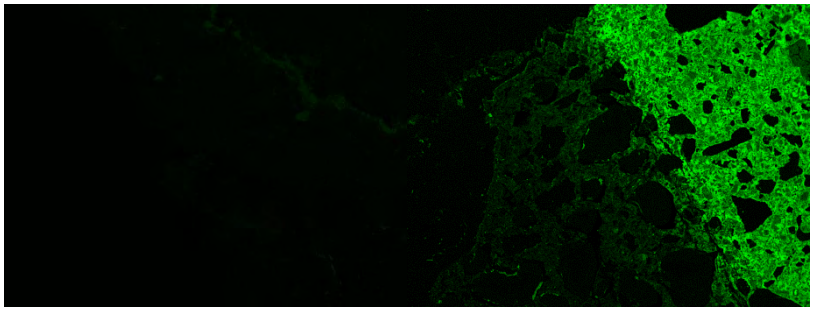

(c) Aluminium mapping (16% CAC)

(d) Magnesium mapping (16% CAC)

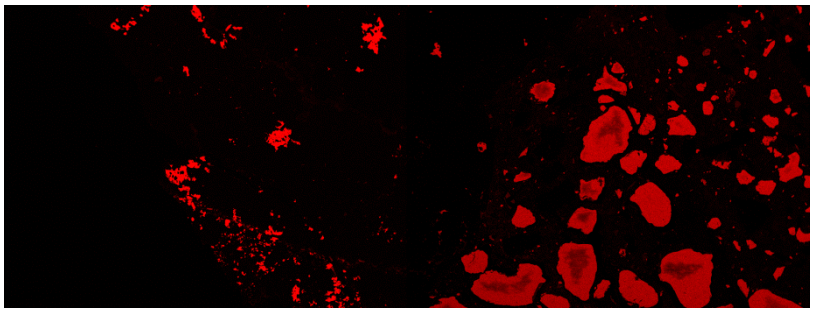

(e) Silica mapping (16% CAC)

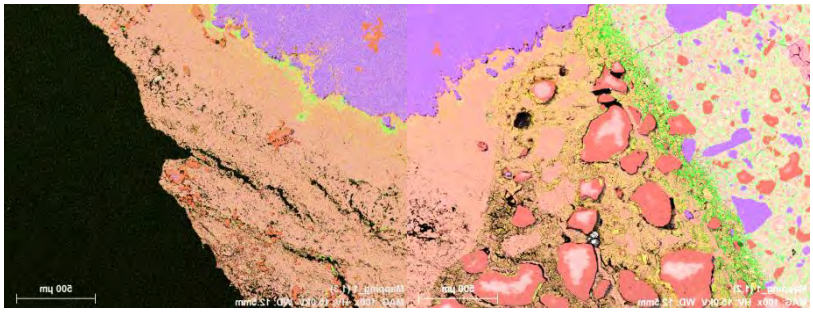

(f) Combined-element (S-Ca-Al-Mg-Si) mapping (16% CAC)

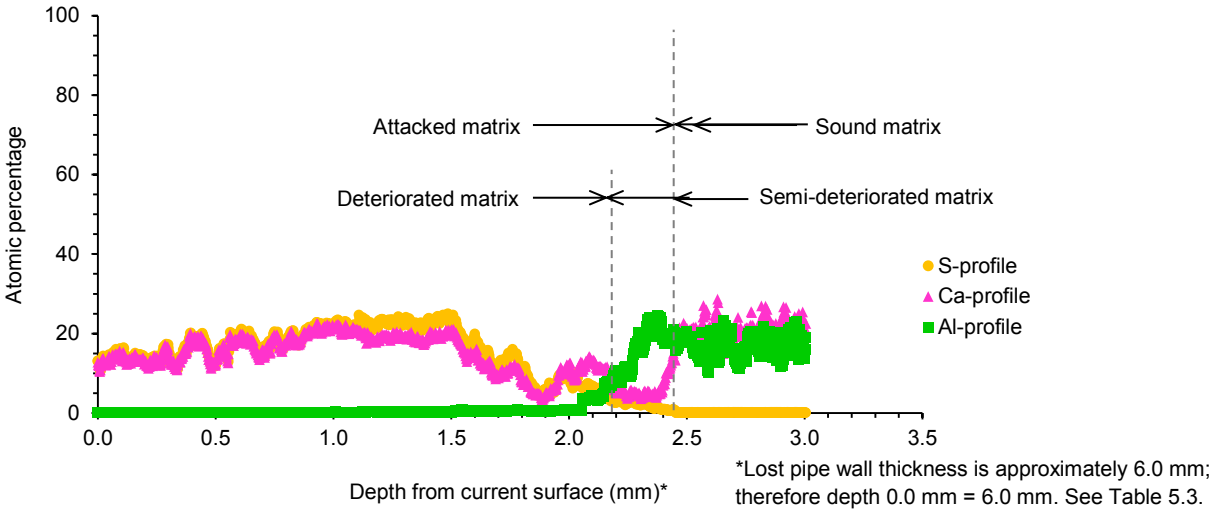

(g) S-Ca-Al concentration vs. depth profiles, up to approximately 0.5 mm into the sound matrix (16% CAC)

Figure 5-27 (a) to (g): Elemental mapping/concentration profiles for concrete mixture with 16% CAC.

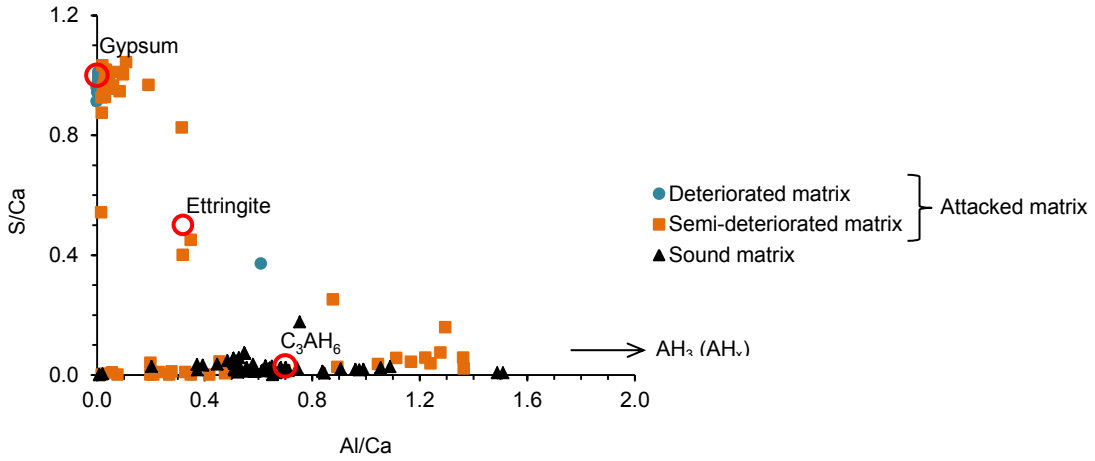

Figure 5-28: EDS point analysis for concrete mixture with 16% CAC, exposed to biogenic H_2SO_4 for 127 months.

5.5.1.2 Elemental mapping of concrete mixture with 18% CAC and dolomite coarse aggregate

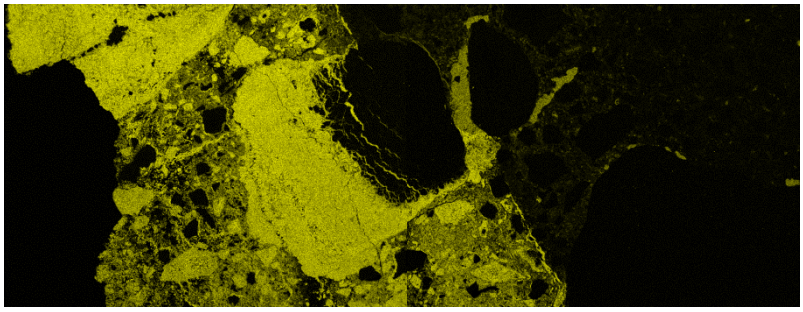

(a) Sulphur mapping (18% CAC)

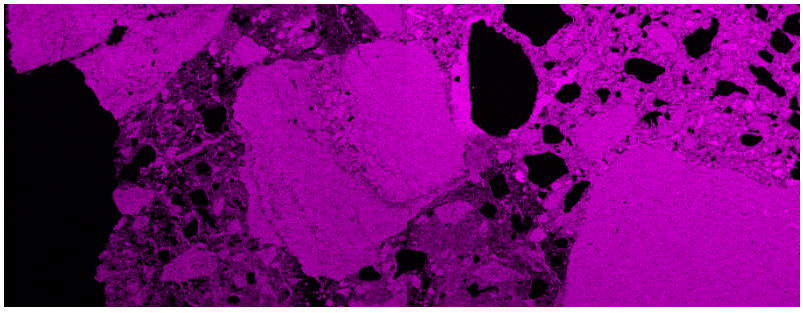

(b) Calcium mapping (18% CAC)

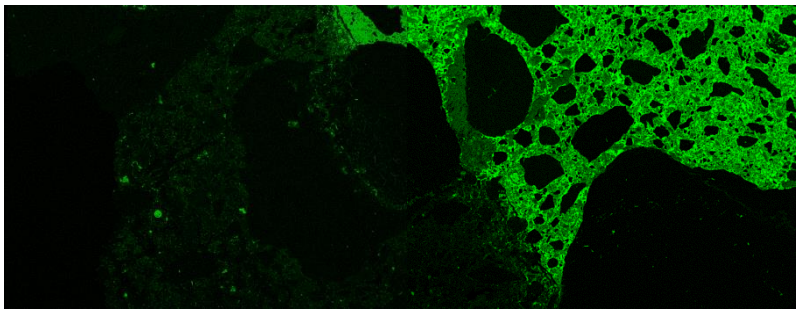

(c) Aluminium mapping (18% CAC)

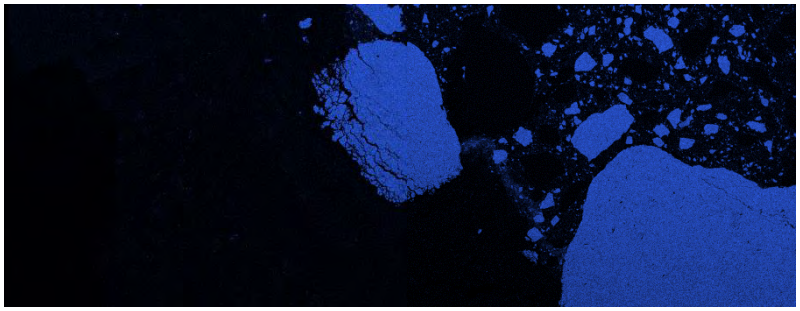

(d) Magnesium mapping (18% CAC)

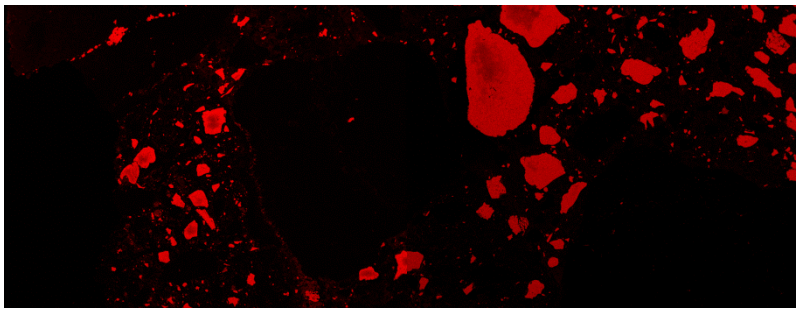

(e) Silica mapping (18% CAC)

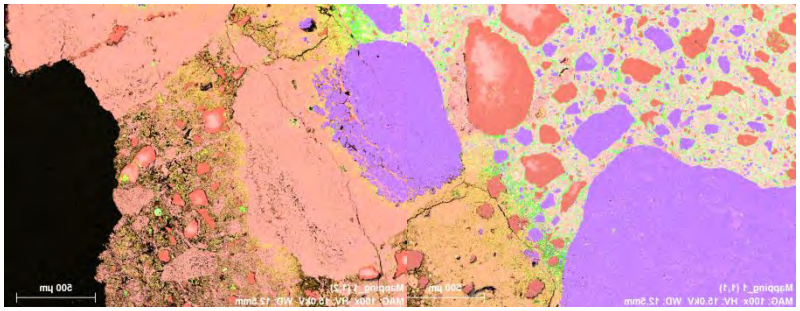

(f) Combined-element (S-Ca-Al-Mg-Si) mapping (18% CAC)

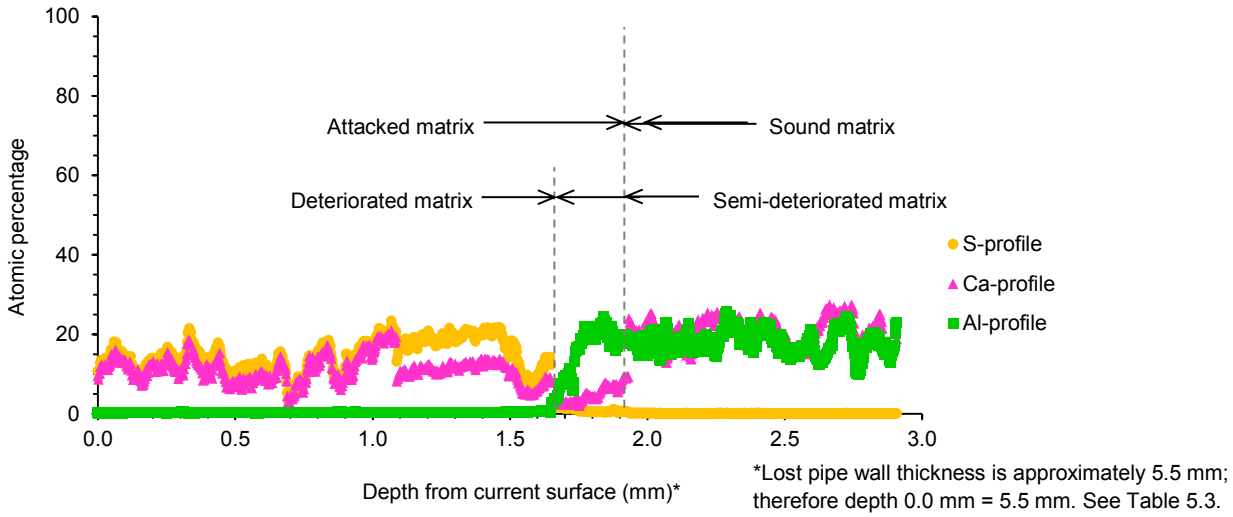

(g) S-Ca-Al concentration vs. depth profiles, up to approximately 1 mm into the sound matrix (18% CAC)
Figure 5-29 (a) to (g): Elemental mapping/concentration profiles for concrete mixture with 18% CAC.

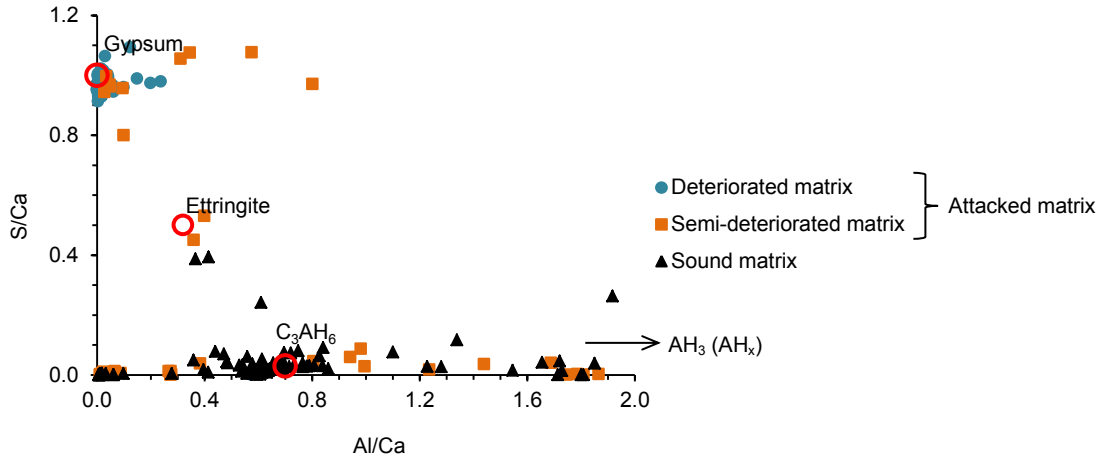

Figure 5-30: EDS point analysis for concrete mixture with 18% CAC, exposed to biogenic H_2SO_4 for 127 months.

5.5.1.3 Elemental mapping of concrete mixture with 23% CAC and dolomite coarse aggregate

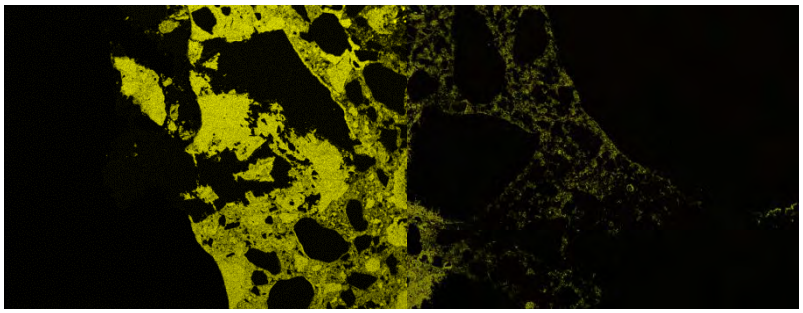

(a) Sulphur mapping (23% CAC + DOL)

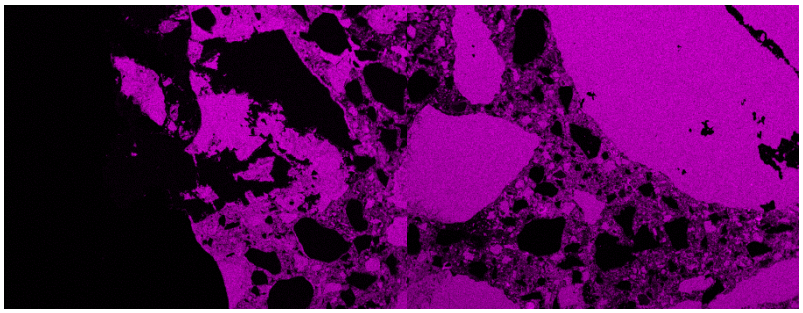

(b) Calcium mapping (23% CAC + DOL)

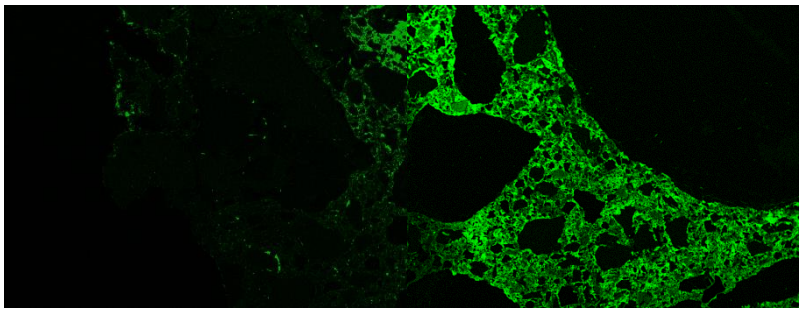

(c) Aluminium mapping (23% CAC + DOL)

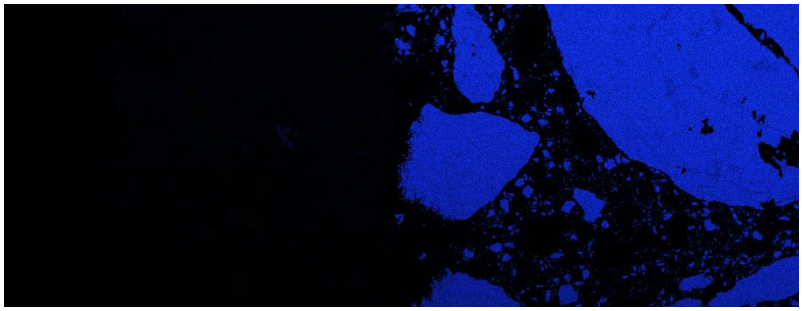

(d) Magnesium mapping (23% CAC + DOL)

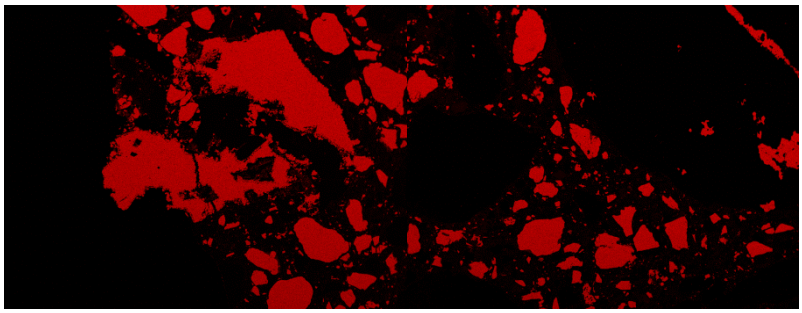

(e) Silica mapping (23% CAC + DOL)

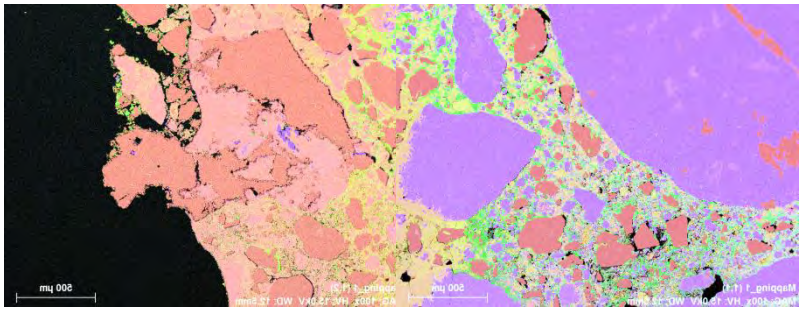

(f) Combined-element (S-Ca-Al-Mg-Si) mapping (23% CAC + DOL)

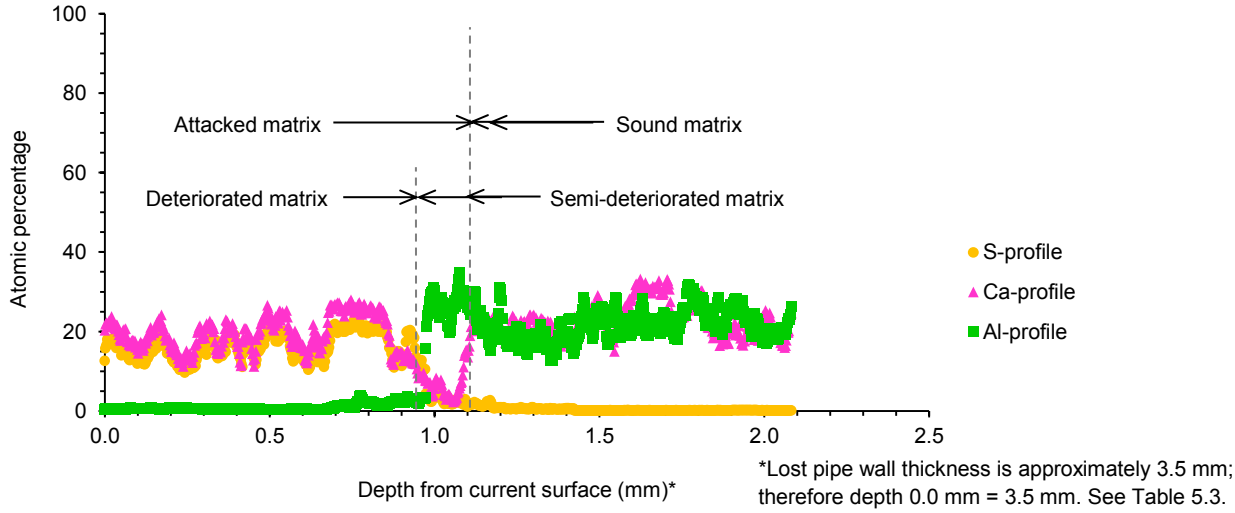

(g) S-Ca-Al concentration vs. depth profiles, up to approximately 1 mm into the sound matrix (23% CAC + DOL)

Figure 5-31 (a) to (g): Elemental mapping/concentration profiles for concrete mixture with 23% CAC + DOL.

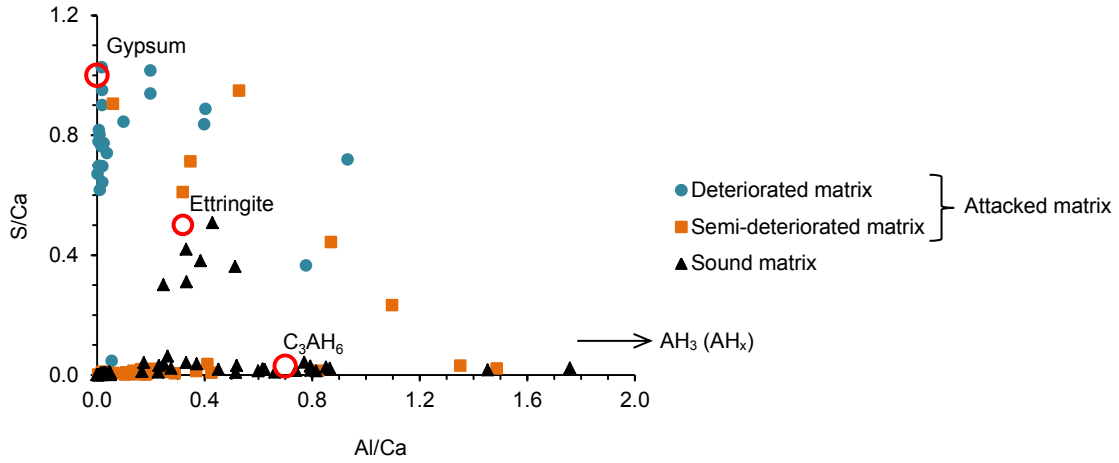

Figure 5-32: EDS point analysis for concrete mixture with 23% CAC + DOL, exposed to biogenic H_2SO_4 for 127 months.

5.5.1.4 Elemental mapping of concrete mixture with 23% CAC and quartzite coarse aggregate

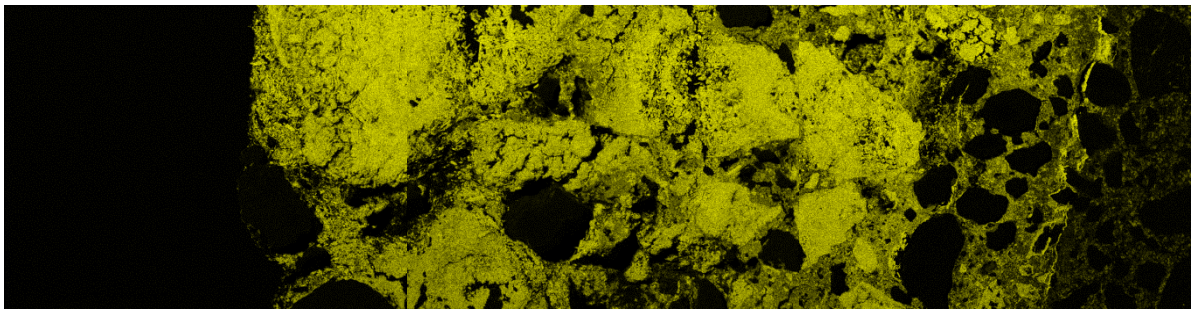

(a) Sulphur mapping (23% CAC + SIL)

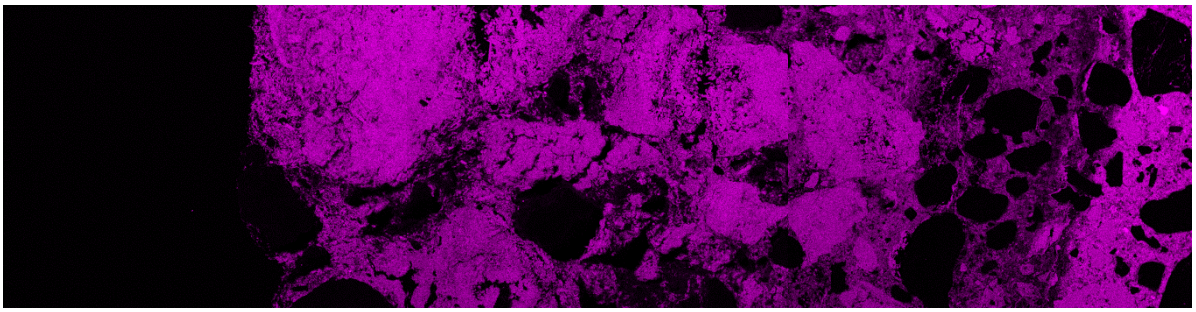

(b) Calcium mapping (23% CAC + SIL)

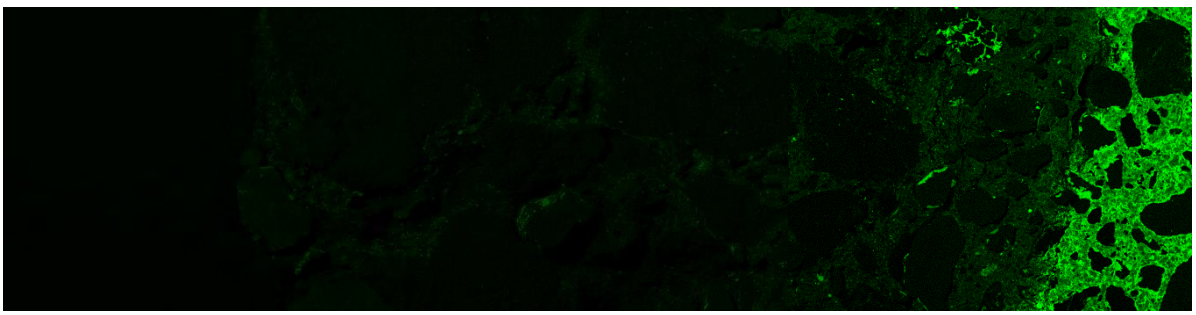

(c) Aluminium mapping (23% CAC + SIL)

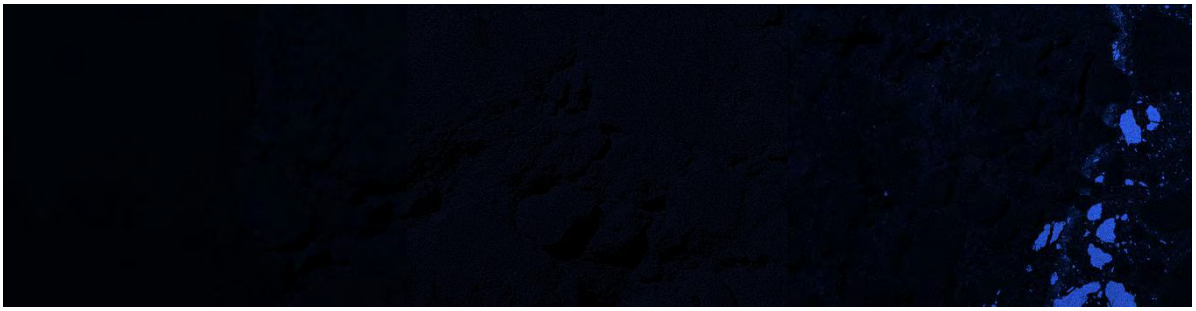

(d) Magnesium mapping (23% CAC + SIL)

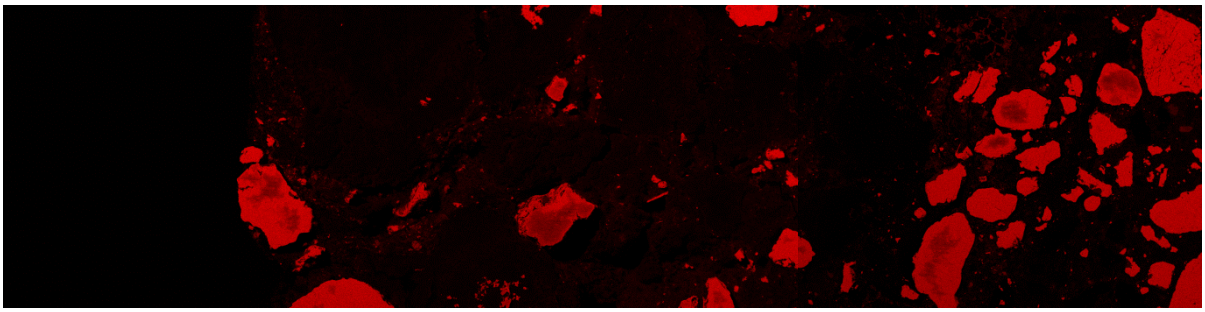

(e) Silica mapping (23% CAC + SIL)

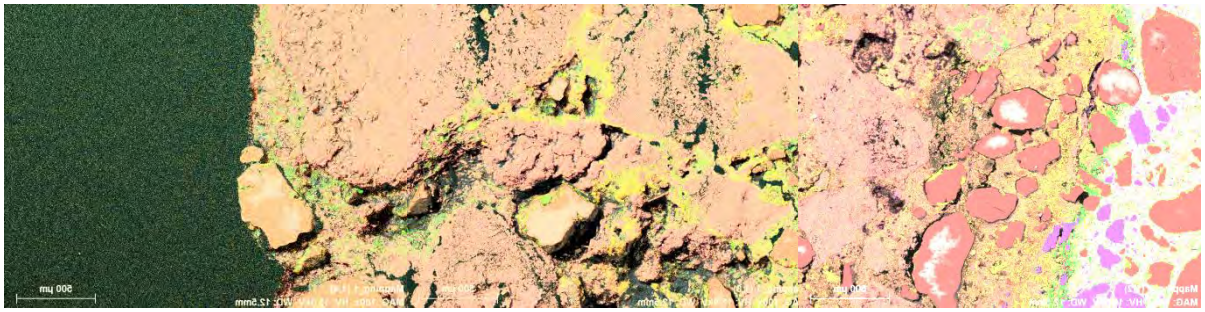

(f) Combined-element (S-Ca-Al-Mg-Si) mapping (23% CAC + SIL)

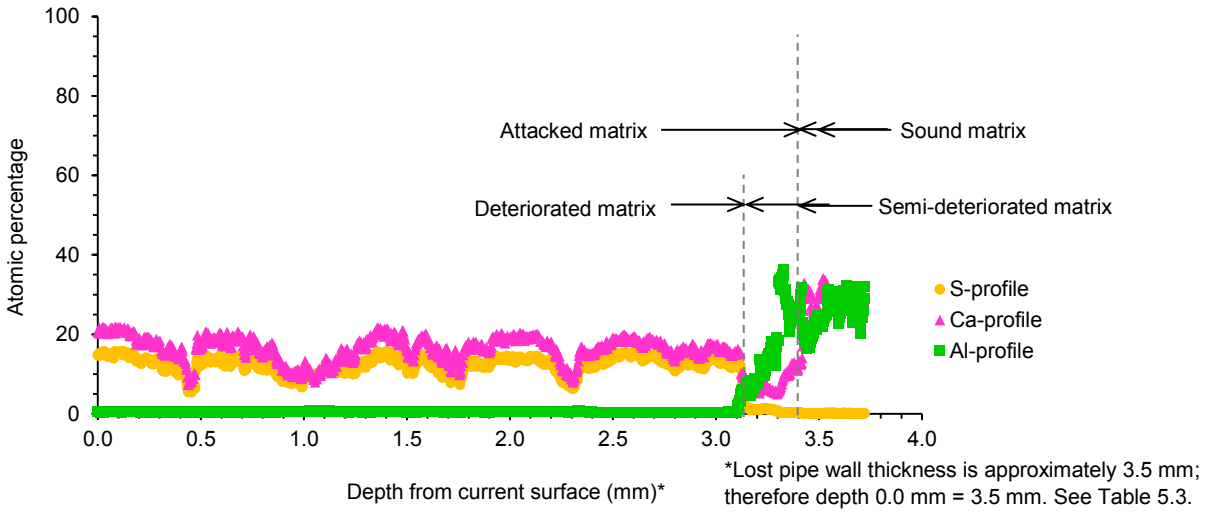

(g) S-Ca-Al concentration vs. depth profiles, up to approximately 0.3 mm into the sound matrix (23% CAC + SIL)

Figure 5-33 (a) to (g): Elemental mapping/concentration profiles for concrete mixture with 23% CAC + SIL.

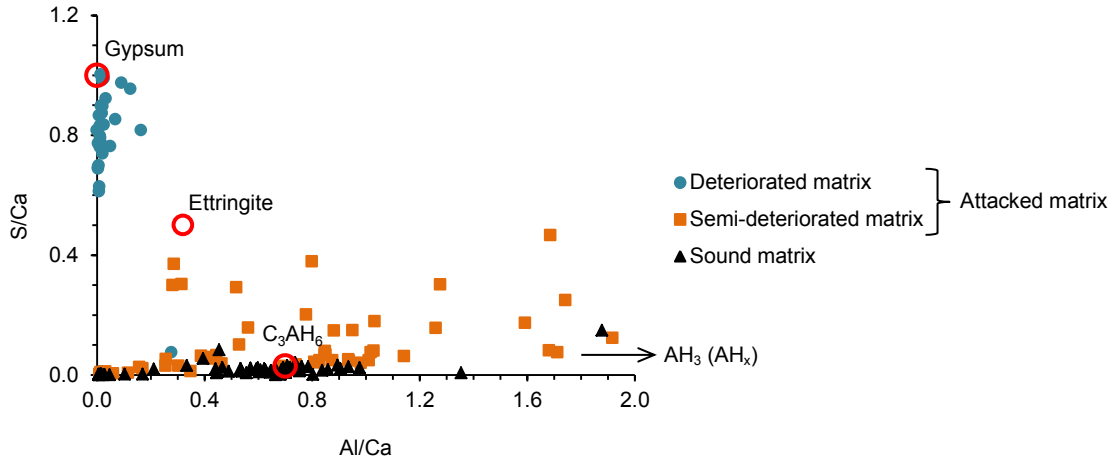

Figure 5-34: EDS point analysis for concrete mixture with 23% CAC + SIL, exposed to biogenic H_2SO_4 for 127 months.

5.5.1.5 Elemental mapping of concrete mixture with 11% CAC + 4.5% FA + 1.5% SF and dolomite coarse aggregate

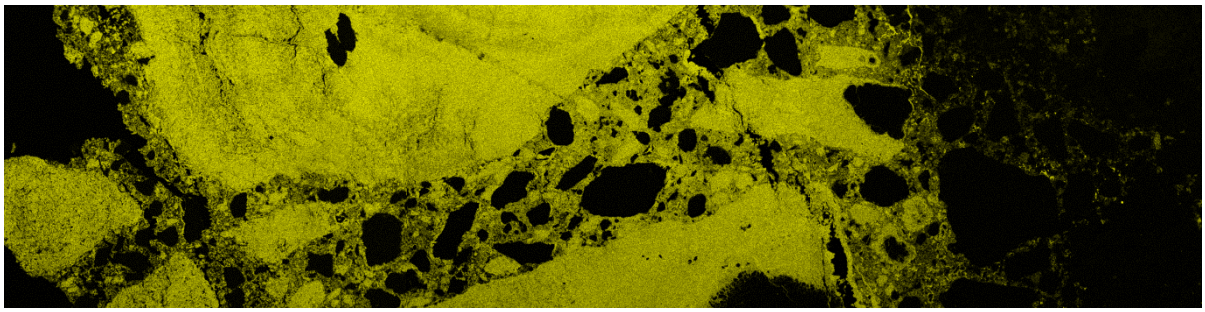

(a) Sulphur mapping (11% CAC + 4.5% FA + 1.5% SF)

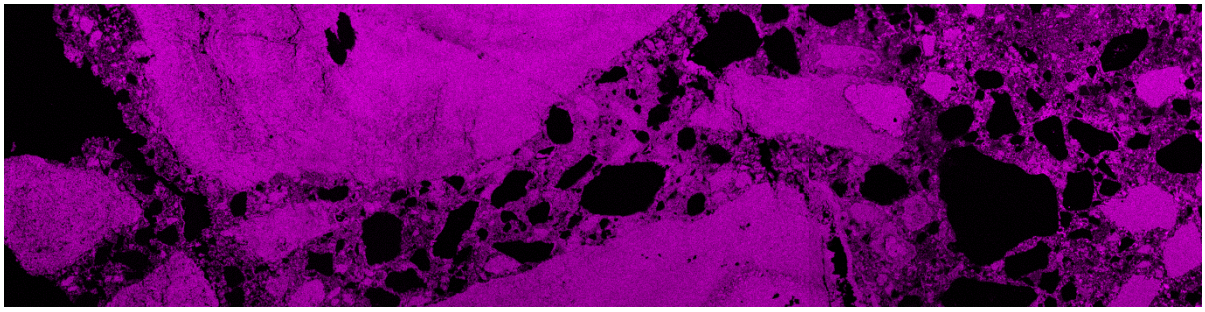

(b) Calcium mapping (11% CAC + 4.5% FA + 1.5% SF)

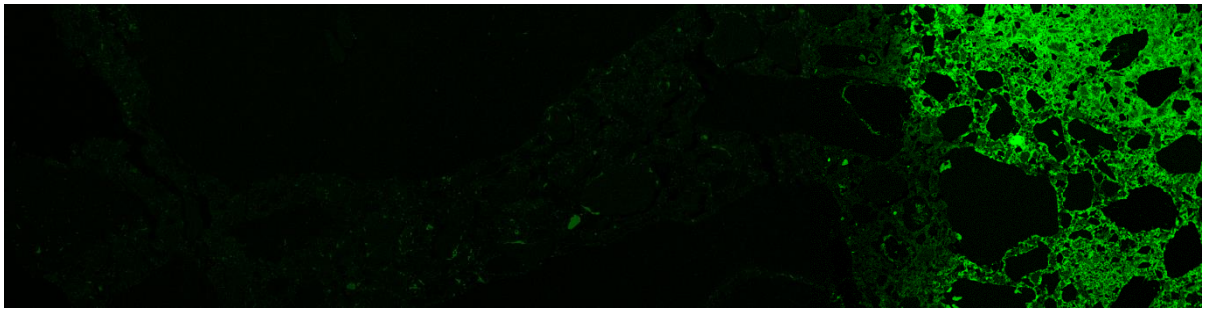

(c) Aluminium mapping (11% CAC + 4.5% FA + 1.5% SF)

(d) Magnesium mapping (11% CAC + 4.5% FA + 1.5% SF)

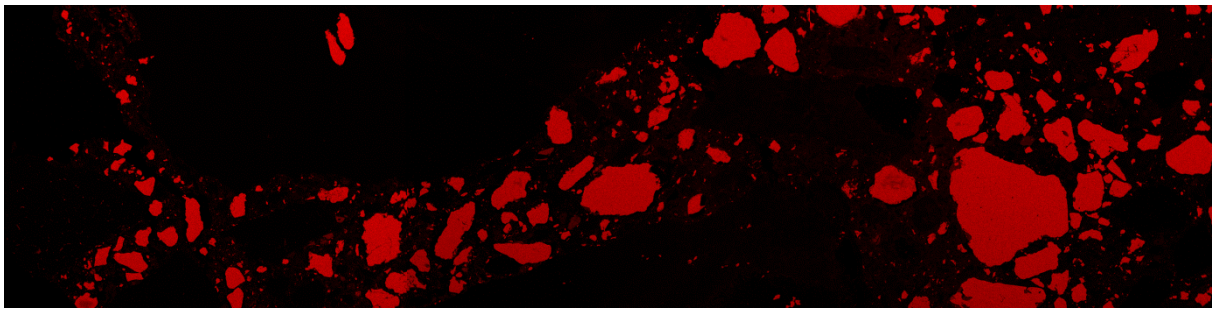

(e) Silica mapping (11% CAC + 4.5% FA + 1.5% SF)

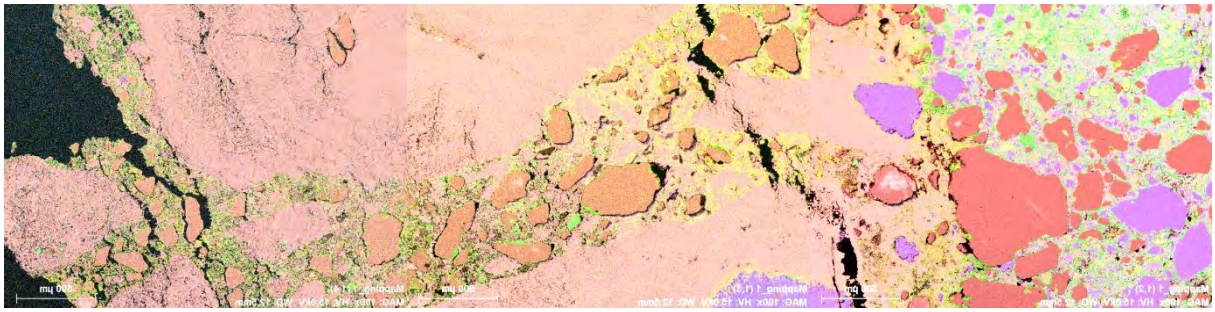

(f) Combined-element (S-Ca-Al-Mg-Si) mapping (11% CAC + 4.5% FA + 1.5% SF)

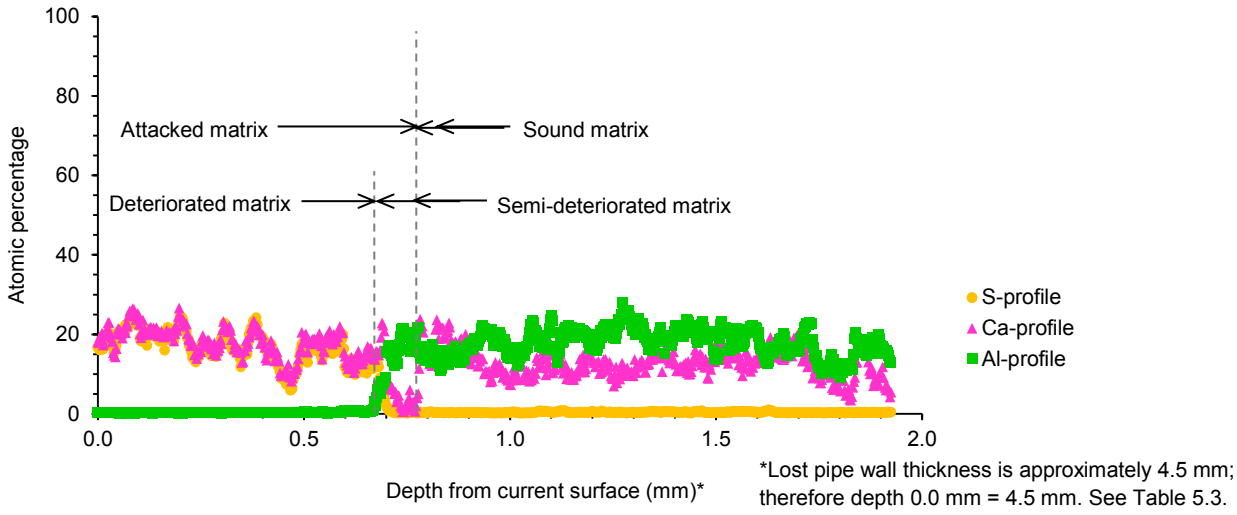

(g) S-Ca-Al concentration vs. depth profiles, up to approximately 1 mm into the sound matrix (11% CAC + 4.5% FA + 1.5% SF)
Figure 5-35 (a) to (g): Elemental mapping/concentration profiles for concrete mixture with 11% CAC + 4.5% FA + 1.5% SF.

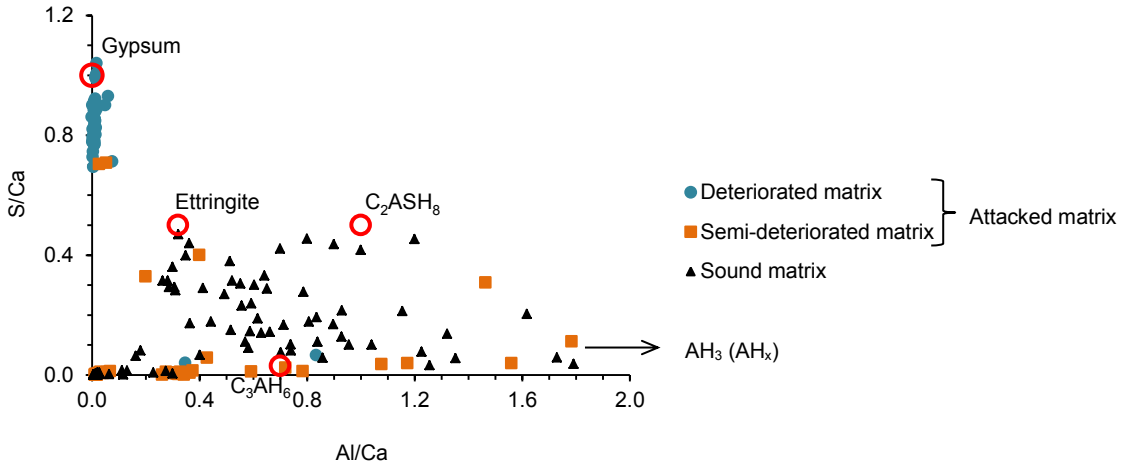

Figure 5-36: EDS point analysis for concrete mixture with 11% CAC + 4.5% FA + 1.5% SF, exposed to biogenic H_2SO_4 for 127 months.

5.5.1.6 Elemental mapping of concrete mixture with 20% CAC and aluminate (Alag™) coarse aggregate

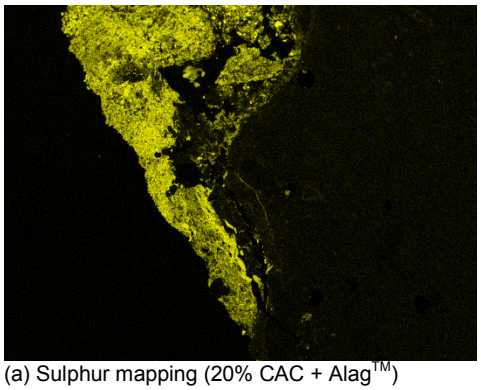

(a) Sulphur mapping (20% CAC + Alag™)

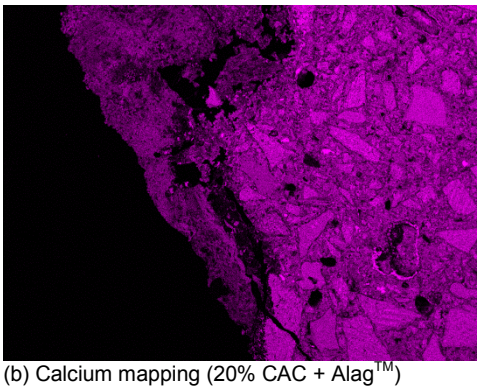

(b) Calcium mapping (20% CAC + Alag™)

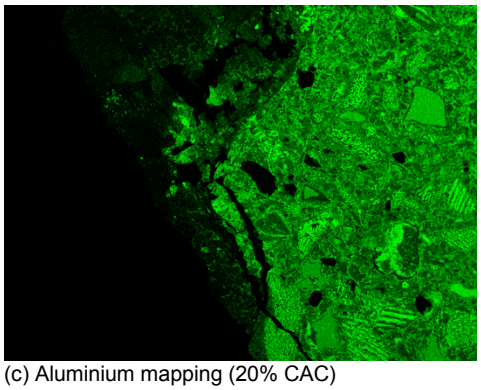

(c) Aluminium mapping (20% CAC)

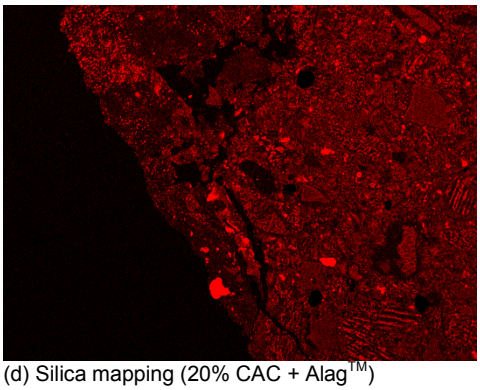

(d) Silica mapping (20% CAC + Alag™)

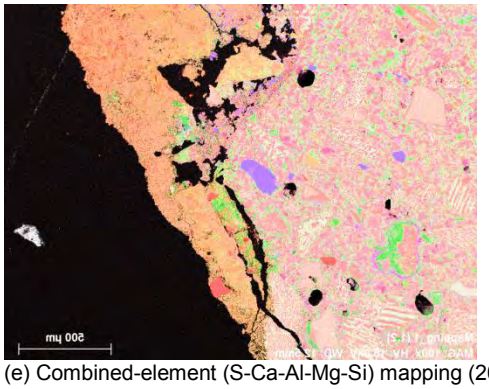

(e) Combined-element (S-Ca-Al-Mg-Si) mapping (20% CAC + Alag™)

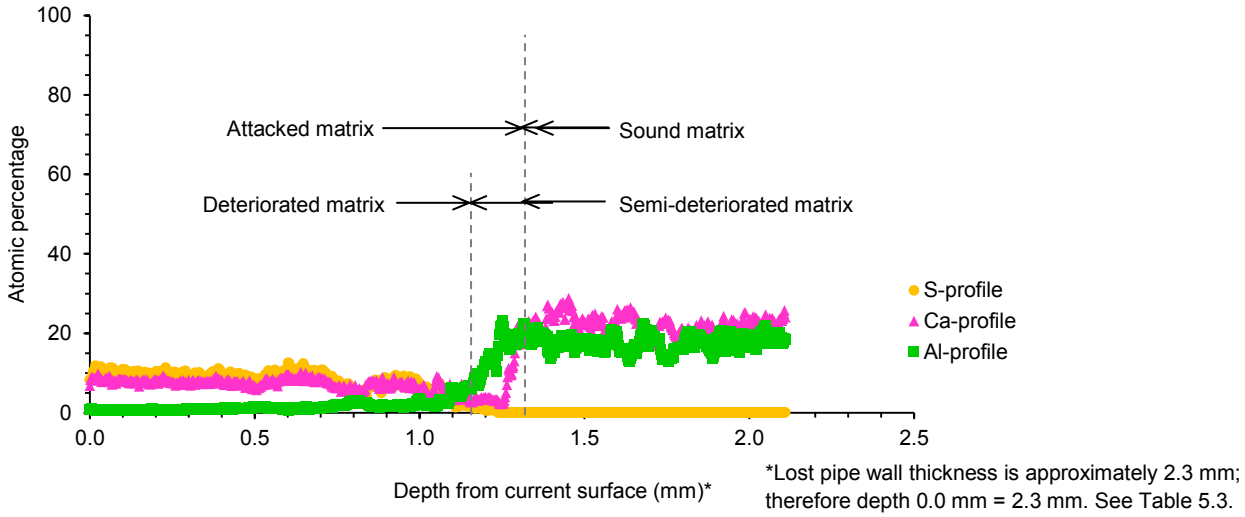

(g) S-Ca-Al concentration vs. depth profiles, up to approximately 0.8 mm into the sound matrix (20% CAC + Alag^{TM})
Figure 5-37 (a) to (g): Elemental mapping/concentration profiles for concrete mixture with 20% CAC + Alag^{TM}.

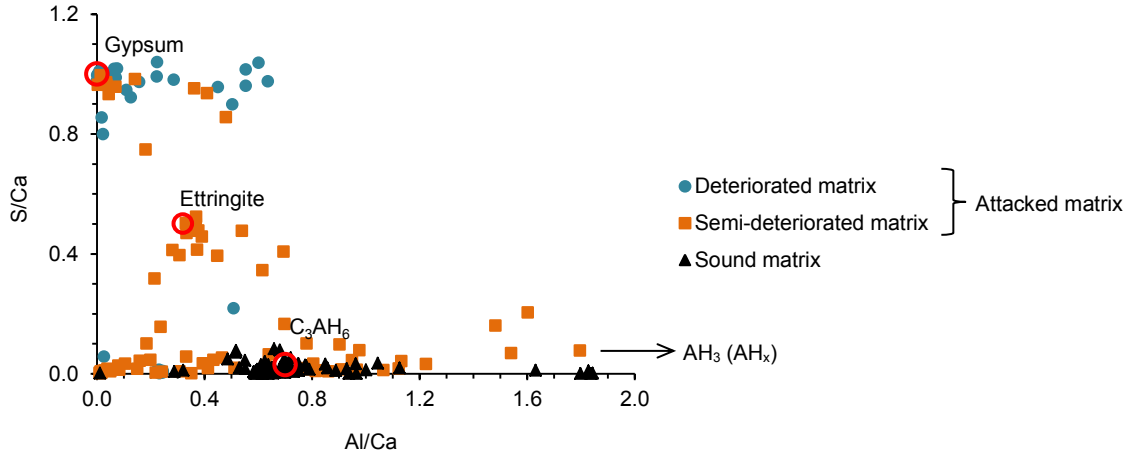

Figure 5-38: EDS point analysis for concrete mixture with 20% CAC + Alag^{TM}, exposed to biogenic H_2SO_4 for 127 months.

The following can be noted from the results presented in Figure 5-27 to Figure 5-38:

(i) The concentration (atomic percentage) of the sulphur (S) species within the attacked (deteriorated and semi-deteriorated) matrices of concrete mixtures with 16% CAC, 18% CAC, 23% CAC, and 11% CAC + 4.5% FA + 1.5% SF (all with DOL) is in the order of 18% whereas the concentration within concrete mixtures with 23% CAC/SIL and 20% CAC/Alag^{TM} is in the order of 15% and 12% respectively. This concentration is attributed to the deposition of elemental sulphur through abiotic transformations (Wilmot et al., 1988; EPA, 1991; Kotronarou and Hoffmann, 1991; Herisson et al., 2014). However, the progression of the micro-cracks in the concrete matrices is due to biogenic sulphuric acid attack mechanisms which will be discussed in detail in Section 5.7. Similar to PC-based mixtures, the concentration of sulphur species in the sound matrices of CAC-based concrete mixtures is less than 0.3%.

(ii) The concentration (atomic percentage) of the calcium species varies across the attacked (deteriorated and semi-deteriorated) and sound matrices of CAC-based concrete mixtures. Within the sound and semi-deteriorated matrices of plain CAC mixtures, the concentrations are in the order of 25% and 5% respectively. Within the deteriorated matrices, the concentrations are in the order of 18%, 12%, 20%, 18%, 18%, and 7% for CAC/DOL 16, CAC/DOL 18, CAC/DOL 23, CAC/SIL 23, CAC/DOL 17 + FA +SF, and CAC/Alag^{TM} 20 respectively.

(iii) The concentration (atomic percentage) of the aluminium species varies across the attacked (deteriorated and semi-deteriorated) and sound matrices of all the CAC-based concrete mixtures. Within the sound matrices of CAC/DOL 16, CAC/DOL 18, CAC/DOL 23, CAC/SIL 23, CAC/DOL 17 + FA +SF, and CAC/Alag^{TM} 20, the concentration of aluminium is in the order of 16%, 16%, 21%, 26%, 18%, and 14% respectively. Within the semi-deteriorated matrices of CAC/DOL 16, CAC/DOL 18, CAC/DOL 23, CAC/SIL 23, CAC/DOL 17 + FA +SF, and CAC/Alag^{TM} 20, the concentration of aluminium is in the order of 24%, 23%, 28%, 35%, 21%, and 21% respectively. Within all the deteriorated matrices, the concentration of aluminium is less than 6%.

(iv) The Al/Ca ratios of the sound matrices in all the CAC-based mixtures are approximately 0.7.

(v) The acid-soluble (dolomite) aggregates in CAC-based mixtures that have been subjected to biogenic sulphuric acid attack are also characterised by micro-cracks (although to a lesser extent in comparison to PC-based mixtures), indicating typical acid-aggregate dissolution characteristics.

(vi) From the EDS point analyses, the deteriorated matrix is characterised as predominantly gypsum, the semi-deteriorated matrix is characterised as ettringite (AFt), while the sound matrix is principally C_3AH_6 (and AH_3 (or AH_x gel)).

Since the sound concrete matrices subjected to biogenic corrosion process undergo external-based attack, both the deteriorated and semi-deteriorated matrices (products of corrosion) play a significant role in the attack mechanisms, for example, by providing a protective barrier to the attacking acid. In this regard, in order to further understand the underlying mechanisms of attack, the products of corrosion were characterised in detail using quantitative XRD (QXRD) and TGA techniques. Results from these techniques are presented in sub-sections 5.5.2 (QXRD) and 5.5.3 (TGA).

5.5.2 Quantitative XRD

The mineralogical characterisation by XRD (Figure 5-39) shows that the deteriorated and semi-deteriorated matrices (products of corrosion) consist predominantly of gypsum, and also silica, calcite, C_3AH_6, AH_3, and dolomite.

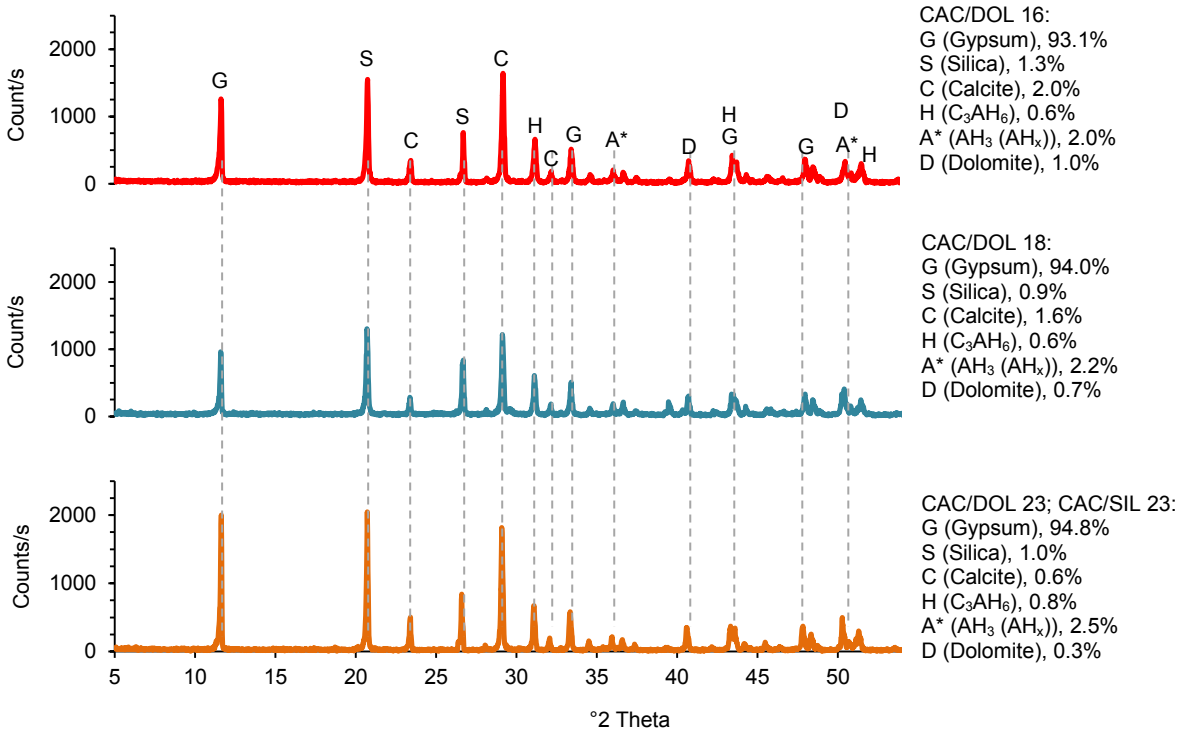

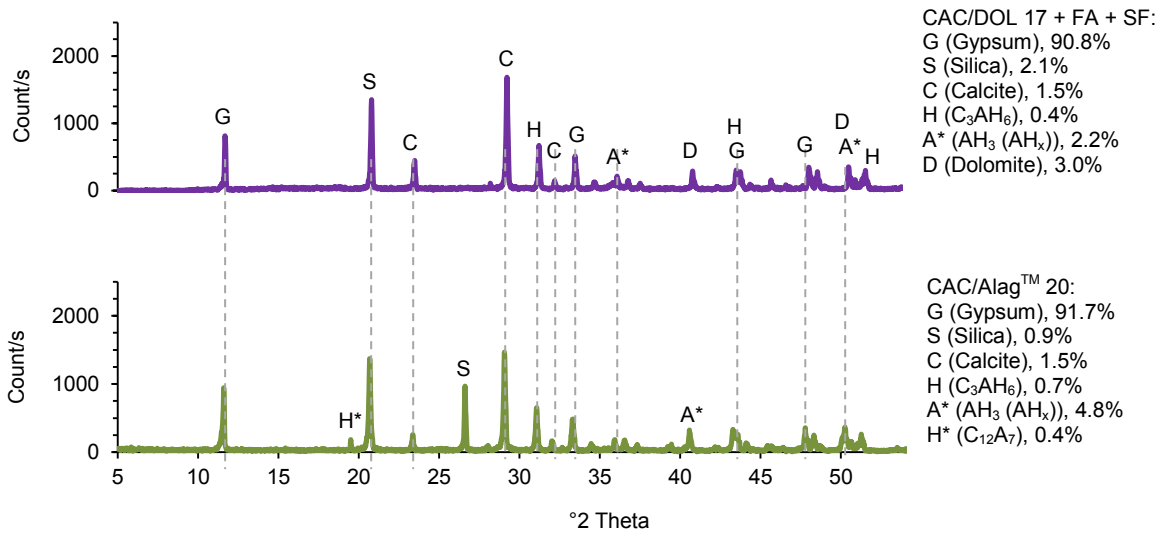

Figure 5-39: QXRD for 'products of corrosion' sampled from CAC-based concrete subjected to biogenic H_2SO_4 for 127 months in the VES.

QXRD results presented above show a slight increase in the amount of gypsum in the products of corrosion as the cement content in plain CAC mixtures increased from 16% (gypsum content approximately 93.1%) to 23% (gypsum content approximately 94.8%). For the blended CAC mixture with 17% total binder (11% CAC, 4.5% FA and 1.5% SF), the amount of gypsum in the products of corrosion was approximately 90.8%, whereas that in the CAC/Alag™ mixture (with 20% CAC) was approximately 91.7%. Also, apart from the increase in the alumina-based phases (C_3AH_6 and AH_3 (or AH_x)) in the products of corrosion with increase in CAC content, the other phases (silica, calcite, and dolomite) within the products of corrosion do not show a clear correlation with binder content in the respective concrete mixtures. More discussion will be given in Section 5.7.

5.5.3 TGA

TGA results on the products of corrosion taken from PC-based concrete mixtures are presented in Figure 5-40 to Figure 5-45.

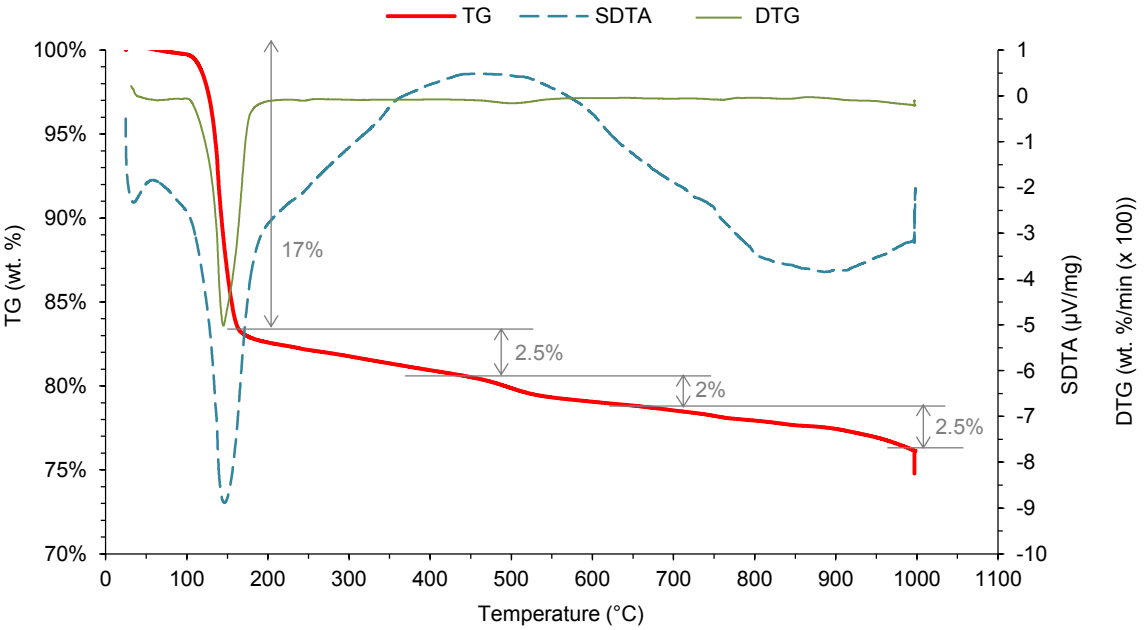

Figure 5-40: TG/SDTA/DTG curves for 'products of corrosion' taken from a concrete sample with 16% CAC.

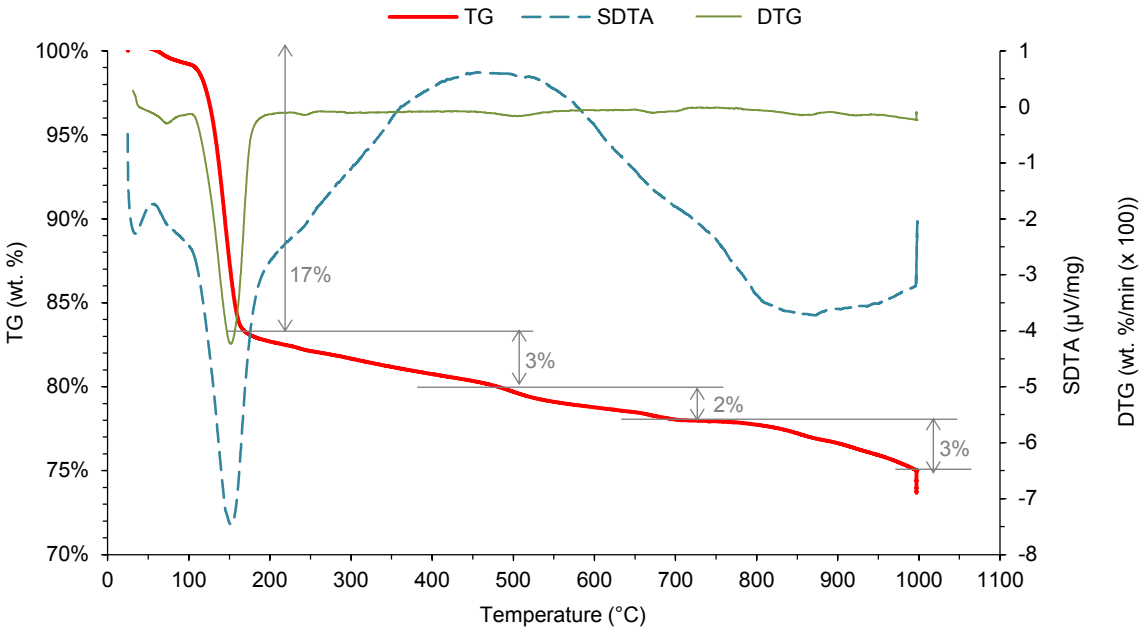

Figure 5-41: TG/SDTA/DTG curves for 'products of corrosion' taken from a concrete sample with 18% CAC.

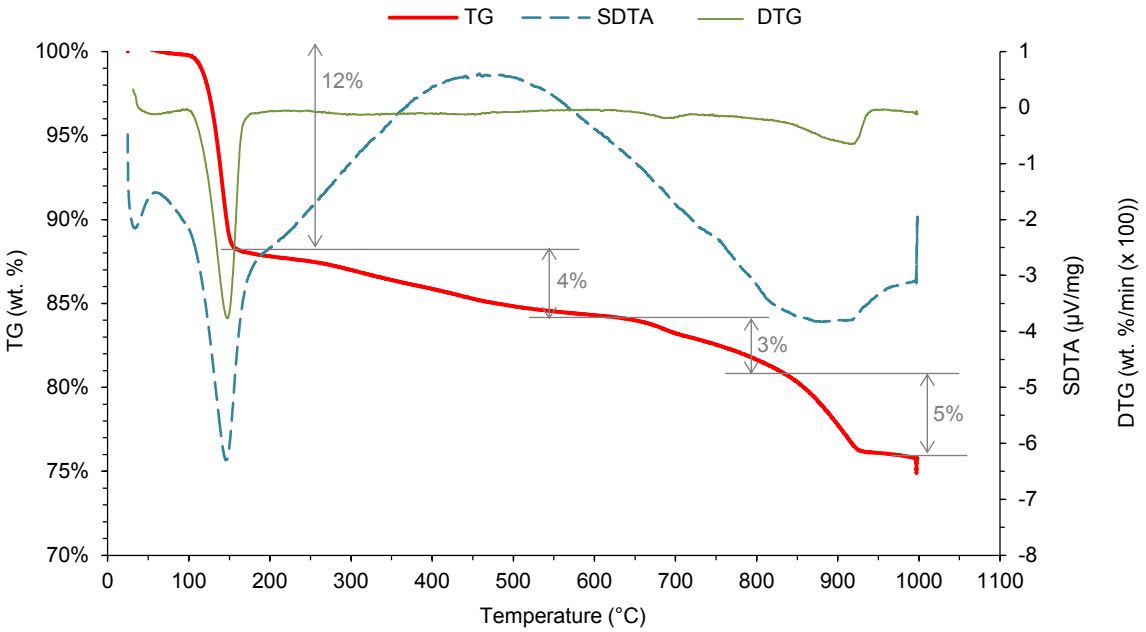

Figure 5-42: TG/SDTA/DTG curves for 'products of corrosion' taken from a concrete sample with 23% CAC + DOL.

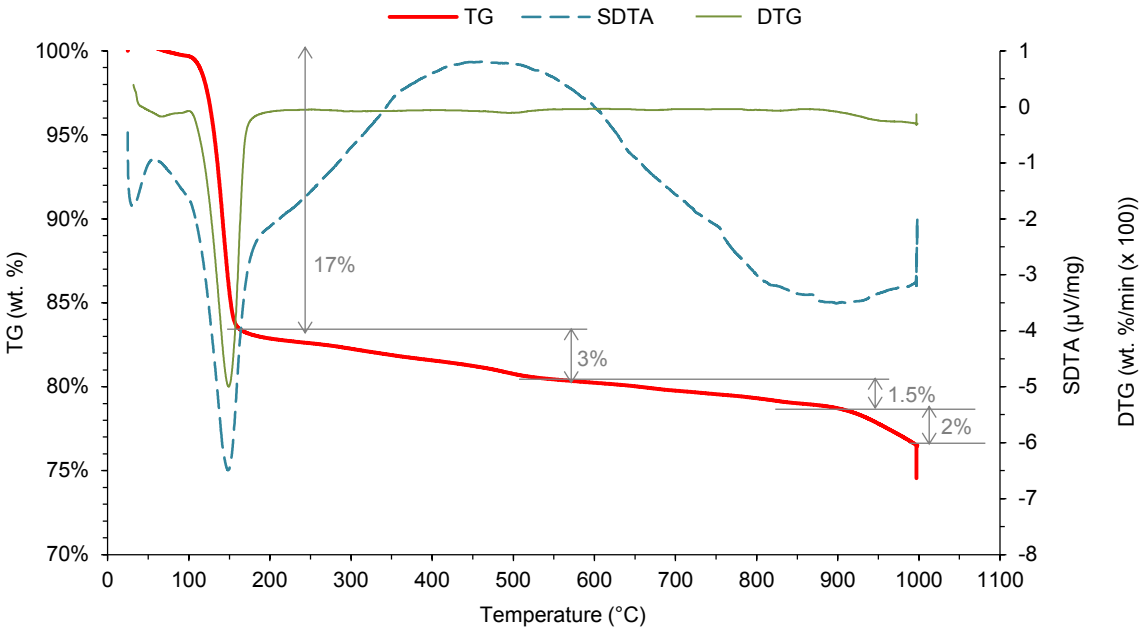

Figure 5-43: TG/SDTA/DTG curves for 'products of corrosion' taken from a concrete sample with 23% CAC + SIL.

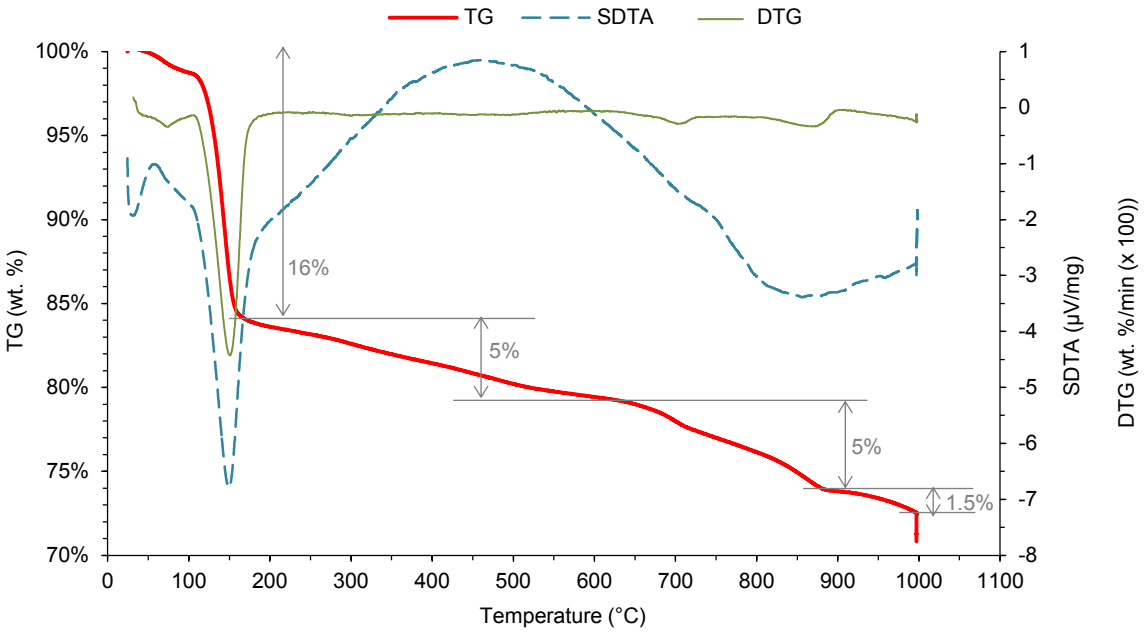

Figure 5-44: TG/SDTA/DTG curves for 'products of corrosion' taken from a concrete sample with 11% CAC + 4.5% FA + 1.5% SF.

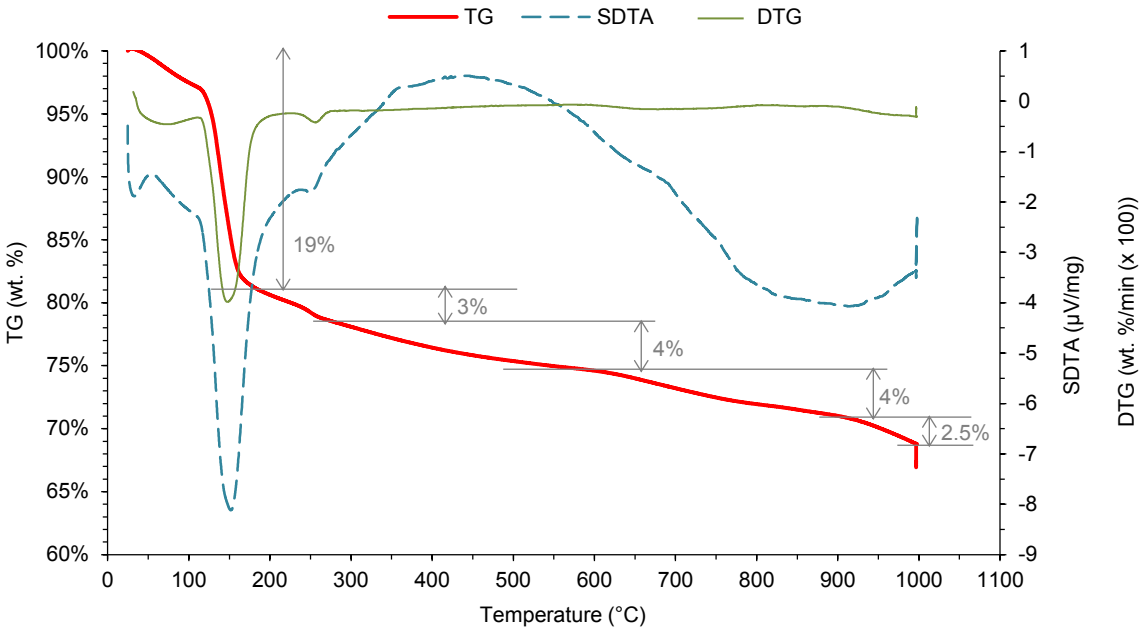

Figure 5-45: TG/SDTA/DTG curves for 'products of corrosion' taken from a concrete sample with 20% CAC + Alag^{TM}.

Similar to results from PC-based mixtures, all the TGA graphs from CAC-based mixtures presented above are typical for dehydration of gypsum, indicating a total weight loss of approximately 23.5% to 32.5%. The first two peaks, at a temperature peak of approximately 50 °C and 154 °C in all these mixtures are a typical representation of the 2-stage weight decrease of between 12% in CAC/DOL 23 mixtures and 19% in CAC/Alag^{TM} 20 mixtures.

In all CAC-based mixtures except that with Alag^{TM}, the third broad peak at approximately 450 °C represents decomposition of AH_3 (weight loss of approximately 2.5% to 5%). At a temperature of approximately 675 °C, there is a weight loss of approximately 1.5% to 5% corresponding to the decomposition of silica (and also traces (<0.2%) of C_3AH_6). Beyond a temperature of approximately 675 °C, there is a weight loss of approximately 1.5% (in blended CAC) to 5% (in CAC/DOL 23) corresponding to the decomposition of carbonates (in calcite and dolomite).

For the CAC/Alag^{TM} mixtures, a third peak appears at approximately 250 °C representing loss of water due to the decomposition of AFm phases (weight loss approximately 3%). A fourth broad peak at approximately 450 °C represents decomposition of AH_3 (or AH_x) (weight loss of approximately 4%). At a temperature of approximately 675 °C, there is a weight loss of approximately 4% corresponding to the decomposition of silica (and also traces (<0.2%) of C_3AH_6). Beyond a temperature of approximately 675 °C, there is a weight loss of approximately 2.5% corresponding to the decomposition of carbonates (in calcite).

5.6 Potential influence of Fe_2O_3 in biogenic corrosion mechanisms

Before proceeding, it is also important to mention that since CAC contains a higher amount of ferric oxide (Fe_2O_3 (F)) than PC, it is highly probable that F also plays an active role during biogenic corrosion mechanisms based on lower corrosion rates exhibited by CAC-based mixtures. However, until recently there has been limited research on Fe-containing hydrates in concrete due to the low (2% to 5%) amount of F in PC, which is the most widely studied binder (Dilnesa, 2011; Dilnesa et al., 2014). Moreover, characterisation of Fe-containing minerals in hydrated binders using standard techniques such as XRD and TGA is difficult due to the overlap of the signals from Fe-containing phases with those of the respective Al analogs (Renaudin et al., 2015). Nonetheless, even though characterisation of the Fe phase in the HCP using both XRD and TGA is outside the scope of the current study, it is hypothesised that this phase probably plays a significant role during biogenic corrosion mechanisms, through the production of reactive oxygen species (ROS) in bacteria, which

results in oxidative stress to SOB (Soenen et al., 2012; Chatterjee et al., 2011; Trun and Gottesman, 1990). Therefore a comparative EDS point analysis of Fe/Ca vs. Al/Ca in the sound matrices of both PC- and CAC-based concrete mixtures is given in Figure 5-46.

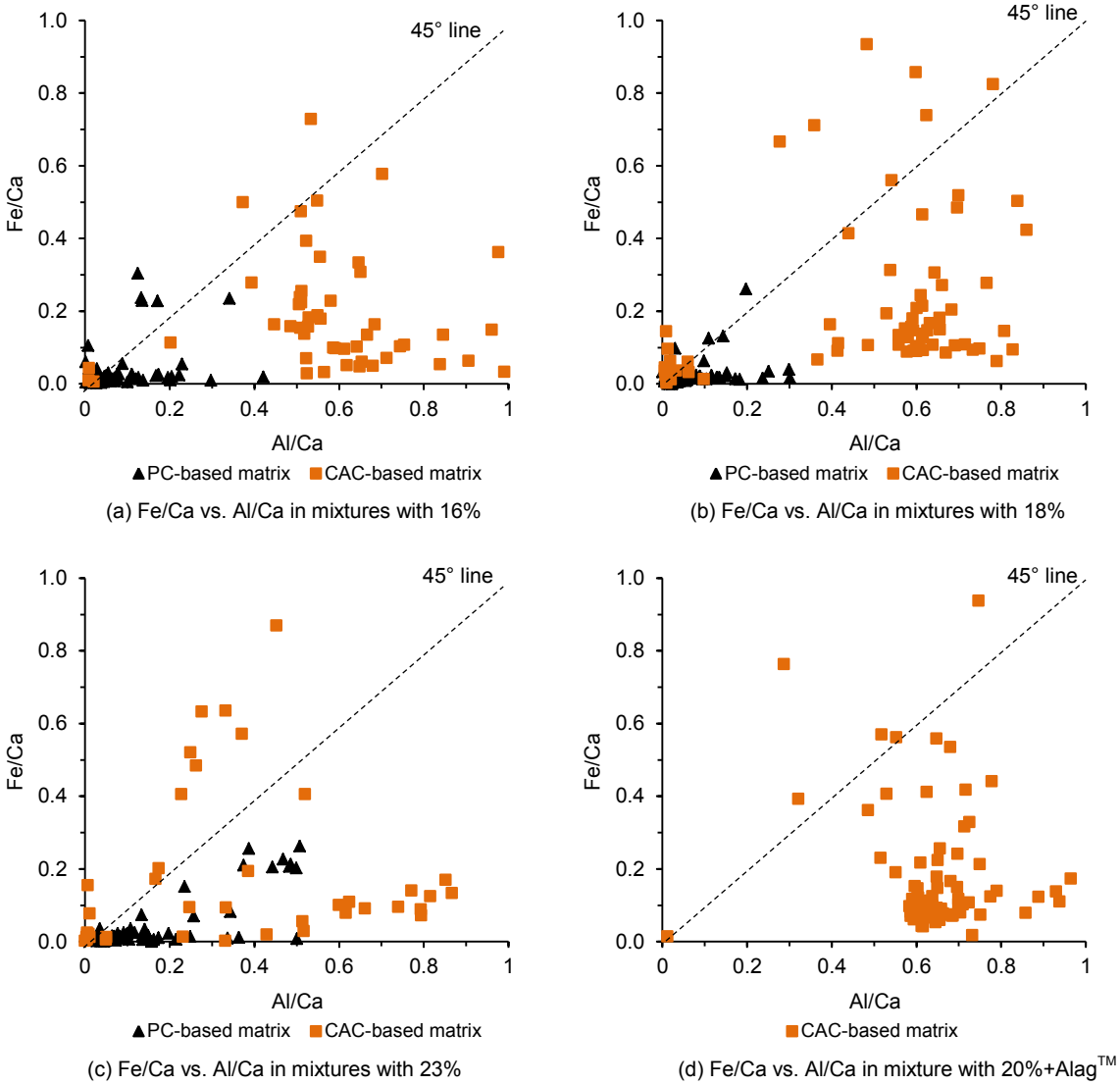

(a) Fe/Ca vs. Al/Ca in mixtures with 16%

(b) Fe/Ca vs. Al/Ca in mixtures with 18%

(c) Fe/Ca vs. Al/Ca in mixtures with 23%

(d) Fe/Ca vs. Al/Ca in mixture with 20%+Alag™

Figure 5-46 (a) to (d): Comparative EDS point analysis of Fe/Ca vs. Al/Ca for sound matrices in concrete mixtures used in the manufacture of sewer pipes

Results presented in Figure 5-46 show a higher concentration of Fe and Al in the sound matrices of CAC-based concrete mixtures than in PC-based concrete mixtures. Moreover, all the mixtures show higher amounts of Al than Fe. This is expected due to the chemical composition of the respective binders.

5.7 Discussion – a comparison of microstructural characteristics of PC- and CAC-based concrete mixtures subjected to biogenic H_2SO_4

From the S-Ca-Al concentration vs. depth profiles presented in sub-sections 5.4.1 and 5.5.1, two distinct characteristics are noted; (i) that within the semi-deteriorated matrices of both PC- and CAC-based concrete mixtures, the concentration of calcium species is lower than that in both the deteriorated and sound matrices of the respective mixtures, and (ii) that within the semi-deteriorated matrices of CAC-based concrete mixtures, the concentration of the alumina species is higher than that of the sound matrix. It is hypothesised that during the destruction of the HCP (decomposition of CH and decalcification of C-S-H in PC-based mixtures, and decomposition of CAH_{10}, C_2AH_8, C_3AH_6

and decalcification of C-A-H in CAC-based mixtures) by the attacking H_2SO_4, dissolution and leaching of Ca^{2+} ions from the sound matrix occurs leaving behind a calcium-deficient layer. These results are in line with the hypotheses that in a $CaO–SiO_2–Al_2O_3$ system, Ca^{2+} ions have a higher mobility than the other ions such as the Al^{3+} (De Keyser, 1955; Weisweiler et al., 1986; Kurdowski, 2014).

Furthermore, it has been shown that the products of concrete corrosion (deteriorated matrix) when both PC- and CAC-based mixtures are subjected to biogenic H_2SO_4 attack are predominantly gypsum, although slightly less gypsum is formed in CAC-based concrete mixtures than in PC-based concrete mixtures (see BSE micrographs of the products of corrosion in Appendix L). From QXRD results presented, this difference varies between 0.7% (in mixtures with 16% cement content and acid-soluble coarse aggregate) and 2.8% (in mixtures with 23% cement content and either acid-soluble or acid-insoluble coarse aggregate). Gypsum is formed through processes that firstly involve the simultaneous destruction of the polymeric nature of calcium species (CH and C-S-H in PC-based mixtures; CH in CAC-based mixtures) and substituting a larger molecule (calcium sulphate ($C\bar{S}$)) (Equation 5.4) into the matrix. Secondly, $C\bar{S}$ precipitates as gypsum ($C\bar{S}H_2$).

$$CH + H_2SO_4 \rightarrow C\bar{S} + 2H \tag{5.4}$$

The higher amount of calcium species in PC-based mixtures than in CAC-based mixtures explains the higher amount of gypsum within the products of corrosion (deteriorated matrix) of PC-based substrates than in CAC-based substrates.

From the literature reviewed (see Section 2.10) and EDS point analyses presented in sub-sections 5.4.1 and 5.5.1, the alumina-rich layer within the semi-deteriorated matrices of CAC-based mixtures is AH_3 (or AH_x gel). When AH_3 is subjected to H_2SO_4 attack, it decomposes to form other *alum compounds* (aluminium sulphate) ($Al_2(SO_4)_3$) (Equation 5.5).

$$2AH_3 + 3H_2SO_4 \rightarrow Al_2(SO_4)_3 + 12H \tag{5.5}$$

Aluminium sulphate *(alum)* has a relatively high surface tension, γ (871 mN/m) than other substances found in the products of corrosion, such as calcium, sulphur and water, which have surface tension values of approximately 360 mN/m, 62 mN/m and 73 mN/m respectively at 20 °C (Ornek et al., 1998). Therefore, due to the decomposition of AH_3, the resultant *alum* creates some internal pressure and binds the other products of corrosion (predominantly gypsum) together. This hypothesis explains the greater depths of the products of corrosion on the surfaces of CAC-based substrates than on the PC-based substrates. Moreover, from the silica mapping, CAC-based mixtures show a higher amount of the acid-insoluble aggregates in the attacked matrices than PC-based mixtures. This implies that, generally there is less aggregate fallout in CAC-based mixtures due to the binding mechanisms that involve *alum*, thereby limiting the exposure of 'fresh' surfaces to aggressive acid conditions.

In addition to the characteristics discussed above, the results presented show that the use of the aluminate aggregate enhances the performance of CAC-based mixtures subjected to biogenic H_2SO_4 attack. The BSE micrograph and elemental mapping for CAC/Alag^{TM} mixture show a more homogenous microstructure with an inferred absence of the ITZ in comparison to all the other mixtures (both PC- and CAC-based).

Similarly, both PC- and CAC-based concrete mixtures with SCMs showed improved performance with regard to corrosion rates. For example, (i) mixtures with 13.5% PC + 4.5% FA experienced lower corrosion rates (by approximately 0.07 mm/yr. or 6%) than plain mixtures with 16% PC, (ii) mixtures with 16.5% PC + 1.5% SF and 12% PC + 6% GGBS experienced lower corrosion rates than plain mixtures with 18% PC (by approximately 0.16 mm/yr. (13%) and 0.04 mm/yr. (3%) respectively), and (iii) mixtures with 11% CAC + 4.5% FA + 1.5% SF experienced lower corrosion rates than plain mixtures with 16% CAC (by approximately 0.13 mm/yr. or 25%) and 18% CAC (by approximately 0.09

mm/yr. or 19%). This improved performance can be attributed to the improved microstructure of blended mixtures and also the chemical influence of alumina in mixtures with FA.

5.8 Biogenic acid attack mechanisms of concrete sewer pipes – chemical and physical factors

From the results and discussions presented in Sections 5.3 to 5.7, it can be seen that the biogenic acid attack mechanisms of concrete in sewers is a complex process which involves both physical and chemical factors. The attack mechanism is predominantly composed of chemical reactions that are linked to physical transformations, which may accelerate the rate of deterioration by promoting the transport of respective aggressive species into the sound matrix.

The attack mechanism of concrete subjected to biogenic H_2SO_4 can be explained by a hypothesis based on the theory of crystallisation pressure (Taber, 1916; Paulini, 1994; Bizzozero et al., 2014). According to Bizzozero et al. (2014), deterioration of porous materials such as concrete can be caused by the precipitation of crystals from the liquid that is present in the matrices' pores, when supersaturation levels are reached. Supersaturation depends on the concentration of the solution, the temperature and on the size of the pores (porosity). According to their analysis of the pore solution, Bizzozero et al. (2014) reported that with an increase in gypsum content in either a PC- or CAC-based system, there is an increase in the supersaturation of ettringite (AFt), which in turn, is proportional to the resultant crystallisation pressure subject to the respective gypsum thresholds (40 mol% for CAC and 56 mol% for PC).

Below the critical gypsum threshold, AFt can only exert pressure in a small number of isolated pores, whereas above the critical gypsum threshold, AFt can form is a bigger fraction of pores. Therefore above the critical gypsum threshold, there is a higher total volume of AFt generating pressure and subsequent onset of unstable expansion. In high expansion systems, this pressure exceeds the elastic limit of the system resulting in cracking and failure.

In general, PC consists of higher calcium content in comparison to CAC, and its Ca/Al ratio is favourable for the formation of CH. Therefore, PC-based systems have more Ca^{2+} ions potentially available to form AFt. Subsequently, the supersaturation of AFt is higher resulting in higher crystallisation pressures within the pores. On the other hand, the Ca/Al ratio in CAC-based systems is favourable for the formation of the stable and amorphous AH_3 (or AH_x) meaning that since most of the alumina is used in the formation of this stable phase, it is no longer available to form AFt, and the supersaturation of ettringite is reduced. This explains the extent of the micro-cracks in PC- and CAC-based BSE micrographs presented in Sections 5.4 and 5.5 respectively, whereas the hypothesis presented in Section 5.7 on the formation of *alum* explains the greater depths of the products of corrosion on the surfaces of CAC-based substrates than on PC-based substrates.

The onset of biogenic H_2SO_4 mechanisms in concrete sewers involves the establishment of microbes that are responsible for generation of the attacking acid. In order to understand the initial stages of these mechanisms, and the microbial ecosystem in the current study, both surface pH vs. time profiling of freshly-cast concrete samples and microbial speciation of the products of corrosion taken from concrete substrates approximately 120 months after installation in the sewer were undertaken. Results are given in the following Section 5.9 (surface pH vs. time profiles) and Section 5.10 (microbial speciation).

5.9 Early-age colonisation and late-age microbial characteristics – surface pH vs. time of concrete mixtures exposed in different sewer environments

This section presents results that characterise 'early-age' and 'late-age' concrete surface colonisation by acid generating bacteria based on changes in surface pH. The results presented herein are also used to highlight the influence of varying exposure conditions on biogenic corrosion mechanisms.

As highlighted in Chapter Four, the current study utilised two sites for a comparative surface pH vs. time profile study, namely the VES (downstream of the inlet manhole (IM)) and a manhole at Langa in Cape Town. A summary of certain parameters which include (i) sewer temperature, H_2S and RH, and (ii) sewage temperature and pH, which influence biogenic corrosion mechanisms in sewers is given in Table 5-4 (measured at the VES and Cape Town (Langa)).

Table 5-4: Summary of temperature, H_2S, RH, and pH characteristics at VES and Langa

Parameter *		Site		
		VES		Cape Town
Daily ambient temp (°C)	Max (in summer)	34		26
	Min (in winter)	0		8
		Inlet Manhole (IM)	Downstream of IM	Manhole at Langa
Sewage temp (°C)		-	21	20
Sewage pH		-	6.98	7.08
Temp of sewer headspace during H_2S profiling (°C)	Summer	32	25	26
	Autumn/Spring	27	22	22
	Winter	19	16	18
H_2S concentration in sewer headspace (ppm)	Summer	51	35	34
	Autumn/Spring	21	13	18
	Winter	9	6	7
RH in sewer headspace (%)	Summer	61	74	75
	Autumn/Spring	68	76	76
	Winter	69	77	80

*Arithmetic mean

Table 5-4 shows higher temperature recordings in the IM than in the downstream experimental section at VES and the manhole at Langa. The H_2S concentration range in the IM, the downstream (of IM) experimental section and the manhole at Langa is 42 ppm, 29 ppm and 27 ppm respectively. Characteristics of the temperature and H_2S concentration in the downstream experimental section at VES and in the manhole at Langa are within ± 2 units in summer and winter. However, even though the recorded sewer temperatures were similar in autumn/spring, higher H_2S concentration (+5 ppm) was recorded in Langa. Moreover, from Figure 5-47 and Figure 5-48 it can be seen that there is a distinct difference in the H_2S profiles of these sites. VES is characterised by 'small peaks' and a general ascent (increase in H_2S concentration) from morning to evening hours while Langa is characterised by cyclic peaks that tend to peak around midday.

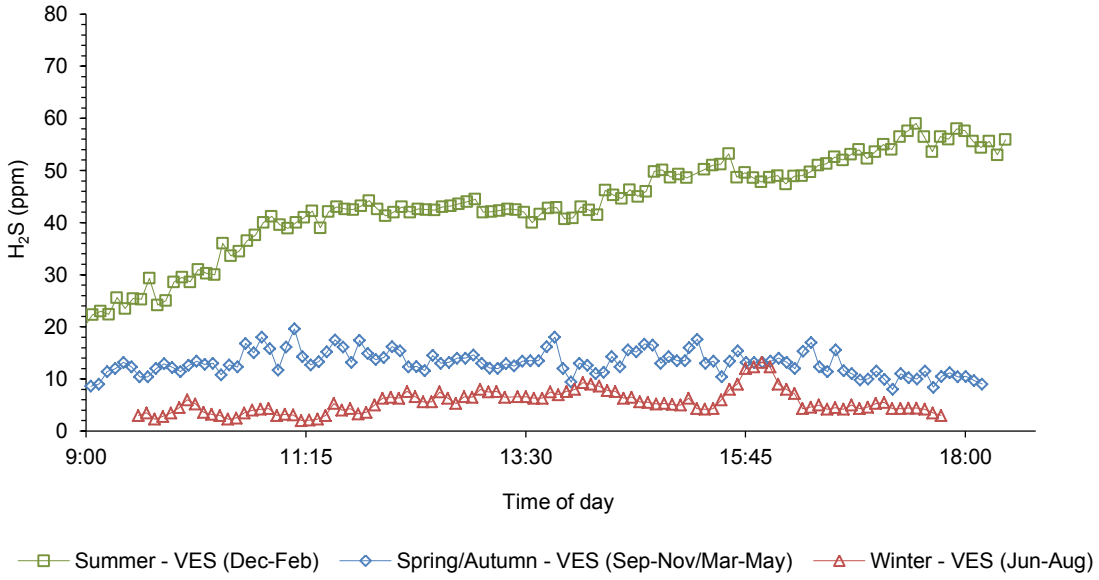

Figure 5-47: Typical daily H_2S profiles in the VES during summer, spring/autumn and winter months (data from current study (2013-2015)).

The durability indices (OPI and WSI) of the concrete mixtures used for surface pH vs. time profiling are given in Table 5-5. Other properties, which include the initial surface pH of the samples at the age of 28 d are given in Appendix I. The surface pH vs. time profiles for these mixtures per site are given in Figure 5-49 (VES) and Figure 5-50 (Langa). Figure 5-51 shows comparative profiles for each mixture in the VES and Langa. Details results are also given in Appendix L (L.5).

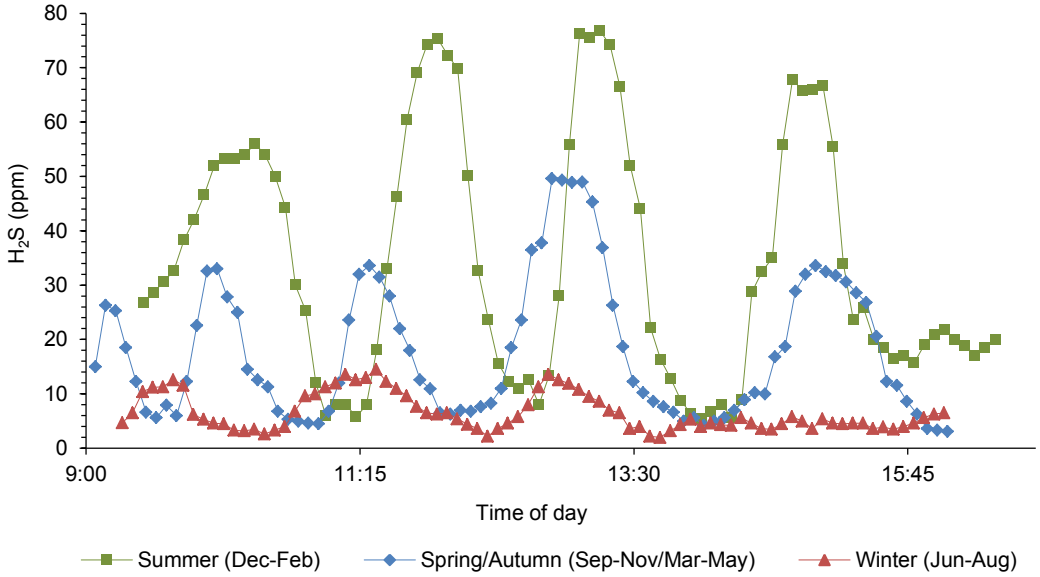

Figure 5-48: Typical daily H_2S profiles in the manhole at Langa during summer, spring/autumn and winter months (data from current study (2013-2015)).

Table 5-5: OPI and WSI of concrete used for surface pH vs. time profiling.

Mixture*	Age (days)	OPI			WSI (mm/√hr)		
		Average#	Standard deviation (σ)	Coefficient of variation (%)	Average#	Standard deviation (σ)	Coefficient of variation (%)
PC 100	28	10.53	0.17	1.57	5.7	0.17	3.01
PC 67/GGBS 33	28	10.78	0.07	0.65	6.0	0.18	3.04
PC 75/FA 25	28	10.48	0.14	1.31	5.9	0.24	4.15
PC 92/SF 8	28	10.89	0.07	0.68	5.6	0.22	3.86
CAC 100	28	9.79	0.12	1.23	11.3	0.22	1.91
CAC 65/GGBS 10/FA 25	28	9.97	0.10	1.04	9.9	0.21	2.11

*See details in Appendix G
#Average of 4 determinations

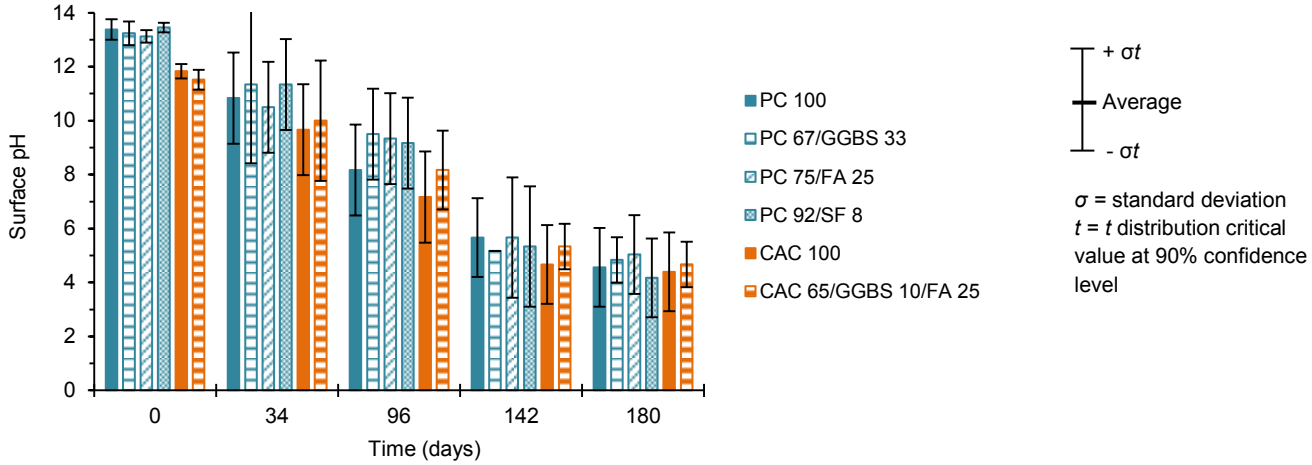

Figure 5-49: Surface pH vs. time profiles for concrete mixtures exposed in the VES for approximately 180 days.

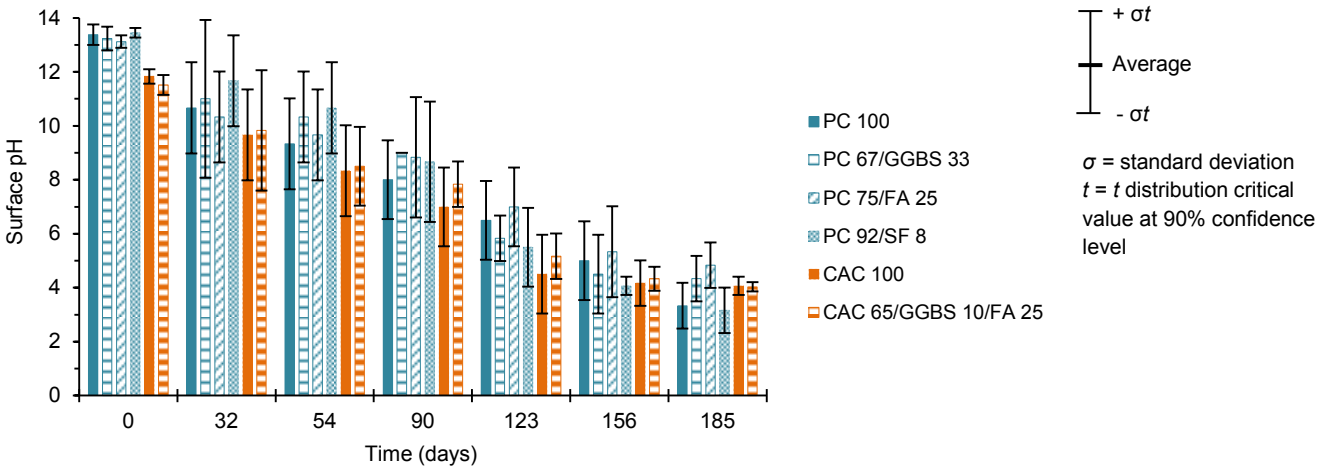

Figure 5-50: Surface pH vs. time profiles for concrete mixtures exposed in the manhole at Langa for approximately 185 days.

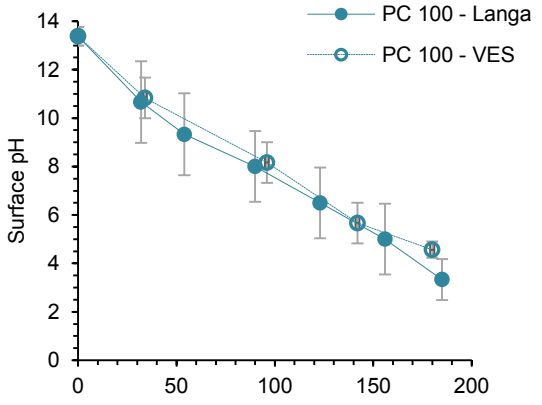

(a) Mixture with 100% PC

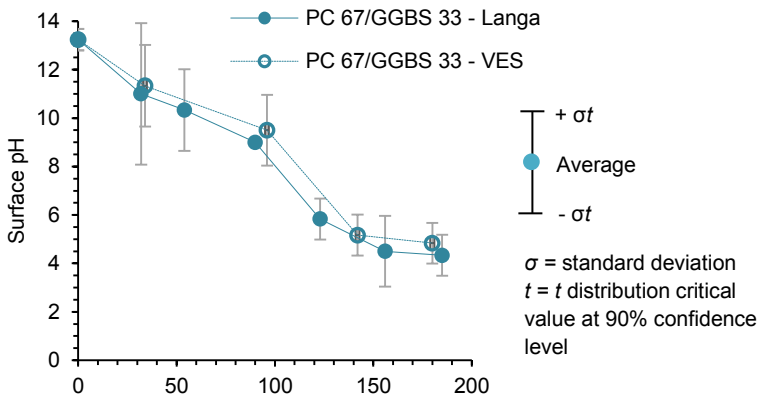

(b) Mixture with 67% PC + 33% GGBS

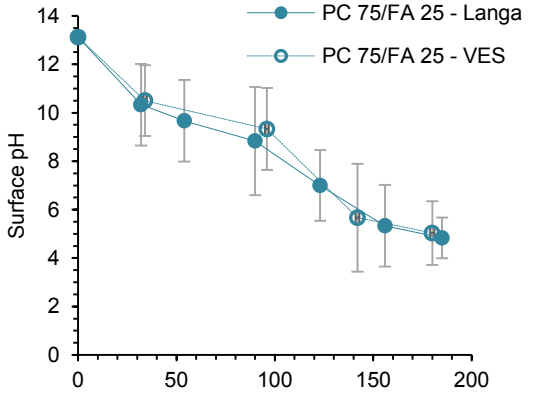

(c) Mixture with 75% PC + 25% FA

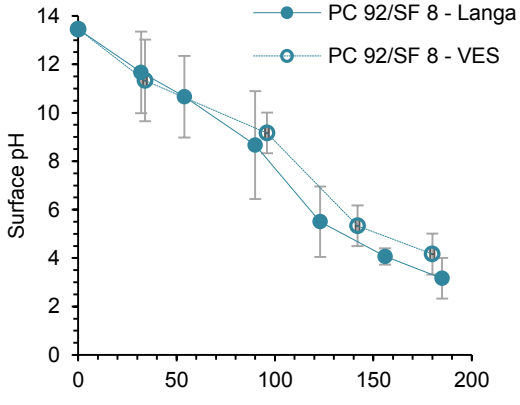

(d) Mixture with 92% PC + 8% SF

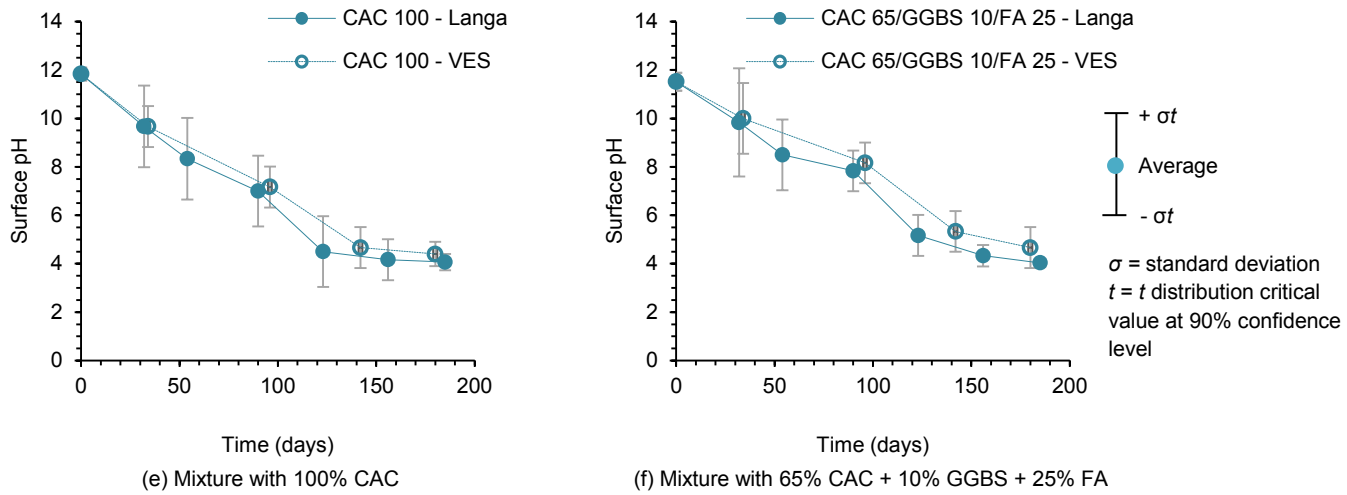

Figure 5-51 (a) to (f): Comparative surface pH vs. time profiles for concrete mixtures exposed in the manhole at Langa and the VES.

The following can be noted from the results presented in Figure 5-49 to Figure 5-51 in conjunction with the characteristics of the respective sites summarised in Table 5-4:

(i) The research sites used in the current study (VES and Langa) have similar characteristics (H_2S concentration and RH) that are deemed to influence biogenic corrosion mechanisms in sewers. For example, the average H_2S results during summer, spring/autumn, and winter months in the VES are 35 ppm, 13 ppm, and 6 ppm respectively, while those in the manhole at Langa are 34 ppm, 18 ppm, and 7 ppm respectively. However, generally, the manhole at Langa in Cape Town has a higher annual average H_2S concentration by approximately 2 ppm than the VES. Moreover, the average RH results during summer, spring/autumn, and winter months in the VES are 74%, 76%, and 77% respectively, while those in the manhole at Langa are 75%, 76%, and 80% respectively. These show that generally, the manhole at Langa in Cape Town has a higher annual average RH by approximately 1.5% than the VES.

(ii) The surface pH of samples installed in the manhole at Langa generally decreased at a higher rate, by a factor of approximately 1.04, than for samples installed in the VES. This factor was computed based on equations of linear trendlines fitted on the respective profiles.

(iii) Prior to exposure to the respective sites described in (i) above, all PC-based concrete mixtures had higher surface pH values than CAC-based mixtures by approximately 1.5 units. However, approximately 180 days after installation in both sewer environments, PC-based mixtures with 100% PC and 92% PC + 8% SF had attained lower surface pH values than CAC-based mixtures by approximately 0.7 units. Nonetheless, the surface pH of PC-based mixtures with 67% PC + 33% GGBS and 75% PC + 25% FA was still higher than that of CAC-based mixtures by approximately 0.3 to 0.7 units.

(iv) Under the in-situ characteristics described in the current study, the profiles reported herein show that the surface pH on CAC-based concrete mixtures started to plateau at approximately pH 4.3, reached approximately 150 days after installation in the respective sewer environments, while that on PC-based did not.

From the results presented in this sub-section, it is possible that similar colonisation patterns by neutrophilic bacteria occur in both PC- and CAC-based mixtures based on the surface pH values reported herein. However, as the surface pH on CAC-based mixtures tends to plateau at a pH of approximately 4.2, it implies that colonisation of acidophilic bacteria on these surfaces is slower than on PC-based mixtures due to the stability of certain products of corrosion, identified by the SEM/EDS technique as AH_3 (or AH_x) (see Section 5.5). Nonetheless, some of the surface pH values recorded at approximately 6 months (185 days) after installation of both PC- and CAC-based concrete mixtures in the VES (and manhole at Langa) were comparable to those measured on samples (with similar

mixture composition) exposed in the VES for approximately 127 months – see Table 5-6. This is an indication that, possibly, the complete destruction of certain binder matrices due to biogenic corrosion mechanisms does not require a consistently low acidic (pH < 2) environment as reported by some researchers (Alexander and Fourie, 2011).

Table 5-6: A comparison of measured surface pH values on concrete mixtures exposed in a 'live' sewer for 6 and 127 months (data from current study (2013 – 2015)).

Mixture	Surface pH range at:	
	6 months[#]	127 months*
PC/DOL	2.49 – 4.18	2.96 – 4.01
PC/GGBS/DOL	3.49 – 5.18	3.11 – 4.23
PC/FA/DOL	3.99 – 5.68	2.04 – 4.62
PC/SF/DOL	2.42 – 4.01	2.44 – 4.17
CAC/DOL	3.73 – 4.40	3.93 – 4.39

[#]Samples installed in the VES during 2015. See mixture composition in Appendix G.
*Samples installed in the VES during 2004. See mixture composition in Appendix E.

In order to understand the microbial ecosystem on the different substrates (PC- and CAC-based) that are responsible for the generation of biogenic H_2SO_4, which attacks the acid-soluble portions in concrete, microbial speciation was undertaken on the products of corrosion taken from these substrates. Results have been presented in the following section.

5.10 Microbial ecosystem on different binder substrates subjected to biogenic corrosion

The results presented in this section are based on the analysis of the products of corrosion taken from both PC- and CAC-based concrete mixtures (a total of 12 concrete mixtures – see details in Appendix E) subjected to biogenic H_2SO_4 attack for approximately 120 months. A description of the analytical techniques is given in Appendix J (J.4).

The microbial speciation in the current study was undertaken twice, during 2014 and 2015. In both instances, the extraction of genomic DNA (gDNA) was successful and characterised as of good quality, based on the absorbance technique of identifying DNA purity (Promega, 2015). A summary of the spectrophotometric quality control values of gDNA extracted during this period is given in Table 5-7.

Table 5-7: Summary of the spectrophotometric quality control values of gDNA extracted during 2014 and 2015.

Mixture*	Results for 2014		Results for 2015	
	Concentration[#] (ng/µl)	DNA purity[#] (260/280)	Concentration[#] (ng/µl)	DNA purity[#] (260/280)
PC/DOL 16	295.4	1.92	209.4	1.87
PC/DOL 18	151.4	1.91	114.1	1.91
PC/DOL 23	130.0	1.90	94.0	1.90
PC/GGBS/DOL 18	104.6	1.89	140.9	1.89
PC/FA/DOL 18	147.7	1.90	134.8	1.89
PC/SF/DOL 18	131.9	1.90	123.7	1.88
CAC/SIL 23	89.2	1.88	96.8	1.84
CAC/DOL 16	33.6	1.85	14.1	1.64
CAC/DOL 18	51.7	1.87	22.9	1.63
CAC/DOL 23	50.7	1.80	343.8	1.69
CAC/FA/SF/DOL 17	106.7	1.87	135.9	1.88
CAC/Alag^{TM} 20	69.4	1.87	14.2	1.55

*See details in Appendix E
[#]See Appendix J.4.1

The extracted gDNA was used in a PCR reaction to amplify the 16S rRNA genes, which were analysed by electrophoresis agarose gel (see Appendix J.4.2). The image of the agarose gel amplified during 2014 is given in Figure 5-52. From the amplified genes, the resulting unique clones were sequenced based on the ARISA analysis, and compared to 16S rRNA sequences deposited on the NCBI database. A summary of the identified microbial diversity (phylogenetic relatives) is given in Table 5-8, while unrooted 16S rRNA gene phylogenetic trees are given in Appendix L (L.7).

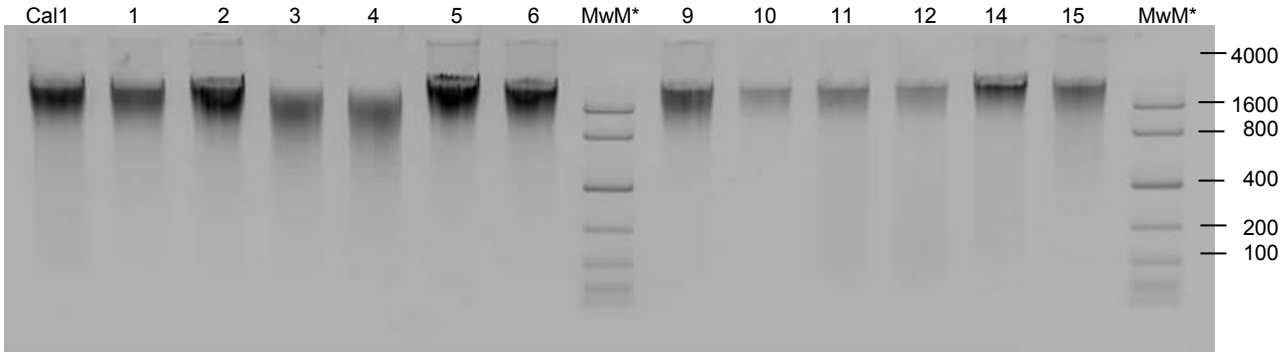

Cal1 = positive control (standard liquid culture of *E.coli*); 1 = PC/DOL 16; 2 = PC/DOL 18; 3 = PC/DOL 23; 4 = PC/GGBS/DOL 18; 5 = PC/FA/DOL 18; 6 = PC/SF/DOL 18; MwM = Molecular Weight Marker; 9 = CAC/SIL 23; 10 = CAC/DOL 16; 11 = CAC/DOL 18; 12 = CAC/DOL 23; 14 = CAC/FA/SF 17; 15 = CAC/Alag^{TM} 20.
*The MwM used was a Kapa Biosystems Express ladder, whose sizes have been indicated on the right-hand side of the figure.
Figure 5-52: Image of agarose gel of the PCR amplification of the 16S rRNA genes from gDNA extracted during 2014.

Table 5-8: Phylogenetic relatives obtained from different concrete substrates exposed to biogenic H_2SO_4 for 120 months.

Mixture *	Closest isolates#	Number of clones obtained
PC/DOL 16	*Frateuria*	3
	Nevskia	1
	Dyella thiooxidans	7
	Acidithiobacillus thiooxidans	1
PC/DOL 18	*Frateuria*	1
	Nevskia	1
	Dyella thiooxidans	2
	Acidithiobacillus thiooxidans	1
PC/DOL 23	*Nevskia*	2
	Paenibacillus	1
	Dyella thiooxidans	1
	Acidithiobacillus thiooxidans	2
PC/GGBS/DOL 18	*Frateuria*	3
	Nevskia	1
	Dyella thiooxidans	1
	Acidiphilium	2
	Halothiobacillus	7
PC/FA/DOL 18	*Acidiphilium*	1
	Acidithiobacillus thiooxidans	3
PC/SF/DOL 18	*Paenibacillus*	2
	Halothiobacillus	5
	Thermithiobacillus	2
	Acidithiobacillus thiooxidans	2
CAC/SIL 23	*Frateuria*	2
	Halothiobacillus	1
	Acidithiobacillus thiooxidans	2
CAC/DOL 16	*Dyella thiooxidans*	1
	Frateuria	2
	Nevskia	2
	Acidiphilium	1
	Acidithiobacillus thiooxidans	3
CAC/DOL 18	*Alicyclobacillus*	9
	Acidiphilium	2
	Acidithiobacillus thiooxidans	3
CAC/DOL 23	*Alicyclobacillus*	5
	Acidithiobacillus thiooxidans	14
CAC/FA/SF/DOL 17	*Alicyclobacillus*	1
	Acidithiobacillus thiooxidans	16
	Sulfobacillus	2
CAC/Alag^{TM} 20	*Acidocella*	1
	Acidiphilium	3
	Thiomonas	1
	Acidithiobacillus thiooxidans	12

*See details in Appendix E
#See unrooted 16S rRNA gene phylogenetic trees in Appendix L.7

The following can be noted from the microbial ecosystem obtained on the different concrete substrates exposed to biogenic H_2SO_4 for approximately 120 months in the VES:

(i) The microbial ecosystem on all the analysed products of corrosion (both PC- and CAC-based) consists of Alpha-, Beta-, and Gammaproteobacteria classes of the phylum Proteobacteria.
(ii) The products of corrosion from PC-based concrete substrates have a higher concentration (based on the number of clones obtained) of neutrophilic gammaproteobacteria (which include *Frateuria, Dyella* and *Nevskia*) than CAC-based substrates.
(iii) The products of corrosion from all the analysed substrates contain *Acidiphilium* (alphaproteobacteria) and/or *Acidithiobacillus thiooxidans* (gammaproteobacteria) within their microbial ecosystems.

Similar results have been reported by several researchers, showing that biogenic acid production in sewer environments is dominated by species of the genus *Acidithiobacillus* (Sand and Bock, 1984; Islander et al., 1991; Okabe et at., 2007; Valix et al., 2012). Before proceeding, it is important to note that the aim of the current study with regard to microbial speciation was to identify the phylogenetic relatives on the different concrete substrates as an indicator of aggressiveness to respective concrete mixtures.

In order to understand the colonisation and characteristics of the microbial ecosystem in sewer environments with similar environmental and hydraulic design considerations such as the VES, a discussion of the results presented in Sections 5.8, 5.9 and 5.10 will be undertaken concurrently in the following Section 5.11.

5.11 Discussion – microbial colonisation and ecosystem on different binder substrates subjected to biogenic corrosion

The bacteria found in the products of corrosion taken from the VES consist of those that can grow at low levels of nutrients (alphaproteobacteria), those that use nutrient substances that emanate from areas of anaerobic decomposition such as H_2S (betaproteobacteria), and those that oxidise H_2S instead of water to produce sulphur as a waste product (gammaproteobacteria).

Frateuria is capable of growing on glucose and a range of other carbon sources. Their optimal growth is observed at a pH of approximately 6 – 7 and temperature of between 25 °C and 40 °C, although they can also be found at a pH of approximately 4 (Swings et al., 1980). Members of the genus *Dyella* grow between pH 4.5 and pH 8 over a wide range of temperature (4 °C – 42 °C), although optimum growth typically occurs between temperature of 25 °C and 35 °C (Jung et al., 2009; Amandham et al., 2011). Members of the genus *Nevskia* grow optimally at pH 6 – 7, at a temperature range of between 25 °C and 28 °C, although their growth has also been observed at pH 4 (Stürmeyer et al., 1998; Weon et al., 2008). Members of the genus *Paenibacillus* show optimal growth at pH 7 and temperature of approximately 35 °C (Osman et al., 2006).

Members of the genus *Halothiobacillus* and *Thermithiobacillus* oxidise reduced sulphur compounds, and have an optimal growth between pH of 6.5 and 8, at a temperature of between 25 °C and 40 °C (Kelly and Wood, 2000). Members of the genus *Acidithiobacillus, thiomonas* and *Sulfobacillus* can also oxidise reduced sulphur compounds and grow optimally at pH of between 2 and 4. Members of the genus *Alicyclobacillus* and *Acidiphilium* are heterotrophic, although some species of the genus *Acidiphilium* can oxidise reduced sulphur compounds (Rohwerder and Sand, 2003). These heterotrophs grow optimally between pH 4 and 7, at a temperature of between 15 °C and 40 °C.

From the discussions above, and results presented in Section 5.9, it is probable that biogenic corrosion in both PC- and CAC-based concrete mixtures exposed in environments such as the VES or manhole at Langa commence approximately 123 days after installation. However, based on the comparative rates of corrosion presented in Section 5.3, and the characteristics of the respective mixtures presented in Sections 5.4 and 5.5, it can be concluded that the superior performance of CAC-based mixtures is dependent on the reactive nature of its hydrates at low pH (< 5).

5.12 Summary of results

This chapter presented results, analysis and discussion of concrete mixtures subjected to biogenic corrosion mechanisms for durations ranging from approximately 6 months to 127 months in two different sewer environments – the VES and Langa. The aim of this chapter was to draw useful insights on the characteristics of concrete mixtures that influence biogenic deterioration mechanisms with the view of incorporating the findings in practical engineering applications, such as in biogenic concrete corrosion prediction (in sewers). From the reviewed literature and results presented herein, it is seen, from a material (concrete) point of view, that the binder type and content used in a concrete mixture affect the biogenic corrosion rate. In summary, the following conclusions can be made from the results presented in current study:

(1) Biogenic concrete corrosion rate

a. In plain mixtures with similar binder contents PC-based concrete mixtures started losing mass due to biogenic corrosion approximately 24 months (2 years) earlier than CAC-based mixtures.
b. PC-based concrete mixtures with a lower amount of PC (16%) experienced less mass loss than those with higher amounts of PC (18% and 23%).
c. CAC-based concrete mixtures with a lower amount of CAC (16%) experienced more mass loss than those with higher amounts of CAC (18% and 23%).
d. Certain CAC-based mixtures incorporating SCMs but with a lower total binder content (such as CAC + FA + SF ternary mixtures with a total binder content of 17% (content of CAC only at 11%)) experienced less mass loss than those with a slightly higher amount of CAC (18%). However, CAC-based concrete mixtures with a higher amount of CAC (23%) experienced less mass loss than the ternary mixtures.
e. Regardless of the aggregate type (acid-soluble or acid-insoluble), CAC-based concrete mixtures with approximately 23% cement content had similar biogenic corrosion rates.
f. The use of artificial aluminate aggregate (such as alag^{TM}) in CAC-based concrete mixtures resulted in a lower biogenic corrosion rate, even at a lower cement content. CAC/alag^{TM} mixtures with 20% experienced less mass loss than both CAC/DOL and CAC/SIL mixtures with 23% cement content.

(2) Microstructural characteristics of concrete subjected to biogenic H_2SO_4

a. Within the semi-deteriorated matrices of both PC- and CAC-based concrete mixtures, the concentration of calcium species is lower than that in both the deteriorated and sound matrices of the respective mixtures.
b. Within the semi-deteriorated matrices of CAC-based concrete mixtures, the concentration of the alumina species is higher than that of the sound matrix.
c. The products of concrete corrosion (deteriorated matrix) when both PC- and CAC-based mixtures are subjected to biogenic H_2SO_4 attack are predominantly gypsum.
d. From the EDS point analyses, the alumina-rich layer within the semi-deteriorated matrices of CAC-based mixtures was identified as AH_3 (or AH_x gel).
e. The use of the aluminate aggregate enhances the performance of CAC-based mixtures subjected to biogenic H_2SO_4 attack.

(3) Microbial ecosystem in the products of corrosion taken from concrete mixtures subjected to biogenic H_2SO_4

a. The phylogenetic relatives of microbes found in the products of corrosion taken from both PC- and CAC-based concrete mixtures are similar irrespective of mixture composition.
b. The identified microbial community has been reported in literature to thrive in a temperature range of between 4 °C and 42 °C, and a pH range of between 2 and 7.

From the summary of results presented above, it can be seen that the biogenic corrosion mechanism in sewers is complex. Moreover, during the design process of concrete mixtures for sewer applications, it is difficult using the current design guidelines, to establish suitable combinations given a wide range of binders (with distinctly different products of hydration) that are available in the market. It is for this reason that the current study aims to provide a suitable framework for biogenic corrosion prediction, particularly for practising engineers, in order to move the concrete mixture design protocols from empirical to a more scientifically rational basis.

The following chapter presents a practical application of microstructural characterisation of concrete mixtures in the widely used Life Factor Method (LFM) – a deterministic (mechanistic) corrosion prediction model.

5.13 References

Alexander, M. G., & Fourie, C. W. 2011. Performance of sewer pipe concrete mixtures with portland and calcium aluminate cements subject to mineral and biogenic acid attack. *Materials and Structures*. 44 (1): 313 – 330.

Alexander, M. G., Goyns, A. M., & Fourie, C. W. 2008. Experiences with a full-scale experimental sewer made with CAC and other cementitious binders in Virginia, South Africa. *Proceedings of the Centenary Conference on Calcium Aluminate Cements.* June 30 – July 2, Avignon. 279 – 292.

Amandham, R., Kwon, S., Ghandi, P. I., Kim, S., Weon, H. Kim, Y-S., Sa, T., Kim, Y-K., & Lee, H. 2011. *Dyella thiooxidans* sp. nov., a facutatively chemolithotrophic, thiosulphate-oxidising bacterium isolated from rhizosphere soil of sunflower (*Helianthus annuus* L.*). International Journal of Systematic and Evolutionary Microbiology*. 61: 392 – 398.

Bizzozero, J., Gosselin, C., & Scrivener, K. L. 2014. Expansion mechanisms in calcium aluminate and sulfoaluminate systems with calcium sulfate. *Cement and Concrete Research*. 56: 190 – 202.

Chatterjee, S., Bandyopadhyay, A., & Sarkar, K. 2011. Effect of iron oxide and gold nanoparticles on bacterial growth leading towards biological application. *Journal of Nanobiotechnology.* 9: 34.

De Keyser, W. L. 1955. Contribution to the study of solid state reactions between OCa, O_3Fe_2, O_3Al_2. *Bulletin of Chemical Societies.* 64(7 – 8): 395 – 408.

Dilnesa, B. Z. 2011. Fe-containing hydrtaes and their fate during cement hydration: Thermodynamic data and experimental study. PhD dissertation. École Polytechnique Fédérale de Lausanne, Lausanne.

Dilnesa, B. Z., Wieland, E., Lothenbach, B., Dähn, R., & Scrivener, K. L. 2014. Fe-containing phases in hydrated cements. *Cement and Concrete Research.* 58: 45 – 55.

EMPA: The Swiss Federal Laboratories for Materials Science and Technology. 2015. In-house software development. A guideline – Laboratory of Concrete and Construction Chemistry. EMPA.

Environmental Protection Agency. 1991. Hydrogen sulphide corrosion in wastewater collection and treatment systems, Technical Report to Congress, 430/09-91-010. Cincinnati: EPA.

Gosselin, C. 2009. Microstructural development of calcium aluminate cement based systems with and without supplementary cementitious materials. PhD dissertation. École Polytechnique Fédérale de Lausanne, Lausanne.

Goyns, A. M. 2003. Virginia sewer rehabilitation: Progress Report 1. Pretoria: Concrete Manufacturers Association.

Goyns, A. M. 2010. Virginia sewer rehabilitation: Progress Report 4. Pretoria: Concrete Manufacturers Association.

Goyns, A. M., Alexander, M. G., & Fourie, C. W. 2008. Applying experimental data to concrete sewer design and rehabilitation. *Proceedings of the Centenary Conference on Calcium Aluminate Cements.* June 30 – July 2, Avignon. 293 – 308.

Herisson, J. 2012. Biodeterioration of cementitious materials in the wastewater – Comparative study of calcium aluminate cement and Portland cement. PhD dissertation. Université Paris-Est, Paris.

Herisson, J., Guéguen-Minerbe, M., van Hullebusch, E. D., & Chaussadent, T. 2014. Biogenic corrosion mechanism: Study of parameters explaining calcium aluminate cement durability.

Proceedings of the International Conference on Calcium Aluminate Cements. May 18 – 21, Avignon. 633 – 644.

Islander, R. L., Devinny, J. S., Mansfeld, F., Postyn, A., & Hong, S. 1991. Microbial ecology of crown corrosion in sewers. *Journal of Environmental Engineering*. 117(6): 751 – 770.

Johnson, A. C., & Wood, M. 1990. DNA, a possible site aluminium toxicity in *Rhizobium*. *Applied and Environmental Microbiology*. 56: 3629 – 3633.

Jung, H., Ten, L. N., Kim, K., An, D. S., Im, W., & Lee, S. 2009. *Dyella ginsengisoli* sp. nov., isolated from soil of a ginseng field in South Korea. *International Journal of Systematic and Evolutionary Microbiology.* 59: 460 – 465.

Kelly, D. P., & Wood, A. P. 2000. Reclassification of some species of Thiobacillus to the newly designated genera Acidithiobacillus gen. nov., Halothiobacillus gen. nov., and Thermithiobacillus gen. nov. *International Journal of Systematic and Evolutionary Microbiology.* 50: 511 – 516.

Kotronarou, A., & Hoffmann, M. R. 1991. Catalytic autooxidation of hydrogen sulphide in wastewater. Environmental Science and Technology. 25(6): 1153 – 1160.

Kurdowski, W. 2014. *Cement and concrete chemistry*. Dordrecht: Springer.

Motsieloa, N. 2013. Acid resistance of sewer pipe concrete. MSc (Eng) dissertation. University of Cape Town, Cape Town.

Okabe, S., Odagiri, M., Itoh, T., & Satoh, H. 2007. Succession of sulphur-oxidizing bacteria in the microbial community on corroding concrete in sewer systems. *Applied and Environmental Microbiology*. 73(3): 971 – 980.

Ornek, D., Gurkan, T., & Oztin, C. 1998. Physical and chemical properties of a highly viscous aluminium sulphate melt. *Industrial and Engineering Chemical Research.* 37: 2687 – 2690.

Osman, S., Satomi, M., & Venkateswaran, K. 2006. *Paenibacillus pasadenensis* sp. nov. and *Paenibacillus barengoltzii* sp. nov., isolated from a spacecraft assembly facility. *International Journal of Systematic and Evolutionary Microbiology*. 56: 1509 – 1514.

Paulini, P. 1994. A Through Solution Model for volume changes of cement hydration. *Cement and Concrere Research.* 24(3): 488 – 496.

Promega Corporation. 2015. Promega protocals and applications guide. Wisconsin: The Promega Publications Hub.

Renaudin, G., Mesbah, A., Dilnesa, B. Z., Francois, M., & Lothenbach, B. 2015. Crystal chemistry of iron containing cementitious AFm layered hydrates. *Current Inorganics Chemistry.*5(2): 1 – 10.

Rohwerder, T., & Sand, W. 2003. The sulfane sulfur of persulfides is the actual substrate of the sulfur-oxidising enzymes from *Acidithiobacillus* and *Acidiphilium* spp. *Microbiology.*149: 1699 – 1709.

Sahmaran, M. 2010. Deterioration mechanisms – chemical. In: Soutsos, M. Eds. *Concrete durability: A practical guide to the design of durable concrete structures*. London: Thomas Telford.

Sand, W., & Bock, E. 1984. Concrete corrosion in the Hamburg sewer system. *Environmental Technology Letters.* 5(12): 517 – 528.

Scrivener, K. L. 2003. Calcium aluminate cements. In: Newmann, J., & Choo, B. S. Eds. *Advanced Concrete Technology – Constituent Materials*. Oxford: Elsiever.

Soenen, S. J., Cuyper, M., Smedt, S. C., & Braeckmans, K. 2012. Investigating the toxic effects of iron oxide nanoparticles. *Methods in Enzymology.* 509: 195 – 224.

Stürmeyer, H., Overman, J., Babenzien, H., & Cypionka, H. 1998. Ecophysiological and phylogenetic studies of *Nevskia ramose* in pure cultures. *Applied and Environmental Microbiology.* 64: 1890 – 1894.

Swings, J., Gillis, M., Kersters, K., De Vos, P., Gosselé, F., & De Ley, J. 1980. *Frateuria,* a new genus for *Acetobacter aurantius. International Journal of Systematic Bacteriology.* 30: 547 – 556.

Taber, S. 1916. The growth of crystals under external pressure. *American Journal of Science*. 4(41): 532 – 556.

Trun, N. J., & Gottesman, S. 1990. On the bacterial cell cycle: Escherichia coli mutants with altered ploidy. *Genes and Development.* 4: 2036 – 2047.

Valix, M., Zamri, D., Mineyama, H., Cheung, W. H., Shi, J., & Bustamante, H. 2012. Microbiologically induced corrosion of concrete and protective coatings in gravity sewers. *Chinese Journal of Chemical Engineering.* 20(3): 433 – 438.

Weisweiler, W., Osen, E., Eck, J., & Höfer, H. 1986. Kinetic studies in the CaO-SiO_2 system, Part I: Mechanism and kinetic data of the reactions between CaO- and SiO_2-powder compacts. *Cement and Concrete Research.* 16(3): 283 – 295.

Weon, H., Kim, B-Y., Son, J., Song, M., Kwon, S., Go, S., & Stackebrandt, E. 2008. *Nevskia soli* sp. nov., isolated from soil of a ginseng field in South Korea. *International Journal of Systematic and Evolutionary Microbiology*. 58: 578 – 580.

Wilmot, P. D., Cadee, K., Katinic, J. J., & Kavanagh, B. V. J. 1988. Kinetics of sulphide oxidation by dissolved oxygen. *Journal of Water Pollution Control Federation.* 60: 1264 – 1270.

Chapter Six: Practical application of microstructural characteristics of concrete mixtures in improving the prediction capability of the LFM – a deterministic (mechanistic) corrosion prediction model

6.1 Introduction

This chapter presents a framework for practical application of the characteristics of concrete mixtures based on the microstructural characterisation presented in Chapter Five. From discussions presented in Sections 5.7 and 5.8, and referring to the reviewed literature in Chapter Two, Part Three, it was highlighted that during biogenic concrete corrosion in sewer environments, another parameter namely AH_x, (based on the Al_2O_3 of binders) besides *alkalinity* (based on the CaO of binders and aggregates), contributes to the overall *neutralisation capacity* of concrete mixtures. Moreover, from discussions presented in Section 5.6, it is hypothesised that Fe_2O_3 also plays an active role during biogenic corrosion mechanisms due to lower corrosion rates exhibited by CAC-based mixtures (CAC contains up to 18% Fe_2O_3). It is for this reason that the current study focusses on understanding the CaO–Al_2O_3–Fe_2O_3 system in relation to the average corrosion rates of different binder systems given in Figure 5-5, with the view of improving the biogenic corrosion prediction capability of the LFM.

Before proceeding, it is important to note that during biogenic acid attack of concrete, the extent of the destruction of the polymeric nature of calcium species in concrete matrices is dependent on the available calcium hydroxide (CH), which is also involved in neutralising the attacking acid, as discussed in Section 5.7. Therefore, it is hypothesised that during biogenic acid attack of concrete matrices, the significance of CaO content in binders relates to the CH component, whereas the CaO content in acid-soluble aggregates (dolomite, $CaMg(CO_3)_2$) relates to the $CaCO_3$ component. In this regard, the current study further proposes to incorporate a CH component in the LFM. However, from the comparative biogenic corrosion rate time-development trends presented in Section 5.3, it was shown that the higher the PC content (or CH content) in concrete mixtures, the higher the corrosion rate. This is contradictory to the hypothesis of the LFM. Hence, in order for the CH component to be incorporated in the LFM, an inverse value, CH^{-1} is proposed, particularly for PC-based concrete mixtures only, since in CAC-based concrete mixtures, the influence of the AH_x component overrides that of CH.

In order to correlate the average biogenic concrete corrosion rates presented in Section 5.3 with an understanding of the microstructural characteristics of concrete mixtures, equivalent parameters from the CaO–Al_2O_3–Fe_2O_3 system, based on stoichiometry and SEM/EDS point analyses, expressed as ratios, were developed. Stoichiometry calculations for parameters that are deemed to play an active role during biogenic corrosion mechanisms were based on Equations 6.1 to 6.4 (these equations are based on the concept of Equation 2.52).

$$CH_{(equiv.)} = \frac{\left((c \times CaO_{cement})\right)}{d} \times \frac{74}{56} \tag{6.1}$$

where c = cement content (kg cement/m^3 concrete)
CaO_{cement} = CaO content of the cement (kg CaO/kg cement)
d = density of concrete (kg/m^3)
The factor 74/56 is the ratio between the molar masses of CH and CaO

$$CaCO_{3(equiv.)} = \frac{\left((a \times CaO_{aggr})\right)}{d} \times \frac{100}{56} \tag{6.2}$$

where a = aggregate content (kg/m^3 concrete)
CaO_{aggr} = CaO content of the aggregates (kg CaO/kg aggregates)
d = density of concrete (kg/m^3)
The factor 100/56 is the ratio between the molar masses of $CaCO_3$ and CaO

$$AH_{3(equiv.)} = \frac{\left((c \times Al_2O_{3(cement)}) + (a \times Al_2O_{3(aggr)})\right)}{d} \times \frac{78}{102} \quad (6.3)$$

where c = cement content (kg cement/m^3 concrete)
$Al_2O_{3(cement)}$ = Al_2O_3 content of the cement (kg Al_2O_3/kg cement)
a = aggregate content (kg/m^3 concrete)
$Al_2O_{3(aggr)}$ = Al_2O_3 content of the aggregates (kg Al_2O_3/kg aggregates)
d = density of concrete (kg/m^3)

- Applicable for artificial aggregates such as Alag^{TM}
- For natural aggregates = 0

The factor 78/102 is the ratio between the molar masses of AH_3 and Al_2O_3

$$FeO(OH)_{(equiv.)} = \frac{\left((c \times Fe_2O_{3(cement)}) + (a \times Fe_2O_{3(aggr)})\right)}{d} \times \frac{107}{160} \quad (6.4)$$

where c = cement content (kg cement/m^3 concrete)
$Fe_2O_{3(cement)}$ = Fe_2O_3 content of the cement (kg Fe_2O_3/kg cement)
a = aggregate content (kg/m^3 concrete)
$Fe_2O_{3(aggr)}$ = Fe_2O_3 content of the aggregates (kg Fe_2O_3/kg aggregates)
d = density of concrete (kg/m^3)

- Applicable for artificial aggregates such as Alag^{TM}
- For natural aggregates = 0

The factor 106.9/159.7 is the ratio between the molar masses of FeO(OH) and Fe_2O_3

The following section presents mechanistic correlations between ratios obtained from stoichiometry and SEM/EDS point analyses, and respective biogenic corrosion rates.

6.2 Mechanistic correlations between ratios obtained from stoichiometry and SEM/EDS point analyses of the sound (un-attacked) concrete matrices and the respective corrosion rates

A summary of correlations between corrosion rates and certain parameters determined from stoichiometry and EDS point analyses is given in Table 6-1, and also in Figure 6-1 to Figure 6-6 for reference and application in corrosion prediction.

Table 6-1: Summary of correlations between corrosion rates and certain parameters determined from stoichiometry and EDS point analyses

	Corrosion rate (mm/yr)*			Characteristics of sound matrices					
	Ave.	Range		Based on stoichiometry, equivalent#				Based on EDS point analysis	
Mixture		Min	Max	$CaCO_3$+	CH**	AH_3**	FeO(OH)**	Al/Ca**	Fe/Ca**
CAC/Alag^{TM}	0.25	0.17	0.34	0.268	0.099	0.181	0.061	0.734	0.234
CAC/SIL 23	0.33	0.29	0.36	0.093	0.114	0.089	0.034	0.619	0.209
CAC/DOL 23	0.33	0.27	0.38	0.335	0.114	0.089	0.034	0.623	0.217
CAC/FA/SF/DOL 17	0.42	0.30	0.53	0.357	0.057	0.050	0.017	0.412	0.199
CAC/DOL 18	0.51	0.45	0.57	0.357	0.089	0.052	0.020	0.499	0.201
CAC/DOL 16	0.55	0.51	0.60	0.363	0.079	0.038	0.015	0.341	0.175
PC/FA/DOL 18	1.07	0.97	1.17	0.357	0.103	0.015	0.008	0.224	0.101
PC/DOL 16	1.14	0.79	1.48	0.363	0.085	0.005	0.008	0.078	0.016
PC/SF/DOL 18	1.14	0.98	1.30	0.357	0.089	0.005	0.008	0.067	0.020
PC/GGBS/DOL 18	1.26	1.03	1.50	0.357	0.210	0.010	0.007	0.191	0.018
PC/DOL 18	1.30	1.26	1.34	0.357	0.300	0.006	0.008	0.141	0.023
PC/DOL 23	1.48	1.11	1.85	0.321	0.360	0.007	0.009	0.147	0.039

*See Chapter Five
#See Equations 6.1 to 6.4
+Influence of aggregate
**Influence of binder

From the summary given in Table 6-1, it can be seen that the average biogenic corrosion rates between CAC-based mixtures with 23% cement content (CAC/SIL 23 and CAC/DOL 23) are the same (0.33 mm/yr.). However, since the siliceous aggregate (SIL) is acid-insoluble, the calculated $CaCO_{3(equiv.)}$ value of CAC/SIL 23 mixture ($CaCO_{3(equiv.)}$ = 0.093) varies from the average of all the other CAC-based mixtures with acid-soluble coarse aggregates ($CaCO_{3(equiv.)}$ = 0.336) by approximately 72%. Based on the significance of $CaCO_{3(equiv.)}$ (*alkalinity*) in biogenic concrete corrosion mechanisms as highlighted in the reviewed literature, certain correlations (including those in

Figure 6-1 to Figure 6-6) did not incorporate this particular SIL-based mixture, since it appears that the corrosion rate in concrete mixtures with 23% CAC is dependent on the alumina component.

In order to draw conclusions on the *significance* of the various parameters presented in Table 6-1 in relation to the respective biogenic corrosion rates, correlations are presented graphically as given in Figure 6-1 to Figure 6-6. The definition of the *significance* was based on hypothesis testing through computed *P*-values. The *P*-value measures the plausibility of a null hypothesis, where the smaller the *P*-value, the stronger the evidence is against a certain assumption or hypothesis. The 5% rule (P = 0.05) is generally used to reject the null hypothesis (Navidi, 2006). In the current study, the null hypothesis under investigation is that all the characteristics of the sound matrices given in Table 6-1, based on stoichiometry and EDS point analysis, do not influence the biogenic corrosion rate in both CAC- and PC-based concrete mixtures. Discussions are given in the following sections.

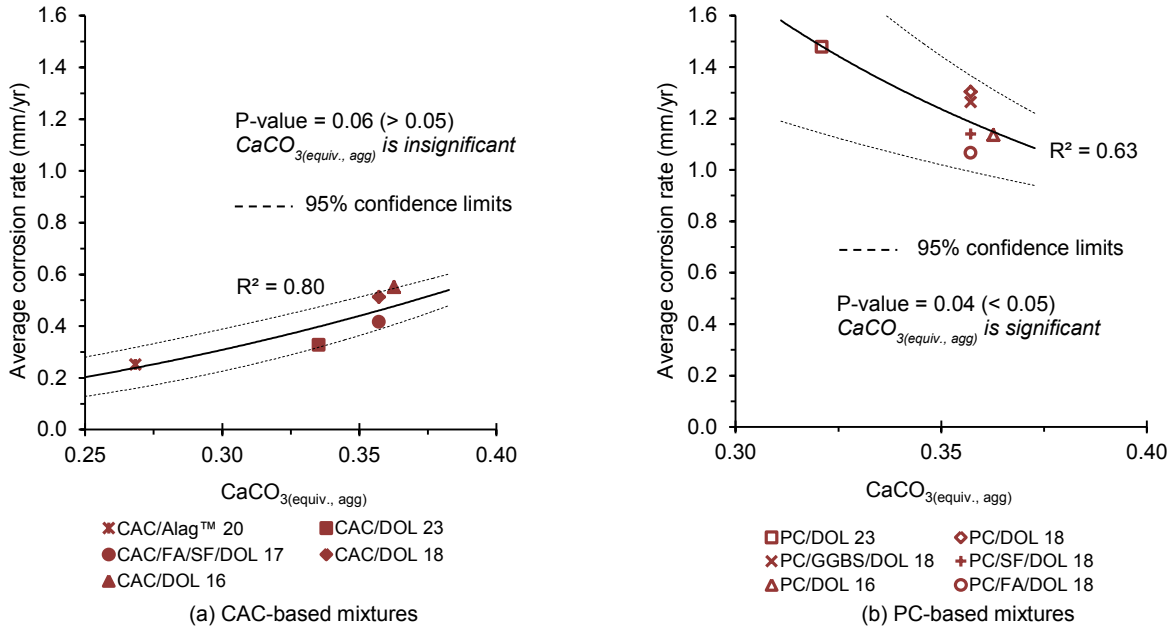

Figure 6-1 (a) and (b): *Significance* of $CaCO_{3(equiv., agg)}$ in CAC- and PC-based binder systems.

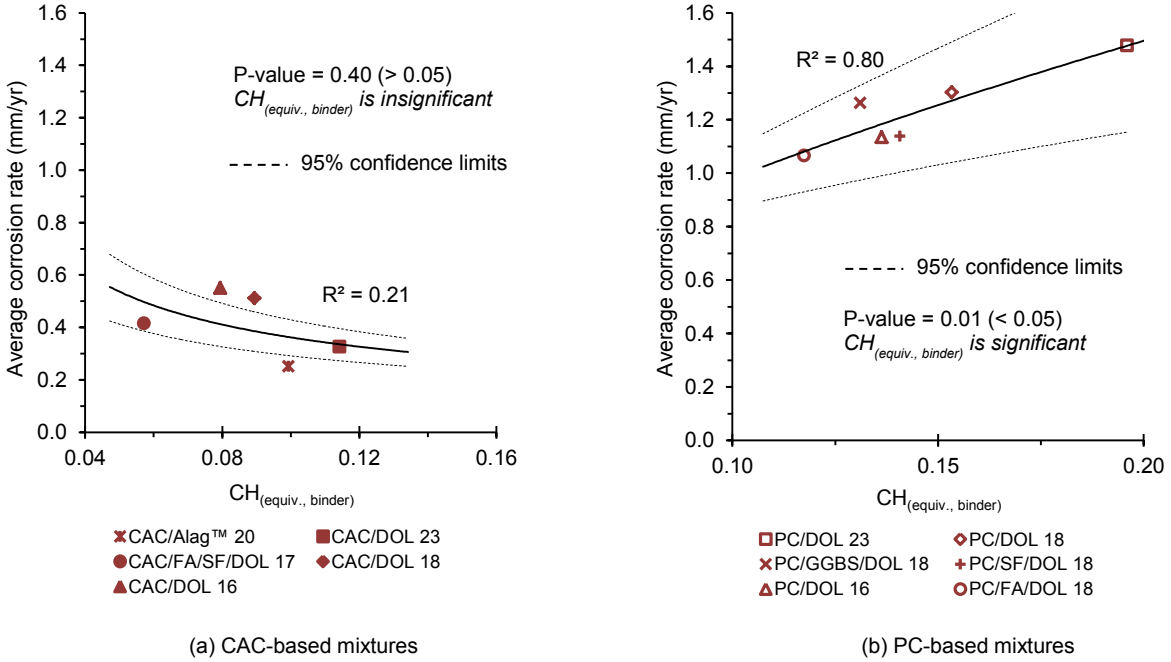

Figure 6-2 (a) and (b): *Significance* of $CH_{(equiv., binder)}$ in CAC- and PC-based binder systems.

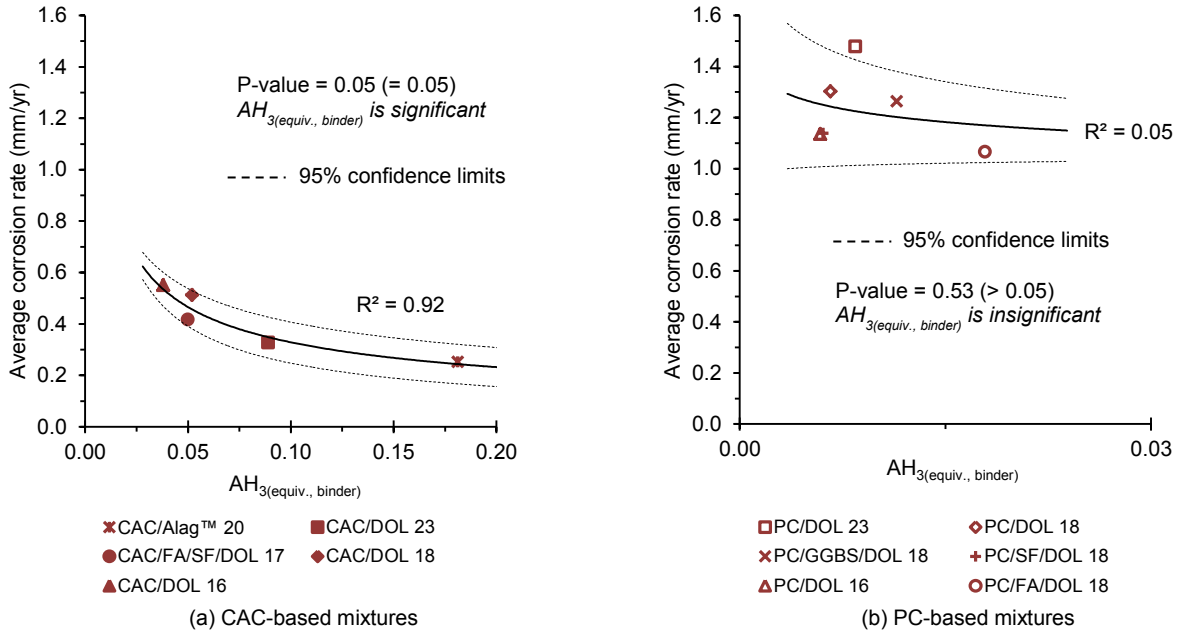

(a) CAC-based mixtures (b) PC-based mixtures

Figure 6-3 (a) and (b): *Significance* of $AH_{3(equiv., binder)}$ in CAC- and PC-based binder systems.

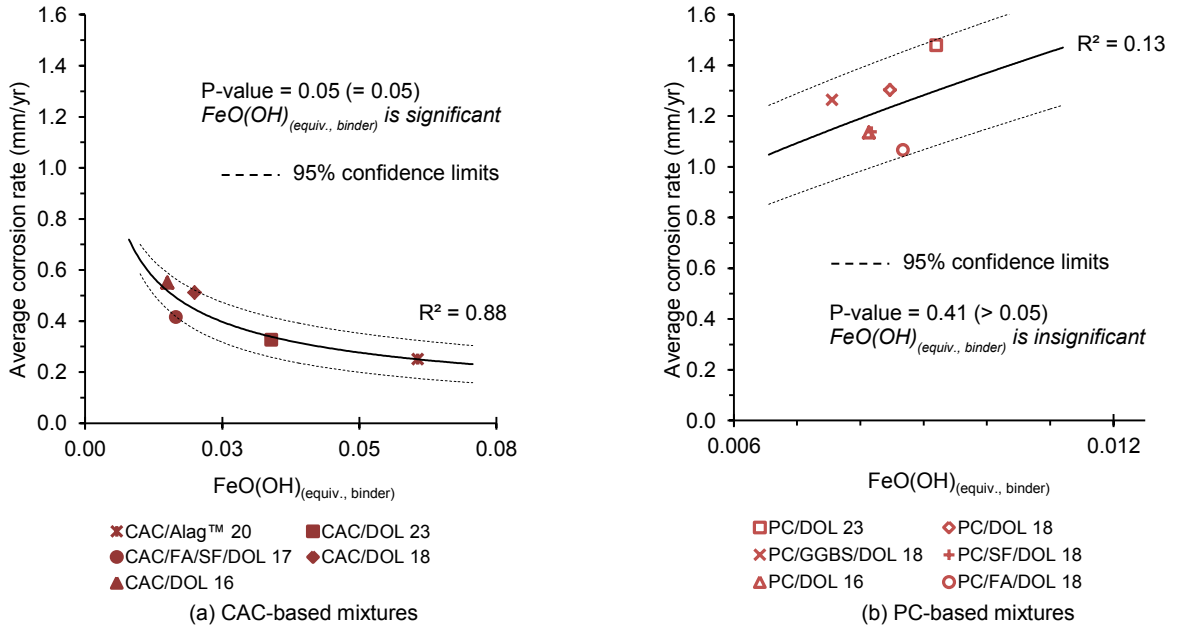

(a) CAC-based mixtures (b) PC-based mixtures

Figure 6-4 (a) and (b): *Significance* of $FeO(OH)_{(equiv., binder)}$ in CAC- and PC-based binder systems.

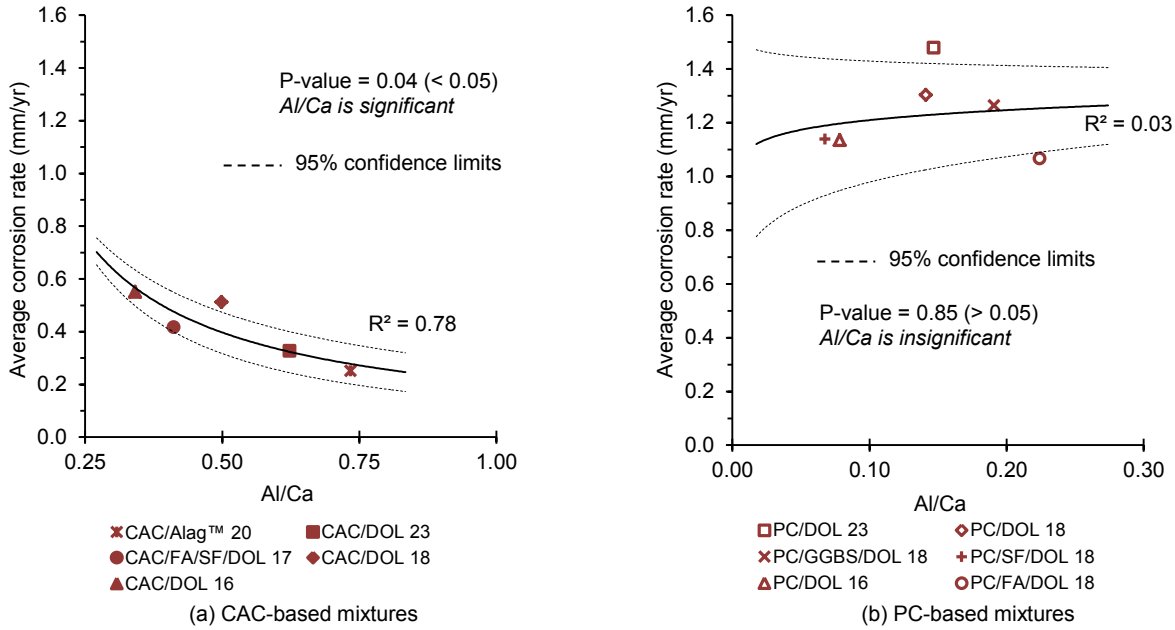

Figure 6-5 (a) and (b): *Significance* of Al/Ca ratios in CAC- and PC-based binder systems.

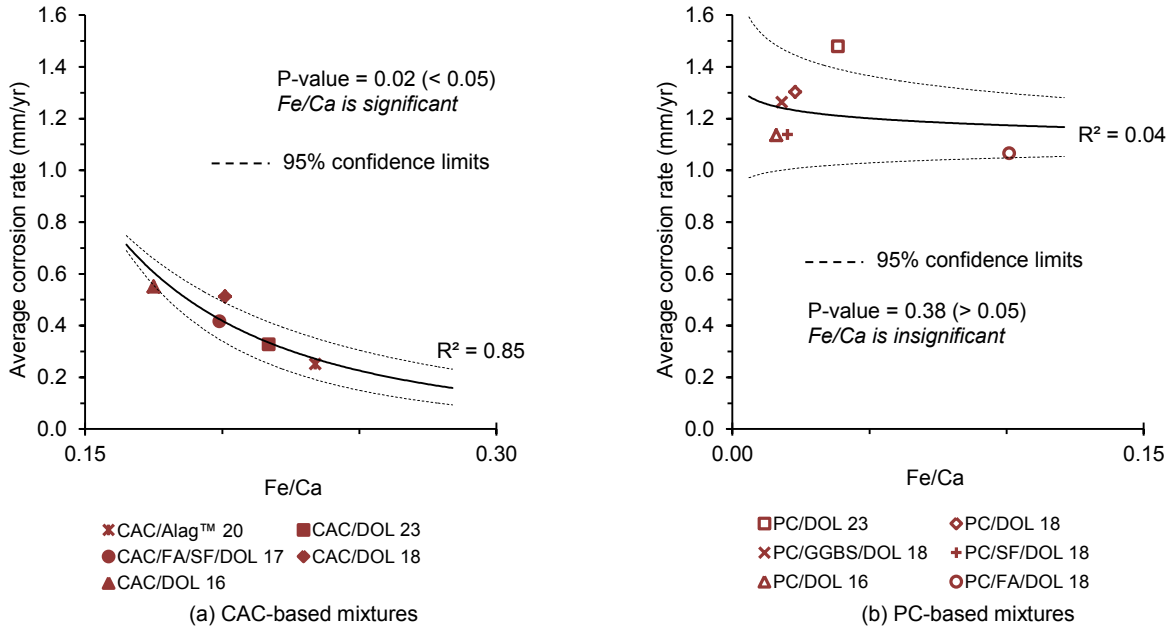

Figure 6-6 (a) and (b): *Significance* of Fe/Ca ratios in CAC- and PC-based binder systems.

Figure 6-1 shows that the calcareous aggregate plays a more active role in PC-based concrete mixtures than in CAC-based concrete mixtures when they are subjected to biogenic acid attack. Figure 6-2 shows that the influence of CH is significant in PC-based concrete mixtures but not in CAC-based concrete mixtures. Moreover, correlations given in Figure 6-3 to Figure 6-6 show that Al and Fe are significant and they influence biogenic corrosion rates of CAC-based concrete mixtures. These correlations further support the hypothesis that, generally, the influence of the alumina and ferrous components override that of the calcium component in biogenic corrosion mechanisms.

The correlations (showing the *significance* of certain parameters) presented in Figure 6-1 to Figure 6-6 are summarised in Table 6-2.

Table 6-2: Summary of significance of certain parameters in CAC- and PC-based concrete mixtures

Mixture	Significance*					
	$CaCO_{3(equiv., agg)}$	$CH_{(equiv., binder)}$	$AH_{3(equiv., binder)}$	$FeO(OH)_{(equiv., binder)}$	Al/Ca	Fe/Ca
CAC-based	0.06 (I)	0.4 (I)	0.05 (S)	0.05 (S)	0.04 (S)	0.02 (S)
PC-based	0.04 (S)	0.01 (S)	0.53 (I)	0.41 (I)	0.85 (I)	0.38 (I)

*Based on *P*-value
I = Insignificant
S = Significant

From the correlations presented in Figure 6-1 to Figure 6-6, and summarised in Table 6-2, it can be seen that of all the parameters that are *significant* in influencing the corrosion rate of both CAC- and PC-based mixtures subjected to biogenic acid attack, it is only the calcium hydroxide (CH) that is proportional to the average biogenic corrosion rate, and this occurs in PC-based mixtures. Moreover, the *P*-values relating to $CaCO_{3(equiv.)}$ for both PC- (= 0.04) and CAC-based (= 0.06) mixtures are relatively close to the 5% level (0.05), although on either side. It is therefore hypothesised that the performance of the PC-based concrete mixtures investigated in the current study is influenced more by the CH content ($CH_{(equiv.)}$) than the $CaCO_{3(equiv.)}$, and this justifies the incorporation of a CH component in the LFM in order to improve its prediction capability. However, it is important to note that since PC-based mixtures with higher cement content experienced greater corrosion rates, values of CH^{-1} are used in order to correlate with the deterioration pattern, because of the inverse relationship of corrosion rate and *neutralisation capacity* of concrete mixtures.

From the literature review and data presented in Section 3.4, it was shown that the multi-equation LFM can be used to predict total sulphide build-up in the sewage, and release to the sewer headspace relatively accurately, based on H_2S concentration levels measured in the inlet manhole to the VES. Therefore the initial equations of the LFM (Equations 2.68 to 2.73) are relatively reliable in this regard. However, the final equation of the LFM (Equation 2.77) considers *alkalinity, A* ($CaCO_{3(equiv.)}$) as the sole rate-controlling parameter during biogenic concrete corrosion. This assumption is simplistic and limited with regard to a broader range of binder systems such as blended PC and CAC, which are available for use in reducing biogenic concrete corrosion rates.

In order to improve the prediction capability of the LFM for a broader range of binders and aggregate types, it is paramount that all the *significant* parameters in both CAC- and PC-based concrete mixtures are correlated with the average biogenic corrosion rates. In this regard, three proposals are made: (i) that the parameters based on stoichiometry provide the *neutralisation capacity (NC)* of concrete mixtures – refer to Equations 2.60 and 2.65, (ii) that the parameters based on SEM/EDS point analyses define the characteristics of the hydrated binder paste, and provide the *bacteriostatic effect* to acid generating bacteria – see Section 2.5.2, and (iii) that the summation of parameters in (i) and (ii) provide the *general effective resistance capacity* ($RC_{eff, gen.}$) of concrete mixtures.

The *general effective resistance capacity* ($RC_{eff, gen.}$), based on Figure 6-1 to Figure 6-6 can be defined as (Equation 6.5):

$$RC_{eff, gen.} = \underbrace{a(CaCO_{3(equiv., agg)}) + b(CH_{(equiv., binder)}) + c(AH_{3(equiv., binder)}) + d(FeO(OH)_{(equiv., binder)})}_{\text{Provides neutralisation capacity}} + \underbrace{e(Al/Ca) + f(Fe/Ca)}_{\text{Provides bacteriostatic effect}} \quad (6.5)$$

where *a, b, c, d, e,* and *f* are multiple regression correlation constants (see details in Appendix L.8), and these are presented in Table 6-3. Figure 6-7 shows the correlation between biogenic corrosion rates and $RC_{eff, gen.}$ of concrete mixtures derived in the current study (see data in Table 6-1).

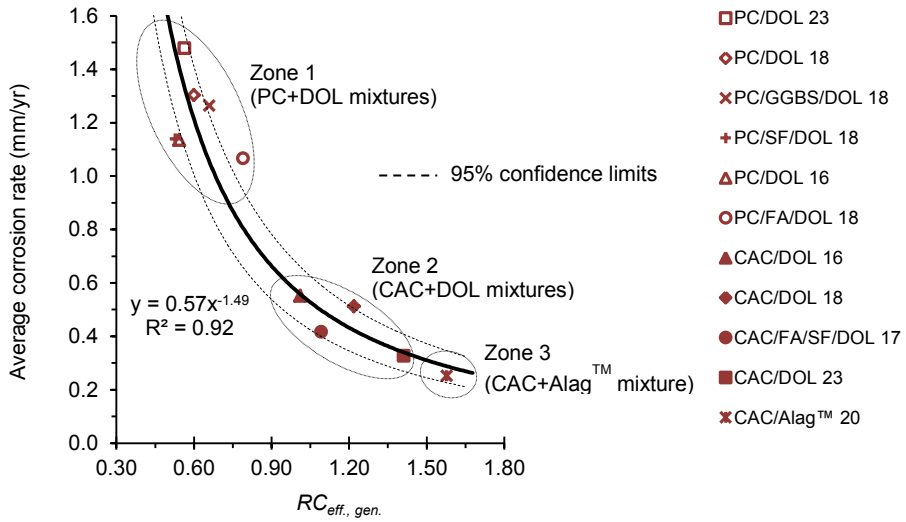

Figure 6-7: Correlation between biogenic corrosion rates and $RC_{eff., gen.}$ of concrete mixtures derived in the current study

Table 6-3: Coefficients for Equation 6.5, used to define the *general effective resistance capacity* of concrete mixtures used in the manufacture of sewer pipes.

Parameter	Coefficients[#]					
	a	*b**	*c*	*d*	*e*	*f*
$CaCO_{3(equiv., agg)}$	-9.52 ± 5.31	-	-	-	-	-
$CH_{(equiv., CAC)}$	-	-0.38 ± 2.68	-	-	-	-
$CH^{-1}_{(equiv., PC)}/100$	-	1.68 ± 0.32	-	-	-	-
$AH_{3(equiv., binder)}$	-	-	-6.31 ± 5.56	-	-	-
$FeO(OH)_{(equiv., binder)}$	-	-	-	-9.27 ± 26.82	-	-
Al/Ca	-	-	-	-	0.84 ± 0.18	-
Fe/Ca	-	-	-	-	-	-2.8 ± 1.22

*For the $RC_{eff.}$ of CAC-based mixtures, input values for $CH_{(equiv., CAC)} \geq 0$ and those for $CH^{-1}_{(equiv., PC)} = 0$; for PC-based mixtures, input values for $CH_{(equiv., CAC)} = 0$ and those for $CH^{-1}_{(equiv., PC)} > 0$

[#]Variability is based on multiple regression correlation between the *significant* parameters summarised in Table 6.2, and the minimum and maximum biogenic corrosion rates (as calculated in Appendix L.2).

The following can be noted from the correlations presented in Figure 6-7, Table 6-3 and the discussions in Section 5.7:

(i) The biogenic corrosion rate of concrete mixtures can be predicted based on the characteristics of the respective materials falling within three distinct zones (although a fourth zone is also hypothesised to occur as highlighted below).

   a. Zone 1 – the key governing factors are based on the CaO content. They include the inverse of the CH content in binders, and the $CaCO_3$ content in the aggregate. This implies that the use of acid-soluble aggregate plays a major role in PC-based concrete mixtures involved in biogenic corrosion mechanisms. This zone applies for PC/DOL mixtures.

      It is hypothesised that in cases where acid-insoluble aggregates are used (with negligible $CaCO_3$ content), a fourth zone (termed 'Zone 4') would occur, defined by higher corrosion rates and lower $RC_{eff, gen.}$ than those of Zone 1 (see Figure 6-8).

   b. Zone 2 – the key governing factors are based on the Al and Fe content. They include AH_x and FeO(OH), where the former is deemed to play a more active role in neutralising the attacking acid and the latter in providing a *bacteriostatic effect* to acid generating bacteria. In this zone, the influence of the natural aggregate type is negligible, and it therefore applies for both CAC+DOL and CAC+SIL mixtures.

c. Zone 3 – the key governing factors are similar to those in Zone 2. Moreover, from the BSE micrographs presented in Chapter Five, the concrete mixture in this zone shows a more homogenous microstructure with an inferred absence of the ITZ due to the use of an artificial aggregate, such as Alag™ which has a similar chemical composition as the binder (CAC). Therefore, this particular zone is characterised by concrete mixtures whose microstructure has an inferred absence of the ITZ and an even higher content of Al and Fe.

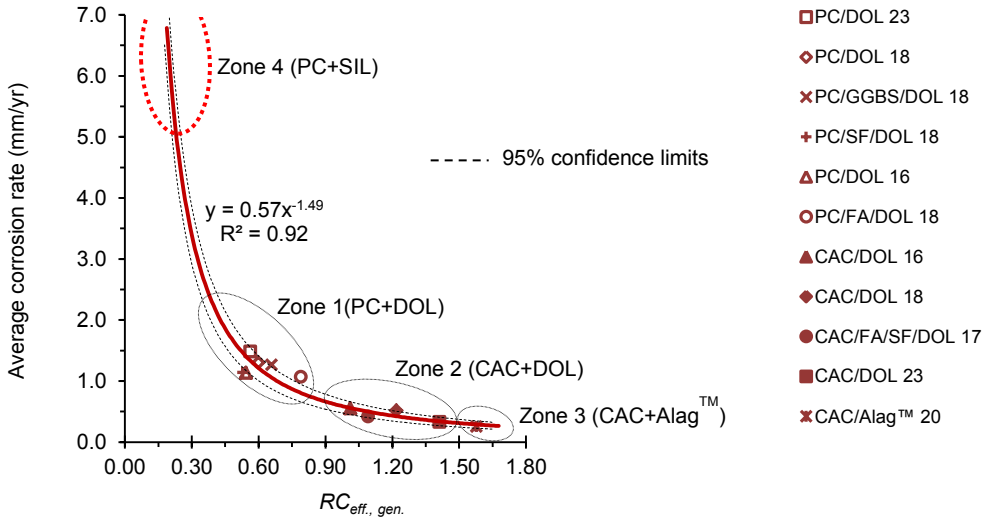

Figure 6-8: 'Zone 4' that can be applied for biogenic corrosion prediction of PC/SIL based concrete mixtures

(ii) The existence of the proposed Zone 4 for application in biogenic corrosion prediction of PC/SIL based concrete mixtures can be validated by corrosion rates measured and reported by Goyns (2003) – see Table 3-5.

(iii) The correlations, expressed by a general relationship in Equation 6.6, can be used in biogenic corrosion prediction. Considering 95% confidence limits, the variability of Equation 6.6 can be defined by Equations 6.7 and 6.8.

$$c_{avg(T,RH,H_2S,t)} = 4.57 - 9.52\left(CaCO_{3(equiv.,agg)}\right) - 0.38\left(CH_{(equiv.,CAC)}\right) + 1.68\left(\frac{CH^{-1}_{(equiv.,PC)}}{100}\right) - 6.31\left(AH_{3(equiv.,binder)}\right) - 9.27\left(Fe(OH)_{2(equiv.,binder)}\right) + 0.84\left(\frac{Al}{Ca}\right) - 2.80\left(\frac{Fe}{Ca}\right) \quad \text{(mm/yr.)} \quad (6.6)$$

$$c_{\min(T,RH,H_2S,t)} = 2.27 - 4.21\left(CaCO_{3(equiv.,agg)}\right) - 3.07\left(CH_{(equiv.,CAC)}\right) + 1.37\left(\frac{CH^{-1}_{(equiv.,PC)}}{100}\right) - 11.88\left(AH_{3(equiv.,binder)}\right) + 17.54\left(Fe(OH)_{2(equiv.,binder)}\right) + 1.02\left(\frac{Al}{Ca}\right) - 1.58\left(\frac{Fe}{Ca}\right) \quad \text{(mm/yr.)} \quad (6.7)$$

$$c_{\max(T,RH,H_2S,t)} = 6.86 - 14.83\left(CaCO_{3(equiv.,agg)}\right) + 2.30\left(CH_{(equiv.,CAC)}\right) - 2.00\left(\frac{CH^{-1}_{(equiv.,PC)}}{100}\right) - 0.75\left(AH_{3(equiv.,binder)}\right) - 36.11\left(Fe(OH)_{2(equiv.,binder)}\right) + 0.66\left(\frac{Al}{Ca}\right) - 4.01\left(\frac{Fe}{Ca}\right) \quad \text{(mm/yr.)} \quad (6.8)$$

In order to use Equations 6.6 to 6.8, for the $RC_{eff.,\ gen.}$ of CAC-based mixtures, input values for $CH_{(equiv.,\ CAC)} \geq 0$ and those for $CH^{-1}_{(equiv.,\ PC)} = 0$; for PC-based mixtures, input values for $CH_{(equiv.,\ CAC)} = 0$ and those for $CH^{-1}_{(equiv.,\ PC)} > 0$.

The coefficients '4.57' (for $c_{avg.}$), '2.27' (for $c_{min.}$), and '6.87' (for $c_{max.}$) in Equations 6.6, 6.7, and 6.8 respectively are Y-intercepts obtained from multiple regression analysis as described in Appendix L.8. It is important to note that (a) the average biogenic corrosion rate, $c_{avg.}$ is also dependent on the temperature (T), RH and H_2S concentration in the sewer environment, and (ii) corrosion of PC-based concrete mixtures commence approximately 2 years (t) before CAC-based concrete mixtures under similar exposure conditions (see Section 5.3, Figure 5-1). Although the influence of sewer headspace temperature and RH is not considered in the current form of the LFM, the current study will propose a factor to address this gap.

(iii) Equation 6.6 can also be used to generate a biogenic concrete corrosion prediction profile, defined by the following alternative Equation 6.9 (refer to equation of line in Figure 6-7):

$$c_{avg,t} = \frac{0.57}{(RC_{eff.})^{1.49}} \tag{6.9}$$

where c_{avg} = average corrosion rate (mm/year)
t = time at start of corrosion. For PC, t = 0; for CAC, t = +2 years
$RC_{eff.}$ is defined by Equation 6.10.

$$RC_{eff.} = (CaCO_{3(equiv., agg)}) + (CH_{(equiv., CAC)}) + (CH^{-1}_{(equiv., PC)})/100) + (AH_{3(equiv., binder)}) + (FeO(OH)_{(equiv., binder)}) + (Al/Ca) + (Fe/Ca) \tag{6.10}$$

where, for CAC-based mixtures, input values for $CH_{(equiv., CAC)} \geq 0$ and those for $CH^{-1}_{(equiv., PC)} = 0$; for PC-based mixtures, input values for $CH_{(equiv., CAC)} = 0$ and those for $CH^{-1}_{(equiv., PC)} > 0$

Before proceeding, it is important to clarify that when Equation 6.10 is substituted in Equation 6.9, the resultant prediction curve is the same as that defined by Equation 6.6. Moreover, unlike Equation 6.6, Equation 6.9 has similarities with the LFM equation for corrosion prediction (see Equation 2.77), as shown in Table 6-4. It is for this reason that Equation 6.9 has been adopted as a basis for improving the LFM.

Table 6-4: Similarity between the LFM and corrosion prediction equation developed in the current study.

Model description	Parameter related to the attacking media/component	Parameter related to the acid-neutralising component
$c_{avg} = 11.4k\frac{\phi_{sw}}{A}$ **	'$11.4k\,\phi_{sw}$'	A = $CaCO_{3(equiv.)}$
$c_{avg,t} = \frac{0.57}{(RC_{eff.})^{1.49}}$ *	'0.57'	$RC_{eff.} = (CaCO_{3(equiv., agg)}) + (CH_{(equiv., CAC)}) + (CH^{-1}_{(equiv., PC)})/100) + (AH_{3(equiv., binder)}) + (FeO(OH)_{(equiv.)}) + (Al/Ca) + (Fe/Ca)$

**The LFM
*Corrosion prediction equation developed in the current study

From Table 6-4, it can be seen that the parameters '0.57' and '$(RC_{eff.})^{1.49}$' in Equation 6.9 relate to '$11.4k\phi_{sw}$' and 'A' respectively in the LFM. These similarities will be explored in Section 6.3 with the view of improving the prediction capability of the LFM.

From the reviewed literature in Chapter Two (Part Three), it was highlighted that biogenic corrosion prediction models, both deterministic and statistical, incorporate only equivalent $CaCO_3$ ($CaCO_{3(equiv.)}$) as the rate-controlling parameter of the corrosion rate of concrete mixtures subjected to biogenic H_2SO_4 attack. However, from the review of studies in the VES (Chapter Three) and results presented in Chapter Five, it has been shown that additional rate-controlling parameters exist. Furthermore, it was also demonstrated (see Table 6-1 to Table 6-3, Figure 6-1 to Figure 6-7, and Equations 6.5 to 6.8) that the hypothesis argued by the LFM that higher equivalent $CaCO_3$ ($CaCO_{3(equiv.)}$) values result in lower biogenic corrosion rates is applicable only to certain PC-based mixtures, and that in fact, CH plays a more active role in biogenic attack mechanisms of PC-based mixtures. Therefore, correlations resulting in Equation 6.9 can be incorporated within the final equation of the LFM with the view of

improving its capability to predict biogenic concrete corrosion rates in sewers. This is undertaken in the following Section 6.3.

6.3 Practical application of microstructural characteristics of concrete mixtures in the LFM

The prediction of biogenic corrosion of concrete sewers is principally a two-step process. The first step entails prediction of the generation of H_2S in the sewer, and the second step entails prediction of the corrosion rate of the concrete pipe materials based on, among other factors, the concentration of H_2S in the sewer's headspace. Whereas the former has been widely researched and documented in other fields such as wastewater engineering and environmental microbiology, the latter has lagged particularly in view of advancement in the cement and SCMs industries. Therefore this section will focus on the materials aspect, particularly the final equation in the multi-equation LFM. In the LFM, the average biogenic corrosion rate is given as (Equation 6.11):

$$c_{avg} = 11.4k\frac{\phi_{sw}}{A} \tag{6.11}$$

where c_{avg} = average corrosion rate (mm/year)
ϕ_{sw} = average H_2S flux to the moist pipe wall (g/m^2/h)
A = alkalinity of the concrete material (g $CaCO_3$ per g concrete material)
k = efficiency factor < 1 (rate constant for H_2S adsorption and oxidation kinetics as a function of temperature and air-flow (Reynolds number)). For systems where ϕ_{sw} is 'low' (such as in large diameter (> 1 m) pipes with less condensate forming on their walls), the value of k approaches 1; for systems where ϕ_{sw} is 'high' (such as in smaller diameter (< 1 m) pipes with more condensate forming on their walls), k may decrease to about 0.3.

Despite the fact that the LFM was developed, principally based on PC-based mixtures, opportunities exist to improve the characterisation of other concrete mixtures with regard to their interaction mechanisms (neutralisation capacity) with the attacking acid, and to incorporate these into the LFM.

The following proposals are made to improve the biogenic corrosion capability of the LFM, based on the studies undertaken in the VES and Figure 6-7;

(a) Introduce a general 'sewer headspace aggressiveness' factor, q, which is hypothesised to introduce the influence of sewer headspace temperature and RH into the LFM, although at this particular point, this factor has not been characterised. For the data relating to the VES, q equates '$11.4k\,\phi_{sw}$' to '0.57' (see Table 6-4), such that numerator part of the *Improved LFM* is of the form '$11.4k\,\phi_{sw}\,q$' (=0.57).
(b) Substitute for the *alkalinity* component 'A' in the denominator part of the LFM with the *alternative effective resistance capacity* '$(RC_{eff.})^{1.49}$,
(c) Therefore, the general *Improved LFM* is of the form:

$$c_{avg,t} = 11.4k\frac{\phi_{sw}}{\left(RC_{eff.}\right)^{1.49}}q \tag{6.12}$$

where c_{avg} = average corrosion rate (mm/year)
t = time at start of corrosion. For PC, t = 0; for CAC, t = +2 years
ϕ_{sw} = average H_2S flux to the moist pipe wall (g/m^2/h)
k = efficiency factor < 1 (as defined in Equation 6.11).
q = sewer headspace aggressiveness factor
$RC_{eff.} = (CaCO_{3(equiv.,\,agg)}) + (CH_{(equiv.,\,CAC)}) + (CH^{-1}_{(equiv.,\,PC)})/100) + (AH_{3(equiv.)}) + (FeO(OH)_{(equiv.)}) + (Al/Ca) + (Fe/Ca)$,
for CAC-based mixtures, input values for $CH_{(equiv.,\,CAC)} \geq 0$ and those for $CH^{-1}_{(equiv.,\,PC)} = 0$; for PC-based mixtures, input values for $CH_{(equiv.,\,CAC)} = 0$ and those for $CH^{-1}_{(equiv.,\,PC)} > 0$

In order to find the 'sewer headspace aggressiveness' factor for the VES, the values for k (= 0.65), and ϕ_{sw} (= 0.0875 g/m^2/h (= 35 ppm H_2S)) were incorporated in the numerator part of the *Improved LFM*, and this was equated to '0.57' in order to solve for q (Equation 6.13).

$$11.4k\,\phi_{sw}\,q = 11.4(0.65)(0.0875)q = 0.57;\ q = 0.88 \tag{6.13}$$

Therefore, in order to predict the biogenic concrete corrosion rate in conditions similar to those in the VES, the applicable *Improved LFM* is of the form;

$$c_{avg,t} = 11.4k\,\frac{\phi_{sw}}{(RC_{eff.})^{1.49}}(0.88) \tag{6.14}$$

Table 6-5 gives a summary of comparative predicted biogenic corrosion rates based on two methods, the LFM (Equation 6.11) and the *Improved LFM* (Equation 6.14). This comparison is also presented in Figure 6-9.

Table 6-5: Summary of predicted biogenic corrosion rates based on the LFM and 'improved LFM'.

Mixture	Predicted biogenic corrosion rate (mm/yr.)	
	Based on the LFM	Based on the *Improved LFM*
CAC/Alag^{TM}	1.61	0.33
CAC/DOL 23	1.32	0.39
CAC/FA/SF/DOL 17	1.49	0.57
CAC/DOL 18	1.36	0.48
CAC/DOL 16	1.38	0.64
PC/FA/DOL 18	1.26	0.90
PC/DOL 16	1.19	1.23
PC/SF/DOL 18	1.18	1.50
PC/GGBS/DOL 18	1.21	1.29
PC/DOL 18	1.15	1.51
PC/DOL 23	1.08	1.58

Other parameters used in the LFM:
- H_2S concentration in the VES (see Table 5-4) = 35 ppm (= 0.0875 g/m^2/h, considering a surface area of 1 m^2, penetration depth of sulphur-based species of approx. 1 mm (estimated from elemental mapping for S) and density of concrete of 2500 kg/m^3)
- Efficiency factor, k = 0.65 (considering a 0.9 m dia. sewer with RH of approx. 75%)

The following can be noted from the comparison given in Table 6-5 and predictions given in Figure 6-9:

(i) The closest correlation between the predicted biogenic corrosion rates based on the LFM, and the measured values is for concrete mixtures with approximately 16% PC (and 16.5% PC + 1.5% SF) with dolomite (acid-soluble) aggregate. This means that, in its current form, the LFM can reliably be used to predict biogenic corrosion rates for concrete mixtures with approximately 16% PC with dolomite aggregate, exposed to conditions similar to those in the VES.

(ii) The greatest variation between the predicted biogenic corrosion rates based on the LFM, and the *Improved LFM* is for concrete mixtures with 20% CAC with Alag^{TM}, and 23% CAC with dolomite aggregate. This means that since the rate-controlling parameter in the LFM is the equivalent $CaCO_3$ ($CaCO_{3(equiv.)}$), this model is not reliable in applications using binder systems other than 16% PC with dolomite aggregate.

(iii) According to the LFM, mixtures with 23% PC + dolomite aggregates have the least biogenic corrosion rate since they have the highest $CaCO_{3(equiv.)}$ value based on stoichiometry, while mixtures with 20% CAC + Alag^{TM} have the highest biogenic corrosion rate since they have the least $CaCO_{3(equiv.)}$ value based on stoichiometry (excluding mixtures with siliceous aggregate). However, both the measured corrosion rates, and those predicted based on the *improved LFM* show the exact opposite of predictions based on the LFM.

(iv) The *Improved LFM* as proposed in the current study reliably predicts the biogenic concrete corrosion rates of different binder systems for conditions similar to those in the VES. Furthermore, q can be characterised (considering sewer headspace temperature and RH) for application in other sewer environments.

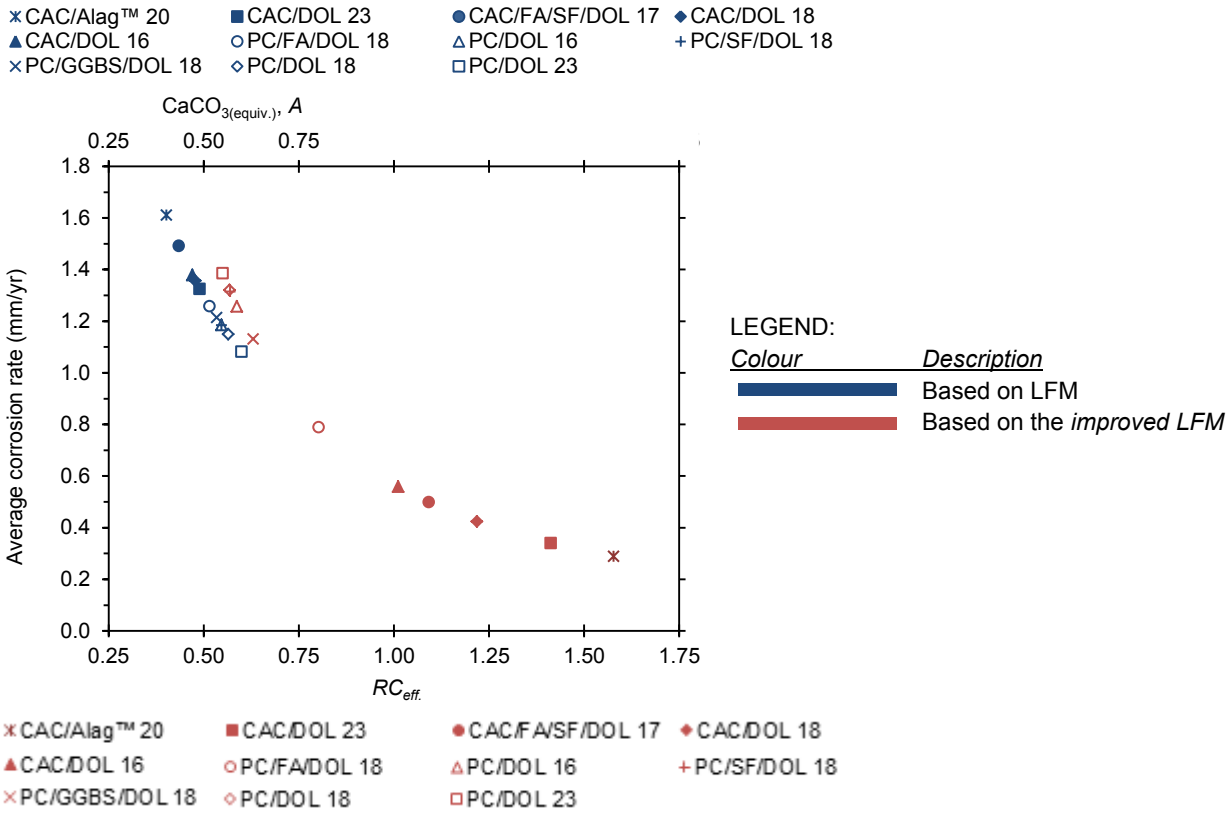

Figure 6-9: Comparison of predicted $c_{avg.}$ based on the LFM and 'improved LFM' proposed in the current study.

6.4 Summary - proposed modification to the LFM

This chapter presented proposed improvements to the existing LFM (EPA, 1985), based on (i) the chemical composition of various plain and blended PC- and CAC-based mixtures, (ii) microstructural characteristics of concrete mixtures used in the manufacture of concrete sewer pipes, and (iii) a sewer headspace aggressiveness factor based on the characteristics of the sewer temperature and RH.

In summary, the proposals presented in this chapter show that:

(1) In its current form, the LFM can be used to predict the biogenic corrosion rate of PC-based concrete mixtures with approximately 16% PC content with dolomite aggregate.

(2) In order for the LFM to be applied to a wider range of binder systems, improvements are required on the *alkalinity* component ($CaCO_{3(equiv.)}$) by incorporating other rate-controlling parameters, namely ($CH_{(equiv.)}$, $AH_{3(equiv.)}$ and $FeO(OH)_{(equiv.)}$). Moreover, since it has been shown that the biogenic corrosion rate is directly proportional to $CH_{(equiv.)}$), values of $CH^{-1}{}_{(equiv.)}$ should be used in calculating the *effective resistance capacity* of concrete mixtures to be applied in the LFM because of the inverse relationship of corrosion rate and *neutralisation capacity* of concrete mixtures.

(3) The *Improved LFM* can be expressed as:

$$c_{avg,t} = 11.4k\frac{\phi_{sw}}{(RC_{eff.})^{1.49}}q \qquad (6.15)$$

where c_{avg} = average corrosion rate (mm/year); t = time at start of corrosion (for PC, t = 0; for CAC, t = +2 years); ϕ_{sw} = average H_2S flux to the moist pipe wall (g/m^2/h); k = efficiency factor (< 1); q = sewer headspace aggressiveness factor (=0.88 for VES)

$RC_{eff.} = (CaCO_{3(equiv.,\ agg)}) + (CH_{(equiv.,\ CAC)}) + (CH^{-1}{}_{(equiv.,\ PC)})/100) + (AH_{3(equiv.)}) + (FeO(OH)_{(equiv.)}) + (Al/Ca) + (Fe/Ca)$,

for CAC-based mixtures, input values for $CH_{(equiv.,\ CAC)} \geq 0$ and those for $CH^{-1}{}_{(equiv.,\ PC)} = 0$; for PC-based mixtures, input values for $CH_{(equiv.,\ CAC)} = 0$ and those for $CH^{-1}{}_{(equiv.,\ PC)} > 0$

(4) For the concrete mixtures (with dolomite aggregates) investigated in the current study, calculated values of $RC_{eff,}$, from stoichiometry and EDS elemental analyses are summarised in Table 6-6.

Table 6-6: Summary of values of $RC_{eff.}$ for concrete mixtures used in the manufacture of sewer pipes in South Africa

Mixture*	$RC_{eff.}$
CAC/Alag™	1.58
CAC/DOL 23	1.41
CAC/FA/SF/DOL 17	1.09
CAC/DOL 18	1.22
CAC/DOL 16	1.01
PC/FA/DOL 18	0.80
PC/DOL 16	0.59
PC/SF/DOL 18	0.57
PC/GGBS/DOL 18	0.63
PC/DOL 18	0.57
PC/DOL 23	0.55

*See details in Appendix E.

Figure 6-10 shows a comparison of prediction curves for average biogenic corrosion rates based on the LFM, and the *Improved LFM* as proposed in the current study, with 95% confidence limits.

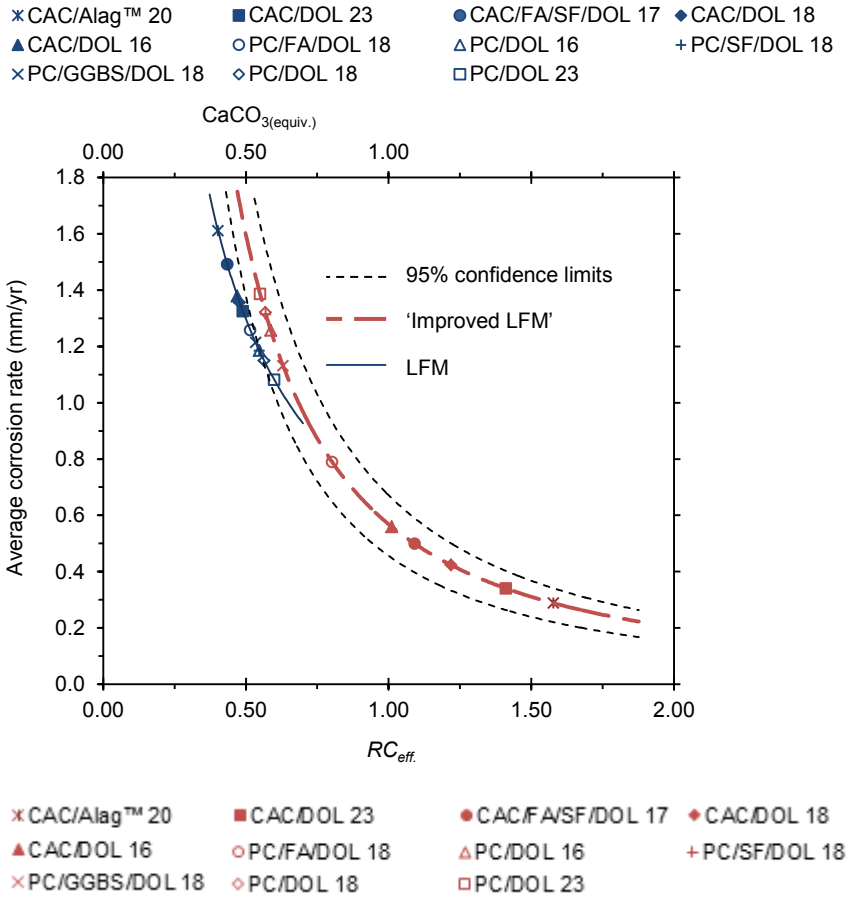

Figure 6-10: Comparison of prediction curves for average biogenic corrosion rates based on the LFM and *Improved LFM* as proposed in the current study.

6.5 Application of the improved LFM in predicting biogenic corrosion rate of concrete sewer pipes – an example

The aim of this example is to illustrate how practising engineers can apply the *Improved LFM* in predicting the biogenic corrosion rate (or thickness of the sacrificial layer) of (new) concrete sewer pipes. The main assumption in this example is that the initial equations that are used to predict sulphide build-up in the sewage and hydrogen sulphide release from the sewage (Equations 2.67 to 2.73) are valid. This is a fair assumption based on the H_2S concentration in the entrance manhole of the VES (approximately 50 ppm) that has been monitored since 1989. This concentration is based on predictions using Equations 2.67 to 2.73 (CSIR, 1996; Goyns, 2001; Goyns, 2010; Goyns, 2014).

This example will consider five concrete mixtures; three PC-based (PC/SIL 16, PC/DOL 16 and PC/DOL 23) and two CAC-based (CAC/DOL 16 and CAC/DOL 23) to be used in an 800 mm diameter outfall sewer with an expected headspace H_2S concentration of approximately 40 ppm. See a summary of various sewer parameters in Table 6-7. These parameters have been intentionally selected to fit the basis of the *Improved LFM* given in Equation 6.14.

Table 6-7: Summary of parameters used in example.

Characteristics of the sewer					Other parameters required in the *Improved LFM**		
Sewer dia. (mm)	Density of concrete (kg/m^3)	$H_2S^{\#}$ (ppm)	Temperature$^{\#}$ (°C)	RH$^{\#}$ (%)	k	φ_{sw} (g/m^2/h)	q
800	2500	40	20	72	0.5	0.10	0.88

*Typical values of k = 0.3 – 1.0; φ_{sw} value (= 0.10 g/m^2/h) equivalent to an H_2S concentration of 40 ppm; q value is for environments with similar sewer headspace temperature and RH as the VES

$^{\#}$Annual average

Applying the proposed biogenic corrosion prediction model in Equation 6.14, and the parameters in Table 6-6 and Table 6-7, respective corrosion rates were calculated – see summary of expected corrosion rates in Table 6-8 and Figure 6-11. Before proceeding, it is important to note that for the PC/SIL 16 mixture used in this example, the assumption is that all the mix proportions are similar to those of PC/DOL 16 except for the substitution of the coarse aggregate fraction, where dolomitic stone is replaced by siliceous stone. In this regard, $CaCO_{3(equiv.,agg)}$ is taken as zero, thus $RC_{eff.}$ = 0.22.

Table 6-8: Summary of expected corrosion rates based on the *Improved LFM*.

Mixture	$c_{avg(pred.)}$ (mm/yr.)
CAC/DOL 23	0.32
CAC/DOL 16	0.53
PC/DOL 16	1.20
PC/DOL 23	1.32
PC/SIL 16	5.01

The expected corrosion rates given in Table 6-8 can then be used to estimate the thickness of the sacrificial layer required for a given service (design) life of a new sewer as shown in Figure 6-11. It is also possible to estimate the remaining service life (RSL) (from Figure 6-11) of a concrete sewer with known parameters such as those presented in Table 6-7.

In this example, it can be seen that, in case of a new 800 mm diameter sewer with (i) a design life of 40 years, (ii) a predicted or measured annual average H_2S concentration of 40 ppm in the sewer's headspace, (iii) an average sewer temperature of approximately 20 °C, and (iv) an average sewer RH of approximately 72%, the required thicknesses of a sacrificial layer made from a CAC/DOL 23, CAC/DOL 16, PC/DOL 16, or PC/DOL 23 concrete mixture are 12 mm, 20 mm, 47 mm, or 53 mm respectively. Moreover, it can be seen that for a PC/SIL mixture with 16% cement, it will take approximately 14 years for the biogenic acid to corrode a 70 mm thick sewer pipe made from this mixture.

The chart presented in Figure 6-11 lends itself to engineering and economic comparisons, based on concrete material properties and expected service lives of respective infrastructure such as sewer pipes. The chart also portrays a 'quality vs. quantity' scenario that can be utilised by design engineers and asset managers in selecting appropriate materials for sewer pipe applications.

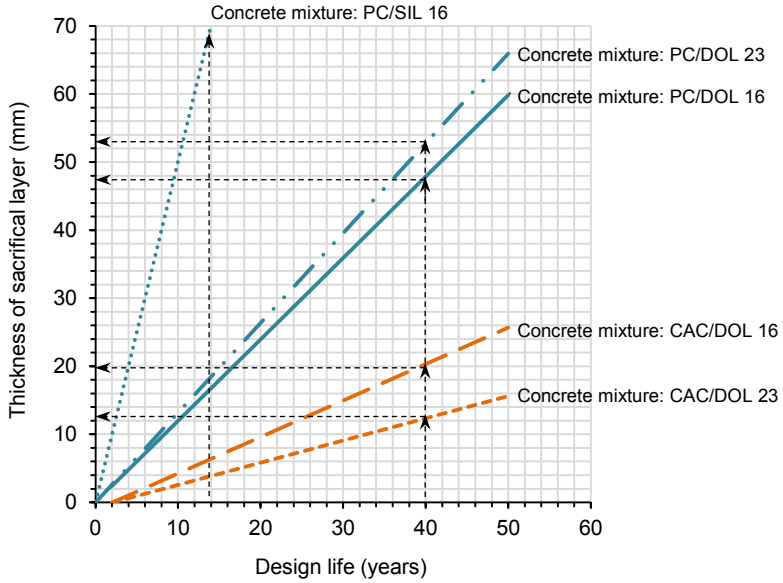

Figure 6-11: Estimating the thickness of a sacrificial layer in concrete sewer pipes based on the *Improved LFM*.

6.6 Critique of the *Improved LFM*

The main aims of the current study were (i) to critically review the widely used deterministic (mechanistic) biogenic corrosion prediction model – the LFM, with the view of improving it based on the microstructural studies of certain concrete mixtures used in the manufacture of concrete sewer pipes, and (ii) to demonstrate that the *Improved LFM* is a practical tool for design engineers with regard to adaptation to the cement and SCM industries. Even though these aims have been sufficiently addressed, there are certain aspects that still need to be addressed. The following section summarises the strengths and weaknesses of the *Improved LFM.*

(1) The strengths of the *Improved LFM* include:

a. The ability to predict biogenic concrete corrosion rates with much greater accuracy based on a wider scope of material properties such as those of blended PC and CAC, that can be incorporated in the model.

b. Provision of a model framework that incorporates two important aspects of concrete mixtures when they are subjected to biogenic acid attack mechanisms; these are (i) the neutralisation capacity, and (ii) the bacteriostatic effect.

c. Provision of a model framework that allows for the application of material characteristics based on microstructural studies using advanced techniques such as scanning electron microscopy and energy dispersive spectroscopy.

d. Provision of a model framework that incorporates the influence of other significant parameters such as sewer headspace temperature and RH (in form of a 'sewer headspace aggressive factor', q) that are involved in biogenic concrete corrosion processes, although at this point, these parameters have not been characterised.

(2) The weaknesses of the *Improved LFM* include:

a. The hypothesis that iron (III) oxide-hydroxide provides a bacteriostatic effect to sulphide-oxidising bacteria is based on (i) the reviewed literature , and (ii) a higher composition of Fe_2O_3 in CAC than in PC, and based on the fact that CAC-based

binder systems experience lower biogenic corrosion rates than PC-based binder systems. This hypothesis needs to be investigated further.

b. The hypothesis that the 'sewer headspace aggressiveness' factor incorporates the influence of sewer headspace temperature and RH in biogenic corrosion prediction. Even though this parameter was not considered in the current LFM, it needs to be characterised.
c. The basis of the proposed *Improved LFM* is the current multi-equation LFM, which predicts biogenic corrosion at a constant rate (linear correlation), considering respective concrete mixtures. Despite the fact that this assumption gives relatively accurate predictions in the proposed model as demonstrated in this Chapter, the true non-linear nature of biogenic corrosion rates in general needs to be investigated further.

6.7 References

Alexander, M. G., Goyns, A. M., & Fourie, C. W. 2008. Experiences with a full-scale experimental sewer made with CAC and other cementitious binders in Virginia, South Africa. Proceedings of the Centenary Conference on Calcium Aluminate Cements. June 30 – July 2, Avignon. 279 – 292.

Council for Scientific and Industrial Research. 1996. *Consolidated report on phase 1 of sewer corrosion research: The Virginia sewer experiment and related research*. Pretoria: CSIR. Report No BOU/C128.

Environmental Protection Agency. 1985. Design manual: Odor and corrosion control in sanitary sewerage systems and treatment plants. Cincinnati: EPA.

Fourie, C. W. 2007. Acid resistance of sewer pipe concrete. MSc (Eng) dissertation. University of Cape Town, Cape Town.

Goyns, A. M. 2003. Virginia sewer rehabilitation: Progress Report 1. Pretoria: Concrete Manufacturers Association.

Goyns, A. M. 2010. Virginia sewer rehabilitation: Progress Report 4. Pretoria: Concrete Manufacturers Association.

Goyns, A. M. 2014. Virginia sewer rehabilitation: Progress Report 6. Pretoria: Concrete Manufacturers Association.

Goyns, A. M., Alexander, M. G., & Fourie, C. W. 2008. Applying experimental data to concrete sewer design and rehabilitation. *Proceedings of the Centenary Conference on Calcium Aluminate Cements.* June 30 – July 2, Avignon. 293 – 308.

Herisson, J. 2012. Biodeterioration of cementitious materials in the wastewater – Comparative study of calcium aluminate cement and Portland cement. PhD dissertation. Université Paris-Est, Paris.

Herisson, J., Guéguen-Minerbe, M., van Hullebusch, E. D., & Chaussadent, T. 2014. Behaviour of different cementitious material formulations in sewer networks. *Water Science and Technology*. 69(7): 1502 – 1508.

Navidi, W. 2006. *Statistics for engineers and scientists*. New York: McGraw-Hill.

Scrivener, K. L., & De Belie, N. 2013. Biogenic sulphuric acid attack of cementitious materials in sewage systems. In: Alexander, M., Bertron, A., & De Belie, N. Eds. *Performance of cement-based materials in aggressive aqueous environments: State-of-the-Art Report, RILEM TC 211-PAE*. Netherlands: Springer. 305 – 318.

Chapter Seven: Conclusions and recommendations for further work

7.1 Introduction

The main objective of the current study was to critically review the widely used deterministic (mechanistic) microbially-induced (biogenic) concrete corrosion prediction model – the Life Factor Method (LFM), with the view of improving its prediction capability based on the microstructural studies of concrete mixtures used in the manufacture of concrete sewer pipes.

Concrete sewers convey sewage which contains compounds such as sulphur (S) and nitrogen (N), which are the main energy sources needed for microbial growth-related processes in sewers and for maintaining the life of already existing biomass (Hvitved-Jacobsen et al., 2013). Both S- and N-compounds are capable of being oxidised to sulphate (SO_4^{2-}) and nitrate (NO_3^-) respectively. Initially, aerobic microorganisms flourish in the sewage but as oxygen used for catabolising organic compounds becomes depleted, anaerobic-anoxic microorganisms occur. It is these anaerobic-anoxic microorganisms such as heterotrophic anaerobic bacteria that are involved in the initial processes of biogenic corrosion mechanisms in sewers, by reducing SO_4^{2-} to sulphides (S^{2-}), and NO_3^- to nitrite (NO_2^-) (and eventually to ammonia (NH_3)) as alternative sources of oxygen (Hvitved-Jacobsen et al., 2013; Kohsaka et al., 2008).

Ammonia (from the nitrogen cycle) exists in the stale sewage as a gas, and it is not corrosive. On the other hand, sulphide exists in the stale sewage as sulphide ions (S^{2-}), hydrogen sulphide ions (HS^-), and hydrogen sulphide molecules (H_2S) both in aqueous and gaseous states, depending primarily on pH. At pH less than 7, H_2S predominates in aqueous solutions and is readily released into the sewer headspace especially under turbulent flow conditions in sewers flowing partly full.

The final processes of biogenic corrosion involve other aerobic microorganisms, namely, sulphide-oxidising bacteria (SOB) that flourish on the non-submerged moist walls of concrete sewers. SOB oxidise the available H_2S in the sewer's headspace to generate energy for assimilation of carbon for synthesis of cell materials, and in the process forms H_2SO_4 on the sewer pipe walls. This process is generally referred to as biogenic H_2SO_4 formation. Biogenic H_2SO_4 attacks the acid-soluble components in concrete matrices in two principle processes. The first process entails destruction of the calcium hydroxide (CH) and substituting a larger molecule (calcium sulphate ($C\bar{S}$)) into the concrete matrix thus causing pressure and spalling of the adjacent concrete and aggregate particles. In the second process, $C\bar{S}$ precipitates as gypsum ($C\bar{S}H_2$) and reacts with various aluminates to form secondary ettringite ($C_6A\bar{S}_3H_{32}$ - AFt). These mechanisms lead to the loss of stiffness and strength, followed by expansion and cracking, and eventually transformation of the affected concrete matrix into a soft and pulpy non-cohesive layer (Sahmaran, 2010).

Concrete sewer pipes can be manufactured from different binder systems such as Portland cement (PC) -based and calcium aluminate cement (CAC) -based. However, due to the different chemical composition of these binders, they form different products of hydration, which react differently when subjected to biogenic acid attack. The major hydrates of PC are calcium hydroxide (CH) and calcium silicate hydrates (C-S-H), and when these are subjected to biogenic H_2SO_4 attack, they are completely transformed to $C\bar{S}$ by four moles of acid (Equation 7.1).

$$CH + H_2SO_4 \rightarrow C\bar{S} + 2H \quad (7.1(a))$$

$$C-S-H + H_2SO_4 \rightarrow C\bar{S} + S + 2H \quad (7.1(b))$$

On the other hand, the major hydrates in CAC are the hydrogarnet (CAH_{10}, C_2AH_8, and C_3AH_6), gibbsite (alumina gel) (AH_3) and CH. When these hydrates are subjected to biogenic H_2SO_4, they are transformed in more phases than PC. The transformation of CH in CAC is similar to that in PC

systems. For the other phases, the dissolution of the calcium component of the hydrogarnet leads to the creation of additional quantities of AH_3 (Equation 7.2), which reacts further with H_2SO_4 to form aluminium sulphate ($Al_2(SO_4)_3$) (Equation 7.3).

$$CAH_{10} + H_2SO_4 \rightarrow C\bar{S} + AH_3 + 9H \quad (7.2(a))$$

$$C_2AH_8 + 2H_2SO_4 \rightarrow 2C\bar{S} + AH_3 + 9H \quad (7.2(b))$$

$$C_3AH_6 + 3H_2SO_4 \rightarrow 3C\bar{S} + AH_3 + 9H \quad (7.2(c))$$

$$2AH_3 + 3H_2SO_4 \rightarrow Al_2(SO_4)_3 + 12H \quad (7.3)$$

Therefore, in general, up to approximately 18 more moles of acid are required to transform the CAC hydrates in comparison to the PC hydrates. This means that CAC-based systems have a higher acid neutralisation capacity than PC-based systems.

The LFM, which was developed principally based on plain PC, is a series of relationships that consider sulphide generation within the sewage and hydrogen sulphide (H_2S) release from the sewage, and relates these to the concrete corrosion rate via two functions; (i) the rate of H_2S consumption (through auto-oxidation and by SOB) on the moist concrete surface, and (ii) the *alkalinity* of the concrete materials, expressed as $CaCO_3$ equivalent, which neutralises the attacking acid. However, neutralisation of biogenic H_2SO_4 attack in binder systems that are Al-rich, such as CAC and PC/fly ash (PC/FA) blends involves other hydrates (AH_x). Therefore, in order for the LFM to be applied to other binder systems such as blended PC and CAC, the characterisation of the acid-neutralising component (alkalinity) needs to be improved. The current study focusses on the acid-neutralising component of various binder systems, with the view of improving the ability to predict the design life of concrete sewers by improving the input parameters in the LFM.

In order to achieve the main objective stated above, the current study was divided into three broad categories, (i) characteristics of the sewer environment, (ii) microstructural characteristics of concrete mixtures subjected to biogenic H_2SO_4 attack in a 'live' sewer, and (iii) proposed improvements to the LFM based on the characteristics in (i) and (ii) above. Therefore the conclusions presented in this chapter are based on these broad categories. Finally, recommendations for further work are also presented in this chapter based on various aspects emanating from the current study.

7.2 Conclusions – characteristics of the sewer environment

The conclusions made from the characteristics of the sewer environment were principally based on a critical review of literature and also on some experimental results. The main objective of reviewing the characteristics of the sewer environment was to highlight the key parameters that influence biogenic corrosion mechanisms, and which form part of the proposed improvements to the LFM as discussed in Section 7.4.

The literature review highlighted that sewer hydraulics, which includes flow velocity, depth of flow, and system turbulence, is one of the significant parameters that influences biogenic corrosion processes. Low flow velocities (typically < 0.6 m/s) with increasing depth of flow are favourable conditions for the establishment of biofilms below the daily sewage flow levels. Due to microbial activities within these biofilms, oxygen is depleted and anaerobic conditions occur. In the presence of both organic substances and SO_4^{2-}, biological production of H_2S occurs, mostly in the anaerobic zones of the biofilms. Therefore, factors that influence the rate of production of H_2S in the biofilms, the concentration of S^{2-} in the sewage, and the rate at which H_2S is released from the sewage include flow velocity, wetted perimeter, flow width, sewage pH, temperature, BOD (or COD) and turbulence.

In as much as these parameters vary in different environments, both geographical and operational, early-age microbial colonisation (see Section 5.9) based on surface pH vs. time profiles of similar samples installed in two different sewer environments, showed similar characteristics. This suggests that the aggressiveness of the sewer environment can be defined by a larger range of headspace H_2S concentration than that reported in literature by Goyns (2003), Alexander and Fourie (2008) and Herisson et al. (2014). This hypothesis is particularly related to the H_2S concentration profiles in the Virginia Experimental Sewer (VES) and manhole at Langa, which have similar sewer temperatures and RH. For example, during summer months (December to February) when sewer temperatures in both locations are favourable for biogenic acid generation (approximately 25 °C), H_2S concentration in the VES varies from approximately 20 ppm to 60 ppm, while in the manhole at Langa, it varies from approximately 5 ppm to 75 ppm; yet generally, the surface pH of concrete samples installed in these environments varies by less than a unit, approximately 180 days after installation.

In addition to the surface pH vs. time profiles, results from microbial speciation showed various phylogenetic relatives that thrive optimally at a pH range of between 2 and 7. Similar results were reported by Sand and Bock (1984), which indicate that the growth of acid-producing bacteria (at pH 5 to 1) requires a mutualistic relationship with certain heterotrophs (which grow at pH 6.5 to 4) that can degrade the organics excreted by the acid-producing bacteria. On the other hand, these results also show that complete destruction of certain PC-based binder matrices due to biogenic corrosion mechanisms does not require a consistently low acidic (pH < 2) environment as reported by Islander et al. (1991), Alexander and Fourie (2011) and Motsieloa (2013). For example, the surface pH measured on certain PC-based concrete samples installed in the VES, 6 months and 127 months after exposure to biogenic attack mechanisms were similar. In particular, the measured surface pH of PC/DOL concrete, 6 months and 127 months after exposure in a 'live' sewer was 4.18 – 2.49 and 4.01 – 2.96 respectively (see Table 5-6), yet after 127 months, these samples had lost approximately 11.2 mm of their wall thickness (a corrosion rate of approximately 1.1 mm/yr.) (see Table 5-2). This implies that such pH values (2 > pH < 4) on surfaces of PC-based concrete sewer pipes can lead to biogenic corrosion of a 25 mm concrete cover in approximately 25 years, which is less than the design life of sewer networks in South Africa, which is traditionally 40 years (Da Silva and Goyns, 2009).

7.3 Conclusions – microstructural characteristics and chemical composition of concrete mixtures exposed to biogenic H_2SO_4

The microstructure of concrete mixtures in the current study was studied using SEM/EDS, XRD and TGA techniques. Contrary to earlier studies by EPA (1974; 1985) and Hvitved-Jacobsen et al. (2013), which hypothesise that concrete mixtures with higher *alkalinity* (A), expressed as the equivalent $CaCO_3$ ($CaCO_{3(equiv.)}$) experience lower biogenic corrosion rates, results from the current study confirmed that this hypothesis is not valid, bearing in mind that CH plays a more active role than $CaCO_3$ in PC-based mixtures. Both CH and $CaCO_3$ are based on the calcium component in a given concrete matrix. From the S-Ca-Al concentration vs. depth profiles presented in Sections 5.4 and 5.5, it was shown that PC-based binder systems have higher calcium content ($CH_{(equiv.)}$ + $CaCO_{3(equiv.)}$) in the sound matrix than CAC-based binder systems (this was also shown by stoichiometry in Section 6.2), and yet they experience higher biogenic corrosion rates. The higher corrosion rate is attributed to (i) increased availability of both CH and C-S-H which are consumed by the attacking acid to form gypsum, and later secondary ettringite ($C_6A\bar{S}_3H_{32}$ - AFt) (Equation 7.4), and (ii) the deterioration mechanism based on the theory of crystallisation pressure, which hypothesises that there is an increase in the supersaturation of AFt in the pores of concrete matrices, which in turn, is proportional to the resultant crystallisation pressure subject to the respective gypsum thresholds (40 mol% for CAC and 56 mol% for PC) (Taber, 1916; Paulini, 1994; Bizzozero et al., 2014).

$$CH + H_2SO_4 \rightarrow C\bar{S} + 2H \quad (7.4(a))$$

$$C-S-H + H_2SO_4 \rightarrow C\bar{S} + S + 2H \quad (7.4(b))$$

$$C_3\overline{S_3}H_6 + C_3AH_{12} + H_{14} \rightarrow C_6A\overline{S_3}H_{32} \quad (7.4(c))$$

On the other hand, the S-Ca-Al concentration vs. depth profiles presented in Chapter Five also show that alternative binders such as CAC, which have lower calcium content but higher aluminium content in the sound matrix than PC, experience lower biogenic corrosion rates due to (i) a higher neutralisation capacity of their stable hydrates, particularly AH_3 (Equation 7.5), and (ii) limited amount of CH resulting in less crystallisation pressures for degrading the concrete matrix. The same effect of alumina could be attributed to the improved performance of PC/FA binder systems which showed less micro-cracks in the deteriorating matrix due to lower crystallisation pressures, in comparison to plain PC mixtures as presented in the BSE micrographs in Section 5.4.

$$C_3AH_6 + 3H_2SO_4 \rightarrow 3C\overline{S} + AH_3 + 9H \quad (7.5(a))$$

$$2AH_3 + 3H_2SO_4 \rightarrow Al_2(SO_4)_3 + 12H \quad (7.5(b))$$

Another significant result from the current study is the potential influence of Fe_2O_3. Even though it was not possible to characterise the Fe-phase to the same degree as S-Ca-Al phases due to the difficulty in characterising Fe-containing minerals in hydrated binders using standard techniques such as XRD and TGA (because of overlapping signals from Fe-containing phases with those of the respective Al analogs (Renaudin et al., 2015)), results presented in Chapter 5 and mechanistic correlations in Chapter 6 showed that concrete mixtures with a higher amount of Fe_2O_3 experienced lower biogenic corrosion rates. This suggests that the Fe-phase either (i) provides a bacteriostatic effect to acid-generating SOB (Soenen et al., 2012; Chatterjee et al., 2011; Trun and Gottesman, 1990), (ii) provides neutralisation capacity to the attacking acid, or (iii) both (i) and (ii). However, identification of which of these possible phenomena had a major effect on the biogenic corrosion rate was outside the scope of the current study, and was therefore not measured.

Moreover, the current study showed that the attack and/or resisting mechanisms of the respective hydrates in various binder systems during biogenic corrosion processes is dependent on the solubility and mobility of the various ions in these systems. For example, CH has a greater solubility (K_{sp} = 5.5 x 10^{-6}) compared with that of AH_3 (K_{sp} = 3.0 x 10^{-34}), and this has a particular effect in PC-based binder systems where the dissolution of the CH (which is a major hydrate) by the attacking acid leads to an increase in the porosity of the concrete matrix resulting in an accelerated rate of attack due to ingress of aggressive medium. The low solubility of AH_3 offers protection against acid attack, particularly in blended PC/FA and CAC-based binder systems.

Ca^{2+} ions have a higher mobility than the other ions, such as Fe^{3+} and Al^{3+} in any binder system. Furthermore, Al^{3+} ions diffuse in the opposite direction to Ca^{2+} and Fe^{3+} ions (De Keyser, 1955; Weisweiler et al., 1986; Kurdowski, 2014). Therefore, during the destruction of the hydrated cement paste (HCP) (i.e. decomposition of CH and decalcification of C-S-H in PC-based mixtures, and decomposition of CAH_{10}, C_2AH_8, C_3AH_6 and decalcification of C-A-H in CAC-based mixtures) by the attacking H_2SO_4, dissolution and leaching of Ca^{2+} ions from the sound matrix occurs leaving behind a calcium-deficient but aluminium-rich layer, which offers protection against acid attack, depending on the aluminium content of the binders.

In addition, the following conclusions can be made on the influence of the chemical composition of a concrete mixture in biogenic corrosion:

(1) $CH_{(equiv.)}$ + $CaCO_{3(equiv.)}$ of a concrete mixture are not the sole rate-controlling parameters in biogenic corrosion mechanisms. The overall neutralisation capacity of any concrete mixture in biogenic corrosion processes incorporates the influence of other parameters, which include Al-based and Fe-based phases.

(2) The influence of both AH_x and FeO(OH) hydrates in concrete mixtures is of greater significance than that of CH and $CaCO_3$ in suppressing biogenic corrosion rates.

7.4 Conclusions – proposed improvements to the LFM

The LFM was critically reviewed in the current study. From the review presented, the following were noted:

(i) The LFM can be used to predict total sulphide build-up in the sewage, and release to the sewer headspace relatively accurately, based on H_2S concentration levels measured in the inlet manhole to the VES.

(ii) $CaCO_{3(equiv.)}$ (*alkalinity*, A) is deemed to be the sole rate-controlling parameter of the predicted biogenic corrosion rates.

(iii) The LFM can be used to predict biogenic corrosion rates for PC-based concrete mixtures with 16% PC and dolomitic aggregate relatively accurately. This conclusion is based on comparative trends of predicted $c_{avg.}$ based on the LFM and *Improved LFM* as proposed in the current study – see Figure 7-1, and the hypothesised 'materials zones' as described in Figure 6-8.

(iv) Even though the LFM can be calibrated using either the crown corrosion factor (CCF), turbulence corrosion factor (TCF) or both factors, it would be inappropriate to apply these factors (some of which propose a factor of up to 10 in turbulent junctions – see Equation 7.6) without considering the influence of other chemical components or hydrates in various binder systems.

$$c_{max} = c_{avg} \times CCF \times TCF \qquad (7.6)$$

where c_{max} = maximum corrosion rate (mm/year)
c_{avg} = average corrosion rate based on the LFM (mm/year) (Equation 6.11)
CCF = crown corrosion factor, ranging from 1.5 to 2.0
TCF = turbulence corrosion factor, ranging from (i) 1.0 to 2.5 for areas with typical turbulent flow conditions, and (ii) 5.0 to 10.0 for turbulent junctions

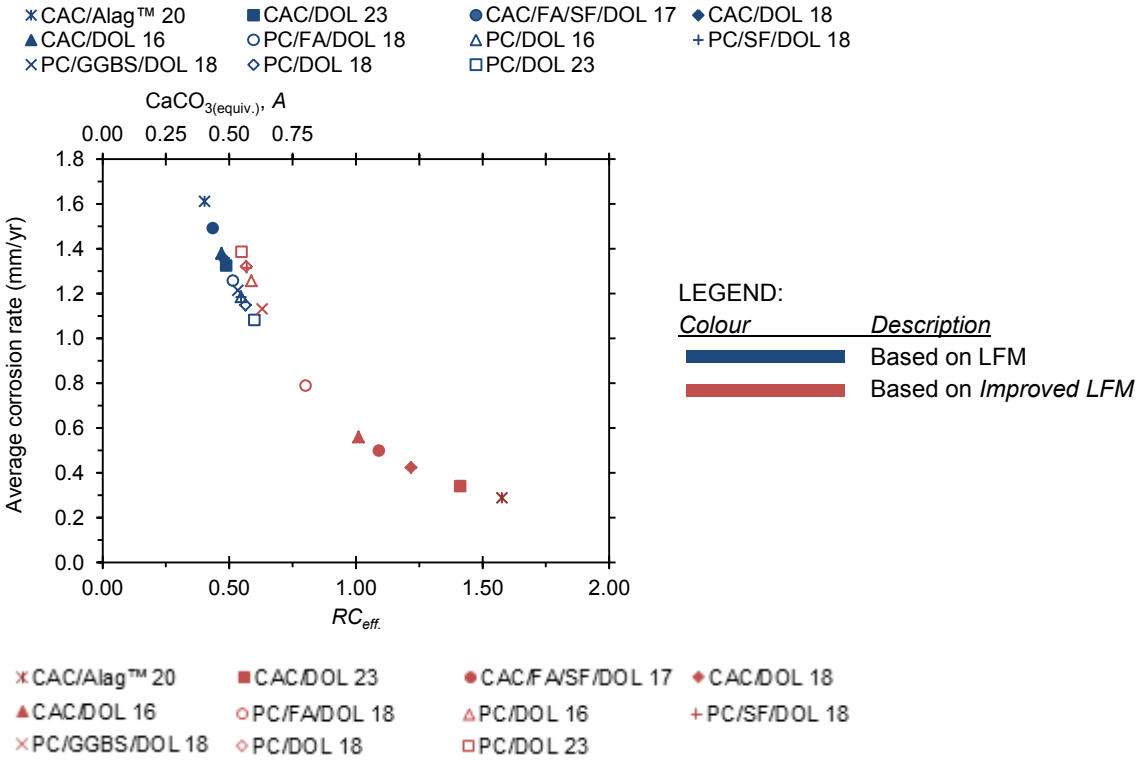

Figure 7-1: Comparison of predicted $c_{avg.}$ based on the LFM and *Improved LFM* proposed in the current study.

(v) From Figure 7-1, it can be seen that biogenic corrosion prediction based on the hypothesis of the LFM is not applicable to other binder systems, which include certain blended PC-based and CAC-based binder systems.

Based on the pros and cons of the LFM as highlighted in (i) to (v) above, the current study proposed improvements to the LFM based on stoichiometry and microstructure characteristics (SEM/EDS analysis) of various binder systems. However, before these improvements were effected, certain relationships were developed that can be used to predict biogenic corrosion rates, *c* in environments similar to the VES. *c* can be predicted using Equation 7.7, which is a shortened general form of Equations 6.6 to 6.8.

$$c = Y \pm RC_{eff.,\,gen.} \tag{7.7}$$

where c = biogenic corrosion rate (mm/yr.)
Y = Y-intercept (from regression analysis) (refer to Table 7-1)
$RC_{eff,\,gen.}$ = *general effective resistance capacity* defined by Equation 7.8.

$$RC_{eff,\,gen.} = \underbrace{a(CaCO_{3(equiv.,\,agg)}) + b(CH_{(equiv.,\,binder)}) + c(AH_{3(equiv.,\,binder)}) + d(FeO(OH)_{(equiv.,\,binder)})}_{\text{Provides } neutralisation\ capacity} + \underbrace{e(Al/Ca) + f(Fe/Ca)}_{\text{Provides } bacteriostatic\ effect} \tag{7.8}$$

where *a, b, c, d, e,* and *f* are multiple regression correlation constants, and these are also presented in Table 7-1.

Table 7-1: Coefficients for the Y-intercept in Equation 7.7, and for the *general effective resistance capacity* in Equation 7.8 of concrete mixtures used in the manufacture of sewer pipes.

Parameter	Coefficients					
	a	*b**	*c*	*d*	*e*	*f*
$CaCO_{3(equiv.,\,agg)}$	-9.52 ± 5.31	-	-	-	-	-
$CH_{(equiv.,\,CAC)}$	-	-0.38 ± 2.68	-	-	-	-
$CH^{-1}_{(equiv.,\,PC)}/100$	-	1.68 ± 0.32	-	-	-	-
$AH_{3(equiv.,\,binder)}$	-	-	-6.31 ± 5.56	-	-	-
$FeO(OH)_{(equiv.,\,binder)}$	-	-	-	-9.27 ± 26.82	-	-
Al/Ca	-	-	-	-	0.84 ± 0.18	-
Fe/Ca	-	-	-	-	-	-2.8 ± 1.22

#Intercept for $c_{avg.}$ = 4.57 ± 2.3 (i.e. for $c_{max.}$ = 6.87; for $c_{min.}$ = 2.27)

*For the $RC_{eff.}$ of CAC-based mixtures, input values for $CH_{(equiv.,\,CAC)} \geq 0$ and those for $CH^{-1}_{(equiv.,\,PC)} = 0$; for PC-based mixtures, input values for $CH_{(equiv.,\,CAC)} = 0$ and those for $CH^{-1}_{(equiv.,\,PC)} > 0$

#The intercept is used together with the *effective resistance capacity* to calculate the corrosion rates

For example, in order to predict the average biogenic corrosion rate, $c_{avg.}$ in environments similar to the VES, Equation 7.9, which is obtained by substituting coefficients in Table 7-1 into Equations 7.7 and 7.8, can be used.

$$c_{avg(T,RH,H_2S,t)} = 4.57 - 9.52\left(CaCO_{3(equiv.,agg)}\right) - 0.38\left(CH_{(equiv.,CAC)}\right) + 1.68\left(\frac{CH^{-1}_{(equiv.,PC)}}{100}\right)$$
$$- 6.31\left(AH_{3(equiv.,binder)}\right) - 9.27\left(Fe(OH)_{2(equiv.,binder)}\right) + 0.84\left(\frac{Al}{Ca}\right) - 2.80\left(\frac{Fe}{Ca}\right) \quad \text{(mm/yr.)} \tag{7.9}$$

It should be noted that due to the distinct difference in the chemical composition and nature of hydrates of PC- and CAC-based binders systems, Equation 7.9 contains different parameters for calcium hydroxide (CH), based on its *significance* (see Table 6-2) on biogenic corrosion rates in the respective binder systems.

A trendline based on Equation 7.9 can also be used to generate an alternative biogenic concrete corrosion prediction profile, defined by the following Equation 7.10 (refer to equation of line in Figure 6-7):

$$c_{avg,t} = \frac{0.57}{(RC_{eff.})^{1.49}} \quad (7.10)$$

where c_{avg} = average corrosion rate (mm/year)
t = time at start of corrosion. For PC, t = 0; for CAC, t = +2 years
$RC_{eff.}$ is defined by Equation 7.11

$$RC_{eff.} = (CaCO_{3(equiv., agg)})+(CH_{(equiv., CAC)})+(CH^{-1}{}_{(equiv., PC)})/100)+(AH_{3(equiv., binder)}) +(FeO(OH)_{(equiv., binder)})+(Al/Ca)+(Fe/Ca) \quad (7.11)$$

where, for CAC-based mixtures, input values for $CH_{(equiv., CAC)} \geq 0$ and those for $CH^{-1}{}_{(equiv., PC)} = 0$; for PC-based mixtures, input values for $CH_{(equiv., CAC)} = 0$ and those for $CH^{-1}{}_{(equiv., PC)} > 0$

Before proceeding, it is important to clarify that when Equation 7.11 is substituted in Equation 7.10, the resultant prediction curve is the same as that defined by Equation 7.9. Moreover, unlike Equation 7.9, Equation 7.10 has similarities with the LFM equation for corrosion prediction (see Equation 2.77), as shown in Table 7-2. It is for this reason that Equation 7.10 has been adopted as a basis for improving the LFM.

Table 7-2: Similarity between the LFM and corrosion prediction equation developed in the current study.

Model description	Parameter related to the attacking media/component	Parameter related to the acid-neutralising component
$c_{avg} = 11.4k\frac{\phi_{sw}}{A}$ **	'$11.4k\,\phi_{sw}$'	A = $CaCO_{3(equiv.)}$
$c_{avg,t} = \frac{0.57}{(RC_{eff.})^{1.49}}$ *	'0.57'	$RC_{eff.} = (CaCO_{3(equiv., agg)}) + (CH_{(equiv., CAC)}) + (CH^{-1}{}_{(equiv., PC)})/100) + (AH_{3(equiv., binder)}) + (FeO(OH)_{(equiv.)}) + (Al/Ca) + (Fe/Ca)$

**The LFM
*Corrosion prediction equation developed in the current study

From Table 7-2, it can be seen that the parameters '0.57' and '$(RC_{eff.})^{1.49}$' in Equation 7.10 relate to '$11.4k\phi_{sw}$' and 'A' respectively in the LFM. By relating these two equations, the current study proposed an *Improved LFM* with the capability to incorporate a wider range of binder systems in biogenic corrosion prediction. The *Improved LFM* is expressed as (Equation 7.12):

$$c_{avg,t} = 11.4k\frac{\phi_{sw}}{(RC_{eff.})^{1.49}}q \quad (7.12)$$

where c_{avg} = average corrosion rate (mm/year)
t = time at start of corrosion. For PC, t = 0; for CAC, t = +2 years
ϕ_{sw} = average H_2S flux to the moist pipe wall ($g/m^2/h$)
k = efficiency factor < 1 (rate constant for H_2S adsorption and oxidation kinetics as a function of temperature and air-flow (Reynolds number)). For systems where ϕ_{sw} is 'low' (such as in large diameter (> 1 m) pipes with less condensate forming on their walls), the value of k approaches 1; for systems where ϕ_{sw} is 'high' (such as in smaller diameter (< 1 m) pipes with more condensate forming on their walls), k may decrease to about 0.3.
q = sewer headspace aggressiveness factor (= $(11.4k\phi_{sw})/0.57$) (hypothesised to introduce the influence of sewer headspace temperature and RH into the LFM, although at this particular point, this factor has not been characterised)

$RC_{eff.} = (CaCO_{3(equiv., agg)}) + (CH_{(equiv., CAC)}) + (CH^{-1}_{(equiv., PC)})/100) + (AH_{3(equiv.)}) + (FeO(OH)_{(equiv.)}) + (Al/Ca) + (Fe/Ca)$,

for CAC-based mixtures, input values for $CH_{(equiv., CAC)} \geq 0$ and those for $CH^{-1}_{(equiv., PC)} = 0$; for PC-based mixtures, input values for $CH_{(equiv., CAC)} = 0$ and those for $CH^{-1}_{(equiv., PC)} > 0$

An example presented in Section 6.5 showed that these proposed improvements can be used in predicting the biogenic corrosion rates or remaining service life for a broader range of binder systems.

7.5 General conclusions

The current study was motivated by the need to improve the design of concrete mixtures for better biogenic corrosion prediction, particularly in sewer applications. The main approach undertaken was microstructural characterisation of various PC- and CAC-based binder systems subjected to biogenic H_2SO_4 attack in a 'live' sewer for more than 10 years, and subsequently, based on the understanding of the underlying mechanisms of attack, proposals were made to the widely used biogenic corrosion model, the LFM. The following conclusions can be made with reference to the aims set out to address the scope of the current study:

(1) The widely used deterministic (mechanistic) model, the LFM provides a sound basis for certain phases in biogenic corrosion prediction, particularly the sulphide build-up phase in sewer systems. It is for this reason that other recent mechanistic models such as WATS are based on the same concept as the LFM. Despite the wide application of these models, they are based on the hypothesis that the rate-controlling parameter, from a material (concrete) point of view, is *alkalinity* expressed as equivalent $CaCO_3$. This hypothesis is also supported by certain statistical models such as SATIR. However, results from the current study have shown that other concrete material parameters, which include equivalent AH_x and equivalent FeO(OH) are involved in neutralising or suppressing the biogenic acid attack mechanism. It is important to note that even though the influence of both AH_x and FeO(OH) is significant, it does not eliminate the effect of $CaCO_3$ in biogenic corrosion mechanisms.

(2) The neutralisation capacity of a concrete mixture to biogenic acid attack is determined by the chemical composition of the binders and the nature of their hydrates. From characterisation of the various binder systems in the current study, it is hypothesised that (i) the calcium component plays an active role in both CH and $CaCO_3$, and the rate-controlling parameter of biogenic corrosion rates, particularly in PC-based systems, is CH, (ii) AH_x offers greater neutralisation capacity than the other phases in a HCP, and (ii) that FeO(OH) (Fe^{3+}) potentially offers greater bacteriostatic effect to acid-generating SOB than the other phases in a HCP.

(3) Under a certain optimum temperature range (between 18 °C and 25 °C) for biogenic corrosion mechanisms, the aggressiveness of the sewer environment can be defined by a wider range of H_2S concentration than in current considerations.

(4) It is possible to incorporate other characteristics of concrete materials (apart from equivalent $CaCO_3$) that influence biogenic corrosion rates in biogenic corrosion prediction models. The current study proposes improvements to the LFM by incorporating (i) equivalent CH, equivalent AH_x and equivalent FeO(OH) based on stoichiometry, and (ii) the nature of the hydrates based on Al/Ca and Fe/Ca ratios as determined by the SEM/EDS technique.

7.6 Recommendations for further work

The current study has made contributions with regard to the focus of the *research motivation and knowledge contribution* section in Chapter One, Section 1.3. However, from the limited scope and research findings presented in sections above, the following principal areas need further research:

(1) Results in the current study showed that the biogenic concrete corrosion rate is influenced by both Al_2O_3 (Al^{3+}) and Fe_2O_3 (Fe^{3+}) in binders, which are hypothesised to provide a bacteriostatic effect to sulphide-oxidising bacteria. However, in order to distinguish between these mechanisms, the extent to which the respective ions are deemed to act needs to be characterised.

(2) Even though the current study showed that concrete mixtures made with binders having a lower amount of CaO (such as mixtures with 16% PC vs. 23% PC) and a higher amount of Al_2O_3 (such as mixtures with 16% CAC vs. 23% CAC) experienced less biogenic concrete corrosion rates due to the influence of the resultant hydrates in neutralising the attacking acid, the respective (most effective) concentration thresholds were not determined. Further work is proposed on this subject.

(3) The role of iron (III) oxide-hydroxide (FeO(OH)) in concrete mixtures subjected to aggressive biogenic H_2SO_4 environments has not been characterised. This should be investigated further.

(4) The *sewer headspace aggressiveness* factor, *q*, which is deemed to incorporate the influence of sewer headspace temperature and RH in the proposed *Improved LFM* is based on biogenic concrete corrosion rates of both PC- and CAC-based concrete mixtures exposed in environments with similar characteristics as the VES. Further work is required to characterise this factor, and also to develop sewer headspace aggressiveness factors in other environments with different conditions from the VES.

7.7 References

Alexander, M. G., & Fourie, C. W. 2011. Performance of sewer pipe concrete mixtures with portland and calcium aluminate cements subject to mineral and biogenic acid attack. *Materials and Structures*. 44 (1): 313 – 330.

Alexander, M. G., Goyns, A. M., & Fourie, C. W. 2008. Experiences with a full-scale experimental sewer made with CAC and other cementitious binders in Virginia, South Africa. Proceedings of the Centenary Conference on Calcium Aluminate Cements. June 30 – July 2, Avignon. 279 – 292.

Bizzozero, J., Gosselin, C., & Scrivener, K. L. 2014. Expansion mechanisms in calcium aluminate and sulfoaluminate systems with calcium sulfate. *Cement and Concrete Research*. 56: 190 – 202.

Chatterjee, S., Bandyopadhyay, A., & Sarkar, K. 2011. Effect of iron oxide and gold nanoparticles on bacterial growth leading towards biological application. *Journal of Nanobiotechnology.* 9: 34.

Da Silva, V. A., & Goyns, A. 2009. The aging of concrete sewers: Replace or rehabilitate. *Concrete Repair, Rehabilitation and Retrofitting II*. London: Taylor & Francis.

De Keyser, W. L. 1955. Contribution to the study of solid state reactions between OCa, O_3Fe_2, O_3Al_2. *Bulletin of Chemical Societies.* 64(7 – 8): 395 – 408.

Environmental Protection Agency. 1974. Process design manual for sulphide control in sanitary sewerage systems. Washington: EPA.

Environmental Protection Agency. 1985. Design manual: Odor and corrosion control in sanitary sewerage systems and treatment plants. Cincinnati: EPA.

Goyns, A. M. 2003. Virginia sewer rehabilitation: Progress Report 1. Pretoria: Concrete Manufacturers Association.

Herisson, J., Guéguen-Minerbe, M., van Hullebusch, E. D., & Chaussadent, T. 2014. Behaviour of different cementitious material formulations in sewer networks. *Water Science and Technology*. 69(7): 1502 – 1508.

Hvitved-Jacobsen, T., Vollertsen, J. & Nielsen, A.H. 2013. *Sewer processes: Microbial and chemical process engineering of sewer networks*. 2nd ed. Boca Raton: CRC Press.

Islander, R. L., Devinny, J. S., Mansfeld, F., Postyn, A., & Hong, S. 1991. Microbial ecology of crown corrosion in sewers. *Journal of Environmental Engineering*. 117(6): 751 – 770.

Kaempfer, W., & Berndt, M. 1999. Estimation of service life of concrete pipes in sewer networks. *Proceedings of the 8th Conference on Durability of Building Materials and Components*. May 30 – June 3. Vancouver. 36 – 45.

Kohsaka, K., Abdul-Talib, S., & Yin, C-Y. 2008. Effect of anoxic transformation processes in municipal wastewater on pH and oxidation reduction potential. *International Symposium on Sanitary and Environmental Engineering.* June 24 – 27. Florence.

Kurdowski, W. 2014. *Cement and concrete chemistry*. Dordrecht: Springer.

Motsieloa, N. 2013. Acid resistance of sewer pipe concrete. MSc (Eng) dissertation. University of Cape Town, Cape Town.

Paulini, P. 1994. A Through Solution Model for volume changes of cement hydration. *Cement and Concrere Research.* 24(3): 488 – 496.

Renaudin, G., Mesbah, A., Dilnesa, B. Z., Francois, M., & Lothenbach, B. 2015. Crystal chemistry of iron containing cementitious AFm layered hydrates. *Current Inorganics Chemistry.*5(2): 1 – 10.

Sahmaran, M. 2010. Deterioration mechanisms – chemical. In: Soutsos, M. Eds. *Concrete durability: A practical guide to the design of durable concrete structures*. London: Thomas Telford.

Sand, W., & Bock, E. 1984. Concrete corrosion in the Hamburg sewer system. *Environmental Technology Letters.* 5(12): 517 – 528.

Soenen, S. J., Cuyper, M., Smedt, S. C., & Braeckmans, K. 2012. Investigating the toxic effects of iron oxide nanoparticles. *Methods in Enzymology.* 509: 195 – 224.

Taber, S. 1916. The growth of crystals under external pressure. *American Journal of Science*. 4(41): 532 – 556.

Trun, N. J., & Gottesman, S. 1990. On the bacterial cell cycle: Escherichia coli mutants with altered ploidy. *Genes and Development.* 4: 2036 – 2047.

Weisweiler, W., Osen, E., Eck, J., & Höfer, H. 1986. Kinetic studies in the CaO-SiO_2 system, Part I: Mechanism and kinetic data of the reactions between CaO- and SiO_2-powder compacts. *Cement and Concrete Research.* 16(3): 283 – 295.

Appendix A: Temperature and relative humidity profiles at Boksburg, Klerksdorp and Virginia

A.1 Typical monthly extreme and average ambient temperature, and monthly average ambient relative humidity profiles at Boksburg, Gauteng Province

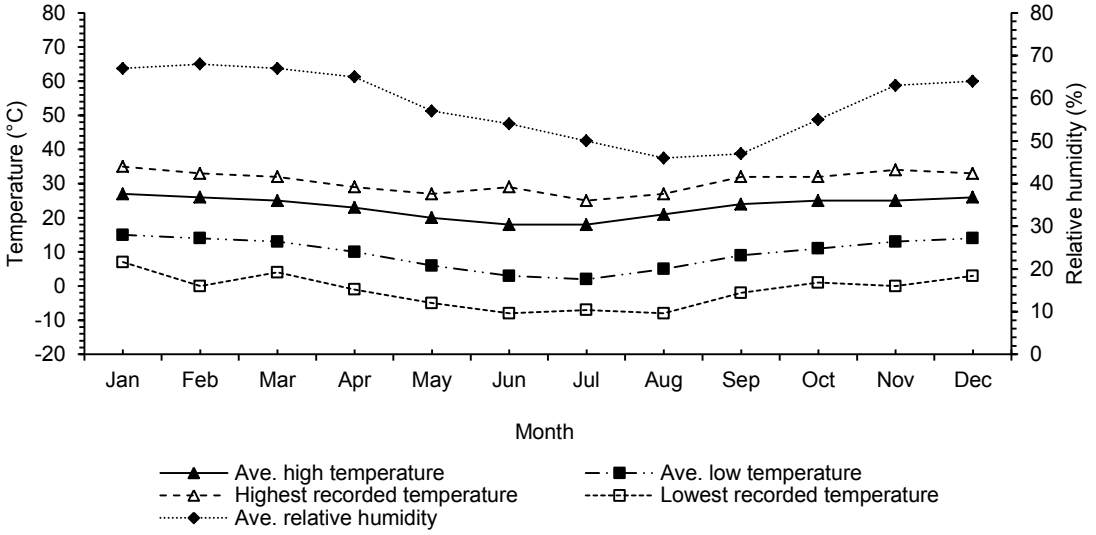

Figure A.1: Typical monthly temperature and relative humidity profiles at Boksburg, Gauteng Province taken over a period of 30 years (Weatherbase, 2015).

A.2 Typical monthly extreme and average ambient temperature, and monthly average ambient relative humidity profiles at Klerksdorp, North West Province

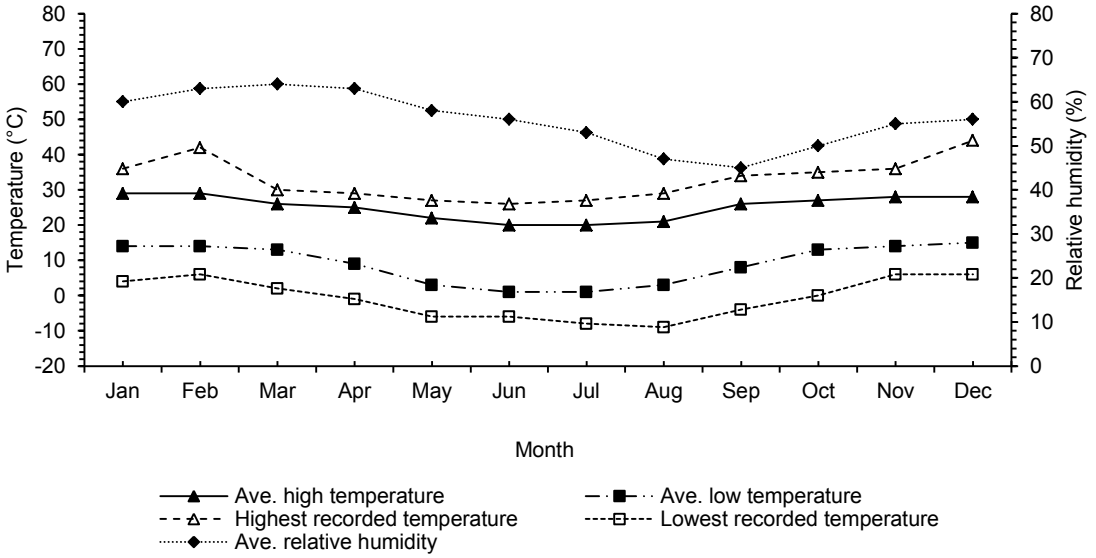

Figure A.2: Typical monthly temperature and relative humidity profiles at Klerksdorp, North West Province taken over a period of 30 years (Weatherbase, 2015).

A.3 Typical monthly extreme and average ambient temperature, and monthly average ambient relative humidity profiles at Virginia, Free State Province

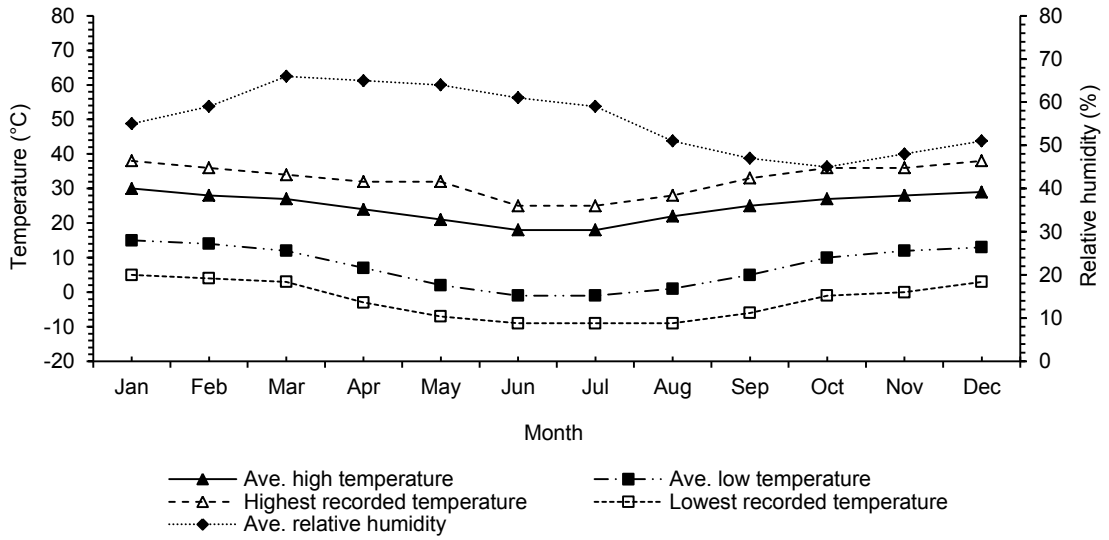

Figure A.3: Typical monthly temperature and relative humidity profiles at Virginia, Free State Province taken over a period of 30 years (Weatherbase, 2015).

A.4 Typical daily temperatures, and average relative humidity profiles in the experimental (VES) section's headspace

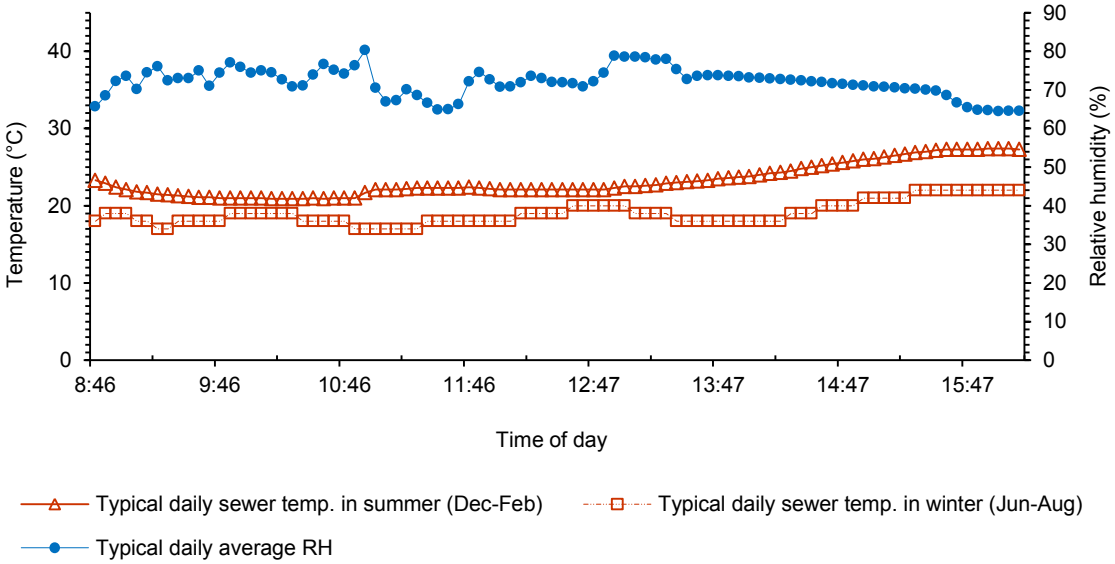

Figure A.4: Typical daily temperature and relative humidity profiles in the experimental (VES) section's headspace (data from current study (2013 – 2015)).

A.5 References

Weatherbase. 2015. http: //www.weatherbase.com, accessed on March 9, 2015

Appendix B: H_2S (gas) profiles in the inlet manhole (IM) to VES, and in the VES

B.1 Typical H_2S profiles in the IM to VES, and in the VES for all climatic seasons

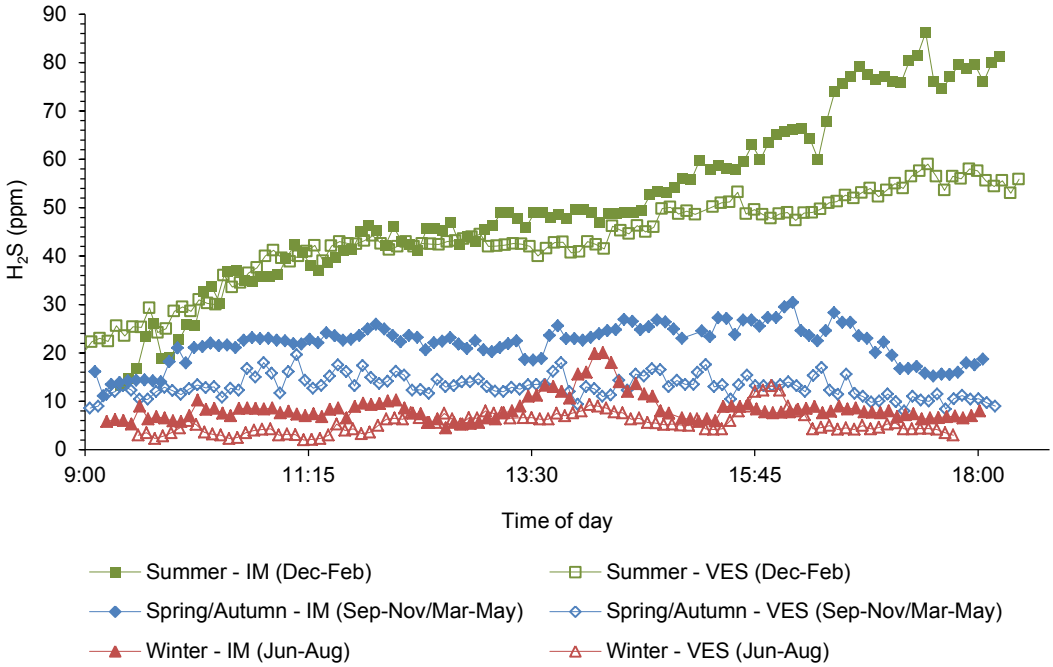

Figure B.1: Typical daily H_2S profiles in the IM to VES, and in the VES for all climatic seasons (data from current study (2013 – 2015)).

Appendix C: Layout of the nine different types of sewer pipes and the mixture composition of the unprotected cementitious category of samples installed in the VES during 1988

C.1 Layout of the nine different types of sewer pipes installed in the VES during 1988 (Goyns, 2003)

Direction of sewage flow	Pipe no.	Description/Type of sewer pipe[#]	Comments
Flow velocity, 2.5 m/s 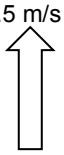	1	Unprotected AC	
	2	AC coated with epoxy tar	
	3	AC coated with polyurethane	
	4	PC/SIL lined with HDPE above the daily sewage flow level	
	5	PC/DOL lined with HDPE above the daily sewage flow level	A half of pipe no. 5, pipe no. 6, and a half of pipe no. 7 were replaced with the so-called MH III after 14 yrs
	6	Unprotected PC/SIL	
	7	Unprotected CAC/SIL	
	8	Unprotected AC	
	9	PC/SIL lined with HDPE above the daily sewage flow level	
	10	PC/DOL lined with HDPE above the daily sewage flow level	A half of pipe no. 10, pipe no. 11, and a half of pipe no. 12 were replaced with the so-called MH II after 14 yrs
	11	Unprotected PC/SIL	
	12	Unprotected CAC/SIL	
	13	Unprotected AC	
	14	AC coated with polyurethane	
	15	AC coated with epoxy tar	Pipe no. 15 and 16 were replaced with the so-called MH IV after 19 yrs
	16	AC coated with epoxy	
	17	HDPE	
	18	PC/DOL lined with HDPE above the daily sewage flow level	
	19	PC/SIL lined with HDPE above the daily sewage flow level	A half of pipe no. 19, pipe no. 20, and a half of pipe no. 21 were replaced with the so-called MH I after 14 yrs
	20	Unprotected PC/SIL	
	21	Unprotected CAC/SIL	
	22	AC coated with polyurethane	
	23	Unprotected AC	
	24	AC coated with epoxy tar	
	25	AC coated with epoxy	

[#]AC = Asbestos cement; PC/SIL = Rapid-hardening Portland cement + siliceous aggregate; PC/DOL = Rapid-hardening Portland cement + dolomite aggregate; CAC/SIL = Calcium (high) aluminate cement + siliceous aggregate; HDPE = High-density polyethylene

C.2 Mixture composition of the unprotected cementitious category of samples installed in the VES during 1988 (Goyns, 2003; CSIR, 1996)

Sewer pipe materials/description	Binder		Aggregate					
			Stone		Sand		Other	
	Type	%	Type	%	Type	%	Type	%
Unprotected PC/SIL	PC*	15	SIL	50	SIL	35	-	-
Unprotected PC/DOL	PC*	15	DOL	50	SIL	35	-	-
Unprotected CAC/SIL	CAC#	20	SIL	42	SIL	38	-	-
Unprotected AC	PC**	85	-	-	-	-	Asbestos fibre	15

*Rapid-hardening Portland cement
**Portland blastfurnace cement
#Calcium (high) aluminate cement

Appendix D: Details of concrete mixtures used in Phase II studies in the VES (1995 to 2001)

D.1 Concrete mixture proportions (ratio by mass to total binder content) of core samples used in the laboratory for mineral acid tests (Alexander and Fourie, 2011)

Mixture[#]	% binder	w/b	Binder		DOL aggregate	
			SCM	Cement	Stone**	Crusher sand
Sewer pipe mixtures:						
PC/DOL 3	18	0.30	-	1.00	2.28	2.28
PC/GGBS/DOL 3	18	0.30	0.50	0.50	2.28	2.28
PC/FA/DOL 3	18	0.30	0.30	0.70	2.28	2.28
PC/SF/DOL 3*	18	0.28	0.10	0.90	2.28	2.28
PC/MK/DOL 3*	18	0.30	0.10	0.90	2.28	2.28
CAC/DOL 3	18	0.30	-	1.00	2.28	2.28
Lining mixtures:						
PC/DOL 3	23	0.28	-	1.00	1.67	1.67
CAC/DOL 3	23	0.28	-	1.00	1.67	1.67
CAC/ Alag^{TM}	18	0.33	-	1.00	2.28	2.28
CAC/Alag^{TM}	23	0.28	-	1.00	1.67	1.67
CAC/SF/Alag^{TM}	23	0.24	0.1	0.90	1.67	1.67

[#]All aggregates crushed; DOL 3 = high quality dolomite (acid insolub. < 6%, 10% FACT = 354)
*SF = silica fume; MK = metakaolin; superplasticiser (1%) used for workability and dispersion
**Nominal 13 mm maximum size used for sewer pipe mixtures and nominal 6 mm maximum size for lining mixtures

D.2 Concrete mixture proportions (ratio by mass to total binder content) of core samples installed in the inlet manhole to VES (Alexander and Fourie, 2011)

Mixture[#]	% binder	w/b	Binder		Aggregate		
			SCM	Cement	Stone**	Crusher sand	Filler sand
Sewer pipe mixtures:							
PC/SIL	14	0.30	-	1.00	3.25	2.89	-
PC/DOL 2	16	0.36	-	1.00	3.45	1.32	0.53
PC/DOL 3	18	0.30	-	1.00	2.28	2.28	-
PC/SF/DOL 2	16	0.32	0.10	0.90	3.45	1.32	0.53
PC/Ag-Zn-Cu/DOL 3[+]	18	0.30	0.01	0.99	2.28	2.28	-
Lining mixtures:							
PC/SIL	23	0.32	-	1.00	1.64	0.82	0.82
PC/DOL 3	23	0.26	-	1.00	1.67	1.67	-
CAC/DOL 3	23	0.26	-	1.00	1.67	1.67	-
CAC/Alag^{TM}	23	0.26	-	1.00	1.67	1.67	-

[#]All aggregates crushed; DOL 3 = high quality dolomite (acid insolub. < 6%, 10% FACT = 354); DOL 2 = low quality dolomite (acid insolub. > 9%, 10% FACT = 130)
[+]Silver-zinc-copper based biocide was used as a corrosion inhibiting additive
**Nominal 13 mm maximum size used for sewer pipe mixtures and nominal 6 mm maximum size for lining mixtures

D.3 Chemical composition of binders in different samples used in Phase II studies in the VES during 2004 (Alexander and Fourie, 2011)

Binder type	Chemical composition (%)										
	CaO	MgO	SiO_2	Al_2O_3	Fe_2O_3	Cl^-	TiO_2	SO_3	Na_2O	P_2O_5	K_2O
CEM I (42.5 R)	64.4	4.2	22.1	4.0	2.5	0.1	0.3	2.0	0.13	0.3	0.64
CAC	37.6	0.7	4.4	39.5	15.1	-	1.8	0.2	0.1	0.1	0.1
FA	4.7	1.3	54.1	32.9	3.3	-	1.7	0.4	0.6	-	0.6
SF	0.6	0.6	92.0	1.5	1.2	-	-	-	-	-	0.6
GGBS	34.0	9.4	35.5	15.4	0.98	-	1.2	2.49	0.16	-	0.87

Appendix E: Layout and mixture details of the seventeen different types of concrete sewer pipe samples installed in the VES during 2004

E.1 Layout of the seventeen different types of concrete sewer pipes installed in Manholes I, II and III in the VES during 2004 (Goyns, 2010)

Manhole I

Direction of flow	Pipe no.	Mixture description[#]
Flow velocity, 2.5 m/s ⇧	22	M CAC/DOL/SIL
	21	M CAC/SIL
	20	M PC/DOL/SIL
	19	M PC/SIL
	16	SCR/R50™
	10	CAC/DOL 16
	15	CAC/ Alag™
	14	CAC/FA/SF/DOL
	12	CAC/DOL 23
	11	CAC/DOL 18
	9	CAC/SIL 23
	1	PC/DOL 16
	6	PC/SF/DOL
	5	PC/FA/DOL
	4	PC/GGBS/DOL
	3	PC/DOL 23
	2	PC/DOL 18

Manhole II

Direction of flow	Pipe no.	Mixture description[#]
Flow velocity, 2.5 m/s ⇧	22	M CAC/DOL/SIL
	21	M CAC/SIL
	20	M PC/DOL/SIL
	19	M PC/SIL
	16	SCR/R50™
	11	CAC/DOL 18
	15	CAC/ Alag™
	14	CAC/FA/SF/DOL
	12	CAC/DOL 23
	10	CAC/DOL 16
	9	CAC/SIL 23
	2	PC/DOL 18
	6	PC/SF/DOL
	5	PC/FA/DOL
	4	PC/GGBS/DOL
	3	PC/DOL 23
	1	PC/DOL 16

Manhole III

Direction of flow	Pipe no.	Mixture description[#]
Flow velocity, 2.5 m/s ⇧	22	M CAC/DOL/SIL
	21	M CAC/SIL
	20	M PC/DOL/SIL
	19	M PC/SIL
	16	SCR/R50™
	12	CAC/DOL 23
	15	CAC/ Alag™
	14	CAC/FA/SF/DOL
	11	CAC/DOL 18
	10	CAC/DOL 16
	9	CAC/SIL 23
	3	PC/DOL 23
	6	PC/SF/DOL
	5	PC/FA/DOL
	4	PC/GGBS/DOL
	2	PC/DOL 18
	1	PC/DOL 16

[#]CAC/DOL/SIL = Calcium aluminate cement + dolomite aggregate + siliceous aggregate; CAC/SIL = Calcium aluminate cement + siliceous aggregate; PC/DOL/SIL = Rapid-hardening Portland cement + dolomite aggregate + siliceous aggregate; PC/SIL = Rapid-hardening Portland cement + siliceous aggregate; SCR/R50™ = Calcium aluminate cement (brand name 'SECAR') + calcium aluminate aggregate (brand name 'R50™'); CAC/DOL = Calcium aluminate cement + dolomite aggregate; CAC/ Alag™ = Calcium aluminate cement + aluminate aggregate; CAC/FA/SF/DOL = Calcium aluminate cement + fly ash + silica fume + dolomite aggregate; PC/SF/DOL = Rapid-hardening Portland cement + silica fume + dolomite aggregate; PC/FA/DOL = Rapid-hardening Portland cement + fly ash + dolomite aggregate; PC/GGBS/DOL = Rapid-hardening Portland cement + ground granulated blast-furnace slag + dolomite aggregate; PC/DOL = Rapid-hardening Portland cement + dolomite aggregate

Note: The calcium aluminate cement (CAC) used in these samples is Ciment Fondu

E.2 Mixture composition (percentage of total mass) of different samples installed in Manholes I, II and III in the VES during 2004 (Goyns, 2010)

Mixture[†]	% total binder	Binder type				% Aggregate		
		% SCM			% Cement	Stone*	Crusher sand**	Filler sand[##]
		GGBS	FA	SF				
Sewer pipe mixtures:								
PC/DOL 16	16	-	-	-	16	48	18	18
PC/DOL 18	18	-	-	-	18	47	18	17
PC/DOL 23	23	-	-	-	23	44	17	16
PC/GGBS/DOL	18	6	-	-	12	47	18	17
PC/FA/DOL	18	-	4.5	-	13.5	47	18	17
PC/SF/DOL	18	-	-	1.5	16.5	47	18	17
Concrete lining mixtures:								
CAC/SIL 23	23	-	-	-	23	44	17	16
CAC/DOL 16	16	-	-	-	16	48	18	18
CAC/DOL 18	18	-	-	-	18	47	18	17
CAC/DOL 23	23	-	-	-	23	44	17	16
CAC/FA/SF/DOL	17	-	4.5	1.5	11	47	18	18
CAC/Alag^{TM}	20	-	-	-	20	40	-	40
SCR/R50^{TM}	20	-	-	-	20	40	-	40
Mortar lining mixtures:								
M PC/SIL	50	-	-	-	50	-	-	50
M PC/DOL/SIL	50	-	-	-	50	-	25	25
M CAC/SIL	50	-	-	-	50	-	-	50
M CAC/DOL/SIL	50	-	-	-	50	-	25	25

[†]PC = CEM I (42.5R); CAC = Ciment Fondu. See chemical composition (also of SCMs) in Appendix E.3

*Nominal 13 mm maximum size used for sewer pipe mixtures and nominal 6 mm maximum size for lining mixtures

**Crusher sand used = dolomite

[##]Filler sand used = siliceous, except for the aluminate-based

E.3 Chemical composition of binders used in different samples installed in Manholes I, II and III in the VES during 2004 (Goyns, 2010; Motsieloa, 2013)

Binder type	Chemical composition (%)											
	CaO	MgO	SiO_2	Al_2O_3	Fe_2O_3	Mn_2O_3	TiO_2	SO_3	Na_2O	P_2O_5	K_2O	LOI
CEM I (42.5 R)	64.5	0.8	21.2	4.0	3.0	0.1	0.3	2.9	0.1	0.2	0.7	2.87
CAC	37.6	0.7	4.4	39.5	15.1	0.2	1.8	0.2	0.1	0.1	0.2	0.2
FA	4.1	1.0	54.9	31.3	3.7	0.06	1.67	0.19	0.36	0.49	0.71	0.78
SF	0.68	0.2	96.0	< 0.1	< 0.1	-	-	0.25	0.18	-	0.45	1.8
GGBS	36.4	8.1	37.1	12.8	0.72	0.98	0.59	2.24	0.5	-	1.07	-

Appendix F: Details of concrete mixtures used for laboratory-based studies of physicochemical properties, and also installed in the VES during 2011

F.1 Concrete mixture proportions (ratio by mass to total binder content) of core samples used in Phase III work by Motsieloa (2013)

Mixture[†]	% total binder	Binder type				% Aggregate		
		SCM			Cement	Stone*	Crusher sand**	Filler sand[##]
		GGBS	FA	SF				
Concrete lining mixtures:								
PC 100	16	-	-	-	1.00	2.89	1.10	1.10
PC 70/FA 30	16	-	0.30	-	0.70	3.04	0.98	0.98
PC 90/FA 10	16	-	0.10	-	0.90	2.89	1.08	1.08
PC 72/FA 20/SF 8	16	-	0.20	0.08	0.72	3.02	0.99	0.99
CAC 100	16	-	-	-	1.00	2.89	1.11	1.11
CAC 85/FA 15	16	-	0.15	-	0.85	2.93	1.04	1.04
CAC 75/FA 25	16	-	0.25	-	0.75	3.01	1.02	1.02
CAC 60/FA 40	16	-	0.40	-	0.60	3.07	0.94	0.94
CAC 75/GGBS 25	16	0.25	-	-	0.75	2.89	1.10	1.10
CAC 60/ GGBS 40	16	0.40	-	-	0.60	2.89	1.09	1.09
CAC 40/ GGBS 60	16	0.60	-	-	0.40	2.89	1.08	1.08
CAC 50/ GGBS 50	16	0.50	-	-	0.50	2.89	1.08	1.08

[†]PC = CEM I (42.5R); CAC = Ciment Fondu. See chemical composition (also of SCMs) in Appendix F.2

*Nominal 13 mm maximum size

**Crusher sand used = dolomite

[##]Filler sand used = siliceous

F.2 Chemical composition of binders in core samples used in Phase III work by Motsieloa (2013)

Binder type	Chemical composition (%)											
	CaO	MgO	SiO_2	Al_2O_3	Fe_2O_3	Mn_2O_3	TiO_2	SO_3	Na_2O	P_2O_5	K_2O	LOI
CEM I (42.5 R)	64.5	0.8	21.2	4.0	3.0	0.1	0.3	2.9	0.1	0.2	0.7	2.87
CAC	37.6	0.7	4.4	39.5	15.1	0.2	1.8	0.2	0.1	0.1	0.2	0.2
FA	4.1	1.0	54.9	31.3	3.7	0.06	1.67	0.19	0.36	0.49	0.71	0.78
SF	0.68	0.2	96.0	< 0.1	< 0.1	-	-	0.25	0.18	-	0.45	1.8
GGBS	36.4	8.1	37.1	12.8	0.72	0.98	0.59	2.24	0.5	-	1.07	-

Appendix G: Details of concrete mixtures installed in the VES and Langa during 2015 for a comparative study on surface pH vs. time

G.1 Concrete mixture proportions (ratio by mass to total binder content) of core samples installed in the VES and Langa during 2015

Mixture[†]	% total binder	Binder type				% Aggregate		
		SCM			Cement	Stone*	Crusher sand**	Filler sand[##]
		GGBS	FA	SF				
Concrete lining mixtures:								
PC 100	16	-	-	-	1.00	2.89	1.09	1.09
PC 67/GGBS 33	16	0.33	-	-	0.67	2.89	1.09	1.09
PC 75/FA 25	16	-	0.25	-	0.75	2.89	1.09	1.09
PC 92/SF 8	16	-	-	0.08	0.92	2.89	1.09	1.09
CAC 100	16	-	-	-	1.00	2.89	1.09	1.09
CAC 65/GGBS 10/FA 25	16	0.10	0.25	-	0.65	2.89	1.09	1.09

[†]PC = CEM II/A-L (52.5N); CAC = Ciment Fondu. See chemical composition (also of SCMs) in Appendix G.1; w/b = 0.36
*Nominal 13 mm maximum size
**Crusher sand used = dolomite
[##]Filler sand used = siliceous

G.2 Chemical composition of binders in core samples used in the current study for surface pH vs. time profile comparison in the VES and Langa

Binder type	Chemical composition (%)											
	CaO	MgO	SiO_2	Al_2O_3	Fe_2O_3	Mn_2O_3	TiO_2	SO_3	Na_2O	P_2O_5	K_2O	LOI
CEM II/A-L (52.5 N)	63.2	0.91	20.2	4.03	3.19	0.1	0.24	2.64	0.18	0.15	0.67	4.08
CAC	37.6	0.7	4.4	39.5	15.1	0.2	1.8	0.2	0.1	0.1	0.2	0.2
FA	4.1	1.0	54.9	31.3	3.7	0.06	1.67	0.19	0.36	0.49	0.71	0.78
SF	0.68	0.2	96.0	< 0.1	< 0.1	-	-	0.25	0.18	-	0.45	1.8
GGBS	36.4	8.1	37.1	12.8	0.72	0.98	0.59	2.24	0.5	-	1.07	-

Appendix H: Particle size distribution of aggregates

H.1 Sieve analysis results

Aggregate	Sieve size (mm)	Mass retained (g)	Percentage of mass retained	Percentage of mass passing
Olifantsfontein dolomite stone	19	0.0	0.0	100.0
	13.2	267.4	11.3	88.7
	9.5	1361.9	57.7	31.0
	6.7	564.9	23.9	7.0
	4.75	60.5	2.6	4.5
	2.36	51.4	2.2	2.3
	1.18	18.4	0.8	1.5
	0.6	8.0	0.3	1.2
	0.3	5.0	0.2	1.0
	0.15	5.1	0.2	0.7
	0.075	5.6	0.2	0.5
	Pan	11.8	0.5	0.0
Olifantsfontein dolomite crusher sand	19	0.0	0.0	100.0
	13.2	18.9	1.0	99.0
	9.5	179.2	9.8	89.2
	6.7	313.6	17.1	72.1
	4.75	246.9	13.5	58.7
	2.36	448.6	24.4	34.2
	1.18	296.1	16.1	18.1
	0.6	159.9	8.7	9.4
	0.3	77.9	4.2	5.1
	0.15	40.8	2.2	2.9
	0.075	19.8	1.1	1.8
	Pan	33.3	1.8	0.0
Roodepoort siliceous pit (filler) sand	6.7	0.0	0.0	100.0
	4.75	0.4	0.0	100.0
	2.36	0.2	0.0	100.0
	1.18	64.1	3.5	96.5
	0.6	198.8	10.8	85.6
	0.3	329.0	17.9	67.7
	0.15	1011.6	55.1	12.6
	0.075	181.2	9.9	2.7
	Pan	49.7	2.7	0.0

H.2 References

South African National Standard. SANS 201: 2008. *Sieve analysis, fines content and dust content of aggregates*. Pretoria: SABS.

Appendix I: A summary of test procedures and results for density (saturated), compressive strength and durability indices of concrete core samples used for surface pH vs. time profiling

I.1 Density of saturated sample

All the core samples that were cast using the static heavy compaction technique measured 75 mm diameter by 220 ± 10 mm. The density of these samples was determined to SANS standards – SANS 6251: 2006. Prior to undertaking this procedure, the test specimens, measuring 75 mm diameter by 80 ± 2 mm were cut from the 28 d air-dried samples (75 mm dia. by 220 ± 10 mm) using a grinding disc, and thereafter immersed in tap water (in a curing tank) at 23 ± 2 °C for 24 h.

Thereafter, the samples were removed from the curing tank, and the water on their surfaces was wiped using a damp cloth. The mass, m_1, of the saturated sample(s) was then determined using a portable bench-top scale. The volume, V, of the sample was also determined by calculation, based on dimensions taken by a digital outside caliper.

The density, D_1, of the saturated sample(s), in kilogram per cubic metre, was calculated using the following Equation I.1.1:

$$D_1 = \frac{m_1}{V} \tag{I.1.1}$$

Results from this test regime are given in Table I.1.

Table I.1: Density of concrete used for surface pH vs. time profiling.

Mixture*	Age (days)	Average density, D_1# (kg/m^3)	Standard deviation (kg/m^3)	Coefficient of variation (%)
PC 100	28	2508	4.94	0.20
PC 67/GGBS 33	28	2514	1.54	0.06
PC 75/FA 25	28	2507	4.48	0.18
PC 92/SF 8	28	2514	5.03	0.20
CAC 100	28	2598	7.80	0.30
CAC 65/GGBS 10/FA 25	28	2560	7.09	0.28

*See details in Appendix G

#Average of 3 readings

I.2 Compressive strength

The core samples (75 mm diameter by 80 ± 2 mm) prepared for density (saturated) tests as described in Appendix I.1 were used for determining the compressive strength of concrete to SANS standards – SANS 5863: 2006 at respective ages of testing. The compressive strength test regime was undertaken immediately after determining the mass and dimensions of the samples as described in Appendix I.1.

During testing, each test sample was centrally positioned between the compressive test machine platens, and a load was then applied at a uniform rate, approximating the rate of stress of about 15 MPa/min, until the test sample failed. The load at failure was recorded in N and the compressive strength, f_{cc}, was calculated to the nearest 0.5 MPa by dividing the load at failure, F, in N, by the area of the contact face, A_c, in mm^2 as given in Equation I.2.1.

$$f_{cc} = \frac{F}{A_c} \tag{I.2.1}$$

Results from this test regime are given in Table I.2.

Table I.2: Compressive strength of concrete used for surface pH vs. time profiling.

Mixture*	Age (days)	Average compressive strength, f_{cc}# (MPa)	Standard deviation (MPa)	Coefficient of variation (%)
PC 100	1	30.5	0.96	3.15
	3	48.0	0.64	1.33
	7	57.0	0.61	1.06
	28	73.0	0.92	1.26
PC 67/GGBS 33	1	25.5	1.32	5.15
	3	34.0	0.56	1.65
	7	45.5	0.73	1.61
	28	60.5	0.84	1.38
PC 75/FA 25	1	25.5	0.78	3.05
	3	38.0	0.44	1.16
	7	53.5	1.14	2.13
	28	70.0	0.55	0.79
PC 92/SF 8	1	31.0	0.99	3.17
	3	46.0	1.55	3.34
	7	59.5	1.05	1.76
	28	77.0	0.59	0.77
CAC 100	1	55.0	0.83	1.50
	3	54.0	0.49	0.90
	7	60.0	3.40	5.67
	28	63.5	0.57	0.90
CAC 65/GGBS 10/FA 25	1	43.5	1.10	2.55
	3	47.5	1.12	2.35
	7	53.5	0.68	1.30
	28	55.0	0.83	1.51

*See details in Appendix G
#Average of 3 readings

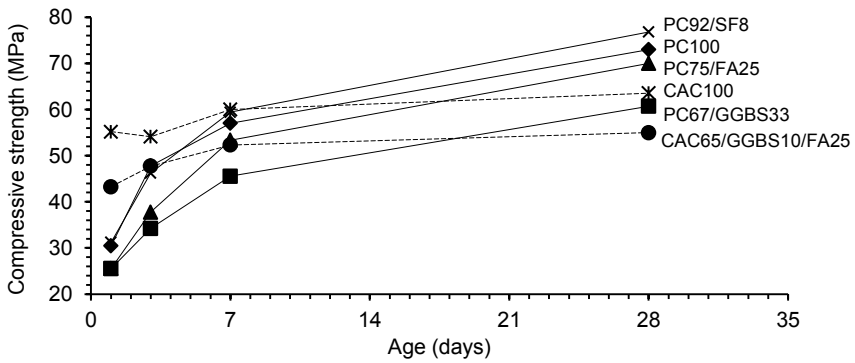

Figure I.2: Compressive strength development curves of concrete used for surface pH vs. time profiling.

I.3 Durability indices

The South African durability index (DI) tests consist of three tests that are used to characterise concrete with respect to penetration of corrosion species. These tests are (i) the oxygen permeability index (OPI), (ii) the water sorptivity index (WSI), and (iii) the chloride conductivity index (CCI. The DI tests used to characterise concrete mixtures in the current study were the OPI and WSI.

The OPI test is useful in characterising concrete mixtures and the effects of the curing method and type of binder used. It is also sensitive to microstructural defects such as voids and is useful in evaluating the effectiveness of the compaction technique of concrete. The typical range of values for OPI test, on the log scale, is 8 to 11 where a higher OPI value indicates lower permeability.

The WSI measures the movement of a wetting front through a porous medium due to capillary action. Typical ranges of sorptivity values vary from 5 mm/√hr for well cured concrete to 20 mm/√hr for poorly cured concrete.

The test samples for these tests consists of a set of four 70 ± 2 mm diameter by 30 ± 2 mm thick concrete discs prepared at the age of 28 d. The samples are conditioned in the oven at 50 ± 2 °C for 7 d ± 4 h prior to testing based on standard procedures given in the SA DI Manual (2009).

Results from this test regime are given in Table I.3.

Table I.3: OPI and WSI of concrete used for surface pH vs. time profiling.

Mixture*	Age (days)	OPI			WSI (mm/√hr)		
		Average[#]	Standard deviation	Coefficient of variation (%)	Average[#]	Standard deviation	Coefficient of variation (%)
PC 100	28	10.53	0.17	1.57	5.7	0.17	3.01
PC 67/GGBS 33	28	10.78	0.07	0.65	6.0	0.18	3.04
PC 75/FA 25	28	10.48	0.14	1.31	5.9	0.24	4.15
PC 92/SF 8	28	10.89	0.07	0.68	5.6	0.22	3.86
CAC 100	28	9.79	0.12	1.23	11.3	0.22	1.91
CAC 65/GGBS 10/FA 25	28	9.97	0.10	1.04	9.9	0.21	2.11

*See details in Appendix G

[#]Average of 4 readings

I.4 Surface pH

Colonisation of acid generating bacteria on surfaces on concrete sewer pipes depends on the pH of the substrate. Therefore this test regime was intended for profiling the surface pH vs. time of concrete cores installed in two different sewer environments; (i) the VES in Virginia, and (ii) manhole at Langa in Cape Town. These profiles were used as a comparative study on mechanisms involved in biogenic concrete corrosion in different geographical locations. However, prior to installing the samples on site, the initial surface pH of the respective concrete mixtures was determined in the laboratory based on the 'powder in suspension' technique (Kakade, 2014).

In order to undertake this test, each air-dried (at a temperature of 22 ± 2 °C and RH of 50%) sample (at the age of 28 d) was first placed on a clean glass plate, and thereafter, their surfaces were sanded (scarified) uniformly using sandpaper. The powder obtained from each scarification process was used to determine the (surface) pH of the concrete. 2 g of the collected concrete powder was transferred to a clean 50 ml plastic container, after which, 40 ml of distilled water was added to the powder. The container was then closed tightly and shaken for approximately 1 minute. Thereafter, the mixture was allowed to settle for 1 h. The digital pH meter (Oakton®) used in the current study was then calibrated using standard buffer solutions prior to taking the pH measurements.

Results from this test regime are given in Table I.4.

Table I.4: Initial surface pH of concrete used for surface pH vs. time profiling.

Mixture*	Age (days)	Average surface pH#	Standard deviation (MPa) #	Coefficient of variation (%)
PC 100	28	13.38	0.13	0.98
PC 67/GGBS 33	28	13.24	0.15	1.14
PC 75/FA 25	28	13.12	0.08	0.61
PC 92/SF 8	28	13.45	0.06	0.45
CAC 100	28	11.83	0.09	0.77
CAC 65/GGBS 10/FA 25	28	11.52	0.13	1.09

*See details in Appendix G
#Average of 3 readings

I.5 References

Kakade, A. M. 2014. Measuring concrete surface pH – A proposed test method. *Concrete Repair Bulletin*. 16 – 20.

South African Durability Index Testing Procedure Manual. 2009. Department of Civil Engineering, University of Cape Town, Cape Town.

South African National Standard. SANS 5863: 2006. *Concrete tests – compressive strength of hardened concrete*. Pretoria: SABS.

South African National Standard. SANS 6251: 2006. *Concrete tests – density of hardened concrete*. Pretoria: SABS.

Appendix J: Test procedures for laboratory analytical techniques

Four types of samples were used for characterisation of concrete mixtures in the current study; (i) dried processed powder samples (from products of biogenic concrete corrosion) – for QXRD and TGA, (ii) dried unprocessed powder samples (products of biogenic concrete corrosion) – for SEM, (iii) polished block samples – for SEM/EDS, and (iv) 'As-sampled' products of biogenic concrete corrosion – for microbial speciation.

For the general preparation procedure of powder samples used for XRD, TGA and SEM, about 30 ml (30 g) of each of the sampled products of biogenic concrete corrosion was transferred from the 50 ml bottles used during field sampling to a new set of similar clean bottles and thereafter subjected to drying. The solvent-exchange sample drying method using isopropanol was used. Isopropanol was added to the bottles to fully immerse the samples. After 5 days of 'soaking', the samples were removed from the 50 ml bottles and vacuum-dried (at 20 ± 2 °C) for 3 minutes prior to undertaking specific sample preparation procedures.

J.1 X-ray diffraction (XRD)

In order to undertake (quantitative) XRD analysis, 20 g of the isopropanol-dried sample was gently 'ground' using a pestle and mortar to obtain a powder (dried processed powder). This powder was sieved through a 63 µm sieve to obtain the final test specimen. About 2.5 g of this powder was tested using a Philips PW 1390 X-ray diffractometer with copper radiation, Cu Kα (wavelength, K = 1.5418 Á), operated at 40 kV and 20 mA over an angular rotation (2θ) from 0° to 70° with a step size of 0.02° and total scan of 20 minutes.

J.2 Thermogravimetric analysis (TGA)

The powder sieved through a 63 µm sieve as described in Appendix J.1 was used for TGA. About 50 mg of this powder was tested using a Mettler Toledo TGA/SDTA 851e microbalance. Samples were tested over a temperature range of 25 °C to 1000 °C, with a heating rate of 10 °C/min, under nitrogen atmosphere.

J.3 Scanning electron microscopy (SEM)

In order to undertake SEM (BSE) analysis on the products of biogenic concrete corrosion, a powder fraction obtained from the remainder 10 g of the sample that was not ground (for XRD/TGA applications as described above) was 'sprinkled' on a carbon-coated holder and left undisturbed for 24 h. After the 24 hours, the holder was mounted in a Nova NanoSEM 230 scanning electron microscope for backscattered imaging and EDS analysis.

For the polished concrete sections used for SEM/EDS analysis, blocks of approximately 20 mm^3 were sawn from the larger blocks obtained from site, and placed in clean, lubricated 30 mm diameter plastic moulds. These moulds (with samples) were then placed in a vacuum impregnation unit (CitoVac®) for 5 – 10 minutes in order to remove all the air prior to adding an epoxy resin. The epoxy resin was added at a pre-determined rate to fill the moulds (completely cover the samples) in 5 minutes. Printed labels for sample identification were then inserted into the mould (whilst the resin was unhardened), and thereafter the moulds were transferred to an oven at 30 °C for 24 h in order for the resin to harden.

The moulds were then removed from the oven and allowed to cool before extracting the embedded samples. The surfaces (of the samples) that were to be scanned were further prepared by a series of grinding and polishing steps (samples were rinsed in soapy water regularly between these steps) to a depth of 1 µm (this was checked using an optical microscope) into the original surface of the concrete blocks. The samples were then placed in an ultrasonic bath for 10 minutes. After removing the samples from the ultrasonic bath, they were rinsed in ethanol, dried and placed in an oven at 30 °C for 1 h. A final check on the quality of the polished section was undertaken using an optical microscope before mounting the samples in the SEM machine for backscattered imaging and EDS analysis. A Philips Quanta 200 SEM with PGT EDS was used for this test regime.

J.4 Microbial speciation

The samples for microbial speciation were transported to the laboratory in an insulated 'Cooler Box' within 36 h after being gently scraped and brushed from the 'lids' in the VES. In the laboratory, all the 'as-sampled' products of biogenic concrete corrosion were stored at 4 °C. Genomic DNA (gDNA) was extracted from approximately 2 g of the respective samples using the Macherey-Nagel Genomic DNA and Roche PCR Template Purification kits,

following neutralisation with sequential phosphate buffered saline washes. A total of three separate gDNA extractions were conducted on the various samples. The quantity and quality** of the extracted nucleic acid material was assessed spectrophotometrically using a Nanodrop, ND-1000 spectrophotometer. Extracted DNA was also stored at 4°C prior to further testing.

Thereafter, the gDNA was diluted to approximately 10 ng/µL and used as the template in a PCR reaction to amplify the 16S rRNA genes using a high fidelity DNA polymerase (Kapa Biosystems Hotstart HiFi DNA polymerase) and the universal 16S rRNA-specific primers, 27F and 1492R. The PCR amplicons were analysed by electrophoresis on a 0.8% (w/v) TAE agarose gel. The PCR product was then cloned into pJET1.2/Blunt and transformed into *E. coli* DH5α. The presence of the expected cloned insert was confirmed by colony PCR, using vector specific sequencing primers pJET1.2 Fwd and pJET1.2 Rev. Clones containing correctly sized insert were de-replicated using *Alu*I and *Hae*III. Thereafter, unique ribotypes were sequenced with pJET1.2 Fwd and pJET1.2 Rev (Inqaba Biotec, Standard Sequencing Service). The sequences were manually edited using Chromas version 2.01 Software and analysed using DNAMAN for windows version 4.13 Software.

Homology and similarity searches of related DNA sequences were performed using the basic local alignment search tool (BLAST) programs (Altschul et al., 1990; Altschul et al., 1997), as provided by the National Centre for Biotechnology Information (NCBI). Phylogenetic analyses were conducted using CLUSTAL X version 2.1 (Higgins and Sharp, 1989) and MEGA version 6 (Tamura et al., 2013) and neighbour-joining (Saitou and Nei, 1987) trees constructed. Bootstrap values were based upon 1000 re-sampled data sets (Felsenstein, 1985) and only bootstrap values greater than 40% are indicated.

**Based on the absorbance technique – see sub-section J.4.1.

J.4.1 Absorbance technique (Promega, 2015)

This is the most common technique to determine DNA yield and purity, based on the measurement of absorbance (common logarithm of the ratio of incident to transmitted radiant power through a material). Absorbance readings are performed at 260 nm (A260) where DNA absorbs light most strongly, and the number generated allows one to estimate the concentration of the solution.

DNA concentration is estimated by measuring the absorbance at 260 nm, adjusting the A260 measurement for turbidity (measured by absorbance at 320 nm), multiplying by the dilution factor, and using the relationship that an A260 of 1.0 = 50 µg/ml pure DNA (Equation J.4.1).

$$\text{Concentration (µg/ml)} = (\text{A260 reading} - \text{A320 reading}) \times \text{dilution factor} \times 50\ \text{µg/ml} \quad \text{(J.4.1)}$$

To evaluate DNA purity, measurements are taken from a full range of 230 nm to 320 nm. DNA purity is calculated as the ratio of the absorbance reading at 260 nm divided by the reading at 280 nm. Good quality DNA will have an A260/A280 ratio of 1.7 – 2.0. However, a reading of 1.6 does not render the DNA unsuitable for any application, but lower ratios indicate presence of more contaminants. The ratio is usually calculated after correcting for turbidity (absorbance at 320 nm) (Equation J.4.2).

$$\text{DNA purity (A260/A280)} = (\text{A260 reading} - \text{A320 reading}) / (\text{A280 reading} - \text{A320 reading}) \quad \text{(J.4.2)}$$

J.4.2 Agarose gel electrophoresis (Promega, 2015)

This technique is also used in estimating DNA concentration. In this method, a horizontal gel electrophoresis tank with an external power supply, analytical-grade agarose, an appropriate running buffer and an intercalating DNA dye along with appropriately sized DNA standards are utilised. A sample of the isolated DNA is loaded into a well of the agarose gel and then exposed to an electric field. The negatively charged DNA backbone migrates toward the anode. Since small DNA fragments migrate faster, the DNA is separated by size. The percentage of agarose in the gel will determine what size range of DNA will be resolved with the greatest clarity. Any RNA, nucleotides and protein in the sample migrate at different rates compared to the DNA, so the band(s) containing the DNA will be distinct.

Concentration and yield can be determined after gel electrophoresis is completed by comparing the sample DNA intensity to that of a DNA quantification standard.

J.5 References

Altschul, S. F., Gish, W., Miller, W., Myers, E. W., & Lipman, D. J. 1990. Basic local alignment search tool. *Journal of Molecular Biology.* 215(3): 403 – 410.

Altschul, S. F., Madden, T. L., Schäffer, A. A., Zhang, Z., Miller, W., Lipman, D. J. 1997. Gapped BLAST and PSI-BLAST: A new generation of protein database search programs. *Nucleic Acids Research.* 25(17): 3389 – 3402.

Felsenstein, J. 1985. Phylogenies and the Comparative Method. *The American Naturilst.* 125: 1 – 15.

Higgins, D. G., & Sharp, P. M. 1989. Fast and sensitive multiple sequence alignments on a microcomputer. *Computer Applications in the Biosciences.* 5(2): 151 – 153.

Promega Corporation. 2015. Promega protocals and applications guide. Wisconsin: The Promega Publications Hub.

Saitou, N., & Nei, M. 1987. The neighbour-joining method: A new method for reconstructing phylogenetic trees. *Molecular Biology and Evolution.* 4(4): 406 – 425.

Tamura, K., Stecher, G., Peterson, D. Filipski, A., & Kumar, S. 2013. MEGA6: Molecular Evolutionary Genetics Analysis Version 6.0. *Molecular Biology and Evolution.* 30(12): 2725 – 2729.

Appendix K: Temperature and relative humidity profiles in the manhole at Langa

K.1 Typical daily temperatures, and average relative humidity profiles in the manhole at Langa

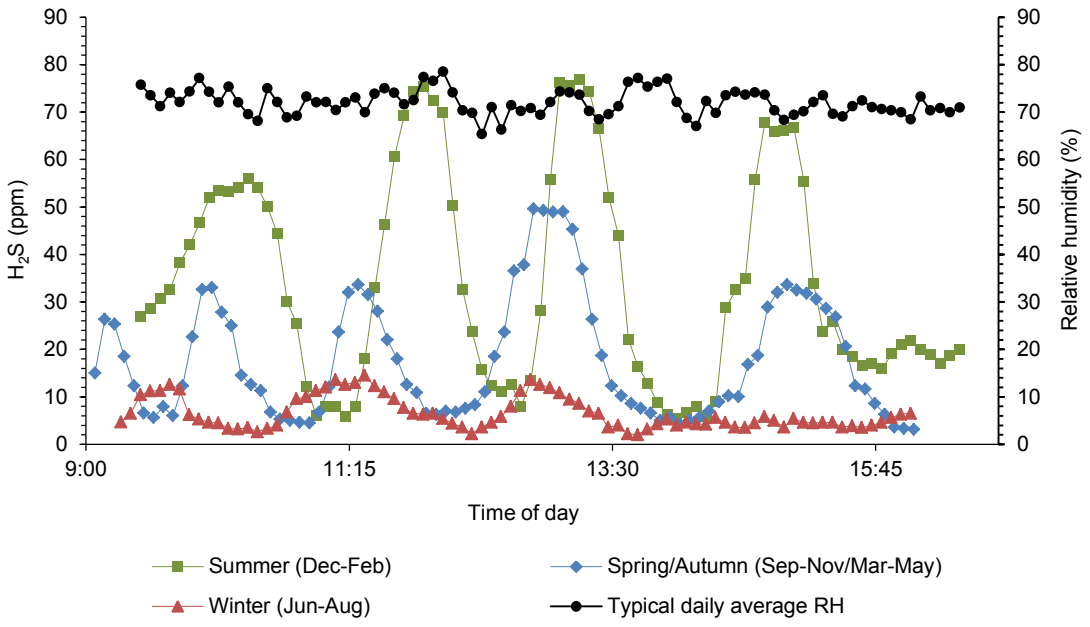

Figure K.1: Typical daily temperature and average RH profiles in the manhole at Langa during summer, spring/autumn and winter months (data from current study (2013 – 2015)).

Appendix L: Detailed results and selected statistical measures

L.1 Detailed corrosion rate time-development trends and data

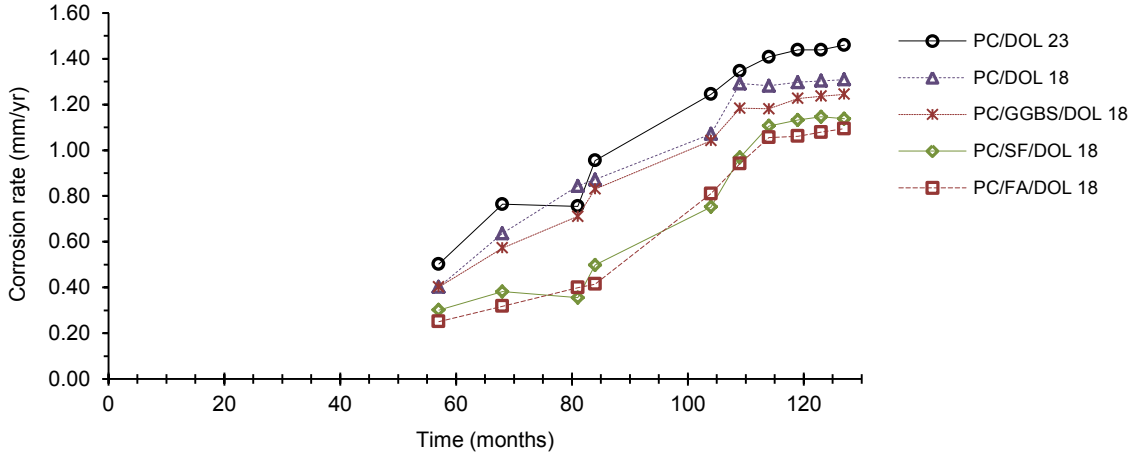

Figure L.1.1: Corrosion rate time-development trends for PC-based mixtures ('lids') located at MH I in the VES

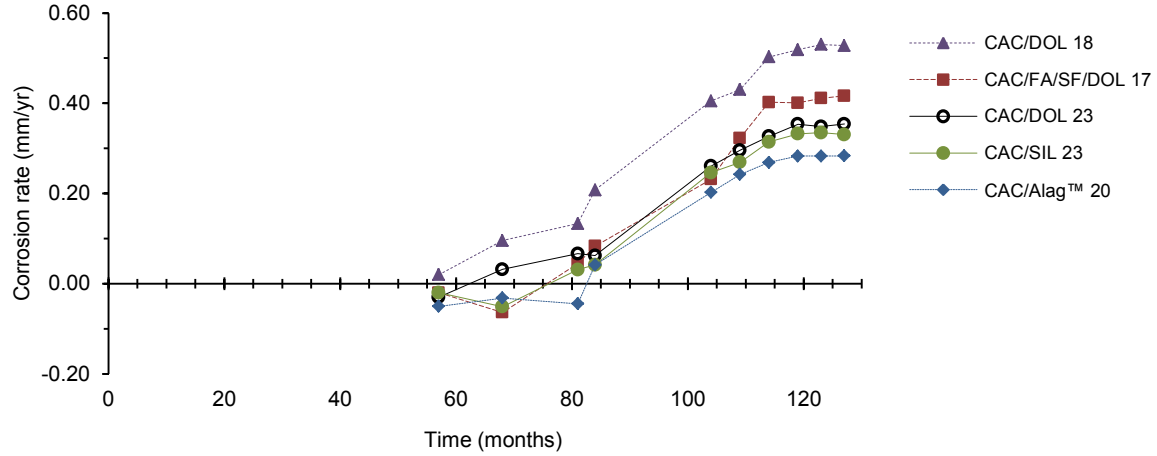

Figure L.1.2: Corrosion rate time-development trends for CAC-based mixtures ('lids') located at MH I in the VES

Table L.1.1: Corrosion rates of concrete mixtures ('lids') located at MH I in the VES.

Month (after installation)	38	57	68	81	84	104	109	114	119	123	127	Average *c** (mm/yr.)	Standard deviation* (mm/yr.)	CoV* (%)
Mixture	Corrosion rate (mm/yr.)													
CAC/Alag™	-	-0.05	-0.03	-0.04	0.04	0.20	0.24	0.27	0.28	0.28	0.28	0.27	0.018	6.56
CAC/FA/SF/DOL 17	-	-0.02	-0.06	0.04	0.08	0.23	0.32	0.40	0.40	0.41	0.42	0.39	0.038	9.85
CAC/DOL 23	-	-0.03	0.03	0.07	0.06	0.26	0.30	0.33	0.35	0.35	0.35	0.34	0.025	7.42
CAC/DOL 18	-	0.02	0.10	0.13	0.21	0.41	0.43	0.50	0.52	0.53	0.53	0.50	0.041	8.26
CAC/SIL 23	-	-0.02	-0.05	0.03	0.04	0.25	0.27	0.31	0.33	0.33	0.33	0.32	0.028	8.73
PC/SF/DOL 18	-	0.30	0.38	0.36	0.50	0.75	0.97	1.11	1.13	1.15	1.14	1.10	0.074	6.73
PC/FA/DOL 18	-	0.25	0.32	0.40	0.42	0.81	0.94	1.06	1.06	1.08	1.09	1.05	0.060	5.78
PC/GGBS/DOL 18	-	0.40	0.57	0.71	0.83	1.04	1.18	1.18	1.23	1.24	1.24	1.21	0.030	2.46
PC/DOL 23	-	0.50	0.76	0.76	0.95	1.24	1.34	1.41	1.44	1.44	1.46	1.42	0.045	3.15
PC/DOL 18	-	0.40	0.64	0.84	0.87	1.07	1.29	1.28	1.30	1.30	1.31	1.30	0.011	0.82

*Calculated for month 109 to month 127. This duration was chosen based on observations from the corrosion rate time-development trends, which tend to start levelling off at month 109.

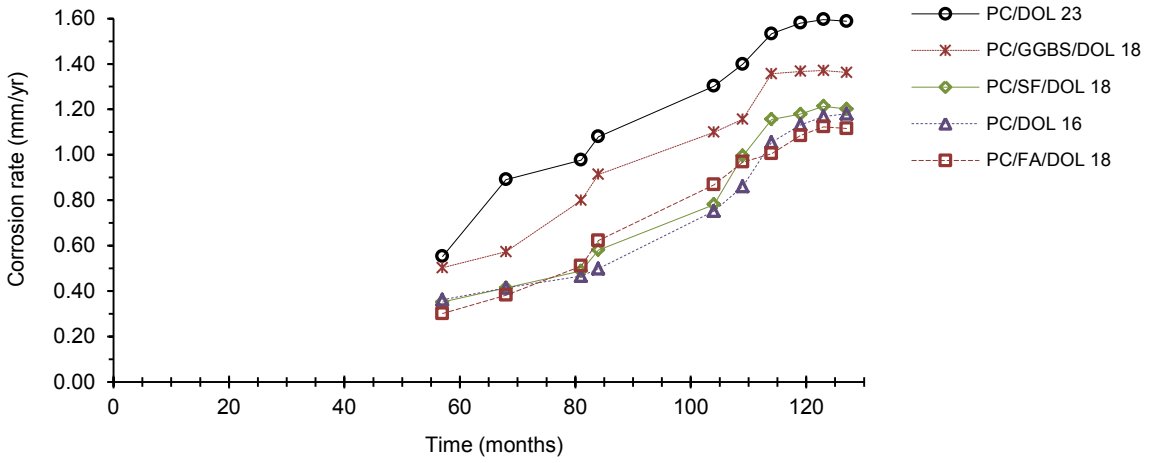

Figure L.1.3: Corrosion rate time-development trends for PC-based mixtures ('lids') located at MH II in the VES

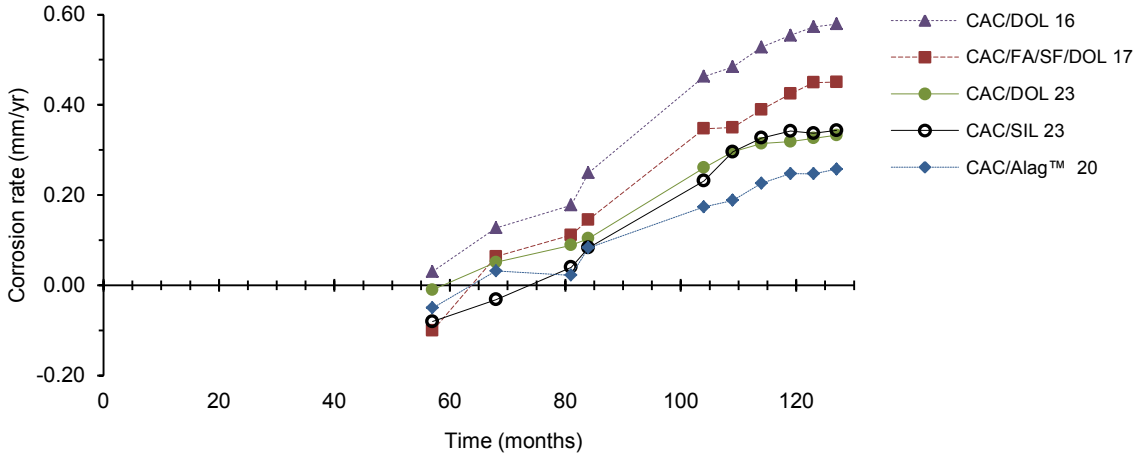

Figure L.1.4: Corrosion rate time-development trends for CAC-based mixtures ('lids') located at MH II in the VES

Table L.1.2: Corrosion rates of concrete mixtures ('lids') located at MH II in the VES.

Month (after installation)	38	57	68	81	84	104	109	114	119	123	127	Average c^* (mm/yr.)	Standard deviation* (mm/yr.)	CoV* (%)
Mixture	Corrosion rate (mm/yr.)													
CAC/Alag™	-	-0.05	0.03	0.02	0.08	0.17	0.19	0.23	0.25	0.25	0.26	0.23	0.028	11.85
CAC/FA/SF/DOL 17	-	-0.10	0.06	0.11	0.15	0.35	0.35	0.39	0.42	0.45	0.45	0.41	0.043	10.44
CAC/DOL 23	-	-0.01	0.05	0.09	0.10	0.26	0.30	0.31	0.32	0.33	0.33	0.32	0.014	4.39
CAC/DOL 16	-	0.03	0.13	0.18	0.25	0.46	0.48	0.53	0.55	0.57	0.58	0.54	0.039	7.14
CAC/SIL 23	-	-0.08	-0.03	0.04	0.08	0.23	0.30	0.33	0.34	0.34	0.34	0.33	0.020	5.96
PC/SF/DOL 18	-	0.35	0.41	0.49	0.58	0.78	1.00	1.16	1.18	1.21	1.20	1.15	0.089	7.72
PC/FA/DOL 18	-	0.30	0.38	0.51	0.62	0.87	0.97	1.01	1.08	1.12	1.12	1.06	0.069	6.53
PC/GGBS/DOL 18	-	0.50	0.57	0.80	0.91	1.10	1.16	1.36	1.37	1.37	1.36	1.32	0.093	7.03
PC/DOL 23	-	0.55	0.89	0.98	1.08	1.30	1.40	1.53	1.58	1.60	1.59	1.54	0.082	5.33
PC/DOL 18	-	0.36	0.41	0.47	0.50	0.75	0.86	1.06	1.13	1.17	1.18	1.08	0.132	12.19

*Calculated for month 109 to month 127. This duration was chosen based on observations from the corrosion rate time-development trends, which tend to start levelling off at month 109.

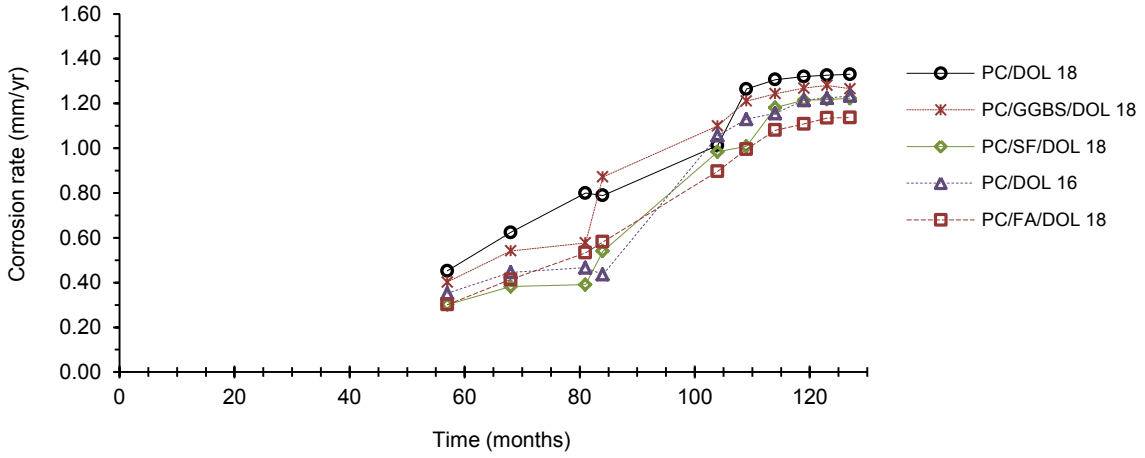

Figure L.1.5: Corrosion rate time-development trends for PC-based mixtures ('lids') located at MH III in the VES

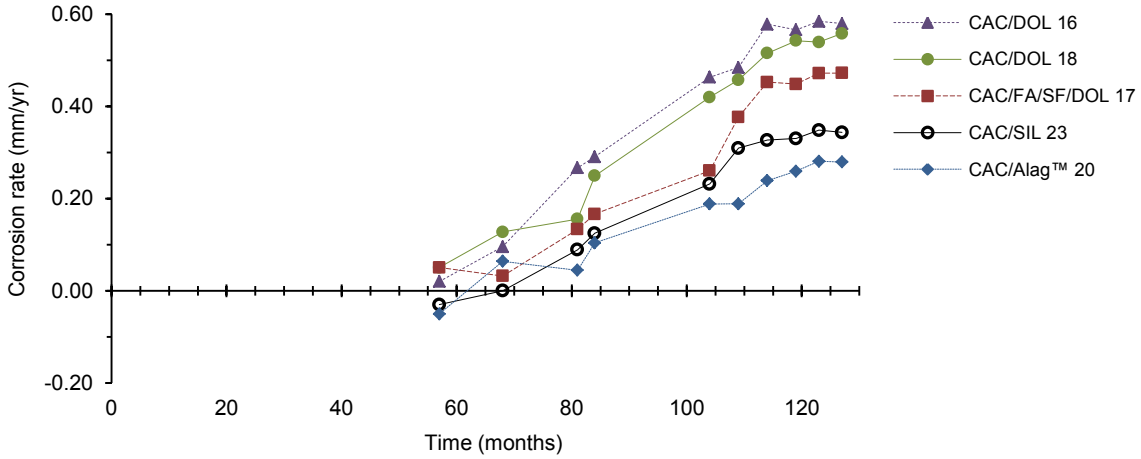

Figure L.1.6: Corrosion rate time-development trends for CAC-based mixtures ('lids') located at MH III in the VES

Table L.1.3: Corrosion rates of concrete mixtures ('lids') located at MH III in the VES.

Month (after installation)	38	57	68	81	84	104	109	114	119	123	127	Average *c** (mm/yr.)	Standard deviation* (mm/yr.)	CoV* (%)
Mixture	Corrosion rate (mm/yr.)													
CAC/Alag™	-	-0.05	0.06	0.04	0.10	0.19	0.19	0.24	0.26	0.28	0.28	0.25	0.038	15.29
CAC/FA/SF/DOL 17	-	0.05	0.03	0.13	0.17	0.26	0.38	0.45	0.45	0.47	0.47	0.44	0.039	8.86
CAC/DOL 18	-	0.05	0.13	0.16	0.25	0.42	0.46	0.52	0.54	0.54	0.56	0.52	0.039	7.56
CAC/DOL 16	-	0.02	0.10	0.27	0.29	0.46	0.48	0.58	0.57	0.58	0.58	0.56	0.042	7.52
CAC/SIL 23	-	-0.03	0.00	0.09	0.12	0.23	0.31	0.33	0.33	0.35	0.34	0.33	0.015	4.62
PC/SF/DOL 18	-	0.30	0.38	0.39	0.54	0.98	1.01	1.18	1.21	1.22	1.22	1.17	0.091	7.79
PC/FA/DOL 18	-	0.30	0.41	0.53	0.58	0.90	1.00	1.08	1.11	1.13	1.14	1.09	0.058	5.35
PC/GGBS/DOL 18	-	0.40	0.54	0.58	0.87	1.10	1.21	1.24	1.27	1.28	1.27	1.25	0.028	2.21
PC/DOL 18	-	0.45	0.62	0.80	0.79	1.01	1.26	1.31	1.32	1.33	1.33	1.31	0.027	2.05
PC/DOL 16	-	0.35	0.45	0.47	0.44	1.06	1.13	1.16	1.21	1.22	1.23	1.19	0.046	3.86

*Calculated for month 109 to month 127. This duration was chosen based on observations from the corrosion rate time-development trends, which tend to start levelling off at month 109.

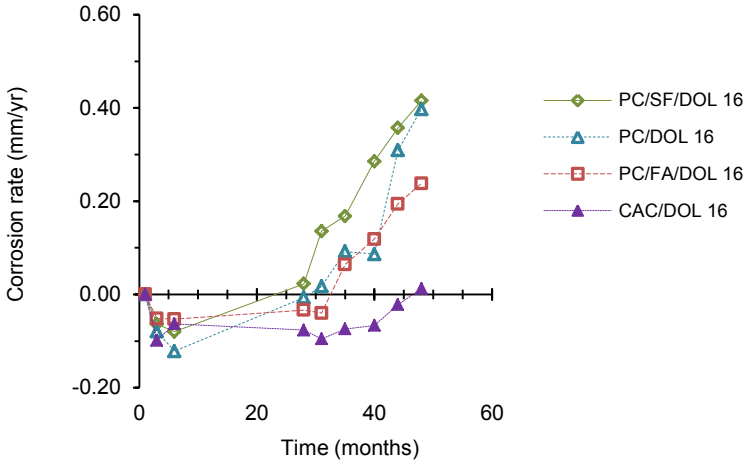

Figure L.1.7: Corrosion rate time-development trends for PC- and CAC-based mixtures (cores) located at MH II in the VES

Table L.1.4: Corrosion rates of concrete mixtures (cores) located at MH II in the VES.

Month (after installation)	0	3	6	28	31	35	40	44	48	Average *c* (mm/yr.)	Standard deviation (mm/yr.)
Mixture											
CAC/DOL 16	-	-0.10	-0.06	-0.08	-0.10	-0.07	-0.07	-0.02	0.01	-0.06	0.038
PC/DOL 16	-	-0.08	-0.12	-0.01	0.02	0.09	0.09	0.31	0.40	0.09	0.182
PC/FA/DOL 16	-	-0.05	-0.05	-0.03	-0.04	0.06	0.12	0.19	0.24	0.05	0.118
PC/SF/DOL 16	-	-0.06	-0.08	0.02	0.14	0.17	0.29	0.36	0.42	0.16	0.188

L.2 Calculations for range of confidence (error bars)

Table L.2.1: Average corrosion rates of concrete mixtures subjected to biogenic H_2SO_4 for 127 months in a 'live' sewer (mm/yr.).

Concrete mixture details*	Cement type	CAC						PC					
	SCM	-	FA+SF	-	-	-	-	SF	FA	GGBS	-	-	-
	Binder content	20	17	23	18	16	23	18	18	18	23	18	16
	Aggregate	Alag™	DOL	DOL	DOL	DOL	SIL	DOL	DOL	DOL	DOL	DOL	DOL
Average#		0.25	0.42	0.33	0.51	0.55	0.33	1.14	1.07	1.26	1.48	1.30	1.14
Standard deviation (σ)		0.02	0.03	0.01	0.01	0.01	0.01	0.04	0.02	0.05	0.09	0.01	0.08
CoV (%)		7.74	6.47	3.98	2.82	1.88	2.53	3.23	2.17	4.35	5.81	0.71	7.00
σ*t***		0.08	0.12	0.06	0.06	0.04	0.04	0.16	0.10	0.24	0.37	0.04	0.34
Min (= average - σ*t)*		0.17	0.30	0.27	0.45	0.51	0.29	0.98	0.97	1.03	1.11	1.26	0.79
Max(= average + σ*t)*		0.34	0.53	0.38	0.57	0.60	0.36	1.30	1.17	1.50	1.85	1.34	1.48

*See details in Appendix E

#Average of 3 computations

**See Table L.2.2 for value of *t*. Degrees of freedom = 2; Probability = 0.05 (95% confidence level); *t* = 4.303

Table L.2.2: *t* distribution critical values

Cumulative probability	$t_{.50}$	$t_{.75}$	$t_{.80}$	$t_{.85}$	$t_{.90}$	$t_{.95}$	$t_{.975}$	$t_{.99}$	$t_{.995}$	$t_{.999}$	$t_{.9995}$
One-tail	**0.50**	**0.25**	**0.20**	**0.15**	**0.10**	**0.05**	**0.025**	**0.01**	**0.005**	**0.001**	**0.0005**
Two-tails	**1.00**	**0.50**	**0.40**	**0.30**	**0.20**	**0.10**	**0.05**	**0.02**	**0.01**	**0.002**	**0.001**
Degrees of freedom											
1	0.000	1.000	1.376	1.963	3.078	6.314	12.71	31.82	63.66	318.31	636.62
2	0.000	0.816	1.061	1.386	1.886	2.920	4.303	6.965	9.925	22.327	31.599
3	0.000	0.765	0.978	1.250	1.638	2.353	3.182	4.541	5.841	10.215	12.924
4	0.000	0.741	0.941	1.190	1.533	2.132	2.776	3.747	4.604	7.173	8.610
5	0.000	0.727	0.920	1.156	1.476	2.015	2.571	3.365	4.032	5.893	6.869
6	0.000	0.718	0.906	1.134	1.440	1.943	2.447	3.143	3.707	5.208	5.959
7	0.000	0.711	0.896	1.119	1.415	1.895	2.365	2.998	3.499	4.785	5.408
8	0.000	0.706	0.889	1.108	1.397	1.860	2.306	2.896	3.355	4.501	5.041
9	0.000	0.703	0.883	1.100	1.383	1.833	2.262	2.821	3.250	4.297	4.781
10	0.000	0.700	0.879	1.093	1.372	1.812	2.228	2.764	3.169	4.144	4.587
Z	0.000	0.674	0.842	1.036	1.282	1.645	1.960	2.326	2.576	3.090	3.291
	0%	**50%**	**60%**	**70%**	**80%**	**90%**	**95%**	**98%**	**99%**	**99.8%**	**99.9%**
	Confidence level										

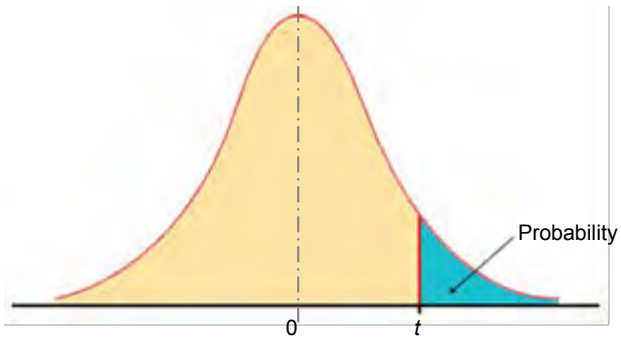

L.3 Biogenic corrosion rates determined from direct measurement of lost wall thicknesses 120 months after installation in the VES

Table L.3.1: Measured biogenic corrosion rates of concrete mixtures ('lids') in the VES.

Mixture	Mixtures in MH I			Mixtures in MH II			Mixtures in MH III		
	Range (mm/yr.)		Average	Range (mm/yr.)		Average	Range (mm/yr.)		Average
	Min	Max	(mm/yr.)	Min	Max	(mm/yr.)	Min	Max	(mm/yr.)
CAC/Alag™	0.20	0.30	0.25	0.20	0.40	0.30	0.10	0.20	0.15
CAC/SIL 23	0.20	0.50	0.35	0.30	0.40	0.35	0.20	0.40	0.30
CAC/DOL 23	0.30	0.50	0.40	0.20	0.40	0.30	0.30	0.40	0.35
CAC/FA/SF/DOL 17	0.30	0.90	0.60	0.30	0.60	0.45	0.20	0.40	0.30
CAC/DOL 18	0.30	0.90	0.60	0.40	0.80	0.60	0.30	0.60	0.45
CAC/DOL 16	0.40	0.90	0.65	0.50	0.80	0.65	0.30	0.70	0.50
PC/FA/DOL 18	0.90	1.60	1.25	0.80	1.30	1.05	0.70	1.00	0.85
PC/DOL 16	1.00	1.60	1.30	0.80	1.40	1.10	0.80	1.10	0.95
PC/SF/DOL 18	1.00	1.80	1.40	0.90	1.50	1.20	0.70	1.20	0.95
PC/GGBS/DOL 18	1.10	1.90	1.50	1.00	1.40	1.20	0.80	1.50	1.15
PC/DOL 18	1.10	1.80	1.45	0.90	1.60	1.25	0.70	1.20	0.95
PC/DOL 23	1.60	2.00	1.80	1.00	2.20	1.60	0.80	1.80	1.30

Table L.3.2: Average biogenic corrosion rates – based on loss of wall thicknesses of samples.

Mixtures	Range (mm/yr.)		Average (mm/yr.)	Standard deviation (mm/yr.)	CoV (%)
	Min	Max			
CAC/Alag™	0.17	0.30	0.23	0.08	32.73
CAC/SIL 23	0.23	0.43	0.33	0.03	8.66
CAC/DOL 23	0.27	0.43	0.35	0.05	14.29
CAC/FA/SF/DOL 17	0.27	0.63	0.45	0.15	33.33
CAC/DOL 18	0.33	0.77	0.55	0.09	15.75
CAC/DOL 16	0.40	0.80	0.60	0.09	14.43
PC/FA/DOL 18	0.80	1.30	1.05	0.20	19.05
PC/DOL 16	0.87	1.37	1.12	0.18	15.72
PC/SF/DOL 18	0.87	1.50	1.18	0.23	19.05
PC/GGBS/DOL 18	0.97	1.60	1.28	0.19	14.75
PC/DOL 18	0.90	1.53	1.22	0.25	20.68
PC/DOL 23	1.13	2.00	1.57	0.25	16.06

L.4 BSE micrographs of the attacked matrix (products of corrosion)

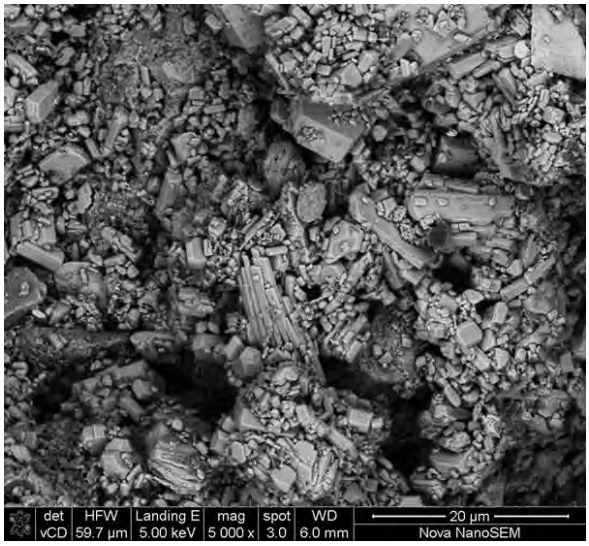

Figure L.4.1: Products of corrosion from a PC/DOL 18 mixture, showing gypsum.

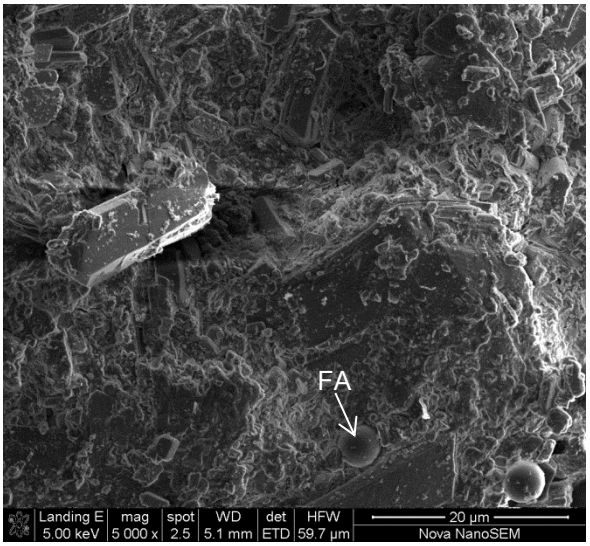

Figure L.4.2: Products of corrosion from a PC/FA/DOL 18 mixture, showing gypsum and some fly ash.

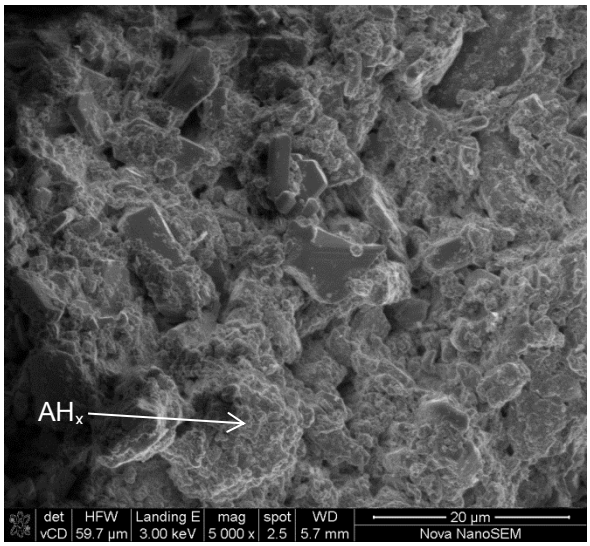

Figure L.4.3: Products of corrosion from a CAC/DOL 18 mixture, showing gypsum and AH_x.

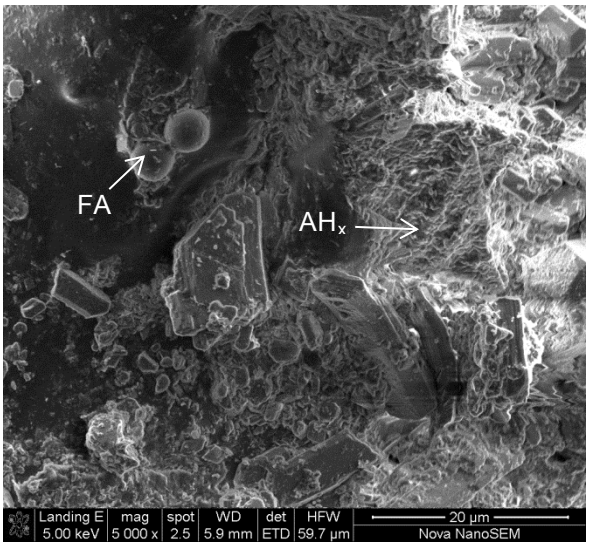

Figure L.4.4: Products of corrosion from a CAC/FA/SF/DOL 17 mixture, showing gypsum, some fly ash and AH_x.

L.5 Surface pH results

Table L.5.1: Surface pH results for concrete samples installed in the manhole at Langa.

Mixture*	Time (days)**	Average surface pH[#]	Standard deviation[#]	Coefficient of variation (%)
PC 100	0	13.38	0.13	0.98
	32	10.67	0.58	5.41
	54	9.33	0.58	6.19
	90	8.00	0.50	6.25
	123	6.50	0.50	7.69
	156	5.00	0.50	10.00
	185	3.33	0.29	8.66
PC 67/GGBS 33	0	13.24	0.15	1.14
	32	11.00	1.00	9.09
	54	10.33	0.58	5.59
	90	9.00	0.00	0.00
	123	5.83	0.29	4.95
	156	4.50	0.50	11.11
	185	4.33	0.29	6.66
PC 75/FA 25	0	13.12	0.08	0.61
	32	10.33	0.58	5.59
	54	9.67	0.58	5.97
	90	8.83	0.76	8.65
	123	7.00	0.50	7.14
	156	5.33	0.58	10.83
	185	4.83	0.29	5.97
PC 92/SF 8	0	13.45	0.06	0.45
	32	11.67	0.58	4.95
	54	10.67	0.58	5.41
	90	8.67	0.76	8.81
	123	5.50	0.50	9.09
	156	4.07	0.12	2.84
	185	3.17	0.29	9.12
CAC 100	0	11.83	0.09	0.77
	32	9.67	0.58	5.97
	54	8.33	0.58	6.93
	90	7.00	0.50	7.14
	123	4.50	0.50	11.11
	156	4.17	0.29	6.93
	185	4.07	0.12	2.84
CAC 65/GGBS 10/FA 25	0	11.52	0.13	1.09
	32	9.83	0.76	7.77
	54	8.50	0.50	5.88
	90	7.83	0.29	3.69
	123	5.17	0.29	5.59
	156	4.33	0.15	3.53
	185	4.03	0.06	1.43

*See details in Appendix G

**Time lapse after installation in the manhole at Langa

[#]Average of 3 readings

Table L.5.2: Surface pH results for concrete samples installed in the sewer (VES).

Mixture*	Time (days)**	Average surface pH[#]	Standard deviation[#]	Coefficient of variation (%)
PC 100	0	13.38	0.13	0.98
	34	10.83	0.29	2.66
	96	8.17	0.29	3.53
	142	5.67	0.29	5.09
	180	4.57	0.12	2.53
PC 67/GGBS 33	0	13.24	0.15	1.14
	34	11.33	0.58	5.09
	96	9.50	050	5.26
	142	5.17	0.29	5.59
	180	4.83	0.29	5.97
PC 75/FA 25	0	13.12	0.08	0.61
	34	10.50	0.50	4.76
	96	9.33	0.58	6.19
	142	5.67	0.76	13.48
	180	5.03	0.45	8.96
PC 92/SF 8	0	13.45	0.06	0.45
	34	11.33	0.58	5.09
	96	9.17	0.29	3.15
	142	5.33	0.29	5.41
	180	4.17	0.29	6.93
CAC 100	0	11.83	0.09	0.77
	34	9.67	0.29	2.99
	96	7.17	0.29	4.03
	142	4.67	0.29	6.19
	180	4.40	0.17	3.94
CAC 65/GGBS 10/FA 25	0	11.52	0.13	1.09
	34	10.00	0.50	5.00
	96	8.17	0.29	3.53
	142	5.33	0.29	5.41
	180	4.67	0.29	6.19

*See details in Appendix G

**Time lapse after installation in the sewer (VES)

[#]Average of 3 readings

L.6 Sewage temperature and pH readings

Table L.6.1: Sewage temperature and pH at the VES and Langa.

Site	Sewage temperature (°C)*				Sewage pH*			
	Reading	Mean	Standard deviation	Coefficient of variation (%)	Reading	Mean	Standard deviation	Coefficient of variation (%)
VES	19.70	20.50	0.59	2.89	6.96	6.98	0.09	1.27
	21.00				7.04			
	20.30				7.12			
	20.80				6.99			
	21.20				6.92			
	20.00				6.87			
Langa	20.13	19.55	0.62	3.15	7.22	7.08	0.10	1.39
	19.05				6.95			
	19.00				7.10			
	20.20				7.14			
	18.93				6.99			
	20.00				7.09			

*Measured between 2013 and 2015

L.7 Unrooted 16S rRNA gene phylogenetic trees

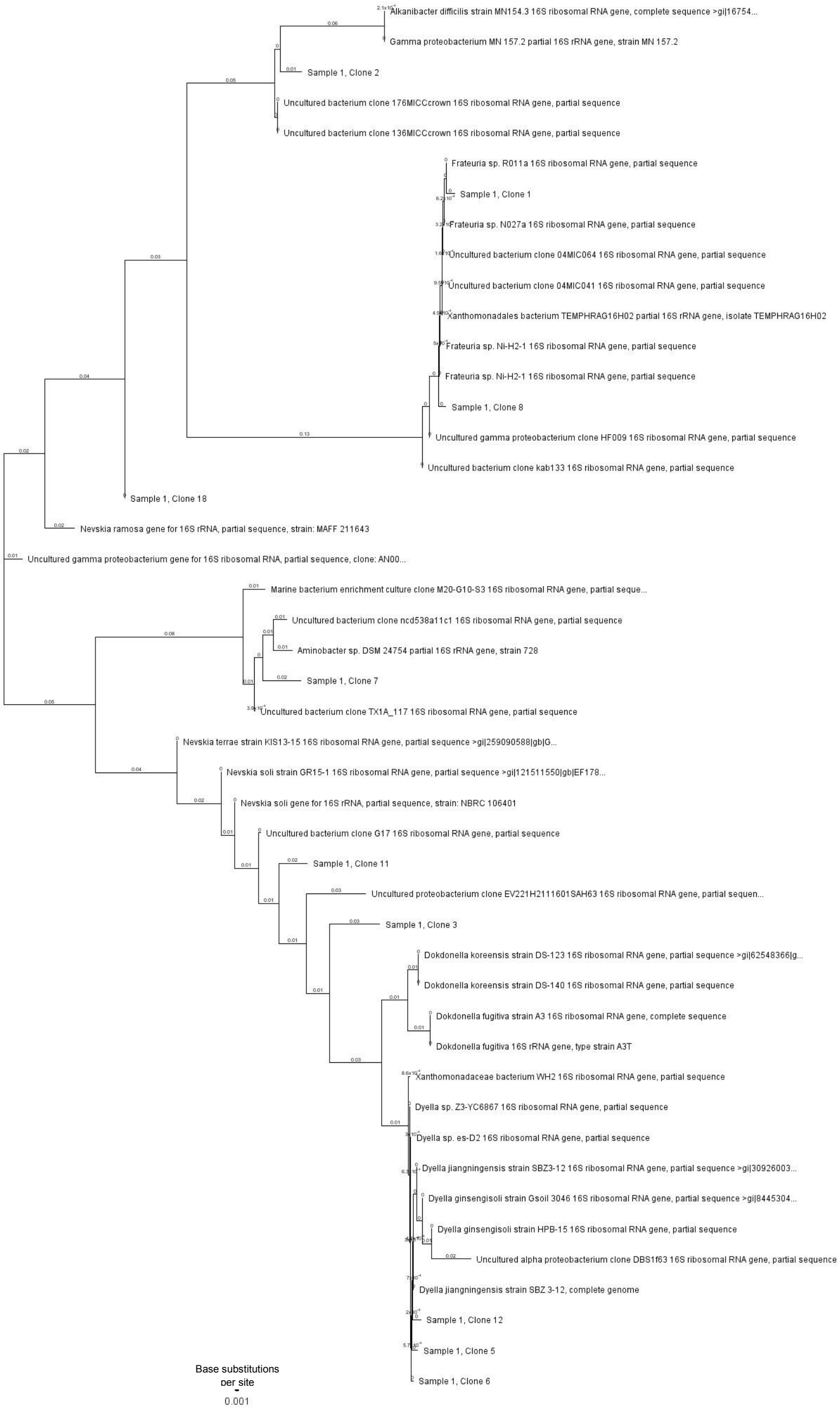

Figure L.7.1: Unrooted phylogenetic tree of 16S rRNA clones identified from the PC/DOL 16 concrete substrate and related sequences, based on the sequence alignment of a common length portion. The tree was constructed using the neighbour joining method.

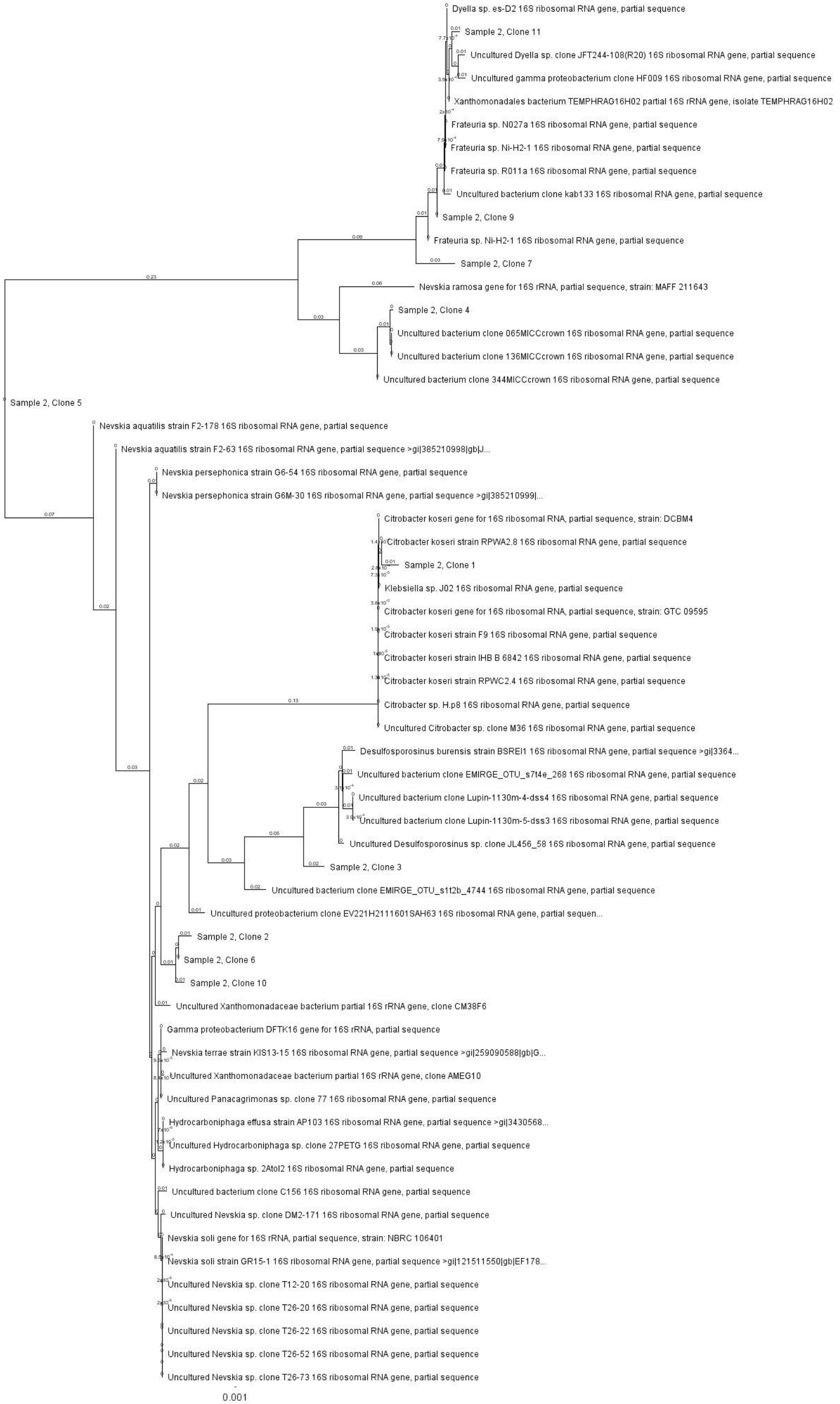

Figure L.7.2: Unrooted phylogenetic tree of 16S rRNA clones identified from the PC/DOL 18 concrete substrate and related sequences, based on the sequence alignment of a common length portion. The tree was constructed using the neighbour joining method.

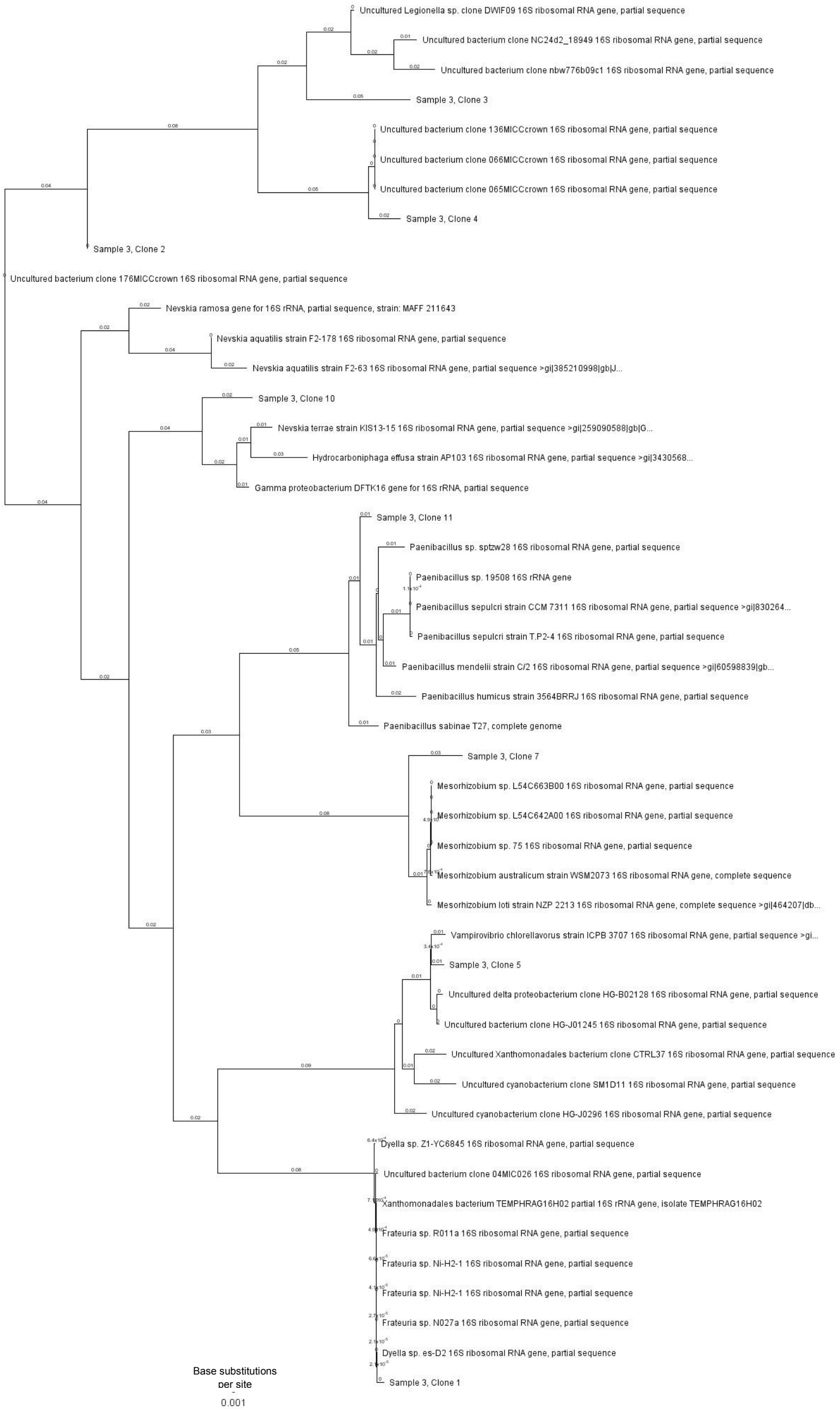

Figure L.7.3: Unrooted phylogenetic tree of 16S rRNA clones identified from the PC/DOL 23 concrete substrate and related sequences, based on the sequence alignment of a common length portion. The tree was constructed using the neighbour joining method.

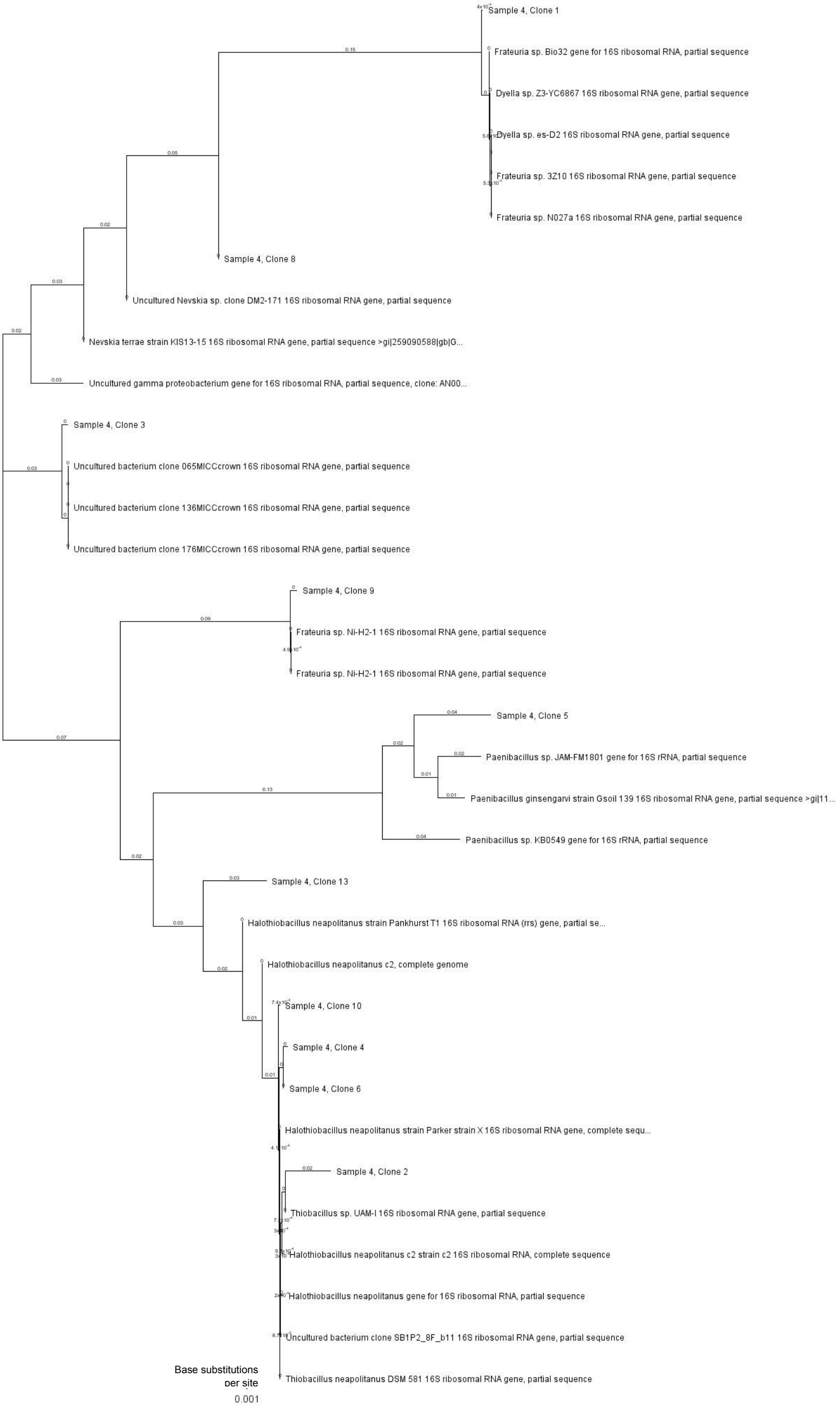

Figure L.7.4: Unrooted phylogenetic tree of 16S rRNA clones identified from the PC/GGBS/DOL 18 concrete substrate and related sequences, based on the sequence alignment of a common length portion. The tree was constructed using the neighbour joining method.

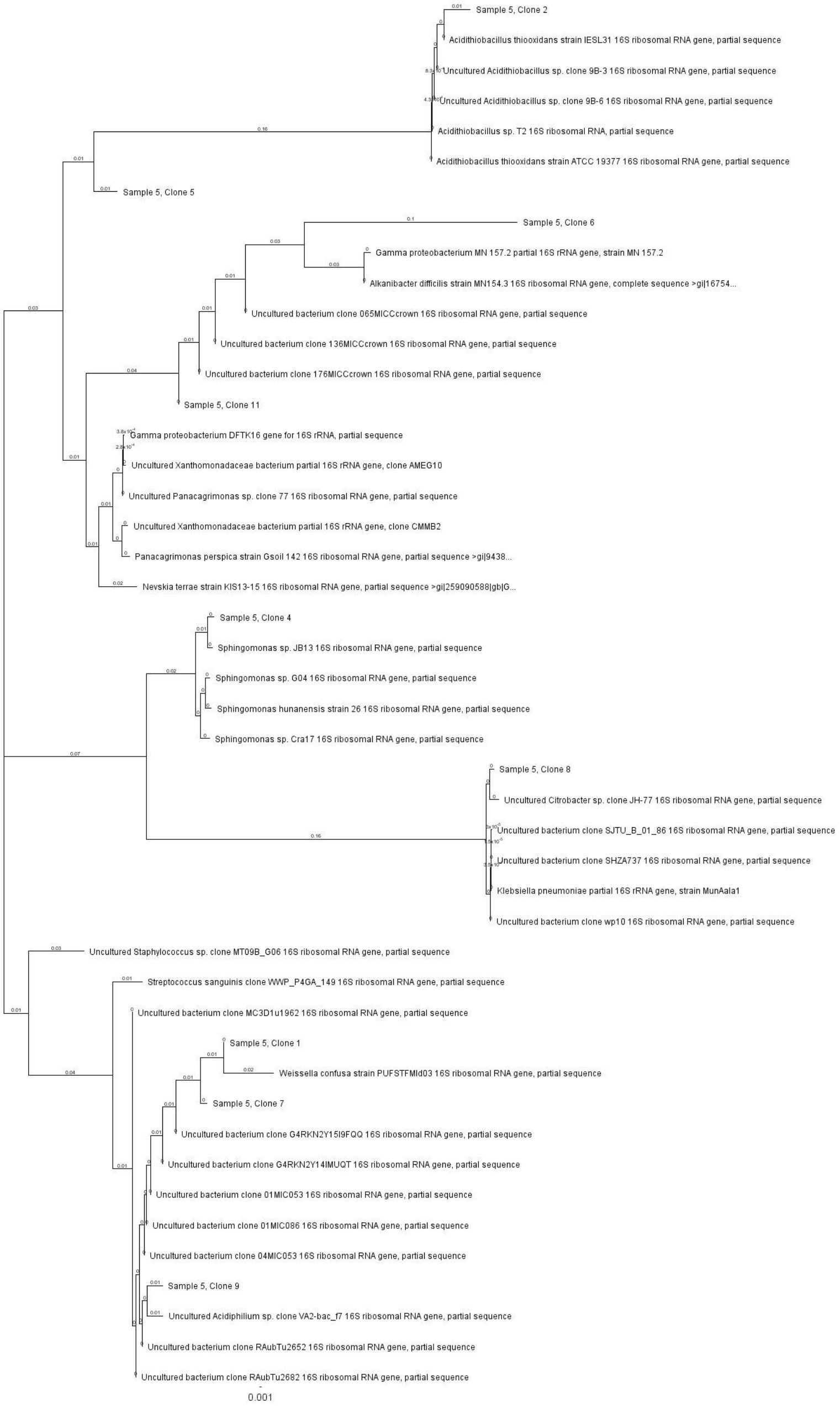

Figure L.7.5: Unrooted phylogenetic tree of 16S rRNA clones identified from the PC/FA/DOL 18 concrete substrate and related sequences, based on the sequence alignment of a common length portion. The tree was constructed using the neighbour joining method.

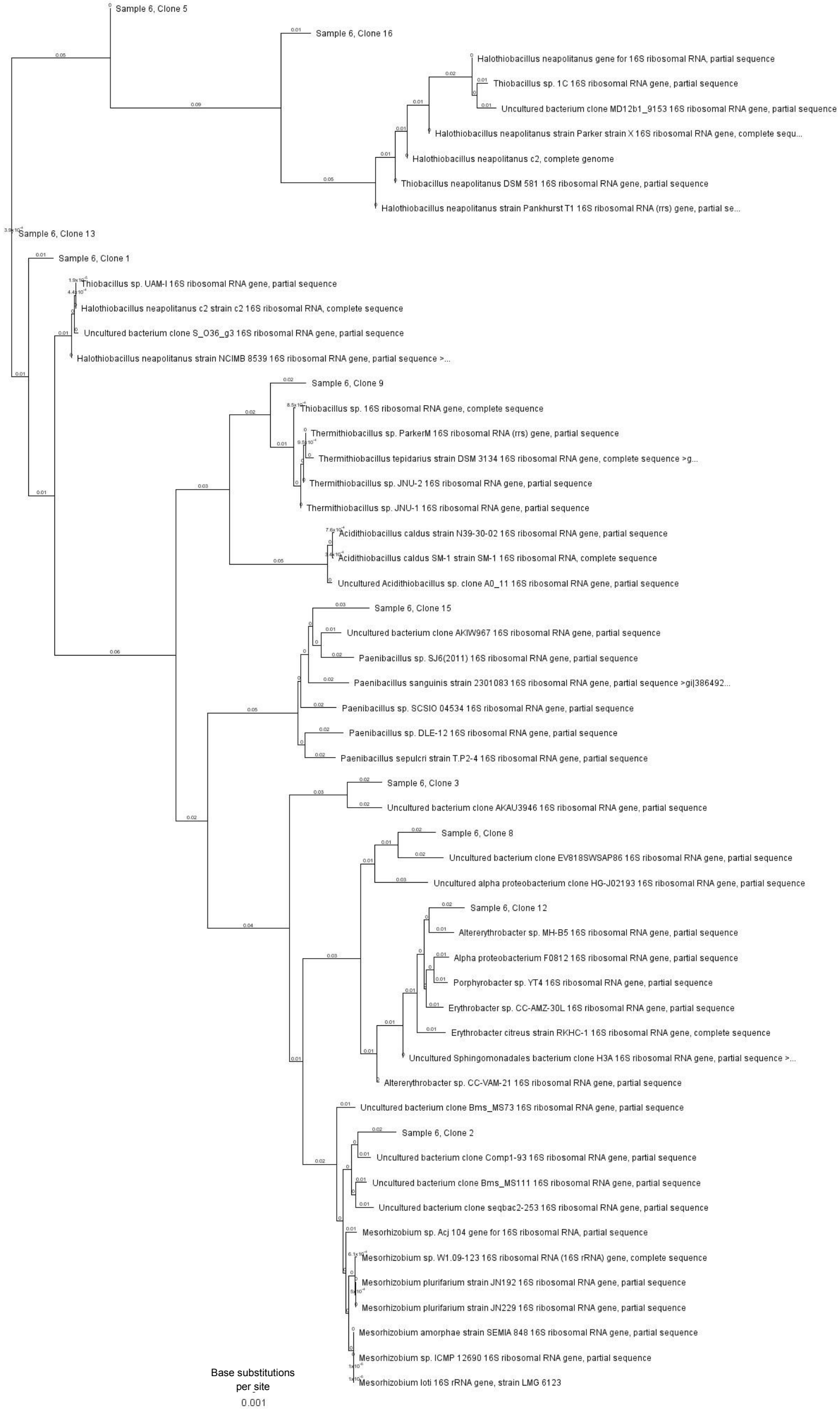

Figure L.7.6: Unrooted phylogenetic tree of 16S rRNA clones identified from the PC/SF/DOL 18 concrete substrate and related sequences, based on the sequence alignment of a common length portion. The tree was constructed using the neighbour joining method.

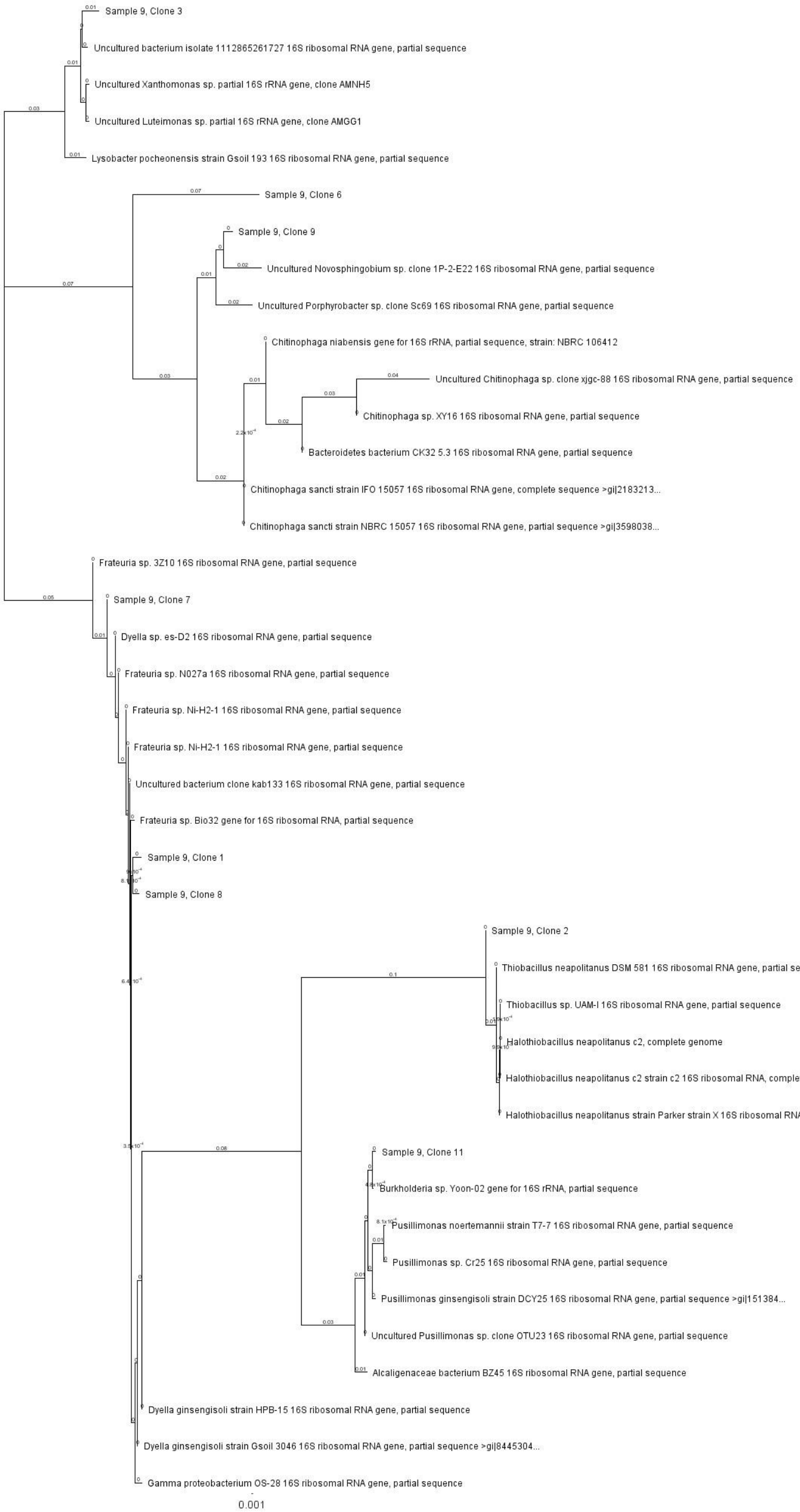

Figure L.7.7: Unrooted phylogenetic tree of 16S rRNA clones identified from the CAC/SIL 23 concrete substrate and related sequences, based on the sequence alignment of a common length portion. The tree was constructed using the neighbour joining method.

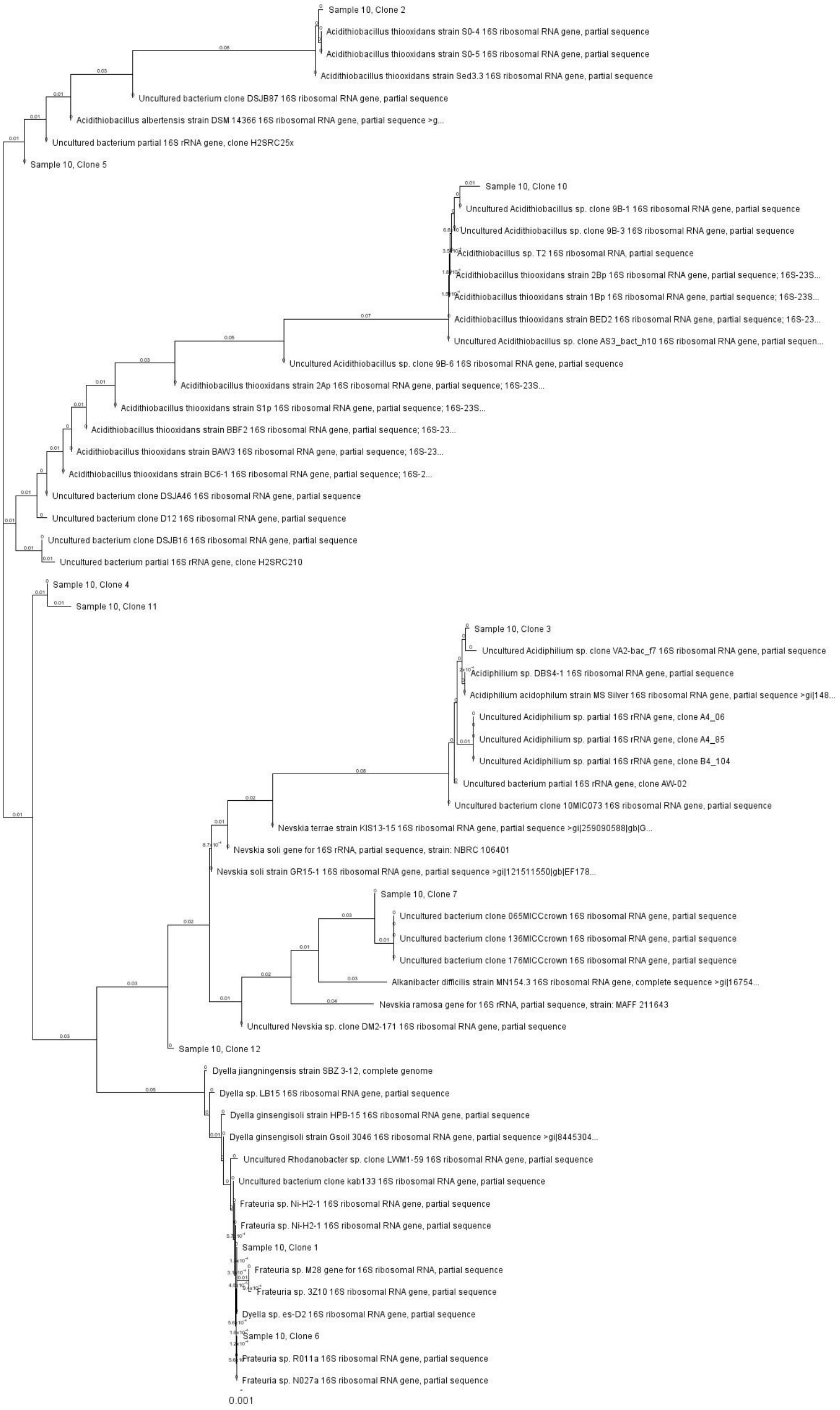

Figure L.7.8: Unrooted phylogenetic tree of 16S rRNA clones identified from the CAC/DOL 16 concrete substrate and related sequences, based on the sequence alignment of a common length portion. The tree was constructed using the neighbour joining method.

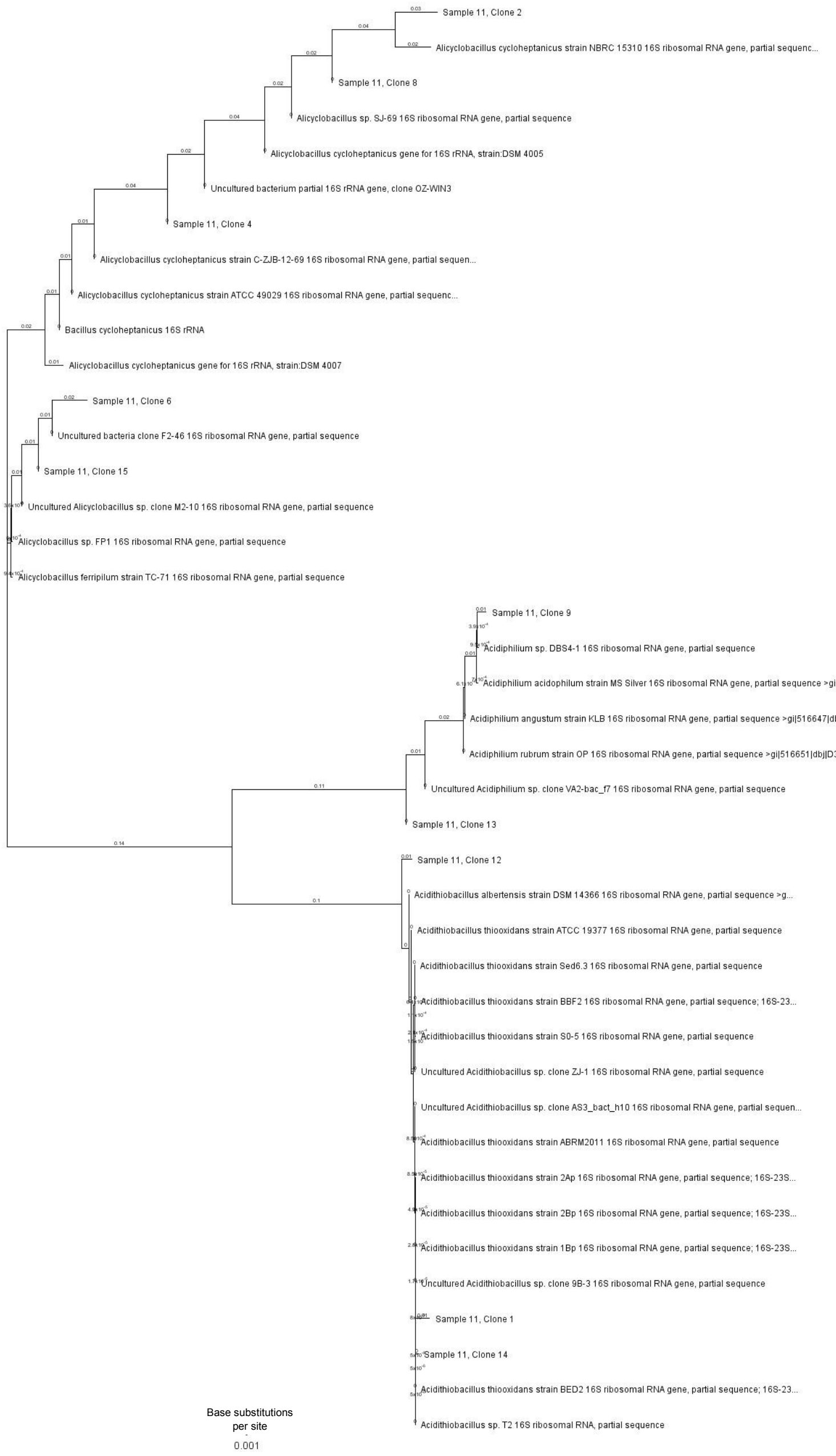

Figure L.7.9: Unrooted phylogenetic tree of 16S rRNA clones identified from the CAC/DOL 18 concrete substrate and related sequences, based on the sequence alignment of a common length portion. The tree was constructed using the neighbour joining method.

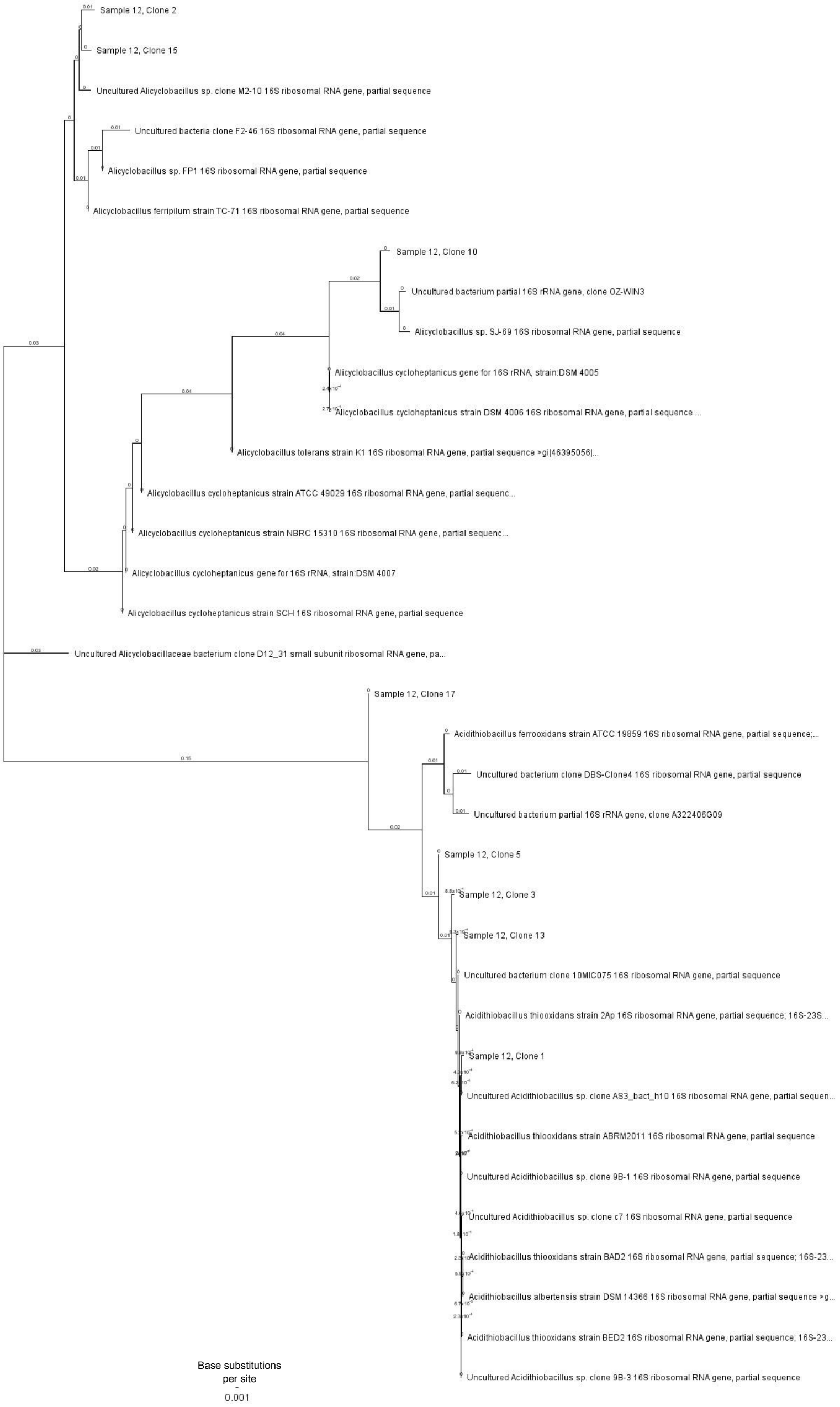

Figure L.7.10: Unrooted phylogenetic tree of 16S rRNA clones identified from the CAC/DOL 23 concrete substrate and related sequences, based on the sequence alignment of a common length portion. The tree was constructed using the neighbour joining method.

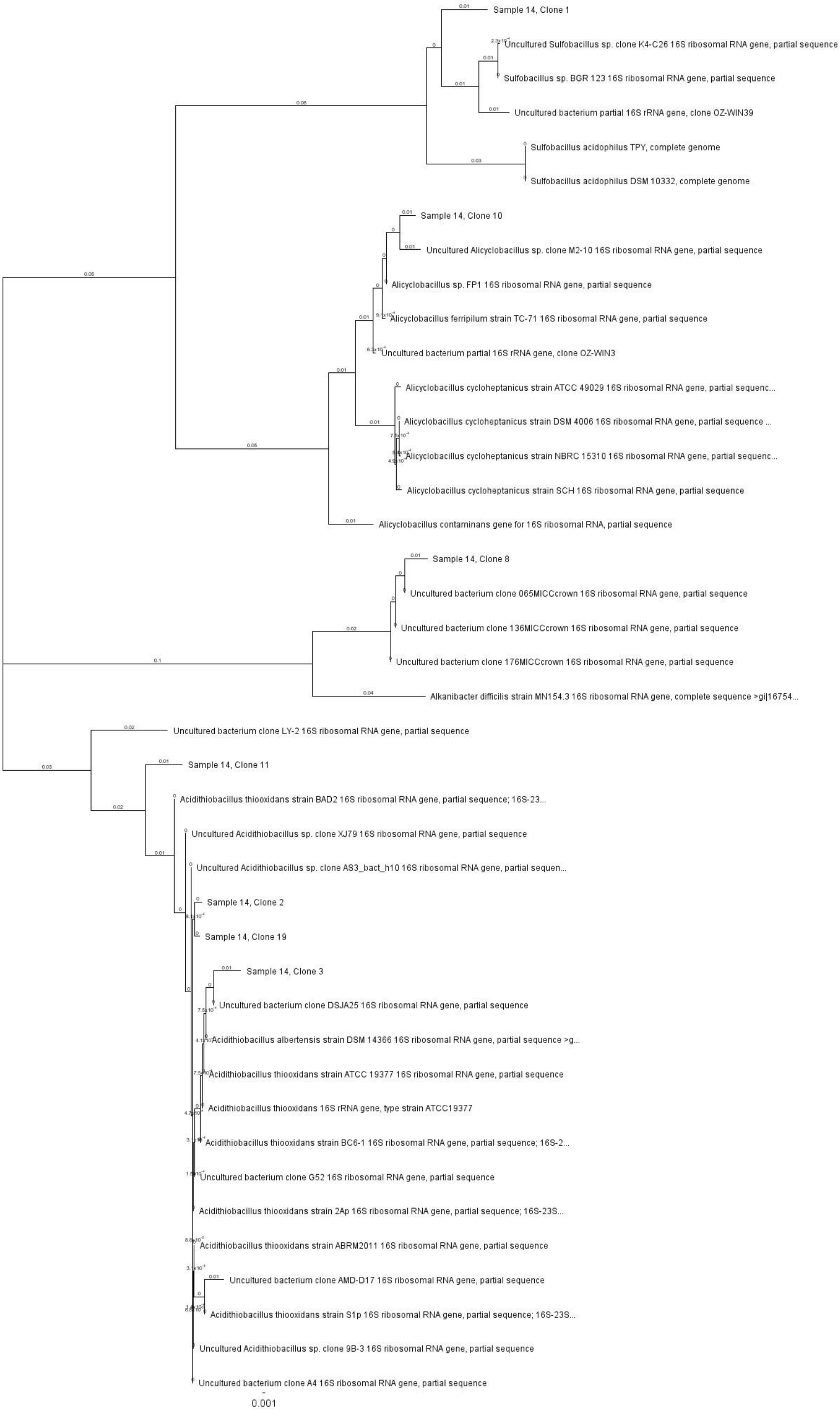

Figure L.7.11: Unrooted phylogenetic tree of 16S rRNA clones identified from the CAC/FA/SF/DOL 17 concrete substrate and related sequences, based on the sequence alignment of a common length portion. The tree was constructed using the neighbour joining method.

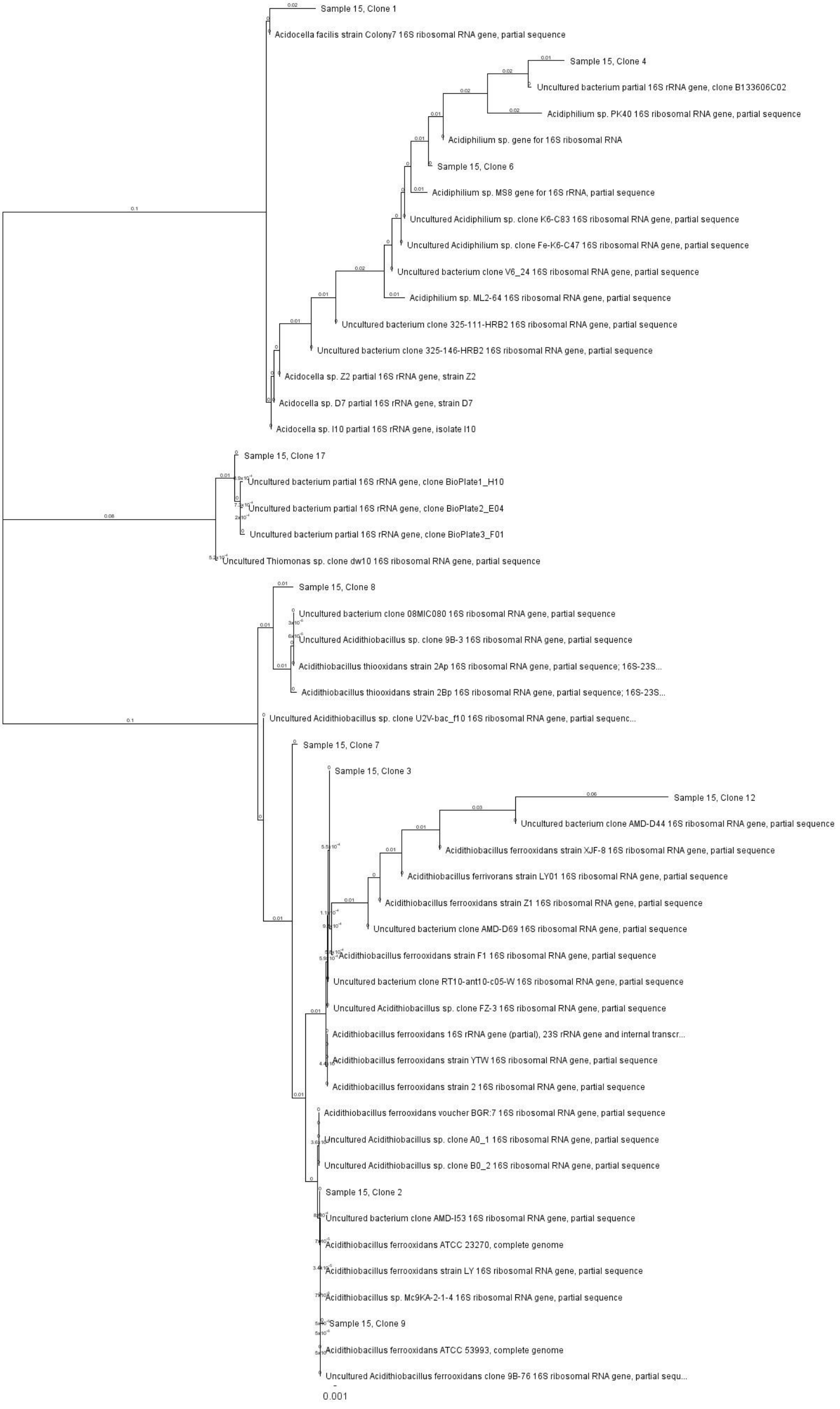

Figure L.7.12: Unrooted phylogenetic tree of 16S rRNA clones identified from the CAC/Alag^{TM} 20 concrete substrate and related sequences, based on the sequence alignment of a common length portion. The tree was constructed using the neighbour joining method.

L.8 Statistical measures: Multiple regression

Multiple regression is applicable in situations where there are several independent variables, $x_1, x_2, x_3, \ldots x_p$ (such as the amount of calcium hydroxide, iron, and alumina gel in a cement), that are related to a dependent variable y (such as corrosion rate of a mixture made from the cement under investigation).

Assume that we have a sample of n items, and that on each item we have measured a dependent variable y and p independent variables $x_1, \ldots\ldots x_p$. The i^{th} sample item thus gives rise to the ordered set ($y_i, x_{1i}, \ldots x_{pi}$). We can then fit the multiple regression model of the form (Equation L.8.1):

$$y_i = \beta_0 + \beta_1 x_{1i} + \ldots + \beta_p x_{pi} + \varepsilon_i \tag{L.8.1}$$

In any multiple regression model, the estimates $\overline{\beta_0}$, $\overline{\beta_1}$, … $\overline{\beta_p}$ are computed by least-squares, just as in simple linear regression, and Equation L.8.2 is called the *least-squares* equation.

$$\overline{y} = \overline{\beta}_0 + \overline{\beta}_1 x_1 + \ldots + \overline{\beta}_p x_p \tag{L.8.2}$$

Now define $\overline{y_i}$ to be the y coordinate of the least-squares equation corresponding to the x values ($x_{1i}, \ldots x_{pi}$). The residuals are the quantities $e_i = y_i - \overline{y_i}$, which are the differences between the observed y values and the y values given by the equation. We want to compute $\overline{\beta_0}$, $\overline{\beta_1}$, … $\overline{\beta_p}$ so as to minimise the sum of the squared residuals $\sum_{i=1}^{n} e_i^2$. To do this, we express e_i in terms of $\overline{\beta_0}$, $\overline{\beta_1}$, … $\overline{\beta_p}$ (Equation L.8.3):

$$e_i = y_i - \overline{\beta}_0 - \overline{\beta}_1 x_{1i} - \ldots - \overline{\beta}_p x_{pi} \tag{L.8.3}$$

Thus we wish to minimise the sum given by Equation L.8.4 by taking partial derivatives of Equation L.8.4 with respect to $\overline{\beta_0}$, $\overline{\beta_1}$, … $\overline{\beta_p}$, and equating them to 0 prior to solving the resulting p + 1 equations in p + 1 unknowns.

$$\sum_{i=1}^{n} \left(y_i - \overline{\beta}_0 - \overline{\beta}_1 x_{1i} - \ldots - \overline{\beta}_p x_{pi} \right)^2 \tag{L.8.4}$$

The expressions obtained for $\overline{\beta_0}$, $\overline{\beta_1}$, … $\overline{\beta_p}$ are multiple regression coefficients, and for each estimated coefficient, there is an estimated standard deviation that can be used for calculating variability.

L.9 References

Navidi, W. 2006. *Statistics for engineers and scientists*. New York: McGraw-Hill.

Appendix M: EBE Faculty: Assessment of ethics in research projects[1]

EBE Faculty: Assessment of Ethics in Research Projects (Rev2)

Any person planning to undertake research in the Faculty of Engineering and the Built Environment at the University of Cape Town is required to complete this form before collecting or analysing data. When completed it should be submitted to the supervisor (where applicable) and from there to the Head of Department. If any of the questions below have been answered YES, and the applicant is NOT a fourth year student, the Head should forward this form for approval by the Faculty EIR committee: submit to Ms Zulpha Geyer (Zulpha.Geyer@uct.ac.za; Chem Eng Building, Ph 021 650 4791). **NB: A copy of this signed form must be included with the thesis/dissertation/report when it is submitted for examination**

This form must only be completed once the most recent revision EBE EIR Handbook has been read.

Name of Principal Researcher/Student: Moses Kiliswa Department: Civil Engineering

Preferred email address of the applicant: KLSWOP001@myuct.ac.za

If a Student: Degree: PhD Supervisor: Prof Mark G. Alexander

If a Research Contract indicate source of funding/sponsorship:

Research Project Title: The influence of sewer environment parameters on the deterioration of concrete sewer pipes

Overview of ethics issues in your research project:

Question 1: Is there a possibility that your research could cause harm to a third party (i.e. a person not involved in your project)?	YES	NO ✓
Question 2: Is your research making use of human subjects as sources of data? If your answer is YES, please complete Addendum 2.	YES	NO ✓
Question 3: Does your research involve the participation of or provision of services to communities? If your answer is YES, please complete Addendum 3.	YES	NO ✓
Question 4: If your research is sponsored, is there any potential for conflicts of interest? If your answer is YES, please complete Addendum 4.	YES	NO ✓

If you have answered YES to any of the above questions, please append a copy of your research proposal, as well as any interview schedules or questionnaires (Addendum 1) and please complete further addenda as appropriate. Ensure that you refer to the EiR Handbook to assist you in completing the documentation requirements for this form.

I hereby undertake to carry out my research in such a way that

- there is no apparent legal objection to the nature or the method of research; and
- the research will not compromise staff or students or the other responsibilities of the University;
- the stated objective will be achieved, and the findings will have a high degree of validity;
- limitations and alternative interpretations will be considered;
- the findings could be subject to peer review and publicly available; and
- I will comply with the conventions of copyright and avoid any practice that would constitute plagiarism.

Signed by:

	Full name and signature	Date
Principal Researcher/Student:	Moses Wopicho Kiliswa	23 Jan 2014

This application is approved by:

Supervisor (if applicable):	Mark Gavin Alexander	24 Jan 2014
HOD (or delegated nominee): *Final authority for all assessments with NO to all questions and for all undergraduate research.*		27.01.14
Chair : Faculty EIR Committee For applicants other than undergraduate students who have answered YES to any of the above questions.		

[1] The research project title at the time of signing this form was tentative

Appendix N: List of papers published in the course of the current study

1. Kiliswa, M. W., & Alexander, M. G. 2014. Towards developing a cementitious lining to withstand biogenic sulphuric acid attack in concrete sewer pipes. *Concrete Plant International*. Issue 5/2014.
2. Kiliswa, M. W., & Alexander, M. G. 2014. Biogenic corrosion of concrete sewer pipes: A review of the performance of cementitious materials. *The 13th International Conference on Durability of Building Materials and Components*. August 30 – September 6. São Paulo.
3. Kiliswa, M. W., Alexander, M. G., & Beushausen, H. 2015. Durability design of concrete mixtures for sewer pipe applications: A review of the Life Factor Method. *The 4th International Conference on Concrete Repair, Rehabilitation and Retrofitting*. October 5 – 7. Leipzig.
4. Kiliswa, M. W., & Alexander, M. G. 2015. Composition and microstructure of calcium aluminate cement systems subjected to biogenic sulphuric acid attack. *The 14th International Congress on the Chemistry of Cement*. October 13 – 16. Beijing.
5. Kiliswa, M. W., Alexander, M. G., & Goyns, A. 2016. Applying an understanding of scanning electron microscopy imaging and energy dispersive spectroscopy mapping/multi-point analysis results to durability assessment of concrete sewer pipes in South Africa. *The 2nd International Conference on Advances in Cement and Concrete Technology in Africa*. January 27 – 29. Dar es Salaam.